UNIVERSITY OF CALIFORNIA SAN DIEGO

SAN DIEGO STATE UNIVERSITY

Design, Synthesis, and Performance of Novel Bifunctional Transition Metal Complexes for Organic Reactions

A Dissertation submitted in partial satisfaction of the
requirements for the degree Doctor of Philosophy

in

Chemistry

by

Braden E. Silva

Committee in charge:

University of California, San Diego

Professor Clifford Kubiak
Professor Charles Perrin

San Diego State University

Professor Douglas Grotjahn, Chair
Professor Temesgen Garoma
Professor Jing Gu

2023

The Dissertation of Braden E. Silva is approved, and it is acceptable in quality and form for publication on microfilm and electronically.

_____

_____

_____

_____

_____

Chair

University of California San Diego

San Diego State University

2023

DEDICATION

Dedicated to the Reader.

TABLE OF CONTENTS

TABLE OF FIGURES

TABLE OF TABLES

ACKNOWLEDGEMENTS

It has been said by many romantic scientists and academics that the years in graduate school are cherished in the highest regard. As a pragmatist, I'll tell you it is indeed every year of one's life that holds such distinction – cherish them all. I'll also tell you that to dedicate such time to scientific leaning and research has truly been a gift in my life. The environment of ambition, challenge, and teamwork is truly profound and hardly replicated in any other pursuit. Under the direction of Professor Douglas Grotjahn, a fine community of science was revealed to me as I started my time at SDSU. Doug taught students to work as he himself does, with fine attention to detail and a highly active imagination. A lesson that will stick with me for life is, "write what you do!" It might be said that a good scientist can do three things at once: set up an experiment, measure the observables, and simultaneously write everything down! The other lesson Doug taught his students is that the best way to understand anything is to talk about it, write about it, and draw it out. Some of my favorite memories are discussions from group meetings – at that time held on weeknights, and with ample food. A full meal provided by two group members each meeting. The food is key. Without it, minds wander and unrest brews. Fill your brother's stomach, and he will surely lend you his mind.

Though I must honestly say I benefited from interactions with every faculty member at SDSU and UCSD, I must call out some by name. Professor Andrew Cooksy, thank for your advice and training in computational and physical chemistries and logical thought. You have a great mind, Dr. Cooksy. Professor Jeff Gustafson, I'm sure I've never met anyone else that can match your enthusiasm, and students love you for it. Professor Jing Gu thank you for being a part of my committee and being a part of my journey.

Professors Josh Figueroa and Joseph O'Connor, thank you both for great lectures on

Organometallic Chemistry. Professor Cliff Kubiak, thank you for the best spectroscopy class I ever attended, Inorganic NMR, and thank you for being a part of my graduate committee and progression through the program. Thank you, Professor Charles Perrin, for both being a part of my graduate committee and for the lectures in Mechanisms of Organic Reactions. I am honored to have learned from all of you.

I must also call attention to those students with whom I did overlap, like sliding doors, only briefly. Dave Marelius, you first introduced me to glovebox work and freshly distilling ethereal solvents. Though we never actually overlapped in the lab, I owe thanks to Gulin Erdogan-Marelius. I read through many of Gulin's notebooks and can surely say my notebook was kept more legible, succinct, and likely accurate through imitation of your style. Reji Nair I must thank for pioneering the first work on biaryl phosphine – the project on which I spent most of my time. Additionally, my efforts were built upon the work of Yi Gong and Abhinandini Sharma, whom I never had the opportunity to meet.

Now I must acknowledge those graduate students that I spent most of my time with; those I must thank for making every day in the lab a pleasure. Erik Paulson, I likely learned more from you than any other graduate student; you have a great mind for science and a great perspective on life. Jayneil Kamdar, you are a great friend, and I must say I am always surprised you have been on this planet longer than I. Aaron Nash; I could always count on you for company in the lab on late nights. Sometimes the only time one can get anything done is after one has spent all day putting his nose in anyone else's work. Erik, Jayneil, and Aaron – you were my closest colleagues, and I thoroughly enjoyed your company. We would discuss our work over coffee, lunch, drinks, and during journeys near and far (LA, SF, Austin, and back to the coffee shop I think I'll need one more espresso). It was all a grand adventure, and I thank you for it.

Farzaneh Saeedifard, it was great to start the graduate program in the same cohort and I am amazed at your productivity. Daniel Sattler, you have the most encyclopedic knowledge of popular culture I have ever seen. Sima Yazdani, your dedication is inspiring. Colton Breyer, you are probably both the best analytical chemist and worst organic chemist to ever work in the Grotjahn research group, and I mean that in the best way possible.

Though not in the Grotjahn research group, there is another group of students that must be acknowledged. Josh Swider, you have become one of my closest friends, and I owe you many thanks. A housemate through six years, we've seen highs, lows, and just about everything in between. Josh and I see the world as a puzzle, and we look for the cracks, as it is the easiest way to let the light in. We spent time doing everything from working on motorcycles, building vegetable gardens, and adopting a border collie named Iodo Dalton. Your friendship has been a great reminder that the journey is usually more important than the destination.

Brian Maniaci and Sean Maddox, you are both great friends and scientists. I can see the positive impact you two leave in your wake. David Onofrei, Haley Swanson, Michael Coste, and Monny Singh I was honored to go through the UCSD year with all of you.

A special mention is due to one graduate student in particular, Sabrina Younan. I can remember the first time we met - you were stumbling around in the NMR lab. A life-threatening virus, lock-down orders, and one brave email. As I write this now, we are engaged to be married, and as they say, the rest is history. You are the love of my life and I learn from you every day. I have never met anyone as wonderful or as organized as you, Sabrina.

I also must thank all the undergraduate students that overlapped with my time in the graduate program. Hanne Henriksen, Kiersten Sukert, Eileen Salsgiver, David Wu, Brett Vincenzini, Esteban Delgado, Derek Aspacio, Daniel Cassaro, Patrick Brklycica, Katrina Ngo,

Susan Andersen, and Mitchell Becker – I know you will all do great things in life. Keep your passions and your energy.

Chapter 1 contains unpublished material and is an introduction to the fields of catalysis and bifunctional catalysis. Contextual information about broader impacts is discussed. The dissertation author was the sole investigator and author of this chapter.

Chapter 2 contains material and data being prepared for publication on the development of functionalized biaryl phosphine ligands for application in gold catalysis. This chapter starts with development of synthetic methods for high efficiency in the synthesis of new iterations on the chemical structure. The use of high throughput screening for reaction discovery is discussed and the result from our trials is discussed. Evaluation of the different ligand candidates is done through NMR studies on two reactions. The first reaction studied is carboxylic acid addition to terminal alkynes. The second reaction studied is isomerization of alkynes. The dissertation author was the sole investigator and author of this chapter.

Chapter 3 contains data currently being prepared for publication on the synthesis of hydrogen-bond-donor-functionalized ferrocenyl bisphosphines, and studies on the coordination chemistry of the novel bisphosphines with platinum and nickel. Development of the synthetic route to yielding the target compounds was necessary, and the major points of concern are discussed. The dissertation author was the sole investigator and author of this chapter.

VITA

2014 Bachelor of Science in Chemistry, California State University, Sacramento

2023 Doctor of Philosophy in Chemistry, University of California San Diego and San Diego State University

ABSTRACT OF THE DISSERTATION

Design, Synthesis, and Performance of Novel Bifunctional Transition Metal Complexes for Organic Reactions

by

Braden E. Silva

Doctor of Philosophy in Chemistry

University of California San Diego, 2023

San Diego State University 2023

Professor Douglas Grotjahn, Chair

CHAPTER 1. This chapter introduces the field of study and motivations steering the direction of development. The topics of catalysis and bifunctional catalysis are discussed.

CHAPTER 2. This chapter describes the development of biaryl phosphines containing functionalization with a pendent base for use in gold catalyzed organic reactions. This chapter starts with development of synthetic methods for high efficiency in the synthesis of new iterations on the chemical structure. The use of high throughput screening for reaction discovery is discussed and the result from our trials is discussed. Evaluation of the different ligand candidates is done through NMR spectroscopic studies on two reactions. The first reaction studied is carboxylic acid addition to terminal alkynes. The second reaction studied is isomerization of alkynes.

CHAPTER 3. This chapter describes the synthesis of hydrogen-bond-donor-functionalized ferrocenyl bisphosphines, and studies on the coordination chemistry of the novel bisphosphines with platinum and nickel. Development of the synthetic route to yielding the target compounds was necessary, and the major points of concern are discussed. Studies on the coordination chemistry of the ferrocenyl bisphosphines with platinum and nickel are discussed.

CHAPTER 1

1.1 Catalysis: Background and Significance

For more than 250 years, human society has been undergoing an amazing period of growth, which can largely be linked with the development and utilization of various forms of technology.[1] Much of this progress is directly dependent upon the results of extensive work on research, development, and application of chemical technologies. Some of the most important developments in chemistry have been, and continue to be, in the area of catalysis. Catalysis impacts sectors ranging from energy and fuel production and storage to construction of functional materials to synthesis of life saving medicines, because facilitates of complex and highly specific bond making and breaking processes between starting materials and products. Evidence of the impact of catalysis can be seen from the estimated global merchant catalysts market in 2017, a staggering $31.3 billion.[2] In fact, it was estimated that over 90% of all industrial chemicals are produced with the use of a catalysts.[1] Since 2001, Nobel Prizes have been given in three different years to recognize research and development of catalytic processes including chiral catalyzed hydrogenation (reduction) and epoxidation (oxidation) reactions[3], alkene metathesis[4], and cross-coupling reactions[5]. It should also be noted that each of these prize-winning research programs has utilized transition metal catalysts. In general, a catalyst is anything that can alter the energy profile of a chemical reaction, and by the final step of the reaction, the catalyst itself is regenerated and released; free to coordinate once again with the starting material to produce another product molecule. Seemingly a simple enough concept, identifying or predicting a catalyst's identity for any given chemical reaction is a non-trivial task, and often will require extensive research and iterative optimization.

In addition to allowing chemists to achieve otherwise energetically demanding reactions with high specificity, catalysts can also improve the efficiency of chemical reactions and reduce the overall environmental impact, a benefit to modern society. Green chemistry is a concept that aims to create sustainability and prevent the waste and pollution that has been so deleterious to the earth's environment. Among the principles of green chemistry that can be advanced by the continued development of catalyst technology are atom economy, less hazardous chemical synthesis, design for energy efficiency, reduce by products, and design to avoid degradation. Furthermore, it should be noted that catalysis itself is one of the twelve principles of green chemistry![6]

Known catalysts range widely in composition, structure, levels of activity, and even state of matter. However, two of the most fundamental categories of catalysts are heterogeneous and homogeneous. Heterogeneous catalysts are in a different phase state or are immiscible with the reactants. Homogeneous catalysts, which will be the topic of this thesis, are completely dispersed and mixed within the reaction media – often being some solvent that can dissolve both the starting materials and the catalysts. Heterogeneous catalysts have proven to be extremely useful in many types of chemical processes and offer the benefit of being easily removed from the products. A pathway for some catalytic development is immobilization of homogeneous catalyst structures to solid supports (a suitable polymer) with the use of some molecular linker.[7] Homogeneous catalysts are generally easier to study mechanistically, resulting in a situation where rational design to create variations in catalyst structure can lead to predictable patterns of reactivity. Often this can be accomplished by variation in the ligands that bind the metal. In the work reported in this thesis the metals will be of the transition series; and much of the focus of the ligand development will center on those with a phosphorus donor atom, known as phosphines.

Bifunctional catalysis has emerged in recent decades as a strategy for improving catalyst activity as well as altering selectivity. In general, bifunctional catalysis can occur any time there are multiple components within a catalyst structure that operate simultaneously to activate substrates and participate in bond-breaking and -making events. Often the various components of a bifunctional catalyst's structure will have opposing roles within the reaction mechanism, for example both a Bronsted acid and base that interact with a substrate, instead of with each other. Within the field of bifunctional catalysis, metal-ligand cooperation occurs in catalyst systems when a substrate undergoes changes in bonding with participation of both the metal center and a functional group within the ancillary ligands bound to the metal.

Withing the Grotjahn research group, there has been extensive development around two bifunctional catalyst system: Ru-1 which is an *anti*-Markovnikov alkyne hydration catalyst, and Ru-2 which is an alkene isomerization catalyst. Both of these catalysts contain pendent basic functionalization that are key to performance of the catalyst.

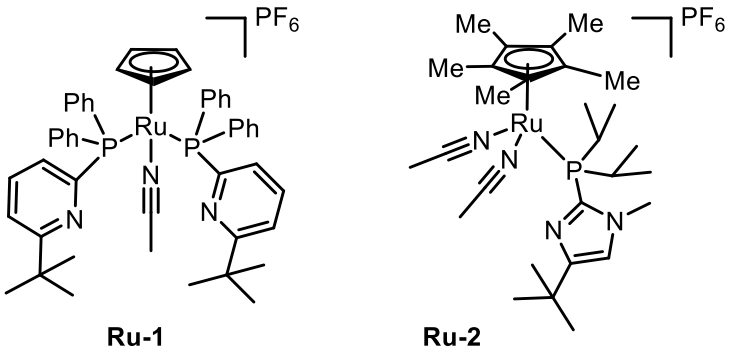

Figure 1. 1 Ru-1: anti-Markovnikov alkyne hydration catalyst, **Ru-2**: alkene isomerization catalyst

Control experiments that compare the heterocycle containing complexes to analogs without any Lewis basic atoms are especially useful at depicting the importance of the heterocycle. The catalyst Ru-1 is able to produce 98.3 % production of nonanaldehyde in 48 hours. A control

compound that is simply $CpRu(PPh_3)_2(PF_6)$ is only able to produce trace amounts of the anti-Markovnikov product, 1%, after 21 hours.

A similar comparison was studied for the alkene isomerization catalyst, **Ru-2**. The control compound $CpRuP(iPr)_3(PF_6)$ is able to produce E-2-heptene from 1-heptene in 1.8% yield after heating for 240 hours. The bifunctional alkene isomerization catalyst **Ru-2** produces 95.6% E-2-heptene after 97 hours. These comparison study show that the incorporation of the pendent base has a drastic effect on the catalyst function. An overarching goal for the work of this thesis is to take the concepts driving the activity of **Ru-1** and **Ru-2** and apply them to new chemical transformations. Besides the function of the pendent base, development on both the alkyne hydration and alkene isomerization catalysts have shown that sterics can play a key role in both driving and limiting accessibility of the catalyst active site to potential substrates as well as providing a driving force for the Lewis basic atom within the pendent base to reach a sufficiently reactive state.

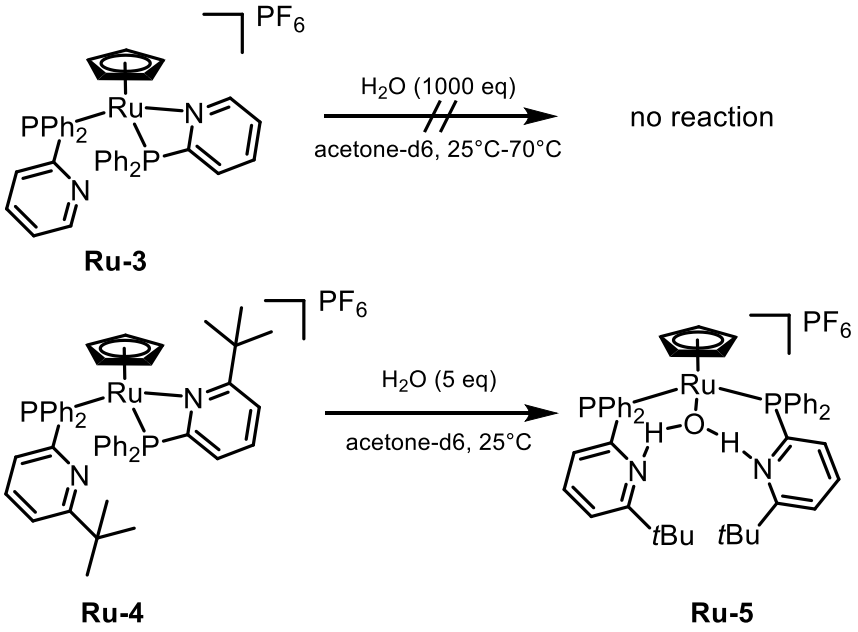

Figure 1. 2 Example in variation in steric bulk around pendent base

A particularly informative experiment compares **Ru-3** and **Ru-4** in the opening of the P,N-chelate to accommodate a water molecule bound to ruthenium. In the presence of even an extreme excess of water, the P,N-chelate in **Ru-3** does not open to accommodate a water molecule to bind to ruthenium. The P,N chelate is able to open with only 5 equivalents of ater when there is a tert-butyl on the heterocycle. Also, a key piece of information is **Ru-5** is the active alkyne hydration catalyst, **Ru-3** does not promote the anti-Markovnikov hydration of alkynes.

ACKNOWLEDGEMENTS

Chapter 1 contains unpublished material and is an introduction to the fields of catalysis and bifunctional catalysis. Contextual information about broader impacts is discussed. The dissertation author was the sole investigator and author of this chapter.

CHAPTER 2

2.1 DEVELOPMENT OF BIARYL DIALKYL PHOSPHINES

The utility of phosphine ligands in transition metal catalyzed reactions can hardly be overstated. The electron-releasing properties of a phosphorus atom in its third oxidation state make phosphines ideal partners to provide stabilization to many highly reactive transition metal atoms. Dialkylbiaryl phosphine ligands, also called biaryl monophosphine ligands, are a special class of phosphine ligands that were initially developed by the research group of Steven Buchwald at MIT. In 1998, the Buchwald group released a communication detailing the use of dialkylbiaryl phosphine ligands for palladium catalyzed aminations (Buchwald-Hartwig cross-couplings).[8] Further research into the design and use of these dialkylbiaryl phosphine ligands has led to improvements in many named palladium catalyzed reactions including the Suzuki-Miyaura[9–14], Heck[15–17], Sonogashira[18], Negishi[19], Hiyama[20–22], and many more unnamed reaction types including: enolate arylation[23–26], reductive cyclization[27], and methylation[28].

The exciting observations made when utilizing challenging aryl chlorides in Buchwald-Hartwig amination included short reaction times, low catalyst loadings, and mild reaction conditions.[29] Although the improved catalysis was observed for some substrates, there were still many observations of little to no product formation in the case of some substrates and palladium pre-catalysts. For example, Buchwald and coworkers were able to achieve high yields with a list of seven distinct aryl chlorides. However, to increase the scope of the cross-coupling to include electron-rich, bulky, or heterocyclic aryl chlorides higher catalysts loadings and reaction temperatures between 80 °C and 110 °C were required.[30] This difference in observed reactivity between similar substrates for a catalyst is common for cross-coupling reactions. Subtle factors such as steric crowding of intermediate coordination complexes can pose a significant roadblock

to product formation. Another likely case may arise wherein an amine or alcohol group within a substrate structure may interfere with equilibrium concentrations of reactive palladium complexes necessary for key cross-coupling steps, thus effectively removing a portion of the palladium from accessing an active catalysts (or pre-catalyst) state. There is not a one-size-fits-all ligand and metal catalyst combination that will work similarly well across steric and electronic variation.

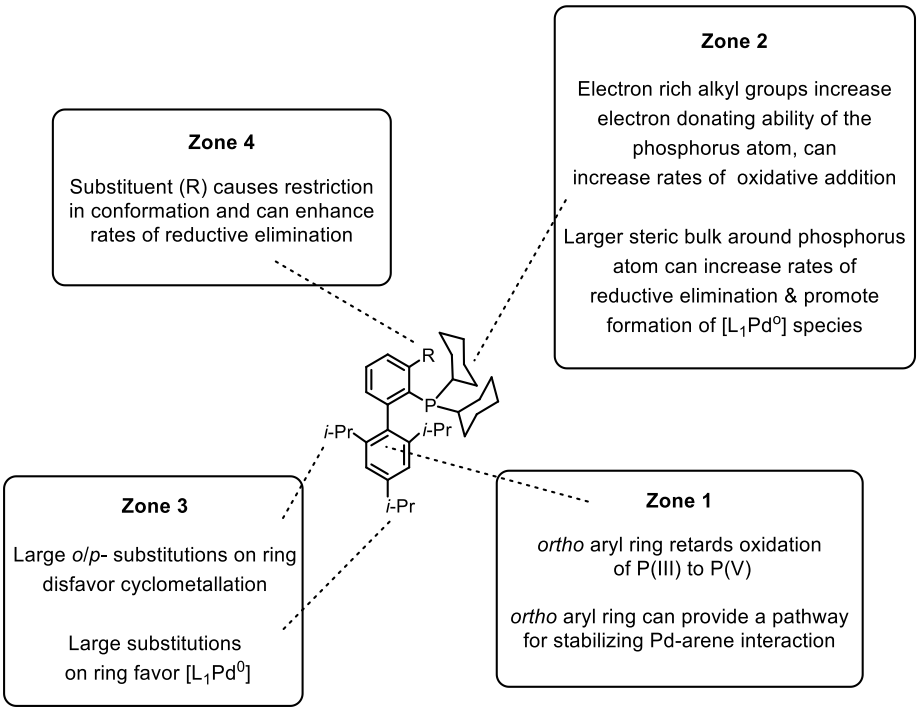

Figure 2.1 Structure activity relationship summary for dialkylbiaryl phosphines in palladium catalysis

Along with these application discoveries, diligent research elucidated mechanism and structure-activity-relationships. Figure2.12 explains some of these conclusions and is adapted from Surry and Buchwald's 2008 review.[29] Key conclusions about the structure activity relationship suggest that not only is the catalyst is a monoligated palladium(0) species [L_1Pd^0] at the start of the cycle, but also that the ligand sterics effect yields by both increasing the rate of reductive elimination and effectively blocking some catalyst deactivation pathways.[29,31]

A particularly illuminating set of experiments compared the normalized reaction rate at 50% conversion for three ligand-to-metal ratios with three different ligands (Figure 2.22).[31]

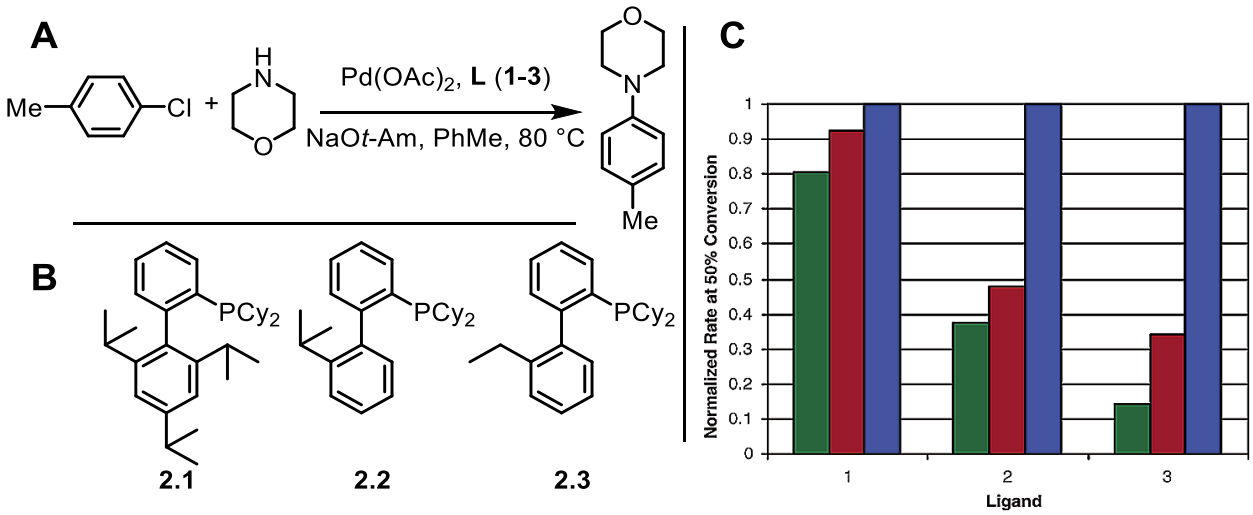

Figure 2.2 Adapted from Buchwald, et al. Study on effect of ligand sterics, Green is 4:1, red is 3:1, blue is 2:1 – Normalized rate is rate at 50% / maximum rate

In the case of **2.1** (the commercially available ligand dubbed XPhos), a mere 20% reduction in the normalized rate is observed when increasing the ligand-to-metal ratio from 2:1 to 4:1, indicating very little effect on the concentration of the $[L_1Pd^0]$ species that participates in oxidative addition with ligand **2.1**. In contrast, ligand **2.3** shows a surprising result. When the ligand-to-metal ratio is increased from 2:1 to 4:1 with ligand **2.3**, the normalized rate decreases by nearly 90%! The large effect indicates the additional amount of phosphine **2.3** is preventing the formation of the active catalytic species, the monoligated $[L_1Pd^0]$ complex. The effect of additional steric bulk clearly prevents extra phosphine molecules from coordinating with a single palladium atom.

In addition to palladium catalyzed reactions, research on dialkylbiaryl phosphine ligands has since expanded to transition metals including rhodium[32,33], ruthenium[34–36], copper[37], silver[38], and gold[39–48]. In 2009, Widenhoefer and coworkers published observations of complexation of JohnPhos with gold (I) chloride dimethyl sulfide, followed by ionization of the gold with silver (I) hexafluoroantimonate while in the presence of electron rich alkenes.[31] The resulting cationic gold

(I) alkenyl phosphane complexes were characterized by low temperature NMR studies and single crystal x-ray crystallography.

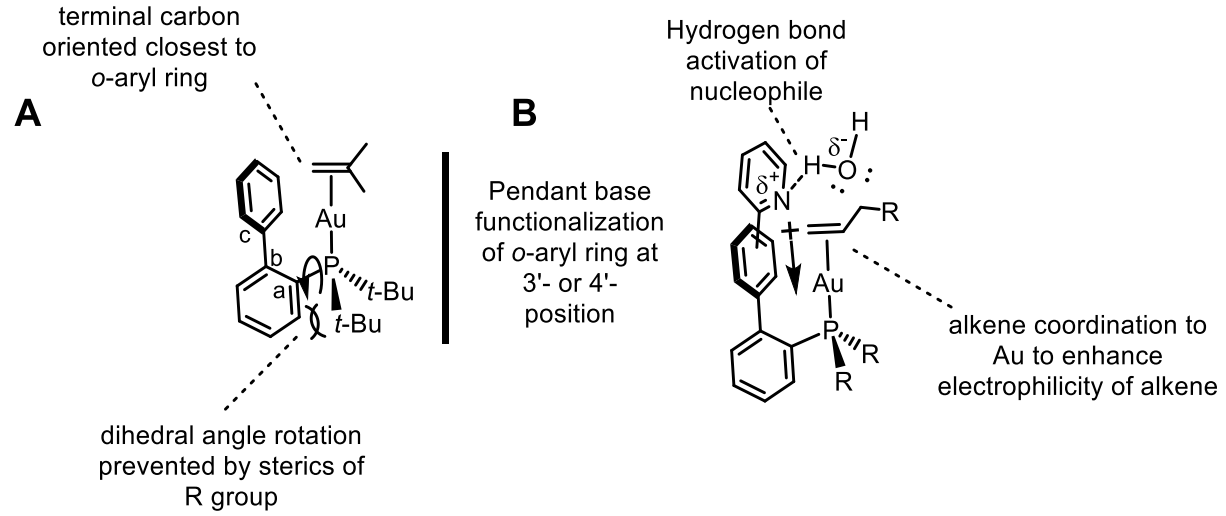

Figure 2.3 A) Summary of observations from Widenhoefer, *Chem. Commun.* **2009**, 6451 – 6453, B) Hypothesis for bifunctional version of biaryl phosphine ligands in gold catalysis

From Widenhoefer's crystal structures, it became apparent that the biaryl framework would be able to provide a rigid backbone. The observations of the gold (I) coordinated η^2- alkene confirmation aided in the formation of the hypothesis that functionalization of the *ortho*-aryl ring with Lewis basic atoms could be an opportune placement of a pendent base within the secondary coordination sphere. Within the Grotjahn research group, this was seen as a way to take lessons learned when studying the alkene isomerization[49,50] catalysts and alkyne hydration[51] catalysts and apply to a completely different molecular geometry. A consistent feature in both the alkene isomerization and alkyne hydration catalysts is the relative positioning of the coordinated substrate and the pendent base component of the phosphine ligand. The pendent base is positioned near the atoms in the alpha position relative to the coordination to ruthenium. The hypothesis for a bifunctional activation of alkene and ROH required for a stable framework and consistent positioning of the pendent base relative to the metal coordination site. Large substituents on the phosphorus atom will cause a high barrier to rotation about the dihedral angle between the

phosphorus-carbon (a) -carbon (b) – carbon (c) atoms (Figure XX, above). The bulky biaryldialkyl phosphine framework appears to be an ideal target to strictly limit conformational flexibility around an open coordination site within a gold(I) linear geometry complex.

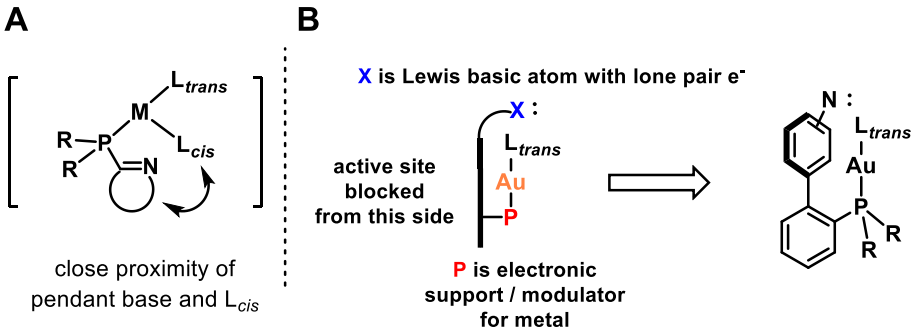

Figure 2.4 Representation of pendent base placement in A) alkene isomerization and alkyne hydration catalysts, B) rigid arm pendent base model

Within the Grotjahn research group, initial studies on functionalization of dialkylbiaryl phosphine ligands was carried out by graduate students Reji Nair[52] and Gulin Erdogan[53]. From the outset of the synthetic work, it was observed that the construction of the functionalized biaryl would not be trivial. The initial methodology was to incorporate the phosphorous atom early in the synthesis, leaving the addition of the pendent base functionality for a late-stage modification to a more generally useful biaryl phosphine precursor. This route was attractive because of the possibility of quickly generating many variations in the pendent base functionality as a final synthetic step. The initial steps gave reason for optimism. The coupling of (4-formylphenyl)boronic acid with 2-bromophenyliodide was accomplished in 85% yield after column chromatography; and the protection of the aldehyde as an acetal was achieved in 98% yield. However, once the initial biaryl moiety was formed, installation of the phosphine proved to be more challenging. Lithiation of the aryl bromide (34-nair thesis) with both *n*-butyllithium and *t*-butyllithium resulted in formation of significant quantities of side products that were not readily separable through column chromatography. The use of the Buchwald methodology (references

needed here) of forming an aryl-Grignard and then reacting with a chlorophosphine in the presence of CuCl was successful in producing the desired general phosphine precursor that could be used to generate different iterations of benzyl amines as the pendent base. Even with this successful strategy, significant amounts of proto-dehalogenation was observed (up to 30%). These synthetic limitations illustrate the need to for development of alternative strategies for functionalized biaryl synthesis.

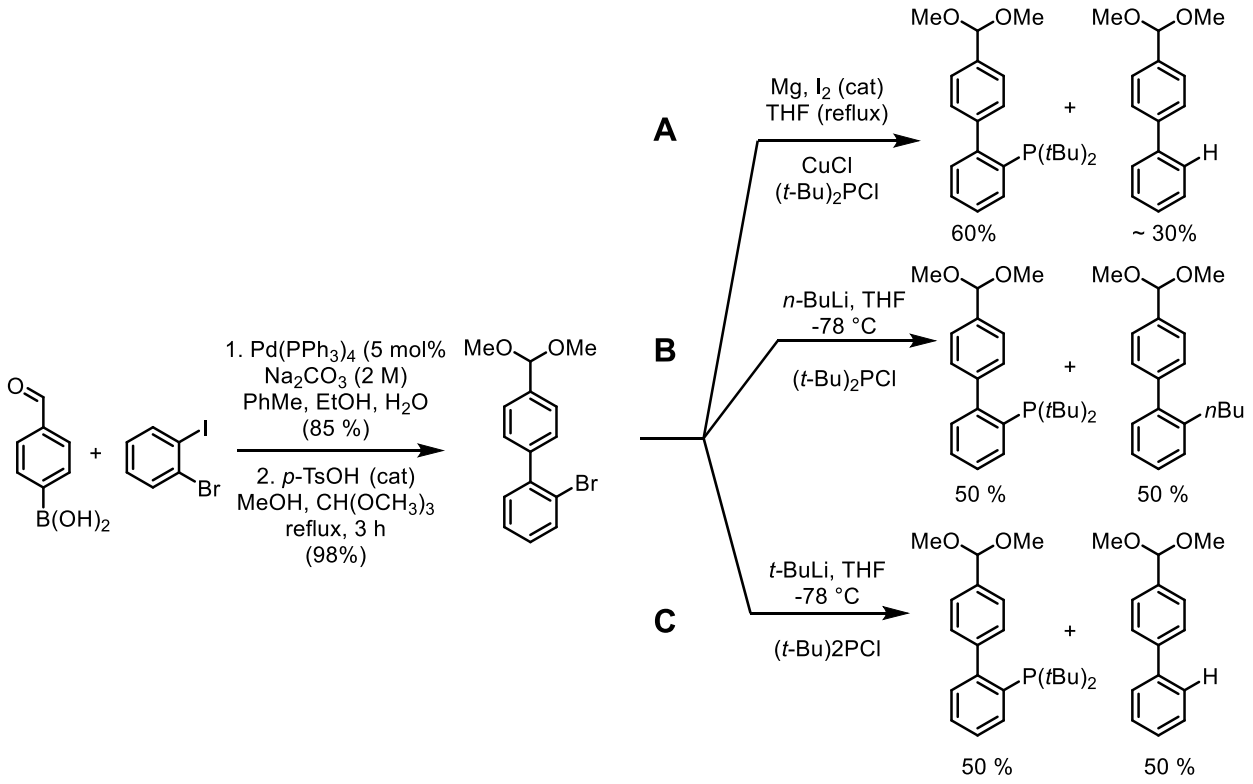

Figure 2.5 Overview of conditions from Reji Nair for installation of phosphine to biaryl fragment

Once the phosphorus connection to the biaryl group was achieved, the acetal could be converted back to the aldehyde, then subject to reductive amination conditions with a secondary amine and sodium cyanoborohydride to yield various benzyl amines.

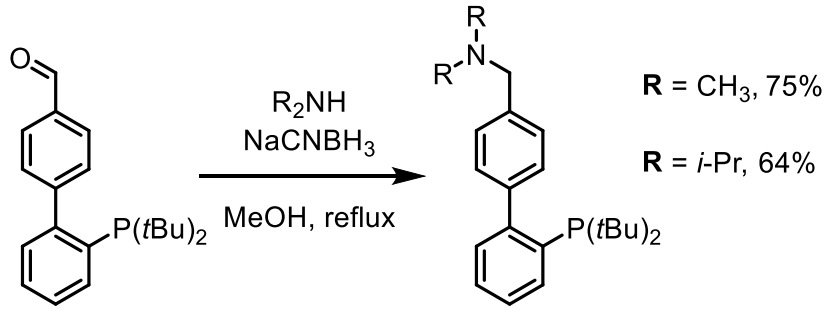

Figure 2.6 Overview of condition from Reji Nair for synthesis of benzylamines on biaryl framework

The initial studies on complexation lead to observation of single crystal x-ray crystallographic data. It was apparent from the x-ray structure that a large degree of conformational freedom would arise from rotation about the C_{sp2}-C_{sp3} bond axis. Additionally, in attempts to use benzyl amine Au complexes, benzyl alcohol was observed, suggesting that the benzylamine was not stable.

A few years later, in 2014, the research group of Liming Zhang commenced publication of what would become a very impressive development of functionalized dialkylbiaryl phosphines and their use as ancillary ligands for Au(I) complexes. The gold(I) phosphine complexes developed were shown to be used as efficient catalysts in reactions targeting alkynes as the substrate. The 2014 Nature Communications report disclosed Lewis base functionalized dialkylbiaryl phosphine gold(I) chloride complexes and their activity as catalysts for addition of carboxylic acids to terminal alkynes and hydration of terminal alkynes. [54] Zhang and coworkers studied the activity of a set of eight dialylbiaryl phosphines functionalized with amines and amides. The optimal ligand, **2.4**, was able to deliver yields of 85% to 99% with catalyst loadings as low as 50 ppm, in some cases. It is interesting to note the optimized solvent for this reaction is fluorobenzene, a somewhat exotic choice. If the solvent is changed to a more commonly used choice, 1,2-dichloroethane, 220 ppm of the gold(I) catalyst with the optimized ligand yields 43%

of the desired product in 12 hours. Also described in the same publication was utilization of the same optimized ligand for gold(I) catalyzed hydration of terminal alkynes to methyl ketones,thus illustrating the practical application of this catalyst across many reactions involving the same key components i.e., RO-H and a carbon-carbon triple bond.

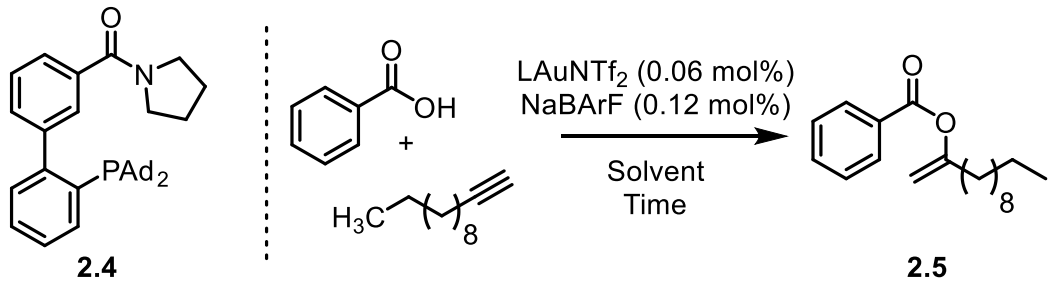

Figure 2.7 Example of 2014 Zhang report on catalyzed synthesis of vinyl esters and optimized ligand structure

Later on, in 2014, Zhang and coworkers published a study on another set of dialkylbiaryl phosphine ligands in which alkynes were isomerized to 1,3-dienes.[55] Seven ligands were screened in the study, three of which were novel from the carboxylic acid addition to alkynes work. The ligand screening revealed that the most active catalyst had added functionality on the biaryl ring structure to produce electronic push and pull effects, as well as increased steric interactions around the pendent base (**2.5**). Yields reported for the different substrates studied varied from 46% to 97% product detection. Again, the choice of solvent for this isomerization reaction was unique: α,α,α-trifluorotoluene. The optimization of conditions to include exotic fluorinated solvents begs to question the details of the cause-and-effect relationship between solvent and performance. What role does the solvent play to increase product formation? One can speculate about potential stabilizing electrostatic interactions between fluorine atoms in the solvent and the cationic gold(I) atom, but there is no evidence clearly supporting that hypothesis. It is important to note that preference for readily available and low-cost solvents should be considered a high priority. Use of

expensive solvents will significantly increase the cost and reduce desirability of using the chemical technology. Compare α,α,α-trifluorotoluene, which costs $70/L (ρ = 1.19 g/mL, B.P. = 103.5 °C) and fluorobenzene, which costs $180/kg (ρ = 1.02 g/mL, B.P. = 85 °C) to 1,2-dichloroethane (ρ = 1.25 g/mL, B.P. = 83 °C) at $14/L. Along with impressive selectivity and activity measures, it is important to optimize catalytic conditions towards accessibility and practicality.

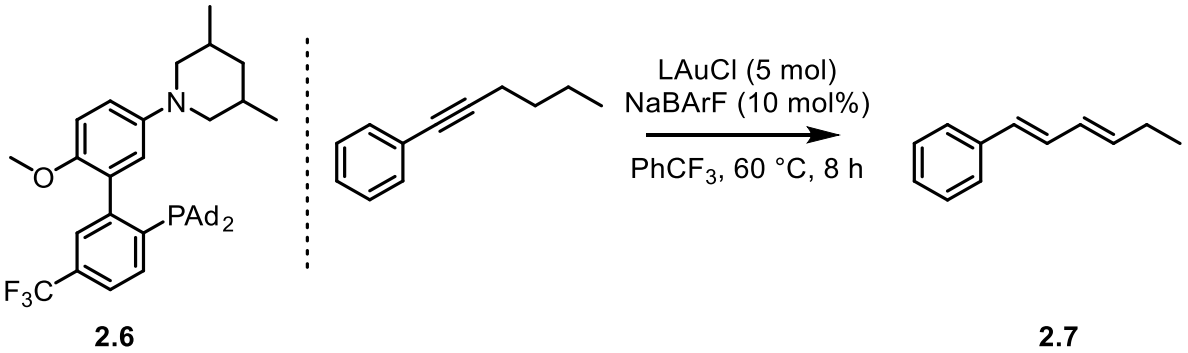

2.6 **2.7**

Figure 2.8 Example of Zhang alkyne isomerization to 1,3-diene catalysis and optimized ligand structure

Continued discovery and development by the Zhang research group over the next 5 years lead to an array of impressive reactions catalyzed by Au(I) complexes of functionalized dialkylbiaryl phosphines. Other notable reactions include a cascading propargylation of aldehydes followed by cycloisomerization[56], isomerization of propargylic esters[57], and hydroalkenylation of propargylic alcohols[58]. Much of this work from the Zhang group was conducted and published concurrently with the novel ligands studied in this work. We saw the results from the Zhang group as encouragement of the rich chemical possibilities for novel, functionalized biarylphosphine ligands. Despite all the reported progress on the functionalized biaryl phosphines, we expected to find unique reactivity through functionalization with aromatics such as pyridyl and imidazolyl moieties on the *ortho*-ring.

2.2 Biaryl mono phosphine ligand design synthesis

An important consideration at the outset of our synthetic efforts was one of methodology. There appeared to be at least three options for a general methodology for ligand synthesis. The initial work form Reji Nair followed a methodology where the biaryl fragment was built first, followed by addition of the phosphine, and finally installation of the pendent base functionality. A path that may offer seemingly faster exploration of the chemical space specifically related to variation in the identity of the pendent base. However, potential complications in synthesis downstream of phosphine installation are likely; consider interference, by the phosphine, with downstream reactions (cross-coupling or otherwise) and oxidative degradation.

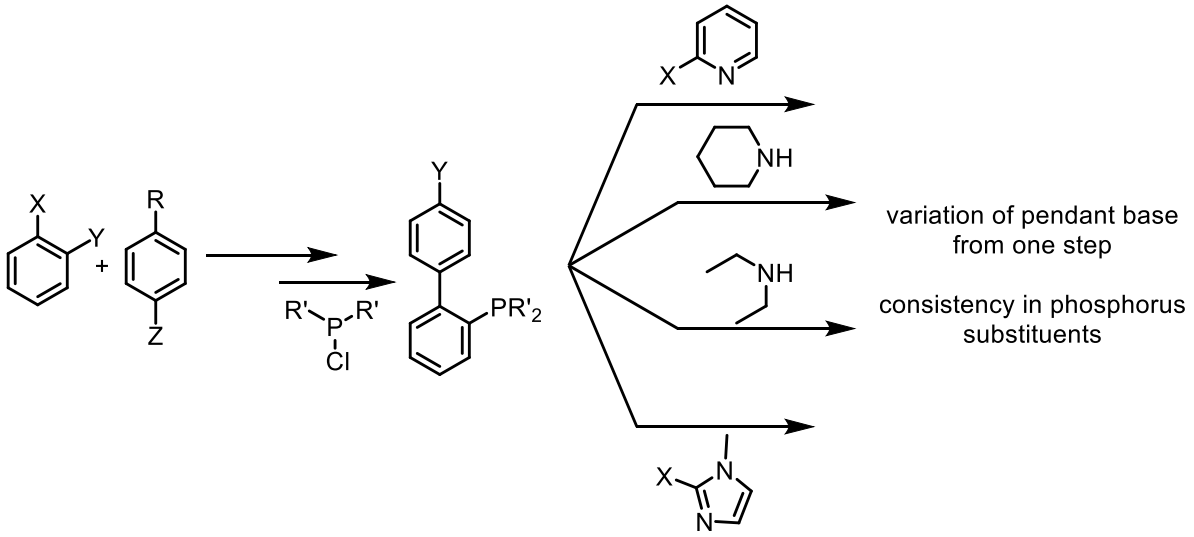

Figure 2.9 Phosphorus-first ligand synthesis strategy

A second framework to consider is construction of a divergent intermediate biaryl molecule that can then undergo installation of the pendent base and the phosphorus group, sequentially. Adding the phosphorus atom last has the advantage of only the product of the very last reaction being reactive (albeit slowly) towards open air. If the phosphine moiety is installed earlier the

downstream intermediates are susceptible to oxidation and loss of yield of high value novel molecules.

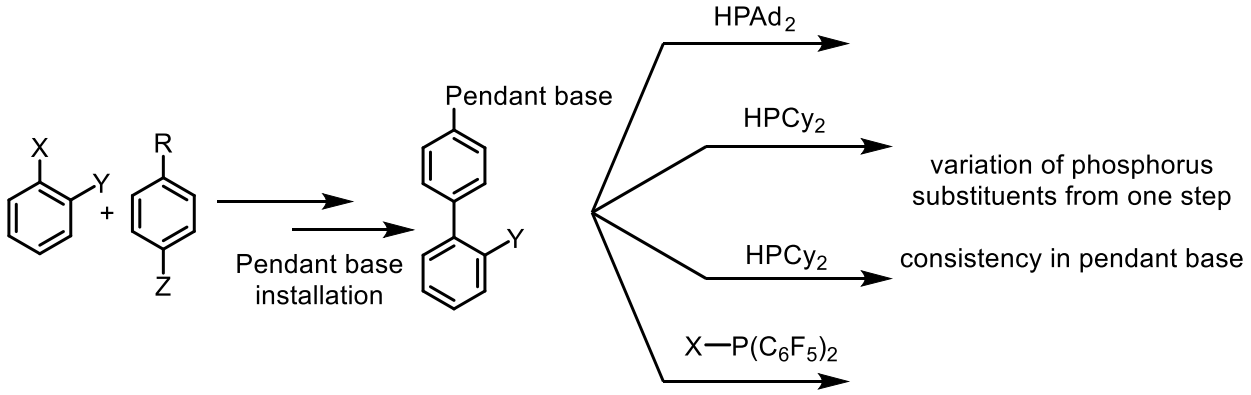

Figure 2.10 Pendent-base-first ligand synthesis strategy

A third, and bolder, methodology is one of cascade-type reaction steps – where more than one bond changing event occurs in the same reaction vessel. For example, the Buchwald synthesis involves formation of the aryl-Grignard reagent and addition of another aryl halide to form the biaryl, followed by carbon-phosphorus bond formation with the addition of a chlorophosphine in the presence of copper(I) chloride.[29] The Buchwald methodology is attractive due to fewer purification steps and an overall shorter list of reactions setup to test the ligand candidate. However, such cascade type reactions are highly sensitive to molecular structure and are often not repeatable with any variation within the starting materials. We were unsuccessful in all attempts with the Buchwald strategy applied towards our target molecules.

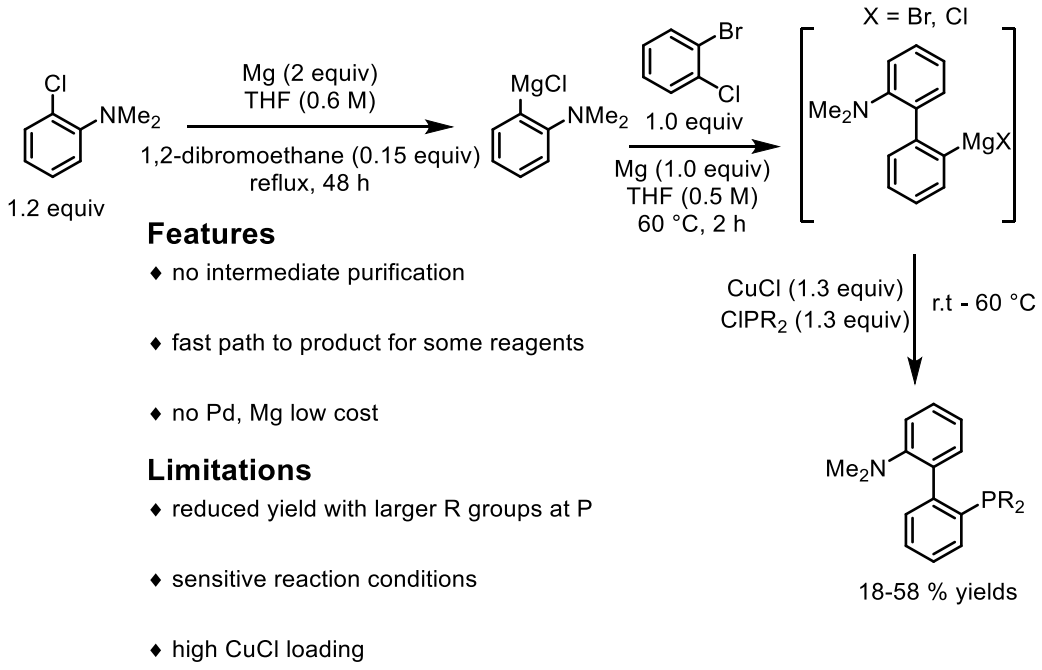

Figure 2.11 Example case of Buchwald ideal strategy for dialkylbiaryl phosphine synthesis

The next consideration focused on degrees of freedom, flexibility, and positioning of the basic atom. The benzyl amine, with its sp^3 hybridized carbon between the ring and the basic nitrogen, appeared too flexible. We imagined a 2-pyridyl substitution at either the 3'- or the 4'-position within the biaryl ring structure would be a good place to start. In the 3'-position, dihedral rotation about the *ortho*-phenyl ring and pyridine ring planes can effectively swipe the basic nitrogen's lone pair electrons across a large portion of the area directly above the open coordination spot on the Au(I) ion; it can be expected that this dihedral angle will have a low barrier for complete rotation. Also considered was a 2-pyridyl-substitution at the 4'-position on the biaryl ring structure, which would allow for nearly full rotation of the pyridine ring dihedral with respect the lower phenyl ring while maintaining the basic nitrogen's lone pair electrons within a constant plane relative to the lower open coordination spot at the gold(I) atom.

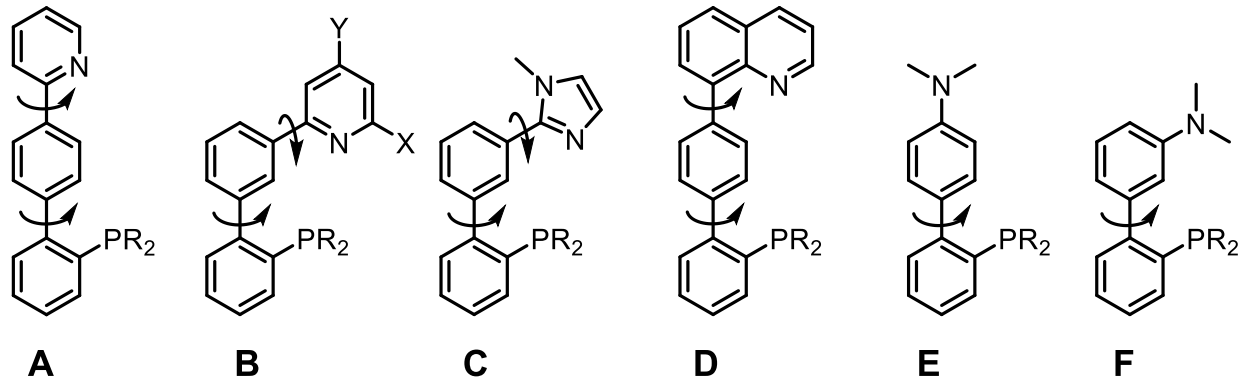

Figure 2.12 Positionings for pendent base functional groups and degrees of rotational freedom

With a variety of catalyst structure candidates, we started to brainstorm how specific components could influence the complex's range of accessible states; and possible push-pull electronic effects through substitution within the biaryl framework. Key areas of chemical space we chose to investigate are illustrated below in **Figure 2.12**. Acyclic and saturated heterocyclic amines directly connected to the *ortho*-aryl ring via nitrogen will have the lowest degree of rotational freedom as well as a high degree of delocalization of the valence electrons (**Figure 2.12 E, F**). Functionalization with a 2-pyridyl moiety at the 3'-position of the *ortho*-aryl ring will allow for significant rotation of the dihedral angle between the two rings (**Figure 2.12 B**). This freedom might prove useful by allowing the nitrogen lone pair electron density access to the Au(I)-coordinated substrate from a variety of angles. On the other hand, the high degree of freedom might encourage rotation of the nitrogen atom away from the zone in which the substrate would coordinate up into the open space remote from the metal.

We also saw an opportunity to vary electron density and sterics with additional functionalization to the pyridine ring. A substitution of X = H to X = *tert*-butyl will offer strong differences in the sterics around the pendent base. Substitution of Y = H to Y = N,N-dimethylamino (Me_2N-) has a strong effect on by increasing the electron density on the aromatic

nitrogen atom. Changing the pyridine ring to imidazole will vary the positioning of the electron density and base strength. (Figure 2.12 C) We also looked to attach the pendent base to the 4'-position which we saw an opportunity to add some limitation to the degrees of rotational freedom by removing the variation in vertical distance between the positioning of the pendent base and the open coordination site on the gold(I) atom.

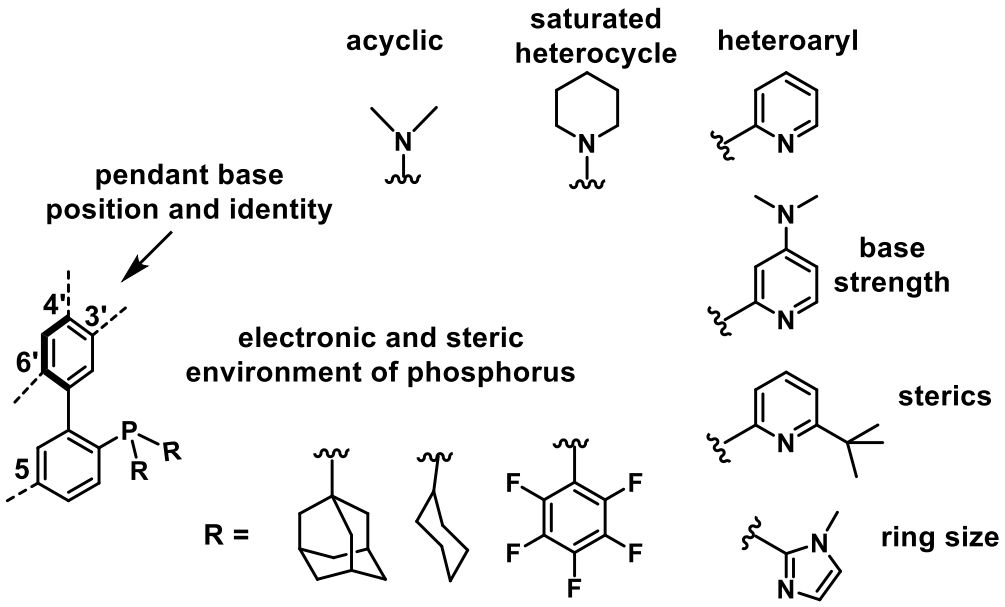

Figure 2.13 Positional and structural variation for ligand functionalization

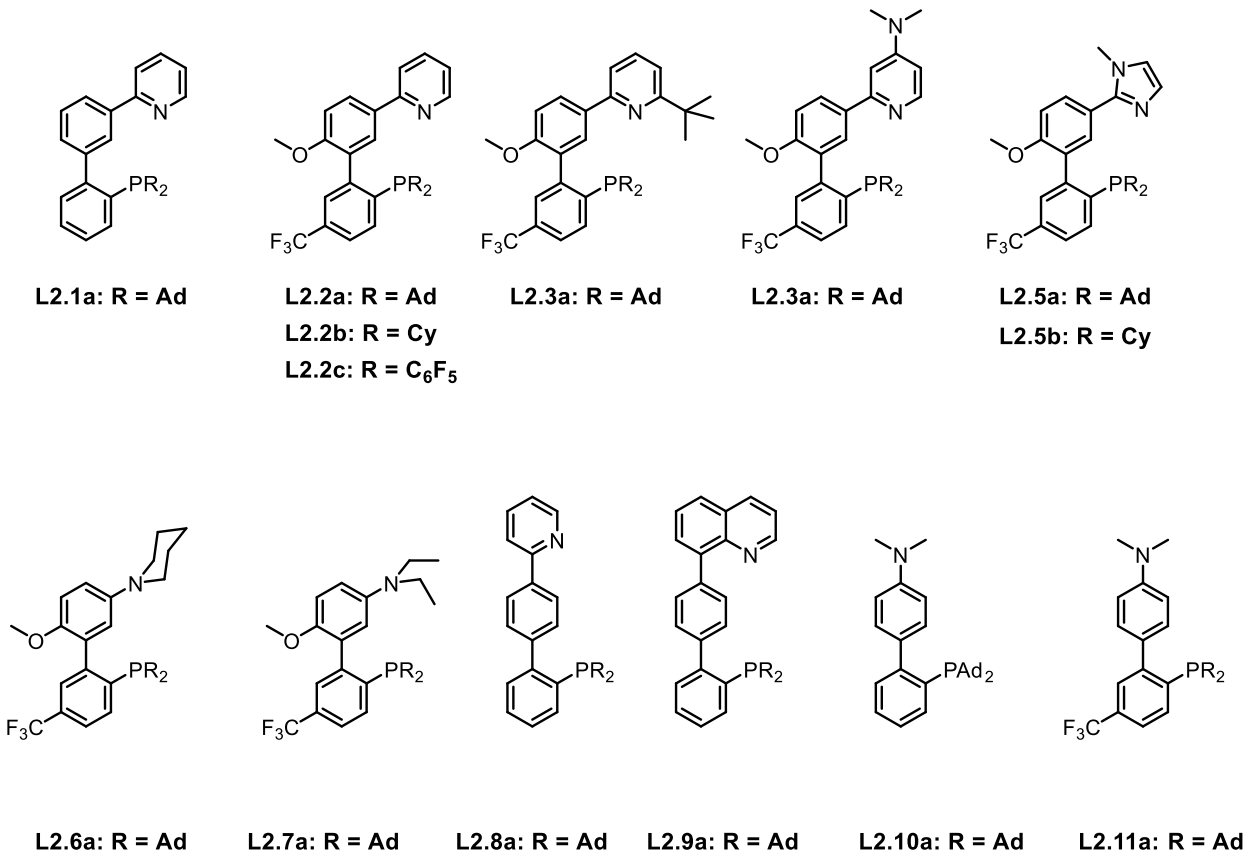

Figure 2.14 Complete set of functionalized biaryl phosphine ligands synthesized for this work

A variety of coupling conditions for the formation of C_{sp2}-C_{sp2} bonds can be found in the chemical literature. Many methods involve palladium catalysis (Suzuki, Stille, Heck, Kumada, Negishi, etc.). A stepwise synthetic pathway will involve converting an aryl halide into a stable cross-coupling partner such as an aryl-boronic acid or aryl-stanane, conducting any necessary purification such as distillation or column chromatography, then using palladium catalysis to build the biaryl framework in a subsequent step. In an effort to push forward synthetic routes that will reduce the number of work-up and purification steps, as well as utilize the same palladium catalyst for multiple cross-coupling steps, we looked to work from the research of Gary Molander and coworkers. In a 2012 *Journal of Organic Chemistry* report[59] a one-pot palladium-catalyzed sequential borylation then Suzuki cross-coupling was reported. The work is notable for utilizing

the same loading of palladium (1-2 mol% loading) for both the borylation step and the Suzuki cross-coupling step. The key difference in reactivity is provided by addition of the stronger base potassium carbonate in the second step, whereas the first step proceeds with the weaker potassium acetate. Of additional note is the optimized ligand for palladium in this two-part reaction sequence. The ligand reported to provide the best yields is XPhos, a dialkylbiaryl phosphine ligand used above in the amination study on sterics.

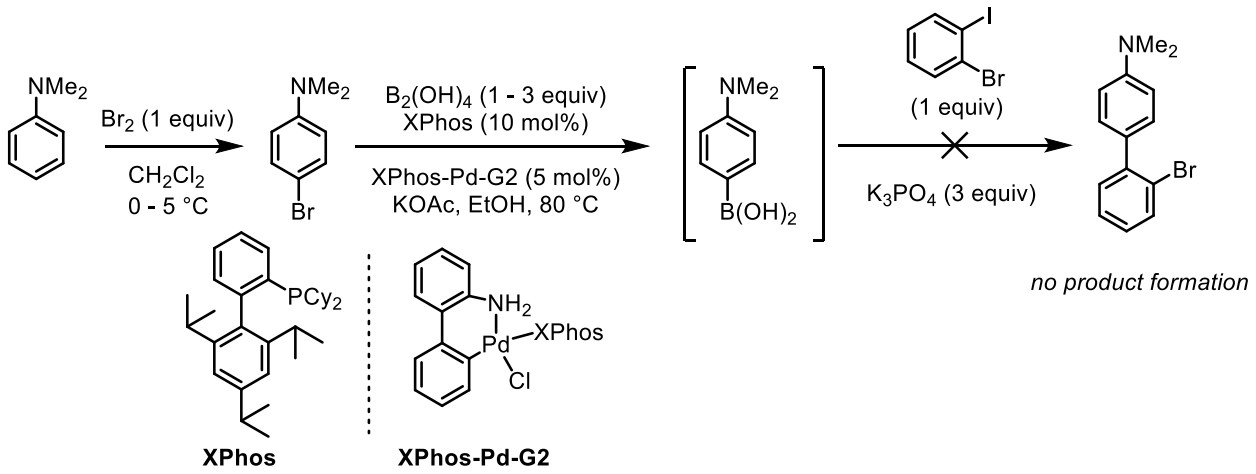

Figure 2.15 Strategy for one-pot cascade type cross-coupling steps

After several unsuccessful attempts at the one-pot sequence with these recycled palladium conditions, as well as variations on the identity of the ligand and palladium precursor, solvent, temperature, and duration of reaction conditions this route was abandoned. TLC analysis showed the formation of a number of new UV-responsive species under many of the conditions, and typically signs of remaining starting material. Our interpretation of these results is that the dimethylamino group is to blame. The key difference in our conditions and those reported in the literature is the dimethylamino group *para* to the intended reaction site. Potentially coordination to palladium from the dimethylamino or an instability in an organometallic intermediate is to specific cause.

A less sophisticated pathway of conversion of an aryl bromide to aryl boronic acid was accomplished with the use of *n*-butyl lithium addition to an air-free and dry solution of the aryl halide **2.7** in THF, followed by the addition of tri-isopropylborate, and finally workup with ammonium chloride. The arylboronic acid **2.8** was sufficiently pure without the need of chromatography. We did see a benefit to washing the crude product with acetone and pentane.

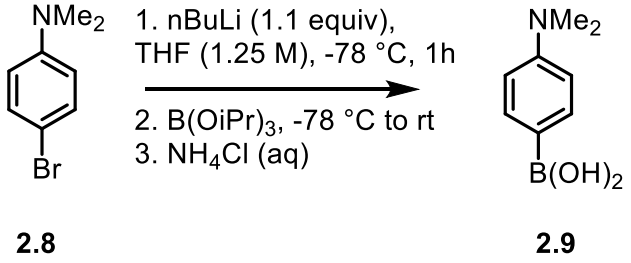

Figure 2.16 Successful synthesis conditions for preparation of aryl boronic acids

Once the intermediate components were reacted to form the biaryl bromide **2.10**, the mixture was purified before installation of the phosphorus moiety. The phosphorus-carbon bond can then be formed, again utilizing palladium catalysis with the diisopropylphosphino ferrocene ligand (DiPPF) and the biaryl bromide.

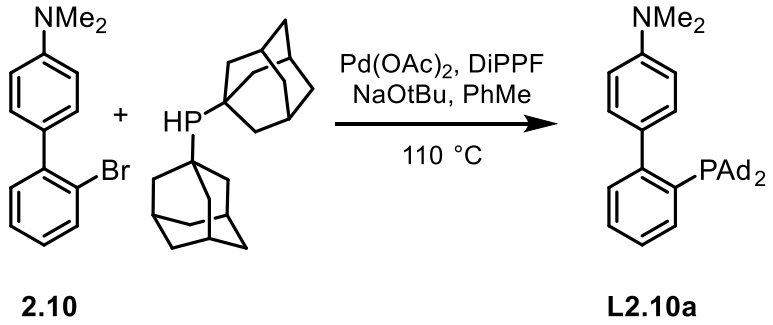

Figure 2.17 Conditions for conversion of biaryl bromide to biaryl dialkyl phosphine

Taking cue from Zhang research group, we decided to utilize the electron electron donating methoxy group in the 6'-position and the electron withdrawing trifluoromethyl group as a substituent in the 5-position.[60] We hypothesized that the difference in electron density in the two

aryl rings could provide additional electron push-pull effects in a bifunctional activation of substrates. Additionally, the electron donation from the methoxy group acts to direct and halogenation in the 3-position – a necessary intermediate step to provide a functional handle for incorporation of a pendent base. To this end, we followed the method published by Zhang to synthesize **I-2.1**. In a small innovation to Zhang's published protocol, we found cleaner results in Suzuki cross-coupling reactions conditions to form **2.17** when additional triphenylphosphine was added to the catalyst $Pd(PPh_3)_4$. We hypothesized undesired cross-coupling products could be prevented by slowing all palladium involved steps.

Once **I-2.1** was in hand, we were able to produce variety in the type of functionalization for inclusion of the pendent base in two synthetic steps (cross-coupling of the heterocycle or Lewis basic group, followed by installation of the phosphino moiety). We found that copper catalyzed amination was successful in production of **2.28** and **2.29**. In some cases, we did find that low conversion and side-product formation pathways led to poor results in attempts to couple the aryl iodide **I-2.1**. In particular, attempts at a Stille cross coupling between 2-(tributylstannyl)pyridine and **I-2.1** were productive in formation of the desired coupling product (**2.18**), but destannylation was a prominent decomposition pathway. In our most successful attempt at the reaction, we were able to product **2.18** in 49% yield relative to the initial loading of **I-2.1**, with 4 equivalents of 2-(tributylstannyl)pyridine added.

During our attempts to couple the bulky, 6-*tert*butyl-2(tributylstannyl)-pyridine, we found that Stille-cross coupling produces yields too low to be synthetically useful. This is due to the electron-poor 2-carbon of the pyridine ring's resistance to form the desired coupling product. With additional complications from steric crowding, the Stille was not an effective protocol to reach

target molecule **2.19**. To circumvent this hurdle, we converted the aryl iodide **I-2.1** into the arylboronic ester **I-2.2** with palladium catalyzed borylation utilizing B_2Pin_2.

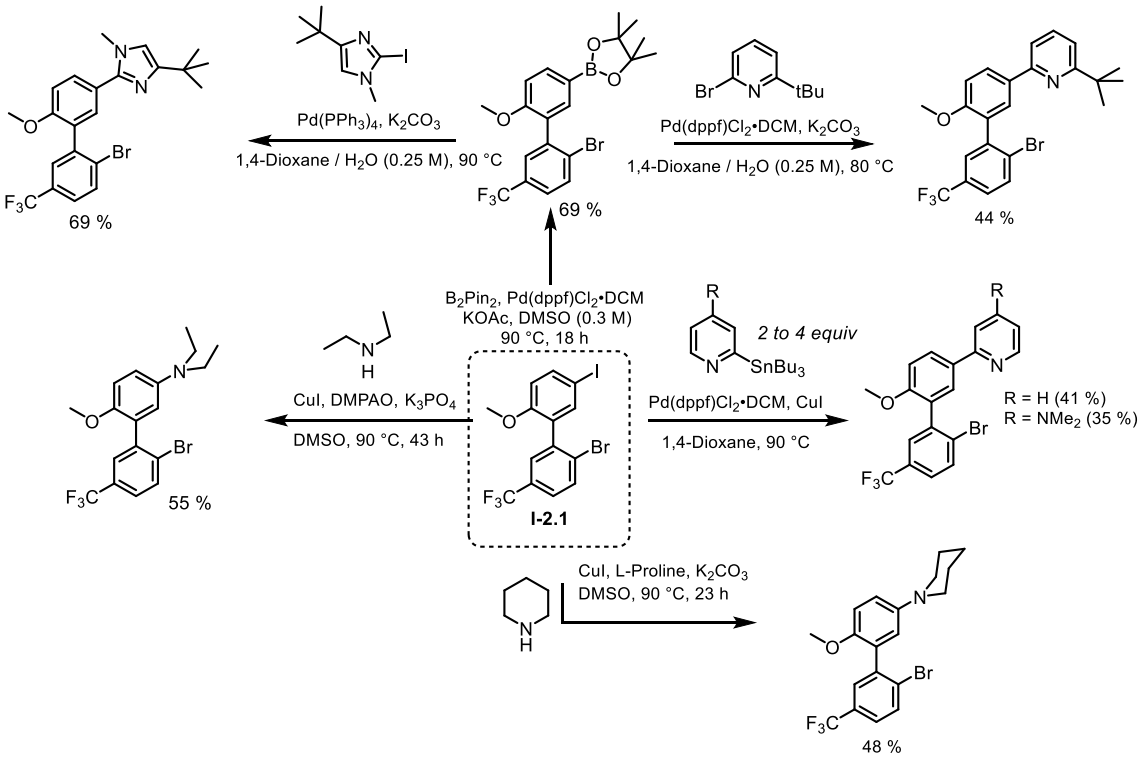

Figure 2.18 Zhang intermediate for efficient diversification of pendent base

We found that use of the highly polar solvent DMSO gave the best results for borylation. Attempts to produce **I-2.2** using 1,4-dioxane as the solvent resulted in non-selective coupling. Our interpretation of these disparate results with DMSO and 1,4-dioxane is in the ability of DMSO to coordinate to palladium. There are many possible coupling results in the borylation of **I-2.1**. Not only can the product **I2.2** react with the starting material **I-2.1** at both the iodide and bromide positions – two molecules of the product **I- 2.2** can potentially react together, these are undesired Suzuki cross-coupling products. The use of the weak base potassium acetate should slow the formation of the Suzuki cross-coupling products. The added steps of coordination and dissociation of solvent molecules will significantly reduce the speed of all cross-coupling steps. In this case, the desired borylation reaction was fortunately still effective under conditions using DMSO as

solvent, while the potential side-reactions were slowed to the point of being non-competitive at moderate heating temperature and times (80 °C for 24 to 30 hours). We found this to be analogous to our addition of triphenylphosphine in the synthesis of **2.10**.

Over the course of the synthesis of the fourteen functionalized biaryl phosphines in this study, there were four key points to our most efficient routes to target molecules. The first driving factor is synthesis of the biaryl carbon-carbon bond very early in the sequence of reactions. Complications from strongly coordinating groups and competing reaction sites severely influence the yield in the biaryl bond formation. The second key feature of the synthetic methodology is the ability for variation in the rolls for a given bond forming step. The aryl iodide **I-2.1** is an effective reaction partner for many conditions. However, the development of conditions to change the role of **I-2.1** from that of the oxidative addition component to the transmetallation component (**I-2.2**) gave us substantially greater power in types of bond-forming conditions available.

The final two take aways from our synthetic efforts are about incorporation of the pendent base and the phosphorus atom. When possible, incorporation of the Lewis basic functional group in the second to last synthetic step is preferred. The final step in the synthesis should be incorporation of the phosphine. Even sterically hindered phosphines such as the biaryl dialkyls will eventually oxidize to a phosphine oxide when handled in open atmosphere. Air-free handling techniques add complexity to even routine reactions and purifications. Additionally, early incorporation of the phosphine to the biaryl structure will almost certainly reduce the effectiveness of many reaction conditions.

2.3 Complexation and Ionization Studies with Novel Biaryl Phosphines

The primary metal we targeted for study of the newly synthesized phosphines was gold, in the first oxidation state. We believed a gold(I) phosphine complex with an opportunely placed

Lewis basic functional group could lead to a two-part activation pathway, after ionization of the chloride. It was shown by Weidenhofer that alkenes would bind to the gold atom with a unique orientation. Additionally, reports of gold catalyzed hydroamination and hydroalkoxylation reactions gave support to studying the new ligands functionality within a gold(I) complex.[61]

We also had some interest in studying the catalytic capabilities of copper(I) complexes containing the novel biaryl phosphine ligands. Copper(I) adopts a similar linear molecular geometry as gold(I), has a similar affinity for coordination to alkenes and alkynes. A highly active copper catalyst would be a breakthrough due to the significantly higher abundance of copper compared to gold on earth. Copper is present in around 70 ppm concentration in earth's crust, gold is around 0.005 ppm.[62]

Formation of the phosphino-gold(I) chloride complexes was accomplished by using chloro(dimethylsulfide)gold(I) as the gold source. This source of gold was chosen due to being readily soluble in organic solvents, and because separation of the liberated dimethylsulfide is easily accomplished under reduced pressure. Although not especially sensitive to oxidative degradation under air, the chloro(dimethylsulfide)gold(I) was stored in a nitrogen filled glovebox and kept away from light in a black bag. Gold complexes can degrade when exposed to light for extended periods. Complexation of the ligands utilized in this study to gold was facile and will complete with adequate stirring in 10 to 15 minutes. A variety of organic solvents are suitable including chloroform, methylene chloride, tetrahydrofuran, 1,2-dichloroethane. A typical choice is complexation in CH_2Cl_2 followed by evaporation to quantitative yield the chloro(phosphino)gold(I) complex. It should be noted that in some cases degradation (potentially polymerization of THF) was observed with the gold complexes in THF solution, especially after addition of an ionizing agent such as $AgPF_6$ or $K[B(C_6F_5)_4]$. In these cases, a solution in d_8-THF

formed a gel-like semi-solid after storage for more than 12 hours in an NMR tube. Formation of the chloro(phosphino)gold(I) complexes was attempted in open air with success. Setup of many of the attempted catalytic reactions with the chloro(phosphino)gold(I) complexes was conducted in open air.

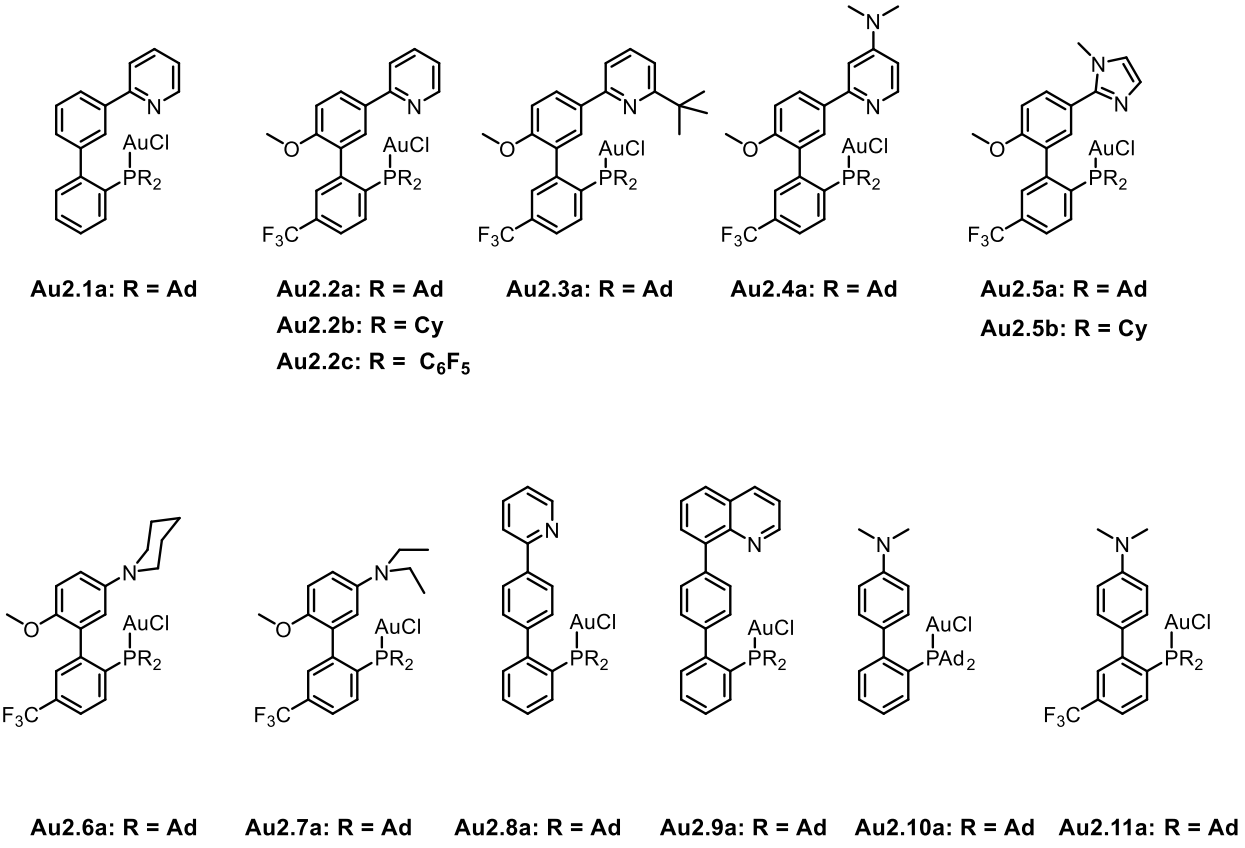

Figure 2.19 Complete set of gold complexes and associated numbering system.

To gain further insights into the relationship between ligand structure and the performance of the gold(I) complex as a catalyst, we decided to study the ionization of the phosphine gold(I) chloride complex with NMR spectroscopy.

2.4 Catalysis and Reactivity

The principal interest for use of the functionalized biarylphosphine gold complexes was towards alkene addition chemistry to yield the anti-Markovnikov product. Knowing this lofty goal would be complex and highly challenging, we began to consider other use cases for the

novel ligands and gold(I) complexes. Known applications for gold catalysis include alkyne isomerization and addition reactions.

2.4.1 High Throughput Screening Approach

A significant challenge in development of catalysts and reaction conditions is often the sheer size of the chemical space that needs exploring. Consider our most aspirational target reaction, addition of and RO-H fragment across an alkene. Along with the ligand structure, also consider that choice of solvent, ionizing reagent, the identity of the metal ion, catalyst loading, ratio of equivalents for substrate loading, time, and temperature are all key parameters to consider and optimize. For the types of addition reactions we were interested in, there are at least 8 parameters to vary. Even to consider a small number of options for each chemical lever, it is quickly apparent that there are potentially hundreds or even thousands of reasonable combinations to consider. Prioritizing conditions most similar to what can be found in the chemical literature will certainly help expedite the discovery, however there is still a significant amount of development necessary.

One method being developed and employed more recently is that of a high throughput experimentation (HTE) approach that utilizes very small-scale reaction sizes to minimize material expense and development time. In a HTE design, a set of possible identities for the relevant reaction conditions are varied in a matrix. A methodology to begin to parse these variables is to sort them into two groups. Discrete variables are those such as the ligand structure, the identity of the solvent. Continuous variables are those such as temperature, time, and molar equivalent ratios of the components. This approach can cast light on non-intuitive connections between different parameters. We worked in collaboration with the Merck High Throughput Experimentation center at the University of Pennsylvania with Dr. Simon Beritt for HTE work conducted in this thesis.

The HTE center was specially designed for organic reaction development and had specialized robotic arms for measuring and dispensing chemicals. However, to effectively conduct HTE for development of new catalytic processes, it is important to consider the challenges unique to the approach. In our experience, the most significant of these challenges are hardware for simultaneous reactions, tools and workflow for the physical set-up and dosing protocols, data management, detection of products, and a strategy for translation of observations from the HTE results to conventional chemical reactions.

Specially designed hardware designed for running multiple, simultaneous reactions is a primary and key place to start. We utilized 24- and 98-well plates specifically designed for running reactions very small-scale reactions. The reaction volumes were 100 µL for the 24-well plates, and 10 µL for the 98-well plates. These glass reaction vessels would be charged small stir bars and a solution of the reaction components dissolved in a semi-volatile solvent, and typically the solvent evaporated after addition across the plate. Multichannel micropipettes were used to dose multiple reaction vessels at once. The reactions were sealed with a cover plate equipment with a disposable PTFE seal. The sealed plates are then heated on a heat plate with temperature monitored via thermocouple and agitation supplied to the reaction vessels via magnetic stirrer.

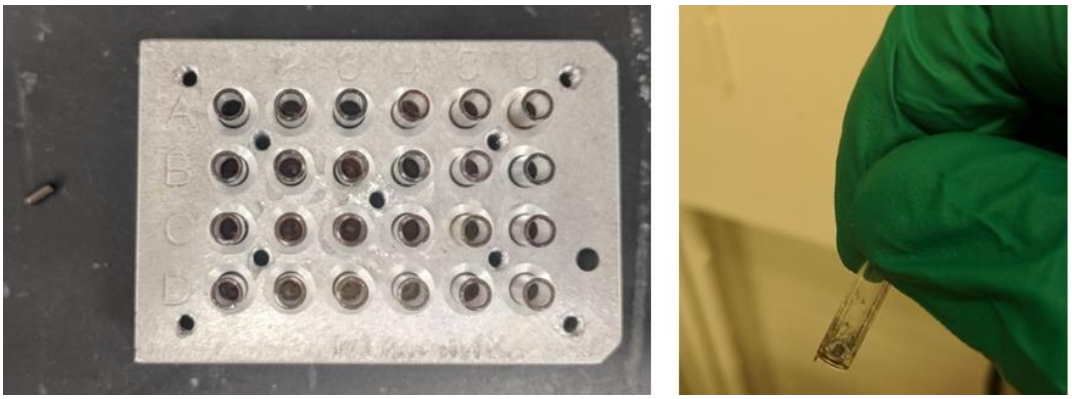

Figure 2.20 Small scale, multi-well reaction plates for high throughput experimentation

When setting up such a large number of simultaneous reactions, it is of crucial importance for completely accurate documentation. Thus, a key feature in design of HTE discovery is management and exact documentation of all experimental steps and the results from analysis of the end products. A preferred option for such a task is a database software. In this project, we used the Freeslate Library Studio software. This software tracked the location and contents of every cell on the matrix, maintained calculations based on molecular weight and our desired molar ratios, and provided an efficient data entry system for transcription of the precise experimental measurements.

For analysis of the products, we relied upon primarily upon a gas chromatography-mass spectrometry system, and with a small number of reactions liquid-chromatography-mass spectrometry analysis. The instrument was also equipped with an autosampler. Reliance on the robotics significantly decreases the laboratory labor required for data acquisition. Additionally, it should be noted that instruments such as gas or liquid chromatography paired with mass spectrometry are a strategic choice. The efficiency gain from combination of the separation and detection steps are crucial for screening disparate reaction conditions small amounts of unusual products.

We ran screenings targeting two reaction types: ROH addition to terminal alkenes, and carboxylic acid addition to terminal alkynes. The alkene addition chemistry was our primary target and received the most thorough treatment and will be discussed in detail here. We chose to vary as many components of the alkene addition test as possible. We included three alkene starting materials, a variety of ionizing agent, and three types of ROH molecules. For alkene variables we chose 10-phenyl-1-decene due to the high degree of insulation between the aromatic ring and the terminal alkene. In the event a catalyst especially competent in alkene isomerization is found, an

intense signal for the conjugated π system will be an obvious signal. Additionally, phenyldecene is a highest molecular weight candidate, thus allowing for the highest level of heating to drive reactivity.

The smallest molecular weight alkene candidate, propene, offers the smallest steric profile. In the event of a certain catalyst combination being highly active for alkene isomerization, the isomerization product for propene, is propene. Thus, a simplification in the outcomes is achieved by removing the effect of extensive alkene isomerization; the concentration of terminal alkene will not diminish due to alkene isomerization. The middle molecular weight alkene chosen was 1-hexene. 1-Hexene offers a high level of simplicity and low steric profile, and significantly more ease of use and dosing when compared to propene. We chose acetic acid, water, and tert-butanol. In the case of tert-butanol, we hypothesized there may be additional steric factors that could potentially bias the regio-chemistry in the event of an addition reaction to a coordinated alkene. Acetic acid was chosen due to its increased level of reactivity compared to water or alcohols. Water, likely the most challenging of the set, was paired with a solvent to solubilize both the non-polar alkene and the catalyst complex in the presence of some amount of water.

Authentic samples of both Markovnikov and anti-Markovnikov addition products of 10-phenyl-1-decene were independently synthesized through established multistep protocols. Hydroboration-oxidation was used to generate the primary alcohol product from 10-phenyl-1-decene. The Markovnikov hydration product was generated through oxymercuration. The primary and secondary alcohols were then reacted with acetic anhydride and di-tert-butyl dicarbonate were used to in the synthesis of the acetyl products and tert-butyl esters, respectively.

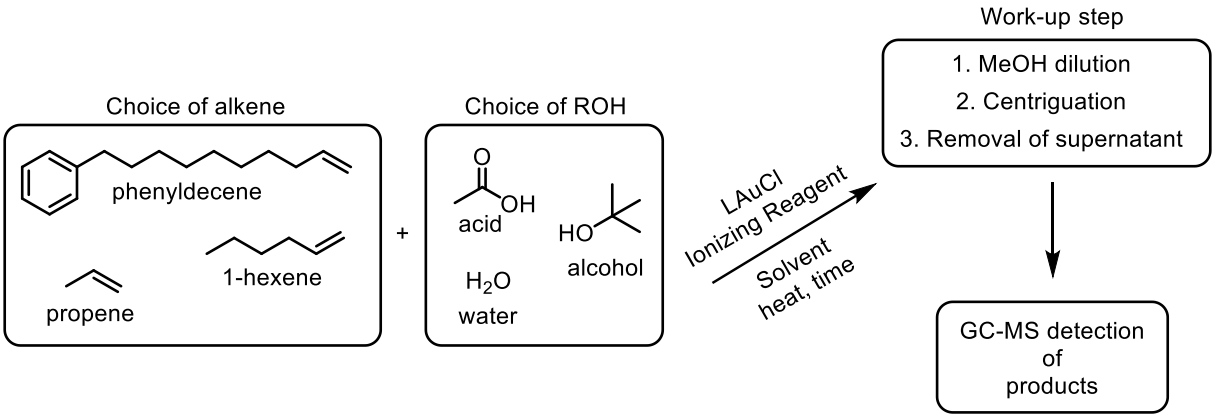

Figure 2.21 Workflow diagram for alkene addition screening

We had seven variants of the biarylphosphine ligands available for the screening. It is important that we included as much variation as possible in the functionalization of the main biaryl fragment as possible. Three of the ligands screened, **L2.2a**, **L2.2b**, and **L2.5a**, have functionalization at the 3'-position. Three of the ligands, **L2.2a**, **L2.5a**, and **L2.6a**, offer a difference in the positioning of the electron density and as well as the steric profile of the pendent base fragment. L2.2b decreases the sterics of the alkyl substituents from very bulky and protruding adamantyl groups to moderately bulky cyclohexyl groups and should thus allow for increased rotation of the Au-P-C-C dihedral angle**. L2.6a** brings the electron density closer to the biaryl framework and removes the possibility to swing the pendent base through a variety of angles relative to the *ortho*-aryl ring (on which the functionalization is attached**). L2.10a and L2.11a** both have low profile N,N-dimethylamino- functionalization at the 4'-position and only differ by the addition of a trifluoromethyl substitution for **L2.11a**, which should somewhat decrease the electron releasing ability of the phosphorus atom to the gold atom within the σ-bonding framework. **L2.9a** is a standout candidate due to the quinolinyl- functionalization at the 4'-position of the biaryl structure. The electron density of the aromatic nitrogen protrudes downward, directly towards the coordination site for a substrate molecule. This molecular diversity allows us to probe

distinct regions of the chemical space we believe could affect such an activation scheme as we hypothesized in Figure 2.3B.

To form the gold complexes, the ligands were dosed onto the reaction plates along with chloro(dimethylsulfide)gold(I) and either CH_2Cl_2 or THF. The gold and ligand mixtures were aged for 1-2 hours, then the ionizing agent was added, and the mixtures aged again for 1-2 hours. The mixtures were then concentrated in a small vacuum chamber under reduced pressure. The targeted gold(I) complex loading for the reactions was 10 mol% relative to the alkene substrate. After the volatile solvent for complexation was evaporated the alkene and ROH mixtures were added, the plate sealed and heated overnight (15-18 hours).

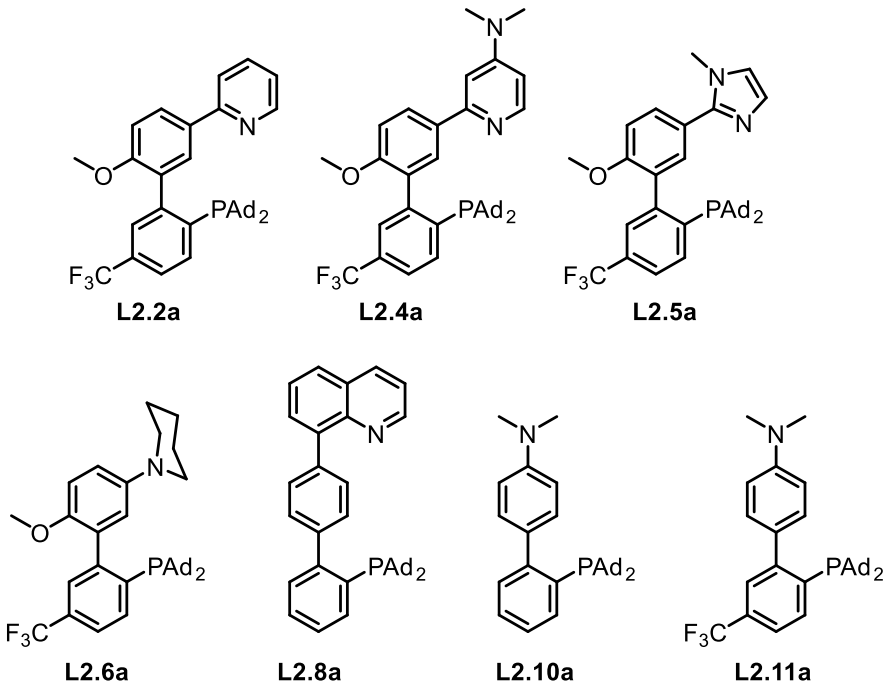

Figure 2.22 Set of ligands studied for alkene addition screening.

Table 2.1 Retention Times of Authentic Products

Compound Name	Retention Time (minutes)	Molecular Weight (g/ mol)
10-phenyldec-1-ene	1.762	216.37
10-phenyldecan-1-ol	1.438	234.38
10-phenyldecan-2-ol	1.425	234.38
10-phenyldecylacetate	1.644	276.42
10-phenyldecan-2-yl acetate	1.634	276.42
9-(*tert*-butoxy)decyl)benzene	1.855	290.49
(10-(*tert*-butoxy)decyl)benzene	1.873	290.49

As can be expected with such a shotgun style approach, most of the screening reactions show no new signals upon analysis. However, we were encouraged to see some signs of potential product formation, albeit in small amounts. In the case of a screening plate run with propene as the alkene and acetic acid, trace signals for m/z of 101.0 were observed in a compound detected at 2.8 minutes in the GC trace. However, the amount detected was at trace levels, 0.7% area count integration; compare to the propene signal showing 86.0% area count. The major conclusion we drew from the screening was can be summarized as a general lack of activity for any reaction of the starting alkene.

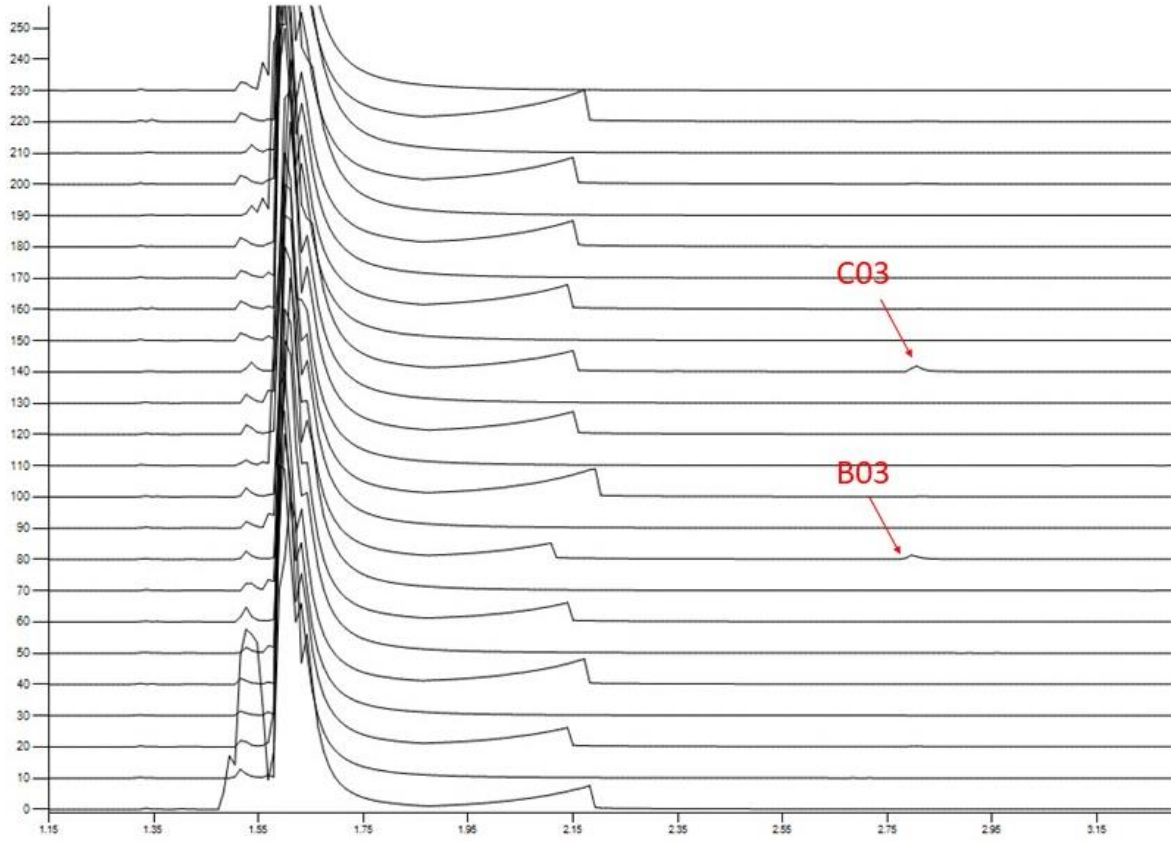

Figure 2.23 Stacked GC trace of 24-well screening plate with propene

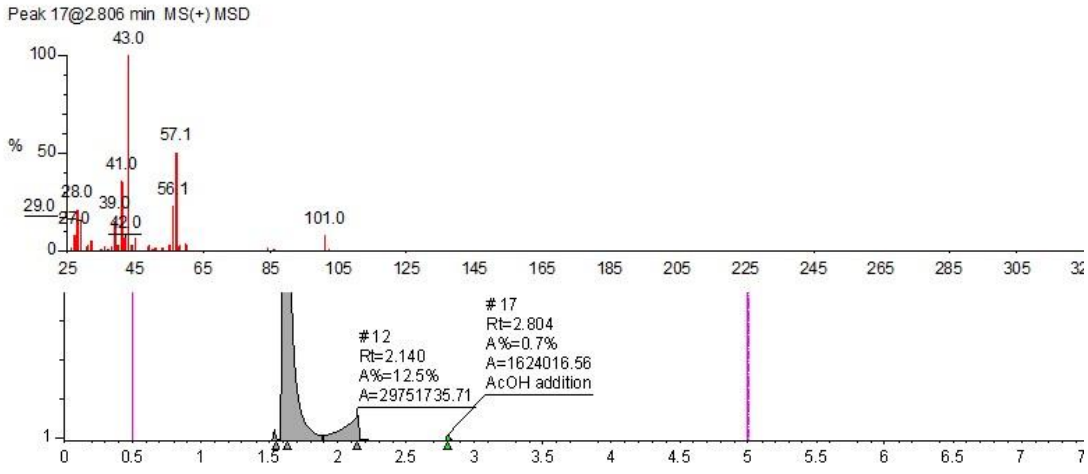

Figure 2.24 GC-MS data for cell B03 with **L2.5a**, acetic acid, propene, and $AgNTf_2$

2.4.2 Addition of carboxylic acids across alkynes

The high throughput screening for addition of terminal alkynes and benzoic acid confirmed the necessity for the tetra-aryl borate anions, either tetrakis(3,5-bis(trifluoromethyl)phenyl)borate or tetrakis(pentafluorophenyl)borate. Next, we sought to compare effectiveness of the different ligand structures as components of the gold catalyzed production of vinyl esters from carboxylic acids and alkynes.

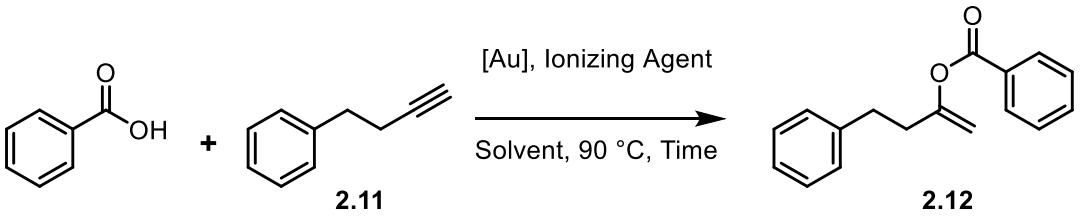

Figure 2.25 Model reaction for carboxylic acid addition to terminal alkynes

The summarized results of the study are presented in Table 2. The most effective ligand structure for this reaction is **L2.2a**. Ligand **L2.1a** was also effective at promoting the formation of vinyl ester **2.12**. Interestingly, the additional steric bulk of **L2.3a** resulted in a significant slowing of product formation, **Table 2** entry 6. Complex **Au2.8a**, with the pendent base located in the 4'-position, also performed well, yielding 76.4% of **2.12** after 5.2 hours heating.

Consistent with findings by Zhang, we observed rapid product formation when the ion exchange agent was present in around double the concentration of the gold complex. With a catalyst loading of 1.8 mol% and the ion exchange loading at 2.0 mol%, use of complex Au2.1a resulted in the product of 50.1% **2.12** after 24 hours heating at 90 °C. When the ion exchange agents loading was more than doubled to 5.3 mol%, 79.2% of the vinyl ester **2.12** was detected after heating for 1.3 hours at 90 °C. The use of DMF as a solvent completed eliminated all product formation. We did find efficient vinyl ester production when HFIP (hexafluoro isopropanol) was used as a solvent (see experimental details).

Table 2.2 Summary of Results for catalyzed addition of carboxylic acids to alkynes

Entry	Au Complex (mol %)	Ionizing Agent (mol %)	Solvent	Time (h)	% Yield 2.12	% Remaining 2.11
1	PPh_3AuCl (5.2)	$K[B(C_6F_5)_4]$ (6.9)	1,2-DCE / C_6D_6 (5/1)	19.25	41.8	29.3
2	**Au2.1a** (1.9)	$K[B(C_6F_5)_4]$ (5.3)	1,2-DCE / C_6D_6 (5/1)	1.3	79.2	12.3
3	**Au2.1a** (1.8)	$K[B(C_6F_5)_4]$ (2.0)	1,2-DCE / C_6D_6 (5/1)	24.0	50.1	36.0
4	**Au2.2a** (1.5)	$K[B(C_6F_5)_4]$ (3.9)	1,2-DCE / C_6D_6 (5/1)	2	84.5	2.0
5	**Au2.2c** (2.7)	$K[B(C_6F_5)_4]$ (2.8)	1,2-DCE / C_6D_6 (5/1)	1	12.4	86.4
6	**Au2.3a** (1.0)	$K[B(C_6F_5)_4]$ (6.0)	1,2-DCE / C_6D_6 (5/1)	24	19.9	69.0
7	**Au2.8a** (2.3)	$K[B(C_6F_5)_4]$ (3.5)	1,2-DCE / C_6D_6 (5/1)	5.2	76.4	21.0
8	**Au2.8a** (2.5)	$K[B(C_6F_5)_4]$ (2.5)	DMF	26	0	70.9
9	None	$K[B(C_6F_5)_4]$ (6.6)	1,2-DCE / C_6D_6 (5/1)	48	0	97.5

2.4.4 Isomerization of alkynes

Another transformation we targeted for application of functionalized biaryl ligands was the isomerization of alkynes. There are at least two major products that can be predicted to form, an allene or an isomerized alkyne. As mentioned above, Zhang and coworkers reported the isomerization of internal alkynes to 1,3-dienes, in this case relying on the extended conjugation of the aromatic system and the two alkenes to act as a thermodynamic sink. We started out with comparing the effect of the pyridine functional substitution to the tertiary amine version used by Zhang.

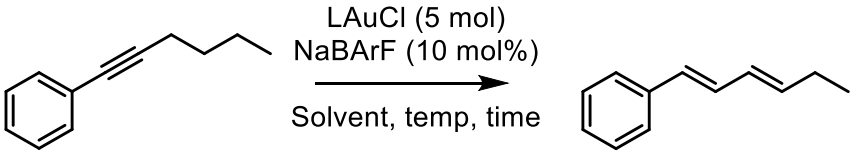

2.7

Figure 2.26 Reaction condition for internal alkyne isomerization

To our surprise, the **Au2.2a** complex did not isomerize the 1-phenyl-1-hexyne starting material to **2.7**. As a benchmark against the 2014 paper, we immediately turned to the case of Au2.6a with 1-phenyl-1-hexyne. Consistent with Zhang's findings, did observe 16 % production of the 1,3-diene product **2.7** after heating at 60 °C for 18 hours. The power and effect of solvent choice can be seen in a comparison of yields with **Au2.6a**. Zhang reports a 77 % yield when α,α,α-trifluorotoluene is used, a striking contrast to the 15.5 % product measured when benzene is the solvent.

We can clearly see from this comparison of yields that the properties of the solvent are crucial for getting the most out of a given catalyst. The dielectric constant for trifluorotoluene is reported as 9.1. The dielectric constant for benzene is 2.2. This contrast in catalyst efficiency with

differing solvents indicates the increased polarity plays a crucial role within the catalytic cycle. Consider the charge and polarity depicted in **Figure 2.27**. The extended, planar structure of the catalyst intermediates will lack stabilization in a non-polar solvent such as benzene. Whereas with a polar, non-coordinating solvent such as α,α,α-trifluorotoluene the charge on catalytic intermediates can be stabilized and allowed to progress towards product formation. Additionally, a potential reduction in ion pairing in the more polar solvent will likely have a positive effect on catalysis. After ion exchange of the chloride to the non-coordinating borate, the gold atom will be able to accommodate a new ligand for coordination. However, in a non-polar solvent, the borate anion will likely be held within a close proximity to the gold(I) cation. This close pairing can inhibit catalysis by blocking the coordination of an incoming substrate from the gold atom.

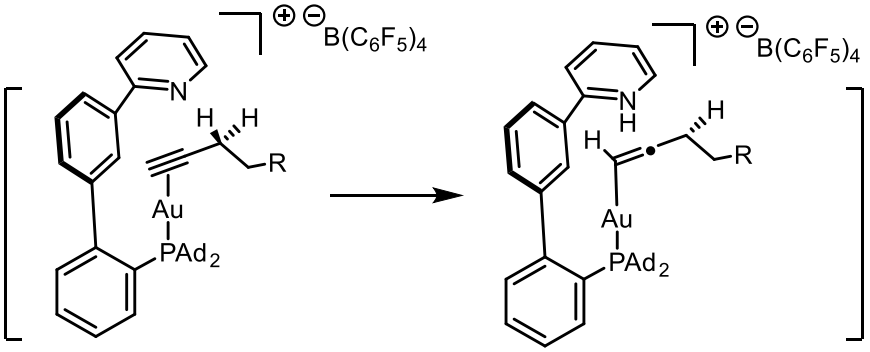

Figure 2.27 Potential intermediates in isomerization of terminal alkynes illustrating likely charge buildup

We attempted isomerization of a terminal triple-bond with the substrate 1-hexyne. Interestingly, **Au2.2a** did produce conversion of the starting material to the allene in 38 % yield, by NMR, after heating for at 60 °C for 31 hours. It is noteworthy that no 2-hexyne was detected, as Zhang showed was formed with the piperidine functionalized ligand. When 1-hexyne was treated for isomerization with **Au2.6a** (Zhang piperidine functionalized biaryl phosphine) we observed not only production of the allene in 67.6 % yield, but also production of 2-hexyne in 15.2 % yield; residual starting material was detected at 8.9 %.

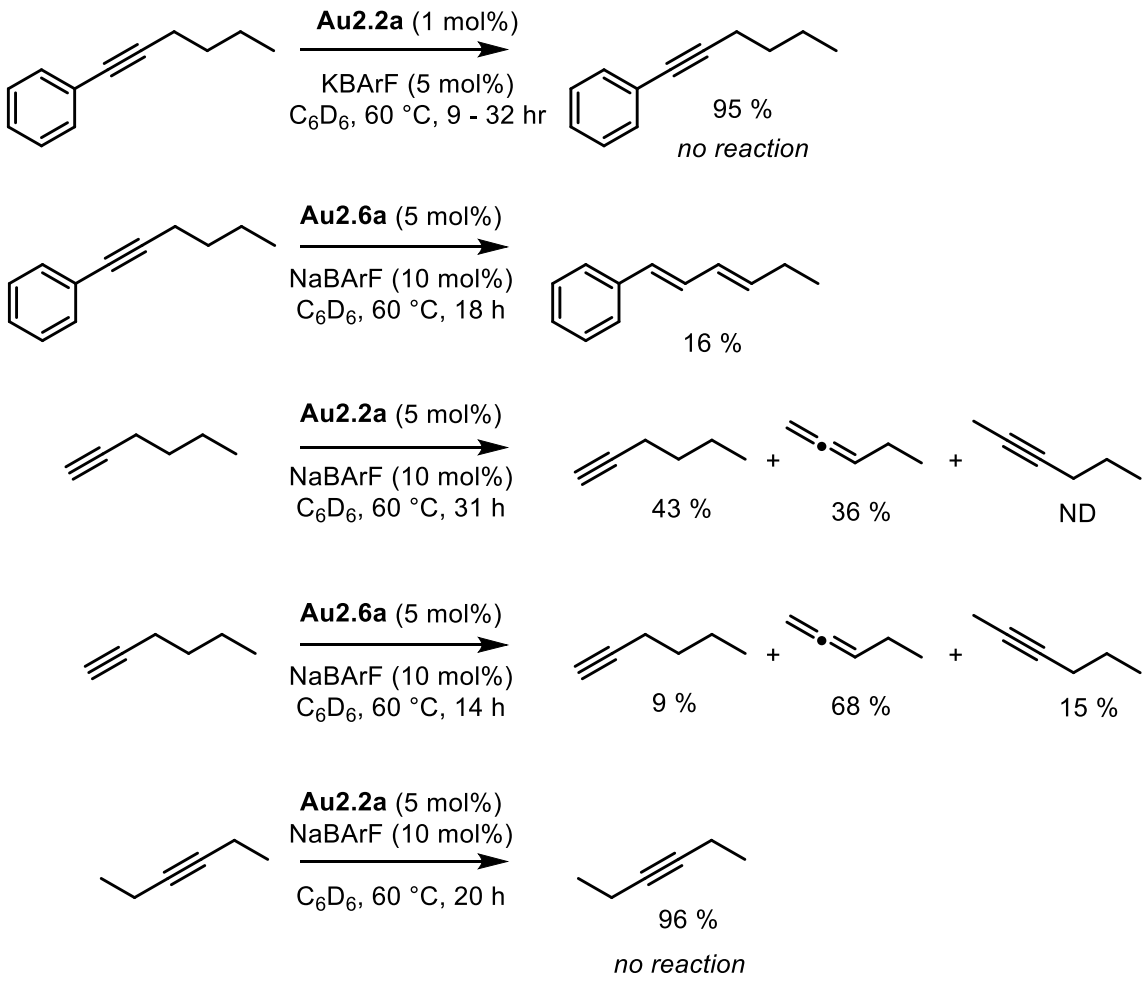

Figure 2.28 Summary of NMR scale alkyne isomerization conditions with functionalized biaryl phosphines in gold(I) complexes

Although slower than Zhang's optimized conditions, we believe there is insight gained from this work. The gold complex bearing the pyridine functionalized ligand Au2.2a is only able to catalyze the transformation of terminal alkynes to allenes, whereas the amino-functionalized **Au2.6a** complex, and those reported by Zhang, produce a mixture of terminal alkyne, allene, and internal alkyne. Further development on alkyne isomerization could benefit from a screening of solvents. For example, a search of dielectric constants for commonly available solvents reveals possible choices of dimethoxyethane ($\varepsilon = 7.23$), dichloroethane ($\varepsilon = 10.42$), and HFIP ($\varepsilon = 16.7$) may be useful for consideration in a solvent optimization screening.

2.5 Conclusion and outlook

Over the course of Chapter 2, we have studied the synthetic methods for biaryl ligand synthesis, some catalytic applications, and have started to develop structure-activity-relationship trends that can be used as groundwork for further development of catalytic applications. Initial development of biaryl phosphines from the Buchwald research group on palladium catalysis shed light on the unique properties the biaryl framework can provide. There are very few other ligand types that can support highly reactive zero-valent palladium in a two- or one-coordinate complex. The reports on functionalization of the biaryl ligand structure by Zhang gave us useful examples for comparison of catalytic performance of some functionalized biaryl phosphines in gold(I) catalyzed reactions of alkynes.

In the research on synthetic methods, we found that multi-step reactions with a single palladium catalyst are incompatible with the heterocyclic and amino functionalized coupling partners we choose to incorporate into the target's structure. Additionally, these Lewis basic and potentially coordinating functional groups often reduce the efficiency of palladium catalyzed carbon-carbon bond forming reactions. To reduce these undesirable effects on yield, we found that formation of the biaryl carbon-carbon bond should be targeted very early in the sequence of reaction steps.

We found that inclusion of certain metal-coordinating components can actually improve product yield in cases where competing reaction sites are an issue. We observed that use of a small excess of triphenylphosphine in Suzuki cross coupling reactions can increase the observed selectivity in product formation. Higher yields were obtained in the synthesis of **2.09** and **2.10**. We also found improvement in yield when DMSO was used as the solvent in the conversion of **I-2.1** to **I-2.2** compared to 1,4-dioxane. We hypothesize this improvement is due to the coordinating

ability of DMSO and the reduction in rate of all potential carbon-boron and carbon-carbon bond forming reactions such that the competing sites of reactivity do not interfere significantly with the formation of the desired product.

Formation of the phosphorus-carbon(sp^2) bond between a biaryl component and a PR_2X component is very efficient when X = H and the reaction proceeds via palladium catalysis. Use of chloro-phosphines in this step is synthetically useful, however a lower yield should be expected, and formation of side-products is often observed.

In the study of catalysis applications of the set of thirteen biaryl phosphine ligands synthesized here, we observed structure-activity trends that can be used to improve outcomes in catalytic reactions. Functionalization of the biaryl structure with acyclic amino is not highly effective for catalysis of alkyne isomerization reactions or addition of carboxylic acids across terminal alkynes. Functionalization of biaryl structure with cyclic amino groups such as **L2.6a** results in the most effective catalyst for the isomerization of terminal alkynes to both 2-alkynes and 1,2-allenes. Surprisingly, functionalization with a 2-pyridyl group at the 3'-position of the biaryl structure such as that in **L2.1a**, **L2.2a-c**, **L2.3a**, **L2.4a**, and **L2.5a** provided the most efficient and selective results in catalysis. In the addition of benzoic acid to 4-phenyl-1-butyne, **Au2.2a** catalyzes product **2.6** formation in 84% yield after heating for 2 hours at 90 °C. For use in isomerization of alkynes, **Au2.2a** will only isomerize terminal alkynes to the corresponding 1,2-allene. **Au2.2a** will not isomerize the 1,2-allene to a 2-alkyne. Additionally, **Au2.2a** will not isomerize internal alkynes, even in the presence of a strong thermodynamic driving force for product formation, such as extended conjugation of 1,3-dienes.

We also observed the need for either $K[B(C_6F_5)_4]$ or $Na[B(C_6H_3\text{-}3,5(CF_3)_2)_4]$ as the ion exchange agent for the carboxylic addition to alkyne reaction. The use of KPF_6 or $AgPF_6$ did not

yield product formation. Additionally, we observed significantly better results when using an excess of molar equivalents of ion exchange agent relative to gold(I) chloride complex equal to 2 or more. An interesting comparison is entries 3 and 4 in **Table 2.2**. After 24 hours only 50% product formation was measured when the amount of $K[B(C_6F_5)_4]$ was equal to 2.0 mol%. While 84 % product formation was measured when the amount of $K[B(C_6F_5)_4]$ was equal to 3.9 mol%.

We found that the solvent used has a drastic effect on efficiency of all ligands within the set studied when used for gold catalysis. The most effective solvents are polar and non-coordinating. An effective measure of solvent polarity is dielectric constant in this case. We observed the best results when the dielectric constant of the reaction medium was near $\varepsilon = 10$. In the case of the carboxylic acid addition to alkynes, 1,2-dichloroethane was an effective choice. In many of the reactions studied we also added C_6D_6 as a co-solvent to expedite analysis. When addition of a carboxylic acid to an alkyne reaction was attempted with the very polar solvent DMF, no product formation was detected. This could be due to coordination of the DMF to the gold(I) catalyst.

The use of high throughput experimentation is effective at scanning a large swath of chemical space for unique reactivity. Although we observed no positive indications of catalysis in our one round of screening on the carboxylic acid addition to alkyne chemistry, we did learn that the ion exchange agent used is a crucial choice for all ligands tested in this work.

Our initial hypothesis for the development of the functionalized biaryl phosphine ligands was to target alkene chemistry. Specifically, we hypothesized that a coordinated alkene would be placed such that a pendent base could activate an ROH type molecule towards addition to the alkene. We did not observe this result in either HTE screenings or NMR studies on the complexes.

Proposed future work on this project includes expansion of the substrate scope for the carboxylic acid to alkyne addition reactions and development of ligands with either carboxylate or phosphonate groups as the pendent base. The focus of this work was on nitrogen containing functional groups. The use of oxygen containing groups as the pendent base may expand the type of catalysis the biaryl phosphine ligands can promote. Additionally, the availability of differing protonation states with the use of carboxylate and phosphonate / phosphonic acid type functionalization on the biaryl ring may offer completely new substrate activation pathways. An interesting question such functionalization could address is: what effects would arise from including the charge balance for a gold(I) cation within the ligand structure in a manner that prevents the anionic portion of the ligand from intramolecular coordination with the gold atom? Would multinuclear complexes form? And if so, would formation of multinuclear complexes hinder catalytic performance?

2.6 Experimental Details

Unless stated otherwise, reactions were performed under dry nitrogen using a combination of Schlenk line and glovebox techniques. NMR spectra were recorded at 30 °C using Varian spectrometers; a 500-MHz INOVA (500 MHz listed below for ^{1}H = 499.940 MHz, 125.7 MHz for ^{13}C = 125.718 MHz, 202MHz for ^{31}P = 202.37 MHz, and 470 MHz for ^{19}F = 470.36 MHz); and 400-MHz Varian NMR-S (400 MHz listed below for ^{1}H = 399.763 MHz, 100 MHz for ^{13}C = 100.525 MHz, 162 MHz for ^{31}P = 161.830 MHz, and 376 MHz for ^{19}F = 376.10 MHz). ^{1}H and ^{13}C NMR chemical shifts are reported in ppm, referenced to residual solvent resonances as internal standards (^{1}H NMR: δ = 7.27 for $C\mathit{H}Cl_3$, 5.32 for $C\mathit{H}DCl_2$, 7.16 for $C_6\mathit{H}D_5$ and ^{13}C NMR: δ = 77.16 for $CDCl_3$, 54.00 for CD_2Cl_2, 128.06 for C_6D_6). ^{1}H NMR signals are given followed by multiplicity, coupling constants *J* in Hertz, and integration in parentheses.

Ethyl acetate (ACS grade), hexanes (ACS grade) pentane (ACS grade) petroleum ether (ACS grade), dimethyl sulfoxide (99.7+ % extra dry), and 1,4-dioxane (99.8% extra dry) were purchased from Fisher Scientific and used without further purification. Tetrahydrofuran, diethyl ether, and dimethoxy ethane were distilled over sodium/benzophenone and sparged with nitrogen prior to use. Methylene chloride was distilled over calcium hydride. Acetonitrile was sparged with nitrogen then stored over 3 Å molecular sieves. Toluene (ACS grade) was sparged with nitrogen then stored over 4 Å molecular sieves. *n*-Butyl lithium was purchased from Fisher Scientific as either a 2.5 M or 1.6 M solution in hexanes and used without further purification.

Palladium tetrakis(triphenylphosphine) ($Pd(PPh_3)_4$) and [1,1'-bis(diphenylphoshino) ferrocene]dichloropalladium (II) complex with dichloromethane ($Pd(dppf)Cl_2$•DCM) were prepared according to literature procedures (need citation here). Water used as cosolvent in cross-coupling reactions was collected from house supplied deionized water line and sparged with nitrogen. Water used to quench reactions was collected from house deionized water line and used without further treatment. Aqueous salt solutions (LiCl, NaCl, NaOH, KOH, HCl, H_2SO_4, etc) were prepared with house deionized water used without further treatment and the corresponding component measured by mass. Other reagents were purchased from commercial suppliers and were used without further purification.

Thin layer chromatography was performed using Sorbtech 200 µm silica gel plates with 254 nm UV absorption. Column chromatography was performed using Sorbtech 60 Å silica gel for flash chromatography under positive pressure of either air or nitrogen gas. Schlenk techniques were performed in a fume hood on a standard two-way Schlenk line with nitrogen and vacuum paths. Vacuum was supplied by use of an Edwards RV8 or RV12 rotary vane vacuum pump.

Liquid nitrogen was used in a glass dewar flask for the cold trap. The cold trap was emptied, cleaned, and dried daily, and whenever full to capacity if necessary multiple times per day.

Ligand Synthesis

Synthesis of **2.13**

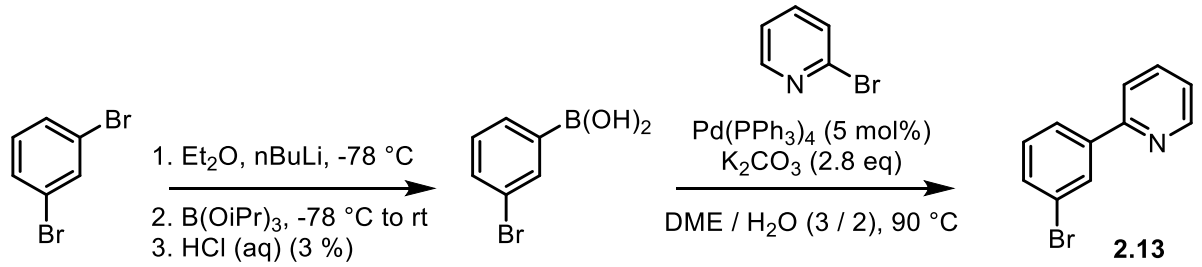

In a nitrogen filled glovebox, an oven dried Schlenk flask was charged with 1,3-dibromobenzene (3.1075 g, 0.0132 mol) and magnetic stir bar. The flask was capped with a rubber septum, removed from the glove box, connected to a Schlenk line under positive pressure of N_2 (g), and 20.0 mL of freshly distilled and de-oxygenated Et_2O was added. The solution was then submerged in a dry ice / *i*PrOH bath with stirring. Via syringe and needle, *n*-BuLi (2.5 M in hexanes) (5.6 mL 0.014 mol) was added dropwise over 7 min. After allowing the reaction to age for 43 min, $B(OiPr)_3$ (3.8082 g, 0.0202 mol) was added dropwise over 3 min, then the mixture was removed from the cooling bath and allowed to slowly warm to rt for 17 h. The reaction was then quenched with saturated NH_4Cl (aq) (30 mL) and then diluted with EtOAc (50 mL) and allowed to mix for 30 min, after which the phases were separated, and the aqueous portion extracted with EtOAc (75 mL). Organic portions were combined and dried over $MgSO_4$, and concentrated *in vacuo* to yield a crude mass of 2.3996 g. The resulting solid was then stirred with 10 mL of HCl (aq) (3 %) for 5 h, then extracted with EtOAc (25 mL). The organic fraction was dried over $MgSO_4$, then concentrated *in vacuo* to yield 1.865 g of an off white solid, which was used without further purification. The solid was taken up in DME (15.0 mL) in a glovebox and added to a pressure

tube containing K_2CO_3 (3.6041 g, 2.608 mmol) and 2-bromopyridine (1.4767 g, 9.29 mmol). To the mixture was added, DI H_2O (10.0 mL) and $Pd(PPh_3)_4$ (532.7 mg, 0.461 mmol). The tube was seal with a teflon cap, then placed in an oil bath pre-heated to 90 °C for 19.5 h. After which time the reaction was diluted with H_2O (150 mL). The mixture was then extracted three times with EtOAc (80 mL), the combined organic fractions were then washed with saturated NaCl (aq) (100 mL), then dried over Na_2SO_4, filtered, and concentrated *in vacuo*. The resulting solid was purified by column chromatography with silica gel (32 g). The mobile phase consisted of hexanes and EtOAc, with 1 % (w/w) NEt_3. The percentage of EtOAc was gradually increased from 5 % initially to a final composition of 15 %, relative to hexanes. Fractions were analyzed by TLC, and similar fractions were combined to yield compound **2.13** as a white solid (1.5277 g, 49 %).

^{1}H-NMR ($CDCl_3$, 400 MHz): δ = 8.71 (ddd, *J* = 4.8, 1.8, 1.0, 1H), 8.18 (t, *J* = 1.9, 1H), 7.92 (ddd, *J* = 7.8, 1.7, 1.0, 1H), 7.78 (ddd, *J* = 8.1, 7.4, 1.8, 1H), 7.71 (dt, *J* = 8.0, 1.1, 1H), 7.55 (ddd, *J* = 7.9, 2.0, 1.0, 1H), 7.35 (t, *J* = 7.9, 1H), 7.29 – 7.25 (m, 1H). Minor signals for residual CH_2Cl_2 (5.30 ppm (s)) and THF (3.76 (m) and 1.85 (m)). Residual 1,4-dixoane (3.71 ppm (s)) and CH_2Cl_2 (5.30 ppm (s)) are observed in the spectrum.

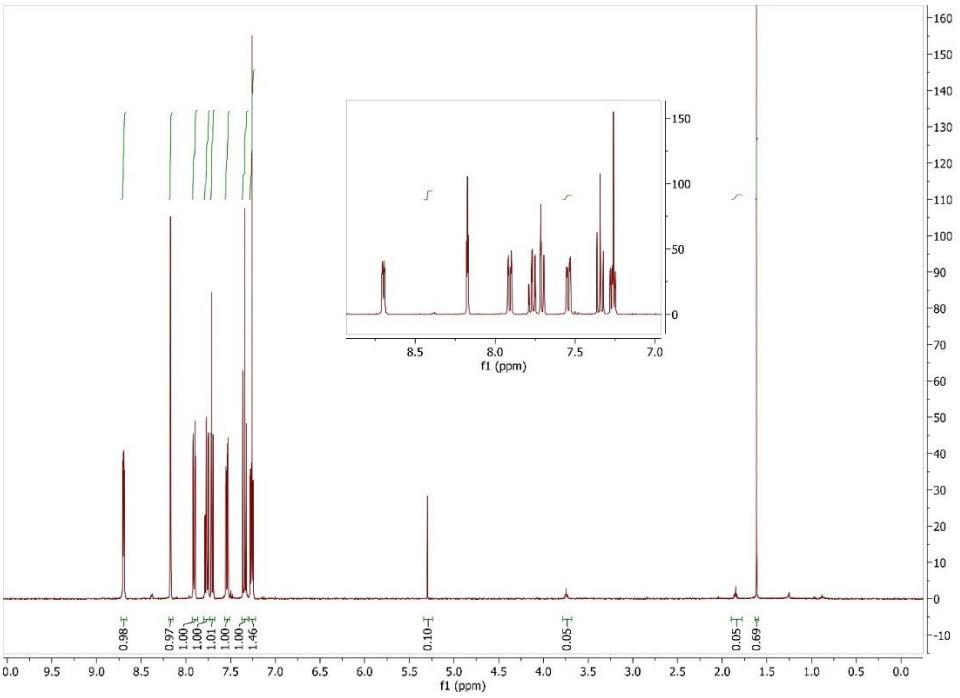

Figure 2.29 ^{1}H-NMR of **2.13** in $CDCl_3$ at 400 MHz, inset showing aromatic region coupling.

Synthesis of **2.14**

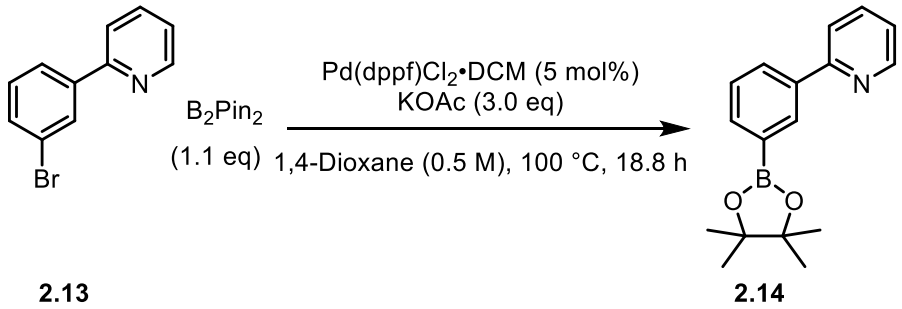

2.13 **2.14**

In a nitrogen filled glovebox, a pressure tube was charged with B_2Pin_2 (1.7607 g, 6.933 mmol), KOAc (1.8604, 18.955 mmol), aryl bromide **2.13** (1.4755 g, 6.303 mmol), then 1,4-Dioxane (20.0 mL). The tube was agitated to facilitate dissolution, then Pd(dppf)Cl_2•DCM (261.2 mg, 0.319 mmol) was added. The tube was sealed with a Teflon cap, removed from the glovebox, and place in an oil bath pre-heated to 100 °C for 18.8 h. After removal from heating, the reaction mixture was diluted with D.I. H_2O (100 mL) and EtOAc (100 mL), which resulted in a large

emulsion layer. Saturated NaCl (aq) (15 mL) was added to break the emulsion, then the layers were separated. The aqueous fractions were then extracted twice more with EtOAc (100 mL). The organic fractions were combined and concentrated *in vacuo* to yield a light brown oil weighing 3.38 g. To the oil, pentane (100 mL) was added, which resulted in formation of a light brown solution and an insoluble solid. The mixture was then filtered, and the solid washed with Et_2O (80 mL). The remaining solid was then washed through the filter with the addition of CH_2Cl_2 (75 mL) and collected in a separate flask, then concentrated *in vacuo* to yield 2.0629 g of aryl boronic ester **2.14** as a brown solid, which was used without further purification. Residual CH_2Cl_2, 1,2-dichloroethane, and water are observable in the ^{1}H-NMR spectrum below.

^{1}H-NMR ($CDCl_3$, MHz): δ 8.71 (m, 1H), 8.39 (s, 1 H), 8.14 (dt, *J* = 7.9, 1.6, 1H), 7.86 (m, could be dt , 1H), 7.83 – 7.78 (m, 1H), 7.77 – 7.70 (m, 1H), 7.50 (t, *J* = 7.5, 1H), 7.23 (ddd,, *J* = 7.3, 4.8, 1.4, 1H), 1.37 (s, 12H)

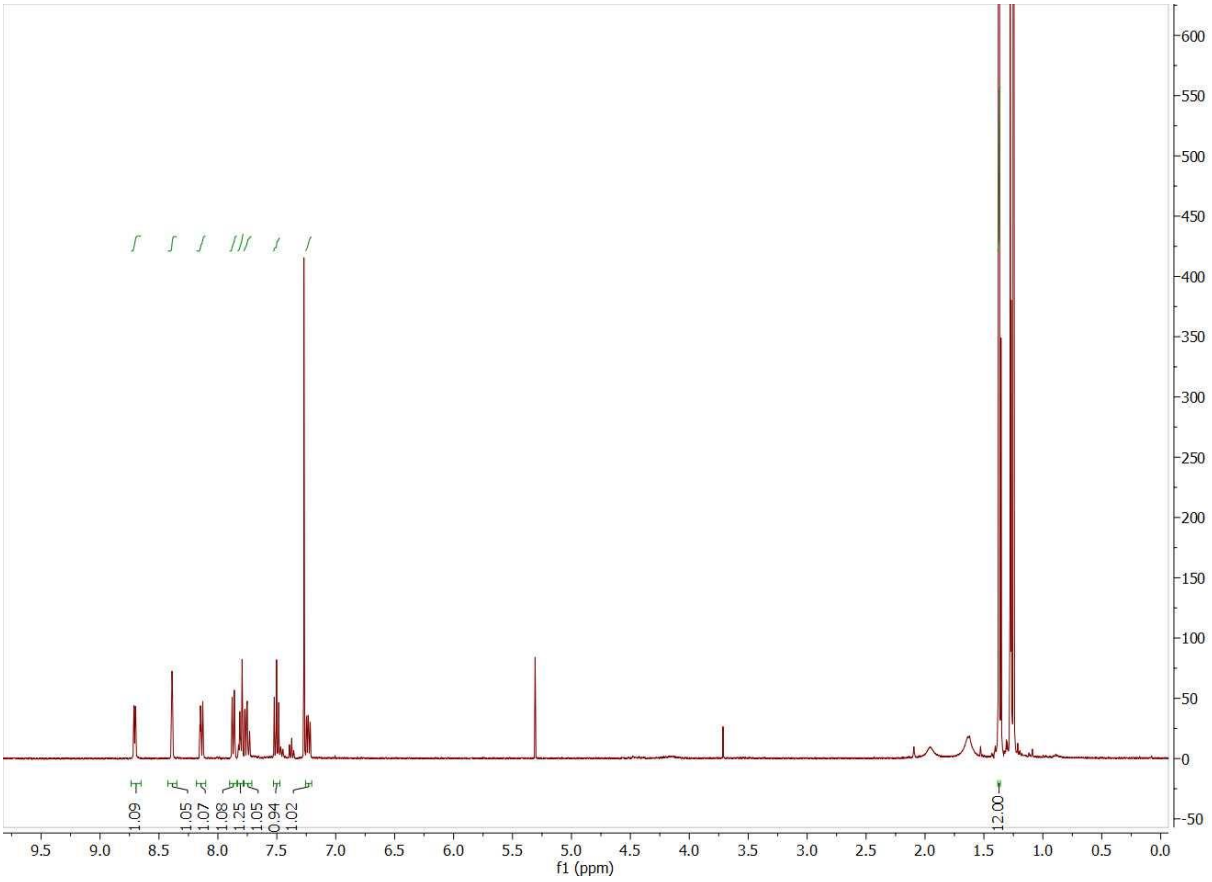

Figure 2.30 ^{1}H NMR spectrum of **2.14** in $CDCl_3$ at 400 MHz

Synthesis of **2.15**

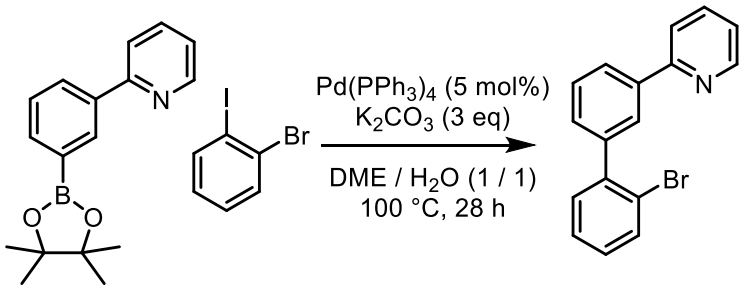

2.14 **2.15**

In a nitrogen filled glovebox, a scintillation vial was charged with crude aryl boronic ester **2.14** (745.6 mg, 2.652 mmol), 1-bromo-2-iodobenzene (684.1 mg, 2.418 mmol), K_2CO_3 (1.0030 g, 7.257 mmol), DME (5.0 mL), D.I. H_2O (5.0 mL), $Pd(PPh_3)_4$ (139.5 mg, 0.121 mmol), and magnetic stir bar. The vial was capped, removed from the glovebox, then place in an oil bath pre-

heated to 100 °C for 28 h. The reaction mixture was cooled to rt, then diluted with D.I. H_2O (50 mL), then extracted four times with EtOAc (50 mL). The combined organic fractions were washed with saturated NaCl (aq) (80 mL), dried over $MgSO_4$, filtered, and concentrated *in vacuo* to yield a crude product of mass 985.8 mg. The crude material was purified by column chromatography on silica gel (30 g). The mobile phase consisted of a mixture of hexanes and EtOAc starting with pure hexanes and ending with 10 % EtOAc in hexanes. Fractions were analyzed by TLC, and similar fractions were combined. ^{1}H-NMR analysis revealed the presence of PPh_3, so the mixture was taken up in CH_2Cl_2 (20 mL) and H_2O_2 (30 %) (20 mL) was added. The biphasic mixture was allowed to stir for 30 min, after which time the phases where separated, and the organic fraction was passed through a short plug of silica, eluting with a mixture of pet. Ether (93 %) and EtOAc (7 %) (150 mL). Concentration *in vacuo* yielded of aryl bromide **2.15** as light brown wax (501.1 mg, 56.8 %).

^{1}H-NMR ($CDCl_3$, MHz): δ = 8.71 (dt, *J* = 4.8, 1.4, 1H), 8.06-8.01 (m, 2H), 7.81-7.74 (m, 2H), 7.70 (dd, *J* = 8.0, 1.2, 1H), 7.58-7.52 (m, 1H), 7.49 (dt, *J* = 7.7, 1.5, 1H), 7.44-7.36 (m, 2H), 7.27-7.21 (m, 2H)

^{13}C-NMR ($CDCl_3$,101 MHz): δ = 157.31, 149.87, 142.52, 141.69, 139.34, 136.91, 133.23, 131.50, 130.11, 128.99, 128.55, 128.16, 127.53, 126.27, 122.80, 122.37, 120.82

EA: Calculated for C17H12BrN (calc. mol wt.): C, 65.83; H, 3.90; N, 4.52. Found: C: 65.50, H: 4.25, N: 4.74

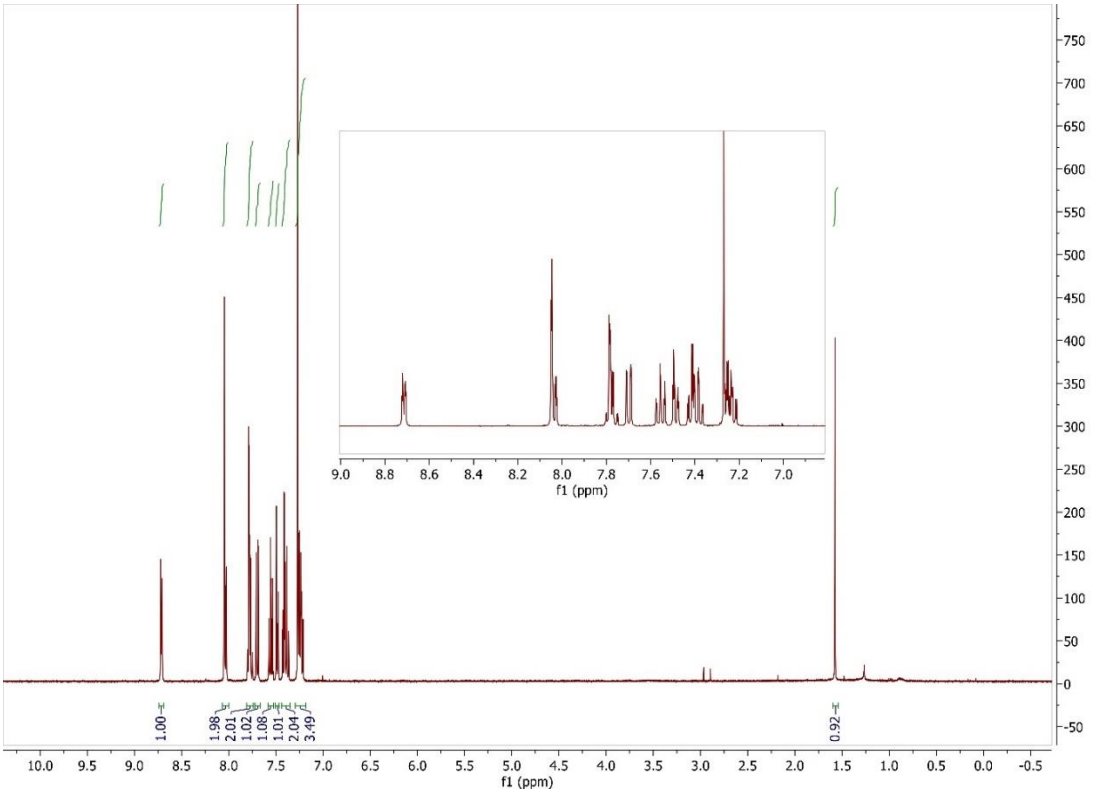

Figure 2.31 ^{1}H NMR spectrum of **2.15** in $CDCl_3$ at 400 MHz

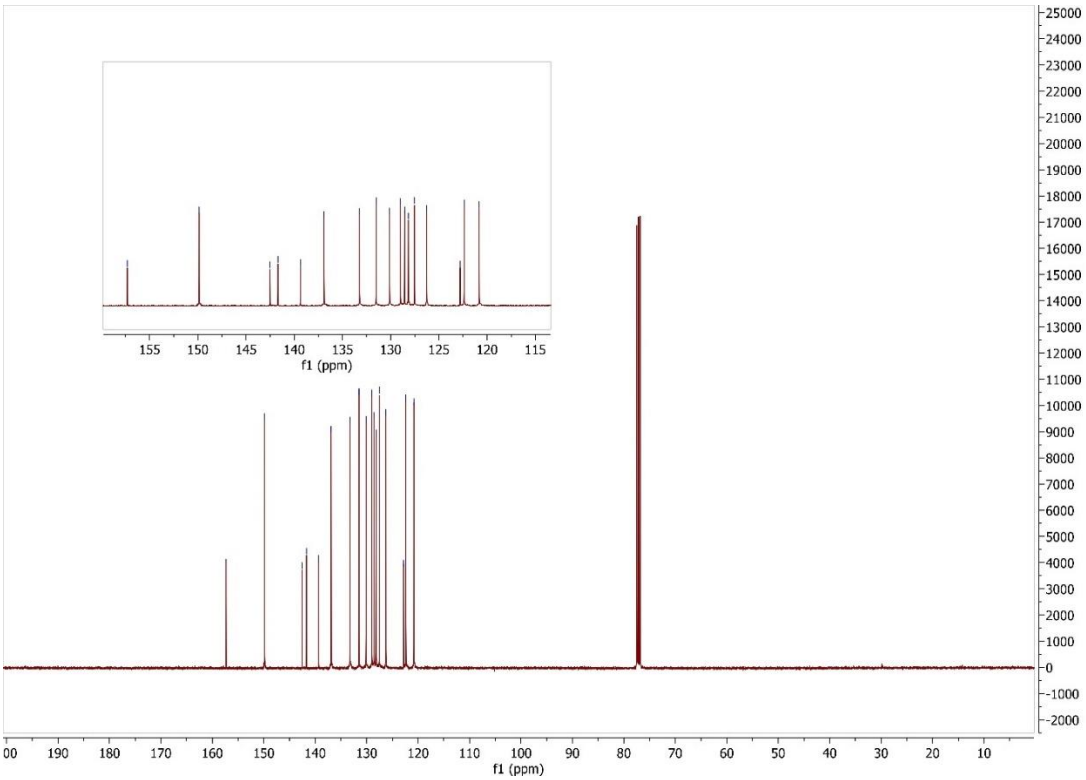

Figure 2.32 $^{13}C\{^{1}H\}$ NMR spectrum of **2.15** in $CDCl_3$ at 100 MHz

Synthesis of **L2.1a**

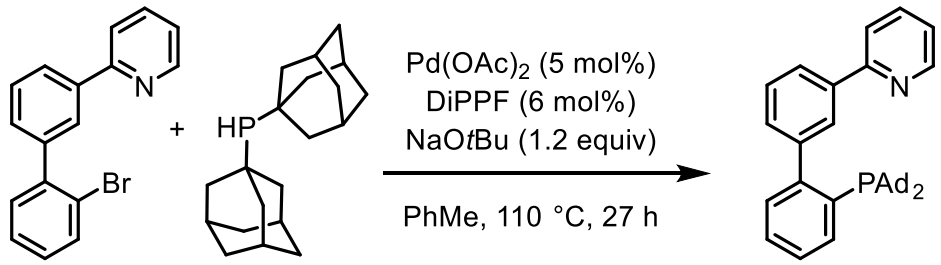

2.15 **L2.1a**

In a nitrogen filled glovebox, an oven dried scintillation vial was charged with magnetic stir bar, DiPPF (38.5 mg, 0.092 mmol), $Pd(OAc)_2$ (17.0 mg, 0.076 mmol), NaOtBu (179.0 mg, 1.863 mmol), and PhMe (1.5 mL). The mixture was allowed to stir at rt for 10 min, then diadamantyl phosphine (520.2 mg, 1.720 mmol), aryl bromide **2.15** (477.5 mg, 1.539 mmol), and PhMe (6.0 mL) were added. The vial was capped, removed from the glovebox, then placed in an

oil bath pre-heated to 110 °C for 27 h. Reaction progress was followed by ^{31}P-NMR analysis. Upon completion, the reaction was allowed to cool to r.t., then purified by column chromatography on silica gel (40 g) without workup. The column was run in a fume hood using de-oxygenated hexanes and EtOAc with positive pressure of N_2 (g). The mobile phase composition was a gradient mixture of increasing polarity starting with pure hexanes and ending with 20 % EtOAc, 1% NEt_3 in hexanes. Similar fractions were combined based on TLC analysis and solvent evaporated *in vacuo* to yield product as an off-white powder (656.1 mg, 80 %).

^{1}H-NMR ($CDCl_3$, 400 MHz): δ = 8.69 (dt, *J* = 4.8, 1.4, 1H), 7.99 (dt, *J* = 7.8, 1.4, 1H), 7.92 (d, *J* = 6.9, 1H), 7.79-7.69 (m, 2H), 7.47 (t, *J* = 7.7, 1H), 7.43-7.30 (m, 4H), 7.21 (ddd, *J* = 6.7, 4.8, 2.0, 1H), 1.98-1.81 (m, 18 H), 1.66 (br s, 12H)

^{31}P-NMR ($CDCl_3$, MHz): δ = 21.01

EA: Calculated C: 83.58, H: 7.96, N: 2.63; Found C: 83.18, H: 8.33, N: 2.91

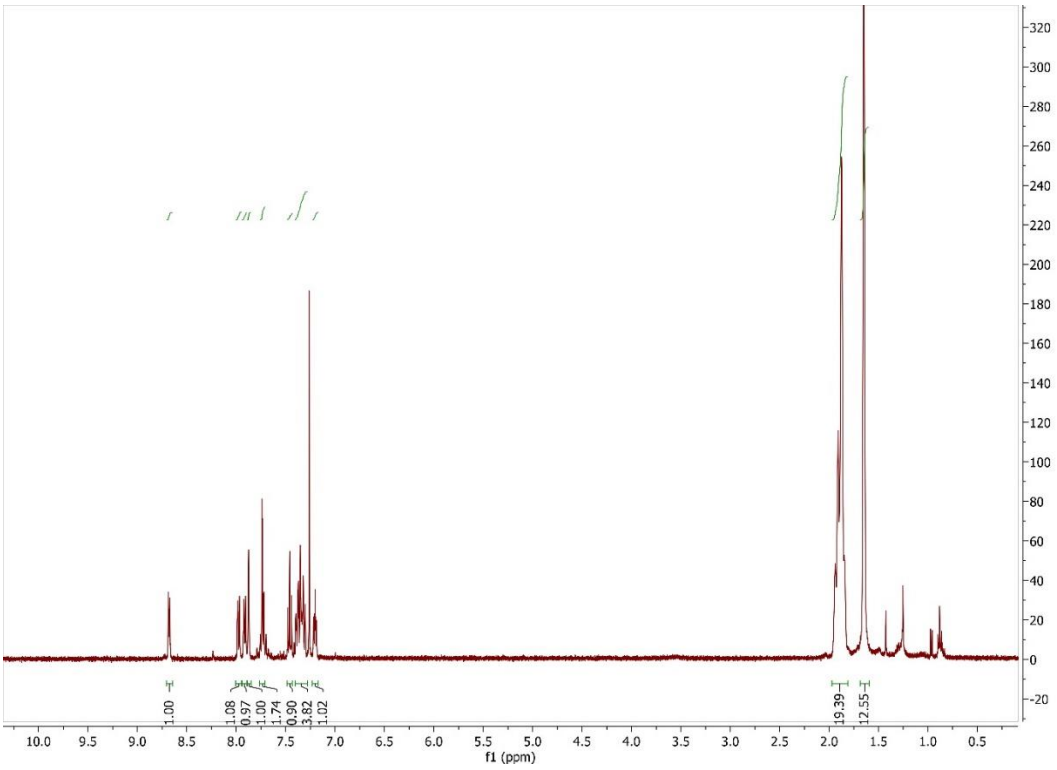

Figure 2.33 ^{1}H NMR spectrum of **L2.1a** in $CDCl_3$ at 400 MHz

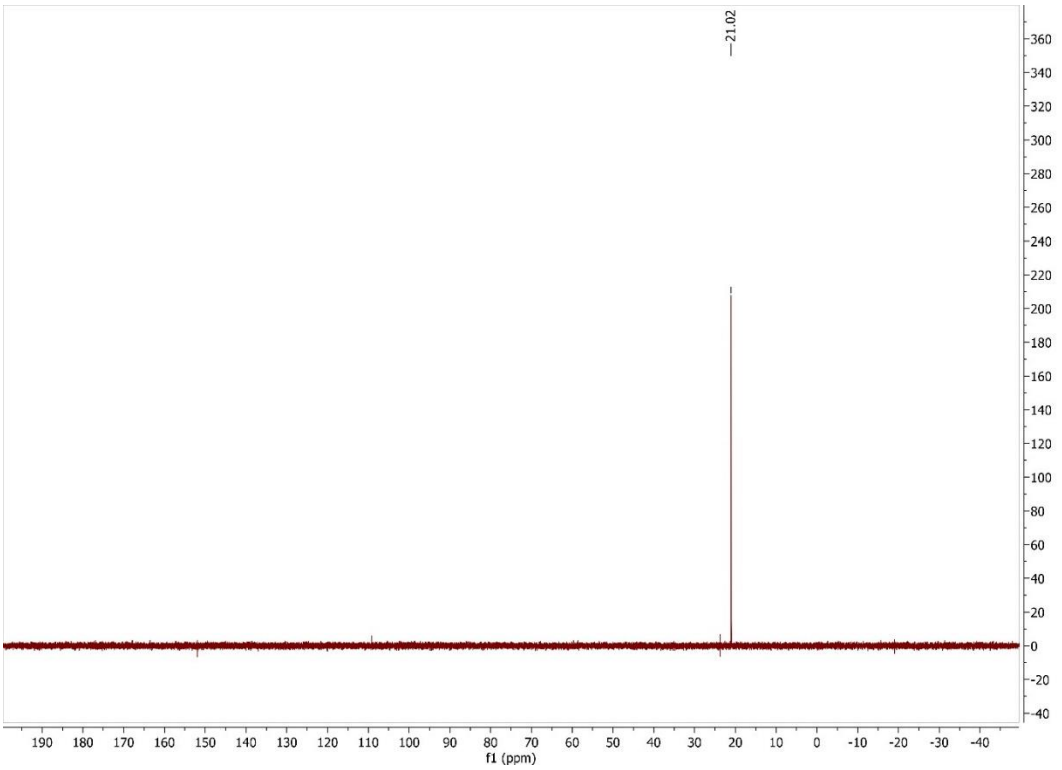

Figure 2.34 ^{31}P NMR spectrum of **L2.1a** in $CDCl_3$ at 162 MHz

Synthesis of **2.16**

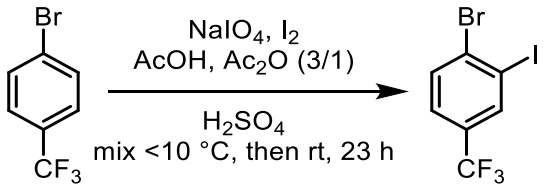

2.16

Following a literature procedure,[55] in open atmosphere, a 3-neck round bottom flask was charged with I_2 (18.5960 g, 0.0733 mol, 1.2 equiv), $NaIO_4$ (15.6820 g, 0.0733 mol, 1.2 equiv.), acetic acid (60 mL), acetic anhydride (30 mL), and magnetic stir bar. The resulting mixture was placed in an ice bath with stirring, while H_2SO_4 (95 % w/w) (83 mL) was added dropwise via addition funnel over 30 min so that the temperature remained below 10 °C. The aryl bromide (para-bromo-α,α,α-trifluorotoluene) was then added via addition funnel over 5 min. After an additional 5-10 min mixing time, the resulting solution was removed from the ice bath and allowed to warm

to room temperature over 23 h. Reaction progress was monitored by ^{1}H NMR spectroscopy. Upon consumption of the starting aryl bromide, the reaction mixture was poured into an aqueous solution of Na_2SO_3 (30 g in 300 mL H_2O) in an ice bath with stirring. This mixture was further diluted with saturated Na_2CO_3 (aq) (200 mL). The resulting mixture was extracted with CH_2Cl_2 (300 mL), separated, and then extracted twice more with CH_2Cl_2 (200 mL). The combined organic layers were washed with sat. Na_2CO_3 (aq) (500 mL) and sat. NaCl (aq) (200 mL), then dried over $MgSO_4$ and filtered. A crude mass of 20.16 g remaining after rotary evaporation was purified by Kugelrohr distillation at 83-87 °C with pressure of 0.28 mmHg. The product **2.16** was isolated as the second fraction, as a clear liquid (17.0584 g, 80 %). Boiling point and NMR spectra were consistent with literature findings.

^{1}H NMR ($CDCl_3$, 500 MHz): δ 8.10 (dd, *J* = 2.2, 0.9, 1H), 7.75 (dd, *J* = 8.4, 0.9, 1H), 7.47 (ddd, *J*= 8.4, 2.2, 0.9, 1H).

^{13}C NMR ($CDCl_3$, 125 MHz): δ 137.19 (q, *J* = 3.8), 134.25, 133.13, 130.85 (q, *J* = 33.2), 126.30 (q, *J* = 3.7), 122.8 (q, *J* = 272.8), 101.55.

^{19}F NMR ($CDCl_3$, 470 MHz) δ -62.81.

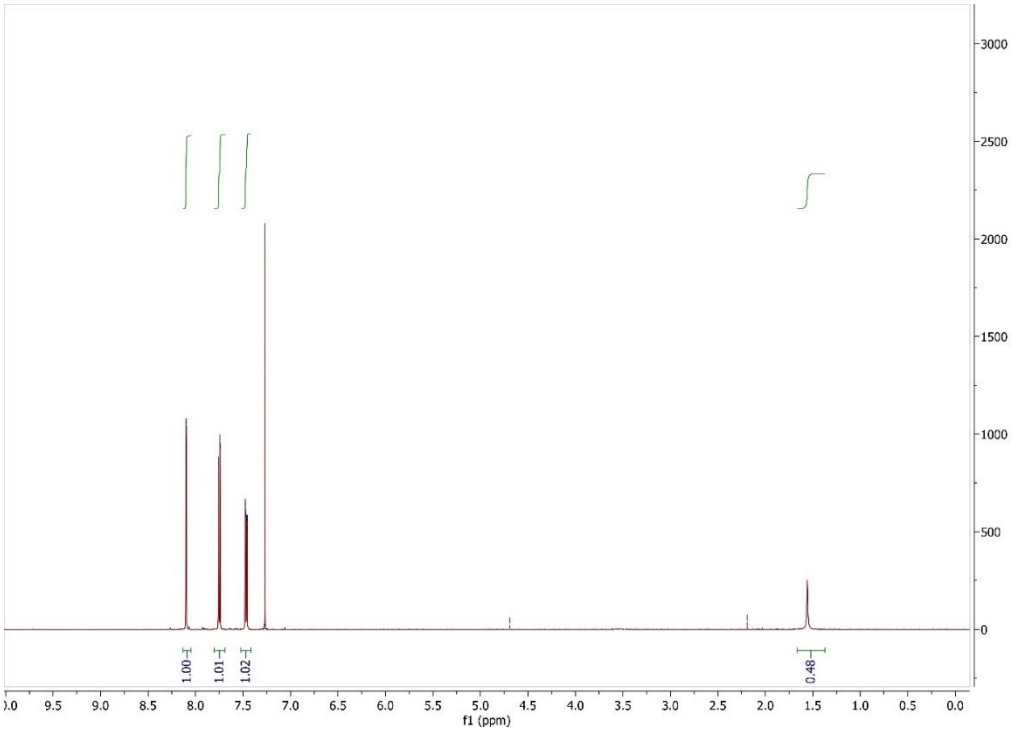

Figure 2.35 ^{1}H NMR spectrum of **2.16** in $CDCl_3$ at 500 MHz

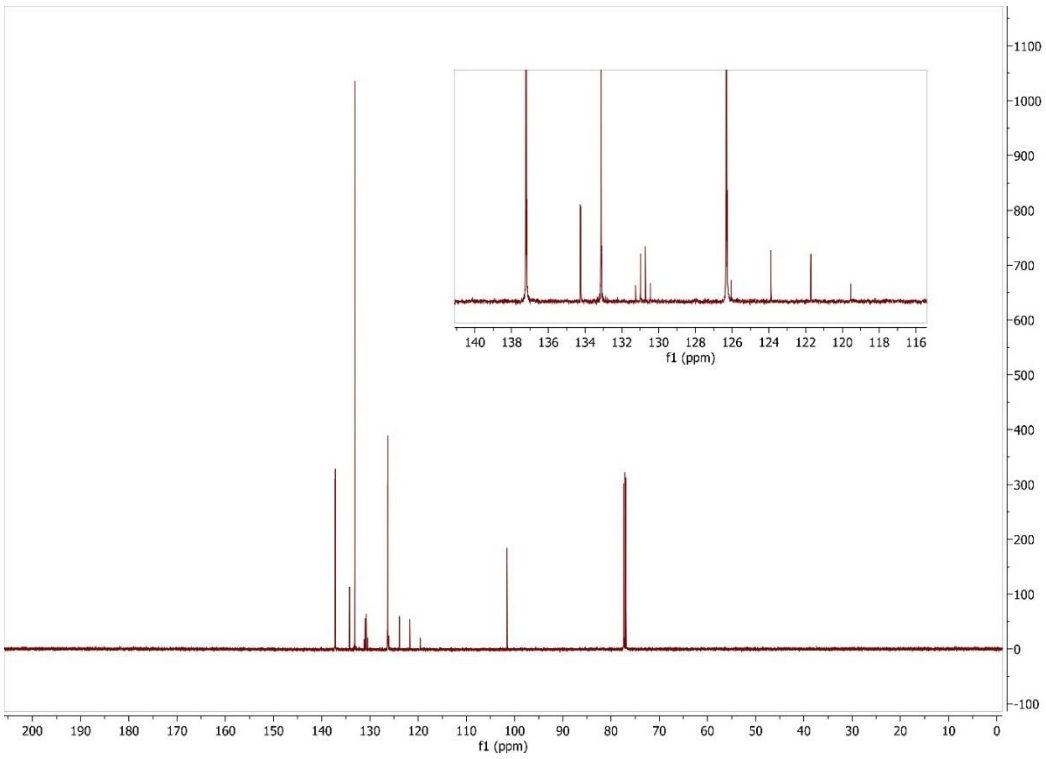

Figure 2.36 $^{13}C\{^{1}H\}$ NMR Spectrum of **2.16** in $CDCl_3$ at 125 MHz

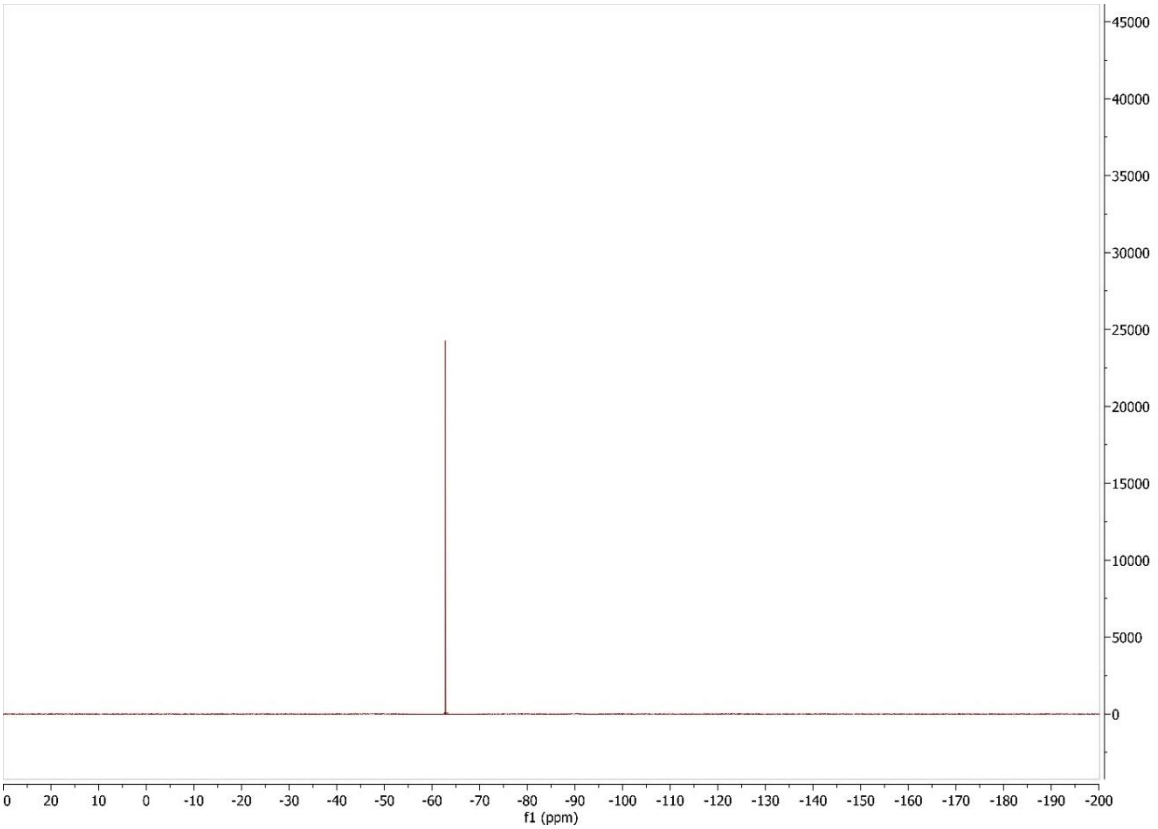

Figure 2.37 ^{19}F NMR spectrum of **2.16** in $CDCl_3$ at 470 MHz

Synthesis of **2.17**

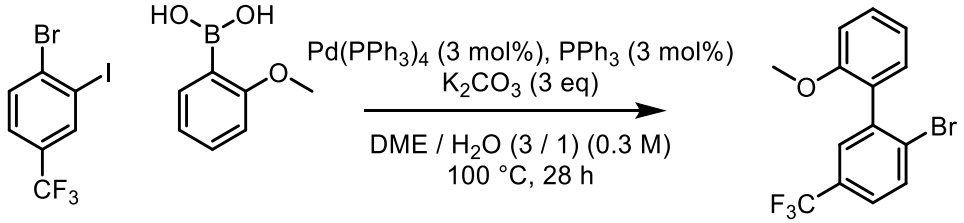

2.16 **2.17**

In a nitrogen filled glovebox, a pressure vessel with Teflon screw cap was charged with magnetic stir bar, 2-methoxyphenyl boronic acid (2.3861 g, 0.0157 mol), aryl iodide **2.16** (5.2532 g, 0.015 mol), triphenylphosphine (119.4 mg, 0.455 mmol), K_2CO_3 (*s*) (6.2103 g, 0.045 mol), then dimethoxyethane (35 mL) and D.I. water (15 mL). The mixture was briefly shaken before palladium tetrakis(triphenyl phosphine) (531.3 mg 0.459 mmol) was added. The pressure vessel was capped, removed from the glovebox, and heated in an oil bath at 100 °C for 27.2 h. Once

cooled, the reaction mixture was filtered, and diluted with D.I. H_2O (50 mL), then extracted three times with EtOAc (50 mL). The organic fraction was then washed with saturated NaCl (aq) (100 mL), then dried over anhydrous $MgSO_4$ and filtered, and concentrated under reduced pressure to yield a light brown colored oil. ^{31}P NMR analysis of the crude product mixture showed resonances for both PPh_3 and $OPPh_3$, -5.2 ppm and 28.9 ppm, respectively. The crude mixture was taken up in CH_2Cl_2 (40 mL) and stirred with 30 % H_2O_2 (15 mL) at room temperature. After 1 h, the phases were separated, and the organic fraction was washed with saturated NaCl (aq), then dried over anhydrous $MgSO_4$, filtered, and the filtrate concentrated under reduced pressure. The mixture was purified by silica gel chromatography (62 g silica). The mobile phase consisted of hexanes and ethyl acetate, in a gradient mixture starting with pure hexanes and ending with 20 % EtOAc by volume. Fractions were analyzed by TLC and similar fractions were combined and concentrated to give product **2.17** as a thick colorless oil after storage under oil pump vacuum (4.1745 g, 84 %).

^1H NMR ($CDCl_3$, 500 MHz): δ 7.78 (d, *J*= 8.4, 1H), 7.55 (d, *J* = 2.2, 1H), 7.47 – 7.40 (m, 2H), 7.18 (dd, *J* = 7.5, 1.8, 1H), 7.06 (td, *J* = 7.5, 1.0, 1H), 7.00 (dd, *J* = 8.3, 1.0, 1H), 3.80 (s, 3H).

^{19}F NMR ($CDCl_3$, 470 MHz): δ -62.54

$^{13}C\{^1H\}$ NMR ($CDCl_3$, 125 MHz): δ 156.55, 140.93, 133.19, 130.78, 130.14, 129.70 (q, *J* = 32.9), 129.04, 128.53 (q, *J* = 3.7), 128.50, 125.42 (q, *J* = 3.8), 124.05 (q, *J* = 272.2), 120.60, 111.17, 55.68.

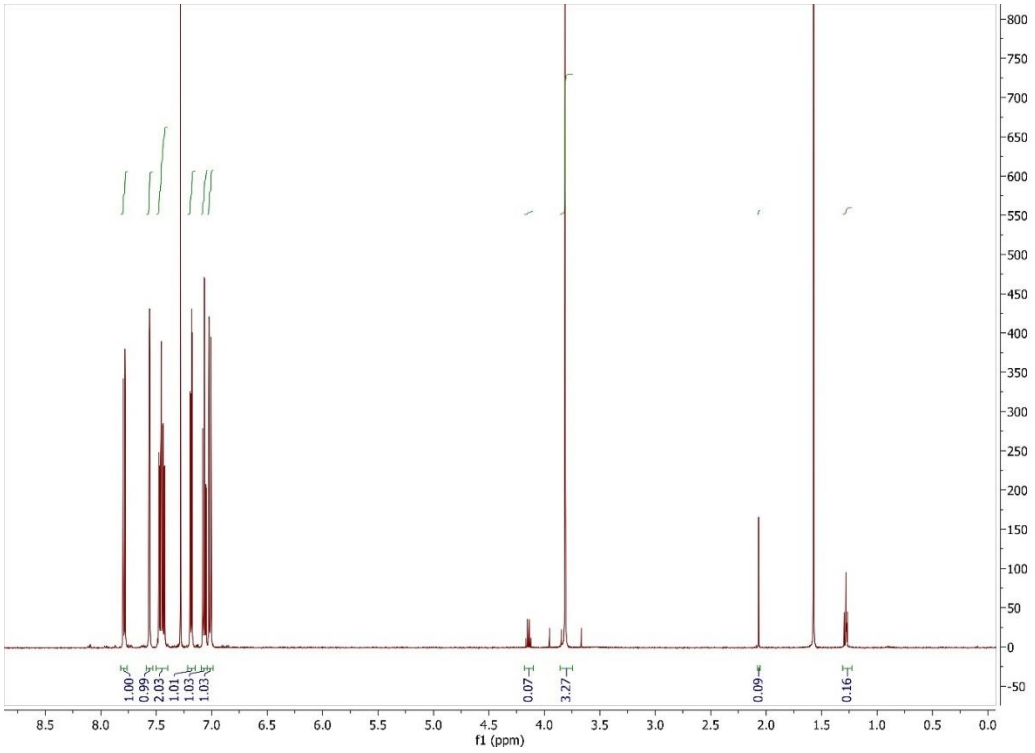

Figure 2.38 ^{1}H NMR spectrum of **2.17** in $CDCl_3$ at 500 MHz

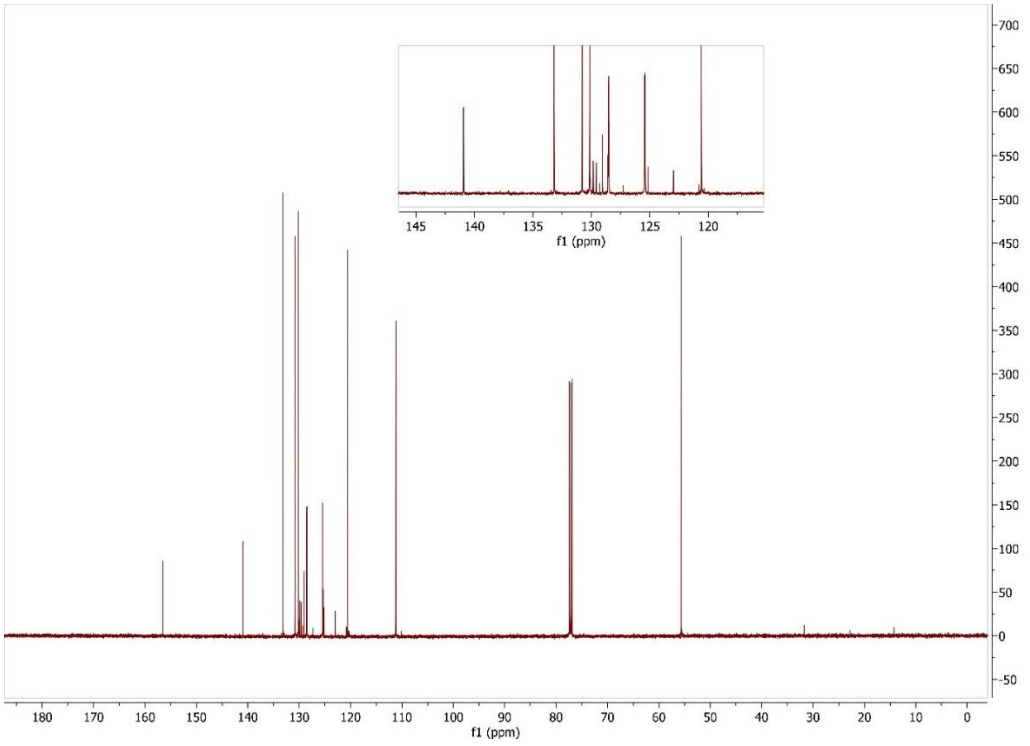

Figure 2.39 $^{13}C\{^{1}H\}$ NMR spectrum of **2.17** in $CDCl_3$ at 125 MHz

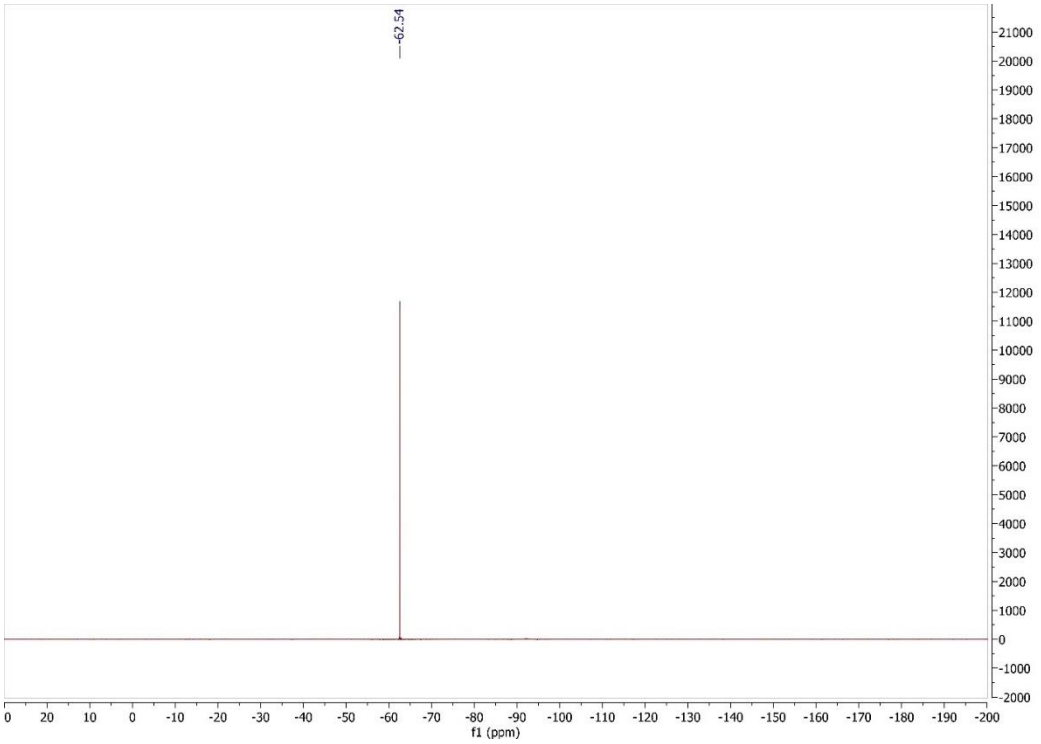

Figure 2.40 ^{19}F NMR spectrum of **2.17** in $CDCl_3$ at 470 MHz

Synthesis of **I-2.1**

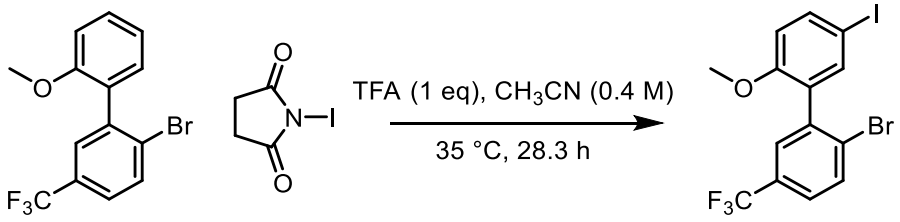

2.17 **I-2.1**

A round bottom flask was charged with a solution of **2.17** (4.0074 g, 0.0121 mol) in CH_3CN (20 mL), *N*-iodo succinimide (3.0013 g, 0.013 mol), then an additional portion of CH_3CN (10 mL) and magnetic stir bar. Next, trifluoroacetic acid (1.3795 g, 0.0121 mol) was added and the flask was capped with a rubber septum. The mixture was placed in a 35 °C oil bath for 28.3 h. Reaction progress was monitored by ^1H and ^{19}F NMR analysis. Upon consumption of the starting material,

the reaction mixture was diluted with 0.23 M Na_2SO_3 (aq) (150 mL) and stirred for 20 minutes. The mixture was then transferred to a separatory funnel and extracted twice with EtOAc (50 mL). The combined organic fractions were then washed with saturated NaCl (aq) (100 mL), then dried over anhydrous $MgSO_4$ and concentrated *in vacuo*. The resulting solid was taken up in pentane (60 mL) and sonicated to facilitate dissolution. The resulting solution was filtered through a fritted funnel and the filtrate was concentrated *in vacuo* to give of aryl iodide **I-2.1** as a white solid (5.1953 g, 94 %).

^{1}H NMR ($CDCl_3$, 500 MHz): δ 7.77 (dd, *J* = 8.3, 0.9, 1H), 7.70 (dd, *J*= 8.7, 2.3, 1H), 7.54-7.45 (m, 3H), 6.77 (d, *J*=8.7, 1H), 3.78 (s, 3H)

^{19}F NMR ($CDCl_3$, 376 MHz): δ -62.57

^{13}C NMR ($CDCl_3$, 125 MHz): δ 156.60, 139.36, 138.98, 138.81, 133.28, 131.35, 129.85 (q, *J* = 32.9), 128.32 (q, *J* = 3.8), 128.27, 125.86 (q, *J* = 3.7), 123.91 (q, *J* = 272.7), 113.46, 82.38, 55.85

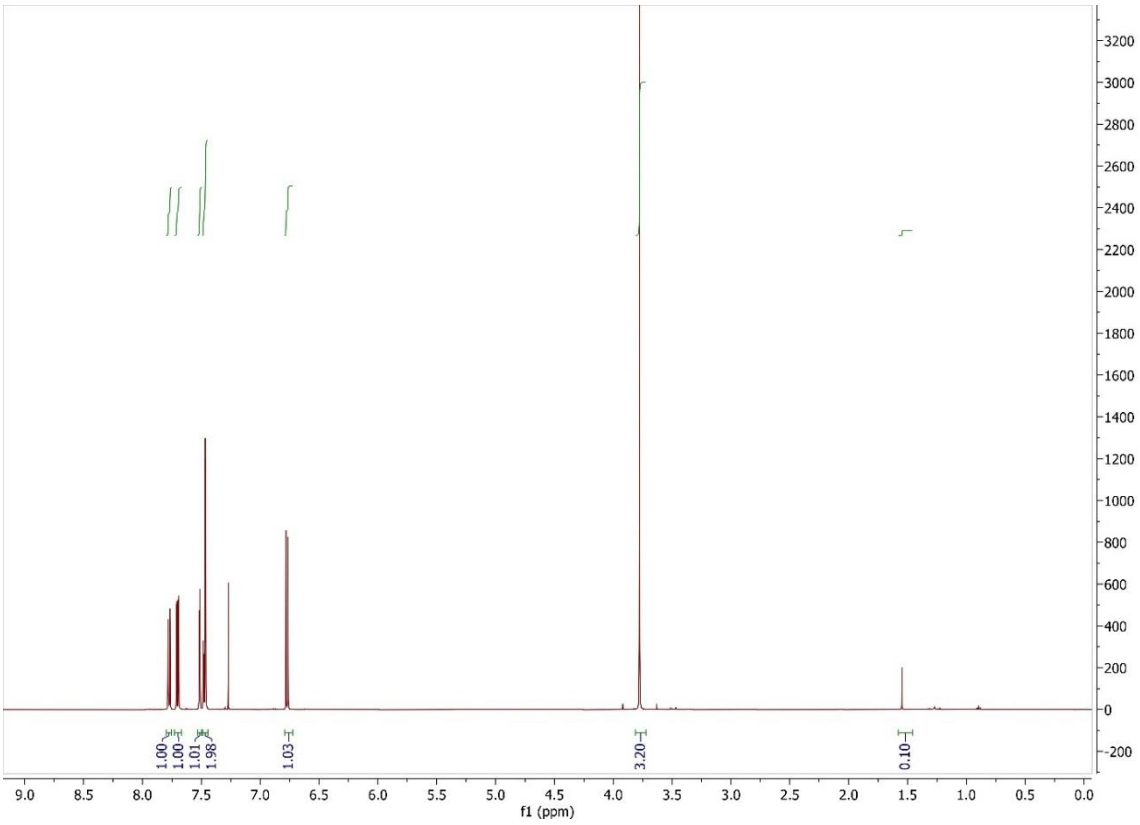

Figure 2.41 ^{1}H NMR spectrum of **I-2.1** in $CDCl_3$ at 500 MHz

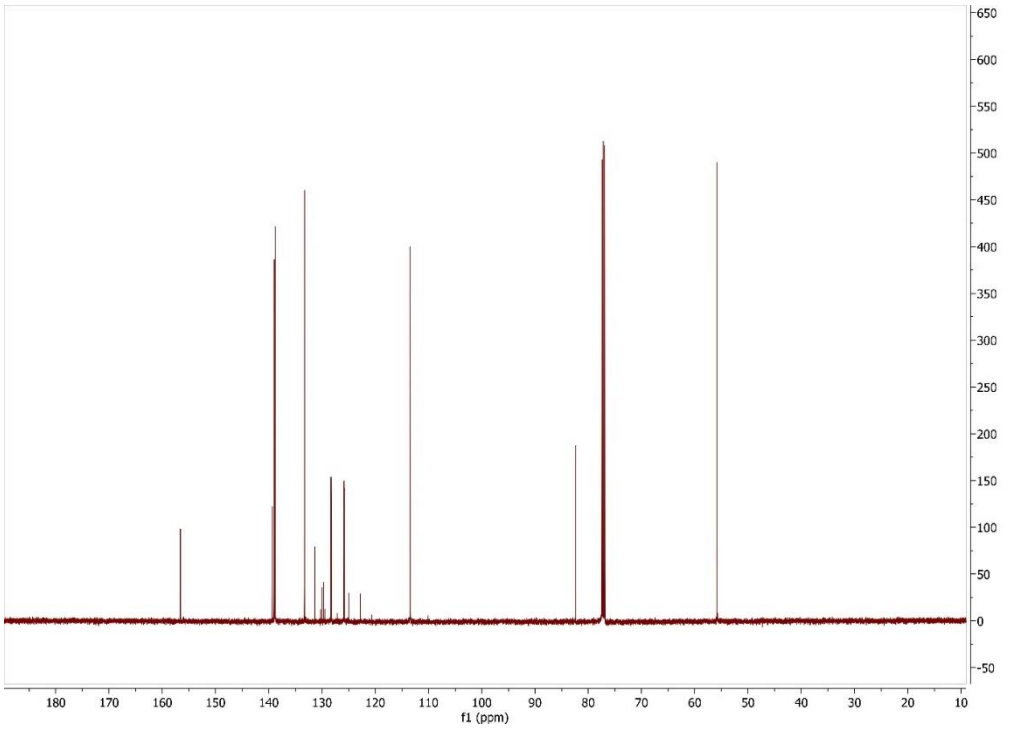

Figure 2.42 $^{13}C\{^{1}H\}$ NMR spectrum of **I-2.1** in $CDCl_3$ at 125 MHz

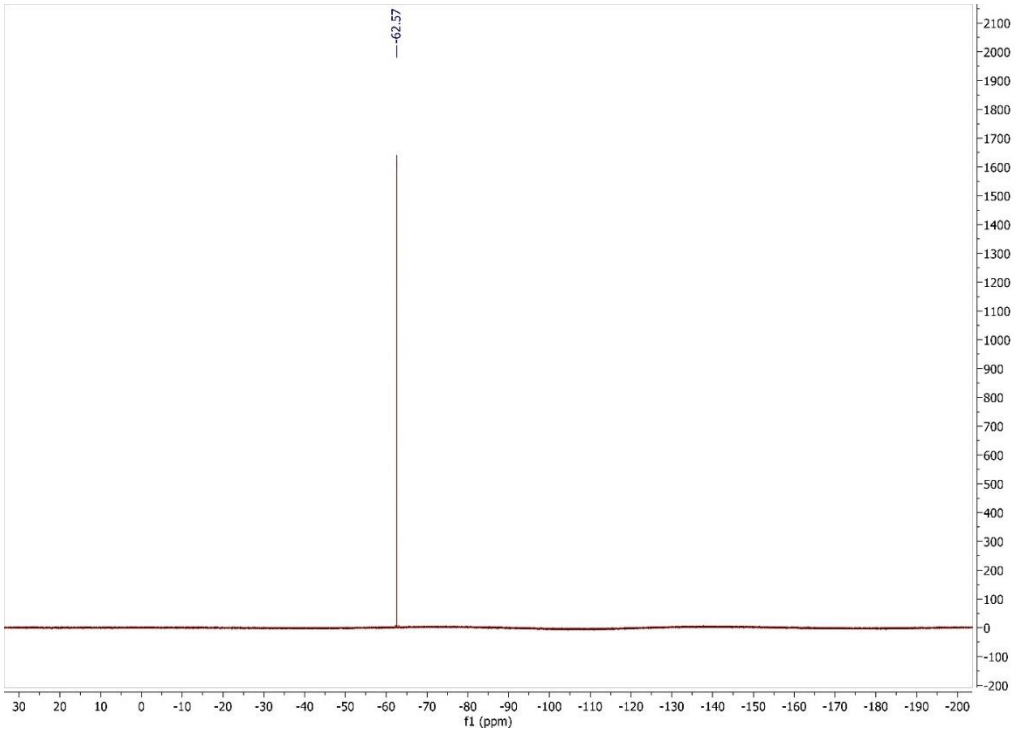

Figure 2.43 ^{19}F NMR spectrum of **I-2.1** in $CDCl_3$ at 470 MHz

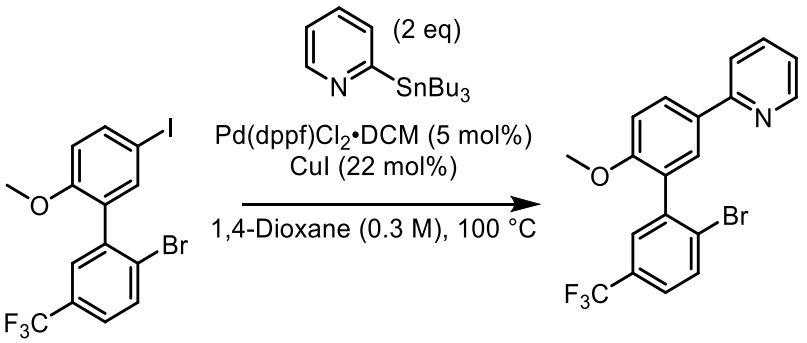

I-2.1
(1 eq)

2.18
41 %

In a nitrogen filled glovebox, a 20 mL scintillation vial was charged with magnetic stir bar, aryl iodide **I-2.1** (438.5 mg, 0.959 mmol), 2-(tributylstannyl)pyridine (448.3 mg, 1.2 mmol), CuI (39.9 mg, 0.210 mmol), and 1,4-dioxane (3.2 mL). The result mixture was briefly agitated, then Pd(dppf)Cl_2•DCM (39.6 mg, 0.0485 mmol). The vial was capped, removed from the glovebox, and placed in a pre-heated 100 °C oil bath. After 19 h heating, reaction progress was followed by ^{1}H NMR analysis (the cooled reaction vial was sampled with a pastuer pipette inside of a nitrogen filled glovebox, and the aliquot diluted with $CDCl_3$). An additional portion of 2-(tributylstannyl)pyridine (297.1 mg, 0.769 mmol) was added to the reaction mixture in the glovebox, then heating continued at 100 °C. After 20 h, the vial was removed from the oil bath and allowed to cool to rt, then diluted with D.I. H_2O (30 mL). The resulting mixture was extracted with EtOAc (30 mL) four times. The combined organic fractions were then washed with saturated NaCl (aq) (50 mL), dried over $MgSO_4$, filtered, and the filtrate concentrated by rotary evaporation. The crude product was purified by column chromatography on silica gel (22 g) with a mobile phase composition consisting of hexanes and EtOAc in a gradient mixture starting with pure hexanes and ending with 20 % EtOAc and 1% NEt_3 in hexanes. The fractions were analyzed by TLC and similar fractions were combined and concentrated by rotary evaporation to give product **2.18** as an off white solid (194.7 mg, 49.7 %).

^{1}H NMR ($CDCl_3$, 400 MHz): δ 8.66 (dt, *J* = 4.9, 1.5, 1H), 8.08 (dd, *J* = 8.7, 2.4, 1H), 7.86 (d, *J* = 2.3, 1H), 7.79 (d, *J* = 8.4, 1H), 7.76-7.71 (m, 2H), 7.62 (d, *J* = 2.0, 1H), 7.47 (dd, *J* = 8.4, 2.2, 1H), 7.20 (ddd, *J* = 5.9, 4.9, 2.0, 1H), 7.10 (d, *J* = 8.7, 1H), 3.86 (s, 3H)

^{13}C{^{1}H} NMR ($CDCl_3$, 376 MHz): δ 157.61, 156.56, 149.48, 140.74, 137.17, 133.21, 131.63, 129.82 (q, *J* = 32.9), 129.46, 129.34, 128.74, 128.60, 128.57, 125.59 (q, *J* = 3.7), 124.04 (q, *J* = 272.4), 121.86, 120.16, 111.42, 55.90

^{19}F NMR ($CDCl_3$): δ -62.5

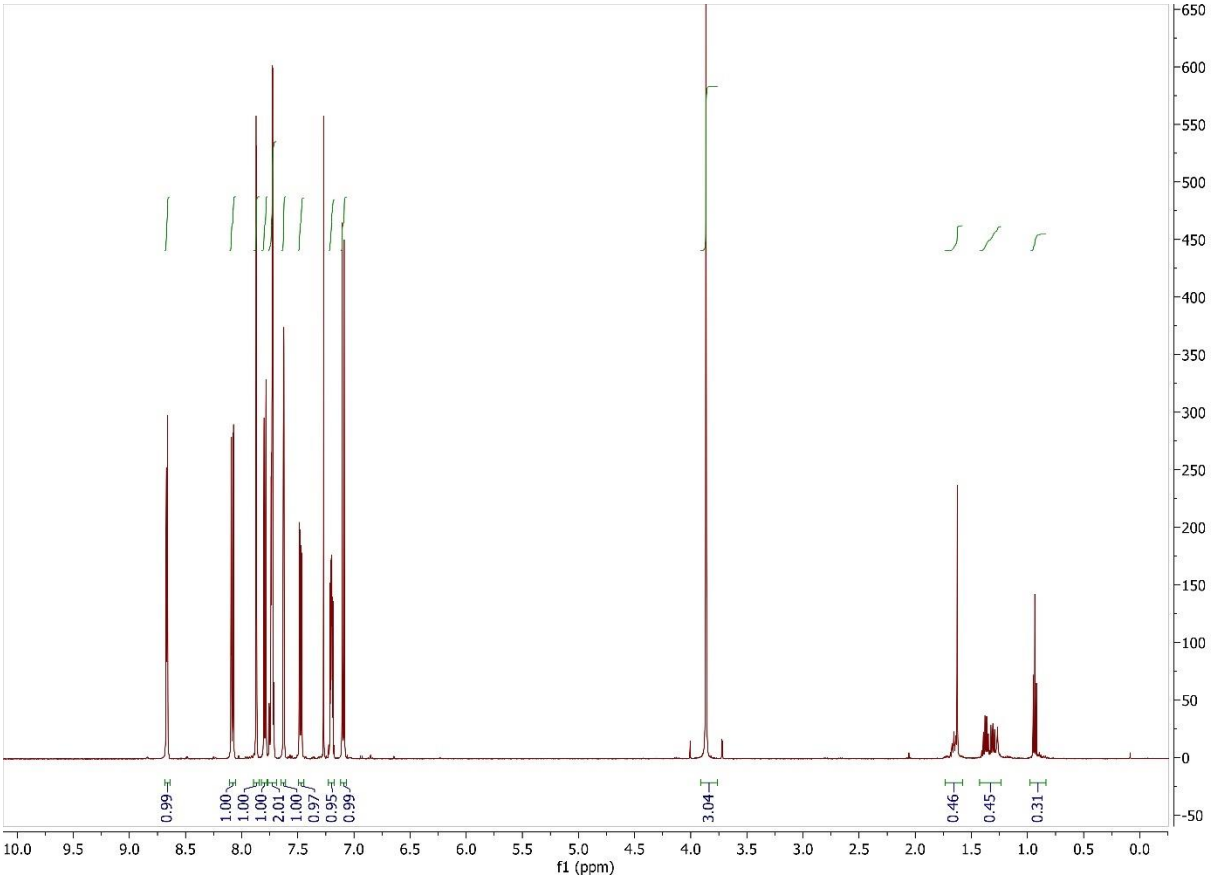

Figure 2.44 ^{1}H NMR spectrum of **2.18** in $CDCl_3$ at 500 MHz

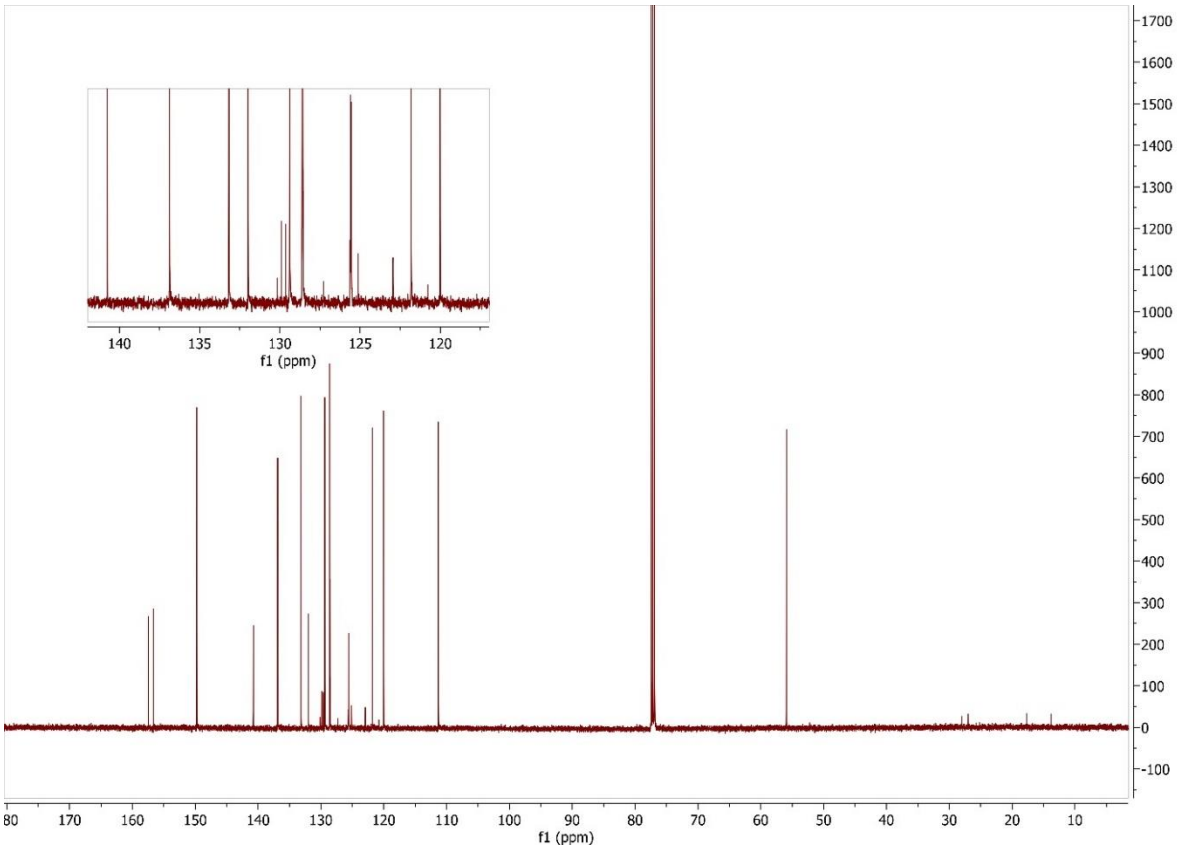

Figure 2.45 $^{13}C\{^{1}H\}$ NMR spectrum of **2.18** in $CDCl_3$ at 125 MHz

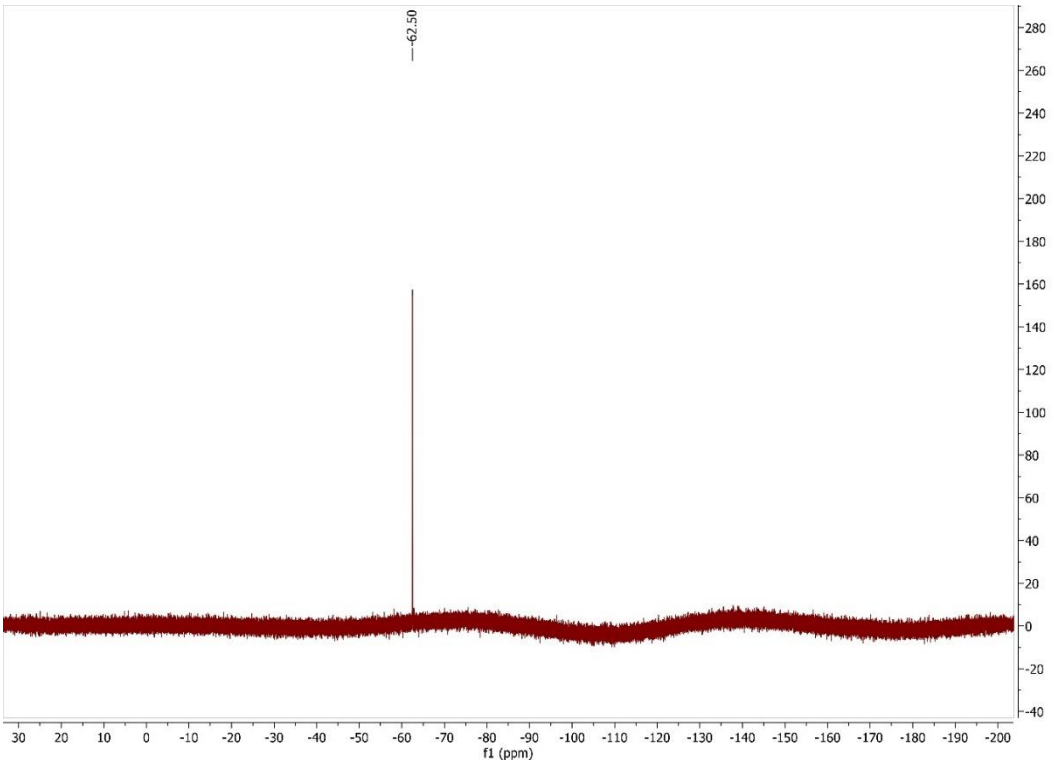

Figure 2.46 ^{19}F NMR spectrum of **2.18** in $CDCl_3$ at 470 MHz

Synthesis of 2.18 (improved yield with Suzuki-Miyaura versus Stille)

In open atmosphere, a scintillation vial was charged with a magnetic stir bar, aryl boronic ester **I-2.2** (507.7 mg, 1.111 mmol). The vial was then covered with a Kim-Wipe and rubber-band, then brought into a nitrogen filled glovebox via antechamber. The vial was then charged with K_2CO_3 (464.0 mg, 3.357 mmol), 2-bromopyridine (265.0 mg, 1.678 mmol), 1,4-dioxane (3.0 mL), and H_2O (1.0 mL). The mixture was brief agitated to encourage dissolution of the solid components. Next $Pd(PPh_3)_4$ (140.3 mg, 0.121 mmol) was added to the reaction vial. The vial was seal, removed from the glovebox, then placed in an oil bath heated to 90 °C for 23 hours. After the heating period was completed, the vial was removed from the oil bath, cooled to room temperature, then work up commenced with the addition of EtOAc (25 mL) and H_2O (25 mL). The mixture was shaken vigorously, then the phases separated in a separatory funnel. The organic phase was again

extracted with H_2O (25 mL). The combined aqueous portions were then extracted with EtOAc (25 mL). The combined organic fractions were then washed with saturated NaCl (aq) (50 mL). To oxidize any remaining triphenylphosphine, H_2O_2 (aq, 15 %) (10 mL), and H_2O (30 mL) were added to the EtOAc solution, and the mixture stirred for 30 minutes. The phases were then separated, the organic phase washed with saturated NaCl (aq) (50 mL), then dried over $MgSO_4$, filtered through a glass fritted funnel, then concentrated by rotary evaporation to yield a crude residue of mass 599.4 mg. The crude product was purified by column chromatography on silica gel with a mobile phase consisting of hexanes, ethyl acetate, and less than 1% NEt_3. The mobile phase composition was varied such that the ethyl acetate concentration was increasing gradually from 5% EtOAc up to 50% EtOAc. The product was collected in fractions 12-16, with some product co-eluting with other species collected in fractions 17-20. The product, an off-white solid, was collected as 357.8 mg (79% yield).

^{1}H NMR ($CDCl_3$, 400 MHz): δ 8.66 (dt, *J* = 4.9, 1.5, 1H), 8.08 (dd, *J* = 8.7, 2.4, 1H), 7.86 (d, *J* = 2.3, 1H), 7.79 (d, *J* = 8.4, 1H), 7.76-7.71 (m, 2H), 7.62 (d, *J* = 2.0, 1H), 7.47 (dd, *J* = 8.4, 2.2, 1H), 7.20 (ddd, *J* = 5.9, 4.9, 2.0, 1H), 7.10 (d, *J* = 8.7, 1H), 3.86 (s, 3H)

^{13}C{^{1}H} NMR ($CDCl_3$, 376 MHz): δ 157.61, 156.56, 149.48, 140.74, 137.17, 133.21, 131.63, 129.82 (q, *J* = 32.9), 129.46, 129.34, 128.74, 128.60, 128.57, 125.59 (q, *J* = 3.7), 124.04 (q, *J* = 272.4), 121.86, 120.16, 111.42, 55.90

^{19}F NMR ($CDCl_3$): δ -62.5

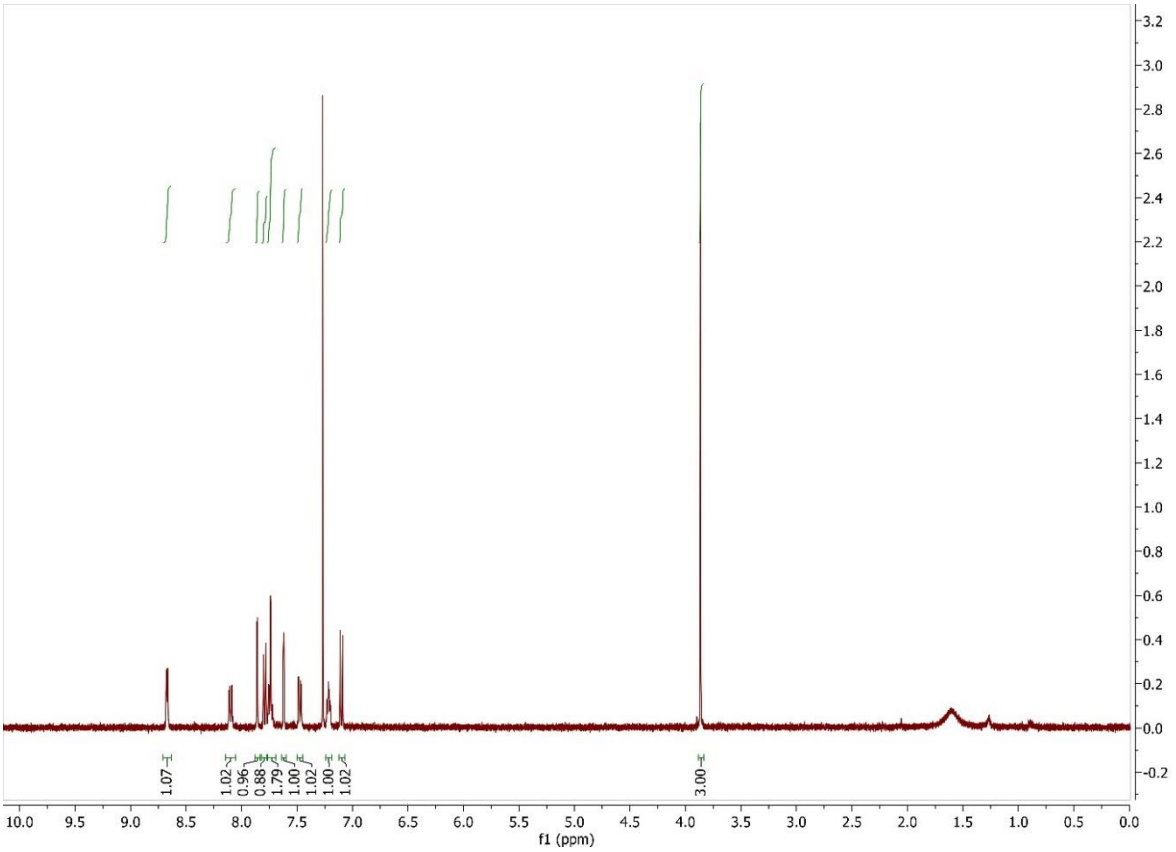

Figure 2.47 ^{1}H NMR spectrum of **2.18** in $CDCl_3$ at 400 MHz

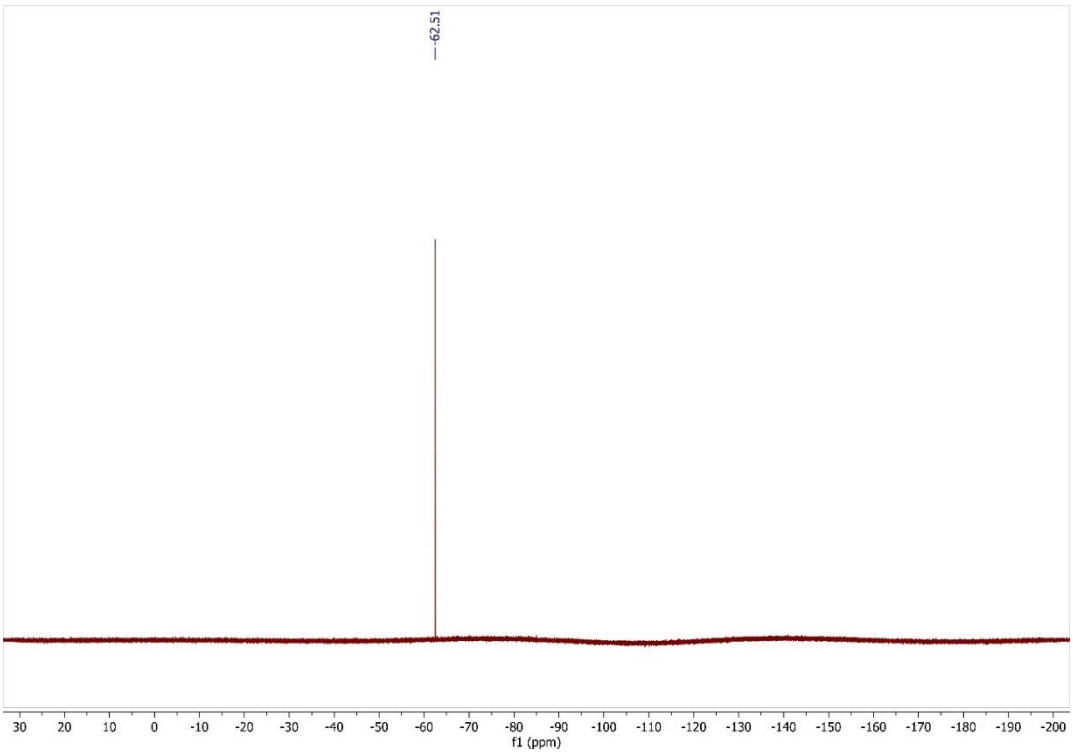

Figure 2.48 ^{19}F NMR spectrum of **2.18** in $CDCl_3$ at 376 MHz

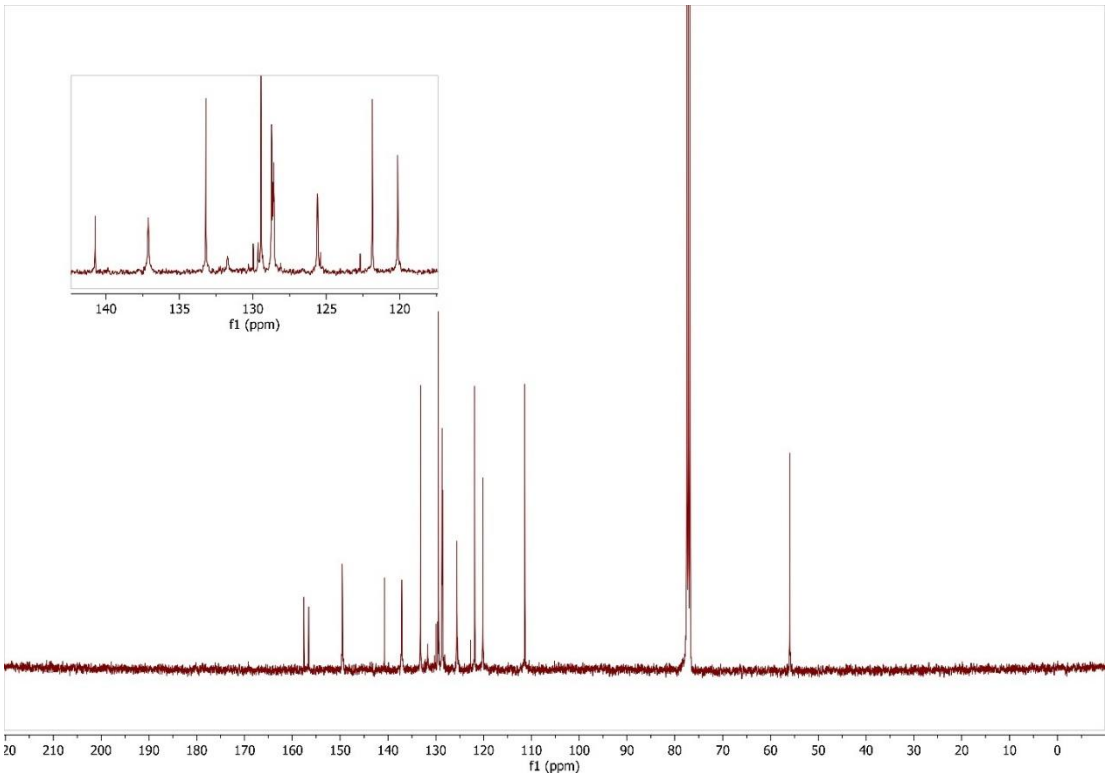

Figure 2.49 $^{13}C\{^{1}H\}$ NMR spectrum of **2.18** in $CDCl_3$ at 100 MHz

Synthesis of **L2.2a**

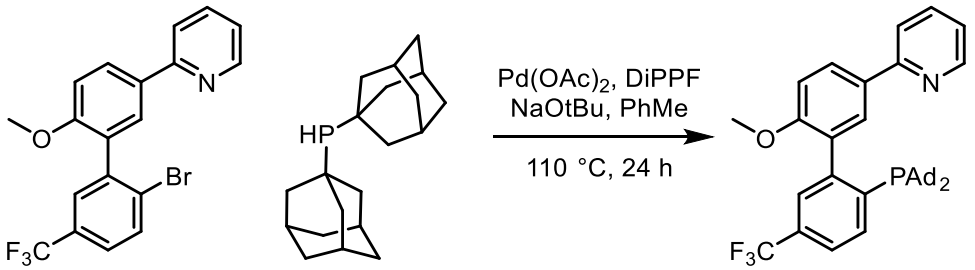

2.18 **L2.2a**

In a nitrogen filled glovebox, an oven dried scintillation vial was charged with $Pd(OAc)_2$ (7.8 mg, 0.035 mmol), DiPPF (16.8 mg, 0.041 mmol), NaOtBu (79.2 mg, 0.824 mmol), PhMe (1.0 mL), and magnetic stir bar. The mixture was allowed to stir at r.t. for 20 min, then aryl bromide **2.18** (279.5 mg, 0.676 mmol), diadamantyl phosphine (224.7 mg, 0.734 mmol), and PhMe (3.0 mL) were added. The vial was capped, removed from the glovebox, then placed in an oil bath pre-heated to 110 °C for 24 h. The reaction vessel was then removed from the oil bath cooled to room temperature. The reaction progress was followed by sampling the reaction mixture in the glovebox, diluting the aliquot with $CDCl_3$, and following the transformation of the ^{31}P NMR spectrum - the disappearance of diadamantylphosphine (δ 17.4 ppm) and the appearance of the tertiary phosphine signal at δ 24.3 ppm. Once the reaction has reached completion, the crude product is purified by directly loading the reaction mixture onto a prepared silica gel column. To avoid oxidation to the phosphine oxide, the solvents used for the chromatography are sparged with nitrogen, and the eluted fractions capped with a rubber septum. The mobile phase consisted of a ethyl acetate and hexanes with less than 1% of triethyl amine added. The mobile phase composition evolved as a gradient mixture starting with pure hexanes (0% ethyl acetate) up to 90% ethyl acetate and 10% hexanes. The product was collected in fractions 24-30, appearance was a while solid of mass 124.4 mg (40.1 %).

^{1}H NMR ($CDCl_3$, 400 MHz): δ 8.65 (d, *J* = 4.9, 1H), 8.06 (dd, *J* = 8.7, 2.4, 1H), 7.78 (d, *J* = 2.4, 1H), 7.72 – 7.65 (m, 3H), 7.60 (d, *J* = 8.1, 1H), 7.55 (s – broad, 1H), 7.17 ppm (ddd, *J* = 5.9, 1.5, 1H), 7.01 (d, *J* = 8.6, 1H), 1.80 – 1.48 (m, 12H), 1.34 – 0.84 (m, 12 H)

^{19}F NMR ($CDCl_3$, MHz): δ -62.5

^{31}P NMR ($CDCl_3$, MHz): δ 24.3

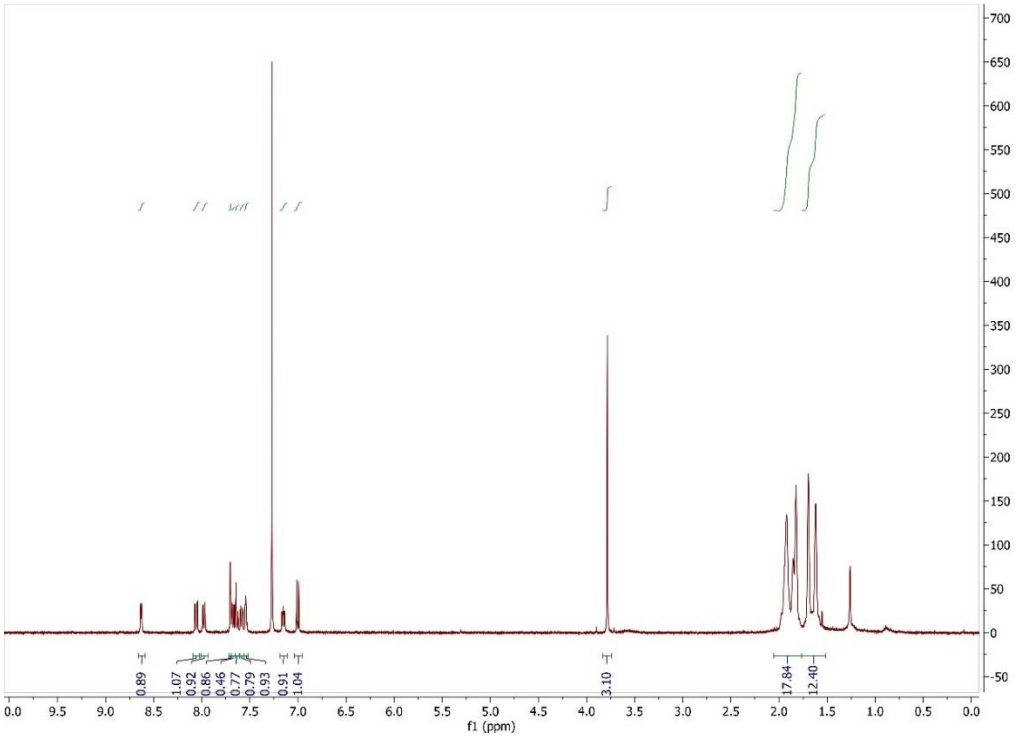

Figure 2.50 ^{1}H NMR spectrum of **L2.2a** in $CDCl_3$ at 400 MHz

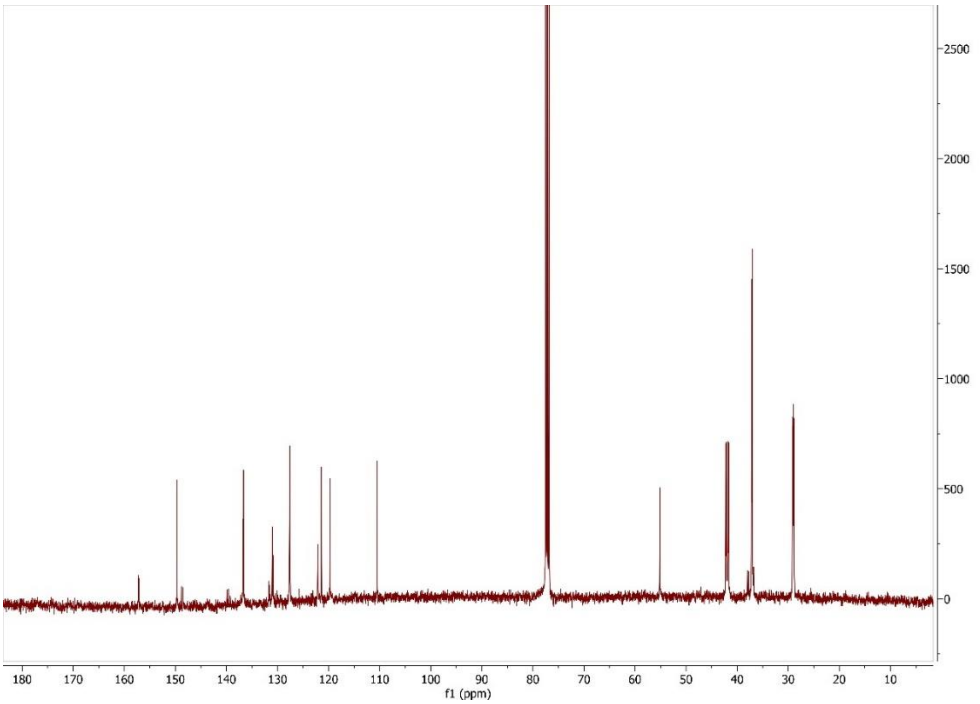

Figure 2.51 ^{13}C NMR spectrum of **L2.2a** in $CDCl_3$ at 100 MHz

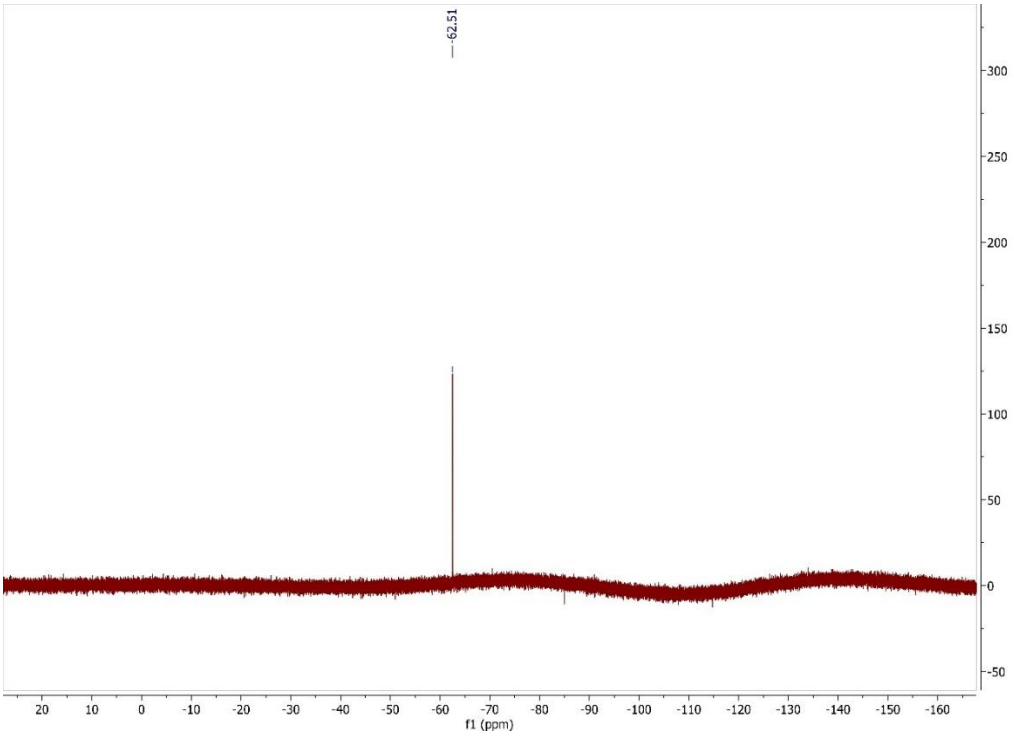

Figure 2.52 ^{19}F NMR spectrum of **L2.2a** in $CDCl_3$ at 376 MHz

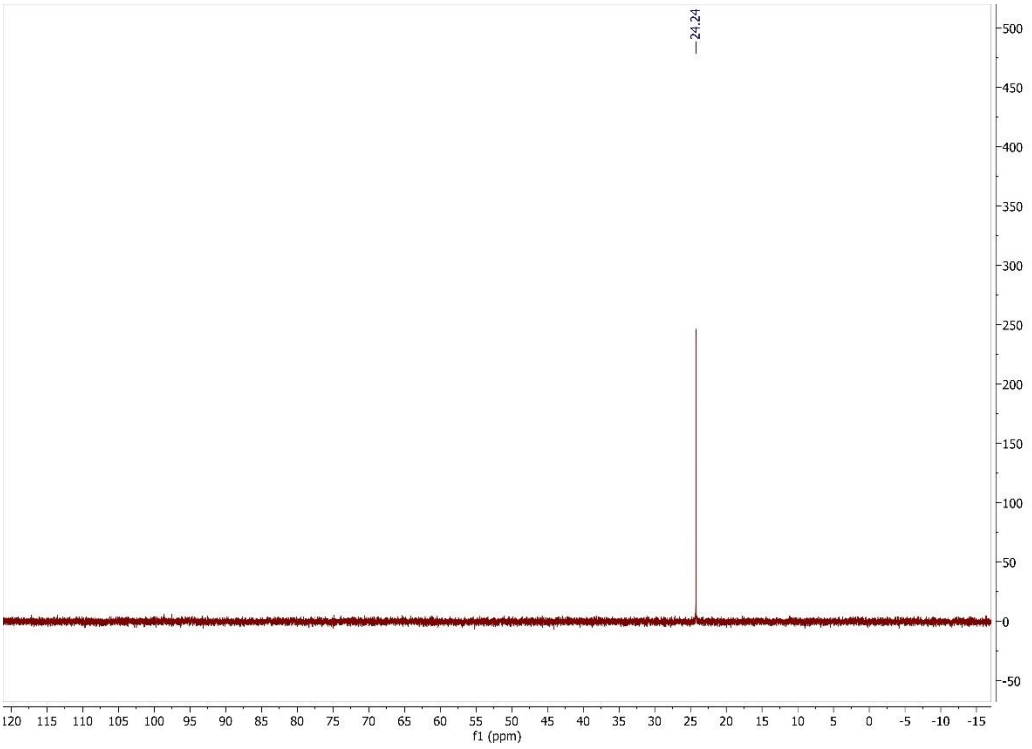

Figure 2.53 ^{31}P NMR spectrum of **L2.2a** in $CDCl_3$ at 16 MHz

Synthesis of **L2.2b**

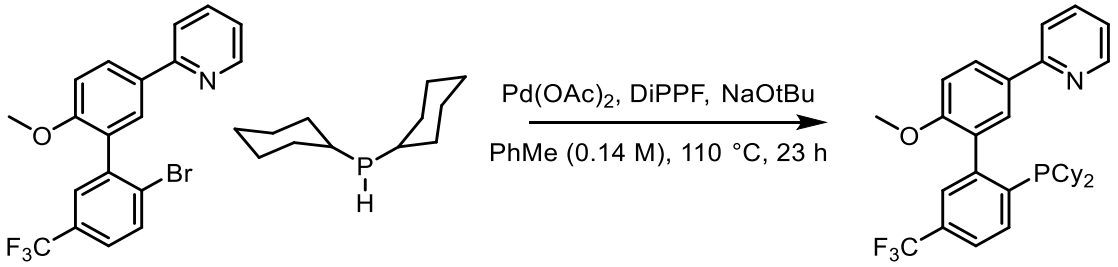

2.18 **L2.2b**

In a nitrogen filled glovebox, an oven dried 20 mL scintillation vial was charged with $Pd(OAc)_2$ (5.7 mg, 0.025 mmol), DiPPF (12.3 mg, 0.029 mmol), NaOtBu (57.4 mg, 0.597 mmol), and toluene (1.0 mL). The mixture was stirred at RT in the box for 40 minutes. The aryl bromide, dicyclohexyl phosphine, and additional toluene (2.5 mL). The vial was sealed, removed from the glovebox, and heated at 110 °C for 23 hours. Reaction progress was analyzed by ^{31}P-NMR. The crude reaction mixture was loaded onto a silica column packed with de-oxygenated hexanes. A

mixture of hexanes and ethyl acetate were used to elute the product from the column in a gradient starting at 99 / 1 and ending at 5/1 with 1 % NEt_3. To protect the phosphine air oxidation the fractions collected in test tubes were capped with a rubber septum. The fractions were analyzed by TLC and 5 fractions were collected, and solvent evaporated with an oil pump and liquid nitrogen trap. The title compound was collected as an off white solid 178.7 mg (69 %).

^{1}H NMR ($CDCl_3$, 400 MHz): δ 8.65 (d, J = 4.8 Hz, 1H), 8.06 (dd, J = 8.6, 2.4 Hz, 1H), 7.78 (d, J = 2.3 Hz, 1H), 7.74 – 7.64 (m, 3H), 7.60 (d, J = 8.0 Hz, 1H), 7.55 (d, J = 2.9 Hz, 1H), 7.17 (td, J = 5.5, 4.8, 2.9 Hz, 1H), 7.01 (d, J = 8.6 Hz, 1H), 3.79 (s, 3H), 1.86 – 1.48 (m, 13H), 1.39 – 0.81 (m, 13H)

^{13}C{^{1}H) NMR ($CDCl_3$, MHz): δ 157.29, 157.09, 149.67, 147.40 (d, *J* = 31.5), 140.97 (d., *J* = 24.6), 136.71, 132.90 (d, *J* = 3.4), 131.18, 130.99 (d, *J* = 6.5), 130.58, 130.35 (d, *J* = 2.0), 127.96, 124.35 (q, *J* = 272.3), 123.16 (q, *J* = 3.7), 121.50, 119.79. 110.48, 55.38, 35.29 (d, *J* = 15.3), 33.55 (d, *J* = 14.4), 30.74 (d, *J* = 16.0) 29.91 (d, *J* = 12.7), 29.85 (d, *J* = 8.2), 28.72 (d, *J* = 4.6), 27.56 (d, *J* = 12.3), 27.38, 26.56 (d, *J* = 24.8)

^{19}F NMR ($CDCl_3$, MHz): δ -62.5

^{31}P NMR ($CDCl_3$, MHz): δ -10.1

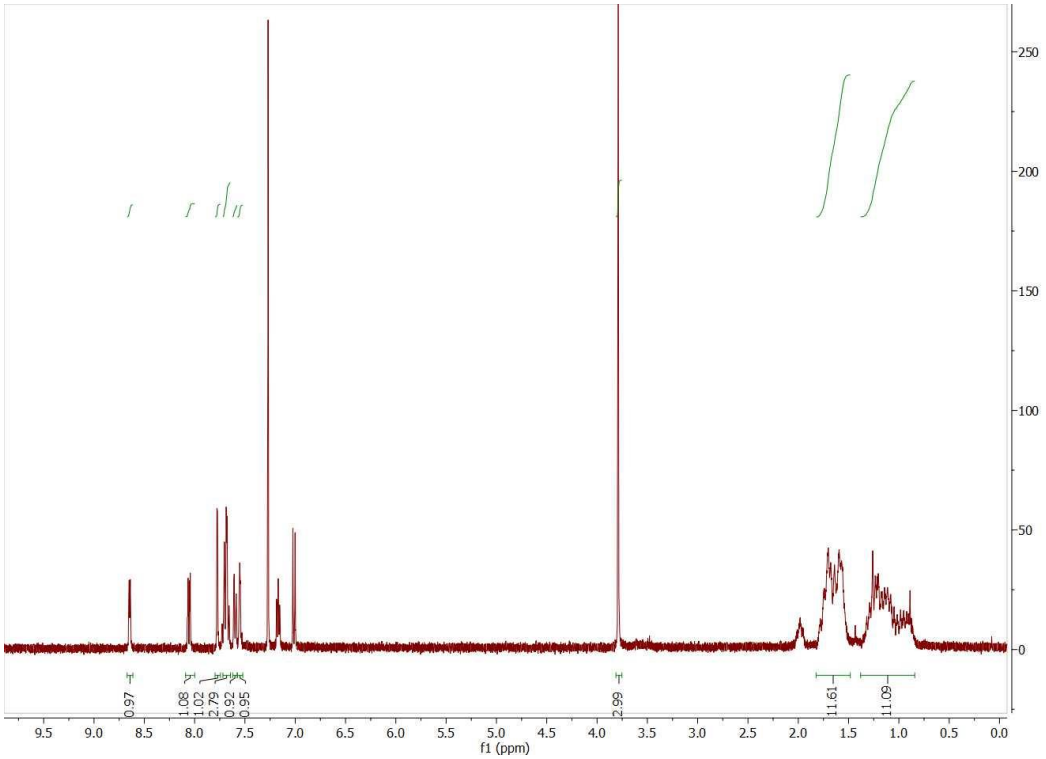

Figure 2.54 ^{1}H NMR spectrum of **L2.2b** in $CDCl_3$ at 400 MHz

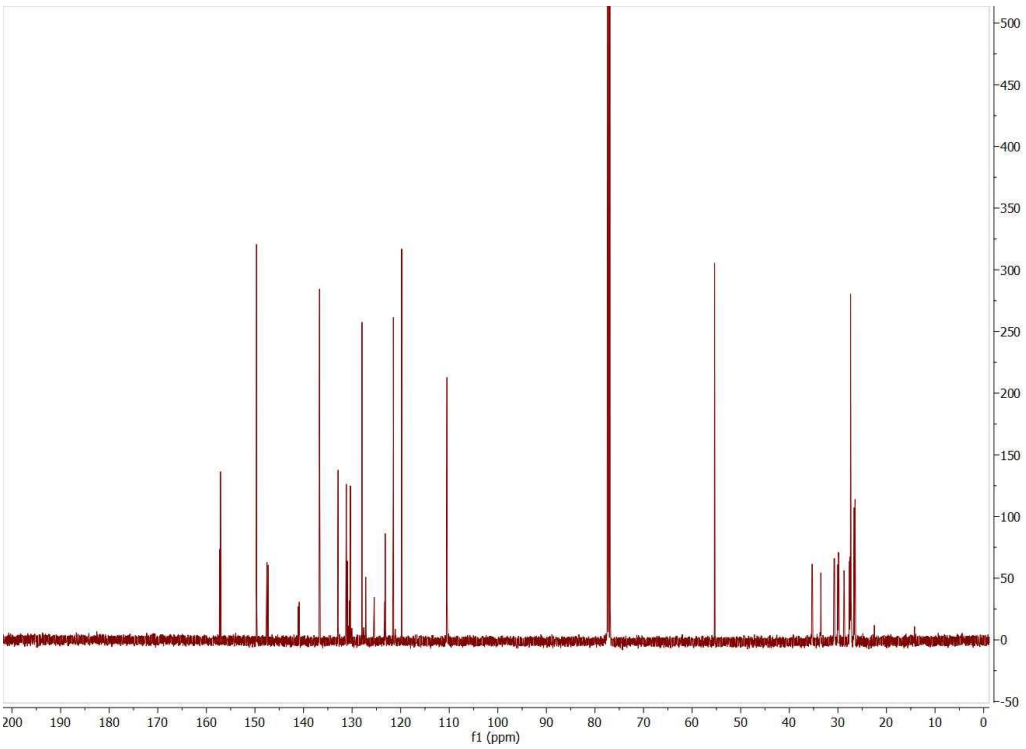

Figure 2.55 $^{13}C\{^{1}H\}$ NMR spectrum of **L2.2b** in $CDCl_3$ at 125 MHz

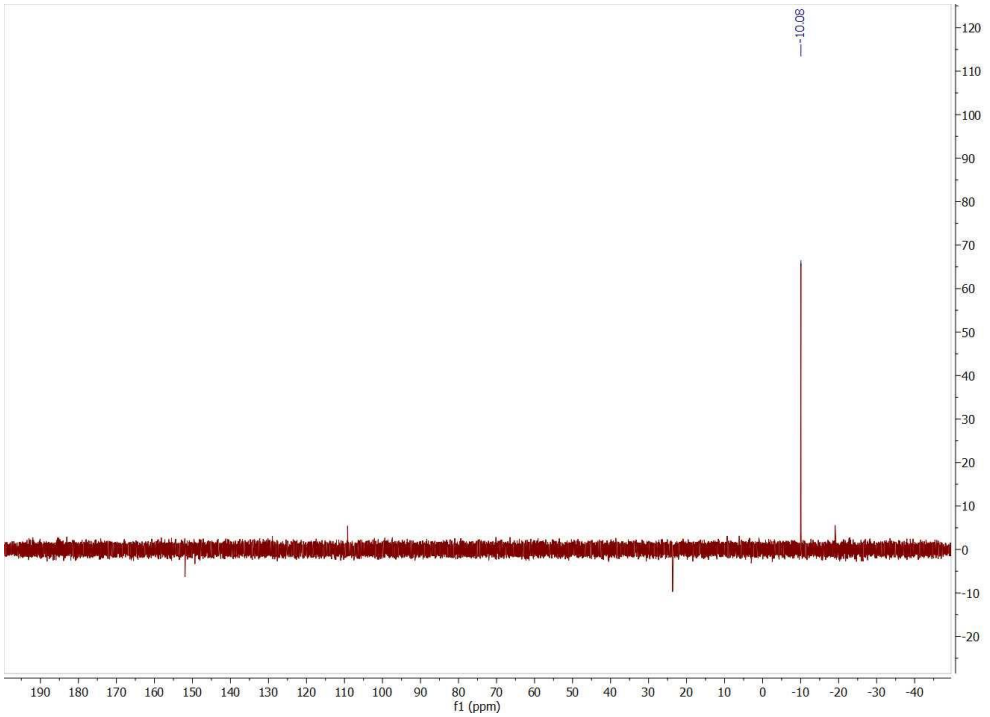

Figure 2.56 ^{31}P NMR spectrum of **L2.2b** in $CDCl_3$ at 162 MHz

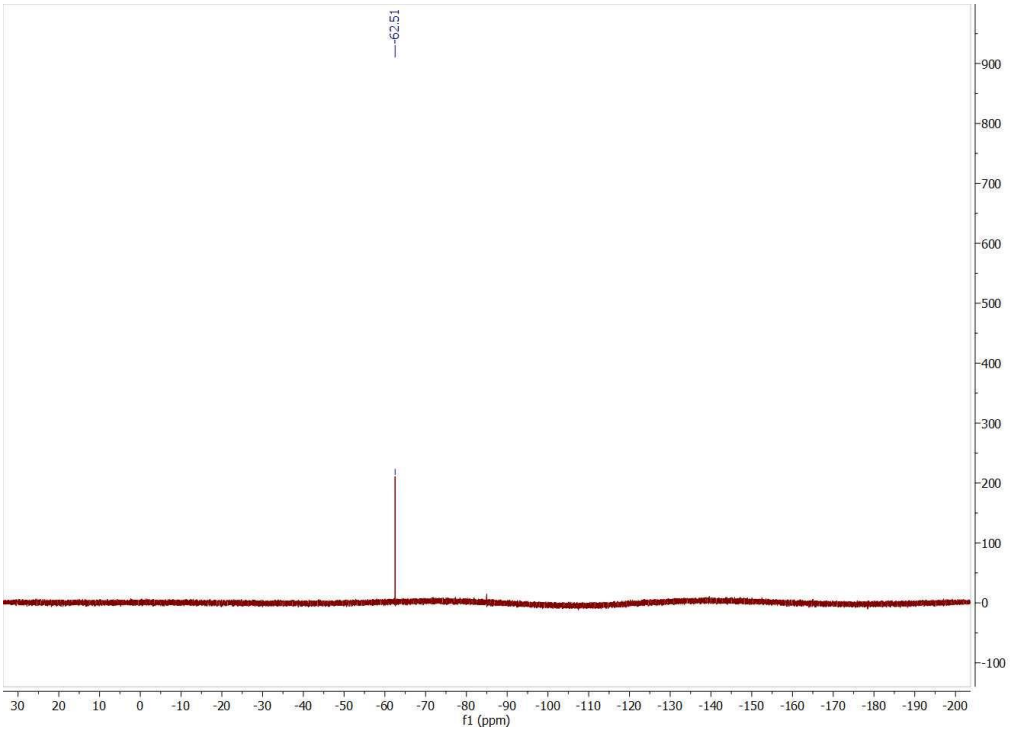

Figure 2.57 ^{19}F NMR spectrum of **L2.2b** in $CDCl_3$ at 376 MHz

Synthesis of **L2.2c**

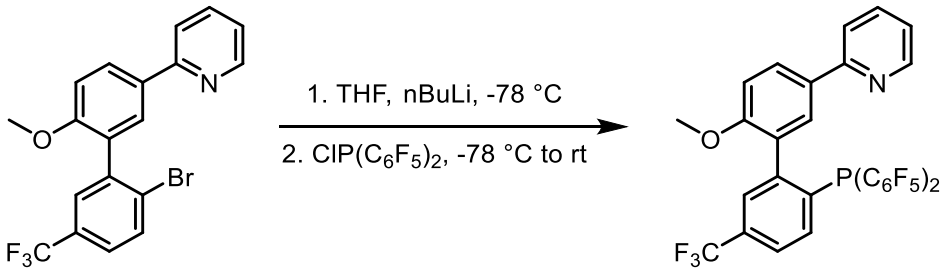

2.18 **L2.2c**

In a nitrogen filled glovebox, an oven dried Schlenk flask was charged with aryl bromide **2.18** (81.7 mg, 0.200 mmol) and magnetic stir bar then capped with rubber septum, removed from the glovebox, and connected to a Schlenk line with positive pressure of N_2(g). Freshly distilled THF (2.0 mL) was added via syringe. The flask was then submerged in a Dry Ice / acetone bath and allowed to cool to -78 °C for ca. 15 min. At this point nBuLi (2.5 M in hexanes) (88.0 µL, 0.220 mmol) was added dropwise via syringe over 8 min. The solution became yellow, and was allowed to stir at -78 °C for 20 min. Next, $ClP(C_6F_5)_2$ (83.0 mg, 0.207 mmol) in THF (0.8 mL) was added dropwise via syringe over 6 min. The mixture was kept cool for an additional 40 min, then allowed to warm to rt and stir for 18 h. Any volatiles were then evaporated *in vacuo* and Et_2O (15 mL) was added in a glovebox. The resulting suspension was filtered, and solvent evaporated *in vacuo* to yield a light-yellow wax (108.8 mg). The crude product was then purified by column chromatography on silica gel (12 g). The column was run in a fume hood using de-oxygenated hexanes, EtOAc, and NEt_3 with a positive pressure of N_2 (g). The mobile phase composition was run as an increasing gradient of EtOAc and hexanes starting with pure hexanes and ending with 50% EtOAc, 1% NEt_3 in hexanes. Fractions were analyzed by TLC and similar fractions combined and concentrated to yield a colorless, clear film (43.7 mg, 32%). Residual hexanes, dichloromethane, diethyl ether, and THF are observed in the ^{1}H NMR spectrum reported.

^{1}H NMR ($CDCl_3$, 500 MHz): δ 8.62 (m, 1H), 7.99 (dd, *J* = 8.6, 2.3, 1H), 7.73 (td, *J* = 7.7, 1.9 Hz, 1H), 7.64 – 7.51 (m, 4H), 7.48 – 7.40 (m, 1H), 7.20 (ddd, *J* = 7.5, 4.8, 1.1, 1H), 7.03 (d, *J* = 8.6, 1H), 3.80 (s, 3H)

^{13}C{^{1}H} NMR ($CDCl_3$, 125 MHz): δ 167.91, 157.12, 155.97, 149.76, 147.90 (dd, $J_{C\text{-}F}$ = 248.2, 44.0), 143.94 (d, *J* = 34.9), 142.82 (dd, $J_{C\text{-}F}$ = 258.3, 40.3), 137.61 (doublet of multiples, $J_{C\text{-}F}$ = 253.2), 136.85, 135.65 (d, *J* = 12.8), 132.29 (q, $J_{C\text{-}F}$ = 32.2), 132.07, 129.99 (d, *J* = 259.8), 129.70 (d, *J* = 2.9), 128.75, 127.77 (d, $J_{C\text{-}P}$ = 7.01), 127.70 – 127.50 (m), 124.40 (q, *J* = 3.7), 123.89 (q, $J_{C\text{-}F}$ (CF_3) = 272.8), 121.93, 119.53, 111.39, 55.80

^{19}F NMR: ($CDCl_3$, 470 MHz): δ -62.84 (s), -127.84 (ddt, *J* = 37.4, 20.9, 5.8), -128.37 (tt, *J* = 19.9, 10.0), -149.00 (tt, *J* = 20.6, 4.7), -149.20 (tt, *J* = 20.5, 4.3), -159.76 to -159.98 (m), -160.45 to -160.67 (m)

^{31}P NMR ($CDCl_3$, 202 MHz): δ -52.85 (m)

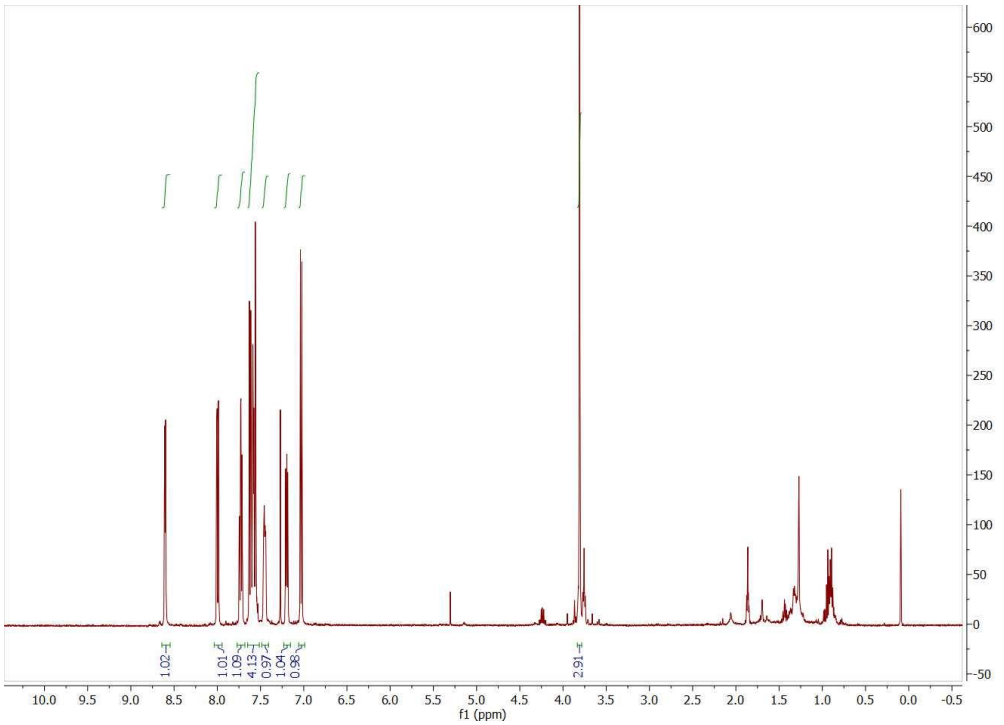

Figure 2.58 ^{1}H NMR spectrum of **L2.2c** in $CDCl_3$ at 500 MHz

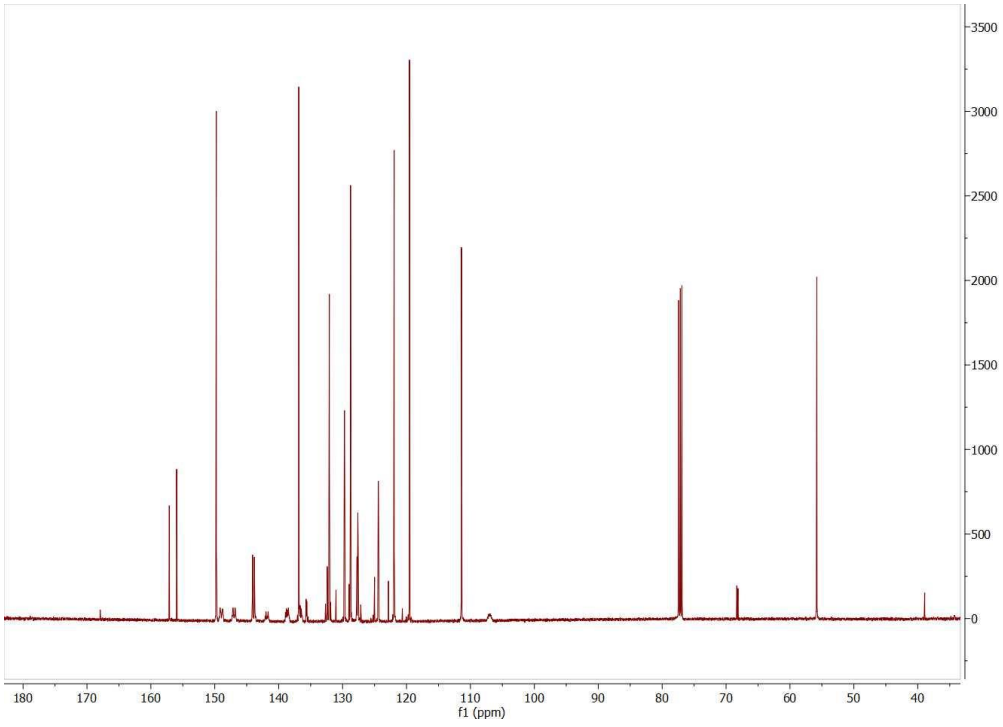

Figure 2.59 $^{13}C\{^{1}H\}$ NMR spectrum of **L2.2c** in $CDCl_3$ at 125 MHz

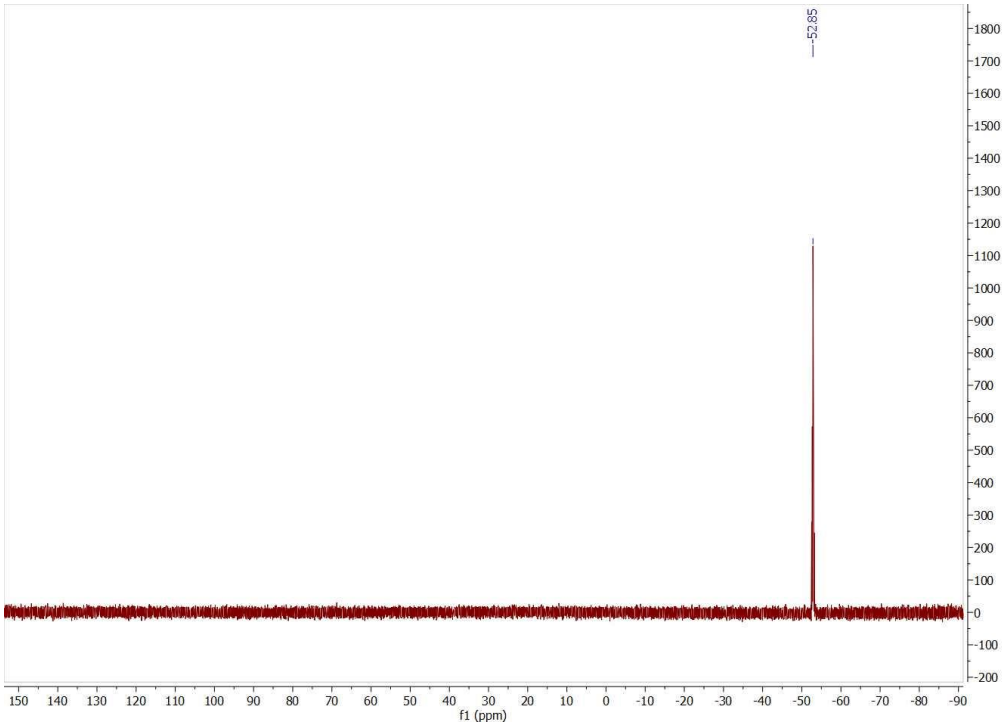

Figure 2.60 ^{31}P NMR spectrum of **L2.2c** in $CDCl_3$ at 202 MHz

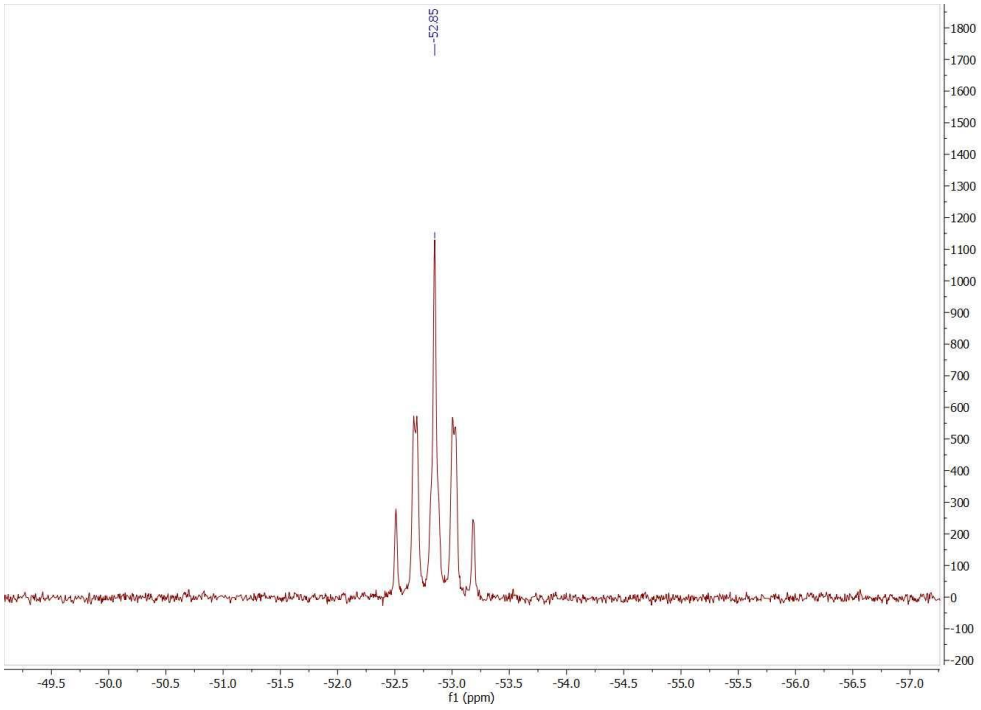

Figure 2.61 ^{31}P NMR spectrum of **L2.2c** in $CDCl_3$ with detailed view of splitting pattern

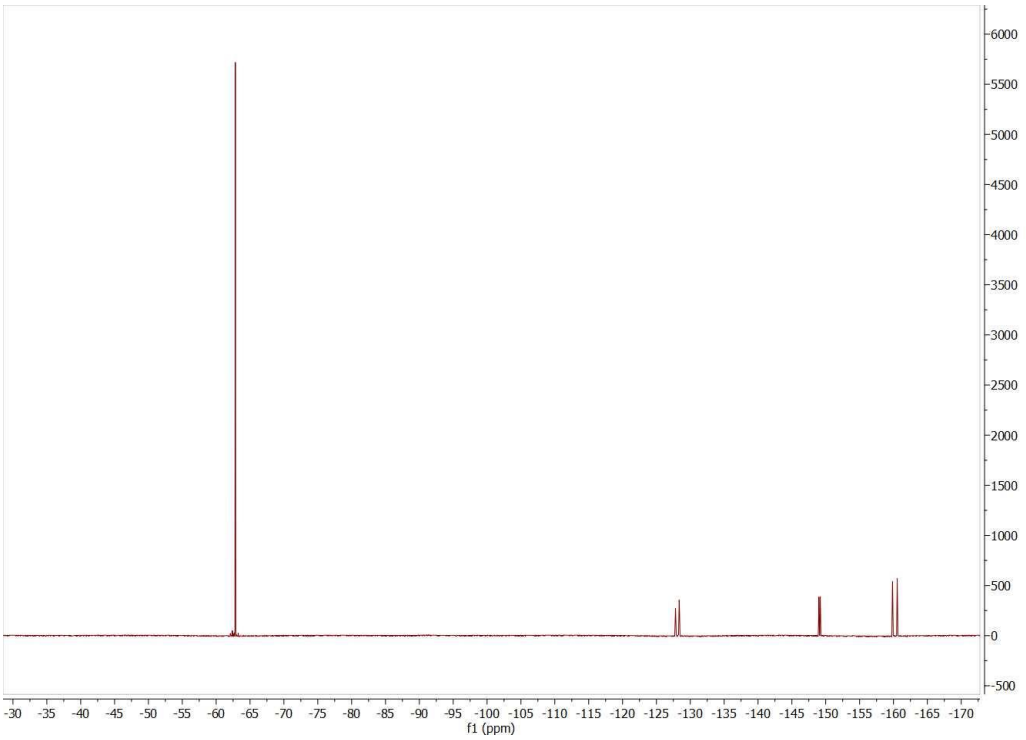

Figure 2.62 ^{19}F NMR spectrum of **L2.2c** in $CDCl_3$ at 470 MHz

Synthesis of **I-2.2**

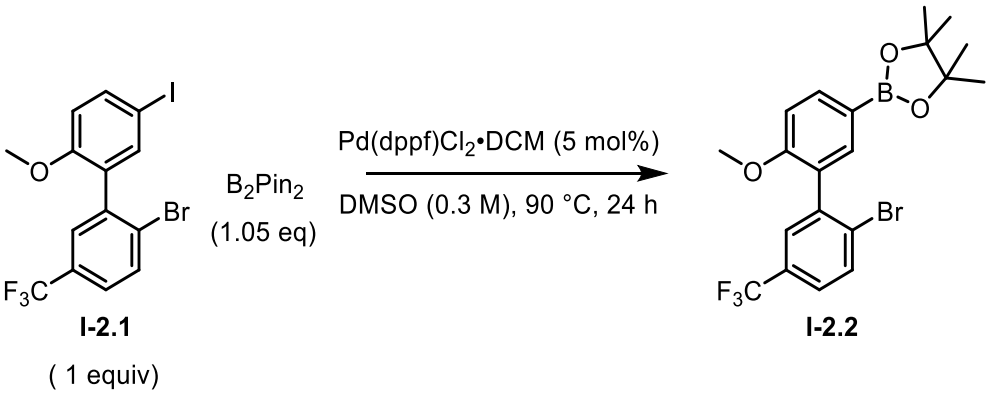

In a nitrogen filled glovebox, an oven dried scintillation vial was charged with magnetic stir bar, aryl iodide **I-2.1** (1.0049 g, 2.20 mmol), B_2Pin_2 (586.9 mg, 2.31 mmol), KOAc (761.3 mg, 7.76 mmol), then DMSO (7.0 mL). The mixture was capped and shaken to facilitate dissolution. Finally, Pd(dppf)Cl_2•DCM (89.5 mg, 0.109 mmol) was added, the vial was capped, and removed from the glovebox. The mixture was placed in an oil bath pre-heated to 90 °C for 24 h. The crude

reaction mixture was then purified by column chromatography without workup on silica gel (36 g). The mobile phase consisted of a mixture of hexanes and EtOAc, starting with pure hexanes and ending with 5 % EtOAc in hexanes. Fractions were analyzed by TLC and similar fractions were combined and concentrated to yield **I-2.2** (699.7 mg, 69 %).

^{1}H NMR ($CDCl_3$, 500 MHz): δ 7.89 (dd, *J* = 8.3, 1.7, 1H), 7.75 (d, *J* = 8.3, 1H), 7.59 (d, *J* = 1.6, 1H), 7.55 (d, *J* = 2.3, 1H), 7.44 (ddd, *J* = 8.2, 2.3, 0.6, 1H), 6.99 (d, *J* = 8.3, 1H), 3.83 (s, 3H), 1.35 (s, 12H)

^{13}C{^{1}H} NMR ($CDCl_3$, MHz): δ 159.14, 141.00, 137.33, 137.18, 132.99, 129.67 (q, *J* = 32.9), 128.66, 128.53 (q, *J* = 3.7), 125.39 (q, *J* = 3.7), 124.06(q, *J* = 272.5), 122.98, 110.42, 83.91, 55.67, 25.04.

^{19}F NMR ($CDCl_3$, 470 MHz): δ -62.48.

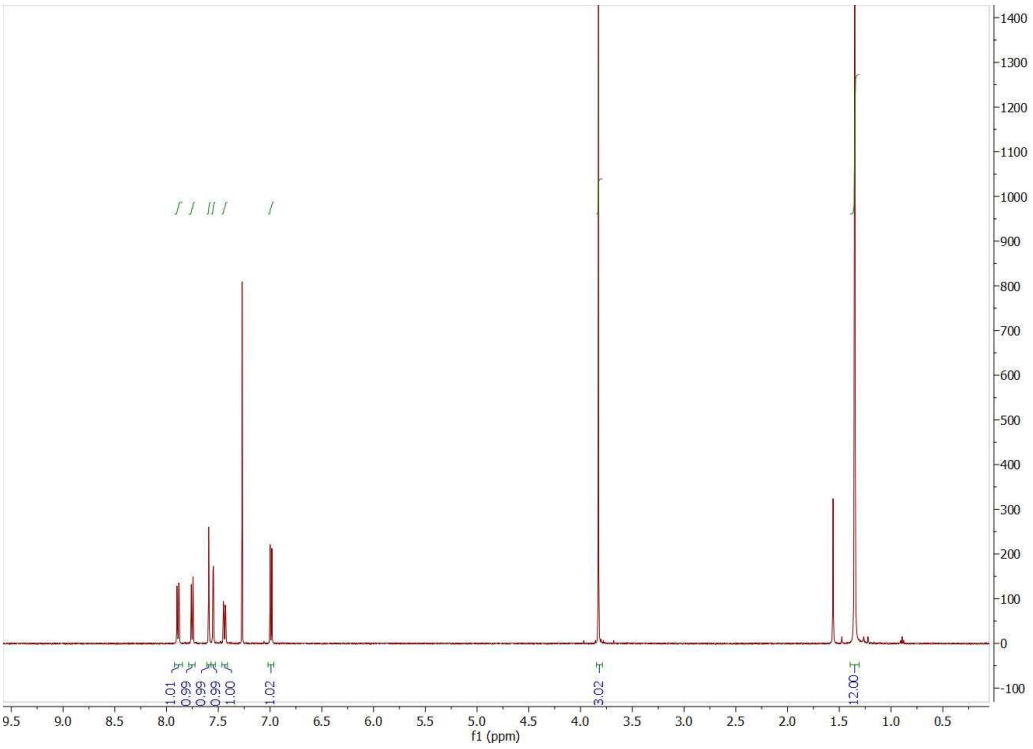

Figure 2.63 ^{1}H NMR spectrum of **I-2.2** in $CDCl_3$ at 500 MHz

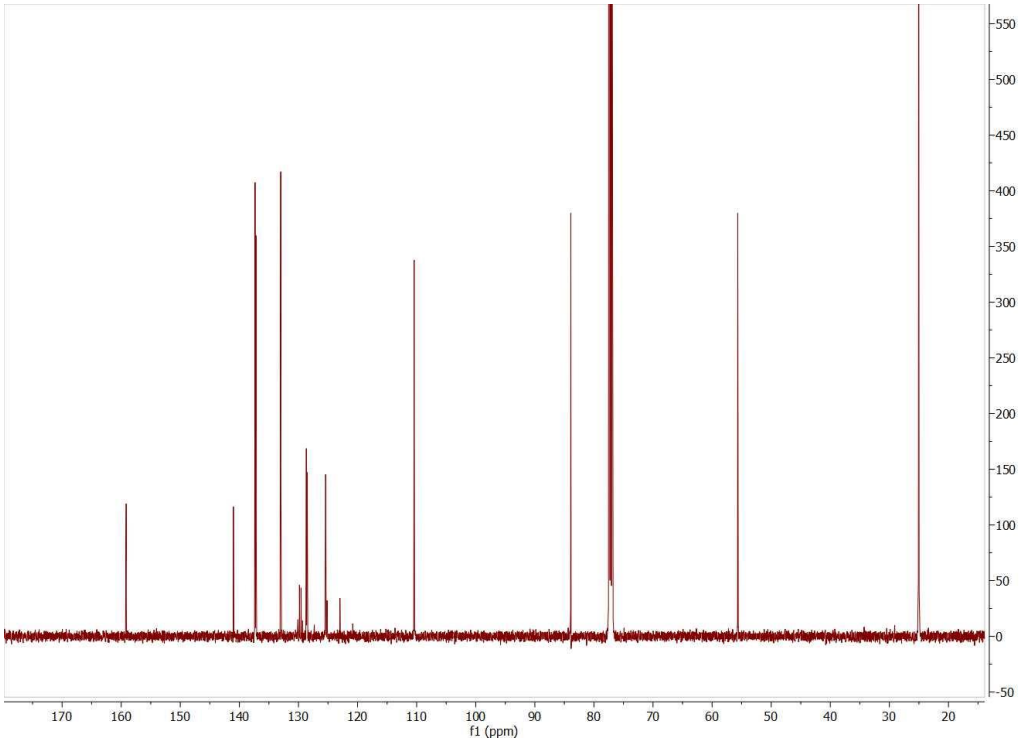

Figure 2.64 $^{13}C\{^{1}H\}$ NMR spectrum of **I-2.2** in $CDCl_3$ at 125 MHz

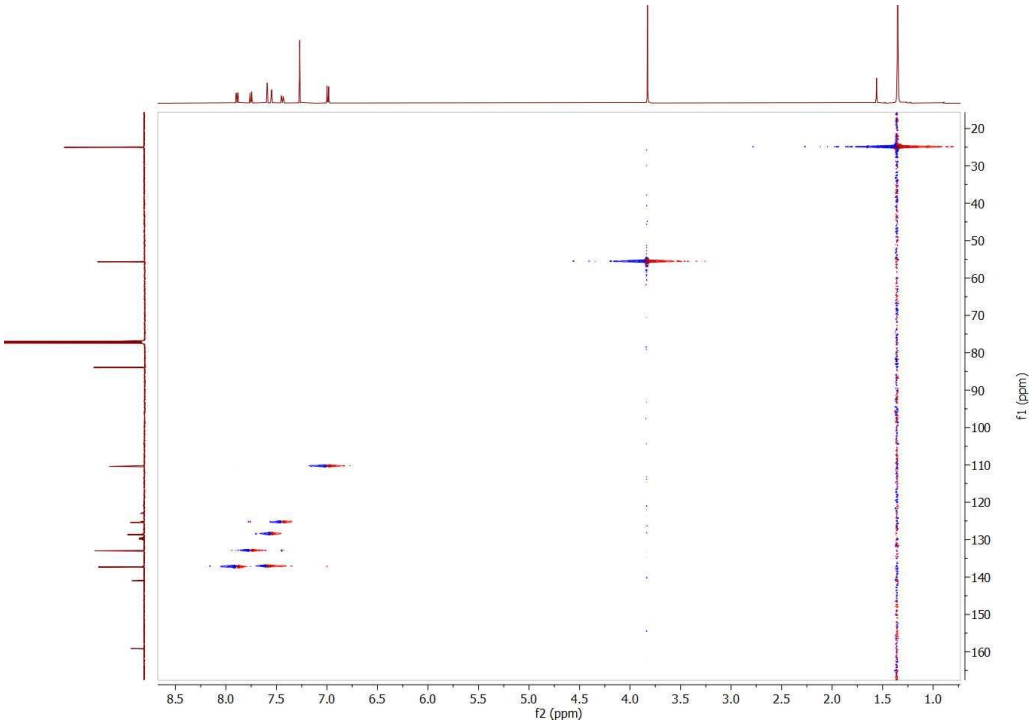

Figure 2.65 ^{1}H-^{13}C gHSQC NMR spectrum of **I-2.2** in $CDCl_3$ at 500 MHz

Synthesis of **2.19**

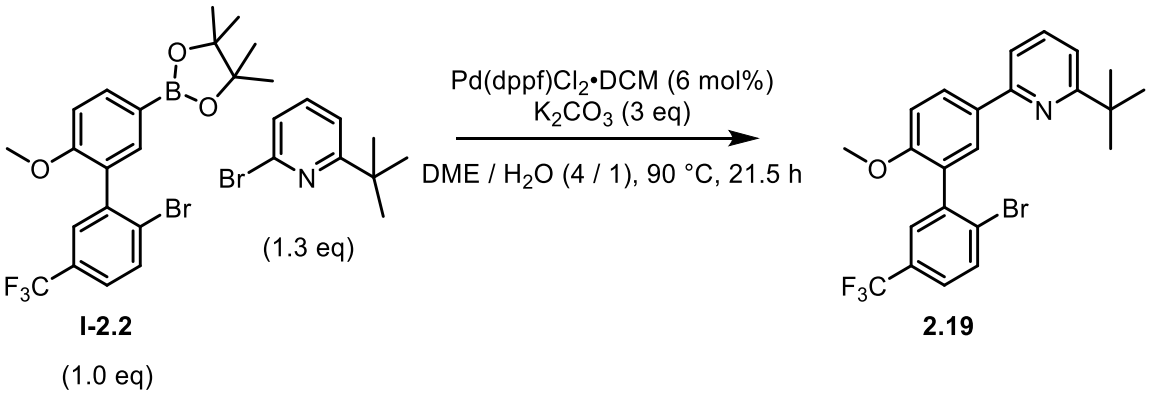

In a nitrogen filled glovebox, a scintillation vial was charged with magnetic stir bar, arylboronic acid **I-2.2** (203.7 mg, 0.446 mmol), 2-bromo-6-tertbutylpyridine (123.0 mg, 0.575 mmol), potassium carbonate (184.8 mg, 1.337 mmol), 1,2-dimethoxyethane (0.8 mL), and water (0.2 mL). The mixture was stirred at room temperature for 10 minutes. Next, $Pd(dppf)Cl_2$•DCM (20.3 mg, 25.0 µmol) was added to the vial. The reaction vessel was sealed, removed from the glovebox, and placed in an oil bath heated to 90 °C for 21.5 hours. After heating, the reaction mixture was cooled to room temperature, then diluted with EtOAc (20 mL) and water (20 mL). The diluted mixture was mixed vigorously in a separatory funnel and the phases separated. The organic phase was reextracted with an additional portion of water (20 mL) and the phases separated. Next the organic phase was washed with a NaCl (sat, aq) brine solution (20 mL) and the phases separated. The washed organic phase was then dried over $MgSO_4$, filtered through a glass fritted funnel, and concentrated by rotary evaporation to yield a brown solid of mass 248.9 mg. This crude product was then purified by column chromatography on silica gel. The mobile phase was comprised of a mixture of ethyl acetate and hexanes, with less than 1% of triethyl amine added. The mobile phase composition was varied in a gradient starting from 5% ethyl acetate and

95% hexanes to 20% ethyl acetate and 80% hexanes. The product was collected in fractions 6 and 7, to yield 121.3 mg (58%) of the desired product as an off-white solid.

^{1}H NMR ($CDCl_3$, 500 MHz): δ 8.2 (dd, *J* = 8.6, 2.3, 1H), 7.91 (d, *J* = 2.3, 1H), 7.82 (d, *J* = 8.3, 1H), 7.67 - 7.62 (m, 2H), 7.53 (dd, *J* = 7.9, 0.8, 1H), 7.49 (dd, *J* = 8.3, 2.4, 1H), 7.46 (t, *J* = 7.8, 1H), 7.29 – 7.26 (m, 2H), 7.25 (dd, *J* = 7.8, 0.8, 1H), 7.10 (d, *J* = 8.6, 1H), 3.86 (s, 3H), 1.43 (s, 9H)

^{19}F NMR ($CDCl_3$, 470 MHz): δ -62.48 (s)

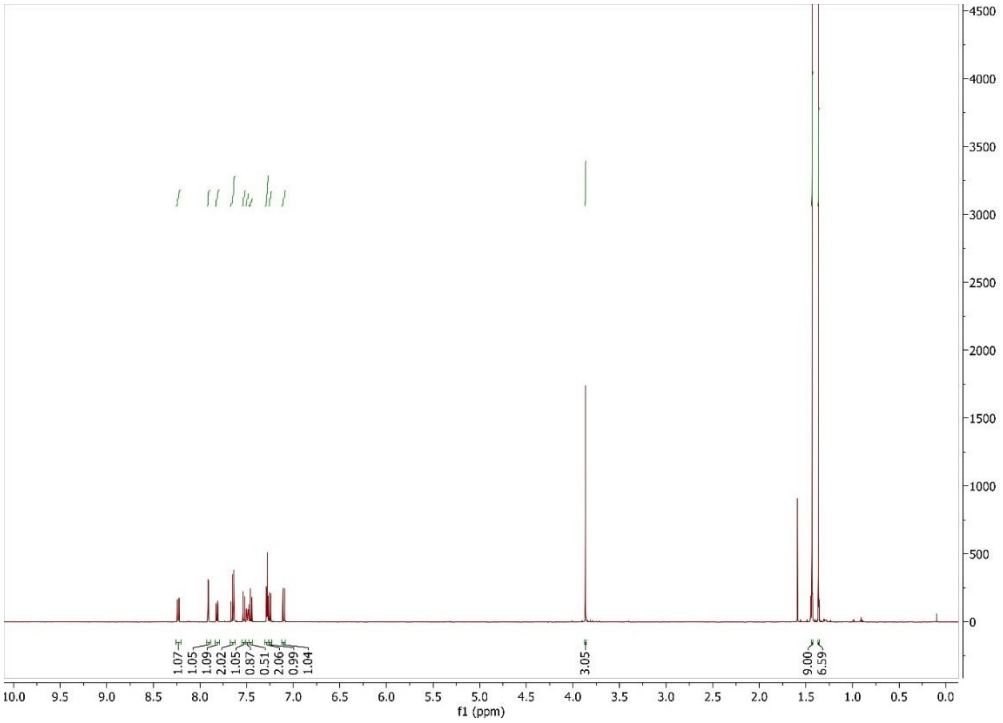

Figure 2.66 ^{1}H NMR spectrum of **2.19** in $CDCl_3$ at 500 MHz

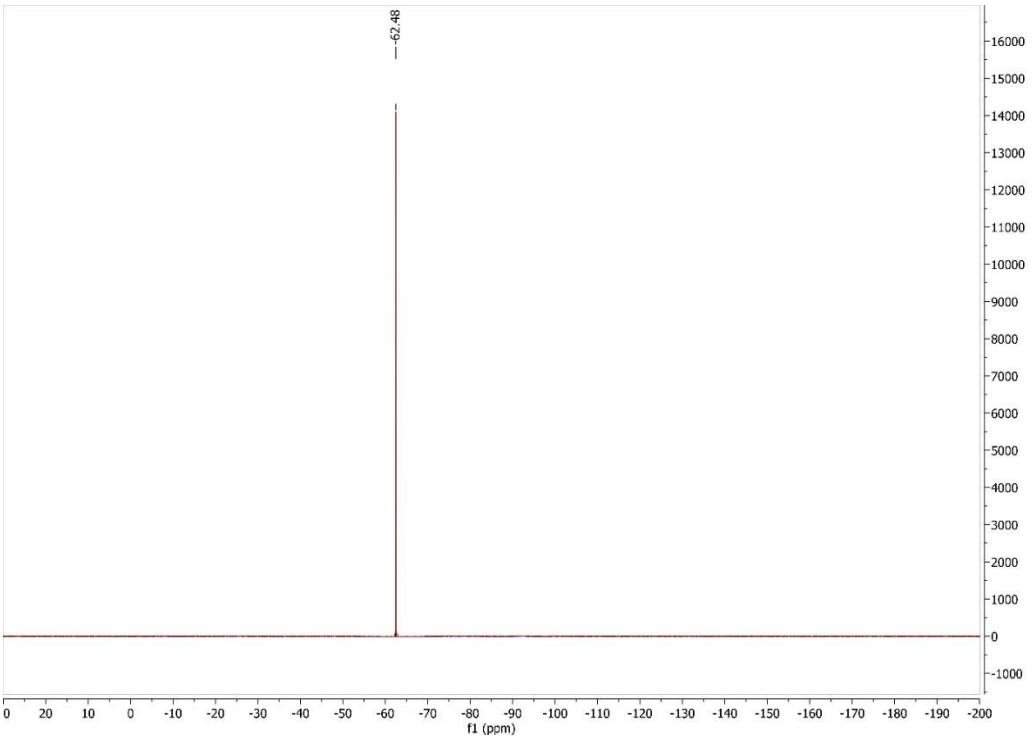

Figure 2.67 ^{19}F NMR spectrum of **2.19** in $CDCl_3$ at 470 MHz

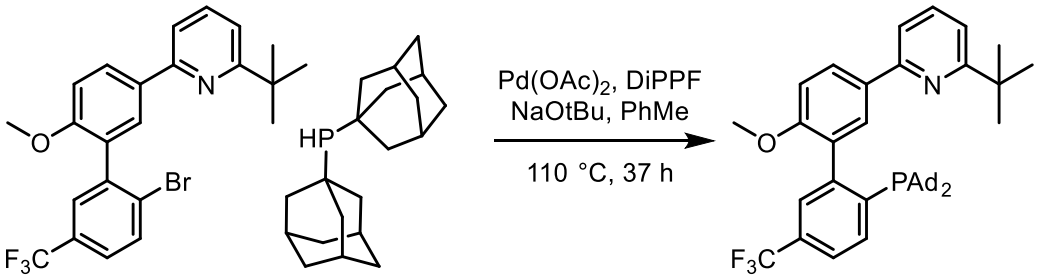

2.19 **L2.3a**

48 %

In a nitrogen filled glovebox, a oven dried scintillation vial was charged with $Pd(OAc)_2$ (3.7 mg, 0.016 mmol), DiPPF (8.7 mg, 0.021 mmol), PhMe (0.5 mL), and magnetic stir bar. The mixture was allowed to stir at rt for 40 min, then aryl bromide **2.19** (133.0 mg, 0.286 mmol), diadamantyl phosphine (95.8 mg, 0.317 mmol), NaOtBu (33.4 mg, 0.348 mmol), and PhMe (2.0 mL) were added, the vial was capped, removed from the glovebox, and place in an oil bath pre-heat to 110 °C for 37 h. Reaction progress was followed by ^{31}P-NMR. Upon completion, the

reaction was allowed to cool to rt, then purified by column chromatography on silica (30 g) without workup. The column was run in a fume hood using de-oxygenated hexanes, EtOAc, and NEt_3 under a positive pressure of N_2 (g). The mobile phase was run as a gradient with increasing EtOAc composition starting with pure hexanes and ending with 15 % EtOAc, 1 % NEt_3 in hexanes. Factions were analyzed by TLC and similar fractions combined and concentrated to yield 191.2 mg of a light brown solid. The solid was then dissolved in a minimal amount of CH_2Cl_2 and placed in a -40 °C freezer to aid crystallization. Upon crystal formation, the mother liquor was removed by pipette, and the solid washed again with cold CH_2Cl_2. Residual solvent was removed *in vacuo* to yield a white solid (94.6 mg, 48.2 %)

^{1}H NMR ($CDCl_3$, 500 MHz): δ 8.14 (dd, *J* = 8.7, 2.3, 1H), 8.00 (d, *J* = 8.1, 1H), 7.81 (d, *J* = 2.3, 1H), 7.63-7.57 (m, 2H), 7.51 (t, *J* = 2.5, 1H), 7.45 (dd, *J* = 7.9, 0.9, 1H), 7.18 (dd, *J* = 7.8, 0.8, 1H), 6.99 (d, *J* = 8.7, 1H), 3.76 (s, 3H), 1.97-1.80 (m, 18 H), 1.72-1.61 (m, 12H)

^{13}C NMR ($CDCl_3$, 120 MHz): δ 168.83, 156.98, 155.18, 148.96 (d, *J* = 35.1), 139.76 (d, *J* = 30.7), 136.74, 136.72, 131.57 (d, *J* = 7.1), 131.37, 130.80 (d, *J* = 2.8), 130.25 (q, *J* = 32.2), 127.69 (singlet, broad) , 127.43, 124.43 (q, *J* = 27, 2.5), 121.99 (2 peaks or doublet? Something else?), 116.54, 116.09, 110.30, 55.10, 53.56, 43.59 (d, *J* = 9.8), 42.08 (d, *J* = 13.4), 41.77 (d, *J* = 12.6), 37.81, 37.78 (d, *J* = 25.5), 37.08 – lots going on here, 30.39, 29.12 (d, *J* = 8.7), 28.93 (d, *J* = 8.4)

^{19}F NMR ($CDCl_3$, 470 MHz): δ -62.49.

^{31}P NMR ($CDCl_3$, 202 MHz): δ 23.72

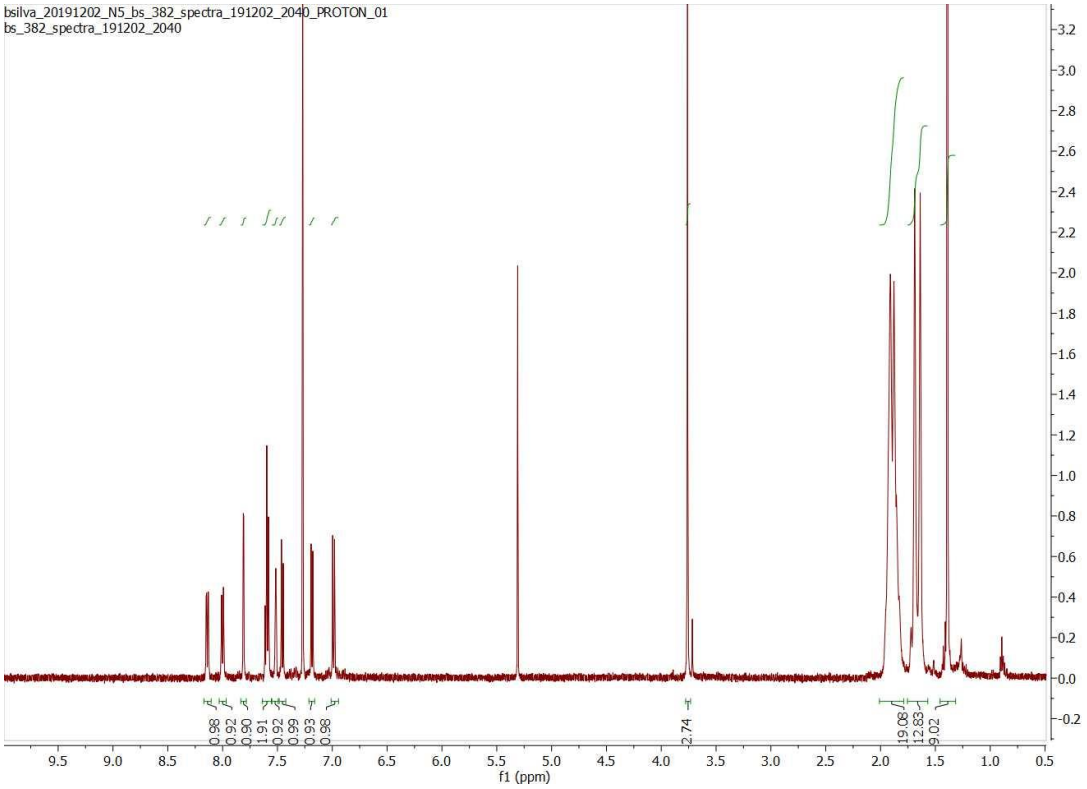

Figure 2.68 ^{1}H NMR spectrum of **L2.3a** in $CDCl_3$ at 500 MHz

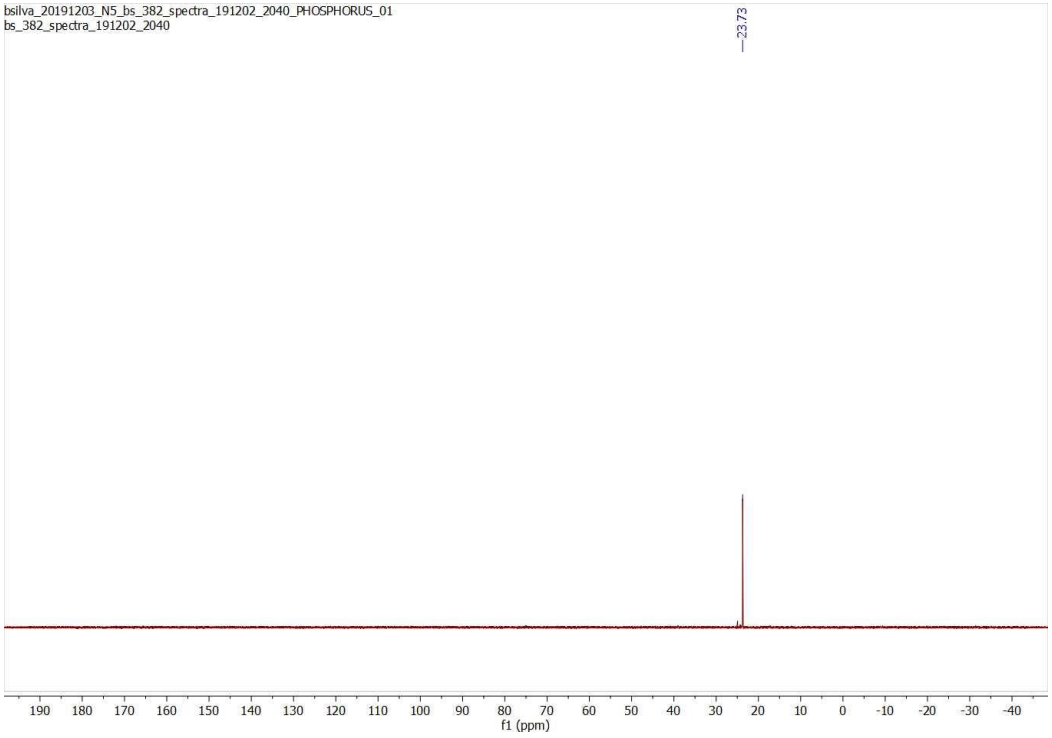

Figure 2.69 ^{31}P NMR spectrum of **L2.3a** in $CDCl_3$ at 162 MHz

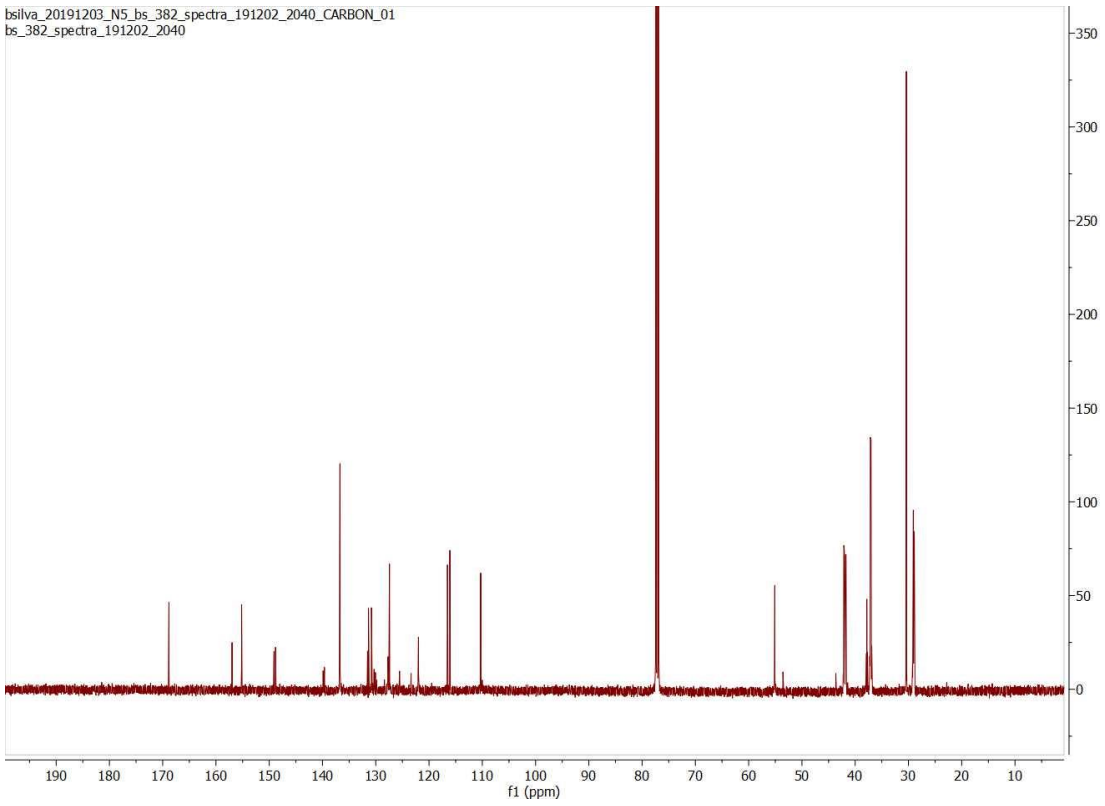

Figure 2.70 $^{13}C\{^{1}H\}$ NMR spectrum of **L2.3a** in $CDCl_3$ at 125 MHz

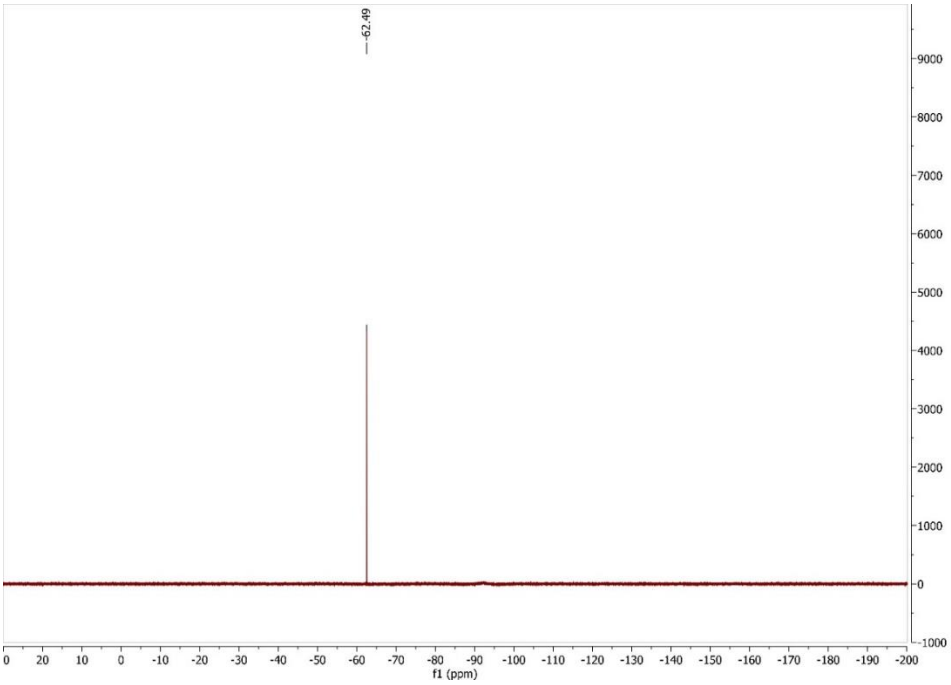

Figure 2.71 ^{19}F NMR spectrum of **L2.3a** in $CDCl_3$ at 470 MHz

Synthesis of **2.20**

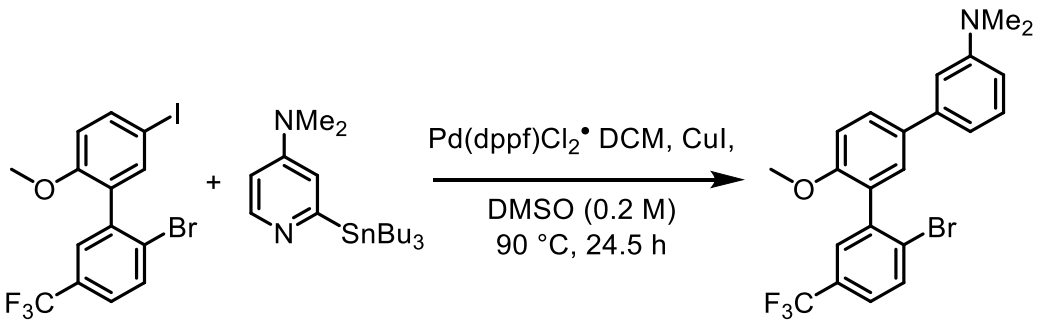

I-2.1 **2.20**

In a nitrogen filled glovebox, an oven dried scintillation vial was charged with a small magnetic stir bar, bs288 (520.0 mg, 1.138 mmol), **I-2.1** (588.3 mg, 1.399 mmol), CuI (66.9 mg, 0.351 mmol), DMSO (dry, de-O_2) (5.7 mL). The mixture was briefly stirred, ~ 5 minutes. Next Pd(dppf)Cl_2•DCM (91.7 mg, 0.112 mmol) was added. The vial was then seal, removed from the glovebox, and place in an oil bath heated to 90 °C for 21 hours. After the initial heating period, the reaction vessel was removed from heating, cooled to room temperature, then under a stream of nitrogen gas, the cap was removed, the reaction mixture sampled (approximately 0.1 mL removed), then the cap quickly replaced on the vial. The aliquot was treated dilution in EtOAc (20 mL) and NH_4OH (aq, 25% by wt) (10 mL), the mixture shaken vigorously, then the phases separated. The organic phase was once again treated with and NH_4OH (aq, 25% by wt) (10 mL), the mixture vigorously shaken, then the phases separated. The organic phase was then dried over Na_2SO_4 (s), filtered through a glass fritted funnel, and concentrated by rotary evaporation. The crude residue (15.5 mg) was dissolved in $CDCl_3$ (0.7 mL) for NMR analysis. As there was still starting material apparent in the crude ^{1}H- and ^{19}F-NMR spectra, the reaction vessel was again placed in the oil bath heated to 90 °C. After an additional 3.5 hours of heating, the reaction was cooled to room temperature and the entire reaction quenched and worked up to a crude product. The work up (described above) consisted of addition of EtOAc (45 mL) and NH_4OH (aq,, 25% by wt) (40 mL),

vigorous mixing in a separatory funnel, separation of the organic and aqueous phases, and re-extraction of the organic phase with NH_4OH (aq, 25% by wt) (30 mL). The organic phase was then extracted twice with LiCl (aq, 10% by wt) (30 mL) in a separatory funnel, dried over $MgSO_4$ (s), then filtered through a pad of celite in a glass fritted funnel. The filtrate was concentrated by rotary evaporation to yield a brown solid (818.7 mg, approximately double theoretical yield). ^{1}H-NMR analysis of this crude solid shows a ratio of about one part product formation to 0.3 parts starting aryl iodide. The crude product was purified by column chromatography on silica gel. The crude product was first dissolved in CH_2Cl_2 (50 mL) and adsorbed to a portion of silica gel. The solvent was evaporated by rotary evaporation, then the free-flowing silica charged with the crude product was poured over the packed glass column charged with silica (40 g). The mobile phase consisted of EtOAc, hexanes, and NEt_3 in the following gradient: of EtOAc (2% by volume) hexanes (~ 98% by volume), and NEt_3 (5 drops) for 200 mL; EtOAc (5% by volume) hexanes (~ 95% by volume), and NEt_3 (10 drops) for 100 mL; EtOAc (10% by volume) hexanes (~ 90% by volume), and NEt_3 (10 drops) for 200 mL; EtOAc (15% by volume) hexanes (~ 85% by volume), and NEt_3 (10 drops) for 100 mL; EtOAc (20% by volume) hexanes (~ 80% by volume), and NEt_3 (10 drops) for 100 mL; EtOAc (30% by volume) hexanes (~ 70% by volume), and NEt_3 (10 drops) for 300 mL; and EtOAc (35% by volume) hexanes (~ 65% by volume), and NEt_3 (10 drops) for 200 mL. Total column solvent volume consumed 1.2 L. The appearance of UV-light response was followed for each fraction. The UV active fractions were compared for TLC R_f values, and those with conserved retention combined, and concentrated by rotary evaporation. Fractions 41-49 were combined to yield 139.6 mg (29%) of a colorless solid that was identified to be the desired product by ^{1}H- and ^{19}F-NMR analysis. Residual ethyl acetate and water can be identified in the ^{1}H-NMR spectrum.

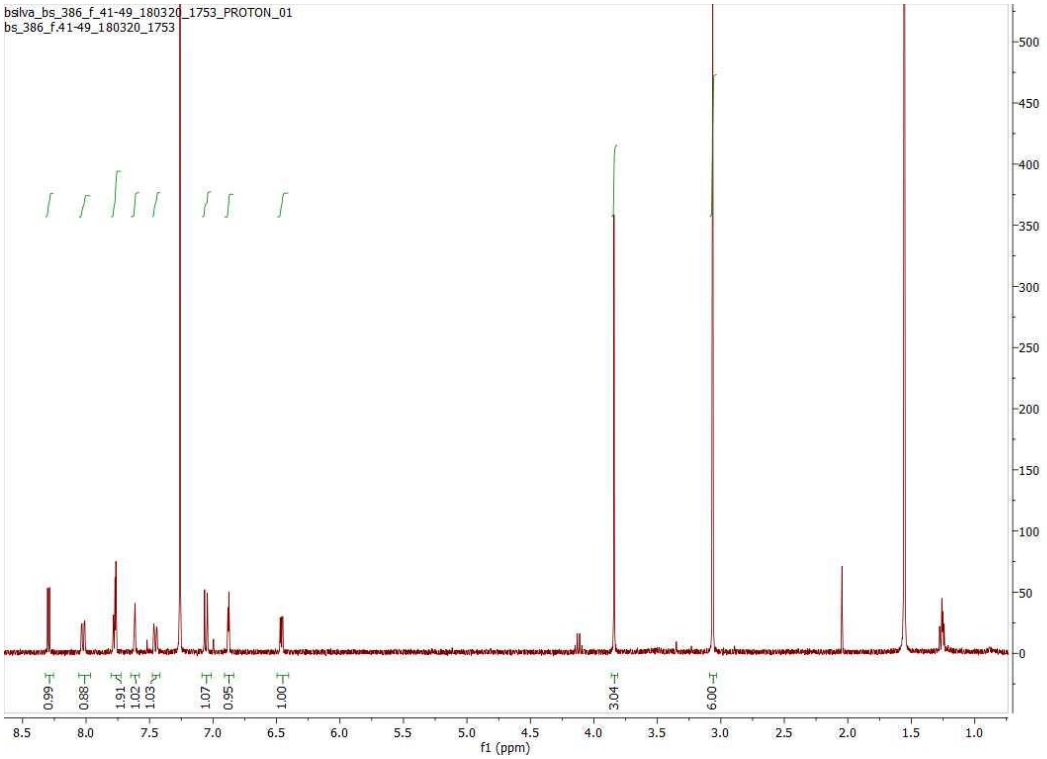

Figure 2.72 ^{1}H NMR spectrum of **2.20** in $CDCl_3$ at 400 MHz

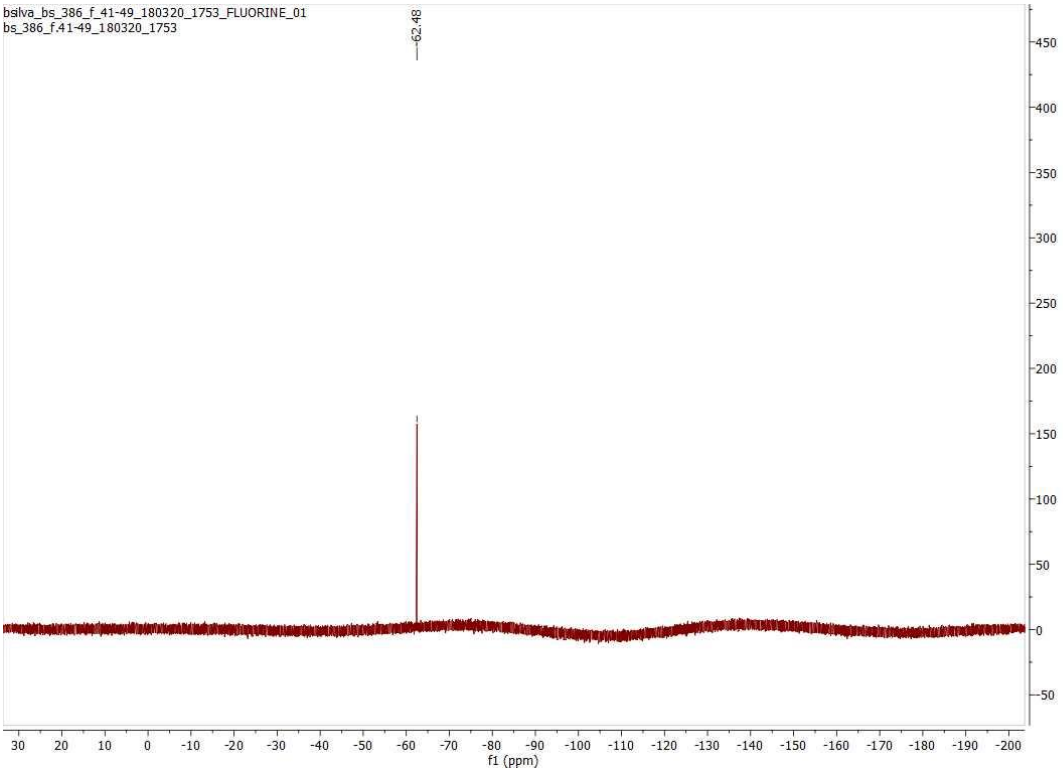

Figure 2.73 ^{19}F NMR spectrum of **2.20** in $CDCl_3$ at 376 MHz

Synthesis of **L2.4a**

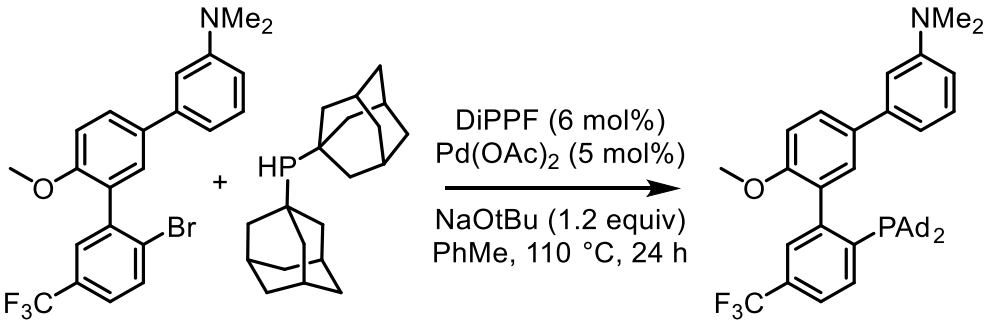

2.20 **L2.4a**

In a nitrogen filled glovebox, a scintillation vial was charged with $Pd(OAc)_2$ (4.5 mg, 0.020 mmol), DiPPF (9.8 mg, 0.023 mmol), and PhMe (dry, deO_2) (0.2 mL). A magnetic stir bar was added, and the mixture stirred at room temperature for 1 hour. Next, diadamantyl phosphine (140.5 mg, 0.465 mmol), sodium tert-butoxide (45.4 mg, 0.472 mmol), and bs714 (174.3 mg, 0.386 mmol) were added to reaction vial with an additional portion of toluene (dry, deO_2) (1.8 mL). The vial was sealed and removed from the glovebox. The vial was then placed in an oil bath heated to 110 °C for 24 hours. After the heating period, the reaction vessel was removed from the glovebox, cooled to room temperature, then subject to column chromatography, loading the crude reaction mixture directly onto a prepared silica column. It should be noted that the mobile phase (ethyl acetate, hexanes, and triethylamine) was prepared by sparging with N_2 (g). This gave sufficiently low O_2 environment to prevent oxidation of the phosphine to the phosphine oxide during the purification process. The composition of the mobile phase was varied in a gradient consisting initially of 2% ethyl acetate, 98% hexanes, and finished with 30% ethyl acetate and 70% hexanes. The product was collected in fractions 25-35, concentrated under reduced pressure. The product presented as a white solid of mass 168.5 mg (65% yield).

^{1}H NMR ($CDCl_3$, 400 MHz): δ 8.28 (d, *J* = 5.9, 1H), 8.03 (dd, *J* = 8.6, 2.3, 1H), 7.97 (d, *J* = 8.0, 1H), 7.60 (d, *J* = 2.3, 1H), 7.59 – 7.51 (m, 2H), 6.97 (d, *J* = 8.6, 1H), 6.83 (d, *J* = 2.4, 1H), 3.76 (s,

3H), 3.03 (s, 6H), 2.01 – 1.77 (m, 18H), 1.73 – 1.55 (m, 12 H). Residual ethyl acetate is observed at δ 4.13 (q, *J* = 7.1), 2.05 (s), 1.27 (t, *J* = 7.1)

^{13}C NMR ($CDCl_3$, 100 MHz): δ 157.72, 156.83, 155.19, 149.76, (148.91 (d, *J* = 36.0)), 139.75 (d, *J* = 30.9), 136.68, not complete here – not seeing key signal for CF3 (should be 272 Hz coupling). Partial ^{13}C NMR spectrum, insufficient signal to noise ratio.

^{19}F NMR: ($CDCl_3$, 376 MHz): δ - 62.50

^{31}P NMR ($CDCl_3$, 162 MHz): δ 24.02

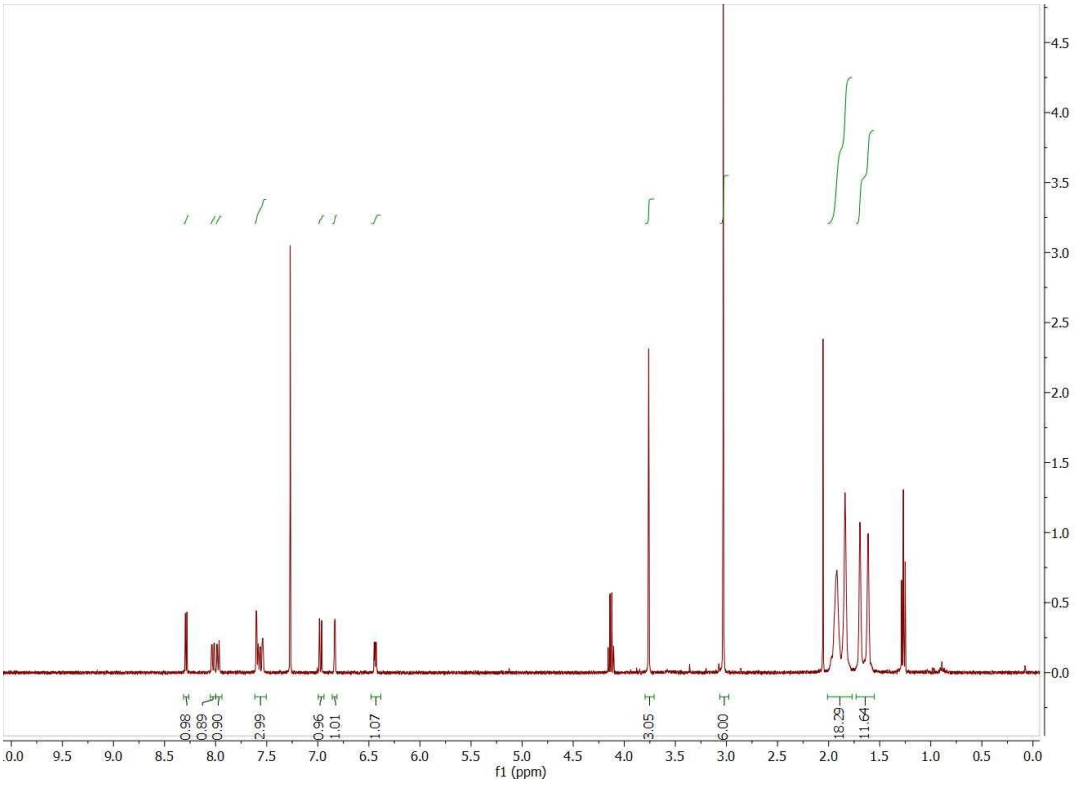

Figure 2.74 ^{1}H NMR spectrum of **L2.4a** in $CDCl_3$ at 400 MHz

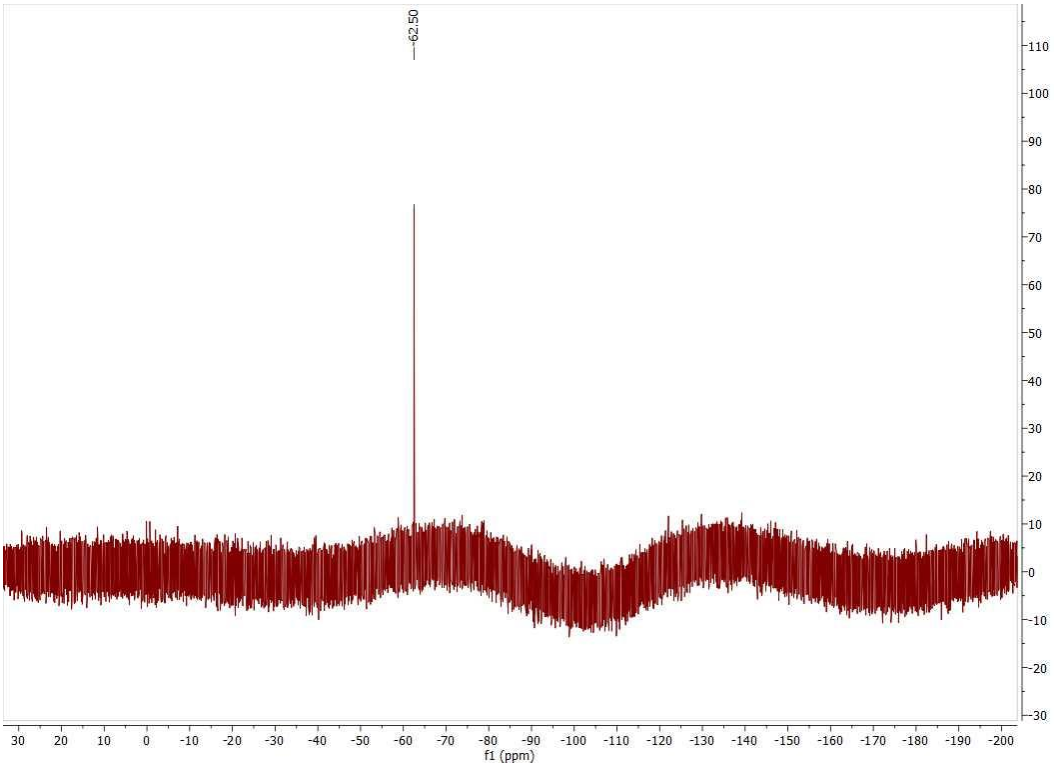

Figure 2.75 ^{19}F NMR spectrum of **L2.4a** in $CDCl_3$ at 376 MHz

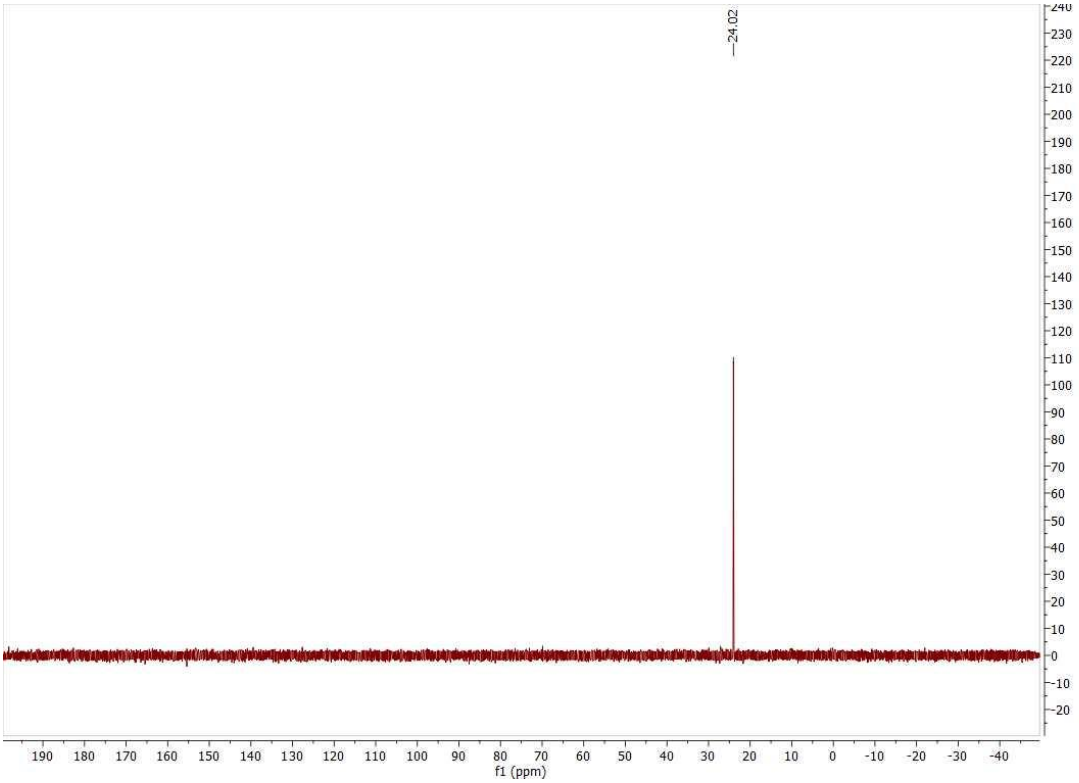

Figure 2.76 ^{31}P NMR spectrum of **L2.4a** in $CDCl_3$ at 162 MHz

Synthesis of **2.21**

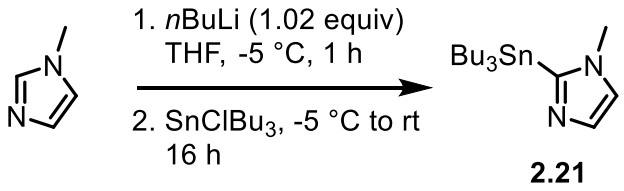

In a nitrogen filled glovebox, a 250 mL Schlenk flask was charged with N-methylimidazole (0.6636 g, 8.083 mmol), THF (10 mL), and magnetic stir bar. The flask was removed from the glovebox, connected to a Schlenk line with nitrogen gas flow, and submerged in an ice bath with NaCl (aq) added. The mixture was stirred for 20 minutes. Next, *n*-BuLi (2.5 M in hexanes) (3.25 mL, 8.050 mmol) was added over the course of 5 minutes. The mixture was stirred for 1 hour. Next, tributylstannylchloride (2.6301 g, 8.079 mmol) was added over the course of 10 minutes. The mixture was stirred and allowed to warm to room temperature over the course of 16 hours.

The reaction was quenched with the addition of water (10 mL), then extracted with diethyl ether (3 portions of 20 mL). The combined organic fractions were dried over $MgSO_4$, filtered through a glass fritted funnel, then concentrated by rotary evaporation. The crude oil was then purified by Kugelrohr distillation at 80 °C for 2.5897 g (86.3%). The product was purified to a mixture consisting of the starting material (N-methylimidazole) in 25% and the desired product in 75%. The mixture was used as is for the next step in the synthetic sequence.

^{1}H NMR ($CDCl_3$, 400 MHz): δ 7.20 (s, 1H), 7.01 (s, 1H), 3.68 (s, 3H), 1.65 – 1.48 (m, 6H), 1.39 – 1.25 (m, 6H), 1.21 – 1.14 (m, 6H), 0.95 – 0.81 (m, 9H)

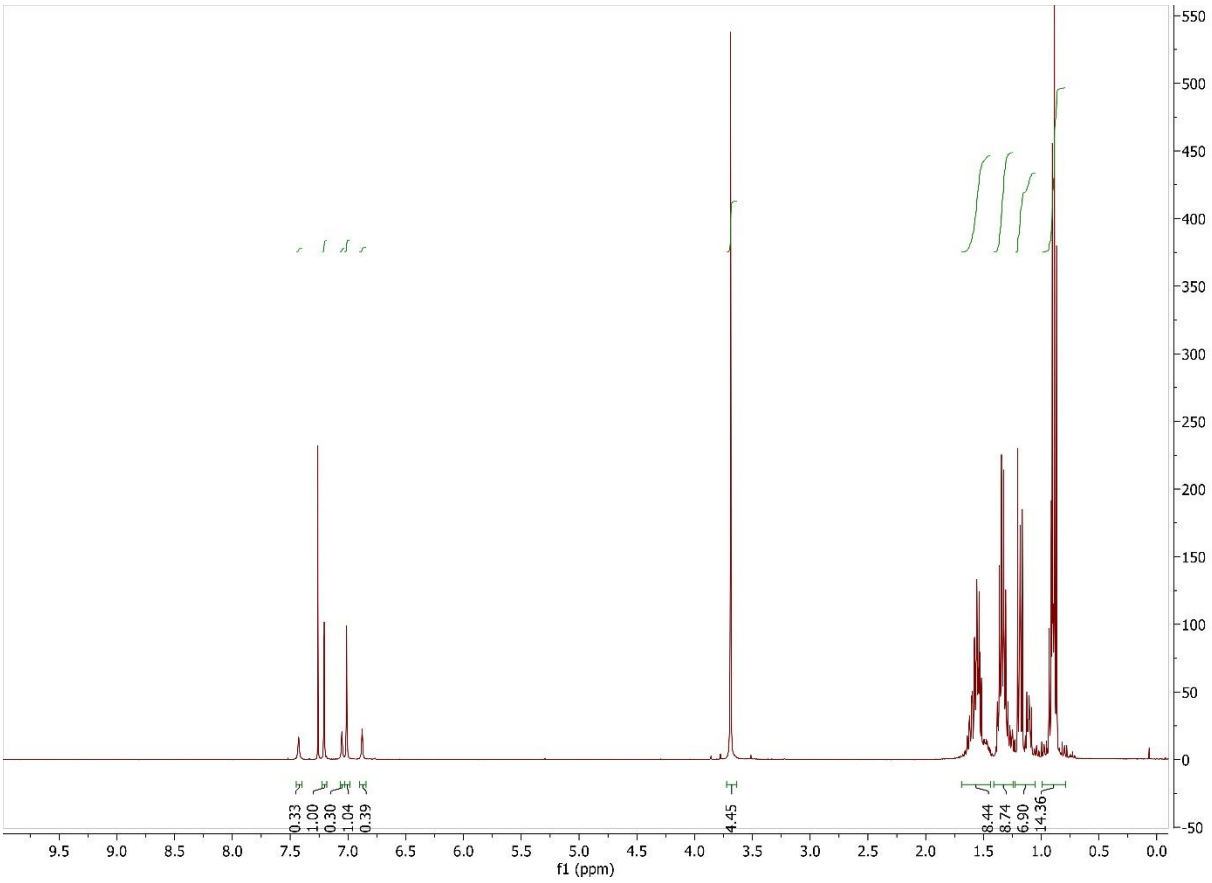

Figure 2.77 ^{1}H NMR spectrum of **2.21** in $CDCl_3$ at 400 MHz

Synthesis of **2.22**

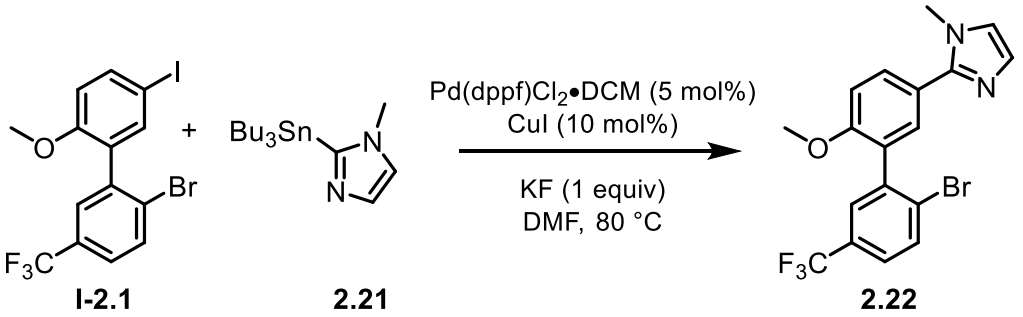

I-2.1 **2.21** **2.22**

In a nitrogen filled glovebox, an oven dried scintillation vial was charged with **2.21** (0.714 g, 1.924 mmol), **I-2.1** (0.4925 g, 1.078 mmol), CuI (0.0257, 0.134 mmol), KF (0.783 g, 1.347 mmol), Pd(dppf)Cl_2•DCM (0.0550 g, 0.067 mmol), and DMF (5 mL). The vial was sealed and removed from the glovebox. The reaction vessel was then placed in an oil bath heated to 80 °C for 72 hours. The reaction was then removed from the heating bath, cooled to room temperature, and quenched with the addition of water (130 mL) and NH_4OH (25%, aq) (20 mL). The mixture was then extracted with CH_2Cl_2 (six portions of 30 mL). The combined organic phases were washed with a saturated solution of NaCl (aq) (100 mL), dried over $MgSO_4$, filtered through a glass fritted funnel, then concentrated by rotary evaporation. The crude product was purified by column chromatography on silica gel. The mobile phase consisted of Et_2O and EtOAc. The product was collected in fractions 5-11 as an off-white solid with mass 169.9 mg (30%).

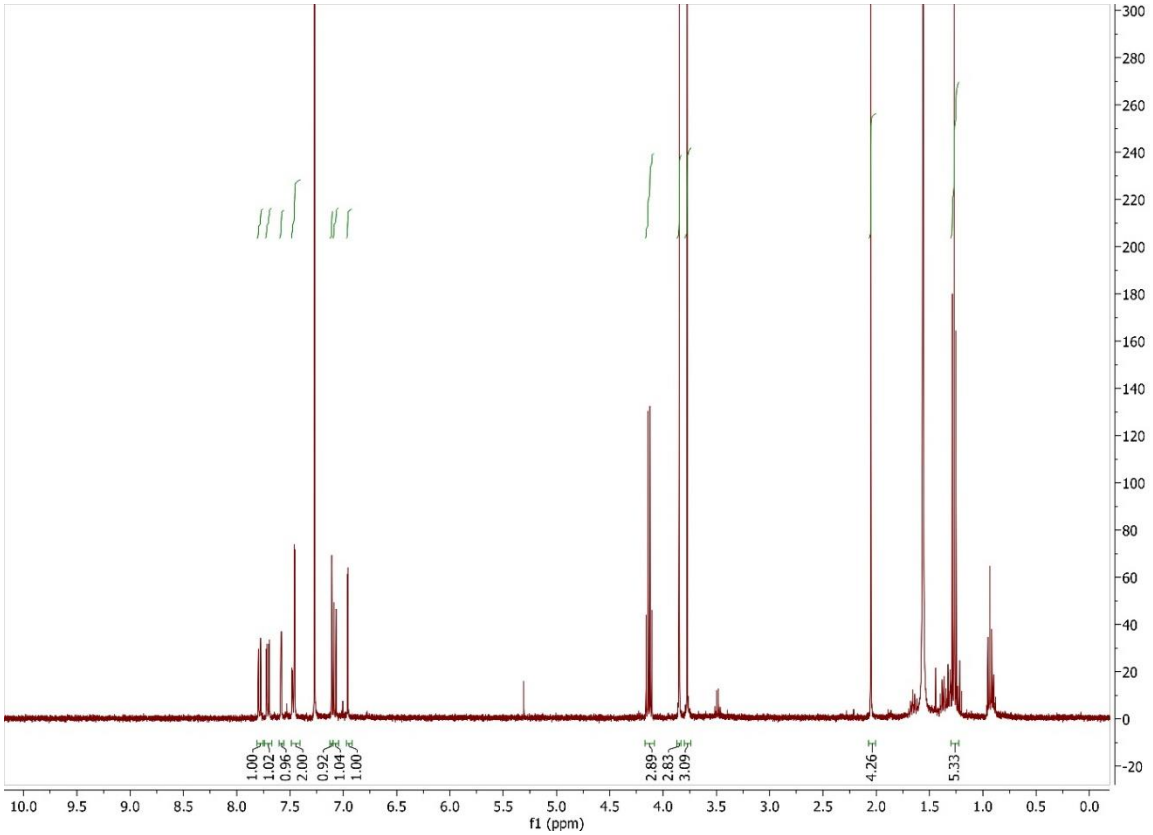

Figure 2.78 ^{1}H NMR spectrum of **2.22** in $CDCl_3$ at 400 MHz

Synthesis of **L2.5a**

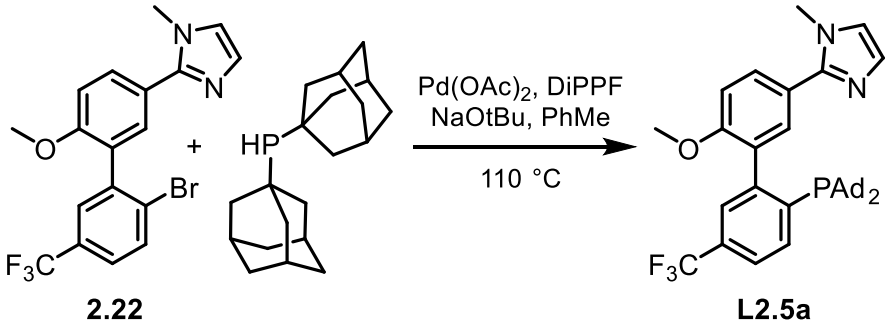

2.22 **L2.5a**

In a nitrogen filled glovebox, an oven dried scintillation vial was charged with $Pd(OAc)_2$ (3.9 mg, 0.017 mmol), DiPPF (8.1 mg, 0.019 mmol), and toluene (1 mL). The mixture was then stirred at room temperature for 30 minutes. Next, **2.22** (133.0 mg, 0.323 mmol), diadamantyl phosphine (107.6, 0.356 mmol), and sodium tert-butoxide (37.3 mg, 0.388 mmol). The reaction

vessel was sealed and removed from the glovebox. The reaction vessel was then placed in an oil bath heated to 110 °C for 43 hours. The reaction vessel was then removed from the oil bath, cooled to room temperature, and directly loaded on a column for chromatography on silica gel. The mobile phase consisted of hexanes and ethyl acetate that was sparged with nitrogen to prevent oxidation of the product. The product was collected in fractions 8-13, concentrated by rotary evaporation and yielded 138.4 mg (31.2%) of a white solid.

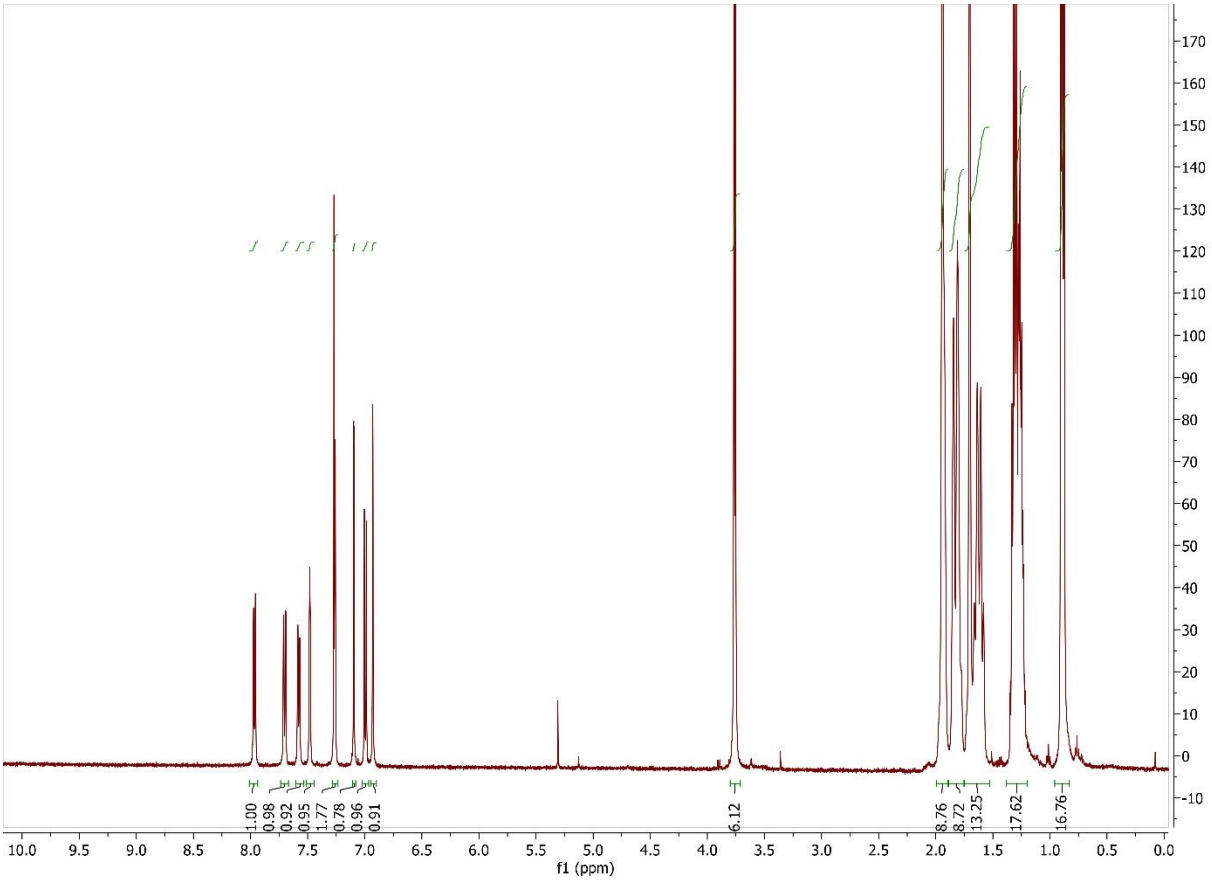

Figure 2.79 ^{1}H NMR spectrum of **L2.5a** in $CDCl_3$ at 500 MHz

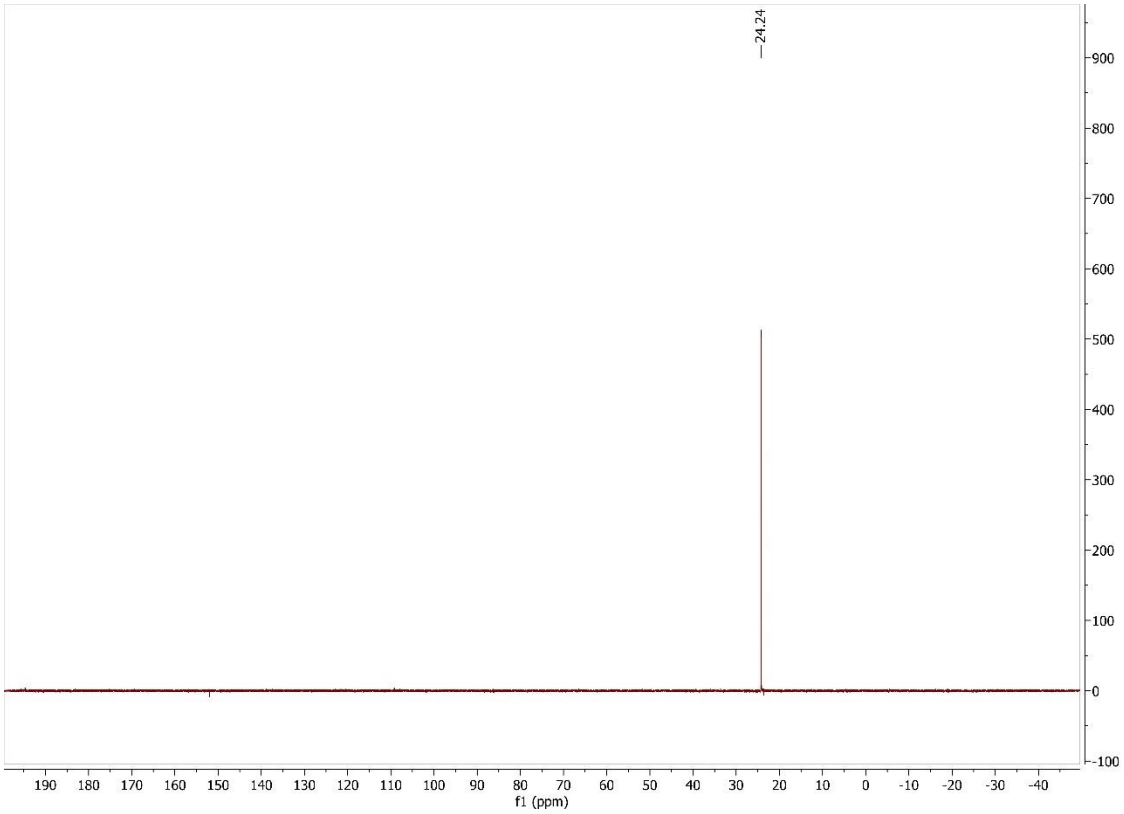

Figure 2.80 ^{31}P NMR spectrum of **L2.5a** in $CDCl_3$ at 162 MHz

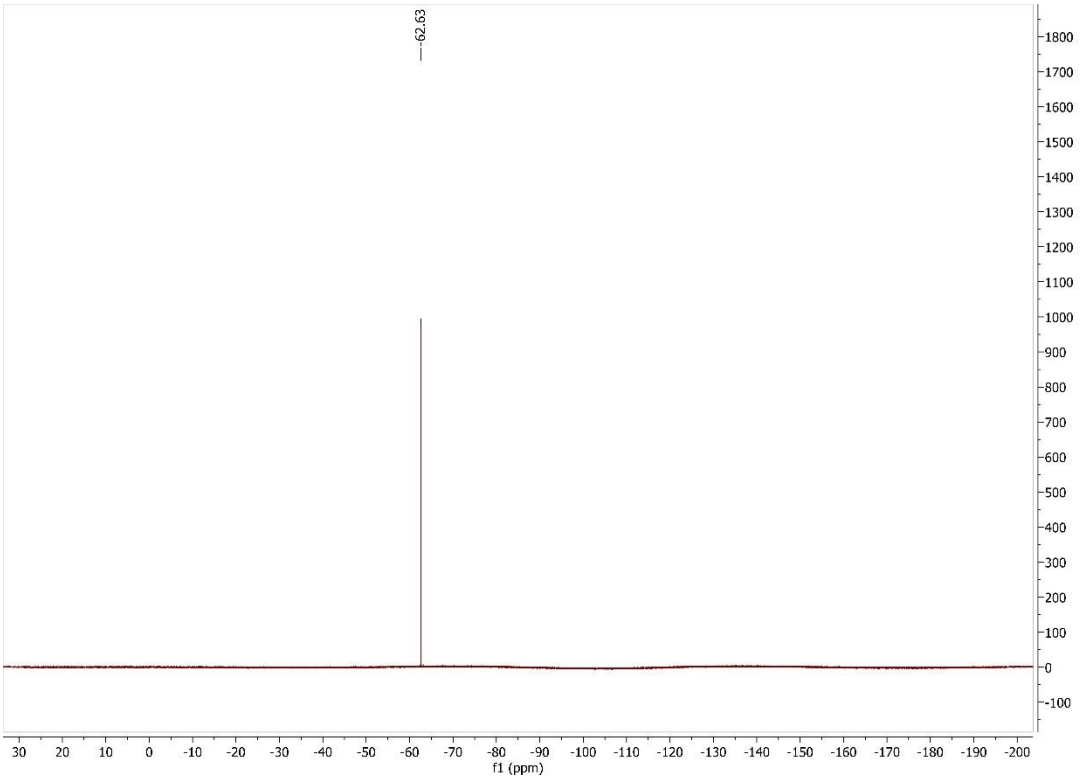

Figure 2.81 ^{19}F NMR spectrum of **L2.5a** in $CDCl_3$ at 3.76 MHz

Synthesis of **2.23**

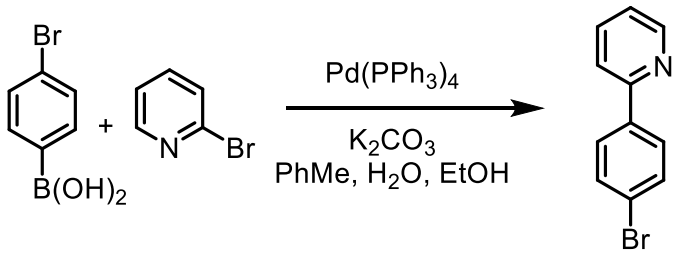

2.23

In open atmosphere, a round bottom flask was charged with 4-bromo-phenyl-boronic acid (2.5616 g, 12.757 mmol), 2-bromopyridine (2.1991 g, 13.918 mmol), potassium carbonate (3.3907 g, 24.534 mmol), toluene (20 mL). The resulting solution was transferred to a pressure vessel, and the round bottom rinsed with H_2O (5.0 mL) and EtOH (5 mL). The rinses were transferred to the pressure vessel. The reaction mixture in the pressure vessel was then sparged with nitrogen for 5

minutes. The pressure vessel was then sealed and brought into a nitrogen filled glovebox via antechamber. Once inside the glovebox, the vessel was charged with $Pd(PPh_3)_4$ (0.1617 g, 0.139 mmol). The pressure vessel was then sealed, removed from the glovebox, and placed in an oil bath heated to 100 °C for 24 hours. The reaction was quenched with the addition of H_2O (30 mL). The work up consisted of extracting the quenched reaction mixture with CH_2Cl_2 (30 mL) three times. The combined organic phase was dried over $MgSO_4$, filtered through a glass fritted funnel, then concentrated by rotary evaporation. The crude product was purified by column chromatography on silica gel with ethyl acetate and hexanes comprising the mobile phase. The mobile phase composition was varied in a gradient starting at pure hexanes and ending with 12% ethyl acetate and 88% hexanes, with a total mobile phase volume of 1100 mL. The product **2.16** was collected in fractions 30 – 38 for 1.159 g, 72%

^{1}H-NMR ($CDCl_3$, MHz): δ = 8.70 (ddd, J = 4.8, 1.7, 1.0, 1H), 7.92 – 7.85 (m, 2H), 7.79 – 7.74 (m, 1H), 7.73 – 7.69 (m, 1H), 7.63 – 7.59 (m, 2H), 7.27 – 7.23 (m, 1H)

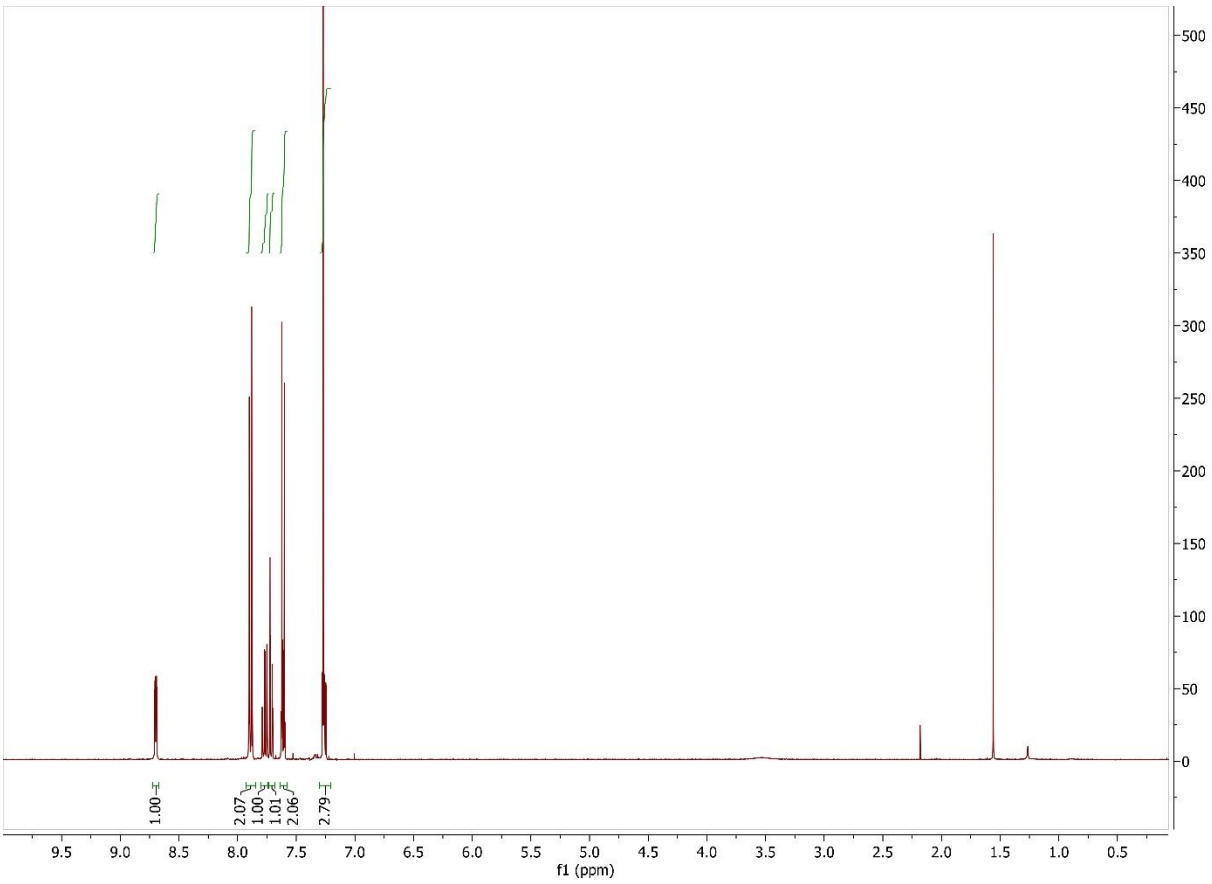

Figure 2.82 ^{1}H NMR spectrum of **2.23** in $CDCl_3$ at 500 MHz

Synthesis of **2.25**

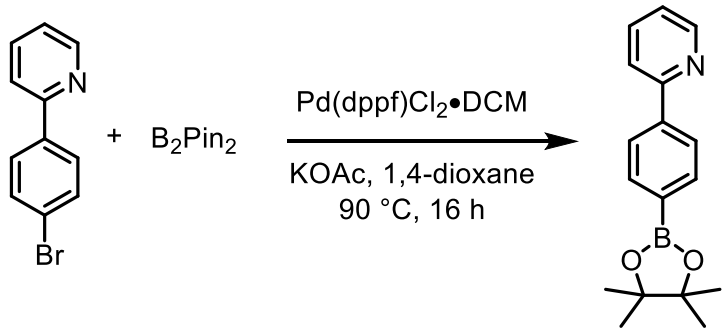

2.24 **2.25**

In a nitrogen filled glovebox, an oven dried pressure vessel was charged with 2-(4'-bromophenyl)pyridine (1.5709 g, 6.711 mmol), B_2Pin_2 (1.7984 g, 7.082 mmol), potassium acetate (2.2440 g, 22.863 mmol), Pd(dppf)Cl_2•DCM (268.3 mg, 0.329 mmol), and 1,4-dioxane (13.0 mL).

The pressure tube was sealed, removed from the glovebox, and placed in an oil bath heated to 90 °C for 16 hours. The reaction was quenched with the addition of H_2O (50 mL). Then the mixture was extracted three times with portions of ethyl acetate (50 mL), dried over $MgSO_4$, filtered through a glass fritted funnel, then concentrated by rotary evaporation. The crude product was purified by column chromatography on silica gel with the mobile phase consisting of petroleum ether and ethyl acetate. The mobile phase composition was varied in a gradient starting with pure petroleum ether and ending with 12% ethyl acetate and 88% petroleum ether. The total mobile phase volume was 900 mL. The product **2.17** was collected in fractions 3-19 and concentrated by rotary evaporation to yield a colorless oil of mass 2.1924 g. NMR analysis suggests the product is only 90% pure, though this proves to be sufficient for the next cross coupling step.

^{1}H-NMR ($CDCl_3$, MHz): δ = 8.72 (dt, *J* = 4.7, 1.3, 1H), 8.02 – 7.98 (m, 2H), 7.94 – 7.90 (m, 2H), 7.79 – 7.74 (m, 2H), 7.28 – 7.20 (m, 1H), (s, 12H). Residue impurities including solvent (1,4-dioxane at 3.70 (s), Et_2O at 3.48 (q) and 1.21 (t), water 1.97 ppm (br)), residual pinacolato-species (1.35 (s), 1.27 (s), 1.24 (s)), and what appears to be a side-product)7.81 (d), 7.49 – 7.43 (m), and 7.42 – 7.34 (m)) are observed in the ^{1}H NMR spectrum.

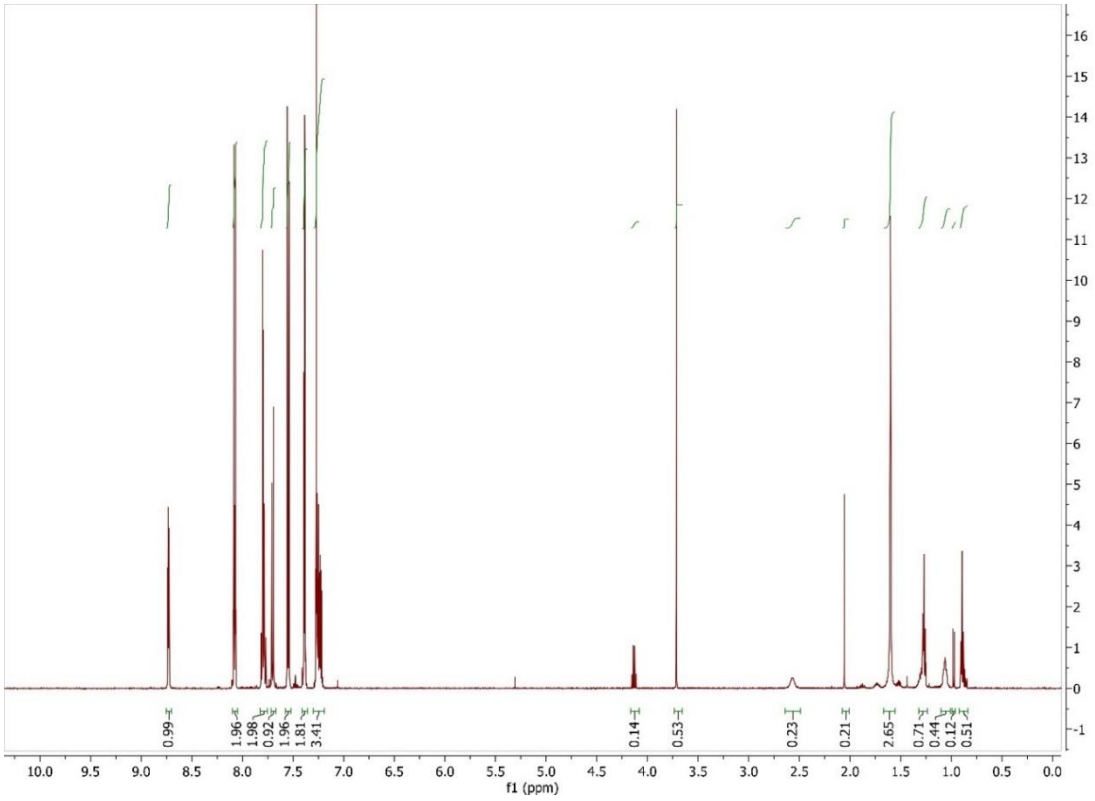

Figure 2.83 ^{1}H NMR spectrum of **2.25** in $CDCl_3$ at 500 MHz

Synthesis of **2.26**

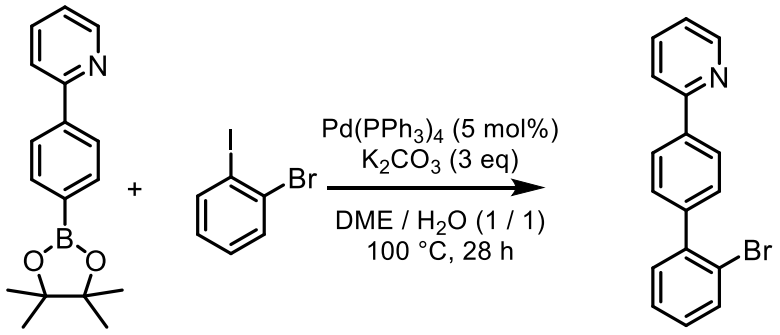

2.25 **2.26**

In a nitrogen filled glovebox, a scintillation vial was charged with **2.17** (1.532 g, 5.449 mmol), 2-bromoiodobenzene (1.6952 g, 5.992 mmol), potassium carbonate (2.288 g, 16.555 mmol), 1,4-dioxane (14 mL), H_2O (3.5 mL), and Pd(dppf)Cl_2•DCM (338.0 mg, 0.4139 mmol). The vial was sealed, removed from the glovebox, and placed in an oil bath heated to 90°C for 22

hours. The reaction was quenched with the addition of H_2O (50 mL). The quenched reaction mixture was then extracted with three portions of ethyl acetate (50 mL). The combined organic phases were then washed with a saturated solution of NaCl (aq) (50 mL), dried over $MgSO_4$, filtered through a glass fritted funnel, and concentrated with rotary evaporation. The crude product was purified by column chromatography on silica gel. The mobile phase composition was varied in a gradient starting at pure hexanes and ending with 12% ethyl acetate and 88% hexanes, with a total mobile phase volume of 1000 mL. The product was collected from fractions 23-29 for mass 0.7908 g, 48%

^{1}H-NMR ($CDCl_3$, MHz): δ = 8.74 – 8.71 (m, 1H), 8.09 – 8.04 (m), 7.82 – 7.75 (m, 2H), 7.70 (d, *J* = 8.0, 1H), 7.56 – 7.52 (m, 2H), 7.41 – 7.36 (m, 2H), 7.28 – 7.18 (m, 1 H). Additional signals in the ^{1}H NMR spectrum are attributed to residual solvent (1,4-dioxane (3.70 (s), EtOAc (4.12 (q), 2.05 (s), 1.26 (t), water (1.60 (s, br)

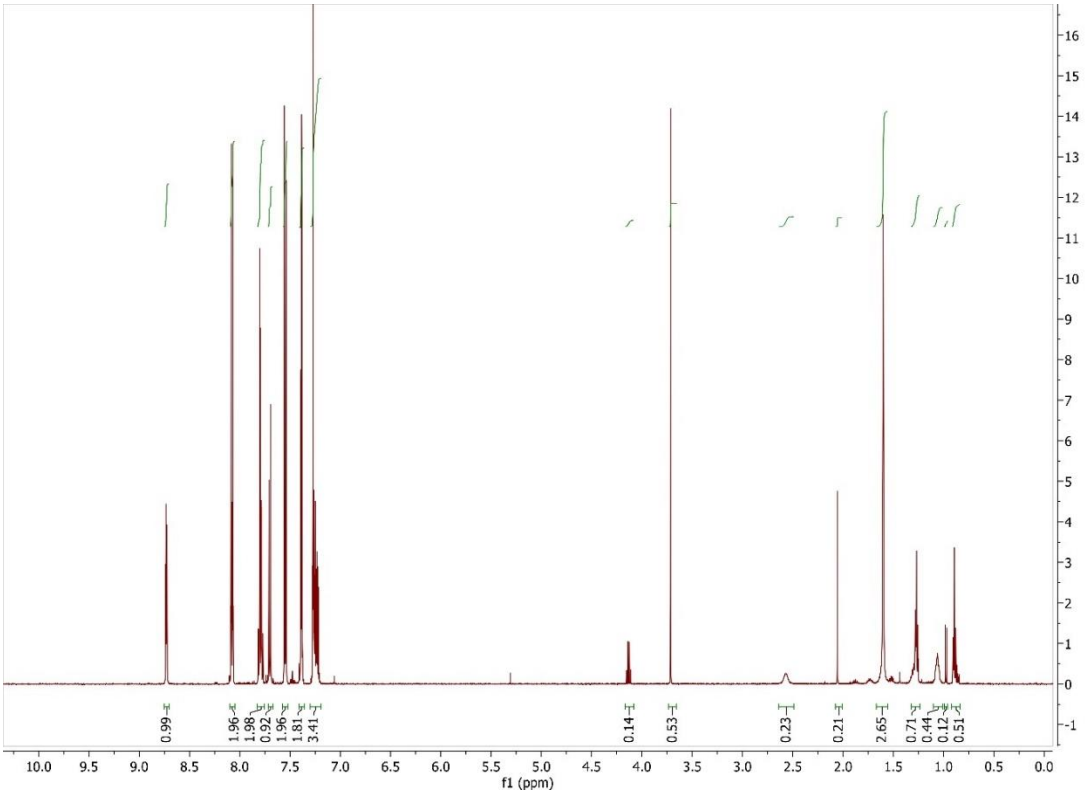

Figure 2.84 ^{1}H NMR spectrum of **2.26** in $CDCl_3$ at 500 MHz

Synthesis of **L2.8a**

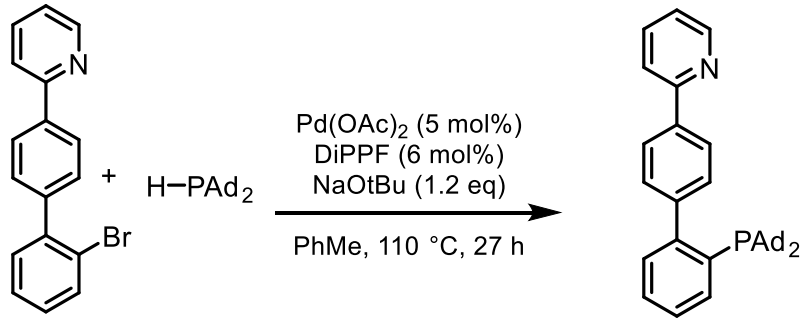

2.26 **L2.8a**

In a nitrogen filled glovebox, an oven dried scintillation vial was charged with DiPPF (52.0 mg, 0.124 mmol), $Pd(OAc)_2$ (50.0 mg, 0.223 mmol), and PhMe (5.0 mL). This mixture was stirred at room temperature in the glovebox for 10 minutes. Next, the reaction vial was charged with **2.26** (676.3 mg, 2.269 mmol), diadamantyl phosphine (764.0 mg, 2.526 mmol), NaOtBu (259.1 mg,

2.696 mmol). The vial was sealed, removed from the glovebox, and placed in an oil bath heated to 110 °C for 24 hours. After the heating period, the vial was removed from the oil bath, cooled to room temperature, and the reaction progress assessed by ^{31}P NMR. After determining the reaction had reached completion, the reaction mixture was loaded directly onto a column of silica gel for purification. The column was run in a fume hood using de-oxygenated hexanes and EtOAc with positive pressure of N_2 (g). The mobile phase composition was a gradient mixture of increasing polarity starting with pure hexanes and ending with 20 % EtOAc, 1% NEt_3 in hexanes. Similar fractions were combined based on TLC analysis. The product was collected in fractions 12-23, then crystallized from a concentrated CH_2Cl_2 at -40 °C. The product was collected as a white solid of mass 466.5 mg (50%)

^{1}H-NMR ($CDCl_3$, MHz): δ = 8.71 (d, *J* = 4.4, 1H), 7.99 (d, *J* = 8.2, 2H), 7.92 (d, *J* = 7.5, 1H), 7.83 – 7.79 (m, 1H), 7.76 (td, *J* = 7.5, 1.7, 1H), 7.44 – 7.33 (m, 4H), 7.32 – 7.28 (m, 1H), 7.25 – 7.19 (m, 1H), 1.98 – 1.81 (m, 18H), 1.66 (s, 12H)

^{31}P NMR ($CDCl_3$, 202 MHz): δ = 20.82

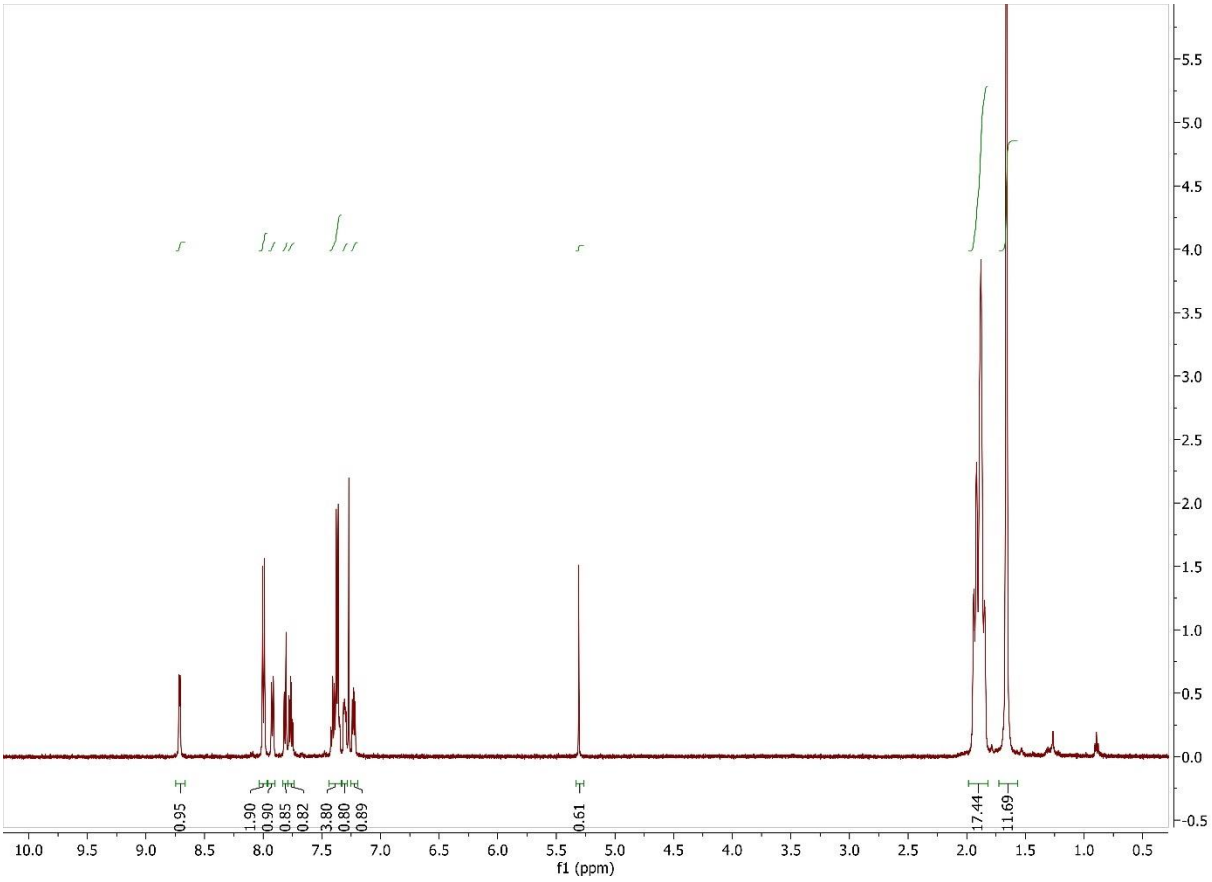

Figure 2.85 ^{1}H NMR spectrum of **L2.8a** in $CDCl_3$ at 500 MHz

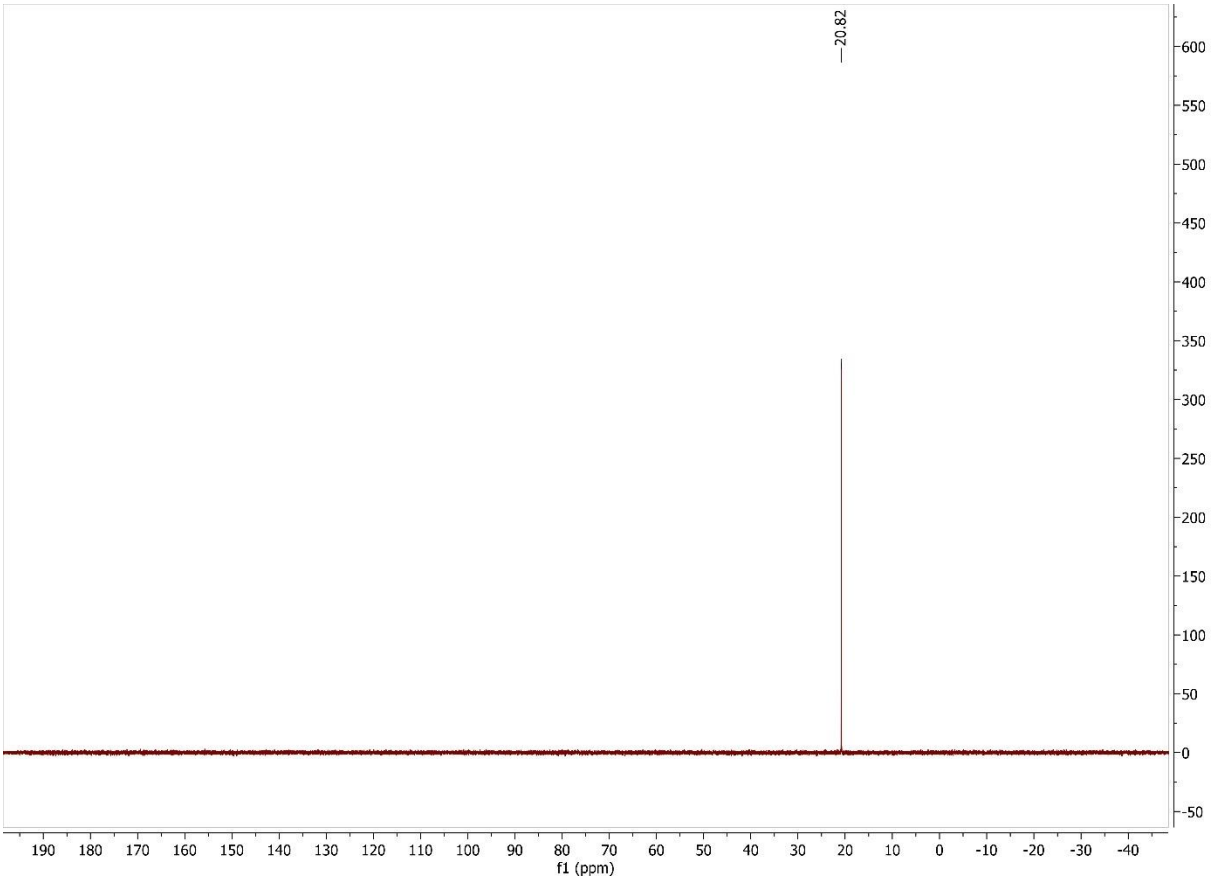

Figure 2.86 ^{31}P NMR spectrum of **L2.8a** in CDCl3 at 202 MHz

Synthesis of **2.8**

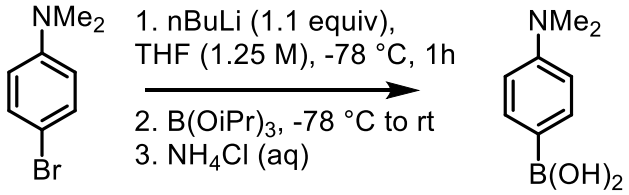

2.7 **2.8**

In a nitrogen filled glove box, an oven dried 2-neck round bottom flask was charged with 4-bromo-N,N-dimethylaniline (504.5 mg, 2.520 mmol), THF (2 mL), and magnetic stir bar. The flask was sealed and removed from the glovebox. The reaction flask was placed in a cooling bath of dry ice and acetone and connected to positive pressure flow of nitrogen gas. After cooling for 30 minutes, *n*-butyl lithium *2.5 M) (1.15 mL, 2.88 mmol) was added to the cold flask dropwise

over 15 minutes. The reaction was stirred, and the cooling bath maintained for 45 minutes. Meanwhile, a syringe was charged with triisopropylborate (0.8560 g, 4.55 mmol) in the glovebox. After the 45 minutes had passed, the triisopropylborate was added to the cold mixture over the course of 3 hours. The reaction was quenched with the addition of NH_4Cl (aq) (5 mL). The mixture was then diluted with water (30 mL) and extracted three times with ethyl acetate (30 mL). The combined organic fractions were dried over $MgSO_4$, filtered through a glass fritted funnel, then concentrated by rotary evaporation. The crude product was washed with acetone, then filtered. The dried product was collected as a grey solid of mass 1.9373 g, 67%.

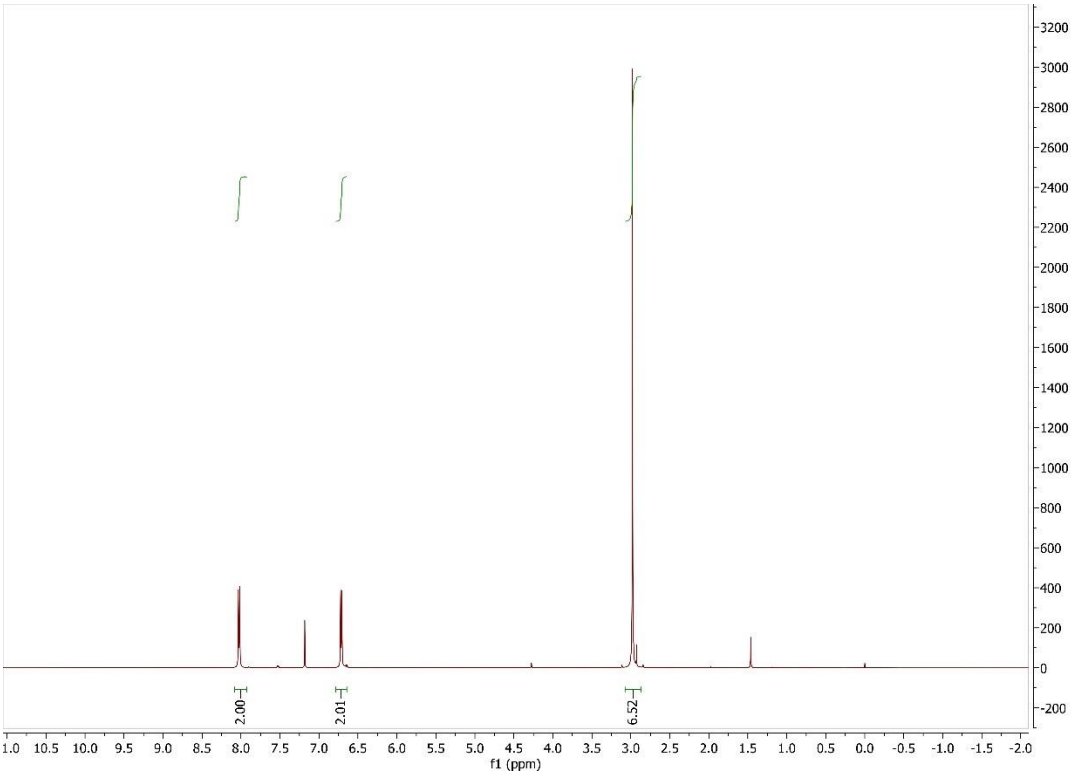

Figure 2.87 ^{1}H NMR spectrum of **2.8** in $CDCl_3$ at 400 MHz

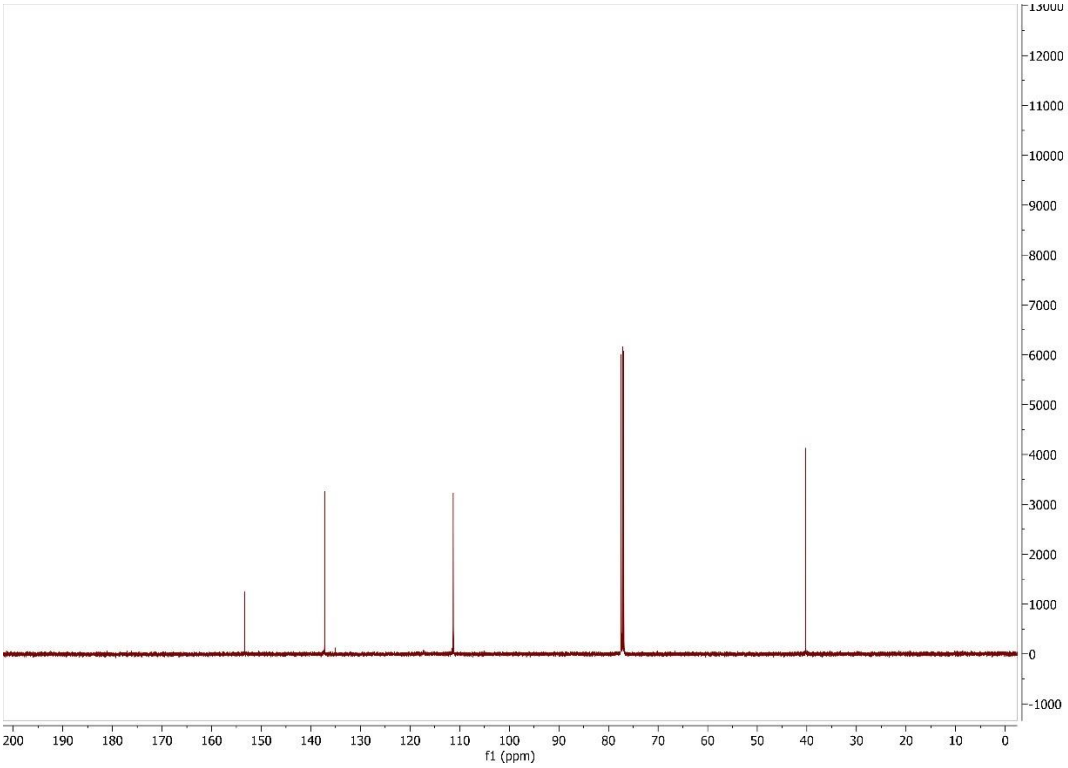

Figure 2.88 $^{13}C\{^{1}H\}$ NMR spectrum of **2.8** in $CDCl_3$ at 100 MHz

Synthesis of **2.9**

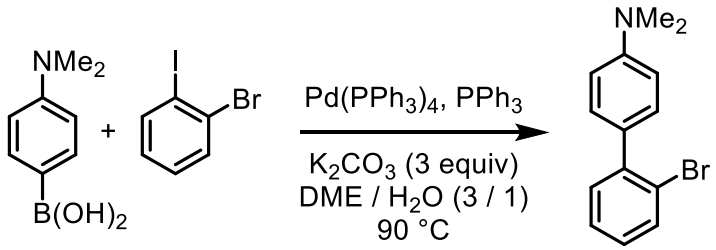

2.8 **2.9**

In a nitrogen filled glovebox, a pressure tube with side arm attachment was charged with **2.8** (503.9 mg, 3.05 mmol), 2-bromo-iodobenzene (780.5 mg, 2.76 mmol), potassium carbonate (1.1491 g, 8.313 mmol), dimethoxyethane (18 mL), water (6 mL), triphenylphosphine (39.3 mg, 0.1498 mmol) and $Pd(PPh_3)_4$ (163.6 mg, 0.142 mmol). The reaction vessel was sealed, removed from the glovebox, then placed in an oil bath heated to 90 °C for 34 hours. The reaction mixture

was cooled to room temperature, then diluted with water (30 mL). The mixture was then extracted with CH_2Cl_2 (25 mL) three times. The organic portions were combined, dried over $MgSO_4$, filtered through a glass fritted funnel, then concentrated by rotary evaporation. The resulting crude product was purified by column chromatography on silica gel. The mobile phase consisted of hexanes and ethyl acetate in a gradient mixture starting at pure hexanes and ending with 20% ethyl acetate and 80% hexanes. The product was collected in fractions 3-8 as a white solid of mass 299.7 mg, 30.3 % yield.

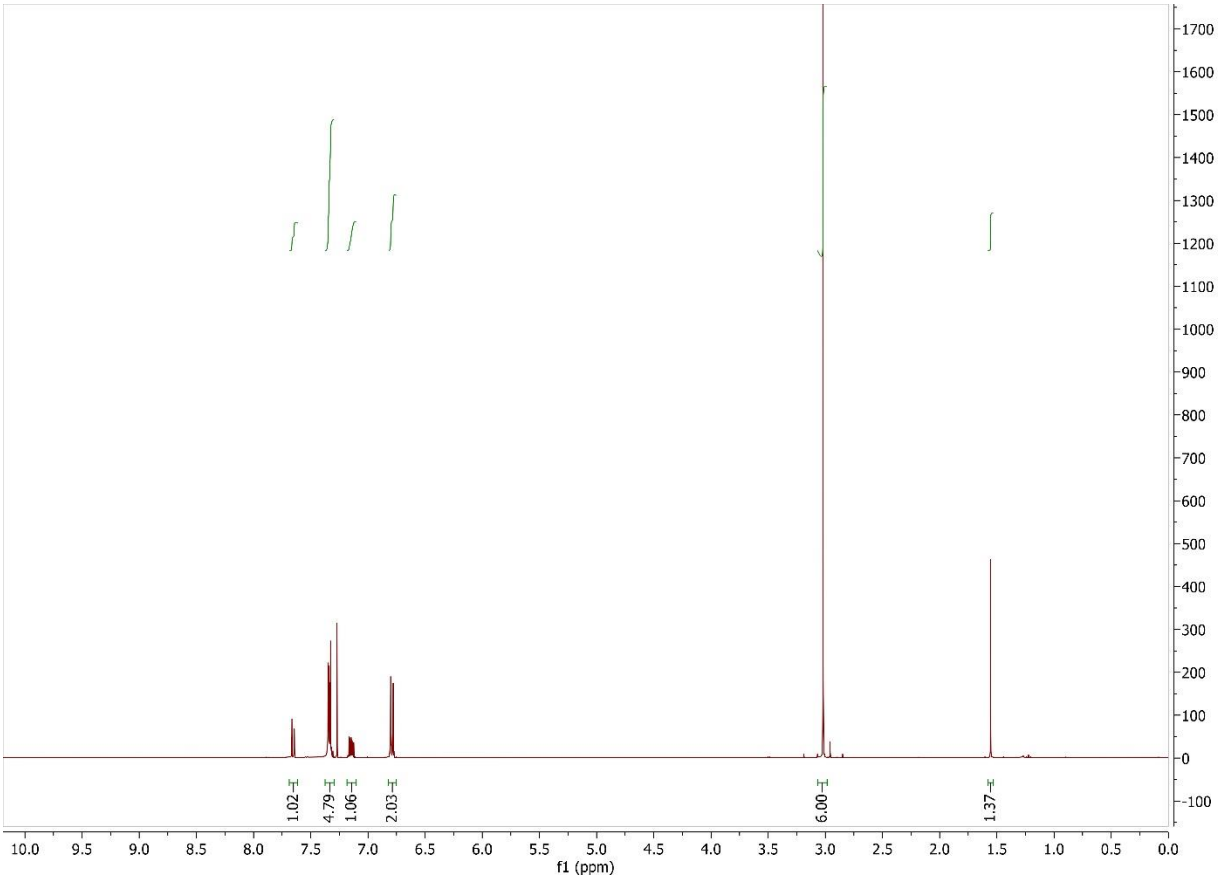

Figure 2.89 ^{1}H NMR spectrum of **2.9** in $CDCl_3$ at 400 MHz

Synthesis of **L10a**

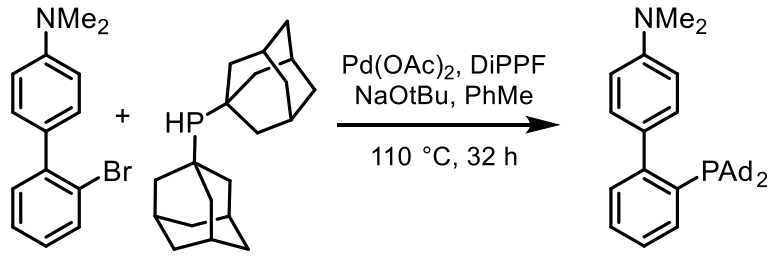

2.9 **L2.10a**

In a nitrogen filled glovebox, an oven dried scintillation vial was charged with $Pd(OAc)_2$ (27.1 mg, 0.121 mmol), DiPPF (53.3 mg, 0.127 mmol), and toluene (0.5 mL). The mixture was stirred at room temperature for 10 minutes. Next, the vial was charged with diadamantyl phosphine (399.1 mg, 1.392 mmol), sodium *tert*-butoxide (129.9 mg, 1.352 mmol), **2.9** (0.3021 mg, 1.094 mmol), and additional toluene (2.5 mL). A stir bar was added, the vial sealed, removed from the glovebox, then placed in an oil bath heated to 110 °C for 32 hours. After consumption of diadamantyl phosphine was confirmed by ^{31}P NMR, the reaction was no longer heated. Purification of the crude product was conducted by directly loading the reaction mixture onto silica. The mobile phase consisted of hexanes and ethyl acetate that were sparged with nitrogen gas before use. The product was collected in fractions 12-15 as a mass of 309.6 mg, 56%.

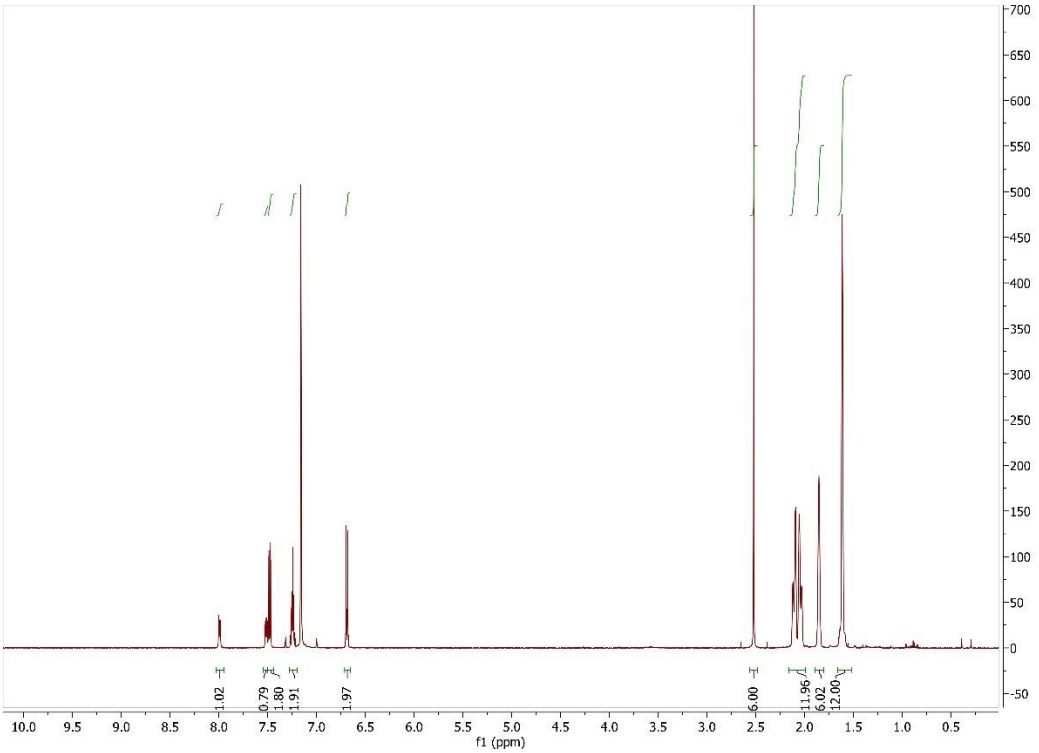

Figure 2.90 ^{1}H NMR spectrum of **L2.10a** in C_6D_6 at 500 MHz

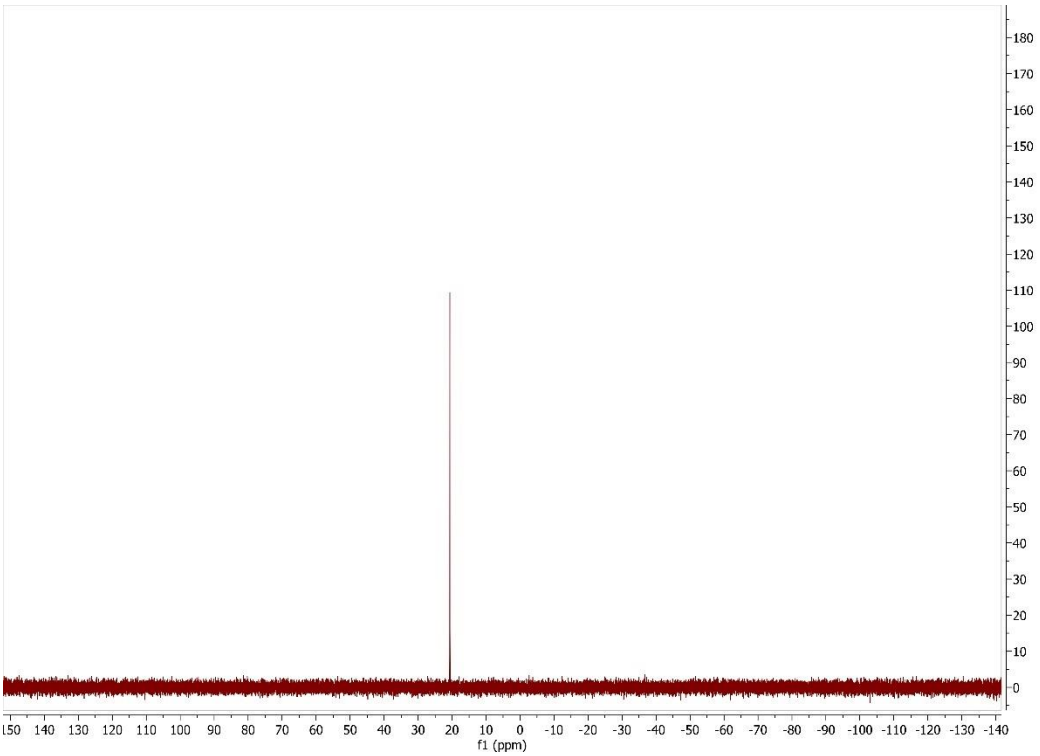

Figure 2.91 ^{31}P NMR spectrum of **L2.10a** in C_6D_6 at 202 MHz

Synthesis of **2.27**

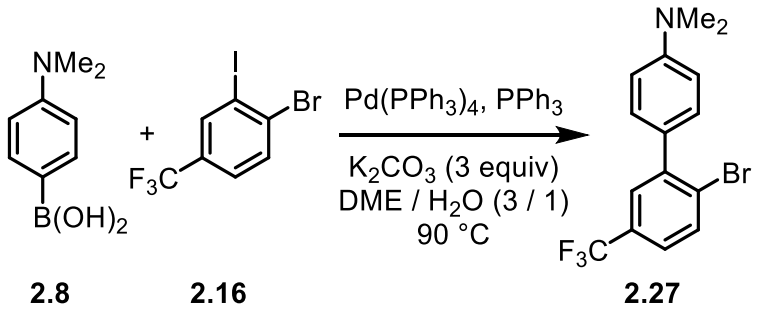

2.8 **2.16** **2.27**

In a nitrogen filled glovebox, a pressure tube with side arm attachment was charged with **2.8** (522.4 mg, 3.16 mmol), 1-bromo-2-iodo-4-trifluoromethylbenzene (1.0070 g, 2.87 mmol), potassium carbonate (1.3196 g, 9.548 mmol), dimethoxyethane (18 mL), water (6 mL), triphenylphosphine (42.0 mg, 0.160 mmol) and $Pd(PPh_3)_4$ (189.8 mg, 0.164 mmol). The reaction vessel was sealed, removed from the glovebox, then placed in an oil bath heated to 90 °C for 40 hours. The reaction mixture was cooled to room temperature, then diluted with water (30 mL). The mixture was then extracted with CH_2Cl_2 (25 mL) three times. The organic portions were combined, dried over $MgSO_4$, filtered through a glass fritted funnel, then concentrated by rotary evaporation. The resulting crude product was purified by column chromatography on silica gel. The mobile phase consisted of hexanes and ethyl acetate in a gradient mixture starting at pure hexanes and ending with 20% ethyl acetate and 80% hexanes. The product was collected in fractions 3-6 as a white solid of mass 404.9 mg, 41% yield.

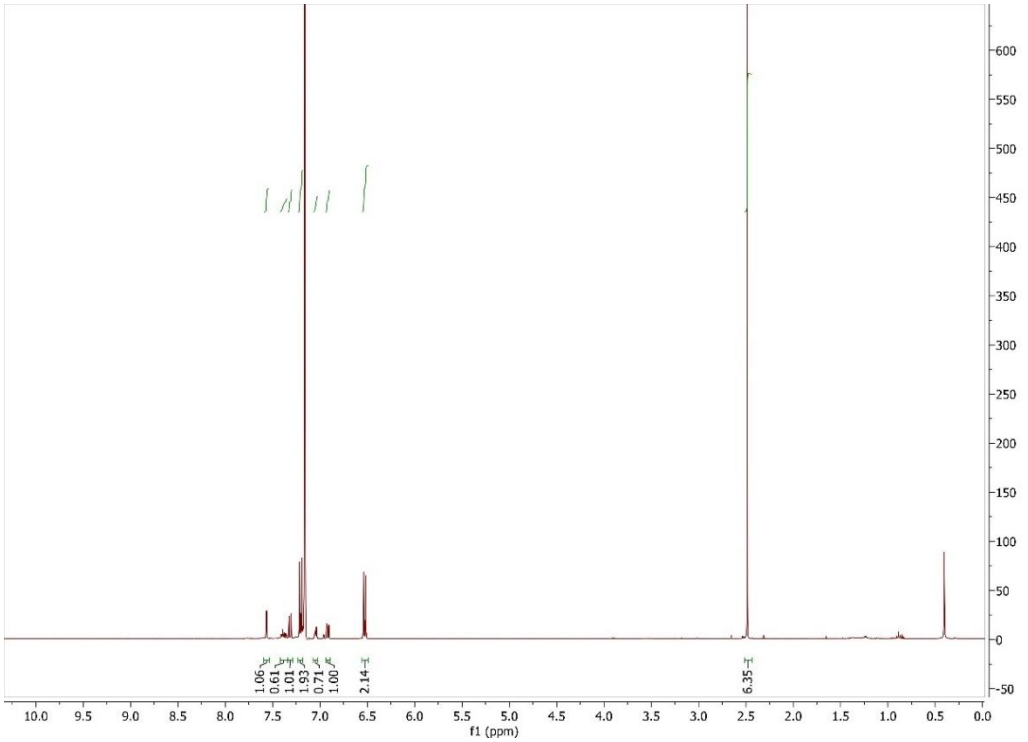

Figure 2.92 ^{1}H NMR spectrum of **2.27** in C_6D_6 at 400 MHz

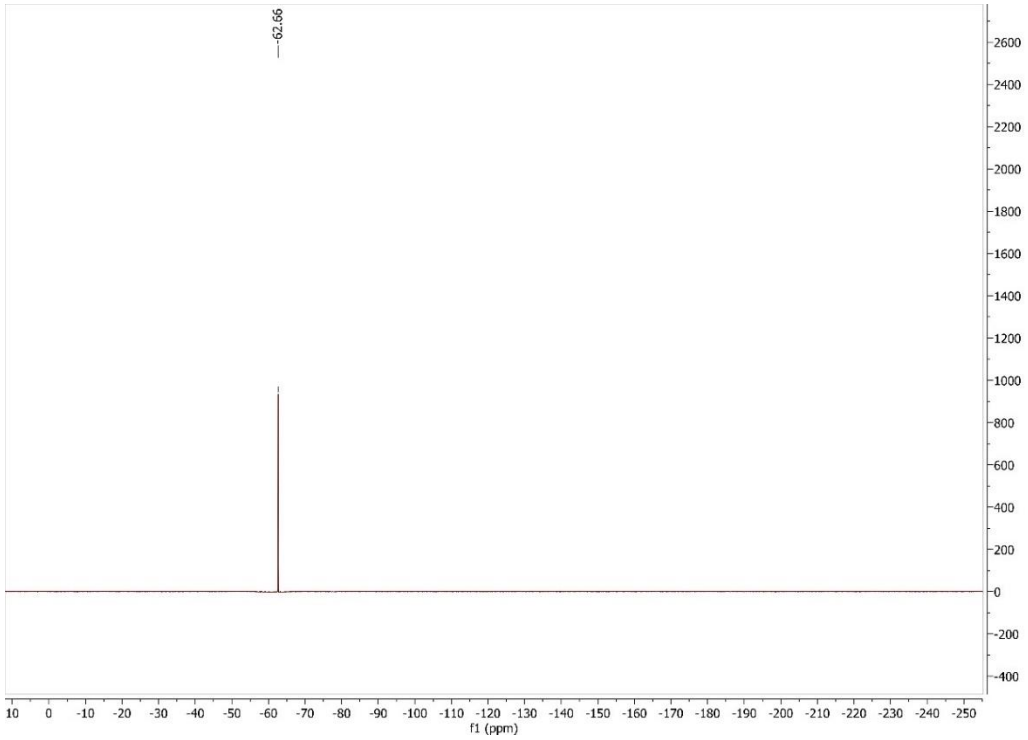

Figure 2.93 ^{19}F NMR spectrum of **2.27** in C_6D_6 at 376 MHz

Synthesis of **L2.11a**

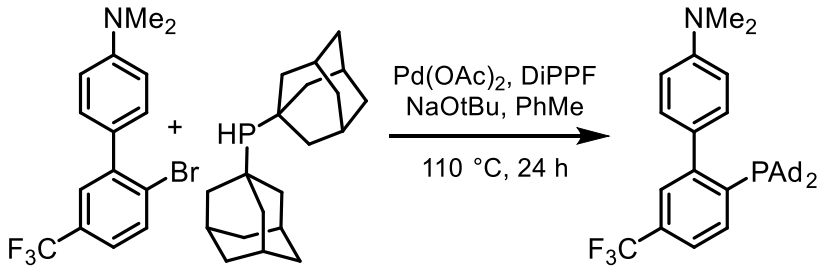

2.27 **L2.11a**

In a nitrogen filled glovebox, an oven dried scintillation vial was charged with **2.**27 (397.9 mg, 1.170 mmol), diadamanyl phosphine (426.1 mg, 1.409 mmol), DiPPF (59.1 mg, 0.141 mmol), NaOtBu (134.5 mg, 1.399 mmol), $Pd(OAc)_2$ (26.8 mg, 0.119 mmol), and toluene (3 mL). A stir bar was added to the mixture, the vial sealed and removed from the glovebox, then placed in an oil bath heated to 110 °C for 24 hours. The reaction progress was assessed by ^{31}P NMR for consumption of diadamantyl phosphine. The reaction was purified by column chromatography on silica gel. The reaction mixture was directly loaded onto the column. The mobile phase consisted of hexanes and ethyl acetate that were sparged with nitrogen before use. The product was collected in fractions 1-4. The product was then crystallized from a concentrated solution of CH_2Cl_2 that was stored in a freezer at -40 °C. The product was collected as the crystallized solid for a mass of 85.4 mg, 13%.

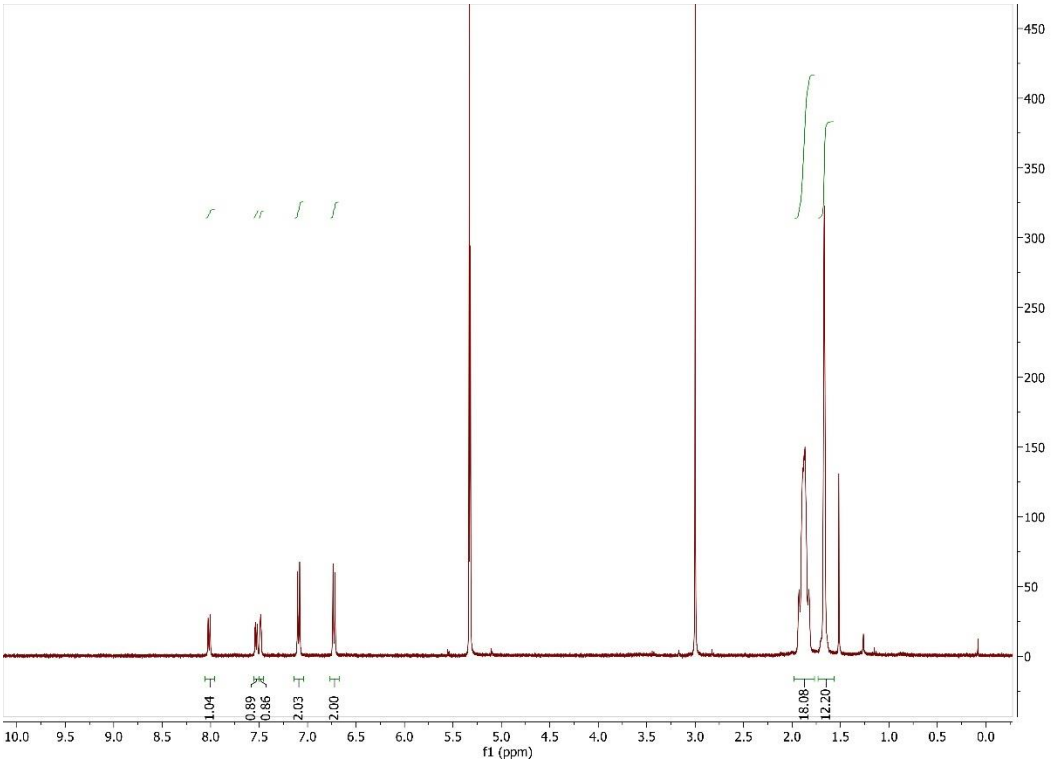

Figure 2.94 ^{1}H NMR spectrum of **L2.11a** in CD_2Cl_2 at 400 MHz

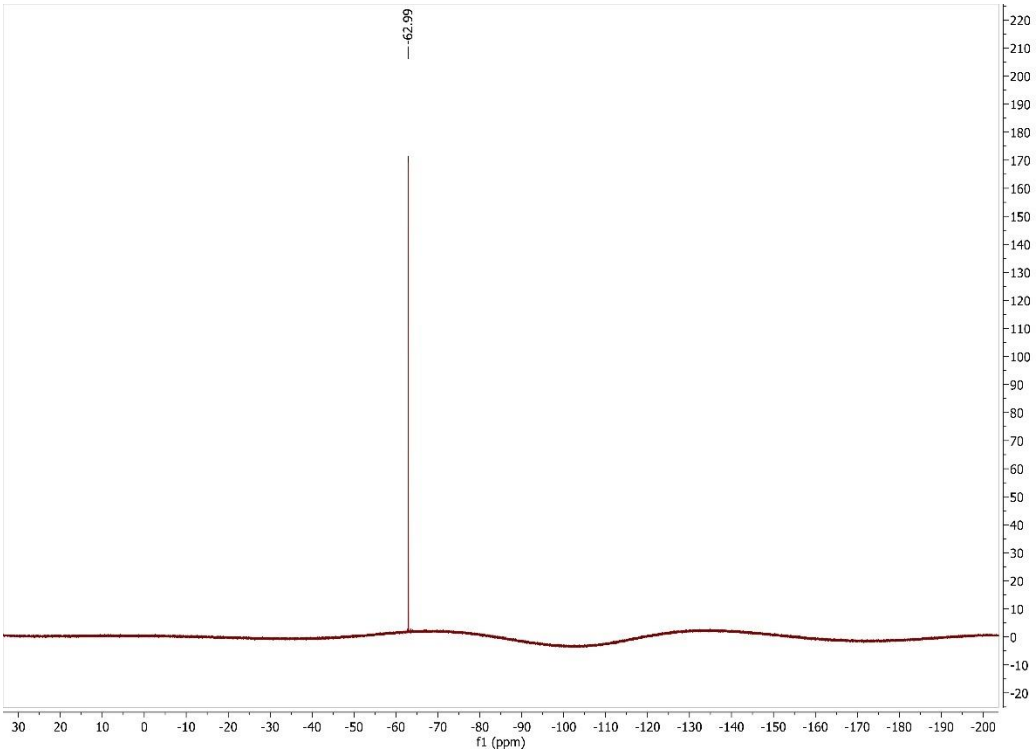

Figure 2.95 ^{19}F NMR spectrum of **L2.11a** in CD_2Cl_2 at 376 MHz

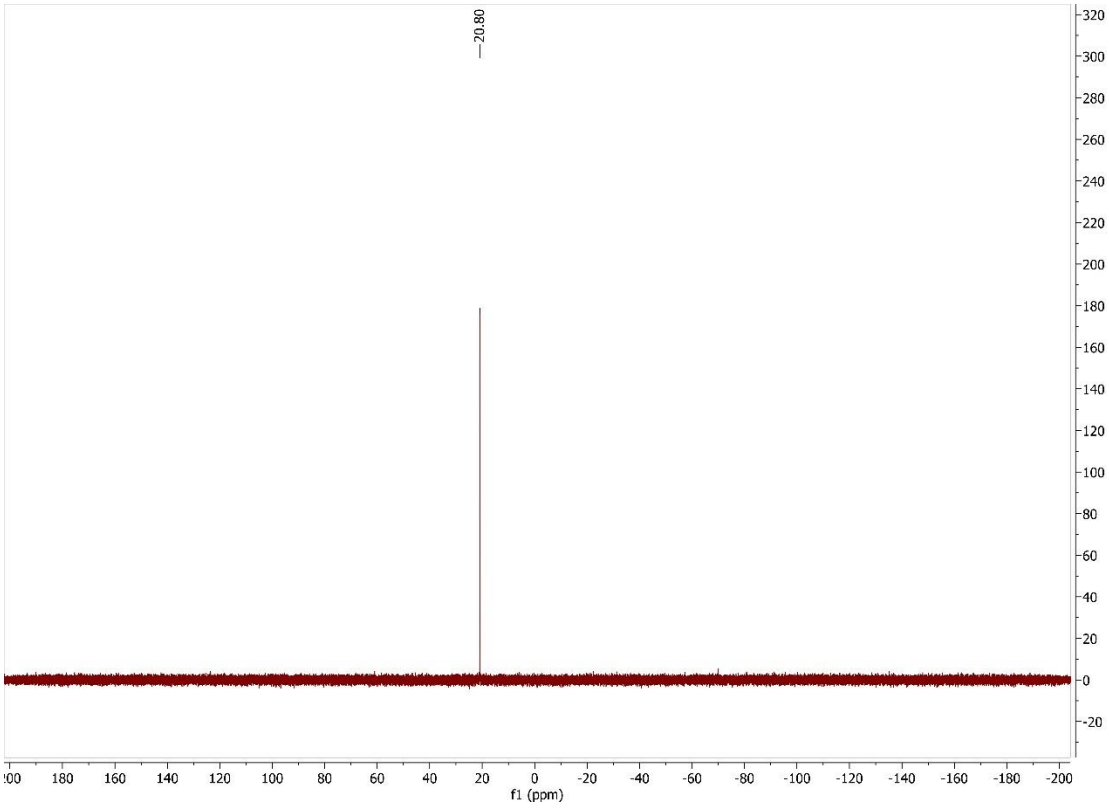

Figure 2.96 ^{31}P NMR spectrum of **L2.11a** in CD_2Cl_2 at 162 MHz

Synthesis of **2.28**

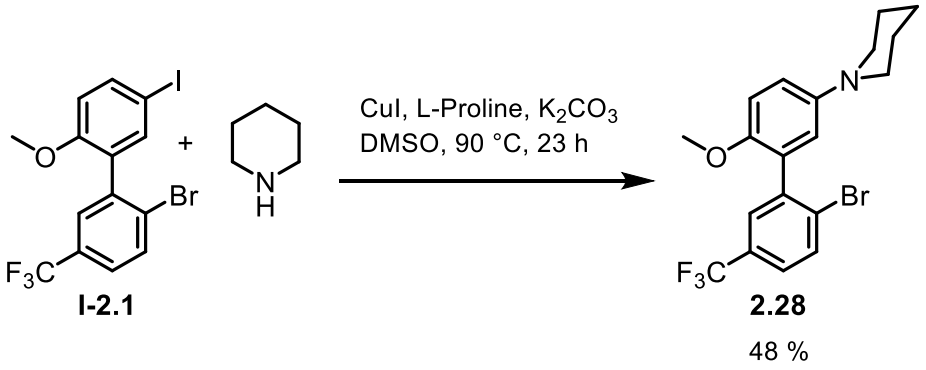

In a nitrogen filled glovebox, a 3-neck round bottom flask was charged with I-2.1 (303.1 mg, 0.664 mmol), L-proline (15.6 mg, 0.139 mmol), potassium acetate (193.1 mg, 0.135 mmol), copper(I) iodide (17.5 mg, 0.0918 mmol), piperidine (116.7, 1.371 mmol), and DMSO (10 mL).The flask was completely sealed using rubber septa, then a water cooled condenser was

attached to the reaction flask flow of positive pressure of nitrogen gas was added via Schlenk line. The reaction was heated at 90 °C for 24 hours. The reaction was quenched with the addition of water (10 mL), then the mixture was extracted with ethyl acetate (10 mL) three times. The combined organic phases were dried over $MgSO_4$, filtered through a glass fritted funnel, and concentrated under reduced pressure. The crude product was further purified by crystallization from a cold and concentrated methanol solution.

^{1}H NMR (C_6D_6, 500 MHz): δ 7.57 (s, 1H), 7.31 (s, 1H), 6.95 (d, *J* = 8.2, 1H), 6.86 (dd, *J* = 8.8, 2.7, 1H), 6.74 (d, *J* = 3.3, 1H), 6.63 (d, *J* = 8.8, 1H), 3.28 (s, 3H), 2.84 (m, 4H), 1.51 (p, *J* = 5.8, 4H), 1.31 (m, 2H).

Synthesis of **2.29**

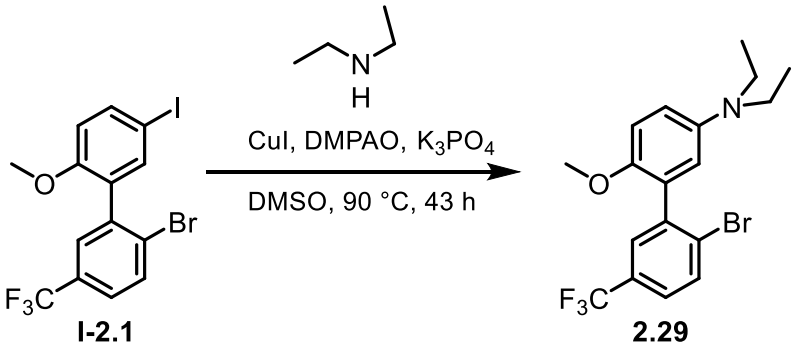

I-2.1 **2.29**

55 %

In a nitrogen filled glovebox, an- oven dried scintillation vial was charged with **I-2.1**(250.0 mg, 0.547 mmol), copper iodide (17.6 mg, 0.092 mmol), 2-(2,6-dimethylphenylamino)-2-oxo-acetic acid (22.7 mg, 0.118 mmol), potassium phosphate (241.2 mg, 1.136 mmol), dimethylamine (74.0 mg, 1.012 mmol), and DMSO (1 mL). The vial was sealed, removed from the glovebox, and heated at 90 °C for 24 hours. The reaction was then removed from the oil bath, cooled to room temperature, and quenched with the addition of water (5 mL). The mixture was then extracted

three times with ethyl acetate (10 mL). The combined organic fractions were dried over Na_2SO_4, filtered through a glass fritted funnel, then concentrated by rotary evaporation. The crude product was then purified by column chromatography on silica gel, eluting with hexanes and ethyl acetate. The product was collected in fractions 6-9 for a mass of 120.5 mg, 54.7%.

^{1}H NMR ($CDCl_3$, 400 MHz): δ 7.77 (d, *J* = 8.1, 1H), 7.58 (s, 1H), 7.43 (d, *J* = 8.5, 1H), 6.91 (m, 1H), 6.77 (m, 1H), 6.55 (s, 1H), 3.71 (s, 3H), 3.29 (br, 4H), 1.14 (t, *J* = 6.9, 6H)

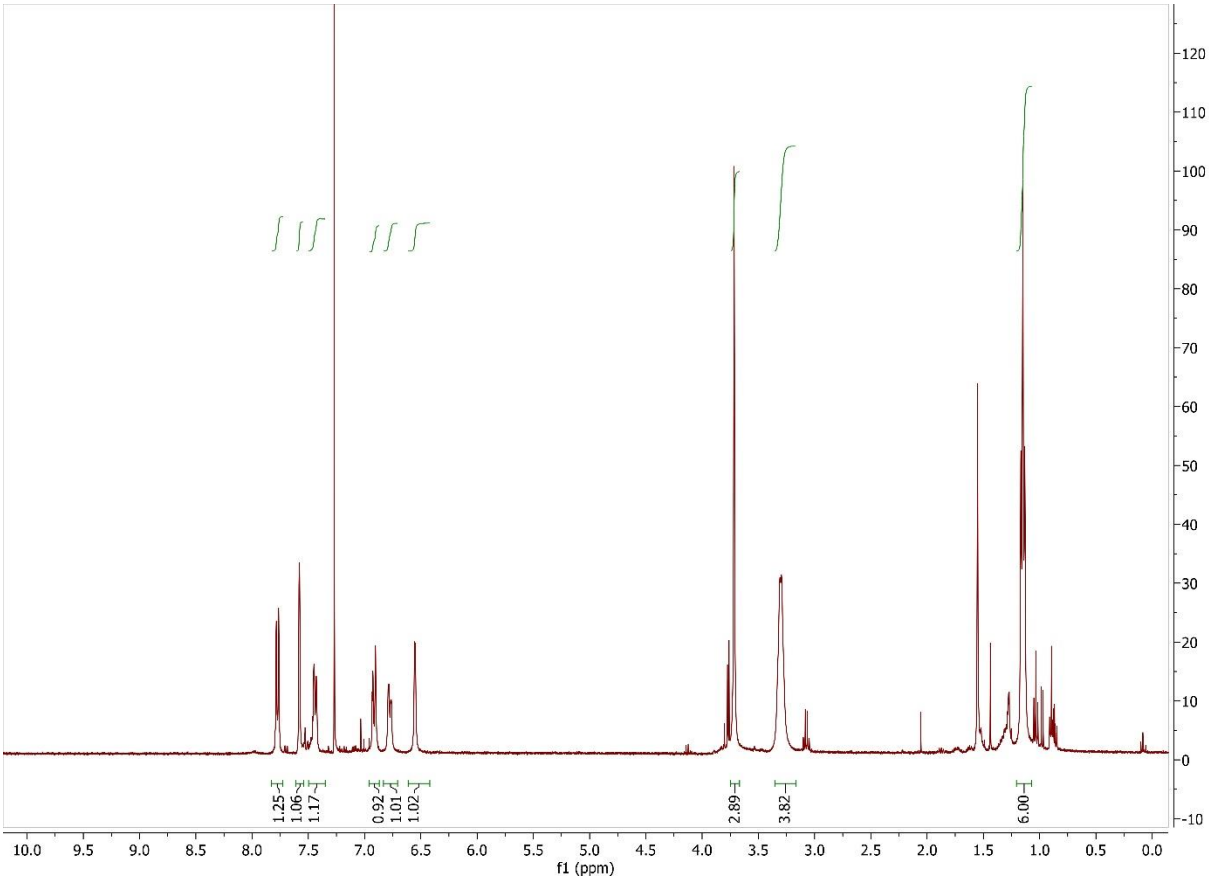

Figure 2.97 ^{1}H NMR spectrum of **2.29** in $CDCl_3$ at 400 MHz

Synthesis of phosphine gold (I) chloride complexes

Synthesis of **Au2.1a**

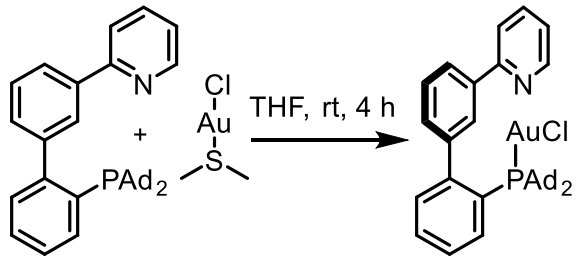

L2.1a **Au2.1a**

In a nitrogen filled glovebox, a scintillation vial was charged with **L2.1a** (43.8 mg, 0.0824 mmol) and CH_2Cl_2 (2.5 mL). A separate scintillation vial was charged with chloro(dimethylsulfide)gold(I) (24.4 mg, 0.0828 mmol) and stir bar, and then the **L2.1a** solution was added by pipette. The mixture was stirred at room temperature for 2 hours. The mixture was then sampled and added to an NMR tube with $CDCl_3$. Observation of the ^{31}P NMR spectrum reveals the full consumption of the free phosphine at δ 21.01 ppm and appearance of the gold complex at δ 61.55 ppm. The reaction mixture was then filted through a small pad of celite 545 in a glass fritted funnel, concentration under reduced pressure to yield the desired complex as a white solid with mass 67.9 mg, quantitative.

^1H NMR ($CDCl_3$, 400 MHz): δ 8.65 – 8.57 (m, 1H), 8.05 – 7.96 (m, 1H), 7.96 – 7.80 (m, 2H), 7.76 (t, *J* = 7.2, 1H), 7.57 – 7.47 (m, 3H), 7.42 (br, 1H), 7.24 - 7.11 (m, 1H), 2.27 – 1.87 (m, 18H), 1.67 (br, 12H)

^{13}C NMR ($CDCl_3$, 100 MHz): δ 157.96, 150.64 (d, *J* = 2.9), 149.46, 143.02 (d, *J* = 6.5), 139.82, 137.02, 134.56 (d, *J* = 2.5), 133.79 (d, *J* = 7.3), 129.75, 128.92, 128.31, 127.16, 126.44 (d, *J* =

6.5), 124.36, 123.93, 122.26, 121.97, 42.86 (d, *J* = 12.5), 42.63 (d, *J* = 12.7), 42.32 (d, *J* = 14.4), 42.30 (d, *J* = 14.4), 36.44 (d, *J* = 3.8), 28.78 (dd, *J* = 9.9), 28.76 (dd, *J* = 9.9)

^{31}P NMR ($CDCl_3$, 162 MHz): δ 61.55 (s)

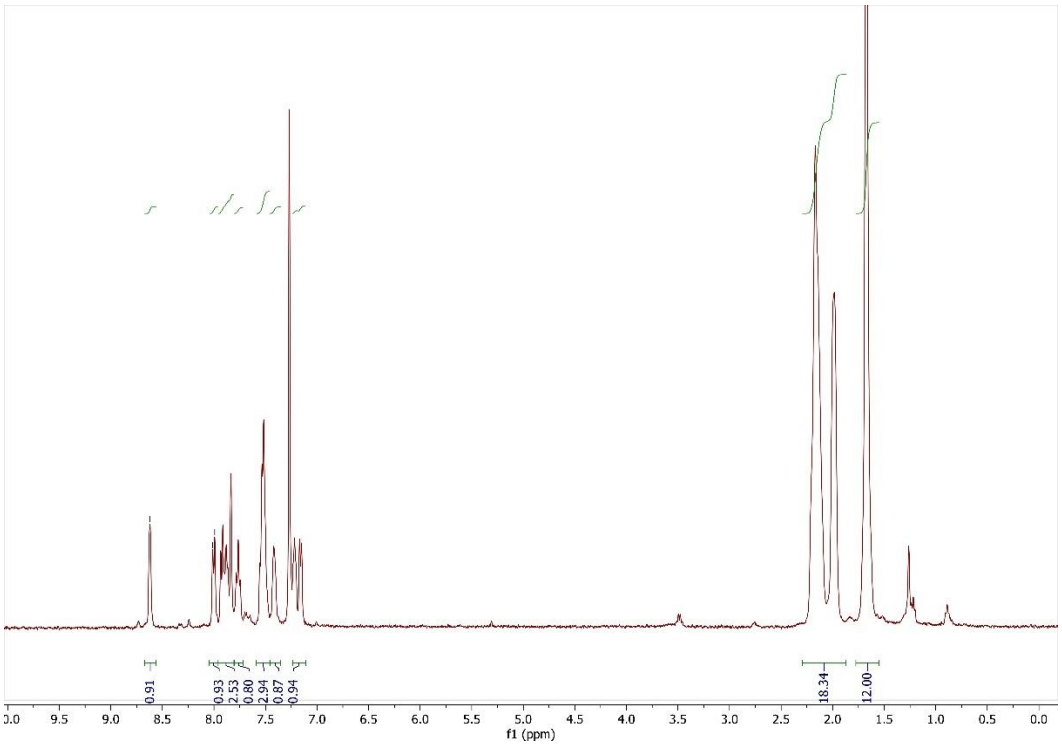

Figure 2.98 ^{1}H NMR spectrum of **Au2.1a** in $CDCl_3$ at 400 MHz

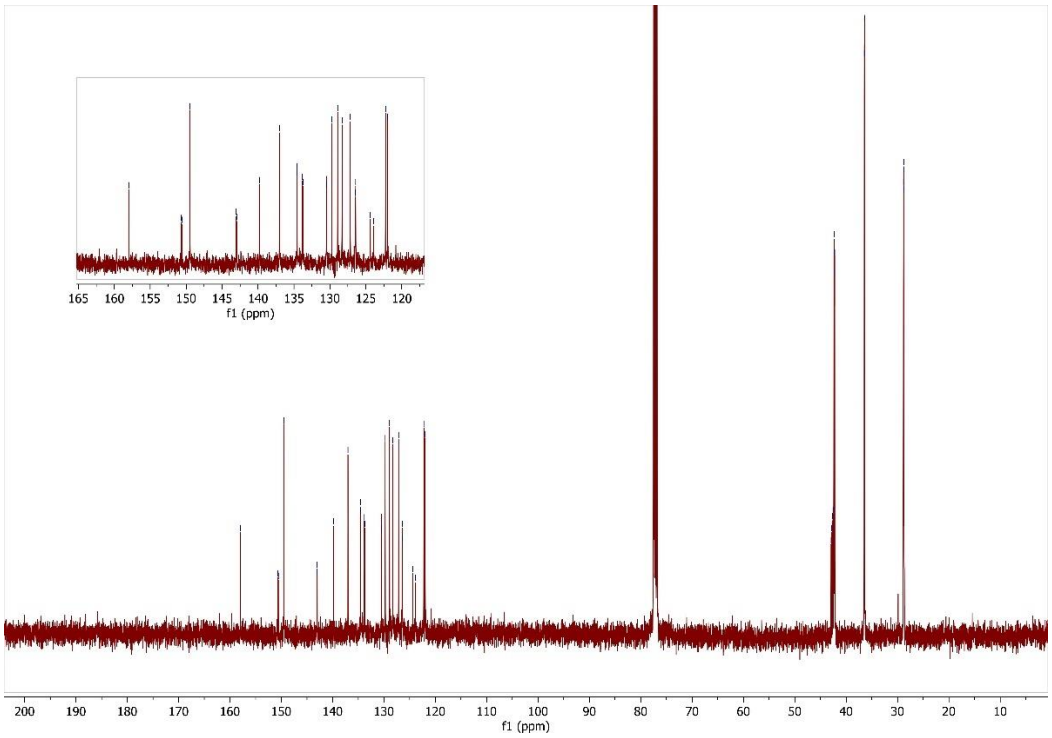

Figure 2.99 $^{13}C\{^{1}H\}$ NMR spectrum of **Au2.1a** in $CDCl_3$ at 100 MHz

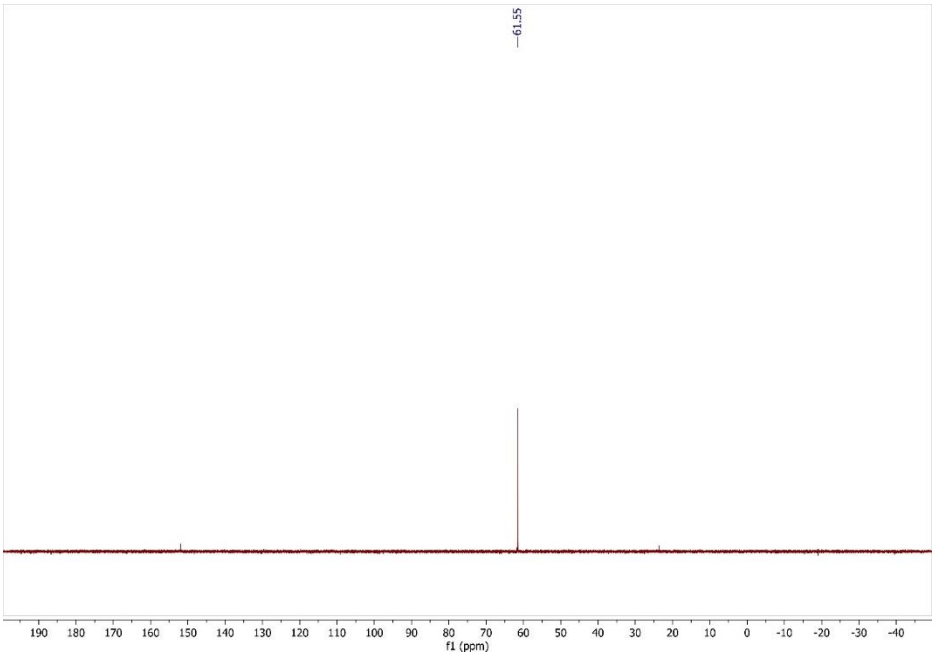

Figure 2.100 ^{31}P NMR spectrum of **Au2.1a** in $CDCl_3$ at 162 MHz

Synthesis of **Au2.2a**

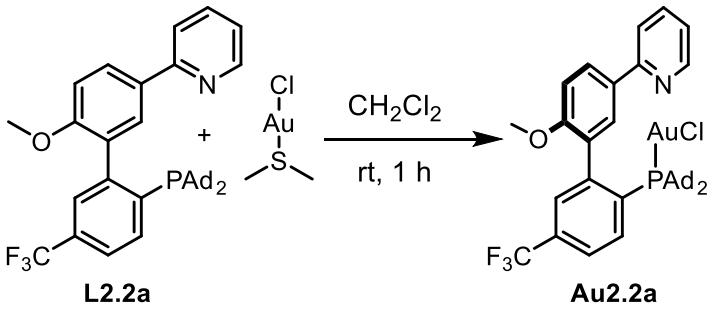

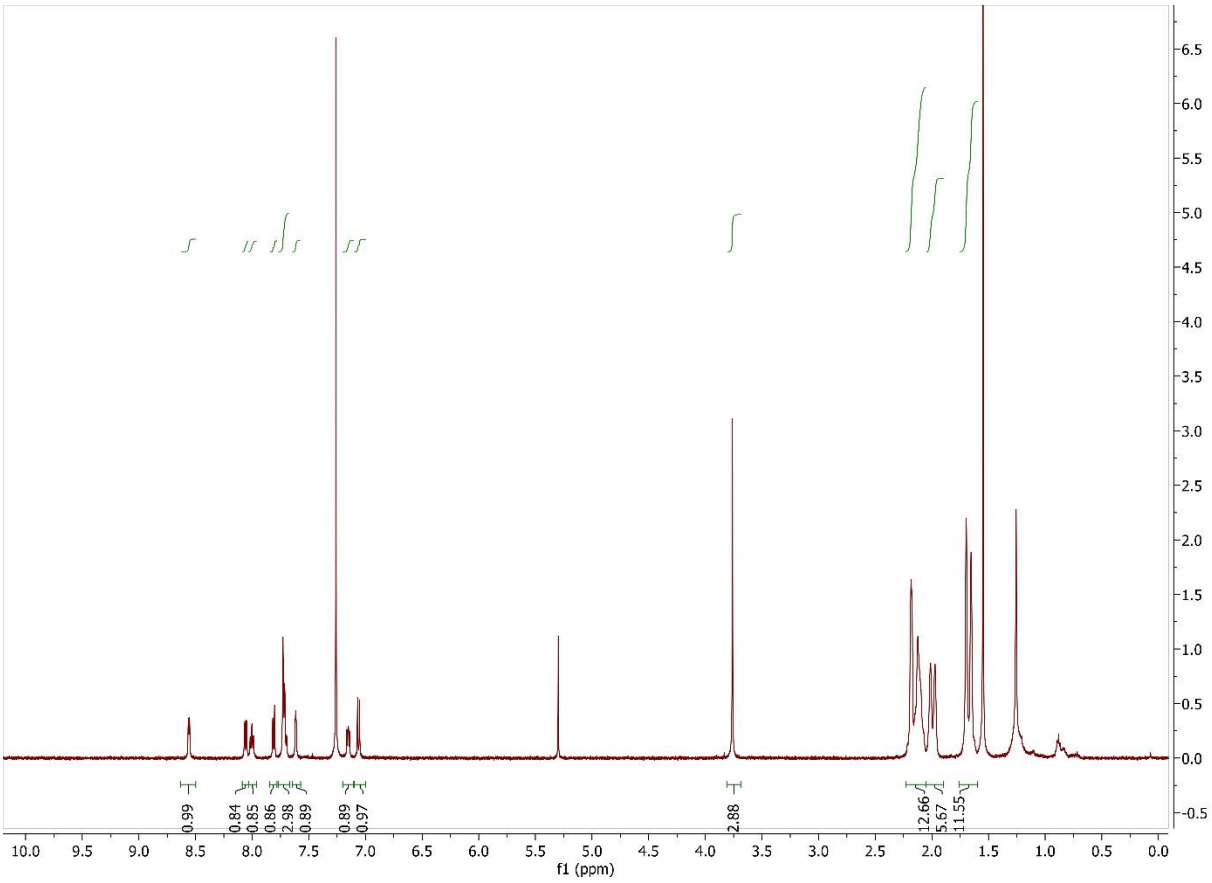

Figure 2.101 ^{1}H NMR spectrum of **Au2.2a** in $CDCl_3$ at 500 MHz

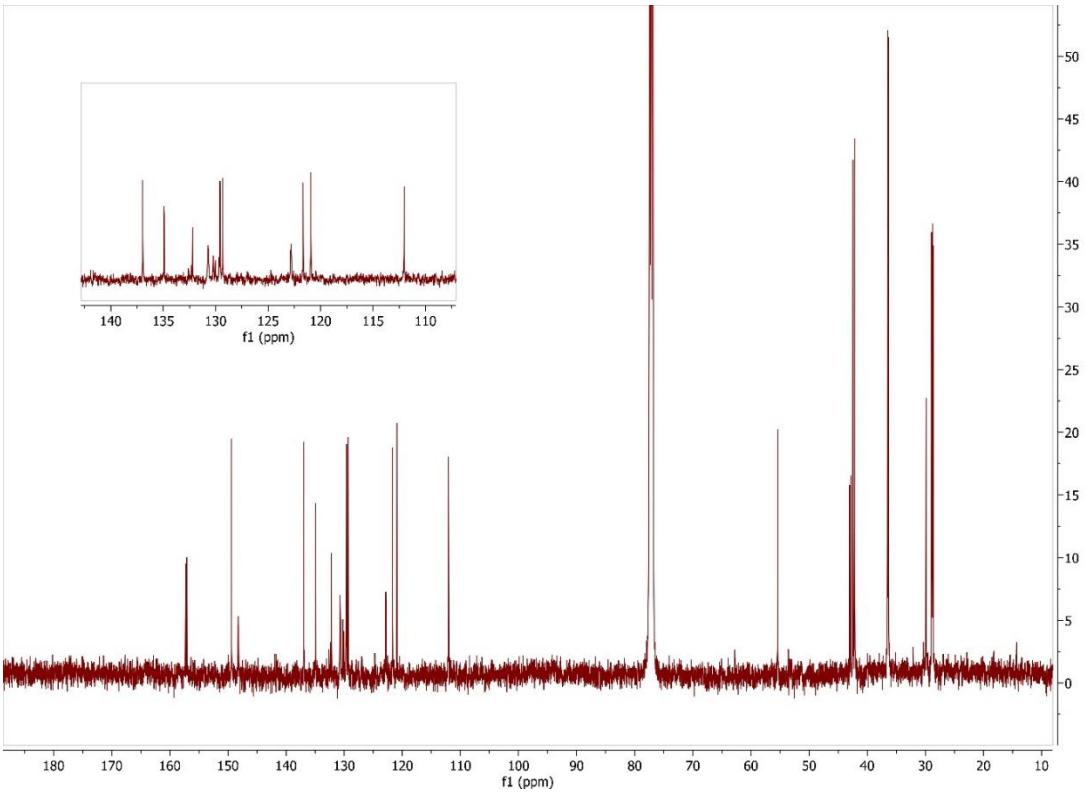

Figure 2.102 $^{13}C\{^{1}H\}$ NMR spectrum of **Au2.2a** in $CDCl_3$ at 125 MHz

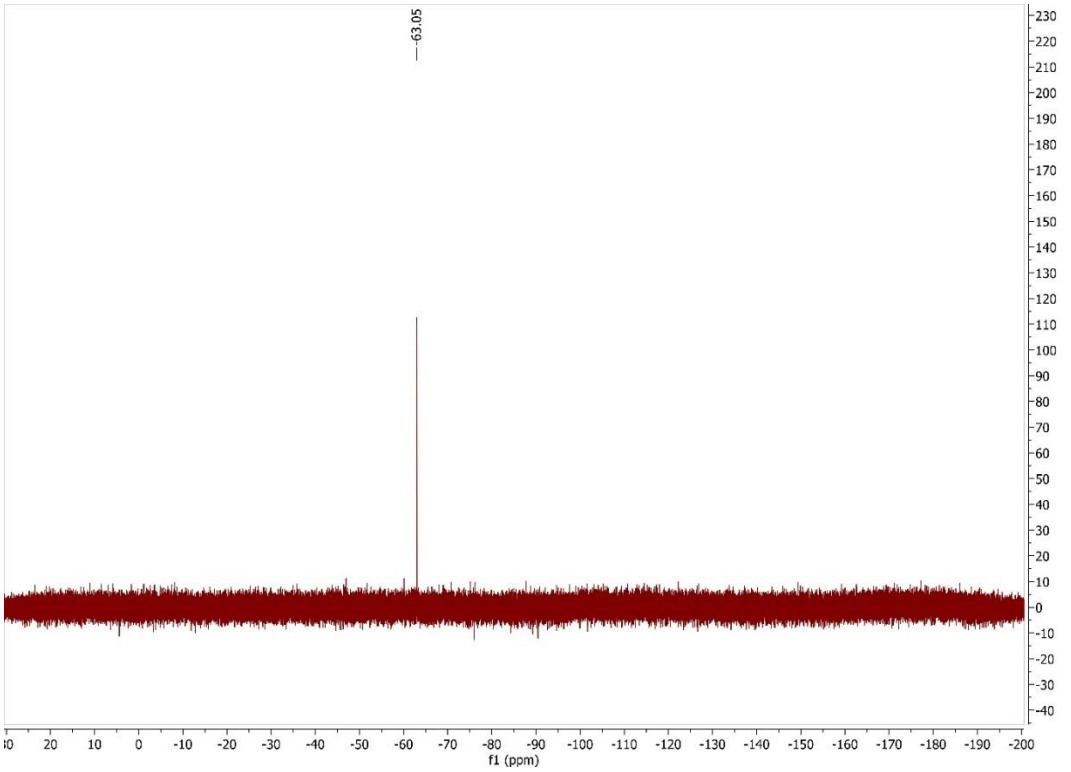

Figure 2.103 ^{19}F NMR spectrum of **Au2.2a** in $CDCl_3$ at 470 MHz

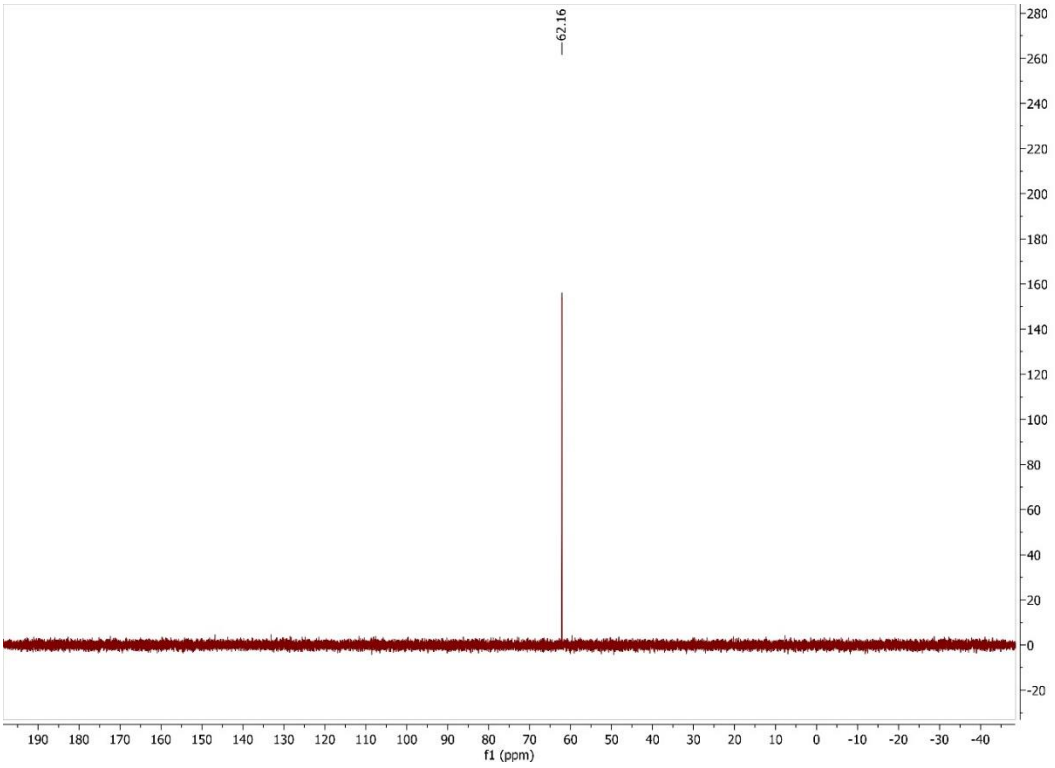

Figure 2.104 ^{31}P NMR spectrum of **Au2.2a** in $CDCl_3$ at 470 MHz

Synthesis of **Au2.2b**

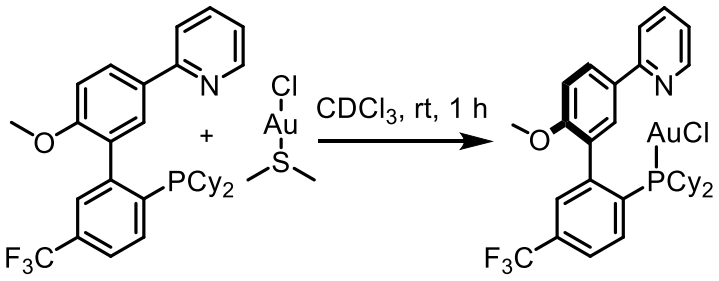

L2.2b **Au2.2b**

In a nitrogen filled glovebox, a scintillation vial was charge with chloro(dimethylsulfide)gold(I) (8.7 mg, 29.7 µmol), L2.2b (15.6 mg, 29.7 µmol), and $CDCl_3$. The reaction mixture was stirred for 1 hour, then the reaction progressed was observed with NMR spectroscopy. Volatile components were removed under reduced pressure. The product was collected as an off-white solid of mass 40.0 mg, 81%.

^{1}H NMR ($CDCl_3$, 400 MHz): δ 859 (ddd, *J* = 4.8, 1.8, 1.0, 1H), 8.06 (dd, *J* = 8.7, 2.3, 1H), 7.86 – 7.69 (m, 5H), 7.62 (s, 1H), 7.18 (dd, *J* = 7.4, 5.4, 1H), 7.09 (d, *J* = 8.8, 1H), 3.81 (s, 3H), 2.35 – 1.48 (m, 14H), 1.43 – 1.03 (8H). Residual CH_2Cl_2 is observed at δ 5.30.

^{31}P NMR ($CDCl_3$, 162 MHz): δ 41.60

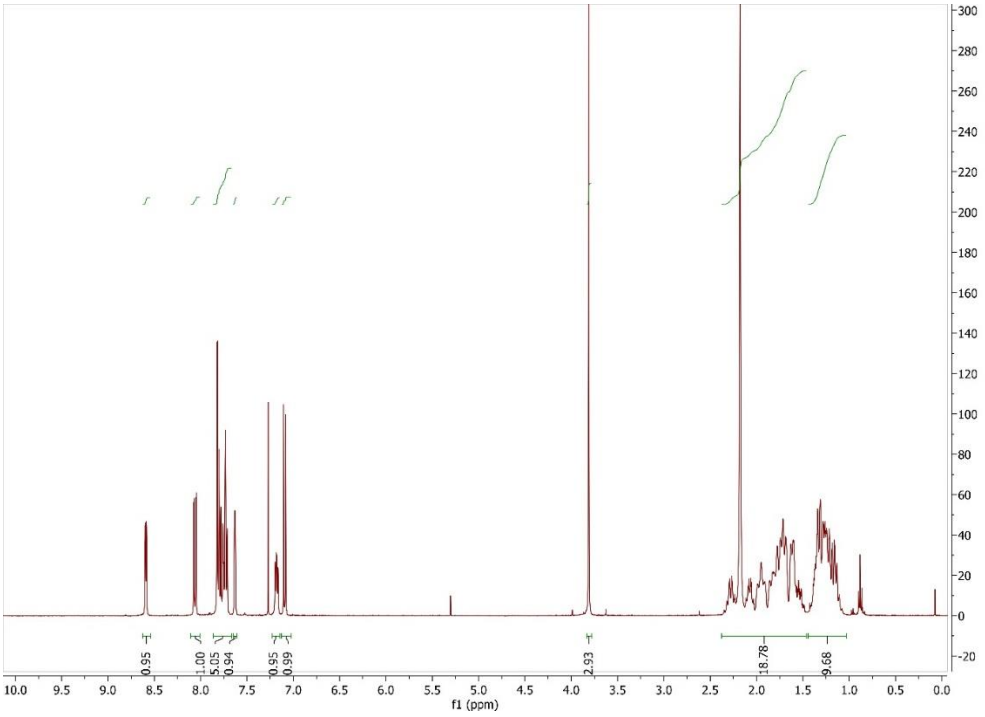

Figure 2.105 ^{1}H NMR spectrum of **Au2.2b** in $CDCl_3$ at 400 MHz

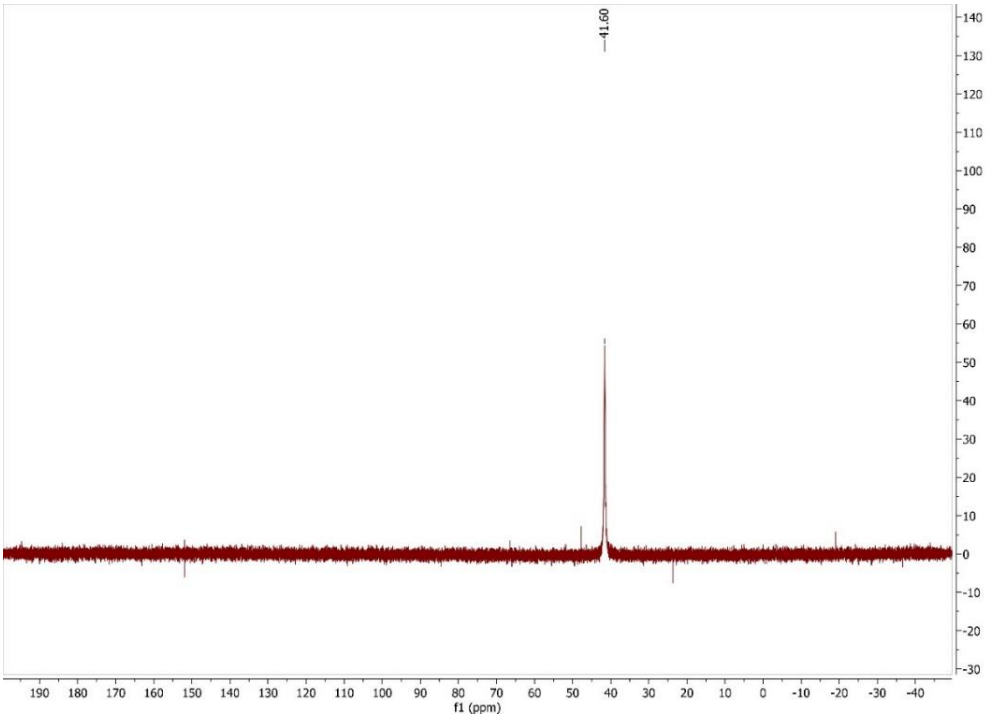

Figure 2.106 ^{31}P NMR spectrum of **Au2.2b** in $CDCl_3$ at 162 MHz

Synthesis of **Au2.2c**

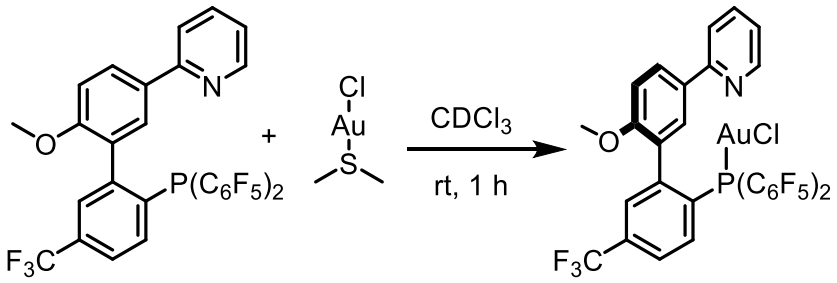

In a nitrogen filled glovebox, a scintillation vial was charged with dimethylsulfide gold (I) chloride (17.8 mg, 60.4 µmol), bs309 (43.0 mg, 62.0 µmol), and $CDCl_3$ (0.7 mL) and magnetic stir bar. The mixture was stirred for 1 hour, and reaction progress monitored by NMR. The mixture was then filtered through a small pad of celite on a glass fritted funnel, and the filtrate concentrated under reduced pressure. The title compound was isolated as an off-white solid of mass 34.8 mg, 62.3%.

^{1}H NMR ($CDCl_3$, 500 MHz): δ 8.45 (d, *J* = 4.2, 1H), 8.04 (dd, *J* = 8.6, 1.6, 1H), 7.80 (m, 5H), 7.42 (s, br, 1H) 7.20 (br, maybe t, 1H), 7.14 (d, *J* = 8.7, 1H), 3.89 (s, 3H)

^{19}F NMR: δ ($CDCl_3$, 470 MHz): δ -63.27 (s), -125.76 (d, *J* = 400.1), -143.14 (dt, *J* = 174.0, 21.4), -157.11 (dt, *J* = 371.3, 19.1 Hz)

^{31}P NMR ($CDCl_3$, 202 MHz): δ -17.04

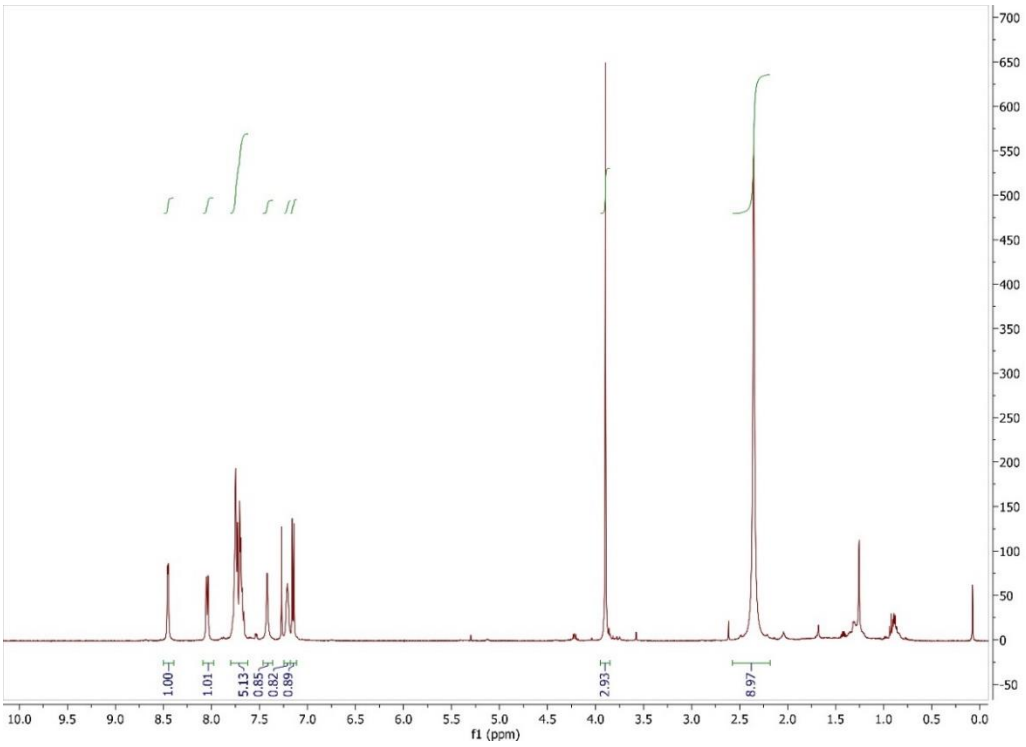

Figure 2.[107] ^{1}H NMR spectrum of **Au2.2c** in $CDCl_3$ at 500 MHz

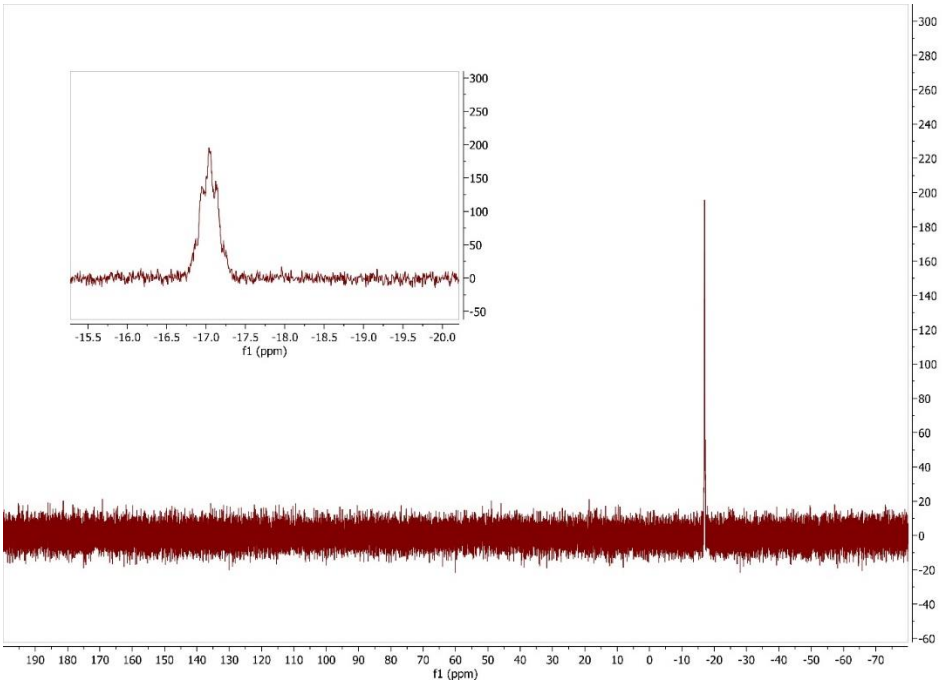

Figure 2.108 ^{31}P NMR spectrum of **Au2.2c** in $CDCl_3$ at 202 MHz

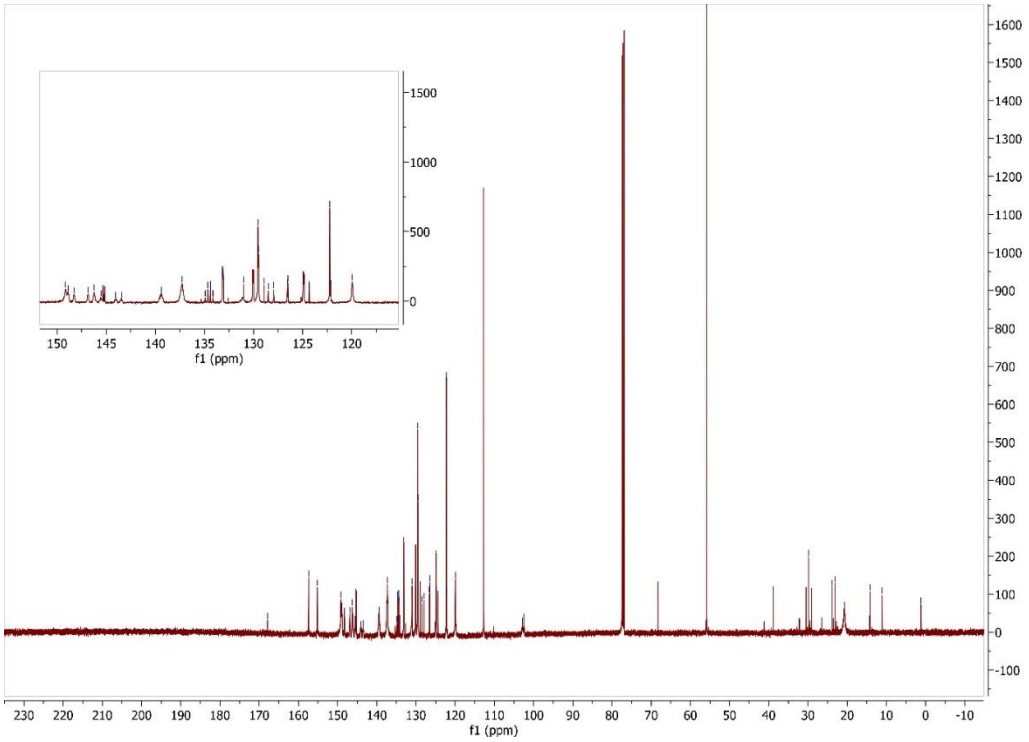

Figure 2.109 $^{13}C\{^{1}H\}$ NMR spectrum of **Au2.2c** in $CDCl_3$ at 125 MHz

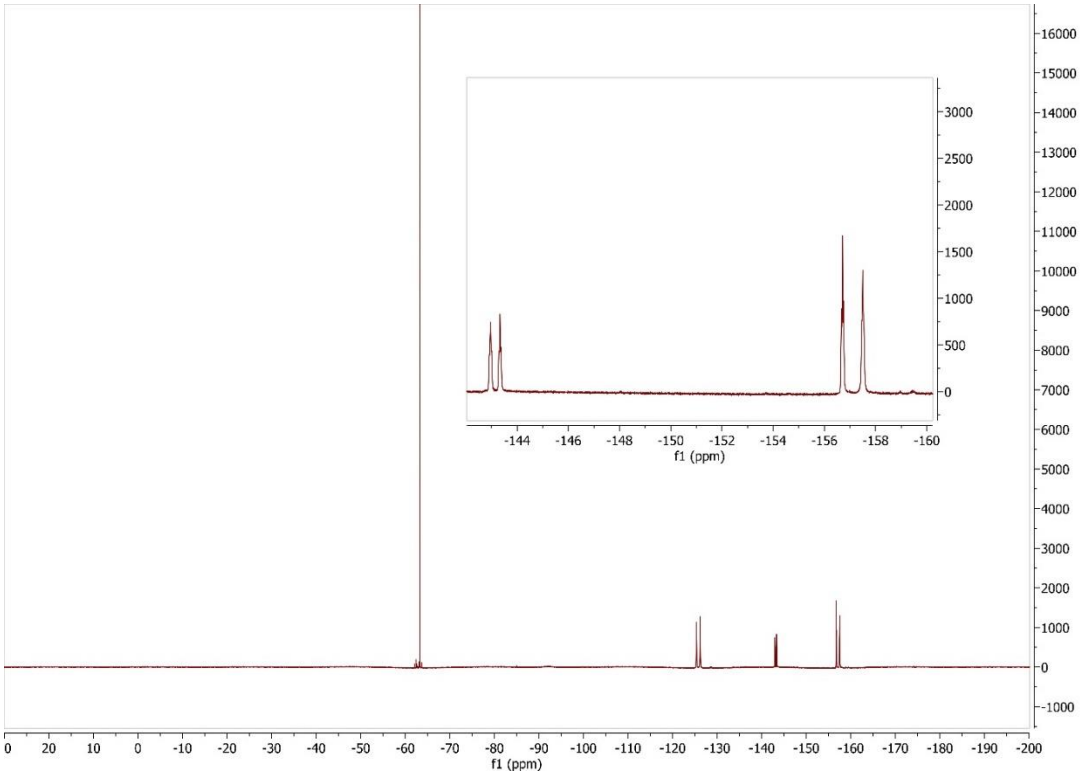

Figure 2.110 ^{19}F NMR spectrum of **Au2.2c** in $CDCl_3$ at 470 MHz

Synthesis of **Au2.3a**

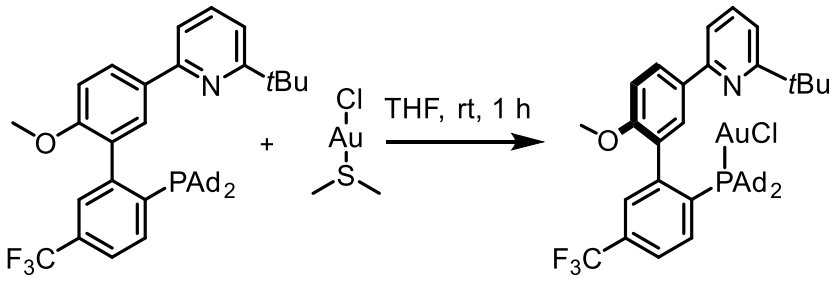

L2.3a **Au2.3a**

In a nitrogen filled glovebox, a scintillation vial was charged with **L2.3a** (23.1 mg, 33.7 µmol), chloro(dimethylsulfide)gold(I) (9.6 mg, 32.6 µmol), magnetic stir bar, and THF (0.25 mL). The mixture was stirred at room temperature for 2 hours. All solids fully dissolved. The volatiles were removed under reduced pressure to yield a white solid (28.5 mg, 31.0 µmol, 95%).

^{1}H NMR ($CDCl_3$, 500 MHz): δ 8.17 (dd, *J* = 8.6, 2.1, 1H), 8.03 (t, *J* = 7.5, 1H), 7.87 (d, *J* = 2.1, 1H) , 7.74 (d, *J* = 8.1, 1H), 7.65 – 7.54 (m, 3H), 7.18 (d, *J* = 7.5, 1H), 7.06 (d, *J* = 8.7, 1H), 377 (s, 3H – coincidence with signal arising from residual THF δ 3.75), 2.25 – 2.08 (m, 12H), 2.03 – 1.96 (m, 6 H), 1.72 – 1.61 (m, 12H), 1.33 (s, 9 H). Residual THF (δ 3.75 (m), 1.86 (m)), CH_2Cl_2 (δ 5.30 (s)), and dimethylsulfide (δ 2.73 (s)) are observed in the spectrum with the product.

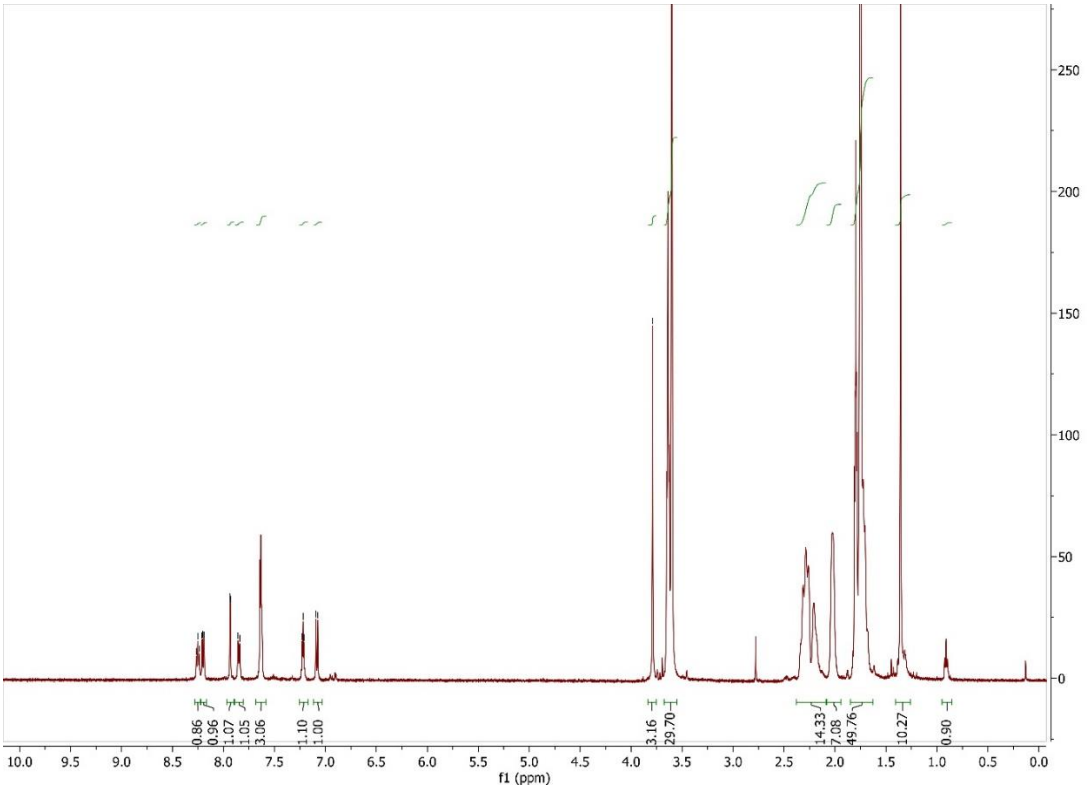

Figure 2.111 ^{1}H NMR spectrum of **Au2.3a** in d_8-THF at 500 MHz

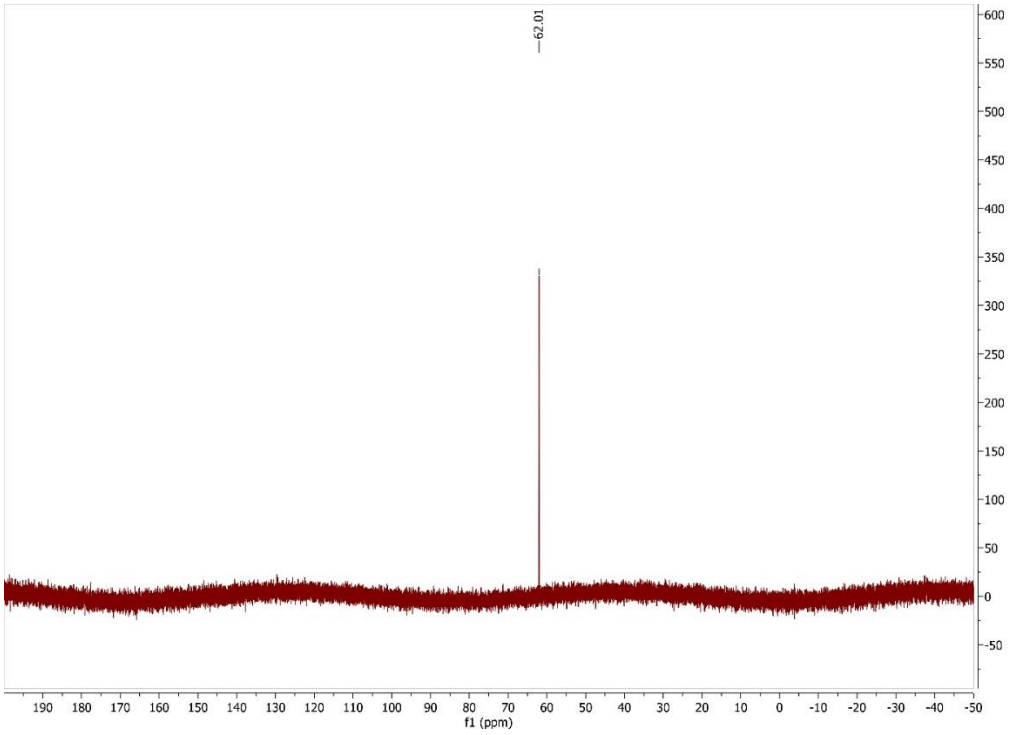

Figure 2.112 ^{31}P NMR spectrum of **Au2.3a** in d_8-THF at 202 MHz

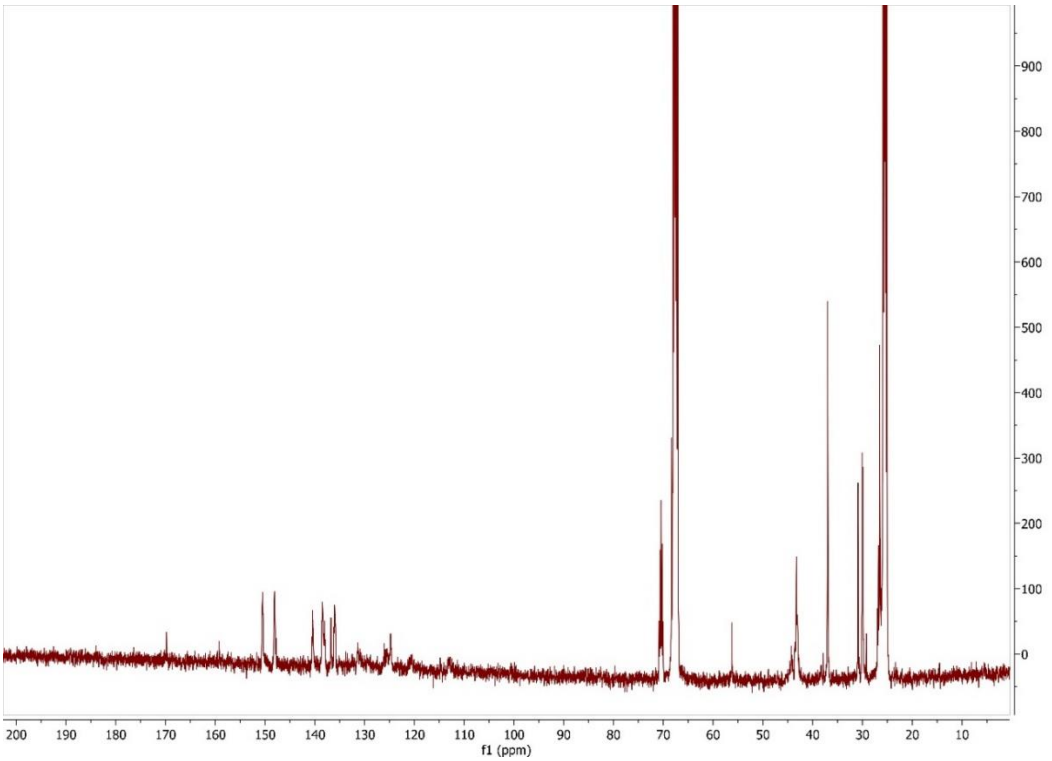

Figure 2.113 $^{13}C\{^{1}H\}$ NMR spectrum of **Au2.3a** in d_8-THF at 125 MHz

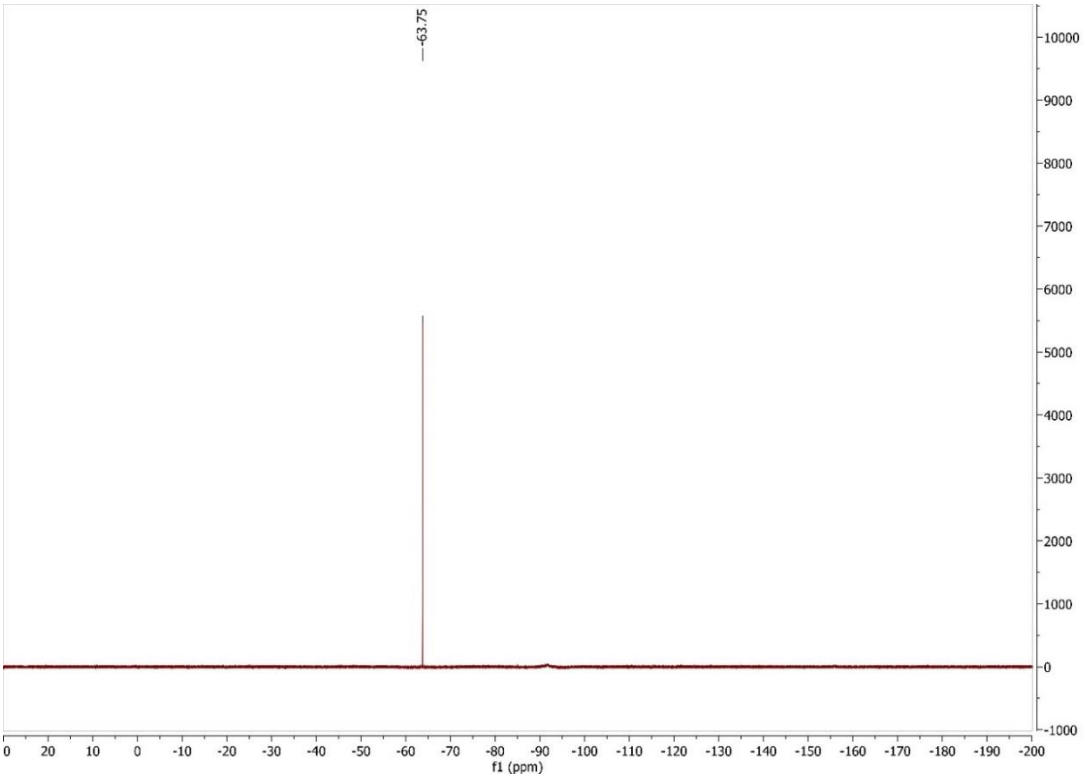

Figure 2.114 ^{19}F NMR spectrum of **Au2.3a** in d_8-THF at 470 MHz

Synthesis of **Au2.4a**

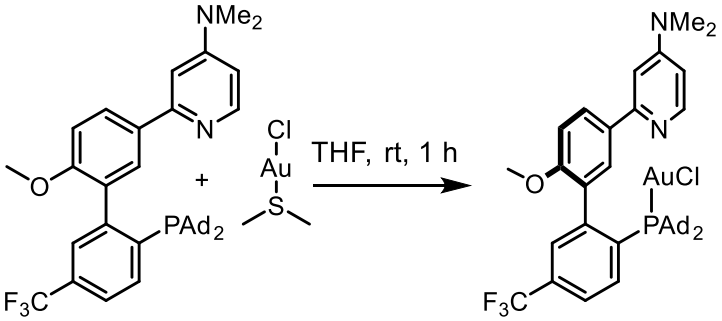

In a nitrogen filled glovebox, a scintillation vial was charged with **L2.3a** (50.2 mg, 0.0746 mmol) and CH_2Cl_2 (2.0 mL), then shaken to fully dissolve. A separate scintillation vial was charged with chloro(dimethylsulfide)gold(I) (21.5 mg, 0.0729 mmol) and magnetic stir bar, then the **L2.4a** solution was added by pipette. The mixture was stirred at room temperature for 1 hour, then completion observed by NMR. The reaction solution was filtered through a pad of celite 545

in a glass fritted funnel, then concentrated under reduced pressure. The resulting white solid was measured at mass 62.5 mg, 92.6% yield.

^{1}H NMR ($CDCl_3$, 400 MHz): δ 8.22 (d, *J* = 6.2, 1H), 8.03 – 7.95 (m, 2H), 7.75 – 7.68 (m, br, 1H), 7.64 (br, 1H), 7.62 (d, *J* = 2.3, 1H), 7.03 (br, 1H), 6.45 (d, br, *J* = 5.8, 1H), 3.74 (s, 3H), 3.09 (s, 6H),

^{31}P NMR ($CDCl_3$, 162 MHz): δ 62.01

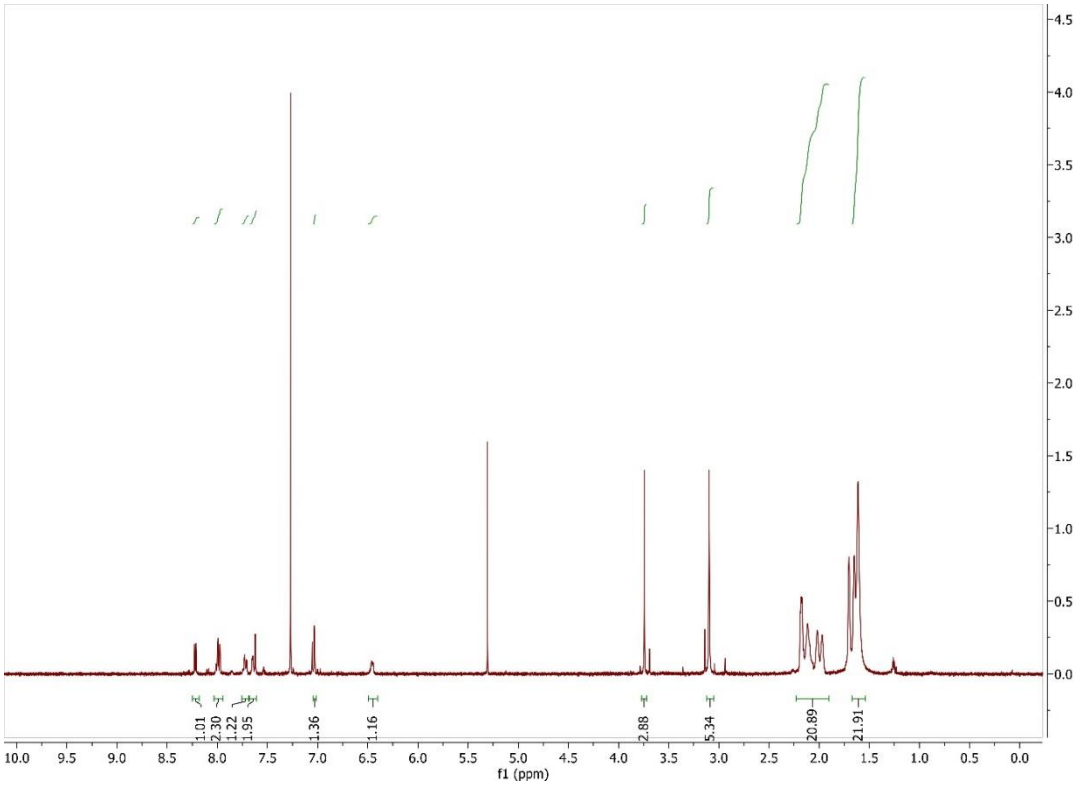

Figure 2.115 ^{1}H NMR spectrum of **Au2.4a** in $CDCl_3$ at 400 MHz

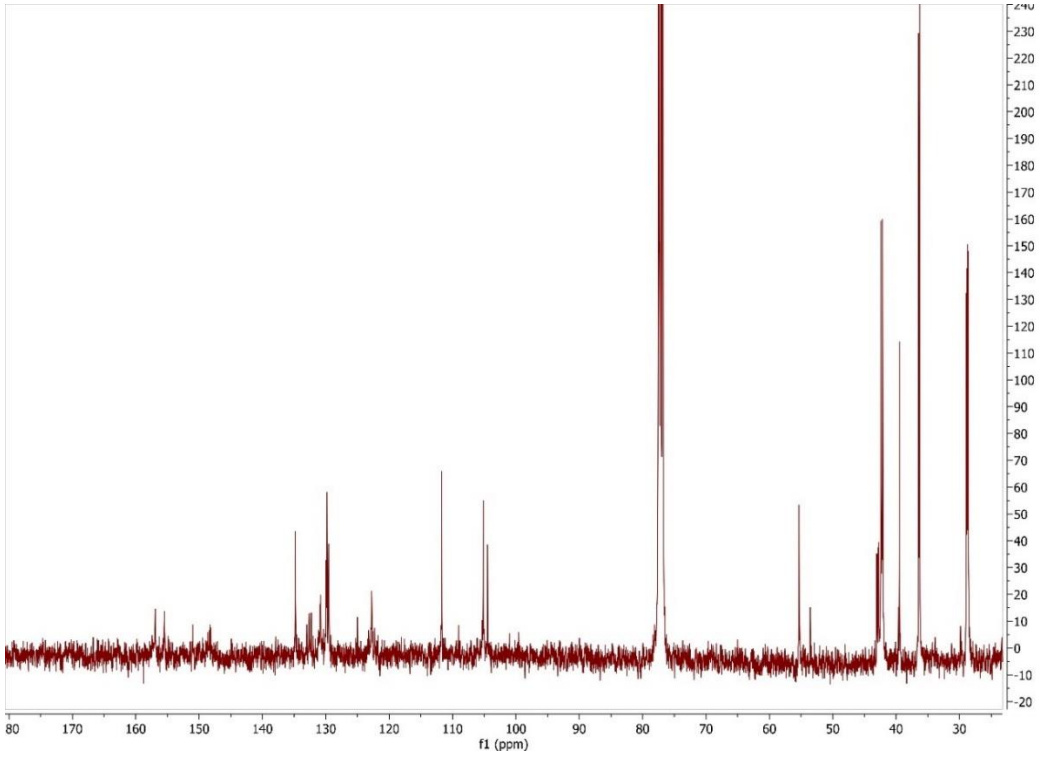

Figure 2.116 $^{13}C\{^{1}H\}$ NMR spectrum of **Au2.4a** in $CDCl_3$ at 100 MHz

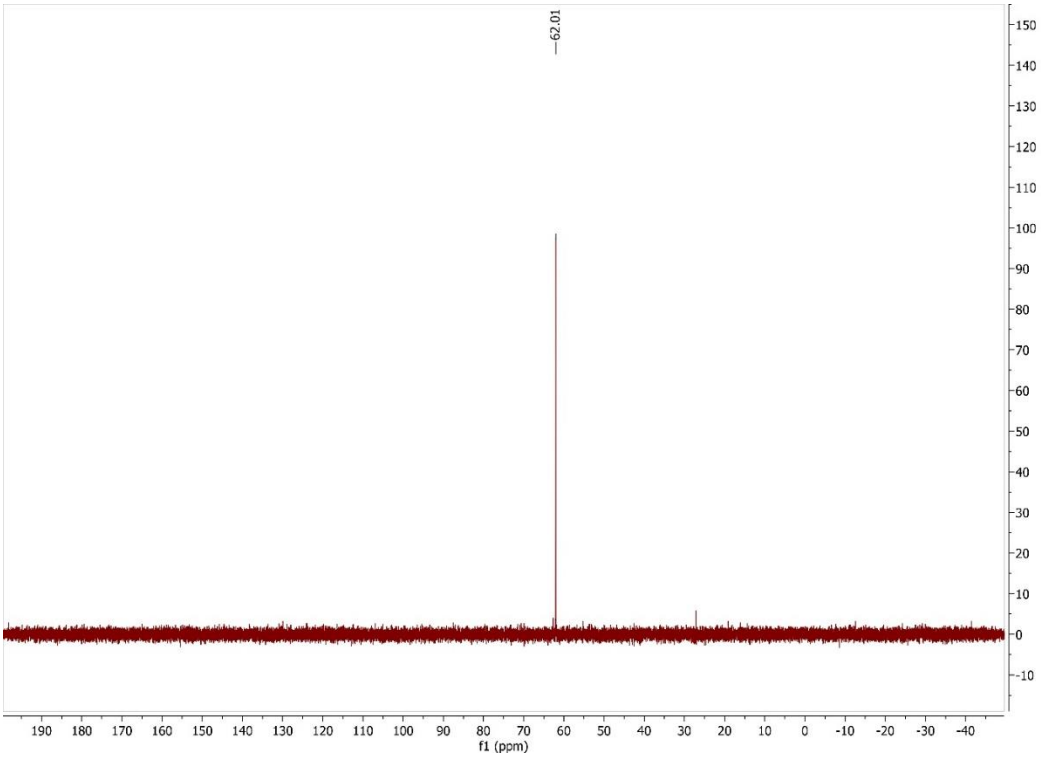

Figure 2.117 ^{31}P NMR spectrum of **Au2.4a** in $CDCl_3$ at 162 MHz

Synthesis of **Au2.6a**

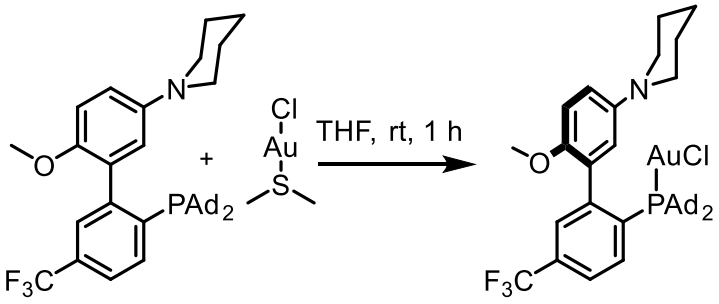

In a nitrogen filled glovebox, a scintillation vial was charged with **L2.6a** (17.8 mg, 0.028 mmol), chloro(dimethylsulfide)gold(I) (8.3 mg, 0.028 mmol), and CH_2Cl_2 (2.0 mL). The mixture was stirred at room temperature for 1 hour, then filtered through a pad of celite 545 on a glass fritted funnel. The volatiles were evaporated under reduced pressure, pentane was added, and the suspension agitated with a spatula, then the volatiles were again removed under reduced pressure to yield the title compound as white solid of mass 17.8 mg, 73.3%.

^{1}H NMR ($CDCl_3$, 400 MHz): δ 8.59 (ddd, *J* = 4.8, 1.8, 1.0, 1H), 8.06 (dd, *J* = 8.7, 2.3, 1H), 7.78 – 7.70 (m, 5H), 7.63 (m, 1H), 718 (m, 1H), 7.09 (d, *J* = 8.7, 1H), 3.81 (s, 3H), 2.37 – 1.08 (m, 22H)

Synthesis of **Au2.8a**

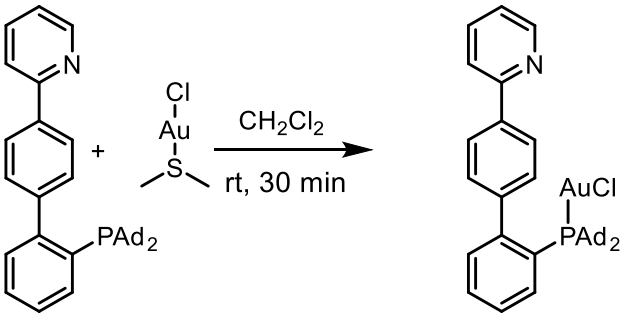

L2.8a **Au2.8a**

Synthesis of **Au2.9a**

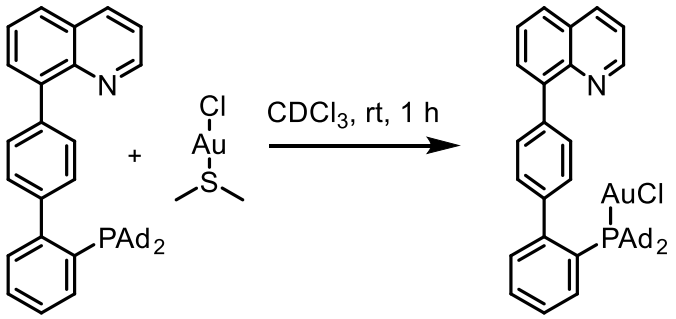

L2.9a **Au2.9a**

In a nitrogen filled glovebox, a scintillation vial was charged with L2.9a (4.7 mg, 0.081 mmol), $CDCl_3$ (0.7 mL), and chloro(dimethylsulfide)gold(I) (2.4 mg, 0.081 mmol) was added. The reaction mixture was stirred at room temperature for 1 hour. Then the volatile components were evaporated under reduced pressure.

^{1}H NMR (CD_2Cl_2, 400 MHz): δ 8.89 (m, 1H), 8.30 (d, *J* = 7.0, 1H), 8.24 (d, *J* = 7.8, 1H), 7.94 (t, *J* = 7.3, 1H), 7.87 (d, *J* = 7.6, 1H), 7.74 – 7.64 (m, 3H), 7.62 – 7.51 (m, 2H), 7.48 – 7.39 (m, 2H), 2.07 (d, *J* = 7.9, 2H), 2.29 – 2.21 (m, 12H), 2.01 (br, 6H), 1.70 (br, 12H)

^{31}P NMR (CD_2Cl_2, 162 MHz): δ 61.54

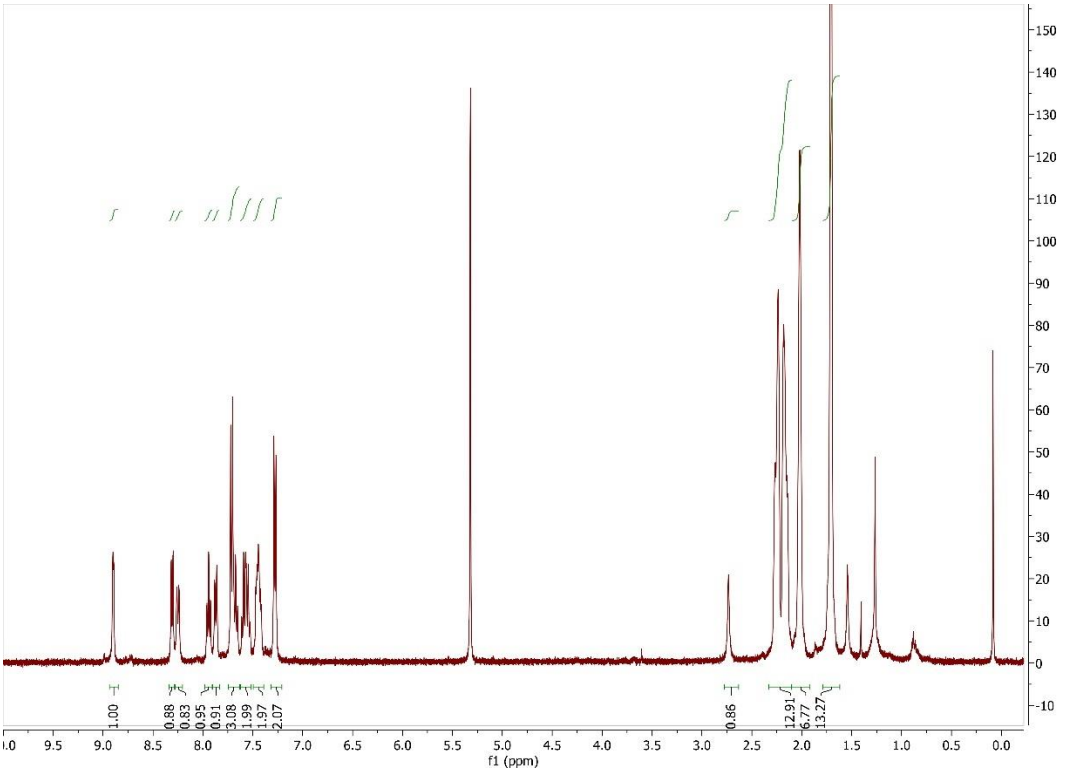

Figure 2.118 ^{1}H NMR spectrum of **Au2.9a** in CD_2Cl_2 at 400 MHz

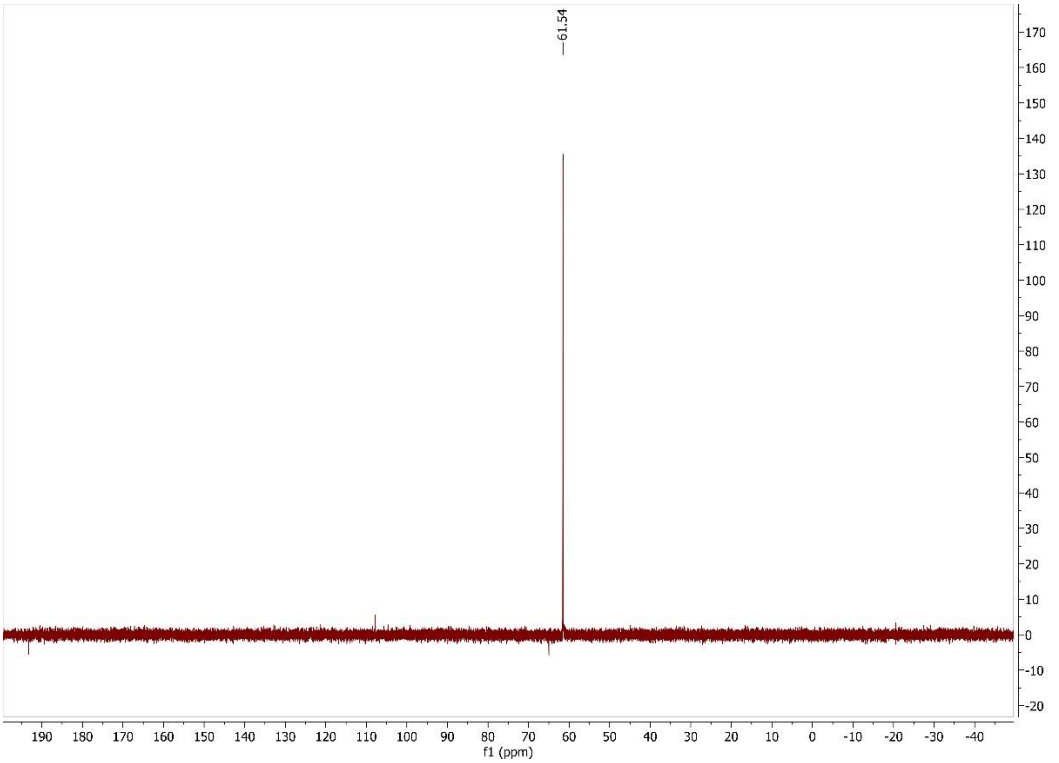

Figure 2.119 ^{31}P NMR spectrum of **Au2.9a** in CD_2Cl_2 at 162 MHz

Synthesis of **Au2.11a**

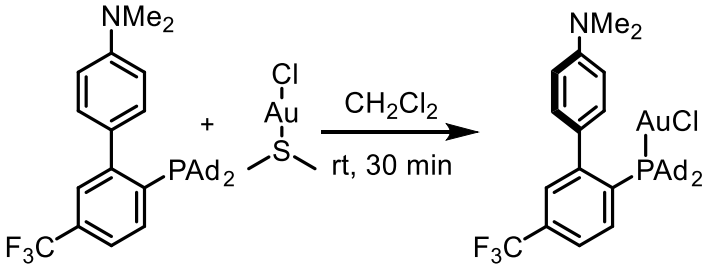

L2.11a **Au2.11a**

In a nitrogen filled glovebox, a scintillation vial was charged with bs080 (21.3 mg, 37.9 µmol), dimethylsulfide gold (I) chloride (11.1 mg, 37.7 µmol), CH_2Cl_2 (1.5 mL), and a magnetic stir bar. The mixture was stirred at room temperature for 45 minutes. The volatiles were then removed under reduced pressure. The gold (I) phosphine complex was collected in quantitative yield as an off-white solid of mass 30.9 mg (37.7 µmol). Residual diethyl ether and 1,2-dichloroethane can be detected in the ^{1}H-NMR spectrum.

^{1}H NMR ($CDCl_3$, 500 MHz): δ 7.97 (m, 1H), 7.69 (d, *J* = 8.2, 1H), 7.62 (s, br, 1H), 6.96 (m, *J* = 8.4, 2H), 6.81 (m, br, 2H)

^{19}F NMR ($CDCl_3$, 376 MHz): δ -63.25

^{31}P NMR ($CDCl_3$, 162 MHz)

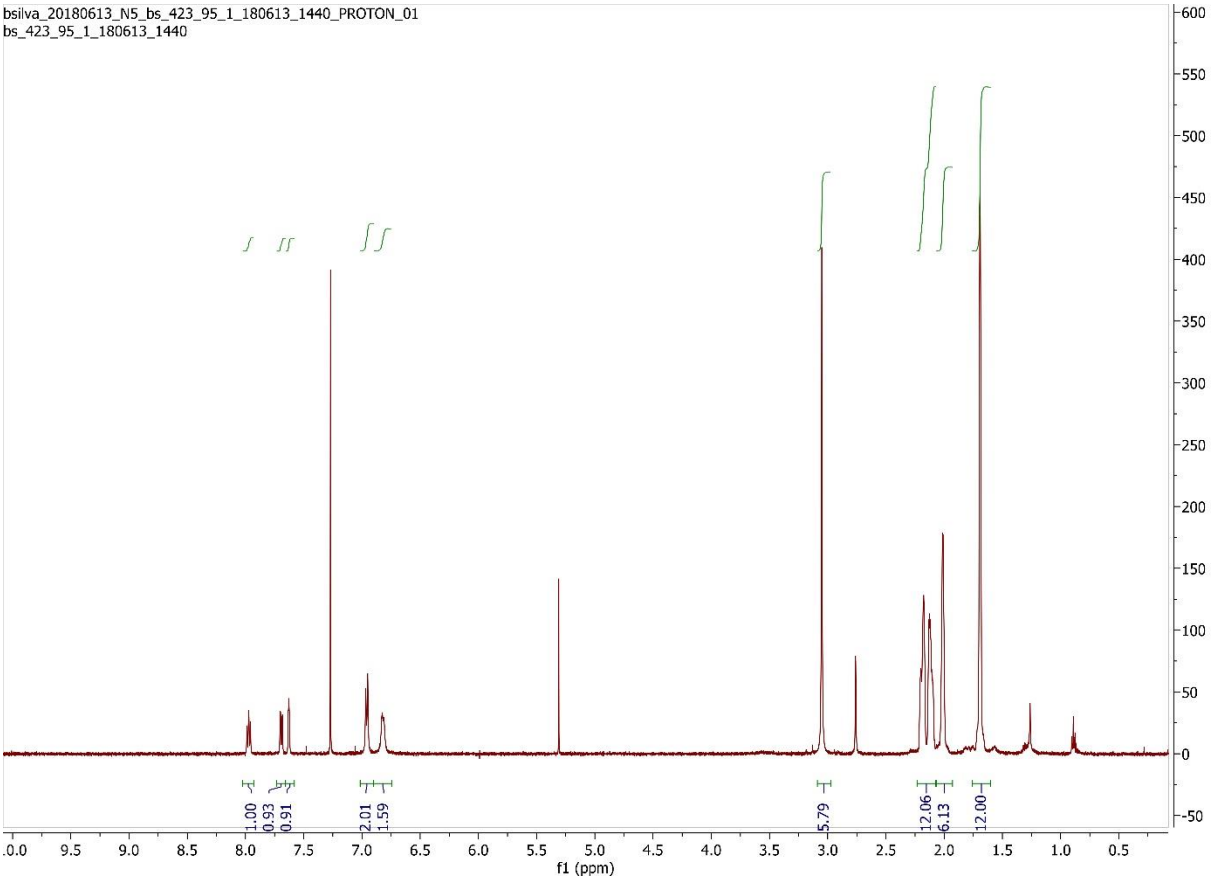

Figure 2.120 ^{1}H NMR spectrum of **Au2.11a** in $CDCl_3$ at 400 MHz

High Throughput Experimentation

Analysis of products by GC-MS was conducted on an Agilent 7890C GC with 5977A MSD (EI & CI probes) and PAL autosampler. The MassHunter software was utilized for interfacing with the instrument. After the heating time was completed and the reaction plates had cooled, the plates were opened and quenched with either methanol Next the plate was resealed, then placed into a centrifuge insert and spun in a centrifuge to settle any precipitates to the bottom of the reaction vessels. The soluble components were then pulled up with a multichannel pipette and placed into 1 mL GC vials. The vials were then diluted with a standard addition of the choice of solvent. In the case of 1000 µL reaction vials, 700µL methanol was added. For the propene

screening conditions methylene chloride was used instead of methanol. The GC oven temperature ramp was set to start at 35 °C, holding for 2 minutes. Then the temperature was ramped at a rate of 25 °C/ minute until the temperature reached 250 °C. Immediately upon reaching 250°C, the temperature ramp rate was increased to 50°C/minute until the temperature reached 300 °C, which was maintained for 1 minute. The sample injection size was 1 µL. Prior to running the parallel reaction plates, we synthesized authentic samples some potential products (detailed below). The independently synthesized products were used as standards to benchmark retention time in the GC.

Synthesis of potential alkene addition products

Synthesis of 10-phenyl-1-decene

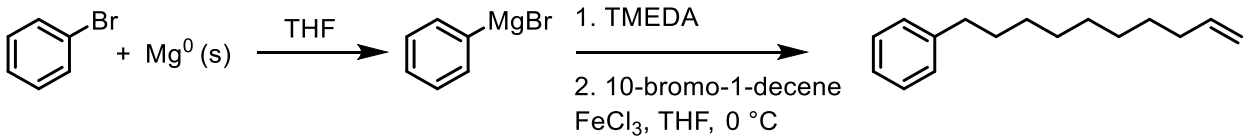

All glassware was oven dried prior to use. 10-bromo-1-decene was treated by passing through basic alumina with pentane (6mL). The pentane was then evaporated by rotary evaporation. In a nitrogen filled glovebox, a 250 mL 2-neck round bottom flask (flask A) was charged with bromobenzene (10.5201 g, 0.0670 mol), THF (40 mL), then magnesium turnings (1.6553 g, 0.0681 mol). Within about 20 minutes the reaction was visibly noticeable as the reaction mixture began to darken in color, starting from a clear and colorless solution and developing a purple color. Concurrent with the Grignard reagent preparation, in a nitrogen filled glovebox, a 250 mL flask (flask B) was charged with $FeCl_3$ (467.2 mg, 2.880 mmol) and THF (20 mL in two portions), 10-bromo-1-decene (12.2137 g, 0.0557 mol), and magnetic stir bar. Flask B was placed in an ice-bath with magnetic stirring. After cooling flask B for 20 minutes, the contents of flask A were transferred via cannula to flask B. The addition was conducted in a dropwise manner over

the course of 6 minutes. The mixture was then stirred slowly warming to room temperature over 24 hours. The reaction was then quenched by the addition of water (20 mL), then a saturated solution of NH_4Cl (aq) (200 mL). The mixture was extracted with CH_2Cl_2 (100 mL) three times. The combined organic fractions were then combined and washed with a saturated solution of NaCl (aq) (50 mL) two times, dried over $MgSO_4$, filtered through a glass fritted funnel, then concentrated by rotary evaporation. The crude product mixture (10.5130 g, 87% of theoretical yield – likely inefficient extraction) was purified by column chromatography on silica gel (312 g). The mobile phase consisted of only petroleum ether and was collected in fractions which were concentrated by rotary evaporation and analyzed by mass and ^{1}H-NMR spectroscopy for the desired pure product. The product was collected in fractions 11-13 then subject to Kuglerhor distillation. The third distillation fraction was most pure and was collected in 0.8073 g, 6.8%.

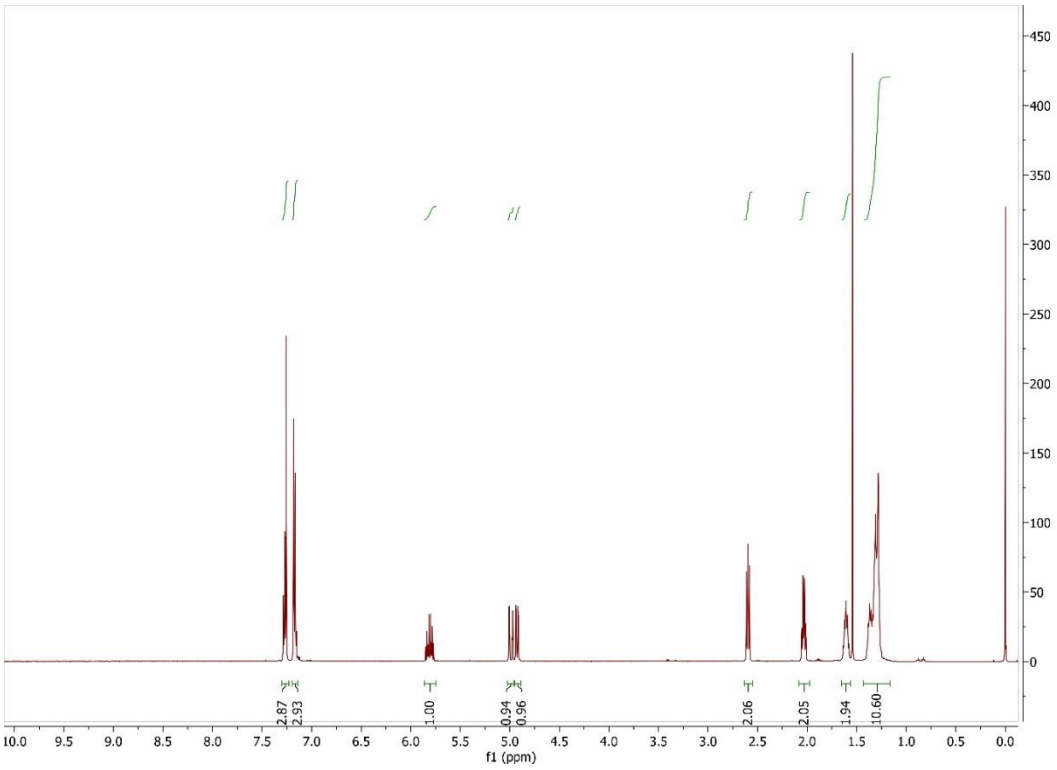

Figure 2.121 ^{1}H NMR spectrum of 10-phenyl-1-decene in $CDCl_3$ at 500 MHz

Synthesis of 10-phenyldecan-1-ol from 10-phenyl-1-decene

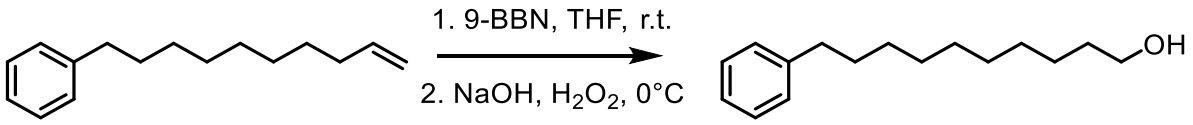

An oven dried and silanized 50 L Schlenk flask was charged with phenyl decene (500.5 mg, 2.313 mmol), THF (2.0 mL), then 9-BBN (0.5 M in THF) (5.2 mL) (2.6 mmol). The mixture was stirred at room temperature for 24 hours. Next the reaction vessel was placed in an ice bath with stirring. A solution of NaOH (3 M, aq) (2.4 mL) was added dropwise over the course of 25 minutes. The reaction was stirred for 16 hours. After that point the reaction was worked up with the addition of potassium carbonate (0.5013 g, 0.0036 mol) followed by extraction with diethyl ether (three portions of 15 mL). The combined organic phase was washed with a saturated solution of NaCl (aq) (50 mL), dried over $MgSO_4$, filtered through a glass fritted funnel, then concentrated by rotary evaporation. The crude product was purified by column chromatography on silica gel (9 grams). The mobile phase consisted of a mixture of hexanes and ethyl acetate.

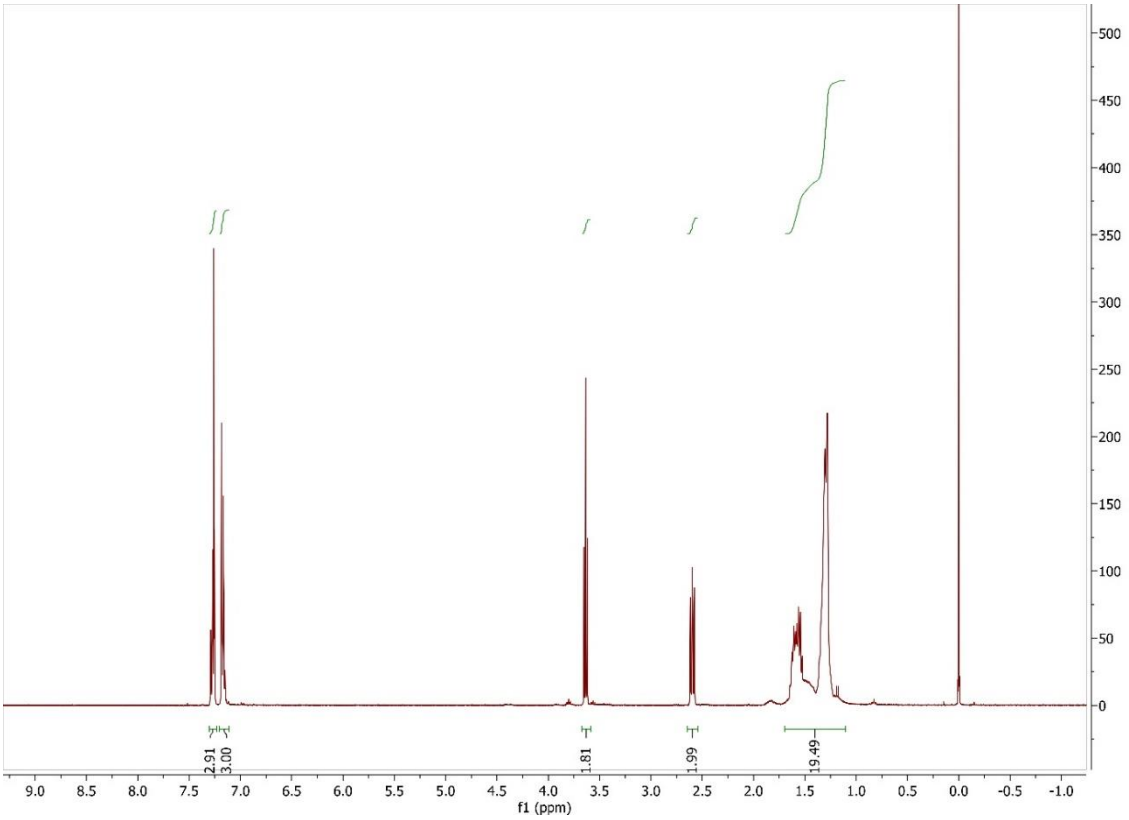

Figure 2.122 ^{1}H NMR spectrum of 10-phenyl-1-decanol in $CDCl_3$ at 400 MHz

Synthesis of (10-(*tert*butoxy)decyl)benzene

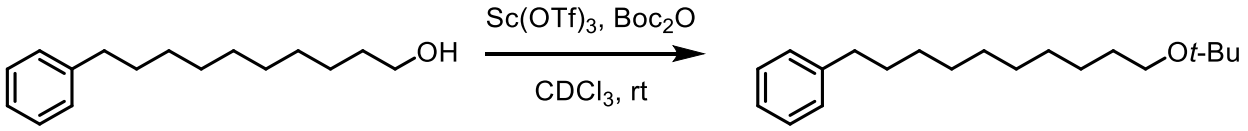

A dried and silanized J. Young NMR tube was charged with bs109(80.0 mg, 0.341 mmol), $CDCl_3$ (0.7 mL), $Sc(OTf)_3$ (22.4 mg, 0.046 mmol), and ditert-butyldicarbonate (200.4 mg, 0.979 mmol). The NMR tube was connected to a Shlenk line with nitrogen flow for off-gassing of the evolving carbon dioxide. After 24 h, the reaction was quenched with addition of water (5 mL) and extracted with CH_2Cl_2 (three portions of 5 mL), dried over $MgSO_4$, filtered through a glass fritted funnel, then concentrated by rotary evaporation. The crude product was purified by column

chromatography on silica gel (9 grams). The mobile phase consisted of a mixture of hexanes and ethyl acetate. The product was collected in fractions 5 and 6 for a mass of 61.4 mg, 61.9%.

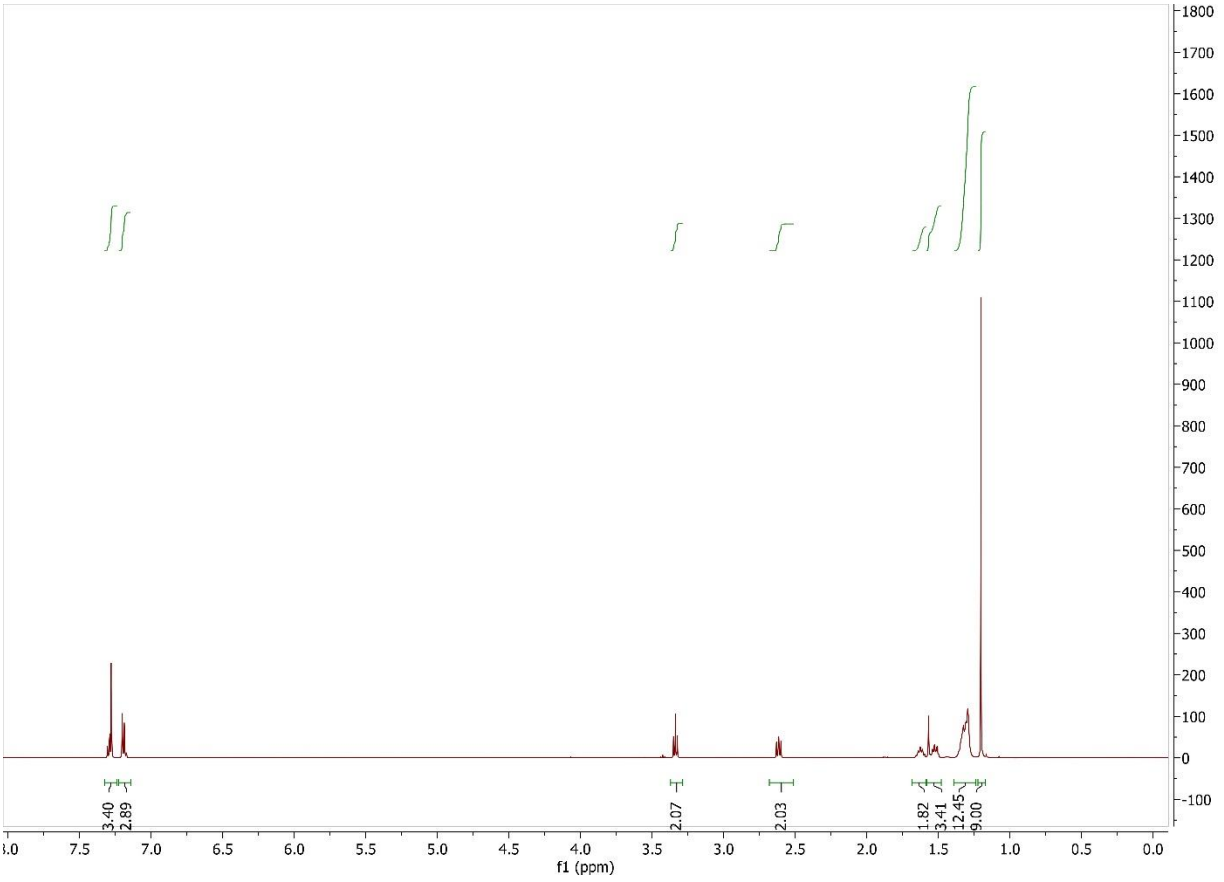

Figure 2.123 ^{1}H NMR spectrum of (10-(tertbutoxy)decyl)benzene in $CDCl_3$ at 500 MHz

Synthesis of 10-phenyldecyl acetate

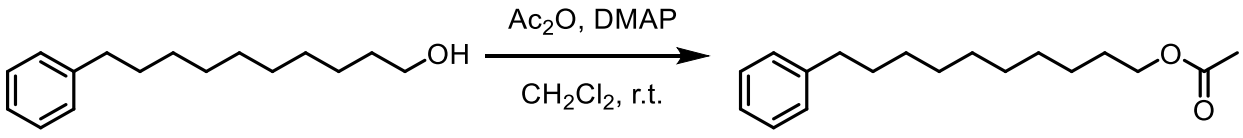

A dried and silanized 50 mL Schlenk flask was charged with 10-phenyldecan-1-ol (80.0 mg, 0.341 mmol), 4-(N,N-dimethylamino)pyridine (3.2 mg, 0.026 mmol), CH_2Cl_2 (2 mL) and magnetic stir bar. Acetic anhydride (329.7 mg, 3.23 mmol) was added slowly over 2 minutes. The reaction was stirred at room temperature for 24 hours. The reaction was then quenched with the

addition of water (5 mL) and a saturated solution of $NaHCO_3$ (aq) (5 mL). The mixture was then extracted with CH_2Cl_2 (3 portions of 5 mL). The combined organic phases were dried over $MgSO_4$, filtered through a glass fritted funnel, then concentrated by rotary evaporation. The crude product was purified by column chromatography on silica gel (9 grams). The mobile phase consisted of a mixture of hexanes and ethyl acetate. The product was collected in fractions 4 and 5 and yielded 63.1 mg, 66.9%.

^{1}H NMR (CD_2Cl_2, 500 MHz): δ 7.28 – 7.21 (m, 2H), 7.19 – 7.11 (m, 3H), 4.01 (t, *J* = 6.8, 2H), 2.64 – 2.55 (m, 2H), 2.00 (s, 3H)

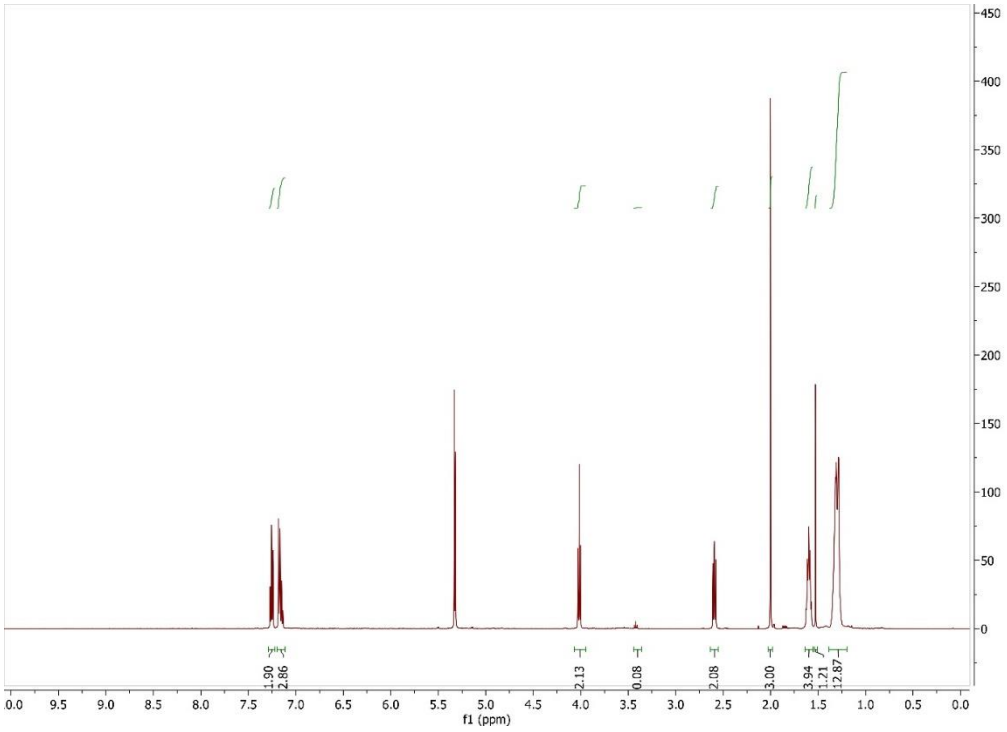

Figure 2.124 ^{1}H NMR spectrum of 10-phenyldecyl acetate in $CDCl_3$ at 500 MHz

NMR Scale Catalyzed formation of vinyl acetates from carboxylic acids and terminal alkynes

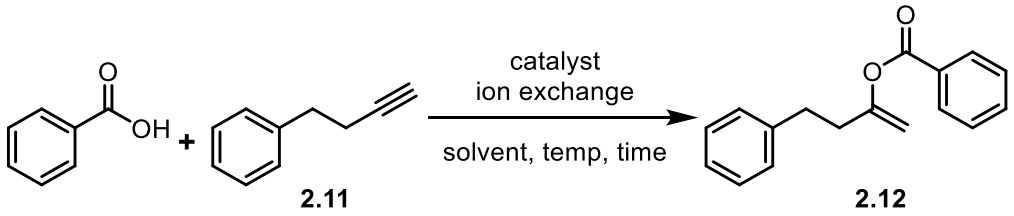

Catalyzed addition of benzoic acid to 4-phenyl-1-butyne with **Au2.1a**

A J. Young NMR tube was charged with 4-phenyl-1-butyne (21.1 mg, 0.162 mmol), benzoic acid (13.7 mg, 0.112 mmol), **Au2.1a** (2.2 mg, 0.003 mmol, 2 mol%), $((CH_3)_3Si)_4C$ (1.2 mg, 0.004 mmol), 1,2-DCE (0.5 mL), and C_6D_6 (0.1 mL). An initial ^1H NMR was recorded, then $K[B(C_6F_5)_4]$ (2.3 mg, 0.003 mmol) was added to the reaction mixture and the tube sealed. The tube was sealed and heated at 90 °C for a total of 24 hours. Yield of vinyl ester is 44% as measured by NMR.

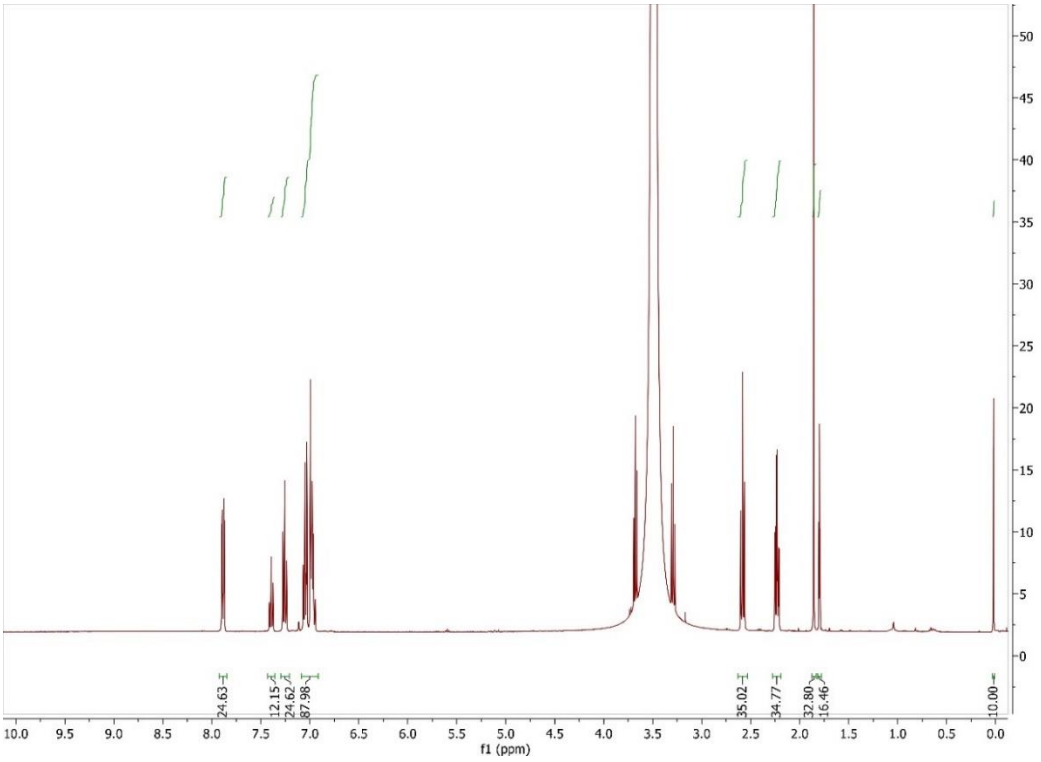

Figure 2.125 ^1H NMR spectrum of starting composition for addition of benzoic acid to 4-phenyl-1-butyne with **Au2.1a**, C_6D_6 lock signal at 400 MHz

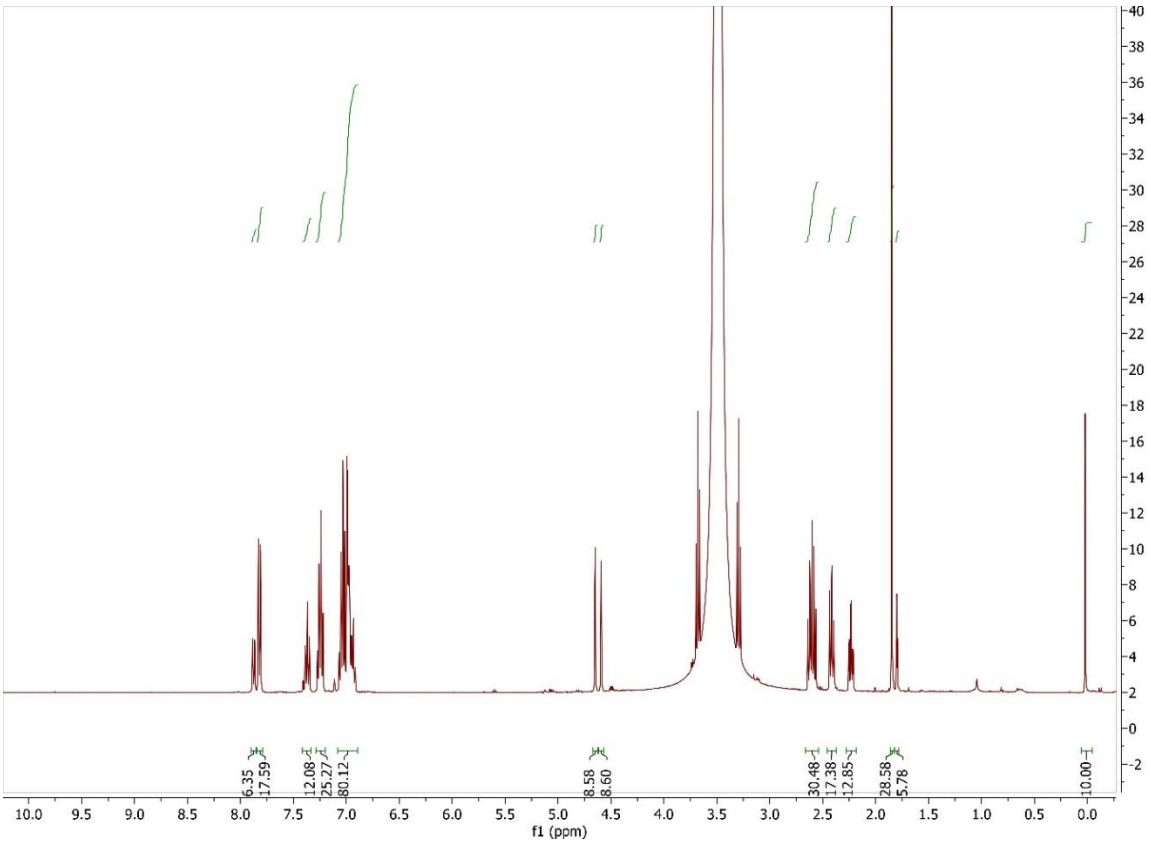

Figure 2.126 ^{1}H NMR spectrum of ending composition for addition of benzoic acid to 4-phenyl-1-butyne with **Au2.1a** with C_6D_6 lock signal at 400 MHz

Catalyzed addition of benzoic acid to 4-phenyl-1-butyne with **Au2.1a**

A J. Young NMR tube was charged with 4-phenyl-1-butyne (13.6 mg, 0.104 mmol), benzoic acid (12.2 mg, 0.100 mmol), **Au2.1a** (1.8 mg, 0.002 mmol, 2 mol%), $((CH_3)_3Si)_4C$ (1.1 mg, 0.004 mmol), HFIP (0.5 mL), and C_6D_6 (0.1 mL). An initial ^{1}H NMR was recorded, then $K[B(C_6F_5)_4]$ (2.1 mg, 0.003 mmol) was added to the reaction mixture and the tube sealed. The tube was sealed and heated at 90 °C for a total of 3.5 hours. Yield of vinyl ester 83% as measured by NMR.

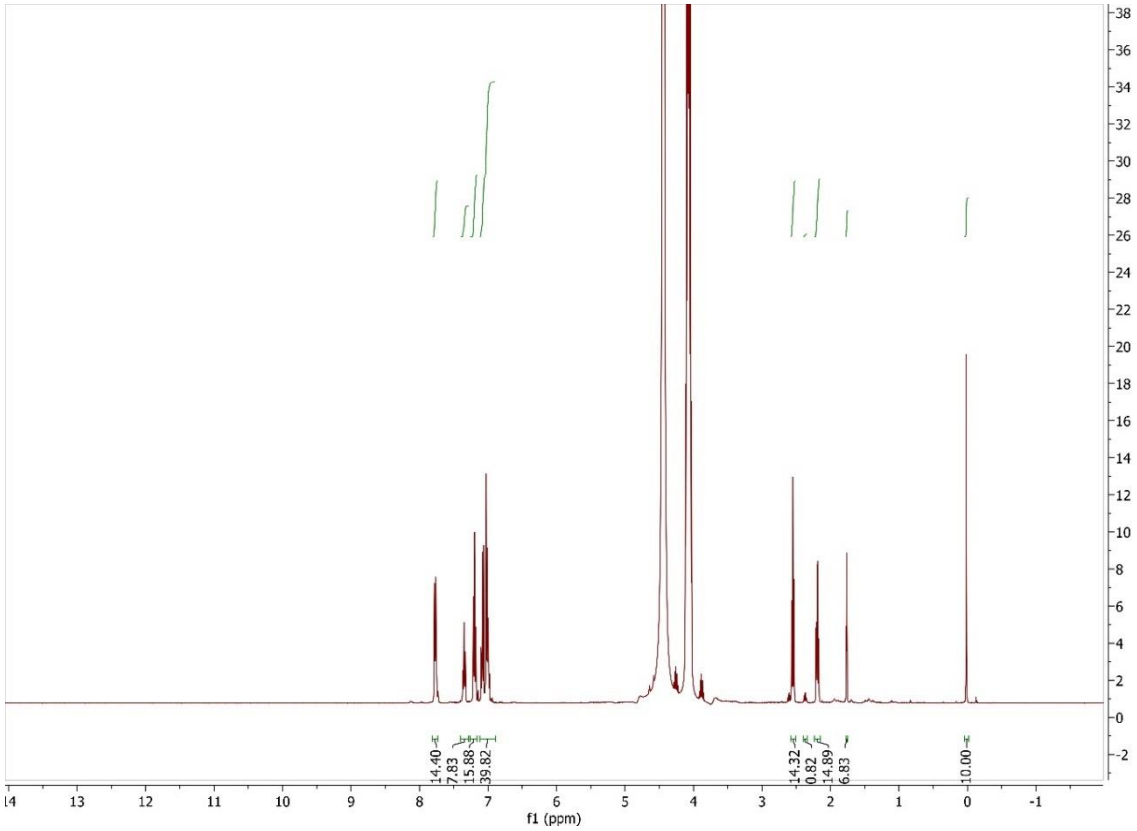

Figure 2.127 ^{1}H NMR spectrum of starting composition for addition of benzoic acid to 4-phenyl-1-butyne with **Au2.1a** with C_6D_6 lock signal at 400 MHz

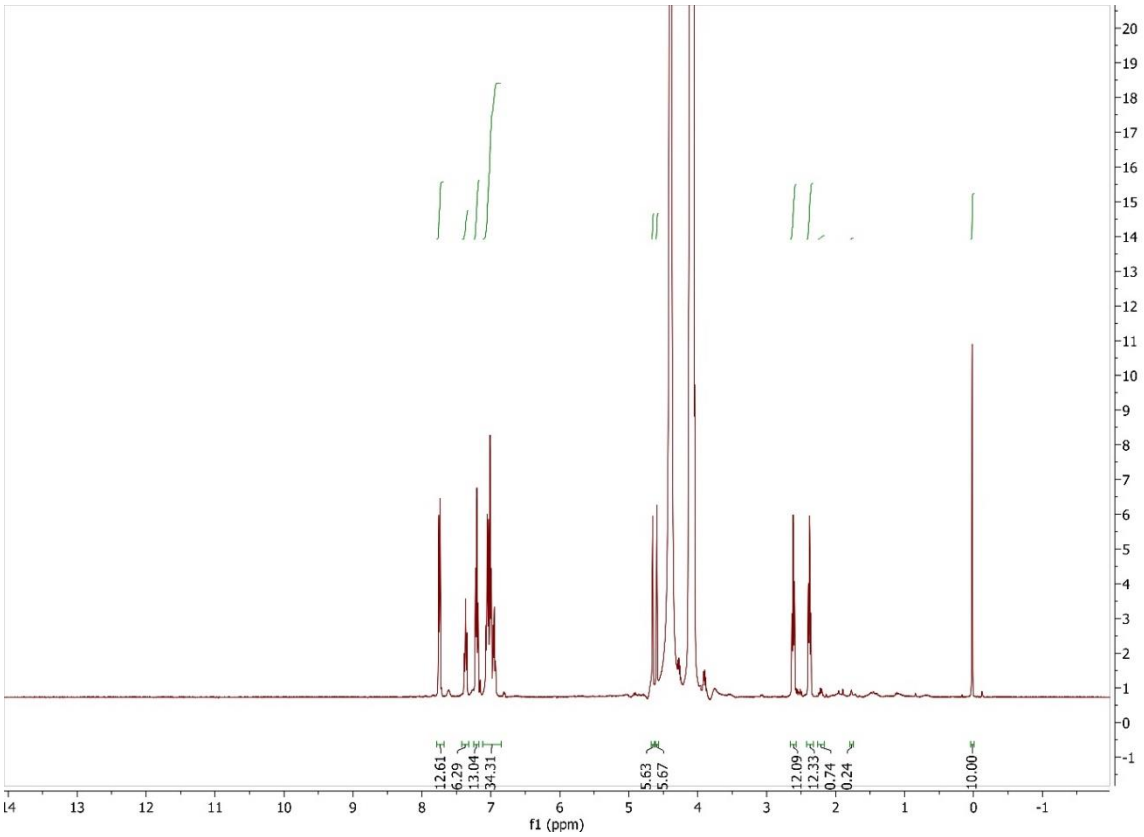

Figure 2.128 ^{1}H NMR spectrum of ending composition for addition of benzoic acid to 4-phenyl-1-butyne with **Au2.1a** with C_6D_6 lock signal at 400 MHz

Catalyzed addition of 4-nitrobenzoic acid to 4-phenyl-1-butyne with **Au2.1a**

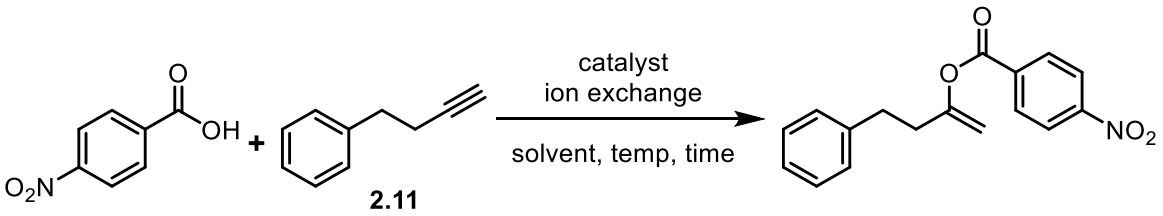

A J. Young NMR tube was charged with 4-phenyl-1-butyne (14.5 mg, 0.111 mmol), 4-nitro-benzoic acid (17.0 mg, 0.102 mmol), **Au2.1a** (2.9 mg, 0.004 mmol, 3 mol%), $((CH_3)_3Si)_4C$ (1.2 mg, 0.004 mmol), 1,2-DCE (0.5 mL), and C_6D_6 (0.1 mL), then $K[B(C_6F_5)_4]$ (3.3 mg, 0.005 mmol). The tube was sealed, an initial ^{1}H NMR spectrum recorded, then the tube was heated at 90 °C for a total of 18 hours. A final ^{1}H NMR spectrum was recorded after the reaction mixture was

removed from the oil bath and cooled to room temperature. Yield of vinyl ester 73% as measured by NMR.

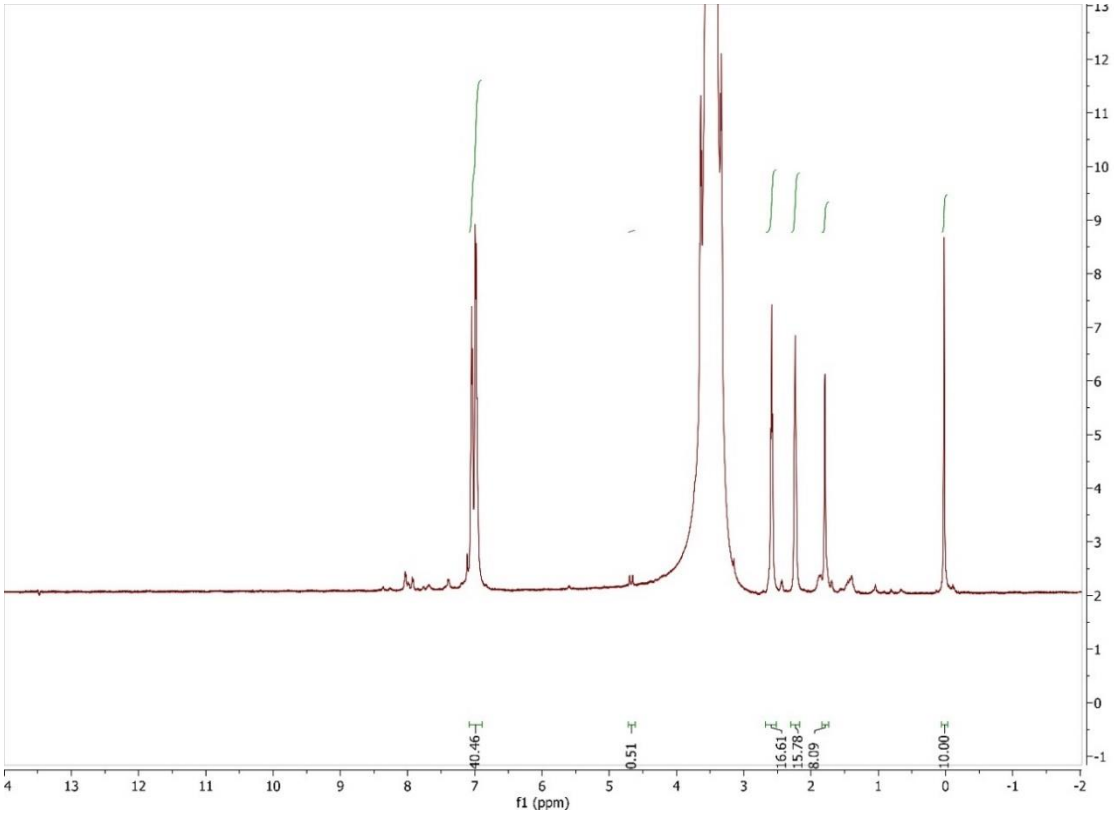

Figure 2.129 ^{1}H NMR spectrum of starting composition for addition of 4-nitrobenzoic acid to 4-phenyl-1-butyne with **Au2.1a** with C_6D_6 lock signal at 500 MHz

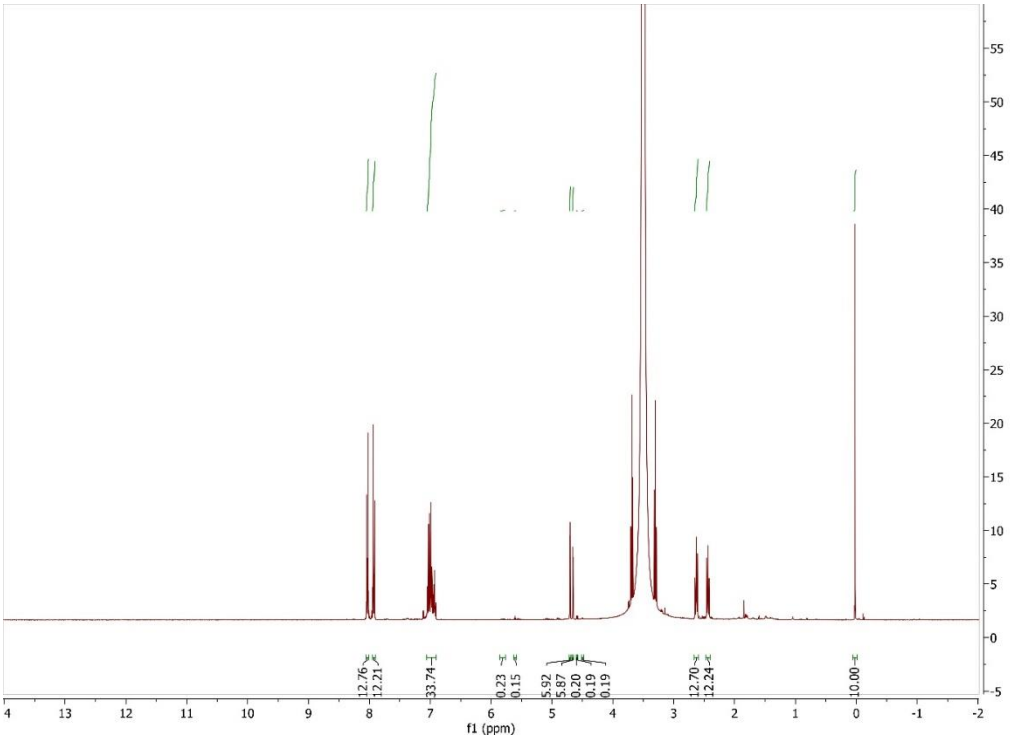

Figure 2.130 ^{1}H NMR spectrum of ending composition for addition of 4-nitrobenzoic acid to 4-phenyl-1-butyne with **Au2.1a** with C_6D_6 lock signal at 400 MHz

Control experiments

Control reaction for uncatalyzed addition of benzoic acid to 4-phenyl-1-butyne (no catalyst no ionizing agent, then ionizing agent addition)

A J. Young NMR tube was charged with 4-phenyl-1-butyne (14.0 mg, 0.108 mmol), benzoic acid (14.5 mg, 0.119 mmol), $((CH_3)_3Si)_4C$ (1.1 mg, 0.004 mmol), 1,2-DCE (0.5 mL), and C_6D_6 (0.1 mL). An initial ^{1}H NMR was recorded the tube was heated at 90 °C for a total of 16 hours. After this point the reaction vessel was charged with $K[B(C_6F_5)_4]$ (5.1 mg, 0.066 mmol). The vessel was sealed and heated at 90 °C for 24 hours. After this time the reaction mixture was cooled to room temperature and again observed by ^{1}H NMR for analysis of any product development.

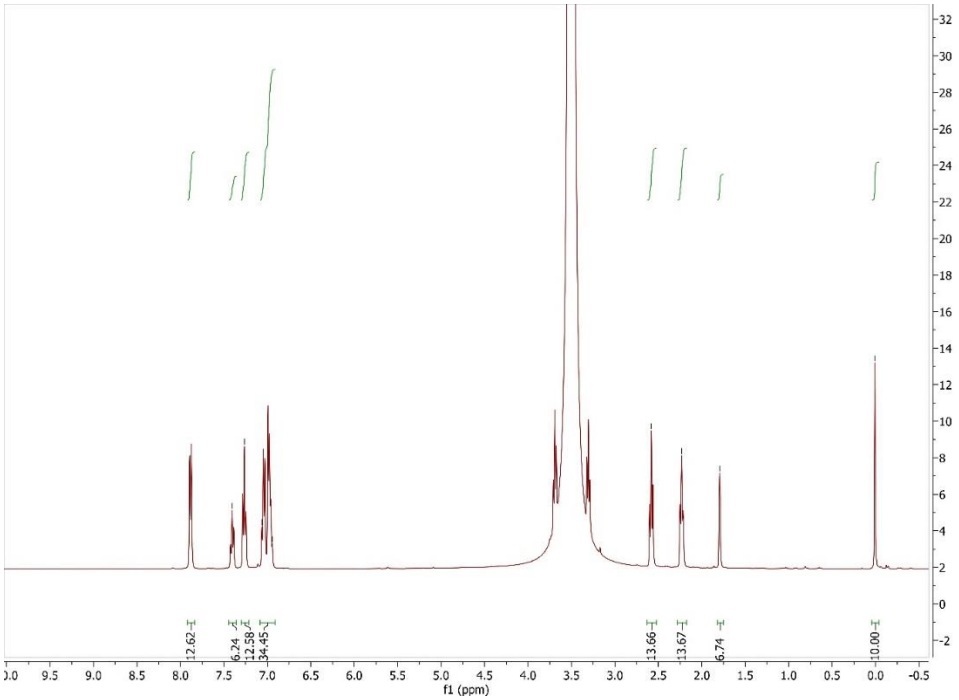

Figure 2.131 ^{1}H NMR spectrum of starting composition for addition of benzoic acid to 4-phenyl-1-butyne without catalyst with C_6D_6 lock signal at 400 MHz.

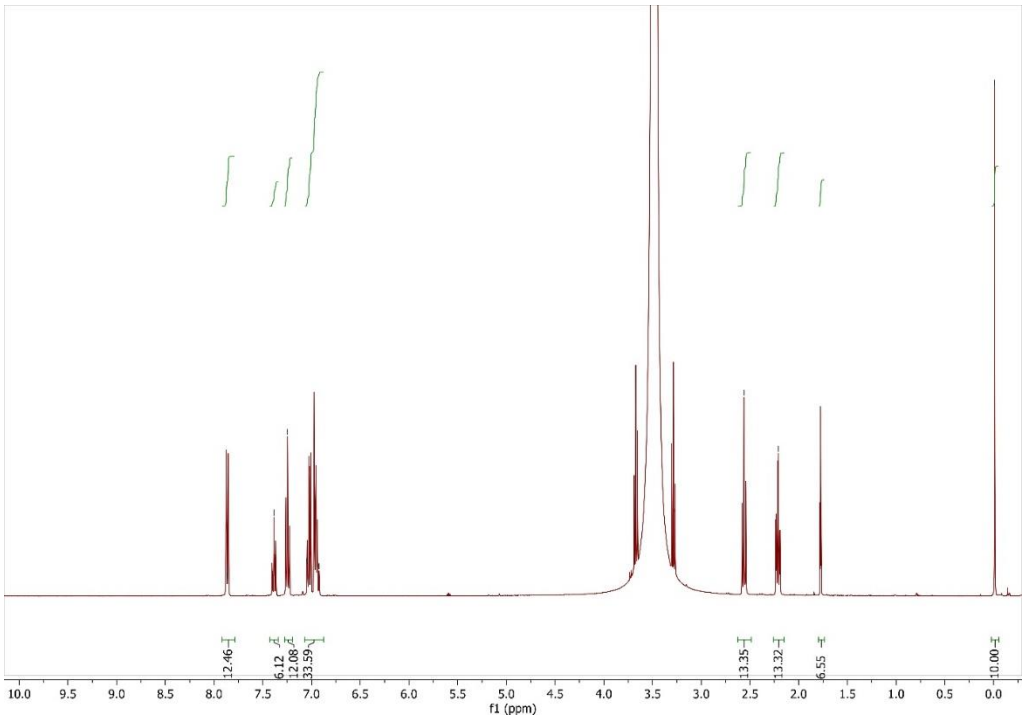

Figure 2.132 ^{1}H NMR spectrum of ending composition for addition of benzoic acid to 4-phenyl-1-butyne without a catalyst with C_6D_6 lock signal at 400 MHz.

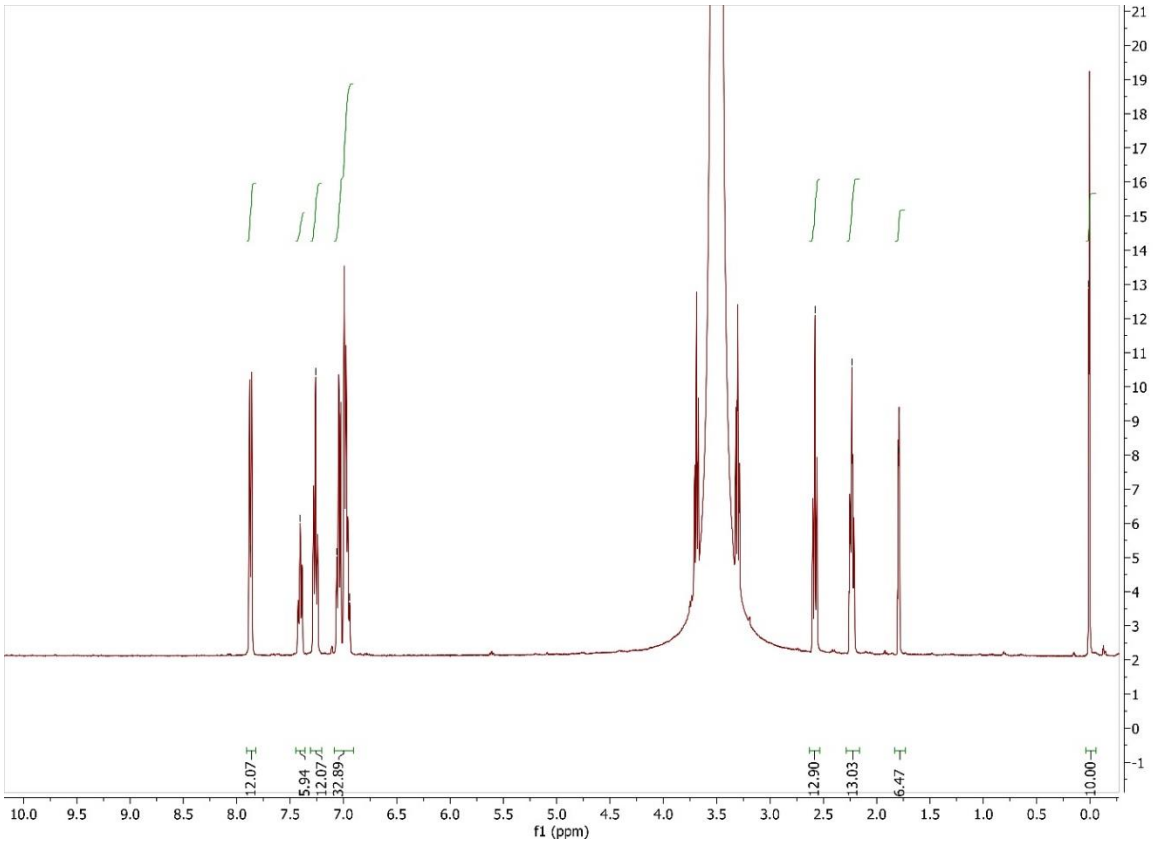

Figure 2.133 ^{1}H NMR spectrum of ending composition for addition of benzoic acid to 4-phenyl-1-butyne with no Au complex, but addition of $K[B(C_6F_5)_4]$ with C_6D_6 lock signal at 400 MHz.

Catalyzed addition of benzoic acid to 4-phenyl-1-butyne with PPh_3AuCl

A J. Young NMR tube was charged with 4-phenyl-1-butyne (13.2 mg, 0.101 mmol), benzoic acid (12.7 mg, 0.104 mmol), PPh_3AuCl (2.6 mg, 0.005 mmol), $K[B(C_6F_5)_4]$ (5.0 mg, 0.007 mmol), internal standard $((CH_3)_3Si)_4C$ (2.4 mg, 0.008 mmol), 1,2-DCE (0.5 mL), and C_6D_6 (0.1 mL). The tube was sealed, then an initial NMR spectrum acquired. The reaction vessel was then placed in an oil bath heated to 90 °C for 19 hours. The reaction vessel was then removed from the oil bath, cooled to room temperature and observed by ^{1}H-NMR for detection of any products.

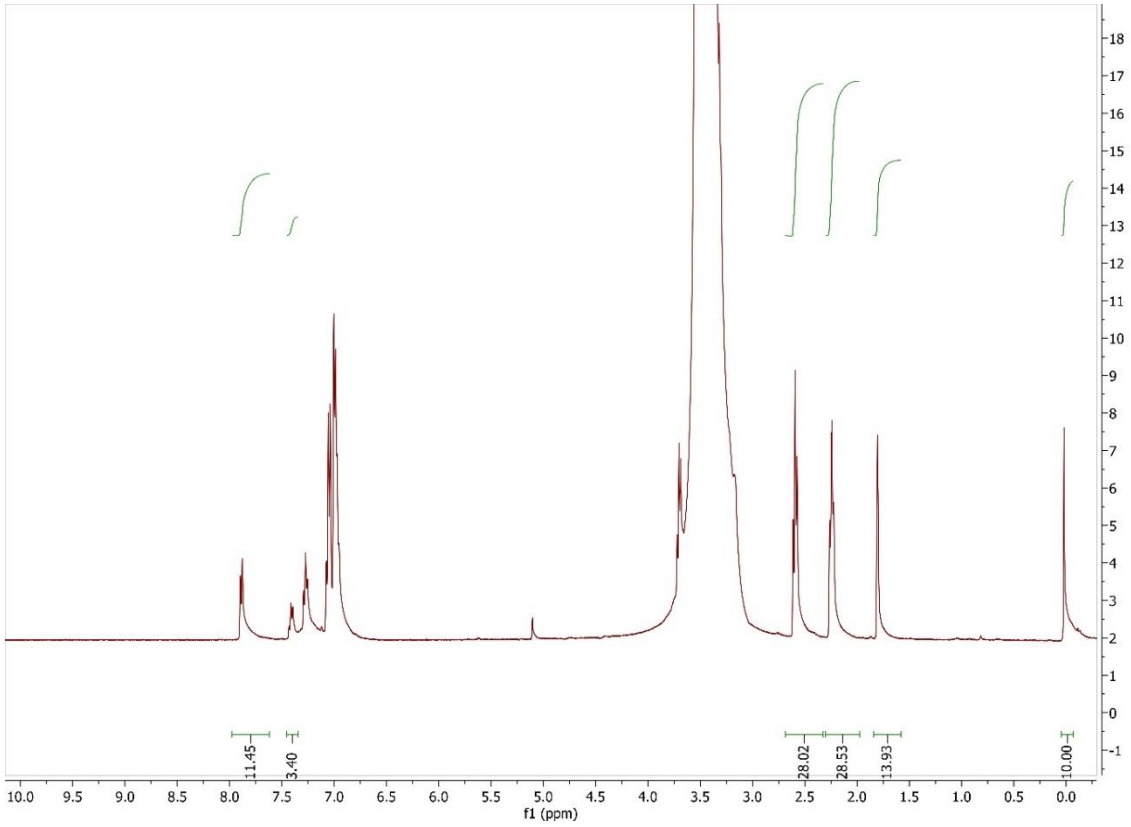

Figure 2.134 ^{1}H NMR spectrum for starting composition for addition of benzoic acid to 4-phenyl-1-butyne with PPh_3AuCl as catalyst, C_6D_6 lock signal at 400 MHz

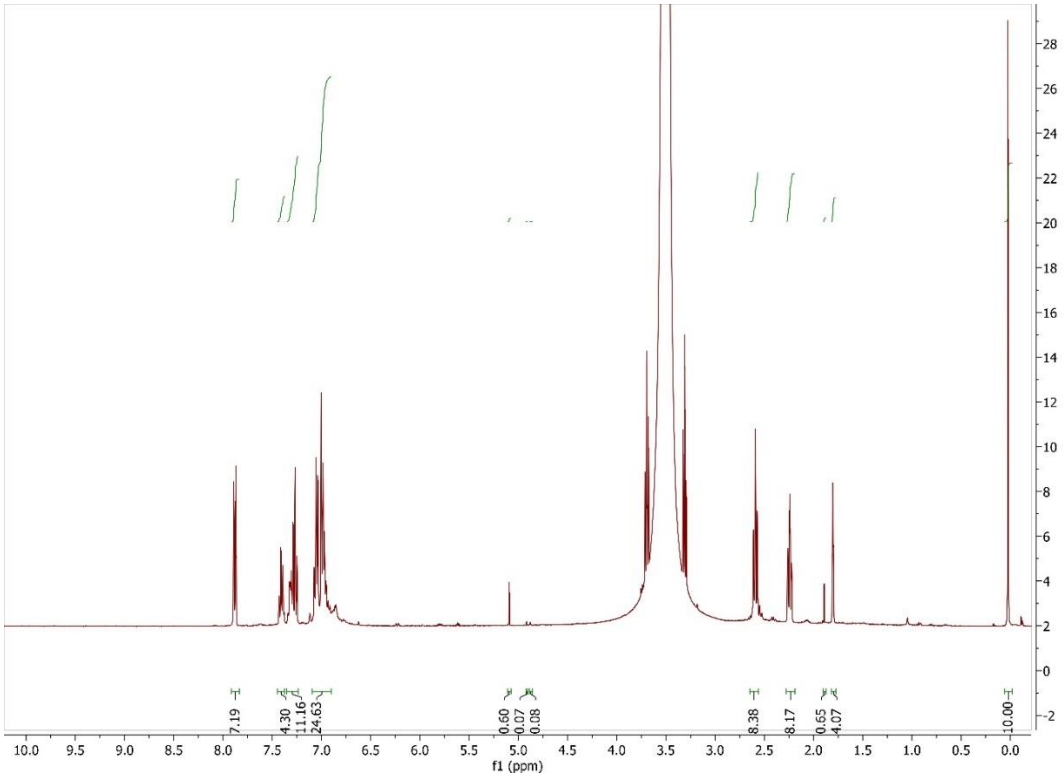

Figure 2.135 ^{1}H NMR spectrum of ending composition for addition of benzoic acid to 4-phenyl-1-butyne with PPh_3AuCl, with C_6D_6 lock signal at 400 MHz

Alkyne Isomerization

Isomerization of 1-phenyl-1-hexyne with **Au2.2a**

In a nitrogen filled glovebox, a J. Young NMR tube was charged with 1-phenyl-1-hexyne (20.0 mg, 0.126 mmol), $((CH_3)_3Si)_4C$ (internal standard), and C_6D_6 (0.7 mL). The tube was then sealed and an initial measurement of the ^{1}H NMR spectrum was observed. Next, the tube was charged with **Au2.2a** (0.036 M in CH_2Cl_2) (35.00 µL, 1.3 µmol) potassium tetrakis[3,5-bis(trifluoromethyl)phenyl]borate (5.2 mg, 7.2 µmol), the tube was sealed, then placed in an oil bath heated to 60 °C for 9 hours. No product formation was detected. To encourage some chemical change, we added additional components to the reaction, and the starting material was detected at

95 % of its initial value. The mixture was charged with **Au2.2a** (0.036 M in C_2Cl_2) (140.0 µL, 5.04 µmol), sodium tetrakis[3,5-bis(trifluoromethyl)phenyl]borate (7.0 mg, 7.9 µmol). The new mixture was then heated at 60 °C for 18 hours. Again, no product formation was detected, and the starting material was measured at 85 % of the initial value.

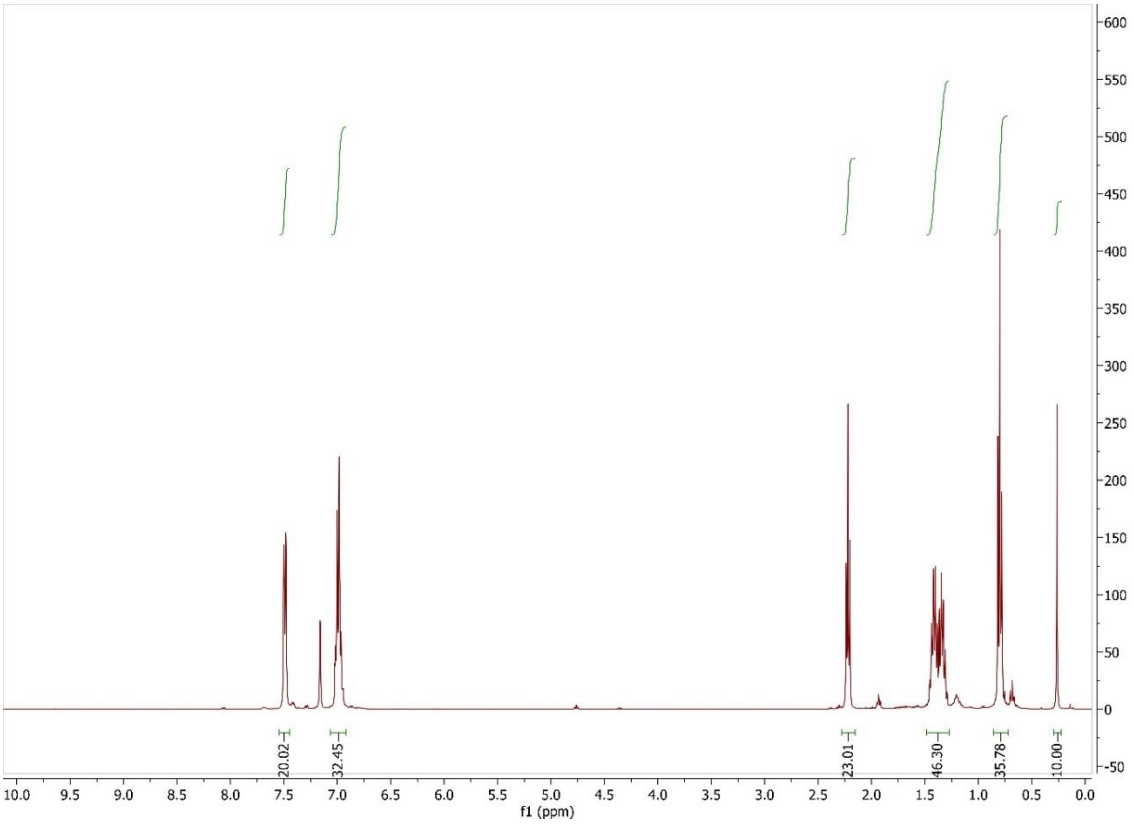

Figure 2.136 ^{1}H NMR spectrum of initial composition for isomerization of 1-phenyl-1-hexyne with **Au2.2a** in C_6D_6 at 400 MHz

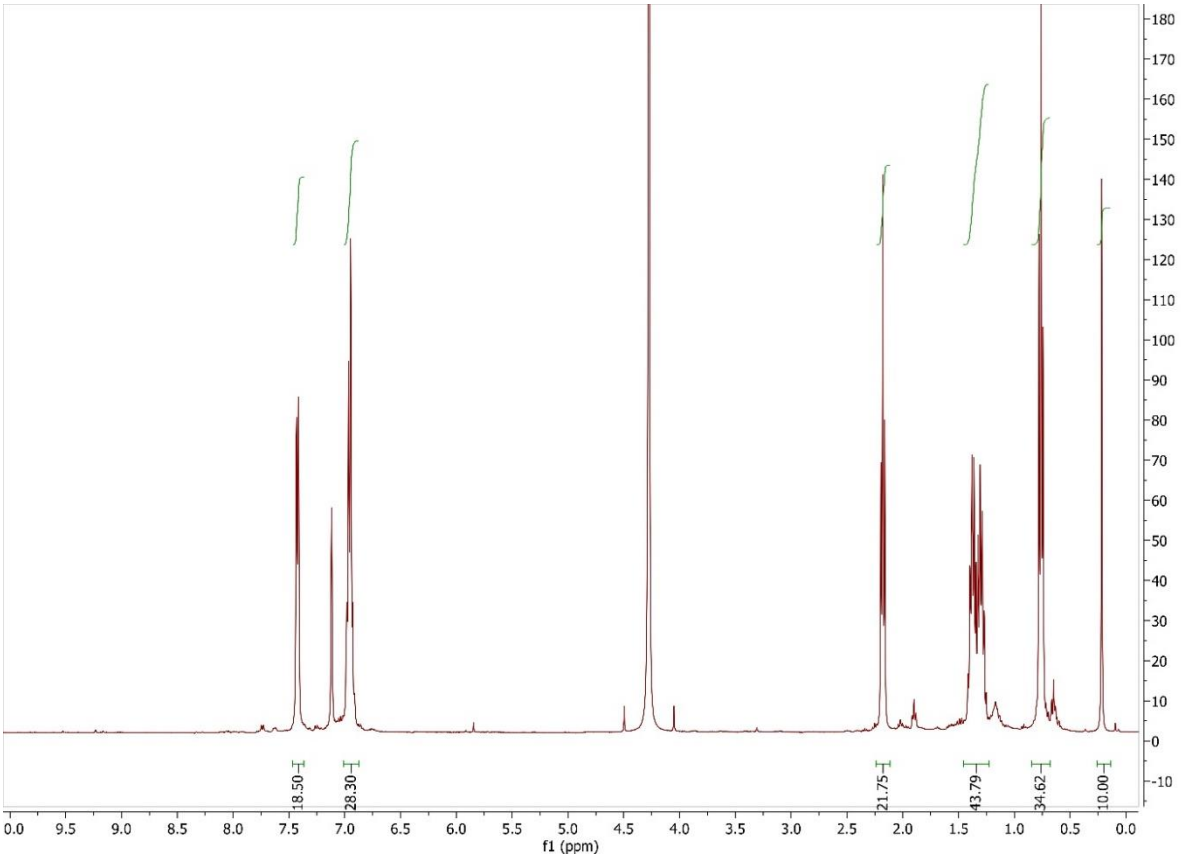

Figure 2.137 ^{1}H NMR spectrum of the ending composition for the isomerization of 1-phenyl-1-hexyne with **Au2.2a** in C_6D_6 at 400 MHz

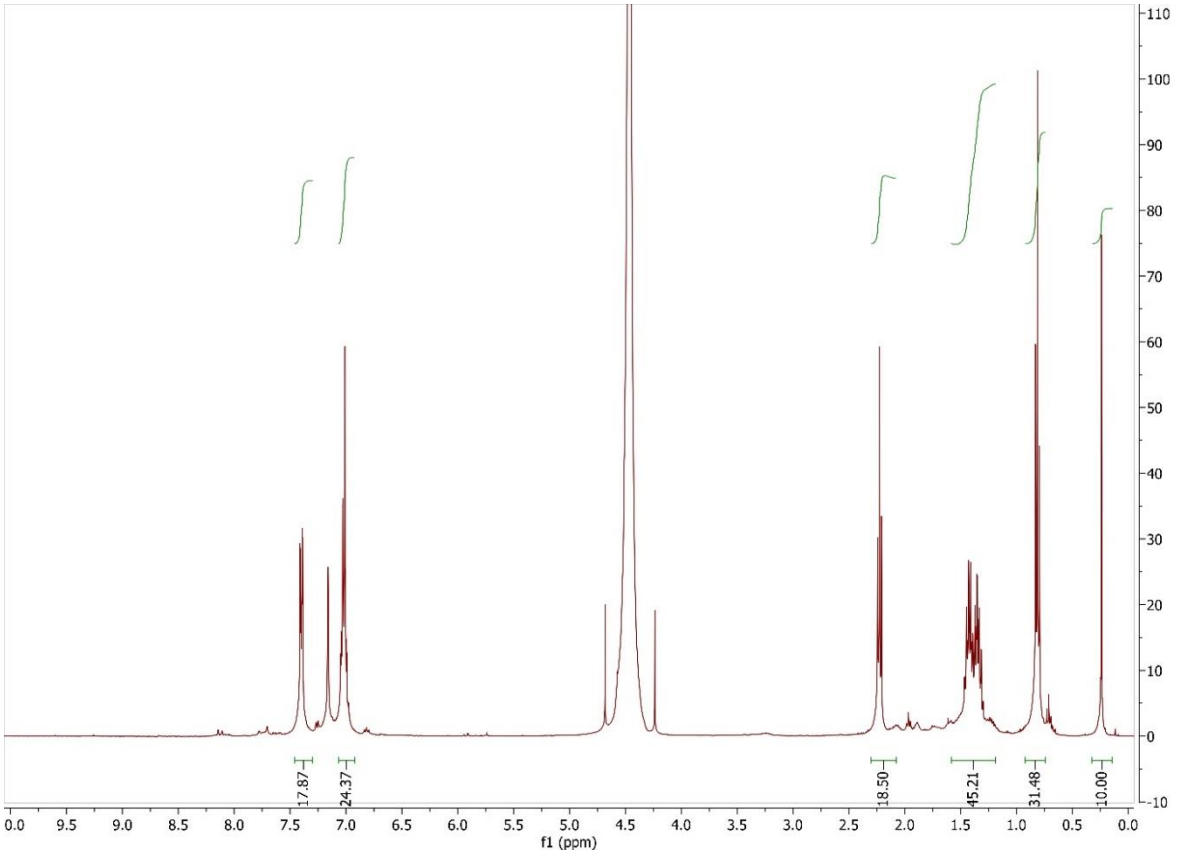

Figure 2.138 ^{1}H NMR spectrum of ending composition for the isomerization of 1-phenyl-1-hexyne with **Au2.2a** after additional catalyst and ionizing agent were added, in C_6D_6 at 400 MHz

Isomerization of 1-phenyl-1-hexyne with **Au2.6a**

In a nitrogen filled glovebox, a J. Young NMR tube was charged with **Au2.6a** (0.026 M in THF) (500.0 µL, 6.5 µmol) then placed under reduced pressure to remove all volatiles. Next the tube was charged with 1-phenyl-1-hexyne (22.9 mg, 0.144 mmol), and $((CH_3)_3Si)_4C$ (internal standard). The tube was then sealed and an initial measurement of the ^{1}H NMR spectrum was observed. Next, sodium tetrakis[3,5-bis(trifluoromethyl)phenyl]borate (11.6 mg, 0.013 mmol) was added to the reaction mixture, the tube sealed, and placed in an oil bath heated to 60 °C for 18 hours. Integration of the 1,3-diene product signals at δ 0.91 (t, *J* = 7.5, 3H), 5.73 – 5.62 (m, 1H),

6.17 – 6.07 (m, 1H), 6.36 (d, *J* = 15.3, 1H), and 6.72 (dd, *J* = 15.8, 10.4, 1H) measure at 14.5% product formation.

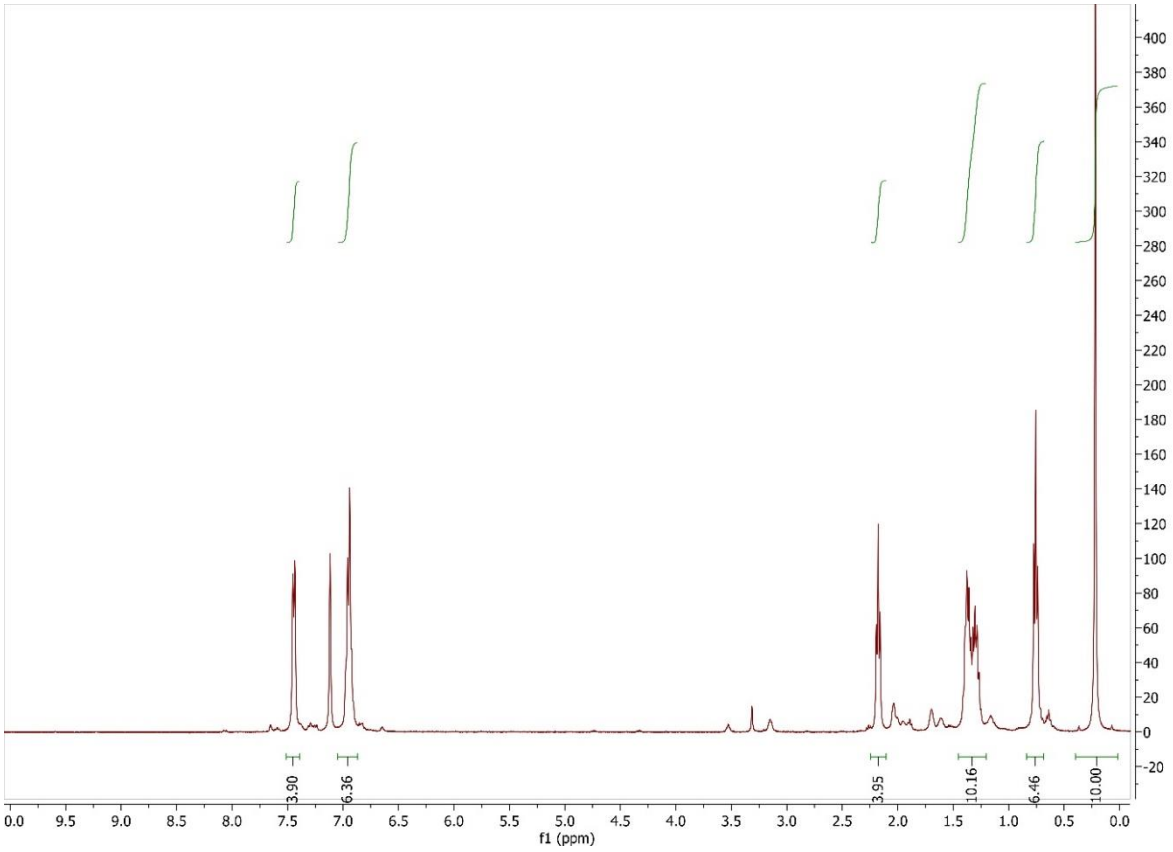

Figure 2.139 ^{1}H NMR spectrum for starting composition for isomerization of 1-phenyl-1-hexyne with **Au2.6a** in C_6D_6 at 400 MHz

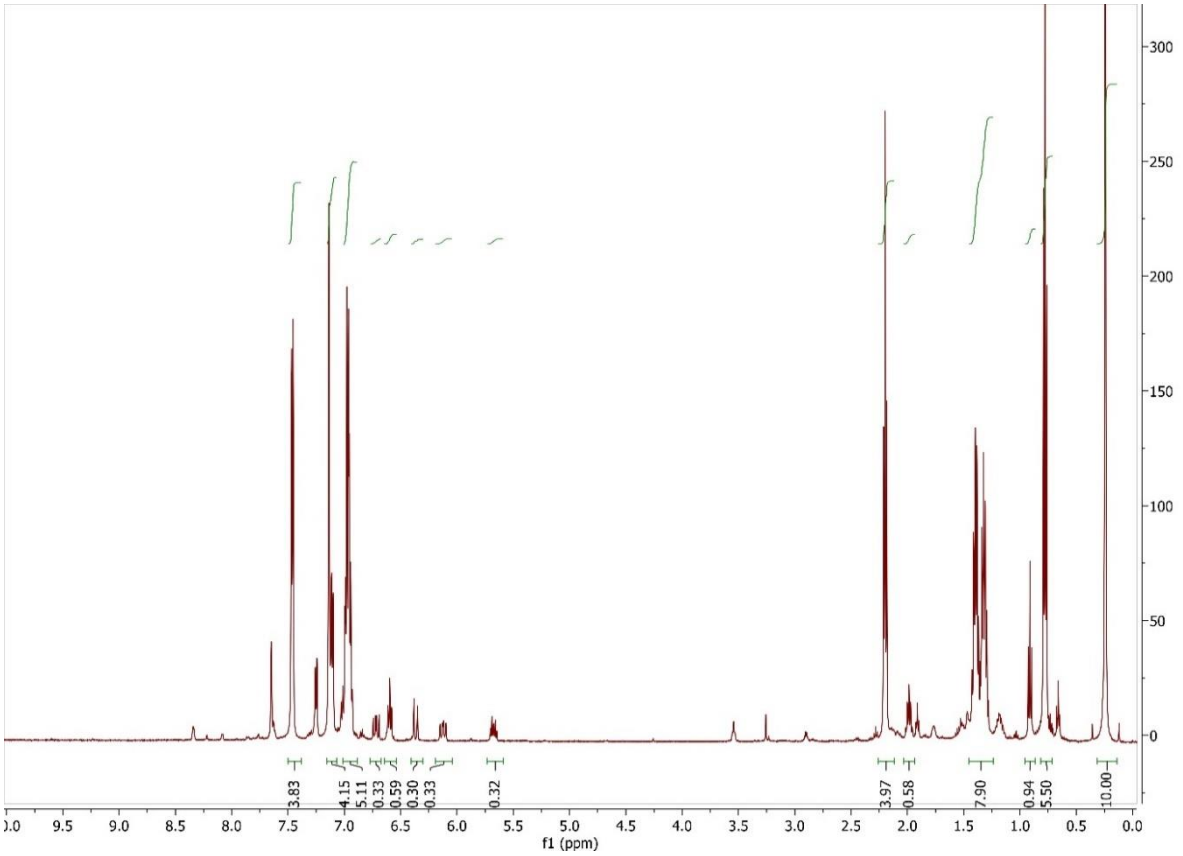

Figure 2.140 ^{1}H NMR spectrum for ending composition in the isomerization of 1-phenyl-1-hexyne with **Au2.6a** in C_6D_6 at 400 MHz

Isomerization of 1-hexyne with **Au2.2a**

In a nitrogen filled glovebox, a J. Young NMR tube was charged with **Au2.2a** (0.036 M in THF) (110.0 µL, 0.0039 mmol). The volatiles were then removed under reduced pressure. Next the tube was charged with 1-hexyne (14.2 mg, 0.173 mmol), $((CH_3)_3Si)_4C$, and C_6D_6 (0.7 mL), sealed, and the initial measurement of the ^{1}H NMR spectrum observed. The tube was then charged with sodium tetrakis[3,5-bis(trifluoromethyl)phenyl]borate (7.6 mg, 0.0085 mmol). Once the tube was sealed, it was placed in an oil bath heated to 60 °C for 31 hours. Integration of the signals at δ 5.03 (p, *J* = 6.8, 1H), 4.61 (dt, *J* = 6.5, 3.2, 2H), 1.87 (dtd, *J* = 10.3, 6.9, 3.2, 2H), and 0.83 (t, *J*

= 7.3, 3H) show production of penta-1,2-diene at 36 %. The starting material, 1-hexyne remains at 43% of the initial value.

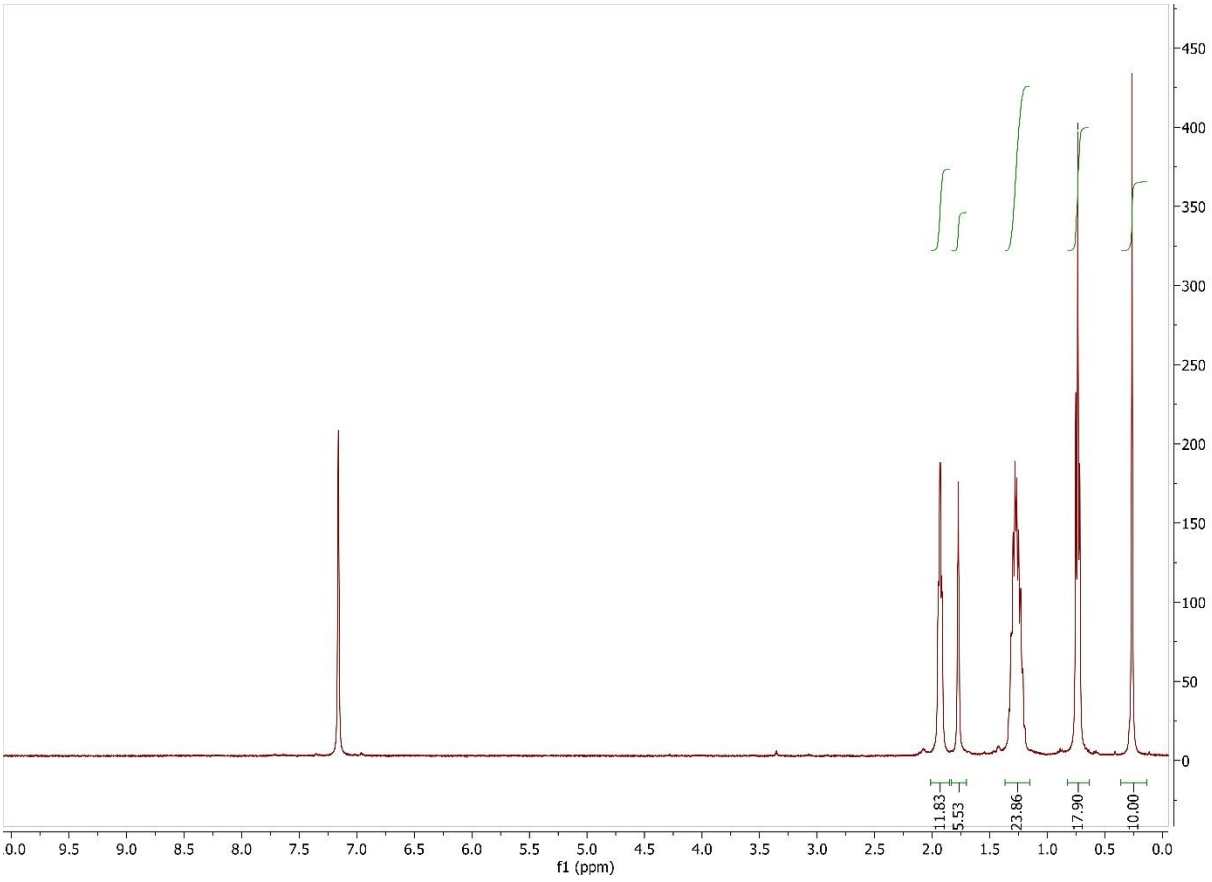

Figure 2.141 ^{1}H NMR spectrum of starting composition in isomerization of 1-hexyne with **Au2.2a** in C_6D_6 at 400 MHz

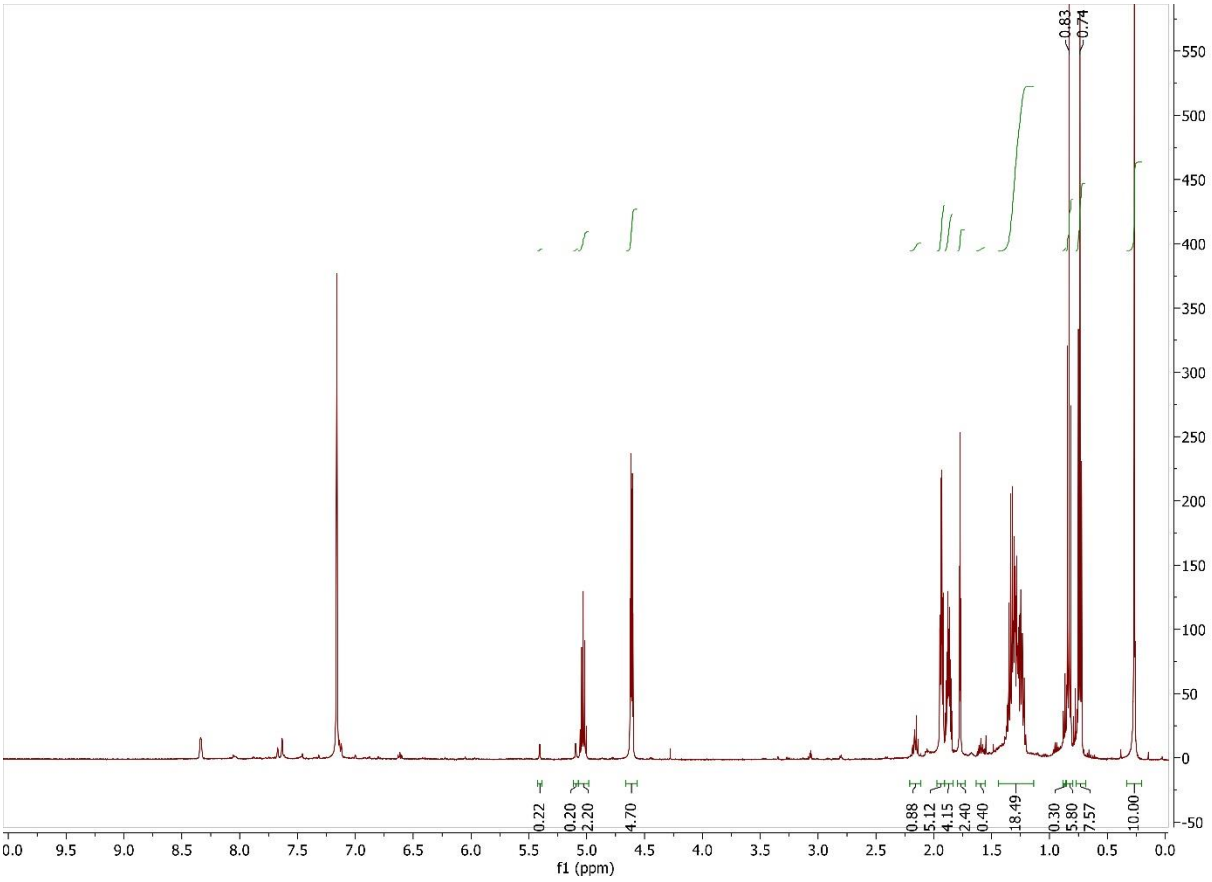

Figure 2.142 ^{1}H NMR spectrum of ending composition in the isomerization of 1-hexyne with **Au2.2a** in C_6D_6 at 500 MHz

Isomerization of 1-hexyne with **Au2.6a**

In a nitrogen filled glovebox, a J. Young NMR tube was charged with **Au2.6a** (0.026 M in THF) (0.25 mL, 0.0065 mmol), then the THF removed under reduced pressure. Next the tube was charged with 1-hexyne (11.2 mg, 0.136 mmol), $((CH_3)_3Si)_4C$, and C_6D_6 (0.7 mL). The tube was sealed and the initial measurement of the ^{1}H NMR spectrum observed. Next the tube was charged with sodium tetrakis[3,5-bis(trifluoromethyl)phenyl]borate (12.2 mg, 0.014 mmol). The tube was then sealed and placed in an oil bath heated to 60 °C for 14 hours. The tube was then removed from the oil bath, cooled to room temperature, and the reaction progress measured by ^{1}H NMR analysis. The detection of allene signals at δ 5.03 (p, J = 6.8, 1H), 4.61 (dt, J = 6.5, 3.2, 2H), and

0.83 (t, J = 7.4, 3H) were used to calculate the amount of penta-1,2-diene production at 68 %. The signals at δ 2.02 (tq, 2H) and 1.56 (t, J = 2.5, 3H) were used to calculate the amount of 2-hexyne production at 15 %. The remaining 1-hexyne was measured to be 9 %.

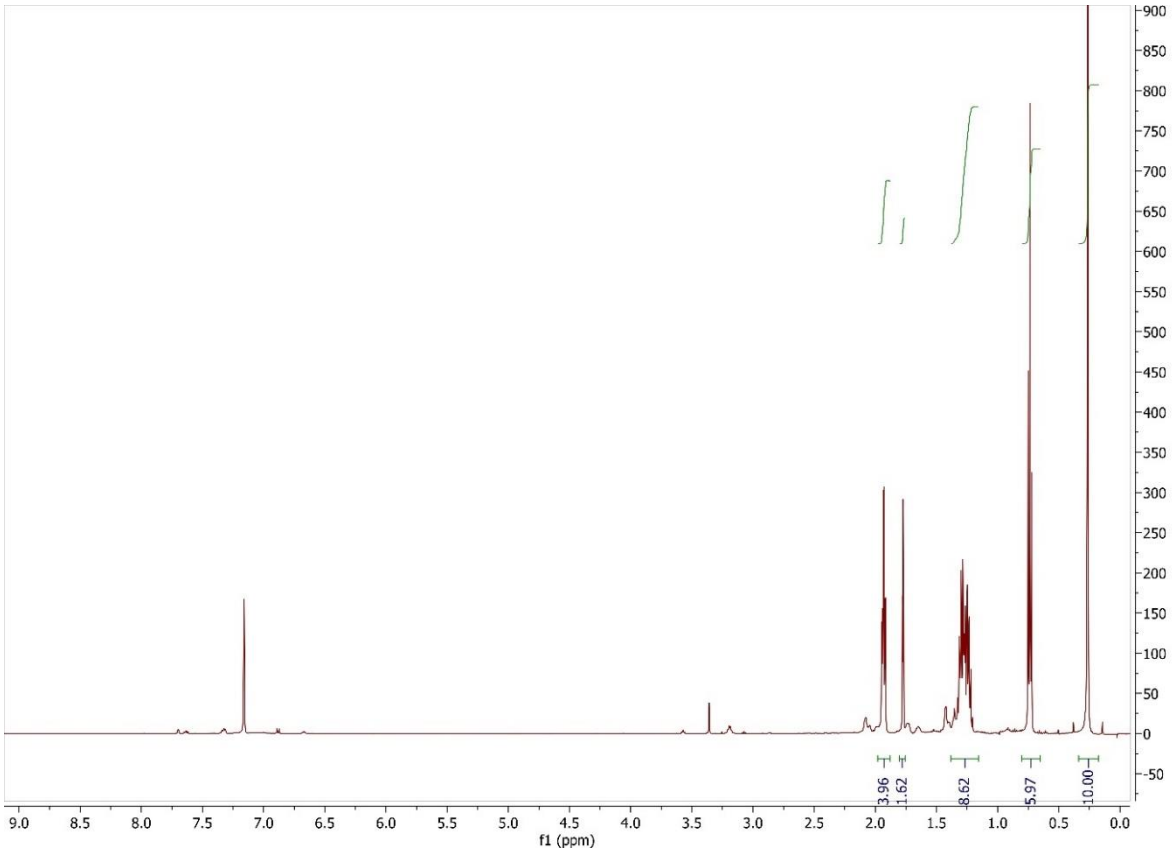

Figure 2.143 ^{1}H NMR spectrum of starting composition in isomerization of 1-hexyne with **Au2.6a** in C_6D_6 at 400 MHz

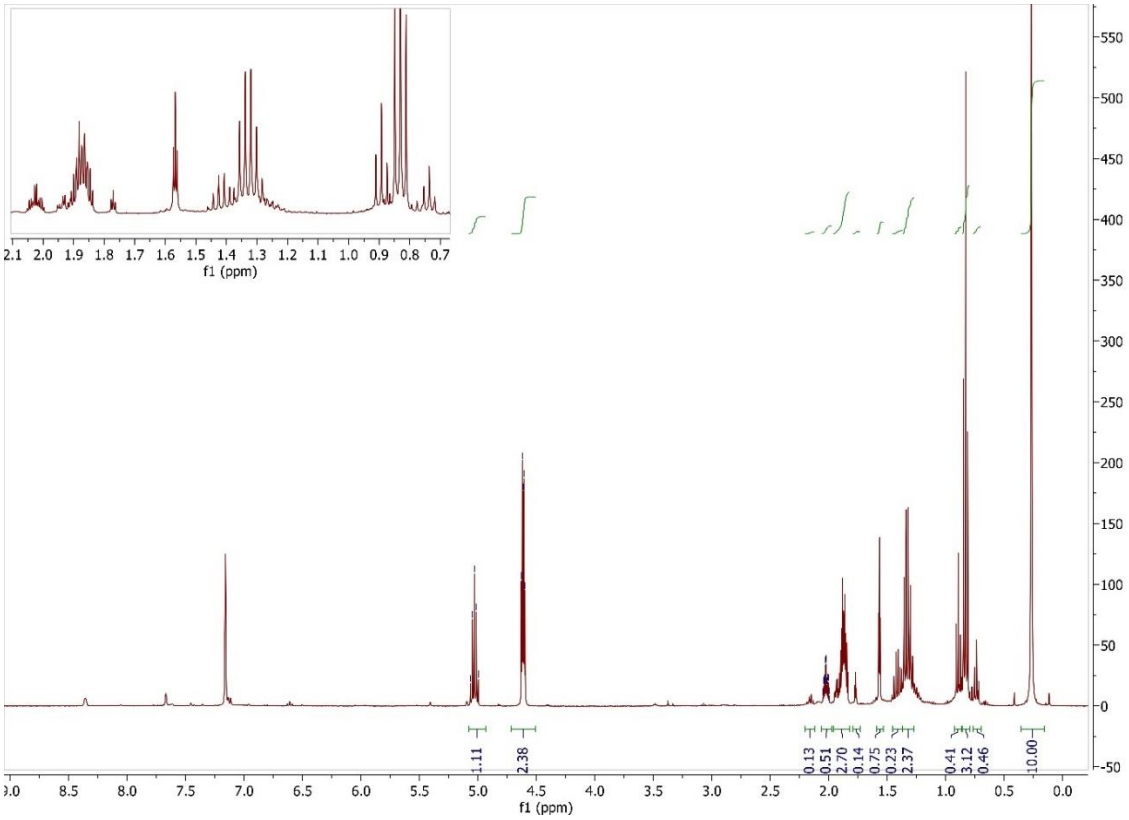

Figure 2.144 ^{1}H NMR spectrum for ending composition in the isomerization of 1-hexyne with **Au2.6a** in C_6D_6 at 500 MHz

Isomerization of 3-hexyne with **Au2.2a**

In a nitrogen filled glovebox, a J. Young NMR tube was charged with **Au2.2a** (4.4 mg, 5.1 µmol), 3-hexyne (10.3 mg, 0.125 mmol), $((CH_3)_3Si)_4C$, and C_6D_6 (0.7 mL). The tube was sealed and the initial measurement of the ^{1}H NMR spectrum observed. Next the tube was charged with sodium tetrakis[3,5-bis(trifluoromethyl)phenyl]borate (9.7 mg, 10.9 µmol). The tube was then sealed and placed in an oil bath heated to 70 °C for 20 hours. The tube was then removed from the oil bath, cooled to room temperature, and the reaction progress measured by ^{1}H NMR analysis. The starting material, 3-hexyne, was detected to be 96.4% of the initial value.

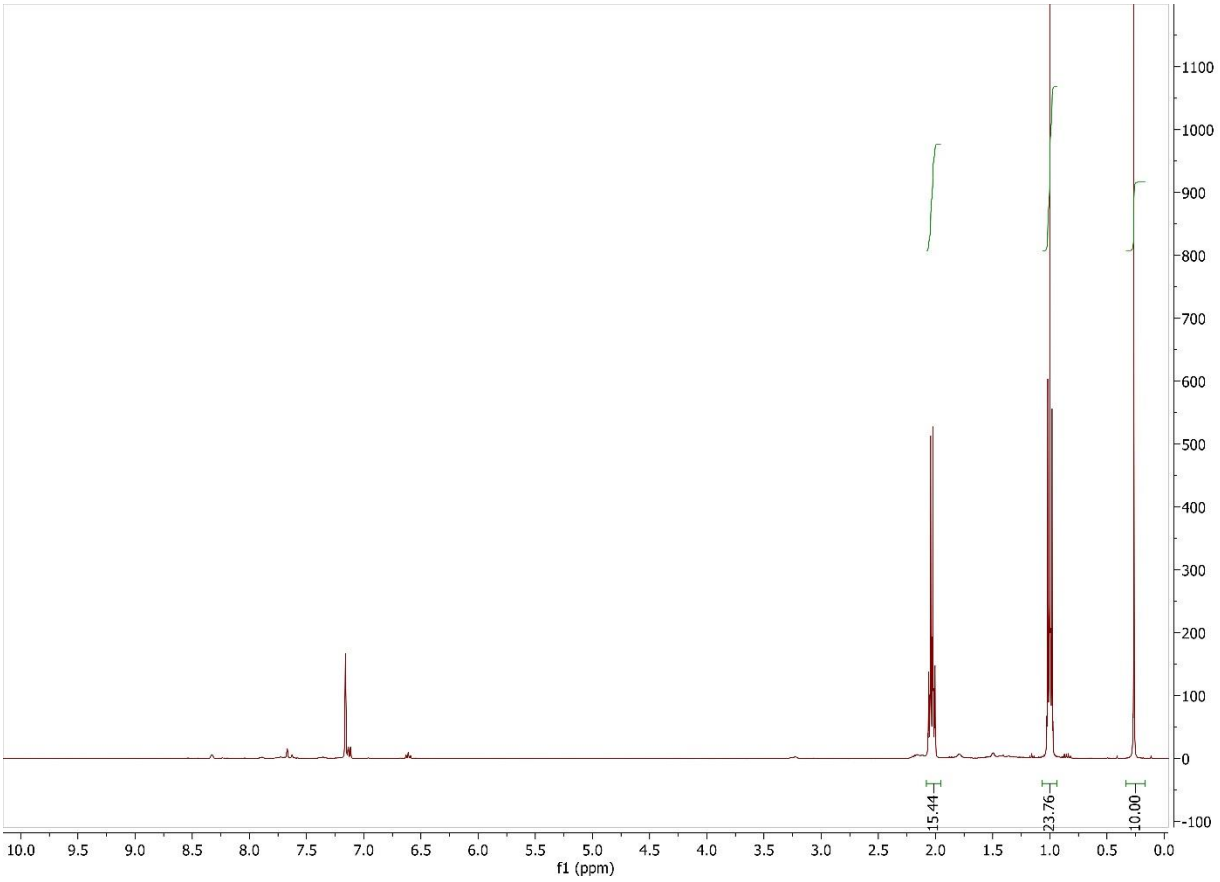

Figure 2.145 ^{1}H NMR spectrum for starting composition in the isomerization of 3-hexyne with **Au2.1a** in C_6D_6 at 400 MHz

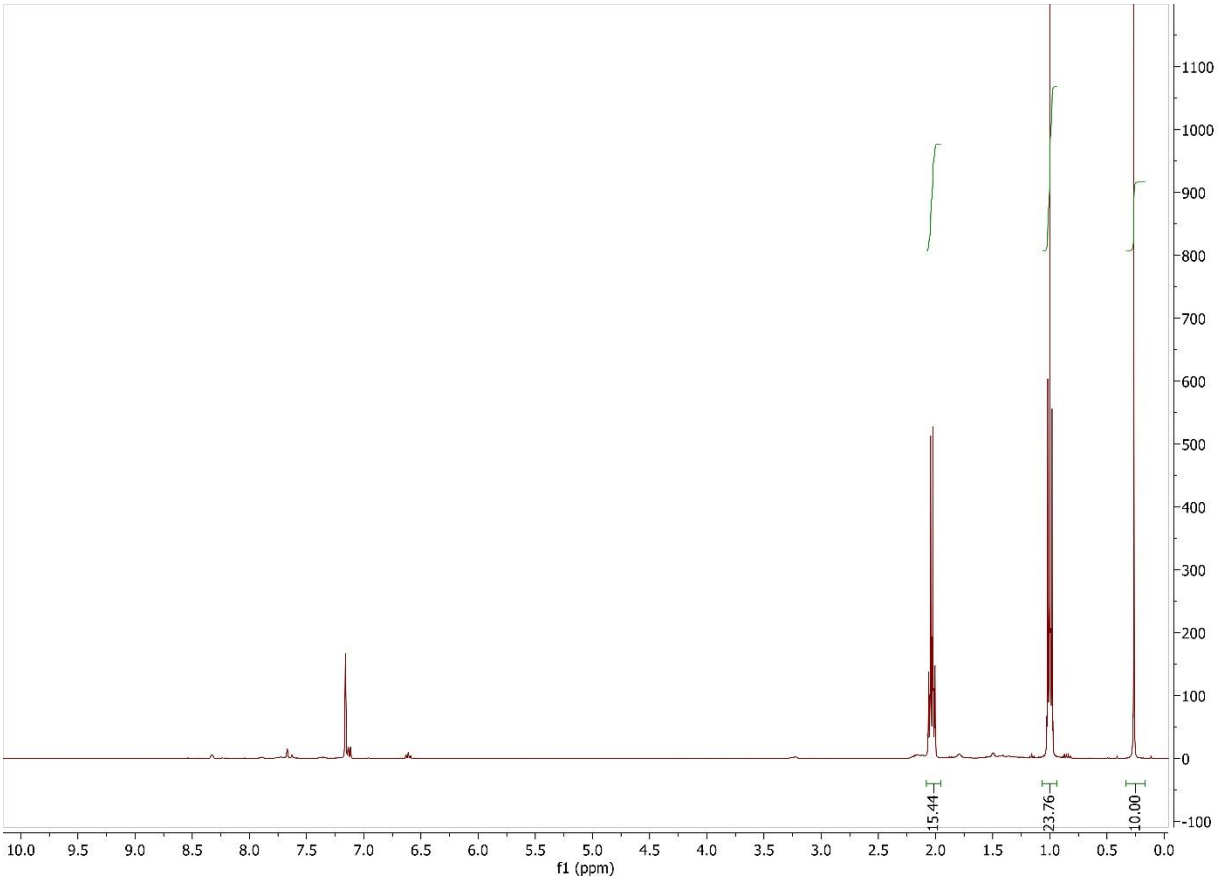

Figure 2.146 ^{1}H NMR spectrum of ending composition in the isomerization of 3-hexyne with **Au2.1a** in C_6D_6 at 400 MHz

ACKNOWLEDGEMENTS

Chapter 2 contains material and data being prepared for publication on the development of functionalized biaryl phosphine ligands for application in gold catalysis. This chapter starts with development of synthetic methods for high efficiency in the synthesis of new iterations on the chemical structure. The use of high throughput screening for reaction discovery is discussed and the result from our trials is discussed. Evaluation of the different ligand candidates is done through NMR studies on two reactions. The first reaction studied is carboxylic acid addition to terminal alkynes. The second reaction studied is isomerization of alkynes. The dissertation author was the sole investigator and author of this chapter.

CHAPTER 3

3.1 Introduction

During mechanistic investigation into the two most successful catalyst systems (in terms of substrate scope, kinetic rates, and selectivity) developed in the Grotjahn research group, a key feature becomes apparent. The bifunctional aspects and overall level of activity of both the alkyne hydration **(Ru-1)** and alkene isomerization (**Ru-2**) systems originate from the heterocycle on the phosphine ligand.[49,50] Once free from coordination with the ruthenium atom, the basic nitrogen can accept a hydrogen bond from a substrate molecule or act as a base to facilitate proton transfer from the incoming substrate, thus altering or enhancing the reactivity of otherwise insufficiently reactive molecules. Studies on these ruthenium catalyst systems indicate that the combined effects of the transition metal and the pendent base allow the mildly basic heterocycles to accept protons from poorly acidic positions such as allylic protons and terminal alkynyl positions because of the acidifying effect of the metal-pi interaction.

For the alkene isomerization catalyst, **Ru-2**, after allylic deprotonation on a coordinated alkene, the imidazolium conjugate acid eventually delivers a proton to a new position within the reacting substrate. A generalized schematic for the existing system's bifunctional activity would follow a path of an initially basic functional group acting on an acidified substrate, then the conjugate acid of the functional group acting as an acid complete the catalytic cycle.

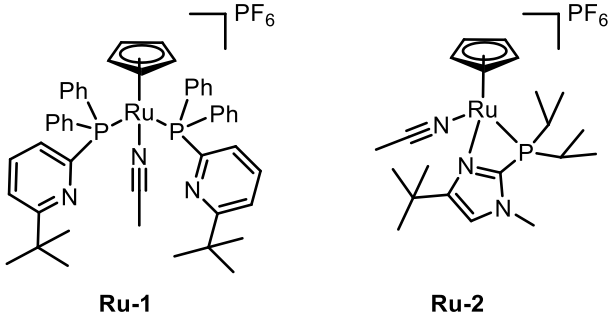

Figure 3. 1 The Grotjahn alkyne hydration catalyst **Ru-1** and alkene isomerization catalyst **Ru-2** structures

A significant aim of this thesis has been to take concepts that govern the reactivity around the **Ru-1** and **Ru-2** systems and expand to new systems that can participate in the same or similar types of interactions in a new context. To that aim, we envisaged a catalyst system that could apply the same mechanistic reaction steps (acceptance of a hydrogen bond, ligand acting as intramolecular base, hydrogen-bond donation, ligand acting as intramolecular acid) but in a rearranged order of operation. A system that displays a reactivity pattern of hydrogen-bond donation / acidic behavior before the hydrogen bond acceptance / basic behavior might offer pathways to new catalytic profiles.

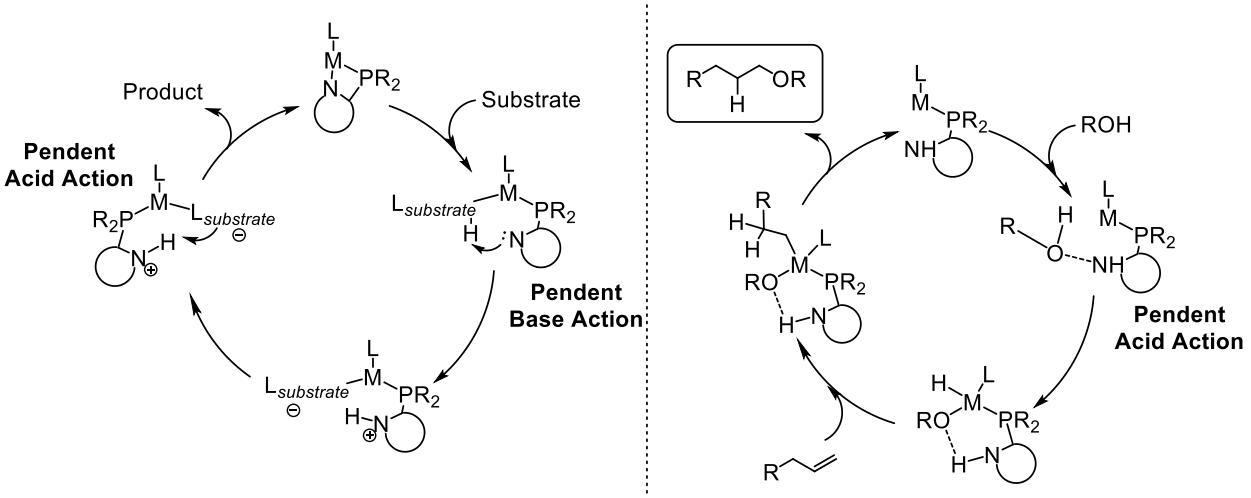

Figure 3. 2 Left) Pendent base first mode of bifunctional activation; Right) Pendent acid first mode of bifunctional activation.

We set our sights on alkene addition chemistry. Specifically, we hypothesized a potential target to be *anti*-Markovnikov type products. Our hypothesis was that an oxidative addition type reaction step between a low valent metal complex and an ROH substrate (water or alcohol) could be accelerated with the pendent acid engagement first pattern of reactivity described above.

Initial work that fueled these concepts was reported in *Organometallics* in 2006[63] on a ditertbutyl-imidizolyl phosphine (**3.1**) and complexation with the zero-valent $Pt(COD)_2$. Then in a 2010 report[64] Grotjahn, *et. al.* expanded the ligand series to include both diisopropyl- and diphenyl-imidazolyl phosphine ligands and their complexes with Cp*Ir moieties.

These initial results indicated some potential usefulness in the system design but left many open questions and a need for innovation. The reactivity observed did show that the hydrogen of the imidazolyl group was able to donate a hydrogen bond to a hydroxo ligand after a reversible oxidative addition, resulting in a Pt^{II} hydride-hydroxo- species (**Pt-3.2**) that was luckily crystallized from the reaction mixture. Furthermore, the system exhibits many opportunities for variation and contains many observables to measure. Both ^{1}H- and ^{31}P-NMR spectra, with coupling to ^{195}Pt observable, as well as x-ray crystal structure data were able to provide ample data documenting the chemical changes.

For example, it is useful to consider some of the remarkable ^{1}H- and ^{31}P-NMR data for the transformations in **Figure 3.3** to illustrate the large set of data readily measurable from this model system. The free ligand **L3.1** shows a $^{31}P\{^{1}H\}$-NMR resonance at δ 16.1 ppm. The chelating hydride species **Pt-3.1** shows $^{31}P\{^{1}H\}$-NMR resonances at δ 52.6 ppm (doublet) with platinum-phosphorus coupling measuring 2940.3 Hz, and a secondary resonance for the chelated moiety at δ 39.4 ppm (doublet) with platinum-phosphorus coupling measuring 2341.2 Hz. The ^{1}H NMR spectroscopic data for **Pt-3.1** reveals an up-field doublet at δ -19.17 ppm with platinum-proton

coupling measuring 1169.3 Hz. Interestingly, decoupling experiments revealed that the hydride proton was coupled only to the ^{31}P nucleus resonating δ 52.6 ppm.

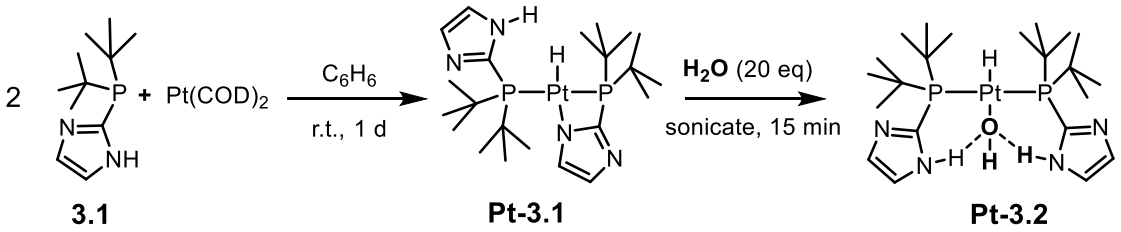

Figure 3. 3 Reactivity described in 2006 *Organometallics* report.

In a further study into this concept, Abhinandini Sharma, Reji Nair, and Doug Grotjahn synthesized the bulkier **L3.2** (diisopropylisopropyl version) and studied its complexation with $Pt(COD)_2$. To their delight, they found that **L2.3** indeed showed differences in reactivity compared to **3.1**. **Figure 3.3** illustrates some of the key differences.

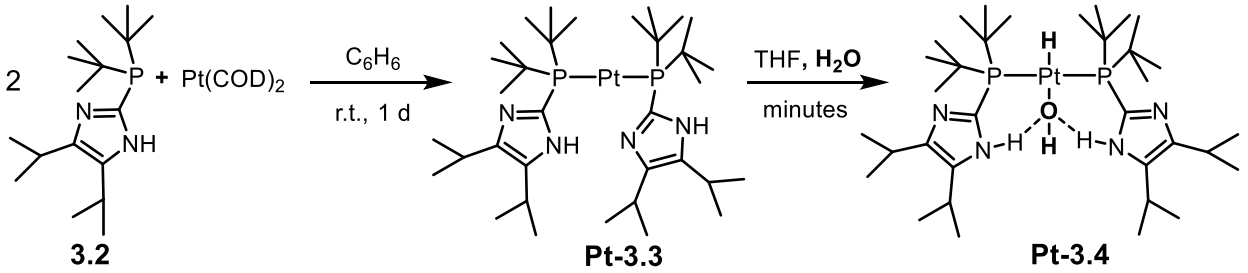

Figure 3. 4 Complexation study of **L3.2** and subsequent reactivity towards water

The two-coordinate Pt(0) complex **Pt3.3** was especially exciting to observe, considering the formal electron count of this compound is only 14 valence electrons. Despite the interesting coordination chemistry of **L3.2** and the structure of its resulting Pt(0) and Pt(II) complexes, **Pt-3.3** and **Pt-3.4**, respectively, no carbon-oxygen bond formation was observed while in the presence of ethylene. Because of this resistance towards catalytic turnover, the project went dormant for several years. Reflection upon this work during the efforts described in chapter two, we were struck with the sense that new ligand design features could push the pendent acid first functionality

towards a catalytic application. For ideas on the next step forward, we brainstormed a possible catalytic cycle would look like for this type of complex acting as an alkene hydration catalyst. Then we considered how to promote these classic organometallic mechanistic steps would benefit from a new ligand design.

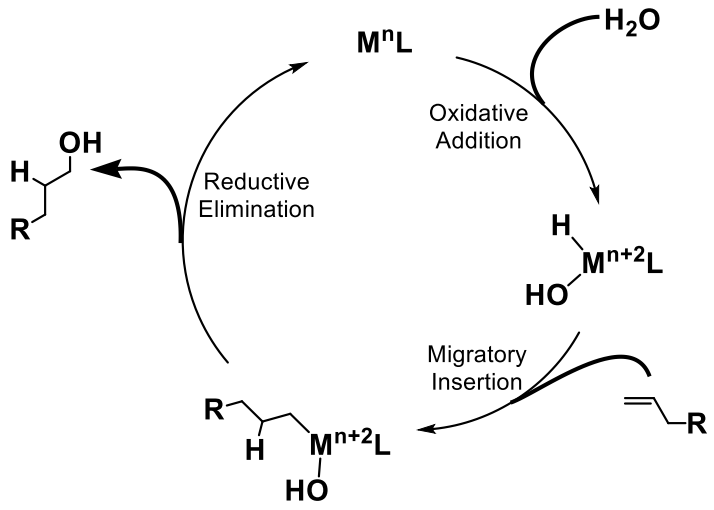

Figure 3. 5 Idealized catalytic cycle for alkene hydration via an oxidative addition / reductive elimination type mechanism.

The protic imidazolyl-ligand framework showed great promise because it was already showing signs of the product of the first step in an idealized catalytic cycle. However, a consistent feature in both systems is the fact that the two phosphine ligands, **L3.1** and **L3.2**, are always observed in the *trans* coordination geometry, thus forcing the hydride and the hydroxo- moieties into an orientation that is unfavorable for a reductive elimination step, assuming an alkene was able to insert into the metal-hydride bond. We set out looking to design a system that encouraged a *cis* coordination geometry of the hydride and hydroxo ligands, gave a driving force for reductive elimination, and conserved the initial reactivity observed in coordination studies with **L3.1** and **L3.2**.

The target scaffold for initial experiments was the ferrocenyl bisphosphine system, which was popularized in the form of 1,1'-bis(diphenylphosphino)ferrocene, commonly referred to as

DPPF. The backbone structure of ferrocene seemed to offer several features that could be useful towards our goals. Specifically, we saw the potential for the bisphosphine system to offer properties that could lower the rearrangement energy and activation barrier for reductive elimination.

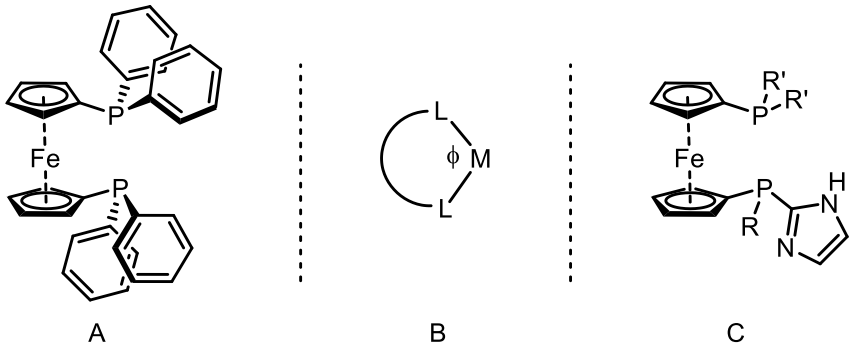

Figure 3. 6 A) DPPF ligand, **B**) Depiction of L-M-L bite angle ϕ; **C**) Generalized concept for new ligand design

Many chemists have studied reductive elimination and found influence on rates to arise from many factors. The bisphosphine ferrocenyl framework and choice of ancillary phosphorus substituents is thought to increase rates of reductive elimination through orbital and steric effects[65,66], symmetry[67,68], bite angle[69–71], coordination number[72], oxidation state[73–79], and degree of σ-donation effects across the entire set of ligands[80]. Depending on the specifics of the conditions, molecules involved in the reaction, and specific type of transformation, these different effects can have varying levels of importance on the ultimate outcome of a chemical event. With these many available levers to adjust reactivity trends, the ferrocenyl backbone was selected for an array of initial ligands. The structures that were targeted for synthesis were specific iterations of the generalized structure shown in **Figure 3.6 C**. This low symmetry system was selected to include a heterocyclic substituent on one phosphorus, while the other phosphorus's substituents could be selected to tune the steric environment and degree of electronic donation from the phosphorus atoms to the transition metal.

3.2 Synthetic Strategy

The first goal to studying any number of these heterocycle-containing bisphosphines was to map an efficient and general synthetic method, ideally allowing later stage generation of several different molecular candidates. We aimed to explore systems both with and without C_2-symmetry. A unique strategy was needed for the lower symmetry structures, so that we could build each phosphine group separately. A stepwise pathway with intermediate points for differentiation to a non-C_2-symmetric ligand system will be described first. Then a more direct route leading to higher symmetry ligands will be described later in this section.

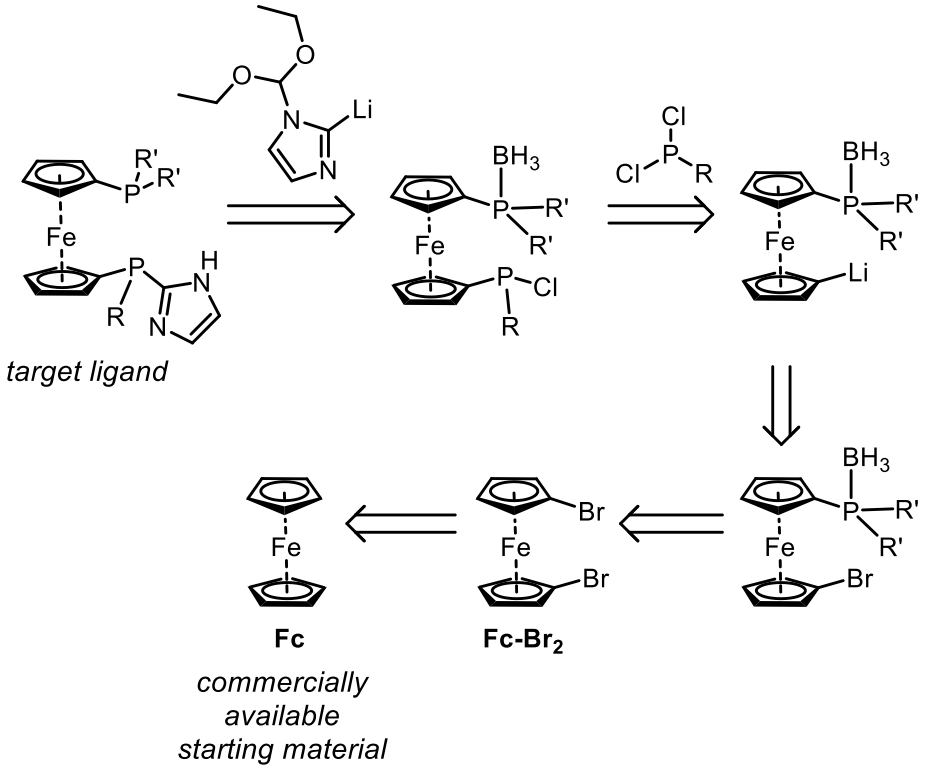

Figure 3. 7 Retro-synthetic strategy for new ligand synthesis with single bifunctional site

We began this synthesis with the commercially available molecule ferrocene (which could be purchased for as low as $0.20 USD/ gram). The reaction of ferrocene with a slight excess of two equivalents of *n*-butyllithium in the presence of a diamine yields the doubly deprotonated dilithoferrocene tetra-(methyl)ethylenediamine adduct can be isolated and stored in a rigorously

air and water free environment.[81] The dilithio-ferrocenyl can be reacted with tetrabromoethane to yield dibromoferrocene via the elimination reaction.[82] A single phosphine can then be added in high yield to generate the mono-phosphine mono-bromo (species after a single equivalent of *n*-butyl lithium is used to generate the mono-bromo-mono-litho-ferrocene. We targeted the use of the borane protecting group on the initial phosphorus group installation to ease the purification of the intermediates. The phosphino-borane adduct is simply removed with the addition of an electron rich secondary amine. In this case pyrrolidine was selected, as the borane-pyrrolidine adduct can be removed by volatilization and captured in a liquid nitrogen cold trap under deep vacuum. Notably, the diisopropylphosphine borane adduct able to be purified by column chromatography without any special care for the air-sensitivity displayed by free dialkyl phosphines.

We attempted the final phase of the synthesis, installing the second phosphine moiety, without removal of the borane protecting group as we were expecting the need for further chromatographic purification to yield an analytically pure sample of the desired ligand. Initial attempts were made by addition of $PhPCl_2$ to the mono-lithioferrocene **3.2** generated in situ (**Figure 3.8**), as the desired product would be immediately ready for the next synthetic step. It is important that the molar ratios of the dichlorophosphine and the lithioferrocene intermediate **3.2** (**or 3.2'**) be kept such that the chlorophosphine is always in excess. If **3.2** was to be in excess of the chlorophosphine, the strongly nucleophilic carbanion would react with the available phosphorus-chlorine bonds, thus creating a possibility where more than one ferrocenyl-group attaches to a single phosphorus atom.

We generated the intermediate **3.2** with the addition of n-butyl lithium to **3.1** in a THF solution that was kept rigorously free of air and water, with the flask in a dry ice and acetone cold bath. Then a cannula and positive nitrogen gas pressure was used to transfer the solution of

lithioferrocenyl intermediate **3.2** to a cold, stirring, and rigorously air and water free solution of dichlorophenylphosphine in THF. A distribution of products was observed, indicated a nonselective reaction. Furthermore, the ^{1}H- and ^{31}P-NMR data indicated a significant change in the structure and bonding.

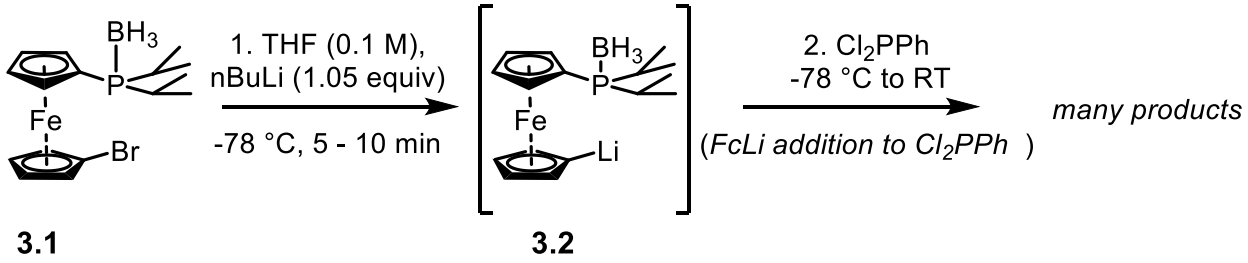

Figure 3. 8 Attempted reaction sequence for installation of the second phosphorus moiety

To further investigate this undesirable result, we ran a series of control experiments to find the most efficient path forward. A particular goal of the synthetic methodology developed in this section is the requirement that very little to no side-product formation occurs. The techniques of purification compatible with the highly reactive synthetic intermediates are very limited. The most reliable separations for chlorophosphines and aminophosphines are filtration and distillation. Chromatography is not possible due to hydrolysis on silica.

To simplify the reaction, we chose to study the formation of the carbon-phosphorus bond using Ph_2PCl instead of $PhPCl_2$. The product of the reaction between **3.2** and Ph_2PCl is not water-reactive, thus allowing all study of conditions to be targeted at the intended chemical step, without unintended interference. We found that the desired substitution product was efficiently formed when the reaction of **3.1** and *n*-butyl lithium was held below -70 °C, **Figure 3.8**. Without the additional phosphorus-chlorine bond, and if the generated carbanion **3.2** is kept below -70 °C, there is no proton scrambling and the desired product is dominant.

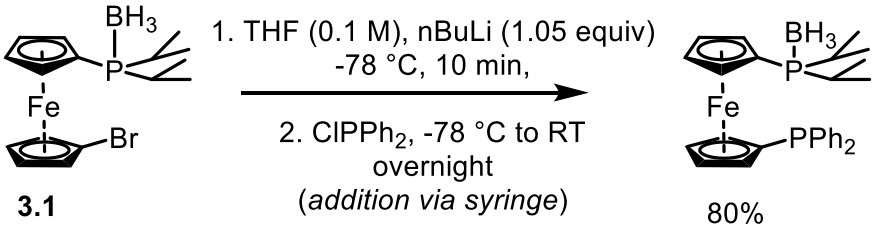

Figure 3. 9 Cold lithium halogen exchange of **3.1**, followed by immediate addition of chlorodiphenylphosphine

In the next control reaction, illustrated in **Figure 3.10**, compound **3.1** was treated with *n*-butyl lithium, again at -78 °C, then after holding for 8 minutes, the reaction vessel was removed from the dry ice and acetone bath and placed in an ice water bath. Then Ph_2PCl was added via syringe to the reaction in the ice bath. A large amount of the product of proton scrambling was detected. The diagnostic evidence of such proton scrambling is the ^{31}P NMR spectrum, showing two doublets resonating at 36.4 and -22.6 ppm with a coupling constant of 229 Hz.

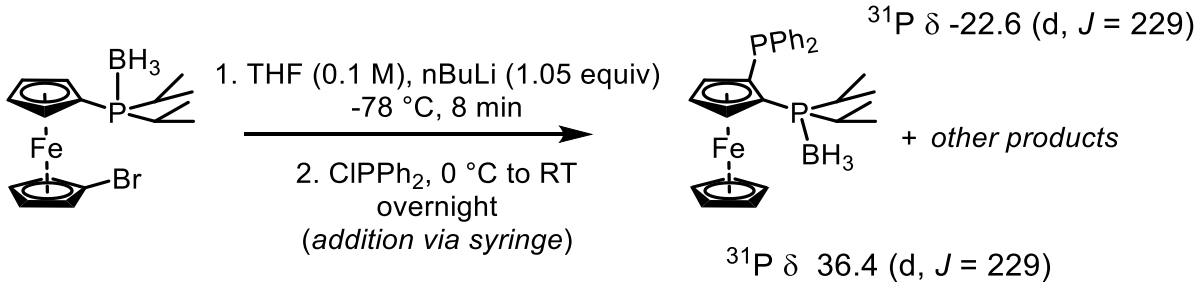

Figure 3. 10 Test of thermal stability of lithioferrocenyl intermediate **3.2** at 0 °C

One hypothesis that was developed was that the borane protecting group was acidifying the protons on the cyclopentadiene ring adjacent the diisopropylphosphine group. To test this, the borane adduct was removed by reaction with pyrrolidine. Once deprotected, the arylbromide **3.1'** was exposed to the same reaction conditions those represented in **Figure 3.8**, addition of *n*-butyl lithium with the solution in a dry ice and acetone bath, then syringe addition of chlorodiphenylphosphine with the temperature maintained near -78 °C. Upon observation of the

products, we were delighted so see the major product was the Fc-T1, in 70-80% yield, from repeated trials, as measured by NMR.

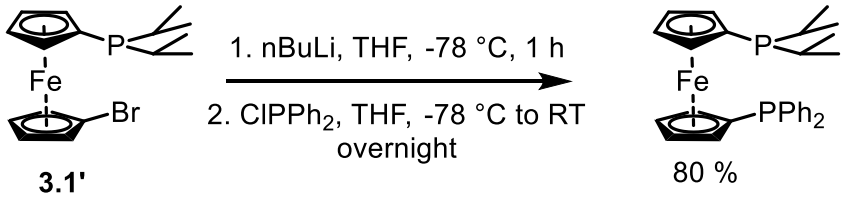

Figure 3. 11 Cold lithium halogen exchange of **3.1'** followed by immediate addition of chlorodiphenylphosphine

We next wished to probe the thermal stability of the intermediate lithioferrocene compound, **3.2'**. In this experiment, after addition of *n*-butyl lithium at -78 °C, the reaction vessel was removed from the dry ice and acetone bath and placed in an ice water bath at 0 °C. Then, at 0 °C, Ph_2PCl was added. In this case we observed the major product to be the desired product. However, rearranged product was observed in 20% relative to the desired product. We also observed small signals for other, unidentified, minor products. This result indicates that even without the borane protecting group, the lithiated ferrocenyl intermediate is unstable at 0 °C.

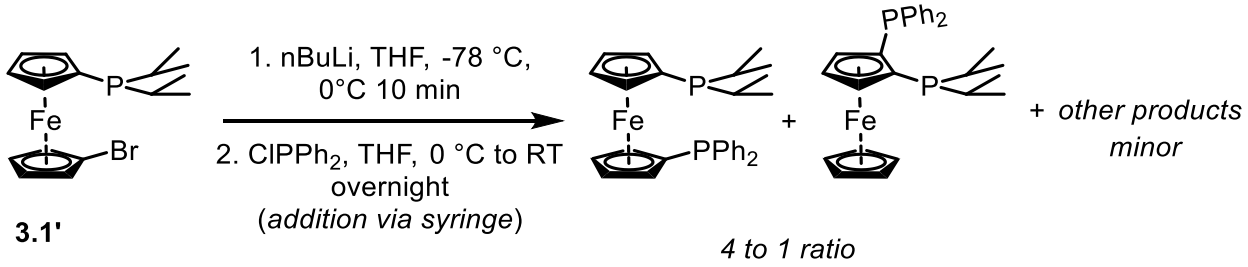

Figure 3. 12 Test of thermal stability of lithioferrocenyl intermediate **3.2'**

We decided to remove the potential for downstream complications due to the thermal instability of both **3.2** and **3.2'**. Instead of attempting to use a dichlorophospine in the reaction with the lithiated ferrocenyl intermediate, we converted the dichlorophosphines of interest to chloro amino phosphines. This additional step is especially useful because the phosphorus-nitrogen bond

is not susceptible to substitution by an alkyl or aryl lithium reagent. Thus, it will be feasible to generate the lithiated ferrocenyl intermediate such as **3.2'**, then add the chlorophosphine to the mixture, without the complication of multiple lithiated molecules reacting with a dichlorophosphine. Conversion of the amino phosphine to a chlorophosphine is easily achieved through the addition of PCl_3 or anhydrous HCl source, and removal of the side product, $PCl_2(NEt)$, under reduced pressure.

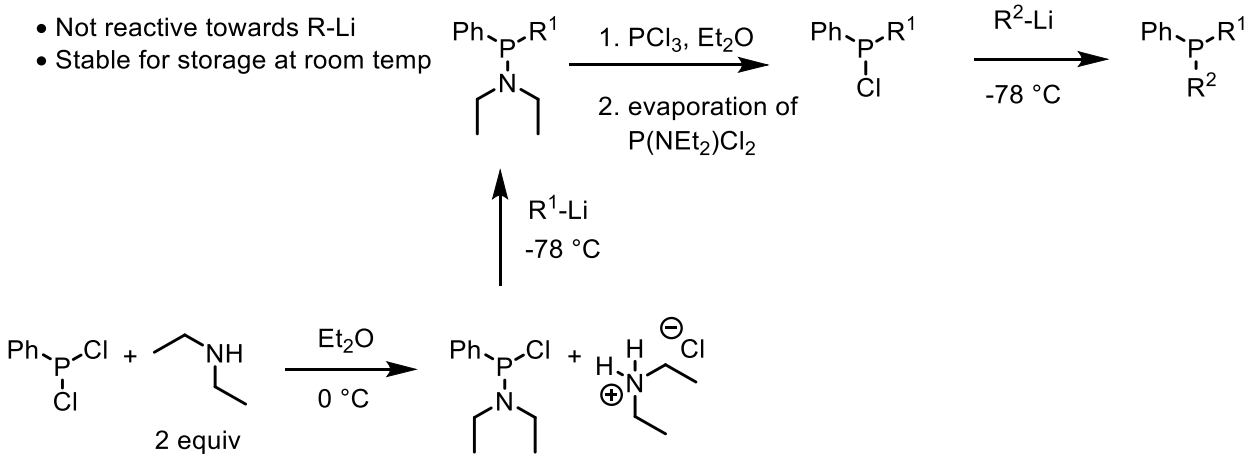

Figure 3. 13 Workflow for utilization of aminophosphine intermediate

After the issues of the thermal instability of the lithioferrecenyl intermediates, **3.2** and **3.2'**, were better understood, the subsequent synthetic steps to reach the target ligand proceeded without complications. It should be noted that once the intermediate amino phosphine is converted to a chloro-phosphine, rigorously air and water-free conditions are required, as well as low temperature storage if not used with a few days.

In the case of the target ligands with higher symmetry, the amino phosphine steps were used, and the synthesis of the target complexes was accomplished as expected from the studies on the non-symmetrical structures. As general note, all of the alkyl-, chloro-, and amino-phosphines are very sensitive to decomposition in air. In the case of the chloro- and amino-phosphines,

exposure to water or other protic molecules will also result in rapid decomposition. Important details include drying all glassware to be used rigorously under vacuum and fresh distillation of distilling solvents to provide sufficiently inert environment for the synthetic steps. In some cases, purification of the starting materials may be necessary to achieve high yielding reaction steps.

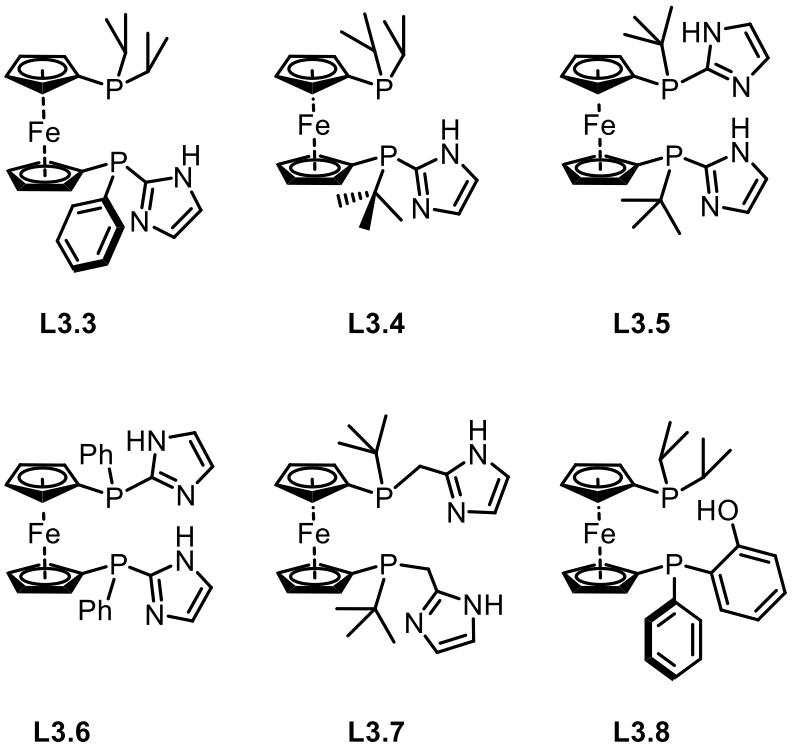

Figure 3. 14 Set of novel ferrocenyl bisphosphines synthesized for study.

L3.3 and **L3.5** were both observed through single crystal x-ray diffraction. The structural data of the free ligands serves as an additional confirmation to the NMR spectral data of molecular identity. However, because of free rotation of the cyclopentadienyl rings when the phosphorus atoms are not coordinated to a metal atom there are no insights gained about potential coordination chemistry or catalytic application.

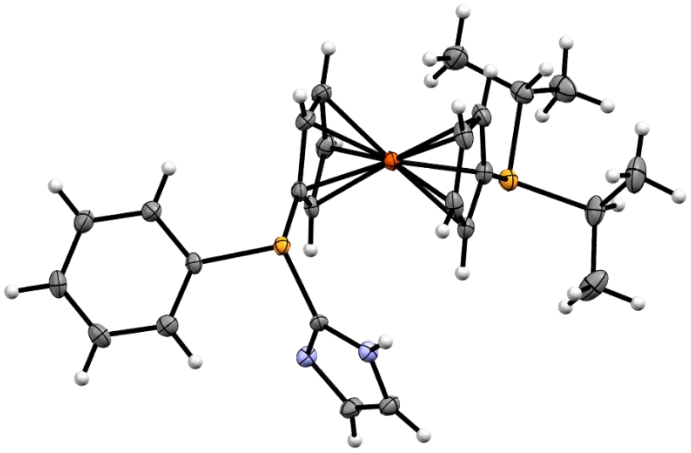

Figure 3. 15 X-Ray crystal structure of **L3.3**, crystals grown by cold storage of a concentrated CH_2Cl_2 solution. Co-crystallized CH_2Cl_2 omitted for clarity.

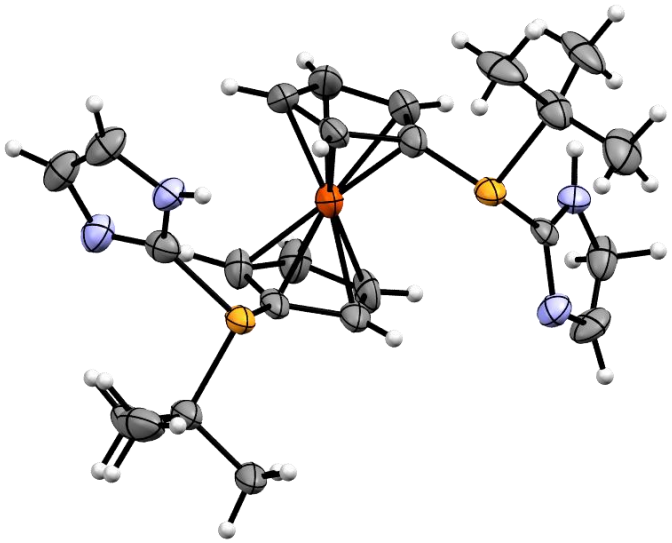

Figure 3. 16 X-Ray crystal structure of **L3.5**, crystallized out of reaction mixture with $Ni(COD)_2$, THF, and H_2O. A co-crystallized water molecule was omitted for clarity.

With the newly synthesized bisphosphinesbisphoshines in hand, we set out to explore trends in coordination chemistry and the reactivity of the resulting metal complexes. We employed

studies monitoring ^{1}H and ^{31}P NMR spectra for insightful observations of the chemistry. We plan on conducting a screening utilizing the HTE methods outlined in chapter 2.4.1 of this thesis.

3.3 Coordination Chemistry with platinum

A key interest for the novel bisphosphines was the coordination chemistry within a platinum complex. The original observation inspiring this work was that of a bisphosphinephosphine platinum complex. We started to probe the coordination chemistry of the new set of bisphosphines when reacted with $Pd(COD)_2$. We prepared a d_8-THF of **L3.3** and mixed with $Pt(COD)_2$. Observation with NMR spectroscopy reveals that Pt(0)-phosphine complex is clearly formed. The two signals for the phosphorus atoms are observed in the ^{31}P NMR to resonate at δ 42.7 ppm (d, $J_{P\text{-}P}$ = 42.5, $J_{Pt\text{-}P}$ = 3395.5) for the diisopropyl phosphine and 6.06 ppm (d, $J_{P\text{-}P}$ = 42.5, $J_{Pt\text{-}P}$ = 3404.5). In the ^{1}H NMR spectrum, signals between δ 4.74 ppm and 4.12 ppm represent four proton equivalents and indicate loss of symmetry of the 1,5-cyclooctadiene signals. Thus the 1,5-cyclooctadiene is bound to platinum in this case.

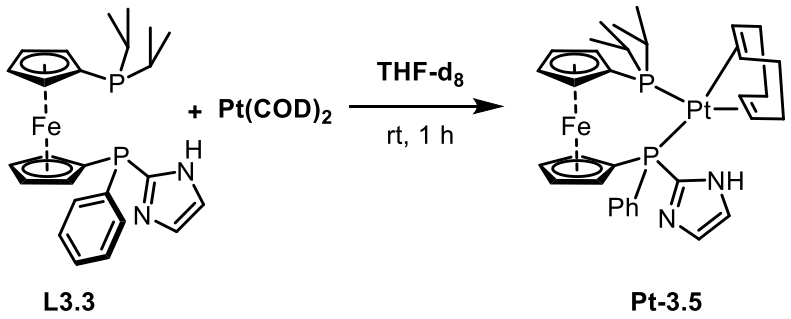

Figure 3. 17 Complexation of **L3.3** with $Pt(COD)_2$

We repeated the experiment in the presence of ethylene and observe the appearance of a broad signal in the ^{1}H NMR spectrum that integrates as four protons at δ 3.0 ppm. This new signal is assigned to coordinated ethylene. It is also noteworthy that the resonances that can be assigned to 1,5-cyclooctadiene are consistent with no coordination to the platinum. Additionally, 20 equivalents of water were added as a THF solution. No definitive signs of activation of the water

oxygen-hydrogen bonds were readily identified. A key feature to look for is a far up-field ^{1}H NMR resonance for metal hydride. Although not fully distinguishable from the spectral noise, a very small signal may be present at δ -6.33 (d, J = 165.6). This sign does indicate that some small degree of O-H bond activation may be possible within this system. However, the relative proportion of this species in the reaction mixture means the concentration is too low to discern further details.

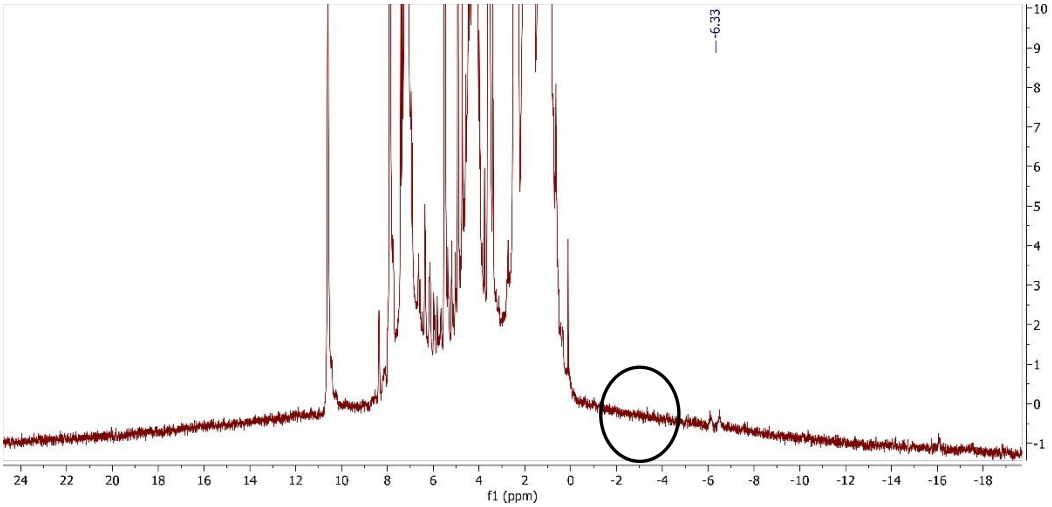

Figure 3. 18 Overview of ^{1}H NMR spectrum of reaction mixture of **L3.3**, Pt(COD)$_2$, and H_2O.

Out of curiosity we again mixed **L3.3** with Pt(COD)$_2$, however this time with the ligand in a two-to-one molar ratio compared to the platinum. The compounds were mixed as a d_8-THF solution and were observed within 1 hour. To our surprise a significantly up-field signal is observed at δ -6.30 ppm (ddd, J = 156.6, 22.6, 10.1) with platinum satellite coupling of $J_{Pt\text{-}H}$ = 835.7 Hz. Also of note is the down field signal at 17.41 ppm, integrating in a roughly one-to-one ratio with the hydride signal. We hypothesize this downfield resonance is due to a strong hydrogen bond between the proton and the two imidazolyl basic nitrogen atoms of the ligands coordinated to platinum. Our assignment of the structure is that of compound **Pt-3.7**. I

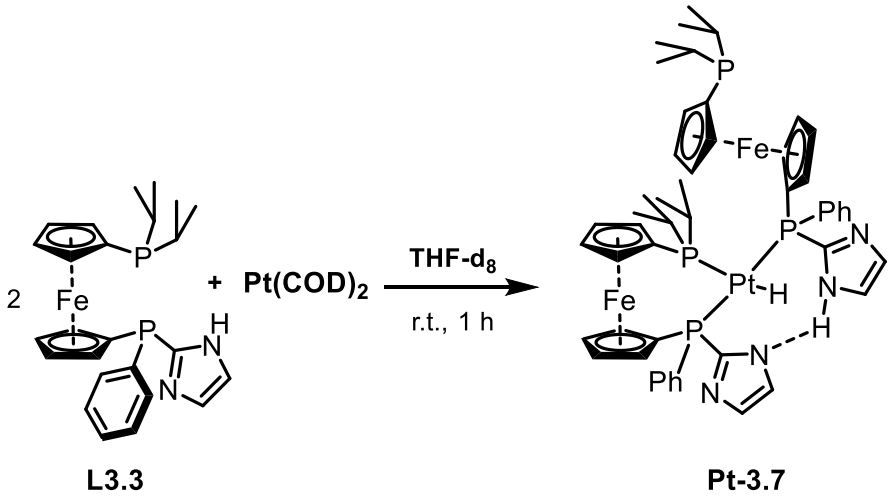

Figure 3. 19 Reaction of two equivalents of **L3.3** and $Pt(COD)_2$

We further probed the hydride formation by complexing **L3.3** with $Pt(COD)_2$ in the presence of different phosphines containing a mildly acid proton. The phosphines **L3.8** (NH-imidazole) and **L3.9** (2-phenolyl) were selected (**Figure 3.20 and 3.21**). We observed similar developments in the ^1H NMR spectra after addition at room temperature. Appearance of a far up-field resonances with platinum coupling satellites was detected as well as the down-field signal assigned to represent a strongly hydrogen bound proton between either the two imidazole rings in the case of **Pt-3.10** or between the imidazole and the phenol in **Pt-3.11**.

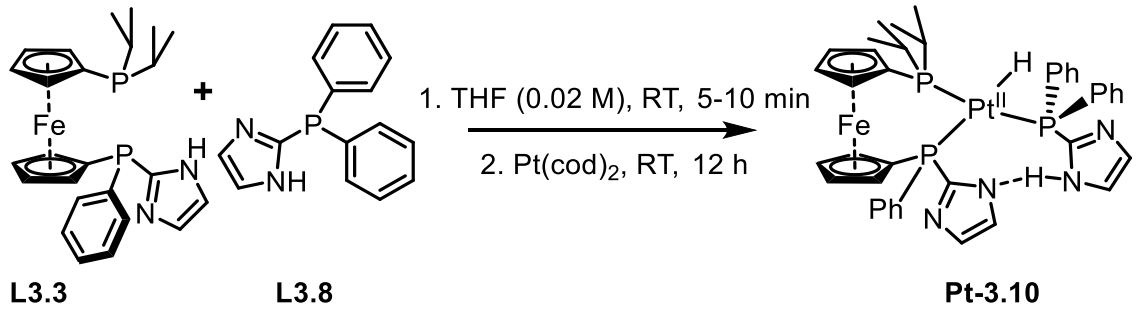

Figure 3. 20 Complexation of **L3.3** and diphenyl-2-imidazolylphosphine with $Pt(COD)_2$

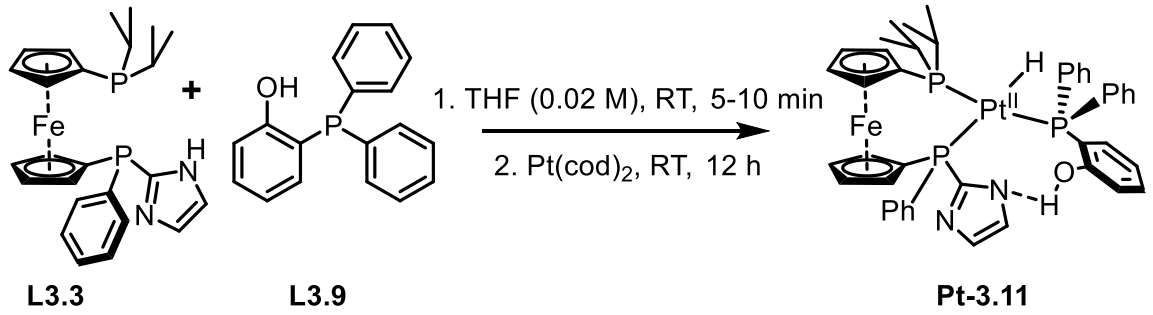

Figure 3. 21 Complexation of **L3.3** and diphenylphosphino-2-phenol with $Pt(COD)_2$

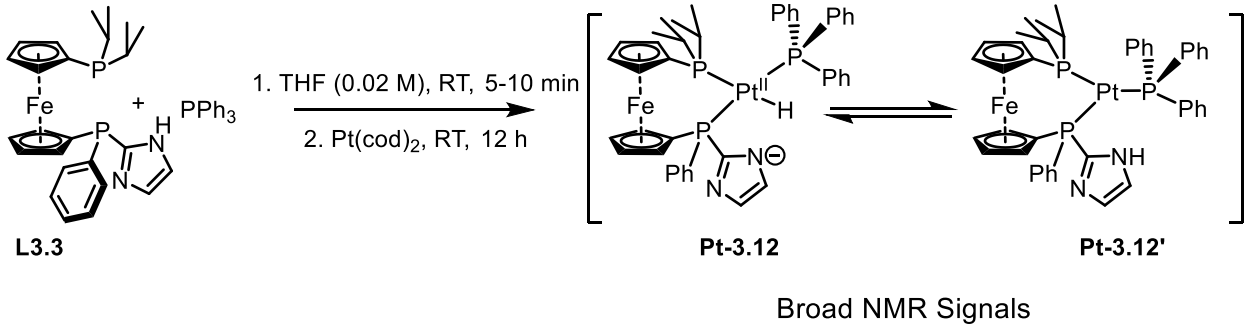

Figure 3. 22 Complexation of **L3.3** and triphenylphosphine with $Pt(COD)_2$

When **L3.3** was complexed with **Pt-3.13** in a one-to-one ratio, two product are formed, **Pt-3.14** and **Pt-3.15**. Initially an even mixture of isomers is observed. The difference in these isomers can be observed in the platinum satellite signals of the ^{31}P NMR spectrum. The atom *trans* to the chloro-ligand has the large platinum-phosphorus coupling, and the atom *trans* to the methyl has the small platinum-phosphorus coupling. After the mixture of these isomers is heated at 70 °C for 6 hours, the system becomes enriched in **Pt-3.14**. We explain this result as hydrogen bonding from the imidazolyl NH and the chloride ligand providing additional stabilization to the complex.

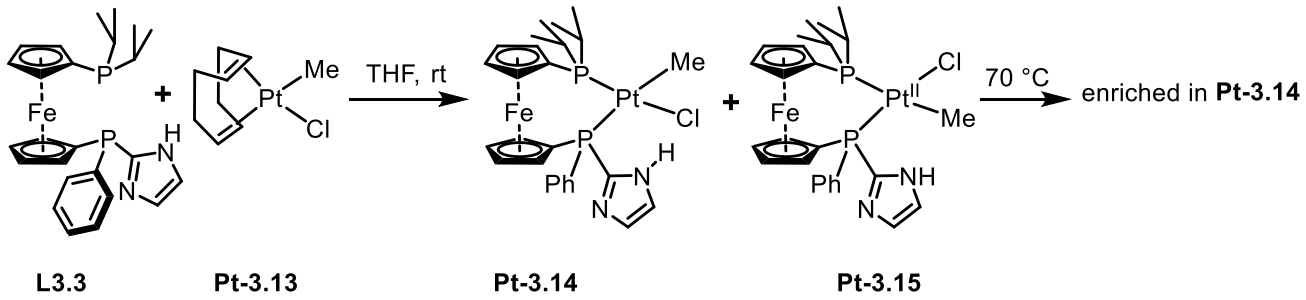

Figure 3. 23 Complexation of **L3.3** with Pt(COD)MeCl, and the observed enrichment in **Pt-3.12** with additional heating

3.4 Coordination Chemistry with Nickel

We had a strong interest in studying the coordination chemistry of the novel functionalized ferrocenyl bisphosphine ligands to many metals. Two obvious points of interest for nickel is its higher abundance on earth compared to palladium and platinum and the long established characteristic resistance of nickel(II)-alkyl complexes to β-hydride elimination[83]. We also received a spark of interest from a bloom of publication on the activity nickel in examples of cooperative catalysis from researcher groups of David MacMillan, Timothy Jamison[84], and others. The cooperative catalysis involves the combination of two different catalysts. In the cases of interest here, a nickel catalyst was paired with photo-redox catalysts such as ruthenium and iridium polypyridine complexes. Studies indicate the nickel complex does much of the work in bond making and breaking steps. The photo-redox catalyst causes oxidation of an intermediate complex from a Ni(II) state to an unstable Ni(III) state, which then quickly reacts in such a step as reductive elimination. Then the resulting Ni(I) complex may be reduced to a Ni(0) state by the reduced state of the photo-redox system.

A great example of such chemistry from the MacMillan group was detailed in *Nature* in 2015.[79] In this work $NiCl_2$•glyme and 4,4′-di-tert-butyl-2,2′-dipyridyl were paired with iridium photo-catalyst to couple primary and secondary alcohols to aryl bromides forming aryl ethers. A key feature of the proposed catalytic cycle is the oxidation of a Ni(II) intermediate is oxidized by

the photocatalyst to a Ni(III) state, which induces reductive elimination and the desired bond formation.

We were encouraged by these results, as one of the key missing steps from the hypothesized catalytic cycle is the carbon-oxygen bond forming step, likely to occur as a reductive elimination step. Additionally, much of the design of the bisphosphine of study in this work was targeted towards encouraging reductive elimination. In fact, an interesting possibility may arise that some co-catalyst or added reagent could oxidize the iron(II) within the ligand structure, at some point within a reaction cycle, to an iron(III) ferrocenium. The oxidized iron atom would likely influence the chemistry elsewhere in the structure through electrostatic (through space) or electron withdrawing (through bond) effects.

Our study of complexation of the bisphosphines to nickel started with complexation to $Ni(COD)_2$. In order to rely on NMR analysis for observation of the chemistry, we specifically targeted Ni(0), a d^{10} atom, to avoid complications from high spin (unpaired electrons). Complexation of **L3.3** with $Ni(COD)_2$ in a one-to-one ratio resulted in the rapid appearance of a color change of the bright yellow nickel solution to a brown colored solution. Observation by NMR revealed there were multiple products formed. Surprisingly, a major resonance is observed at δ 93.79 ppm (dt, J = 154.7, 21.1). This is a significant change in chemical shift from the free ligand which shows resonances at δ -0.24 ppm and -36.23 ppm. Also consider the observed splitting pattern, a doublet of triplets. Further analysis of the signals in the spectrum reveals these three other NMR active nuclei are all phosphorus atoms. The coupling constant match between the resonances at δ 38.13 ppm (ddd, J = 107.8, 20.5, 9.8), 22.56 ppm (ddd, J = 107.7, 21.6, 15.2), and 8.45 ppm (ddd, 154.9, 15.2, 9.8). We ruled out the possibility that simply two L3.1 molecules coordinated to a nickel(0) atom due to the large differences in chemical shift of each signals.

Interesting, possible changes in oxidation state seemed unlikely due to the fact any clearly defined NMR signals are observed at all. Nickel coordination complexes are often paramagnetic, and thus not readily observed by NMR.

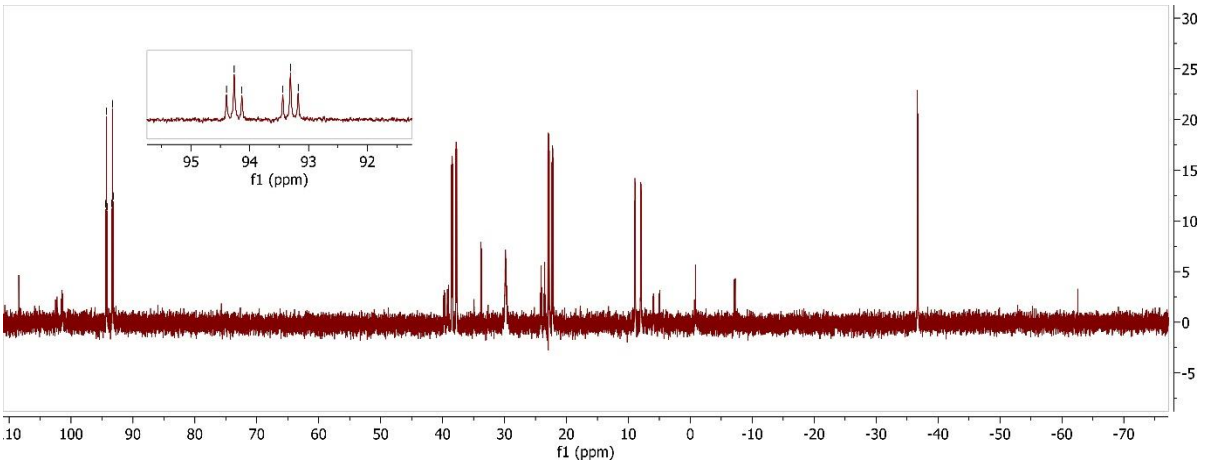

Figure 3. 24 ^{31}P NMR spectrum of reaction of **L3.3** and $Ni(COD)_2$ in a one-to-one molar ratio, in C_6D_6 at 162 MHz

We attempted to crystallize any of the products by vapor diffusion of pentane into the C_6D_6 solution. Luckily crystals did form and were suitable for analysis by x-ray diffraction. The observed result was that of a complex containing two nickel atoms and two molecules of the ligand L3.1, only with one of the molecules missing the imidazolyl group from the phosphorus atom! The net result observed is that of one nickel atom cleaving the carbon-phosphorus bond connecting the imidazolyl fragment to the rest of the ligand.

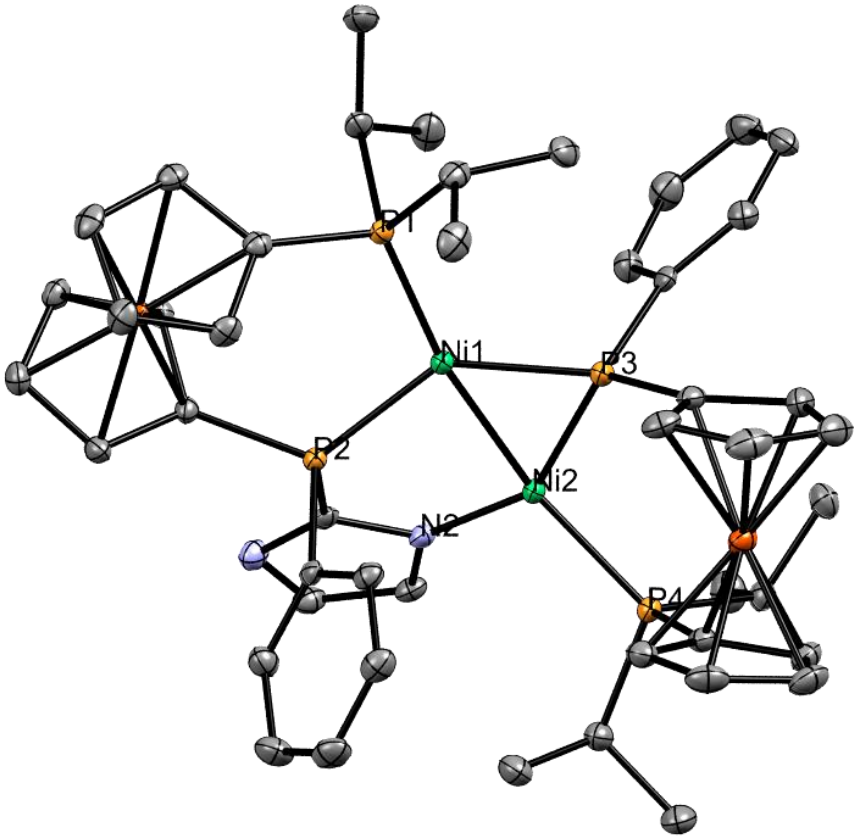

Figure 3. 25 X-ray crystal structure of **Ni-3.1**

The phosphorus atom at the site of the P-C bond cleavage is seen as coordinating to both nickel atoms. A distance of 2.112 Å for the P3-Ni2 bond length is measured, and a distance of 2.137 Å is measured as the P3-Ni1 bond length. The two nickel atoms lie at a distance of 2.529 Å apart from each other. The distance from the diisopropyl phosphorus atom to the nickel atom measures 2.216 Å and 2.184 Å for P1-Ni1 and P4-P2, respectively.

We attempted the complexation of L3.3 to $Ni(COD)_2$ at 0 °C, and in the presence of addition components such as ethylene and water. In all cases, we eventually observed the appearance of the four diagnostic resonances indicative of the multinuclear complex Ni-3.1.

To investigate if sterics around the phosphorus atom could affect cleavage of the phosphorus-carbon bond connecting the imidazolyl fragment to the phosphine we attempted the complexation of **L3.4** with $Ni(COD)_2$. The ligand **L3.4** has the bulkier *tert*-butyl substituent compared to the phenyl substituent in L3.3. In this case we also sparged the ligand solution with ethylene gas, in the hopes of forming a nickel bisphosphine ethylene complex. To our delight, when the reaction mixture was observed by ^{31}P NMR analysis, the appearance of two new phosphorus resonances at δ 37.48 ppm (d, J = 26.5) and 27.24 (d, J = 26.5) was observed along with the disappearance of the free ligand resonances, formerly observed at δ -0.70 ppm and -18.16 ppm.

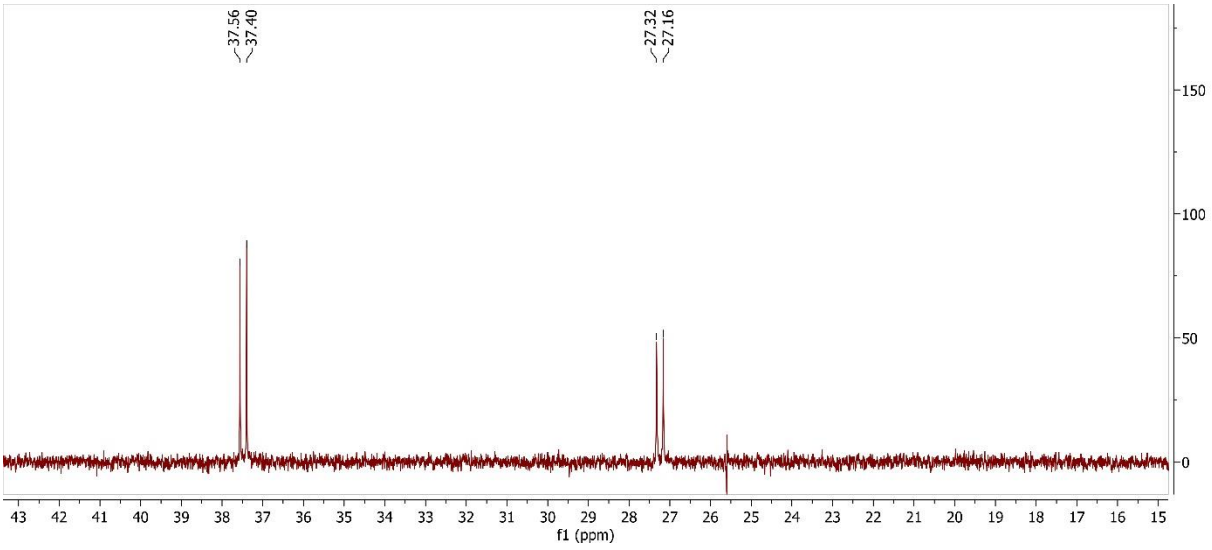

Figure 3. 26 ^{31}P NMR spectrum of **Ni-3.2** in C_6D_6 at 162 MHz

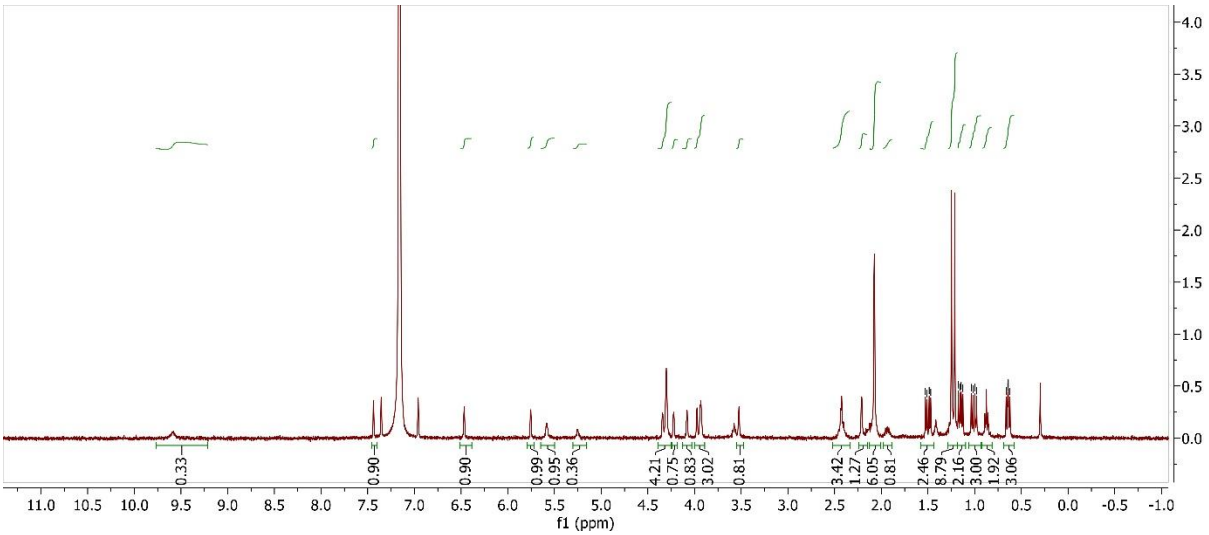

Figure 3. 27 ^{1}H NMR spectrum of **Ni-3.2** in C_6D_6 at 400 MHz

The ^{1}H NMR spectrum also provides detailed information about the newly formed complex. Four distinct signals are observed for the isopropyl methyl groups: δ 1.50 (dd, *J* = 15.9, 7.0 Hz), 1.15 (dd, *J* = 12.8, 7.1 Hz), 1.01 (dd, *J* = 15.8, 7.4 Hz), and 0.64 (dd, *J* = 9.7, 6.9 Hz). This indicates each methyl being in a unique chemical environment. Signals at δ 2.07 ppm (s) and 4.30 ppm (s) integrate in two to one ratio and are taken to indicate a non-coordinated state for the cyclooctadiene.

A new signal at δ 2.42 ppm (br, s) integrates to 3.42 relative to an assigned integration of 3.00 for an isopropyl methyl resonance. Our interpretation is that this broad signal is due to coordination of ethylene. A possible reason for the lack of area under the peak at 2.42 ppm could be a large enough difference in relaxation times for the relative integration to differ from the actual value. The expected slower spin-lattice relaxation rate of the sp^2 protons of ethylene compared to the methyl protons support the 15% deficit in signal. The up field chemical shift relative to free ethylene (*ca*. 5.25 ppm) is consistent with expected results due to the electron rich nature of a nickel(0) atom and the availability for π-back bonding into the ethylene anti-bonding molecular

orbitals. Attempts to induce crystallization through vapor diffusion of pentane into the C_6D_6 solution were not successful.

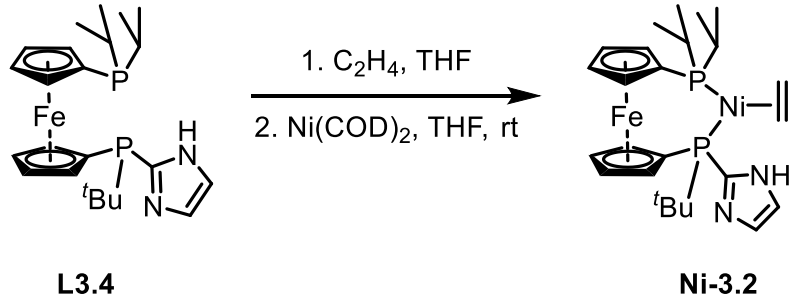

L3.4 **Ni-3.2**

Figure 3. 28 Synthesis of **Ni-3.2** by coordination of **L3.4** and $Ni(COD)_2$ in the presence of ethylene

The three-coordinate nickel complex **Ni-3.2** is proposed as the resulting structure. It may also be likely that a solvent molecule (THF) could bind to form a four-coordinate complex, or two of the three coordinate **Ni-3.2** species could come together and potentially coordinate to the basic nitrogen of the imidazole. To further investigate this proposed complex **Ni-3.2** we took portions of the C_6D_6 NMR solution and added phenol and acetic acid, in separate experiments. Interestingly, the two different experiments returned rather similar spectral details.

When the solution with **Ni-3.2** was mixed with acetic acid in a two-to-three ratio, the ^{31}P NMR siganals assigned to **Ni-3.2** were still observed. However, new resonances are observed at δ 29.62 ppm (br) and -12.15 (d, J = 9.6), as well as minor signals at 31.79 ppm and 11.81 ppm. When the **Ni-3.2** solution was mixed with phenol in a one-to-two ratio similar ^{31}P NMR signals were observed at δ 29.48 ppm (br) and -13.69 ppm (d, J = 9.0). In both experiments the ^{1}H NMR spectrum became significantly less interpretable compared to that used to assign the **Ni-3.2** structure. Because of the lack of clarity in the ^{1}H NMR spectrum and the little information provided from the ^{31}P NMR spectrum no assignment of structure is made. We considered the possibility of the oxygen atom from either phenol or acetic acid coordinating to form four coordinate nickel

complexes. Attempts to induce crystallization by diffusion of pentane into the C_6D_6 solutions were not successful.

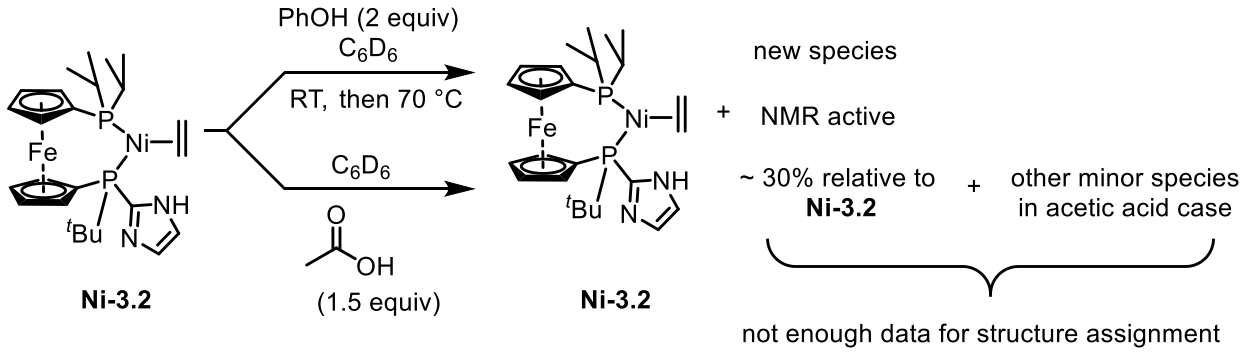

Figure 3. 29 Summary of reactivity studies with **Ni-3.2** and protic molecules

To futher investigate the coordination chemistry between the bifunctional ferrocenyl bisphosphines and nickel, we studied complexation with nickel(II) sources, and reactivity of the corresponding complexes. An additional complication arises in the study of nickel(II) coordination complexes as most are paramagnetic. This paramagnetism often renders ^{31}P NMR analysis useless, and ^{1}H NMR significantly less detailed. Nevertheless, we had hopes that we could gain insights into potential for catalytic applications through such investigations.

To this end, we took the ligand **L3.4** and added one molar equivalent of $NiCl_2$•DME as a THF solution and heated at 70 °C overnight. The resulting product was not identifiable by NMR. Although we acted under the assumption that the nickel(II) dichloride bisphosphine complex **Ni-3.3** was the major complexation product, as this was seen as a reasonable coordination complex in our eyes.

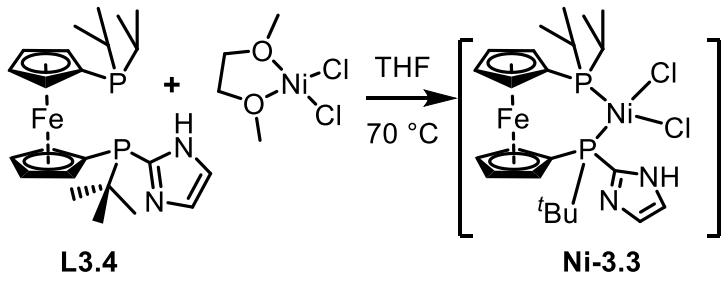

Figure 3. 30 Coordination study between **L3.4** with $NiCl_2$•DME

Next, we took the dark green solid powder recovered after evaporation of the volatile components from **Ni-3.3** and dissolved it in a THF solution that was sparged with ethylene gas. To this solution we added solid zinc(0) powder. Over the course of five minutes a precipitate was noticeable at the bottom of the flask and the solution had changed from a deep green to a yellow / green color. The reaction mixture was filtered, and the filtrate aliquoted for NMR analysis. The aliquot prepared in an NMR tube was sparged with ethylene gas and the solution was partially concentrated as the solvent slowly evaporated. To ensure a lock signal d_8-THF was added to the NMR tube. The resulting ^{31}P NMR spectrum contained identical resonances to those observed in the assignment of **Ni-3.2**! The ^{31}P NMR spectrum, which previous to the zinc addition totally silent, now revealed a major species with two resonances as doublets, appearing at δ 37.72 ppm (d, J = 26.8) and 27.15 (d, J = 27.0). Resonances for a minor product were also observed at δ 62.19 ppm (br) and 18.02 ppm (br). This new minor species integrates to 30 % of the integration of the signals matching the assignment of structure **Ni-3.2**. As a significant amount of non-deuterated THF was still present, the ^{1}H NMR spectrum was not informative.

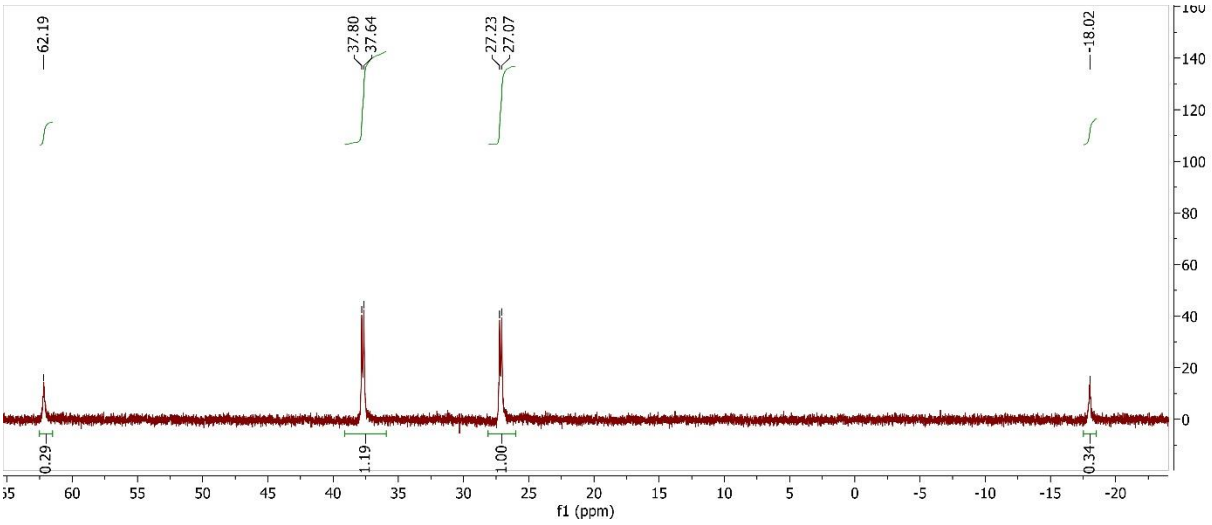

Figure 3. 31 ^{31}P NMR spectrum of reaction of **Ni-3.3** with zinc powder and ethylene, in d_8-THF at 162 MHz

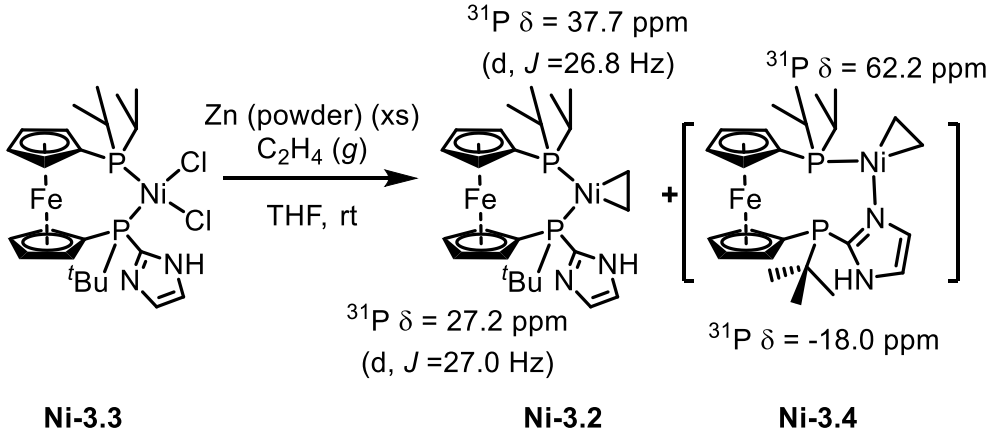

Figure 3. 32 Proposed structures for products generated through reduction of **Ni-3.3** with zinc

Ni-3.4 is considered as a potential candidate for the minor species. The chemical shift of the up-field resonance in matches closely with that of the free phosphine. Although the reduction did not cleanly produce only one product, we were encouraged to see the return of signal in the ^{31}P and ^{1}H NMR spectra. We see this as a proof of concept for utilization of a nickel(II) precurser to generate zero-valent nickel-phosphine complexes. Storage and handling of $Ni(COD)_2$ must be done in a rigorously air and water free environment. $Ni(COD)_2$ decomposes over time, even when stored in a cold air and water free environment.

3.5 Conclusion

In conclusion, we developed synthetic conditions and methodology for the synthesis of novel functionalized ferrocenyl bisphosphine ligands. Effective reactions in the early stages of the synthesis include use of the borane protecting group of electron rich phosphines such as the diisopropylphosphine fragment. Attachment of the second phosphorus group to the ferrocenyl backbown is most efficient when an amino-chlorophosphine is used. Examples of which are phenylchloro aminophosphine and *tert*-butylchloro aminophosphine, which were effectively used in this study.

We found that without protection from sterically large substituents at the phosphorus, the carbon-phosphorus bond linking imidazole to the phosphine structure, highly reactive metal atoms such as nickel(0) can cleave the carbon-phosphorus bond and degrade the ligand structure. When the bulkier *tert*-butyl group was used instead of phenyl, the reaction with $Ni(COD)_2$ did not result in C-P bond breaking. We found that complexation of **L3.4** with a nickel(II) dichloride precursor, followed by reduction with excess zinc powder can yield reduced nickel(0) complexes that may be useful for catalysis.

With some understanding of some coordination chemistry trends with platinum and nickel, the next phase of development should focus on reaction screening with pre-coordinated phosphine-metal complexes as catalysts candidates. The high throughput screening methods discussed in Chapter 2 would be well utilized at this point in the development of the functionalized ferrocenyl bisphosphines towards catalytic application.

Complexation of the ferrocenyl bisphosphine to a nickel dichloride provides a metal complex that is stable when handled in open atmosphere conditions. Once weighed out for use, a

reducing agent such as zinc (and potentially others) has been shown to effectively produce a nickel(0) complex containing the functionalized bisphosphine. Reaction targets for these complexes should include reactions of alkenes. Additional reaction components to target should include water, alcohols, carboxylic acids, and amines. The protic functionalization included in the ferrocenyl bisphosphines is specifically targeted for interaction with molecules that will accept a hydrogen bond. Additional reaction types that might be responsive to the functionalizations of the ferrocenyl bisphosphines include Buchwald-Hartwig amination and transfer hydrogenation. Additional development on the coordination chemistry of the ferrocenyl bisphosphines should include transition metals from groups 7,8,9, and 10.

3.6 Experimental Details

Synthesis of **3.3**

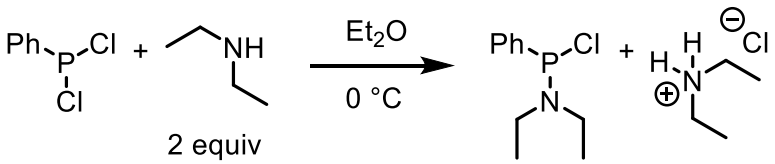

3.3

In a nitrogen filled glovebox, an oven dried and silanized 500 mL Schlenk flask was charged with dichlorophenylphosphine (16.6052 g, 0.09278 mol), diethyl ether (140 mL), and magnetic stir bar. An oven dried and silanized addition funnel was charged with diethylamine (13.5699 g, 0.1855 mol). The vessels were sealed with rubber septa and removed from the glovebox. The vessels were connected and attached to nitrogen flow via a Schlenk line. The flask was placed in an ice water bath with stirring. The diethylamine was then added dropwise through the addition funnel over the 20 minutes and the temperature maintained at 0 °C for 1 hour. Formation of white precipitate was observed. The reaction was stirred at room temperature for 90 minutes, then the reaction progress was assessed by ^{31}P NMR. The reaction was judged to have

reached completion and was then brought into a nitrogen filled glovebox and filtered through a glass fritted funnel. The solid diethylammonium chloride was washed with additional portions of diethyl ether. The filtrate was concentrated under reduced pressure. The crude product was purified by distillation through a perkin triangle at 0.3 mbar between the temperatures of 59-65 °C. The product was collected as the second fraction of mass 17.8161 g, 89%.

^{1}H NMR ($CDCl_3$, 400 MHz): δ 7.73 (m, 2H), 7.48 – 7.37 (m, 3H), 3.13 (m, 4H), 1.11 (t, J = 7.2, 6H)

^{13}C NMR ($CDCl_3$, 100 MHz): δ 139.46 (d, $J_{C\text{-}P}$ = 29.1), 130.64 (d, J = 20.4), 129.59 (d, J = 1.4), 128.34 (d, J = 4.2), 43.84 (d, J = 12.8), 14.05 (d, J = 6.0

^{31}P NMR ($CDCl_3$, 162 MHz): δ 142.34

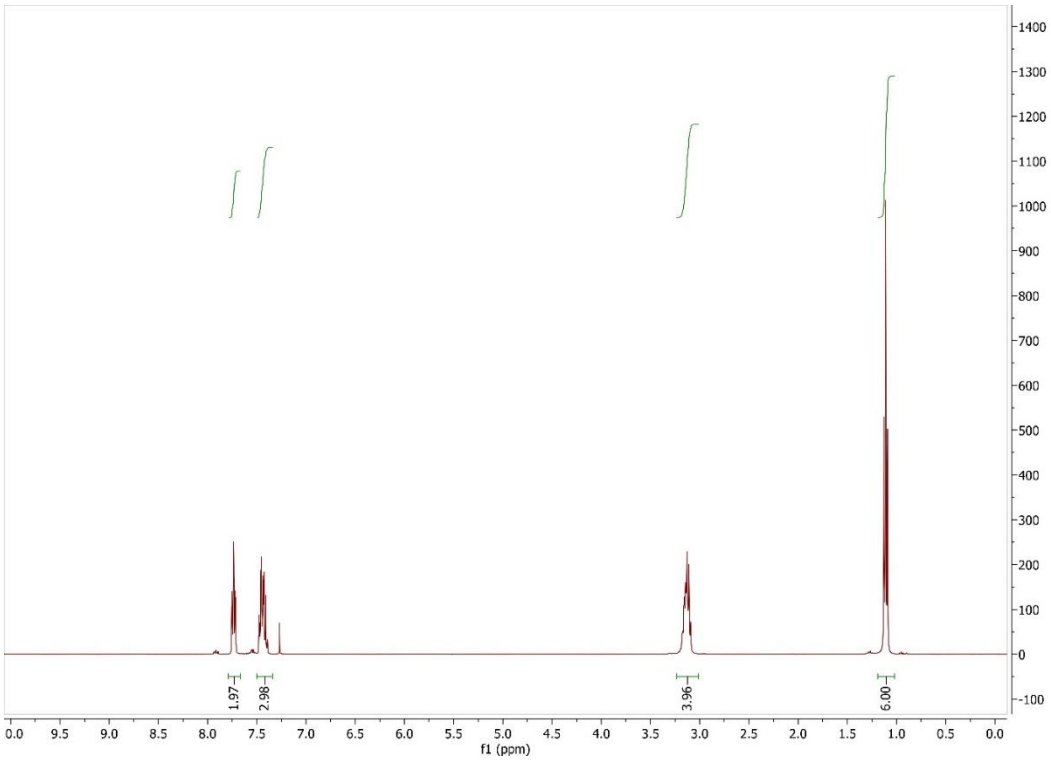

Figure 3. 33 ^{1}H NMR spectrum of **3.3** in $CDCl_3$ at 400 MHz

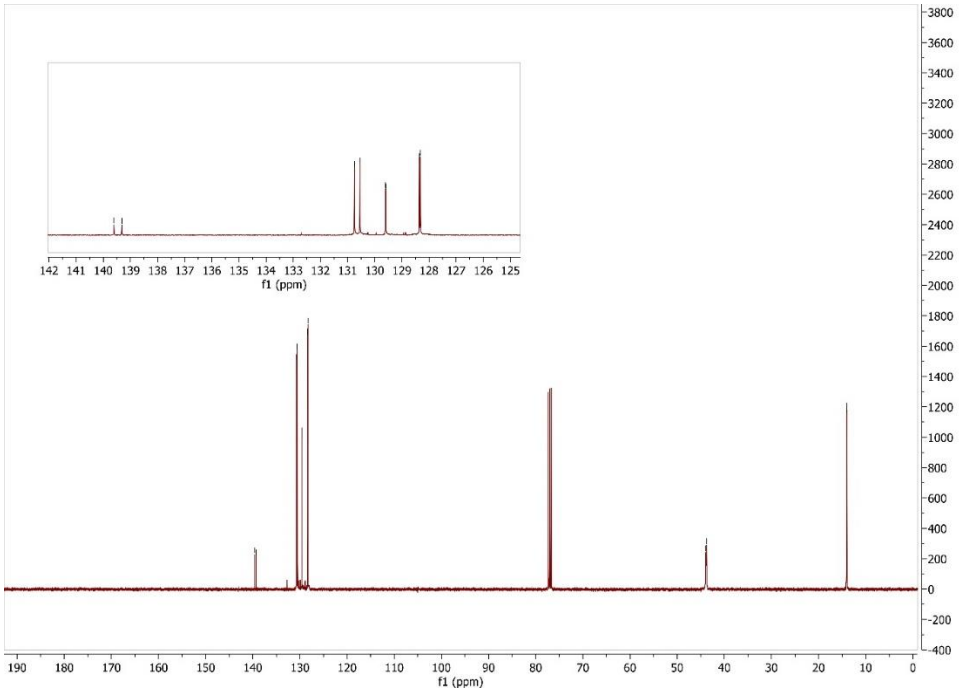

Figure 3. 34 ^{13}C NMR spectrum of **3.3** in $CDCl_3$ at 100 MHz

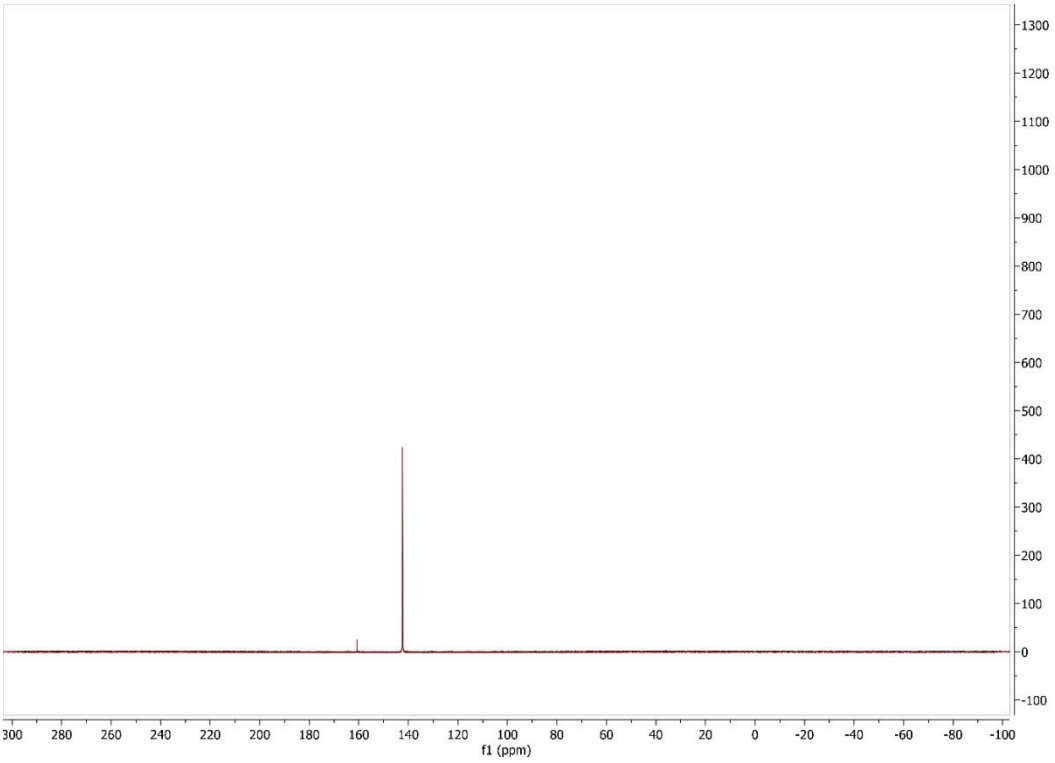

Figure 3. 35 ^{31}P NMR spectrum of **3.3** in $CDCl_3$ at 162 MHz

Synthesis of **3.4**

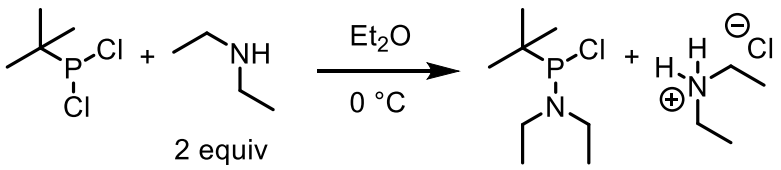

3.4

In a nitrogen filled glovebox, a dried and silanized 100 mL Schlenk flask was charged with tert-butyldichlorophosphine (10.0991 g, 0.0635 mol), diethyl ether (50 mL), and magnetic stir bar. A dried and silanized addition funnel was charged with diethyl amine (9.2971 g, 0.1271 mol). The vessels were sealed with rubber septa and removed from the glovebox. The reaction apparatus was assembled and connected to a Schlenk line for a flow of positive pressure of nitrogen gas. The flask was placed in an ice water bath with stirring. Triethylamine was added dropwise from the addition funnel over the course of 5 minutes. The mixture was stirred in the ice bath for 1 hour, then the bath was removed, and the mixture stirred for 20 hours. The reaction vessel was sealed, brought into a nitrogen filled glovebox via antechamber. The mixture was filtered through a glass fritted funnel and washed with additional diethyl ether. The filtrate was concentrated under reduced pressure to yield the product as a colorless liquid. The crude product was distilled with a Perkin triangle distillation apparatus with a pressure of 0.3 mbar and 48 - 53 °C (vapor temperature). The product was collected in three fractions for a total mass of 9.8409 g, 79%.

^{1}H NMR ($CDCl_3$, 400 MHz): δ 3.22 - 3.02 (m, 4H), 1.17 (d, J = 14.7, 9H), 1.13 (t, J = 7.1, 6H)

^{31}P NMR ($CDCl_3$, 162 MHz): δ 160.98

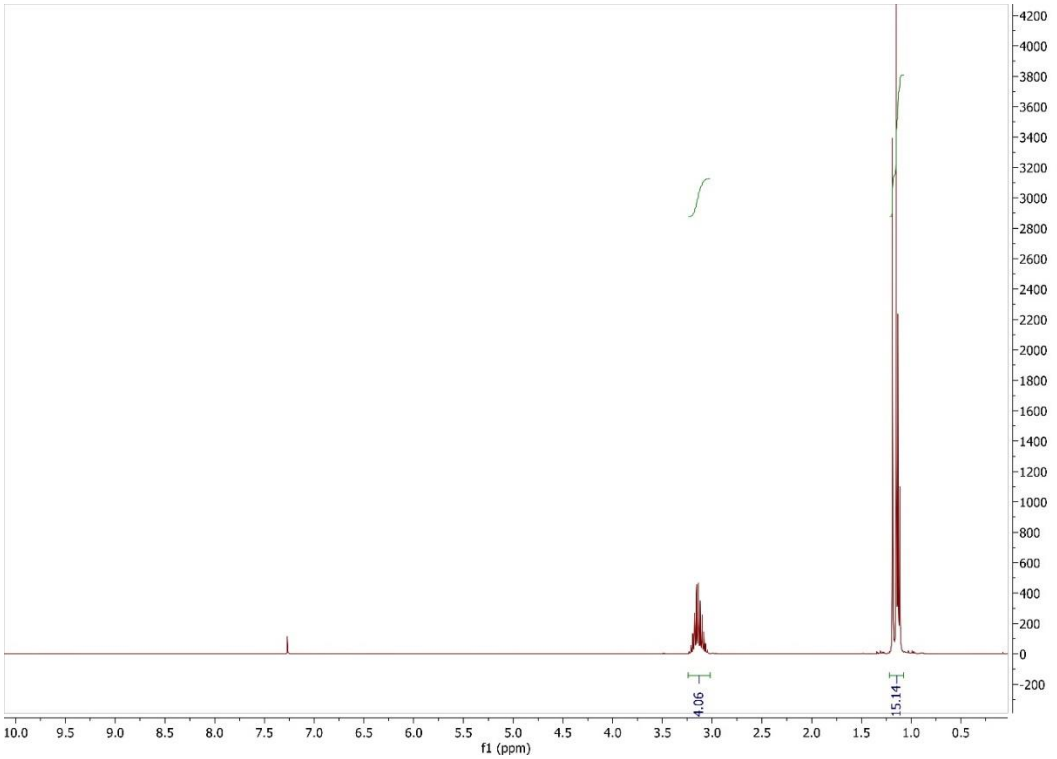

Figure 3. 36 ^{1}H NMR spectrum of **3.4** in $CDCl_3$ at 400 MHz

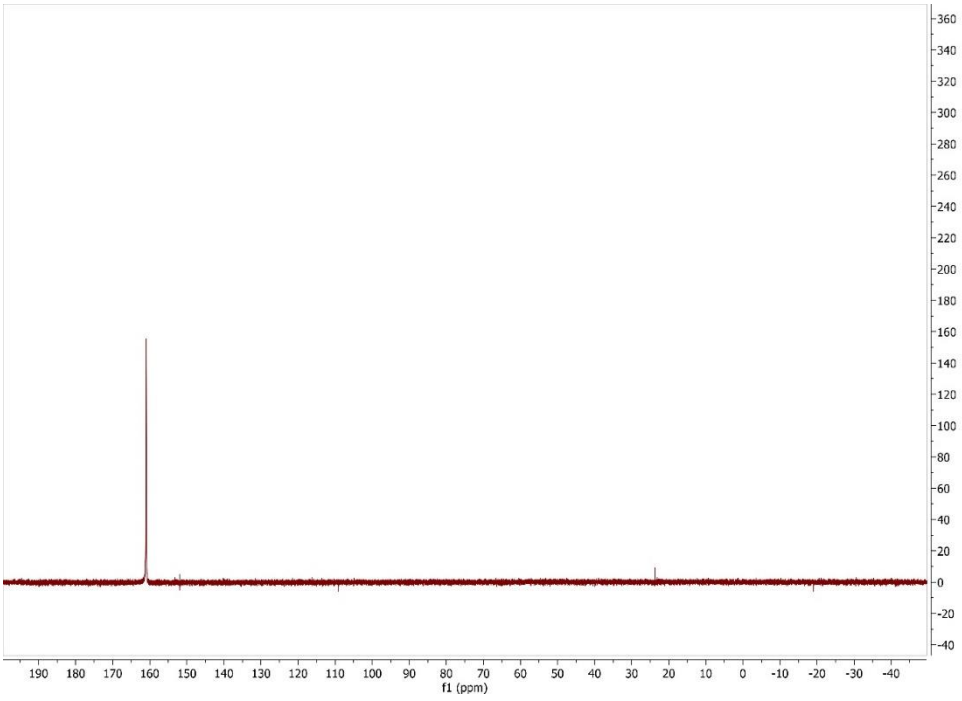

Figure 3. 37 ^{31}P NMR spectrum **3.4** in $CDCl_3$ at 162 MHz

Synthesis of **3.5**

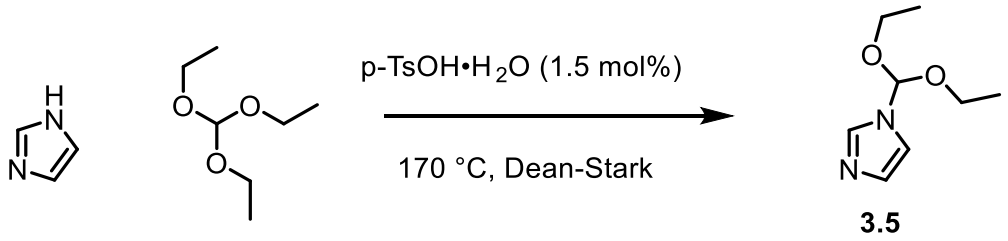

3.5

An oven dried 300 mL 2-neck round bottom flask was charged with imidazole (19.81 g, 0.291 mol), triethylorthoformate (153.76 g, 1.04 mol), and *p*-toluenesulfonic acid monohydrate (753.5 mg, 4.38 mmol) and magnetic stir bar. The flask was connected to a Dean-Stark condenser and heated under a constant nitrogen flow. The temperature was slowly raised to 170 °C and heated for a total time of 5.3 h. The reaction mixture was purified by fractional distillation with ana insulated distilling column. Pure product was collected at a pressure of 320 mtorr and a temperature of 88-90 °C, (21.52 g, 43 %).

^{1}H-NMR (400 MHz, $C_6D_6C_6D_6$): δ 7.69 (s, 1H), 7.29 (t, *J* = 1.1, 1H), 6.91 (t, *J* = 1.1, 1H), 3.19 – 3.01 (m, 4H), 0.88 (t, *J* = 7.1, 6H).)

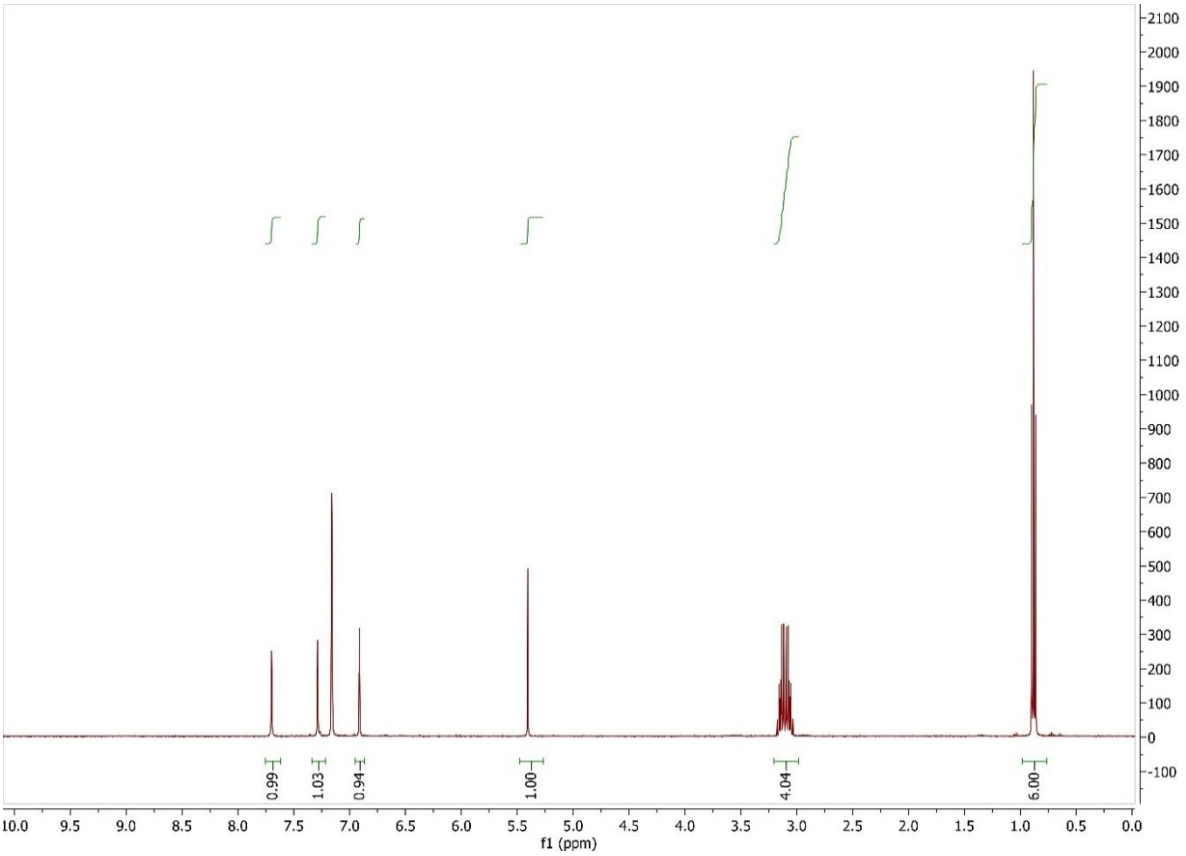

Figure 3. 38 ^{1}H NMR spectrum of **3.5** in C_6D_6 at 400 MHz

Synthesis of **3.1**

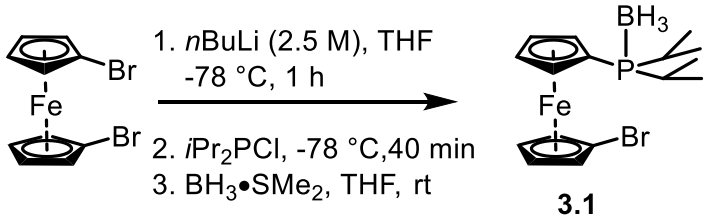

3.1

^{1}H NMR ($CDCl_3$, 400 MHz): δ 4.52 (t, *J* = 1.9, 1H), 4.47 (br, 1H), 4.42 (q, J = 1.7, 1H), 4.30 (t, J = 1.9, 1H), 2.23 – 2.08 (m, 2H), 1.21 – 1.13 (m, 12H), 1.06 - 0.05 (m, 3H)

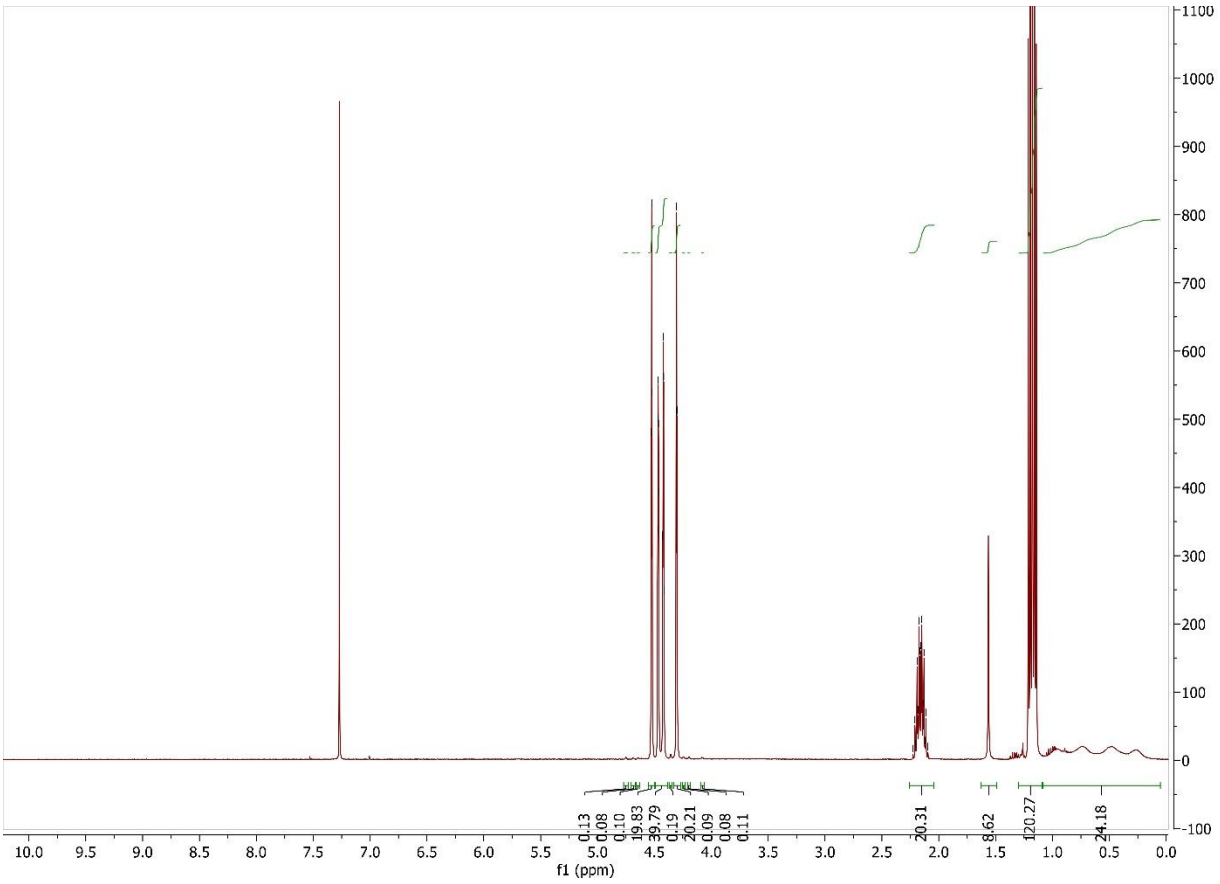

Figure 3. 39 ^{1}H NMR spectrum of **3.1** in $CDCl_3$ at 400 MHz

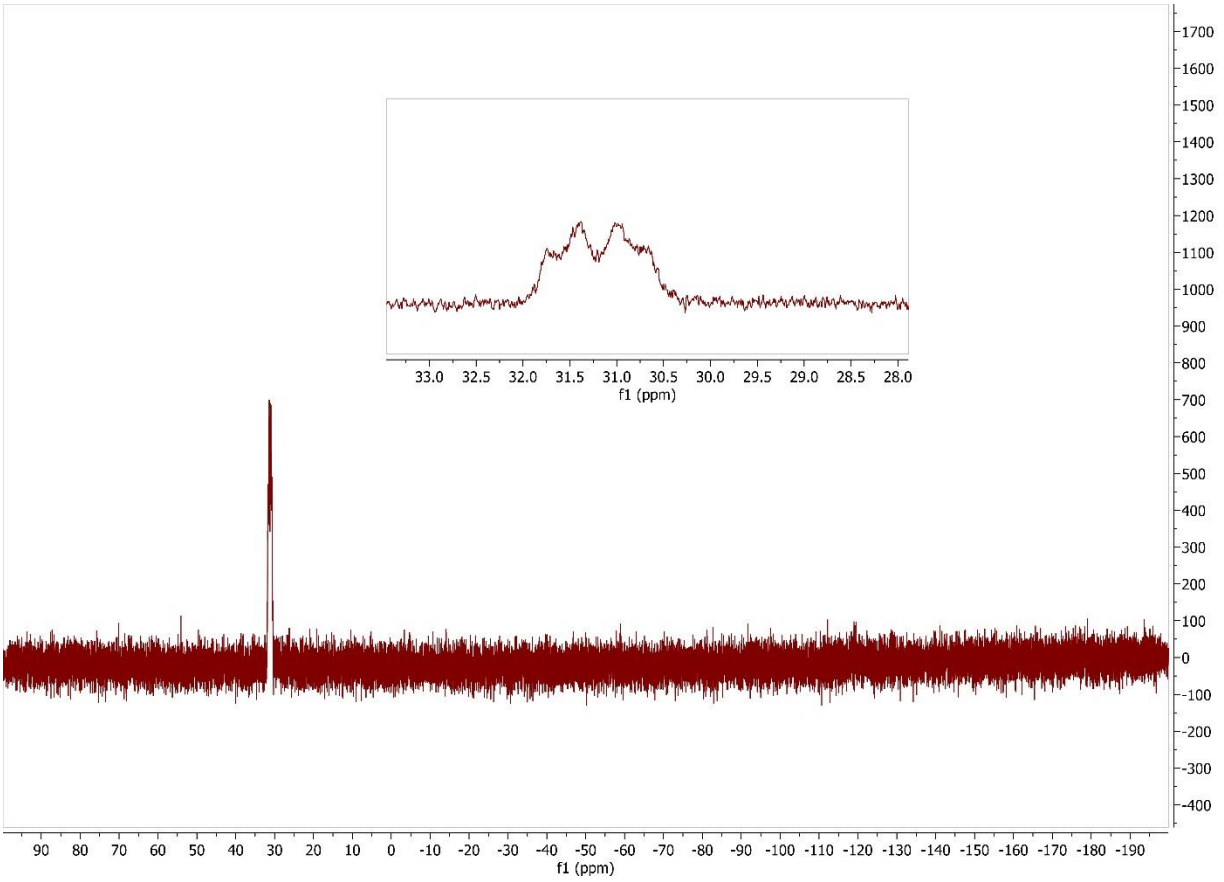

Figure 3. 40 ^{31}P NMR spectrum of **3.1** in $CDCl_3$ at 162 MHz

Synthesis of **3.2'**

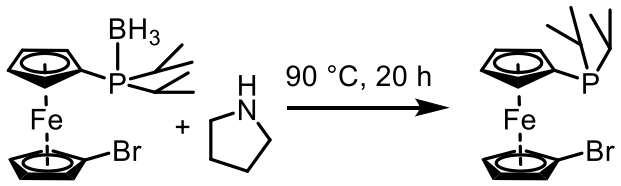

In a nitrogen filled glovebox, a pressure vessel was charged with **3.1** (8.2921 g, 0.02099 mol) and pyrrolidine (10.650 g, 0.149 mmol). A magnetic stir bar was added to the vessel then the top sealed. Once removed from the glovebox, the vessel was placed in an oil bath heated to 90 °C for 36 hours. The reaction progress was assessed by ^{31}P NMR analysis. Once consumption of the phosphino-borane adduct was achieved the reaction mixture was concentrated under reduced

pressure with heating at 70 °C. The product was collected as a dark orange solid of mass 7.5775 g, 94.7%.

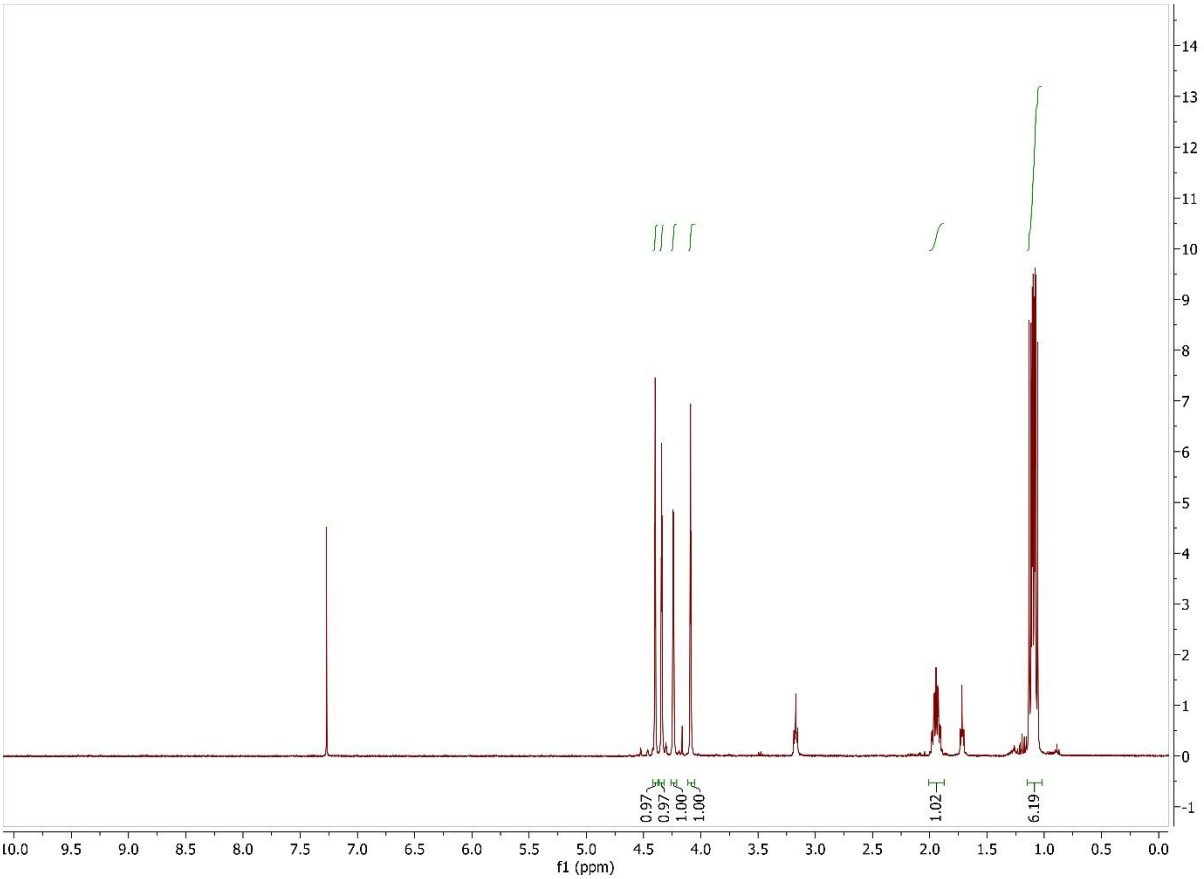

Figure 3. 41 ^{1}H NMR spectrum of **3.2'** in $CDCl_3$ at 400 MHz

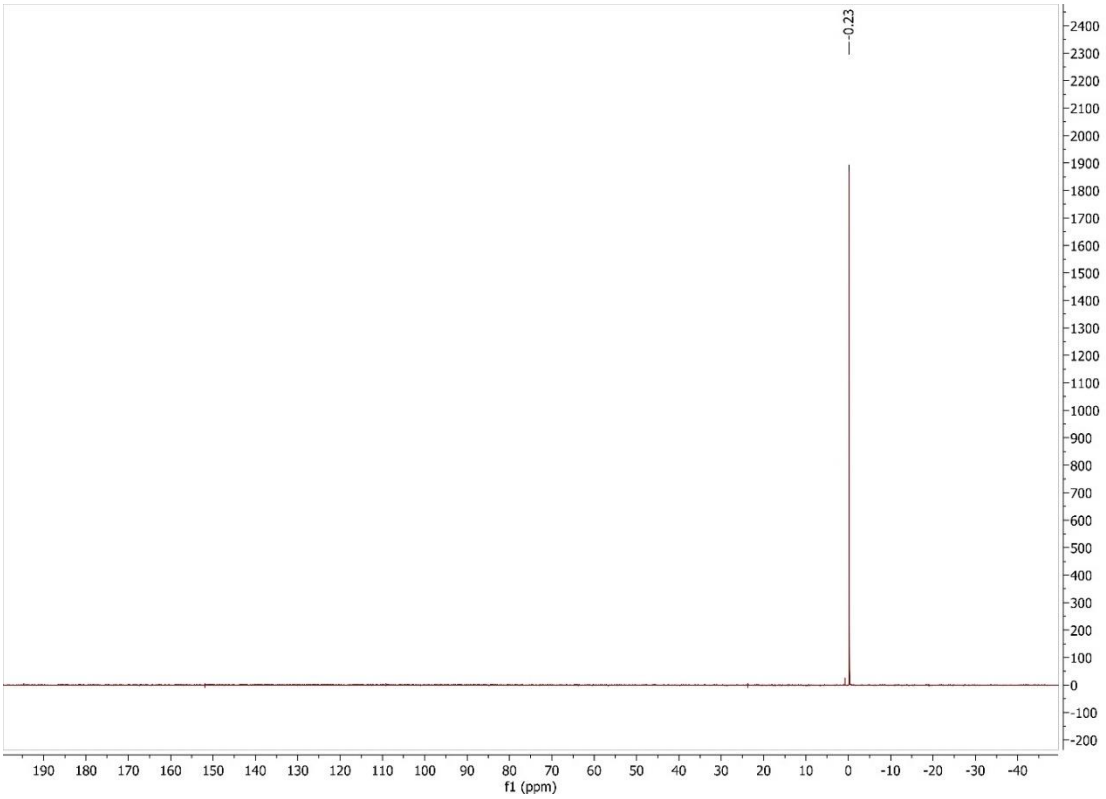

Figure 3. 42 ^{31}P NMR spectrum of **3.2'** in $CDCl_3$ at 162 MHz

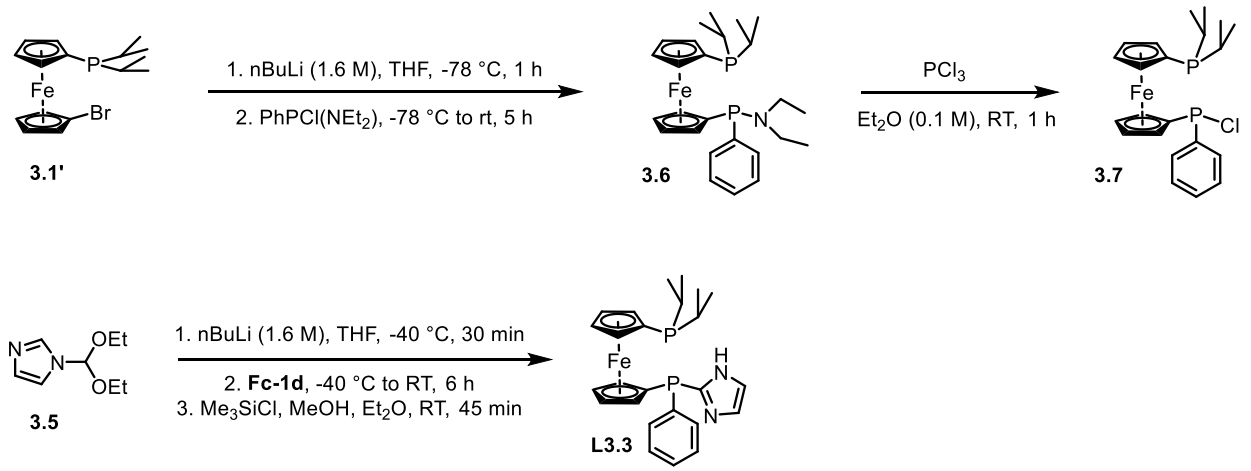

Synthesis of **3.6**

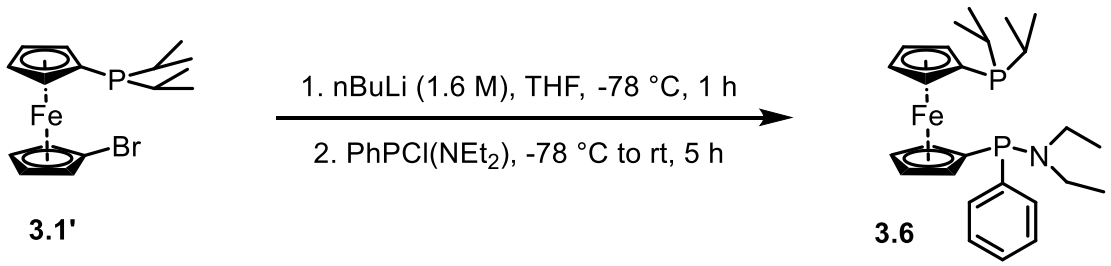

3.1' **3.6**

In a nitrogen filled glove box, a dried and silanized 100 mL Schlenk flask was charged with magnetic stir bar**, 3.1'** (982.1 mg, 2.577 mmol), and C_6H_6 (3.5 mL). The solution was stirred, and solvent evaporated via oil pump 16 h. The flask was brought into a glove box and THF (25 mL) was added. The solution was removed from glove box, connected to N_2 (g) line, and submerged in a dry ice / acetone bath, aged for 15 min. A solution of nBuLi (1.69 mL, 2.704 mmol) (1.6 M in hexanes) was added dropwise via syringe over 6 min, then the mixture was allowed to react for 1 h. A solution of **3.3** (593.3 mg, 2.751 mmol) in THF (6.5 mL) was added via syringe over 6 min. The solution remained in the bath for 3.5 h, at which point the bath was removed and the mixture stirred for 13 h at ambient temperature. All volatiles were then evaporated with an oil pump (4.5 h), the solid residue taken up in pentane (30 mL) and filtered in glove box, then concentrated on an oil pump to yield an orange oil **3.6** (1.2459 g, quantitative).

^{1}H-NMR $CDCl_3$, 400 MHz) δ 7.53 (ddd, J = 7.9, 6.4, 1.4, 2H), 7.34 (td, J = 7.3, 1.7, 2H), 7.30-7.24 (m, 1H), 4.43-4.40 (m, 1H), 4.39-4.34 (m, 3H), 4.31-4.27 (m, 2H), 4.24-4.21 (m, 1H), 4.04-4.01(m, 1H), 3.07-2.96 (m, 4H, overlapping signals), 2.01-1.89 (m, 2H), 1.15-1.04 (m, 12H), 1.00 (t, J = 7.1, 6H)

^{31}P-NMR (CDCl3, 162 MHz) δ 53.4 (s), 0.24 (s)

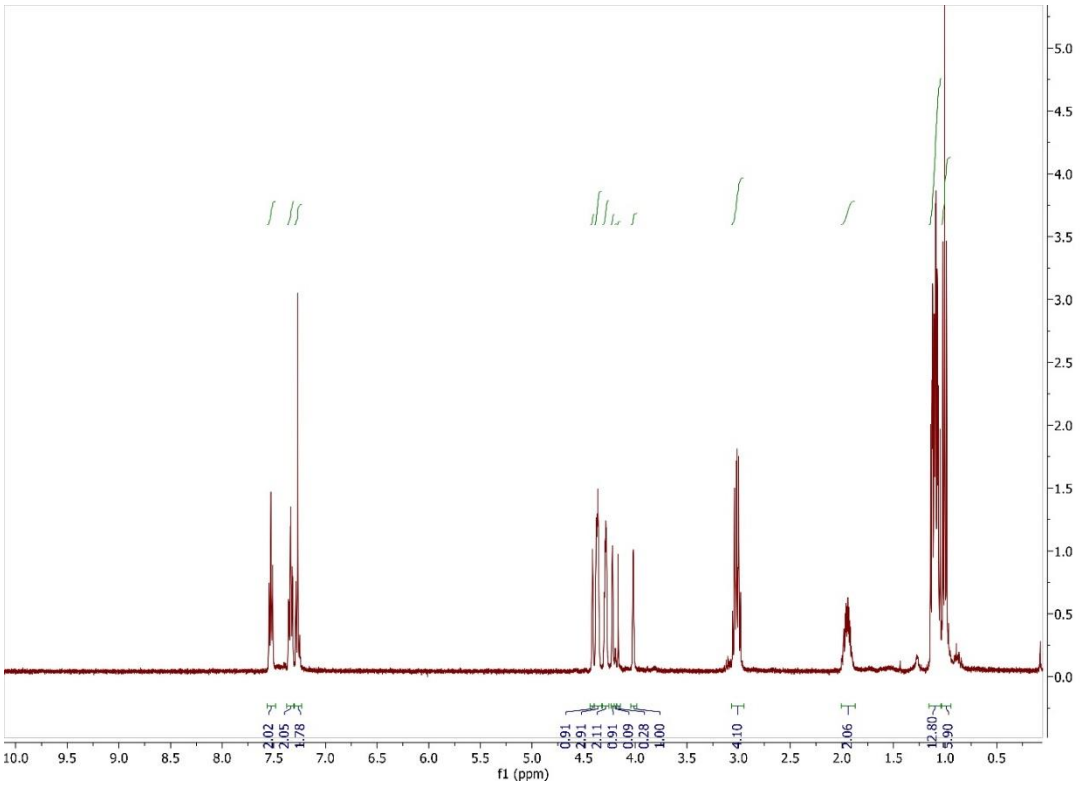

Figure 3. 43 ^{1}H NMR spectrum of **3.6** in $CDCl_3$ at 400 MHz

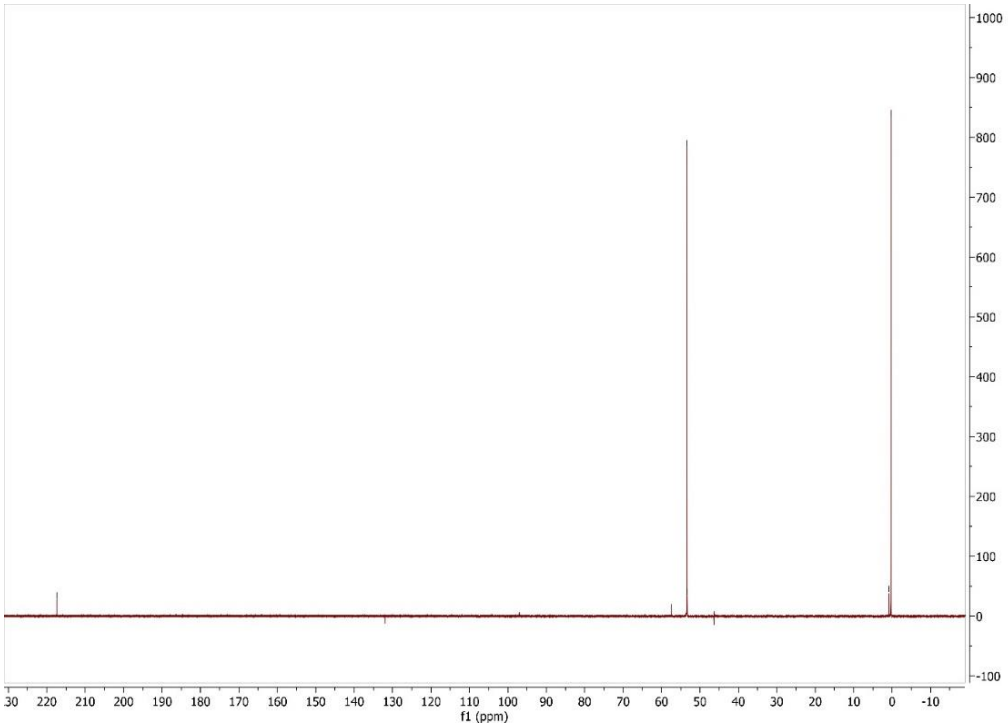

Figure 3. 44 ^{31}P NMR spectrum of **3.6** in $CDCl_3$ at 162 MHz

Synthesis of **3.7**

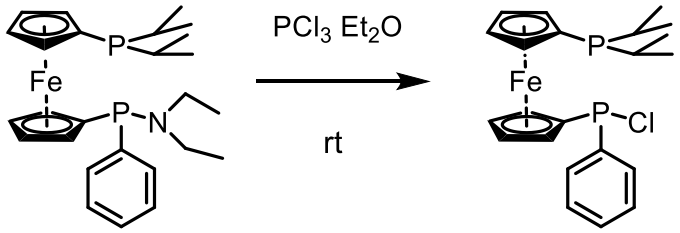

3.6 **3.7**

In a nitrogen filled glove box, a 100 mL Schlenk flask was charged with magnetic stir bar, **3.6** (1.2179 g), and Et_2O (25.0 mL). To the stirring solution a solution of PCl_3 (419.3 mg, 3.05 mmol) in Et_2O (5.0 mL) was added dropwise via syringe over 2 min. The resulting mixture was stirred at RT for 1.5 h, at which point all volatiles were evaporated with an oil pump. In the glove box, pentane (20 mL) was added to the orange residue, and then filtered and washed with additional pentane (10 mL). The filtrate was concentrated on an oil pump to yield an orange oil (1.0895 g, 97 %) which was used in the next step without further purification.

^{1}H-NMR (CDCl3, 400 MHz) δ 7.83-7.74 (m, 2H), 7.47-7.41 (m, 3H), 4.67-4.12 (br m, overlapping signals, 8 H), 2.33-1.84 (m, 2H), 1.23-0.95 (m, 12H)

^{31}P-NMR (CDCl3, 162 MHz) δ 72.4 (s), 7.0 (s)

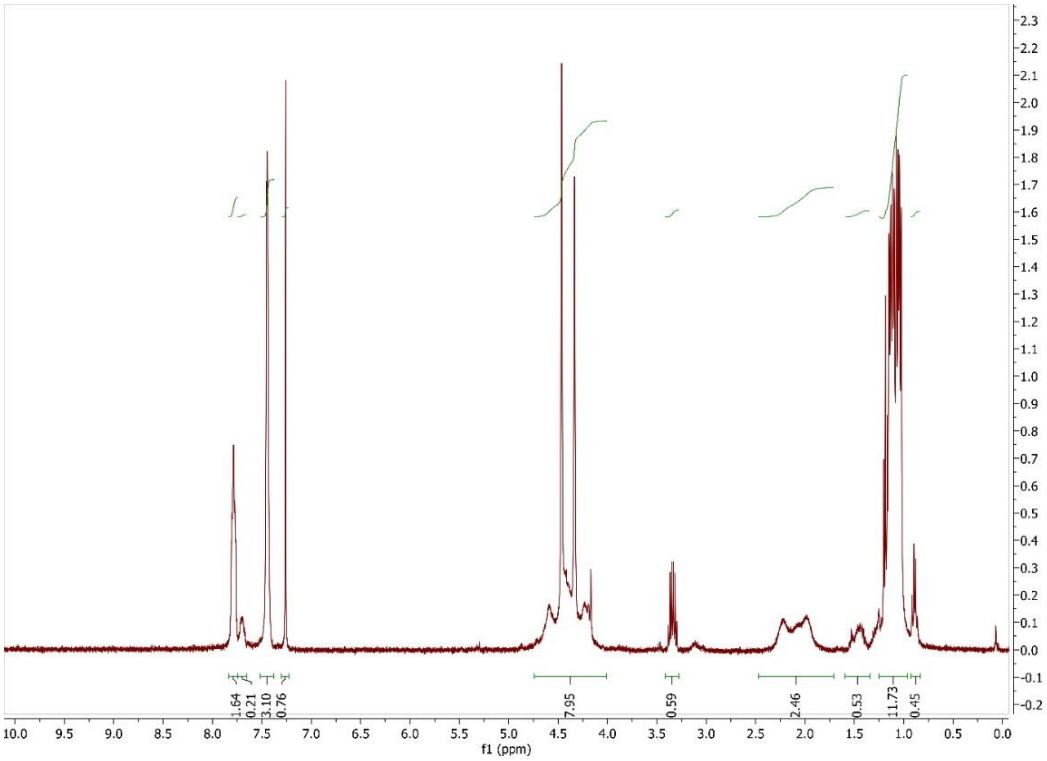

Figure 3. 45 ^{1}H NMR spectrum of **3.7** in $CDCl_3$ at 400 MHz

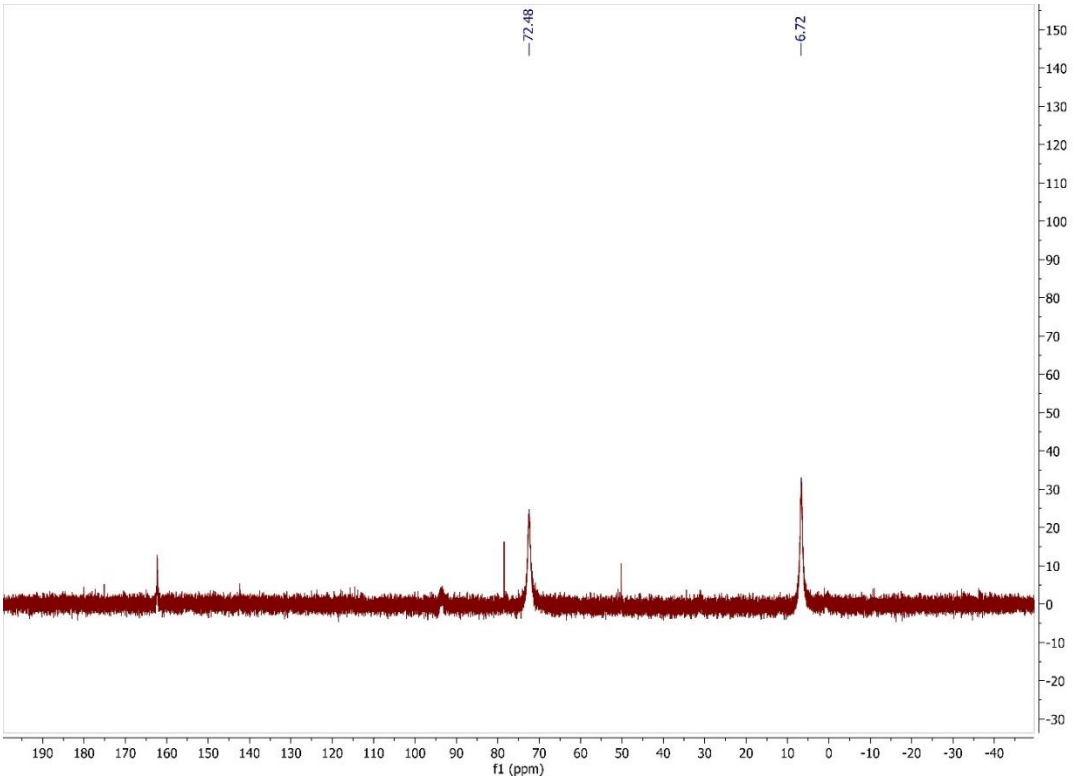

Figure 3. 46 ^{31}P NMR spectrum of **3.7** in $CDCl_3$ at 162 MHz

Synthesis of **L3.3**

In a nitrogen filled glove box, a dried and silanized 250 mL Schlenk flask (Flask-1) was charged with magnetic stir bar, **3.5** (1.5673 g, 9.218 mmol), and THF (60.0 mL), then capped with rubber septum, removed from the box, connected to a N_2 (g) Schlenk line, then placed in a CH_3CN / N2 (l) bath (temp between -40 °C and -35 °C. After aging for 20 minutes, *n*-BuLi (1.6 M) (3.70 mL, 9.25 mmol) was added via syringe and needle over 5 minutes, then the mixture was allowed to stir for 50 minutes with the temperature held between -40 °C and -35 °C. Meanwhile, in the glove box a dried and silanized 100 mL Schlenk flask (Flask-2) was charged with Fc-1d (3.9027 g, 8.776 mmol) and THF (30.0 mL). The flask was capped, removed from the box, and placed in a dry ice acetone bath. The solution of Fc-1d was then transferred via cannula to Flask-1 over the course of 7 minutes, then an additional portion of THF (5 mL) was added to rinse Flask-2 and the

cannula into Flask-1. The resulting mixture was allowed to stir and slowly warm to room temperature. After 10 hours, all volatiles were removed with an oil pump over the course of 10 hours. In the glovebox, pentane was added to the residue, then the suspension filtered, and the filtrate saved and concentrated to yield 11.985 g of an impure dark wax. The wax was dissolved in CH_3OH (35 mL), then $(CH_3)_3SiCl$ (200 µL) was added to the solution. The mixture was stirred at room temperature for 1 hour, then all volatiles were removed with an oil pump. The residue was dissolved in CH_2C_{l2} (50 mL), then H_2O (50 mL) and saturated K_2CO_3 (aq) (5 mL). After thorough mixing, an emulsion layer formed, and all phases were passed through a coarse filter. The phases were then separated, and the organic phase re-extracted with H_2O (30 mL). The solid collected on the coarse filter was continually washed with CH_2Cl_2, and the filtrate added to the organic phases. The combined organics were dried over MgSO4, then filtered and concentrated to yield a yellow solid. A minimum amount of acetone was added to dissolve the solid with light heating. The concentrated solution was cooled, then placed in a -40 °C freezer. After crystal formation the mother liquor was removed, and the crystals washed with cold acetone. The mother liquor was partially concentrated and placed in the freezer to yield 2 more crops of crystals. All isolated solid was combined to yield 2.5201 g (57.5 %) of the yellow solid Fc-1.

^{1}H-NMR (d6-acetone, MHz) δ 11.39 (s, 1H), 7.41-7.36 (m, 2H), 7.33-7.20 (m, overlapping signals, 5H), 4.51 (br, 1H), 4.35 (br, 2H), 4.32 (br, 1H), 4.22-4.15 (m, 3H), 3.96 (br, 1H), 1.94-1.88 (m, 2H), 1.09-0.97 (m, 12H)

^{13}C-NMR (d6-acetone, 125 MHz) δ 146.17 (s), 139.87 (d, J = 6.8), 133.06 (d, J = 19.1), 131.38 (d, J = 8.0), 128.98 (d, J = 7.4), 128.88 (s), 119.13 (s), 78.40 (d, J = 20.9), 76.55 (d, J = 32.5), 75.71 (d, J = 3.3), 73.37 (d, J = 5.0), 73.35 (s), 73.33 (d, J = 8.2),72.48 (d, J = 8.9), 71.79 (s), 71.66 (s),

24.14 (d, J = 12.8), 23.96 (d, J = 12.8), 20.58 (d, J = 7.9), 20.49 (d, J = 8.0), 20.40 (d, J = 3.4), 20.25 (d, J = 11.1)

^{31}P-NMR (d6-acetone, 162 MHz) δ -0.23, -0.25, -36.22, -36.24

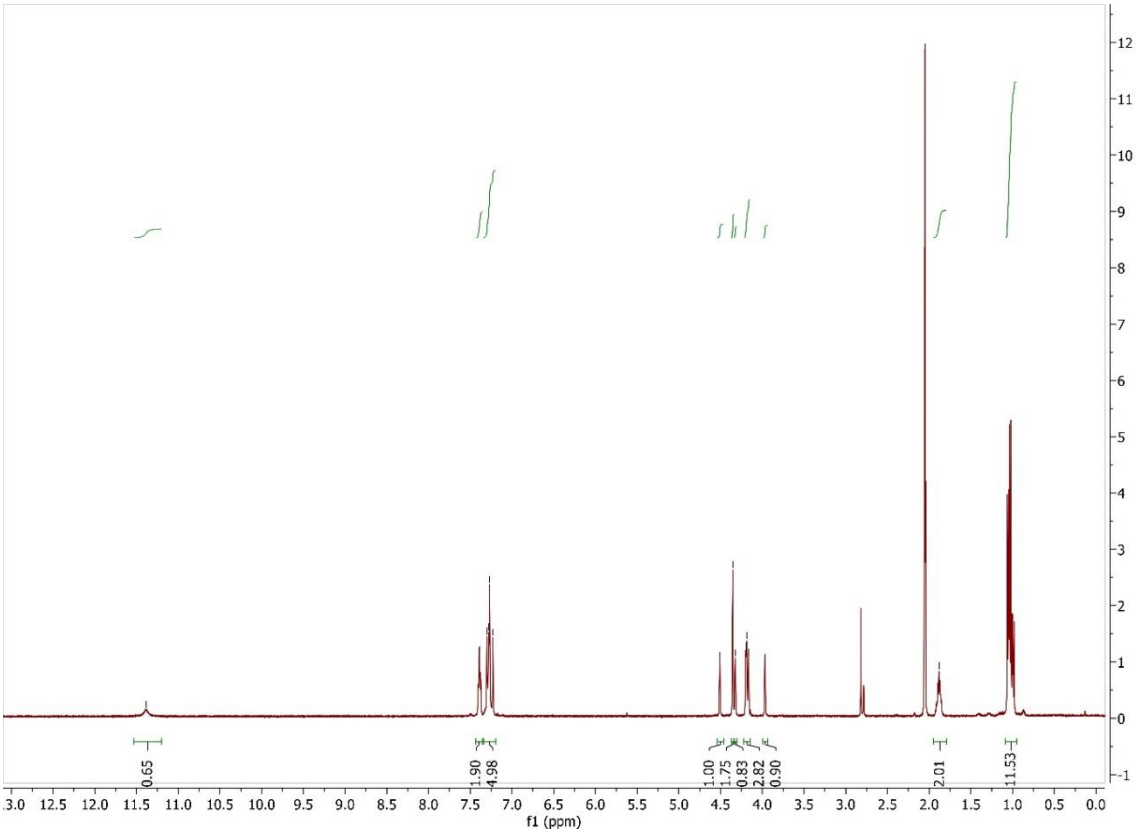

Figure 3. 47 ^{1}H NMR spectrum of **L3.3** in d_6-acetone at 500 MHz

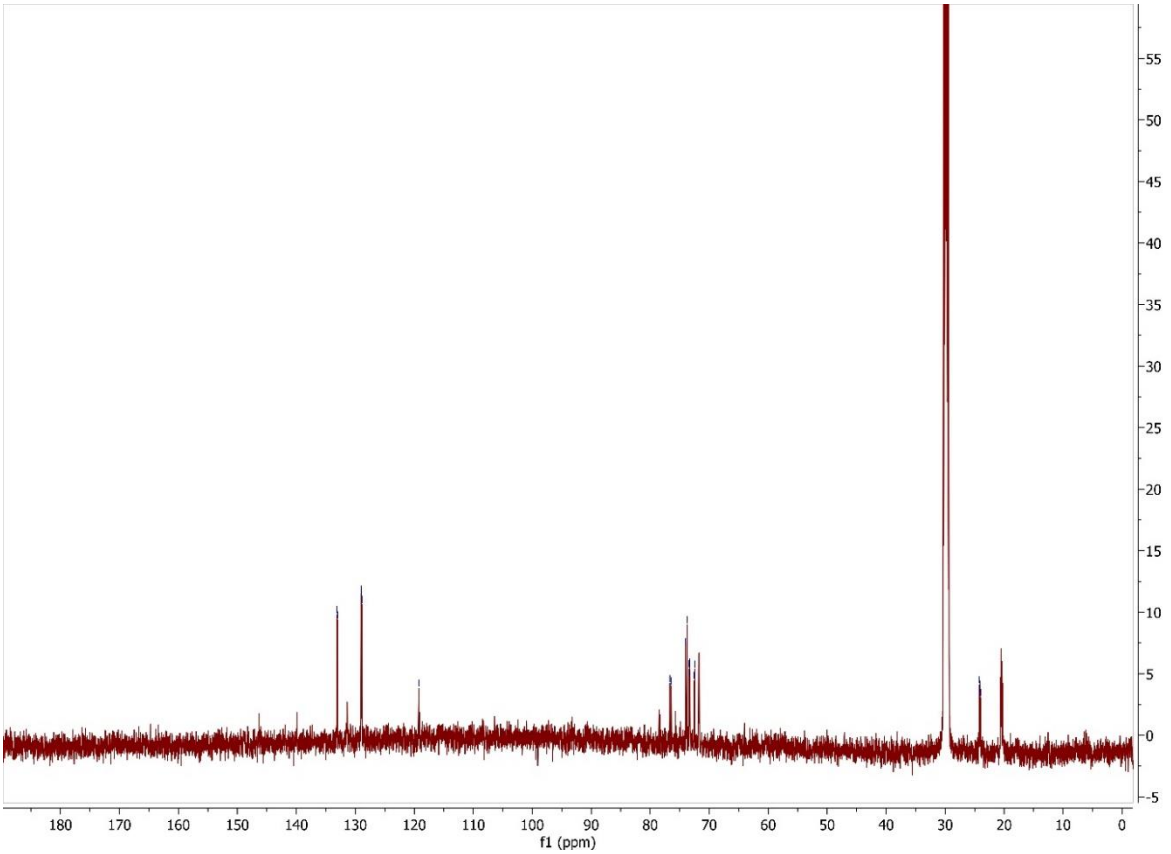

Figure 3. 48 $^{13}C\{^{1}H\}$ NMR spectrum of **L3.3** in d_6-acetone at 125 MHz

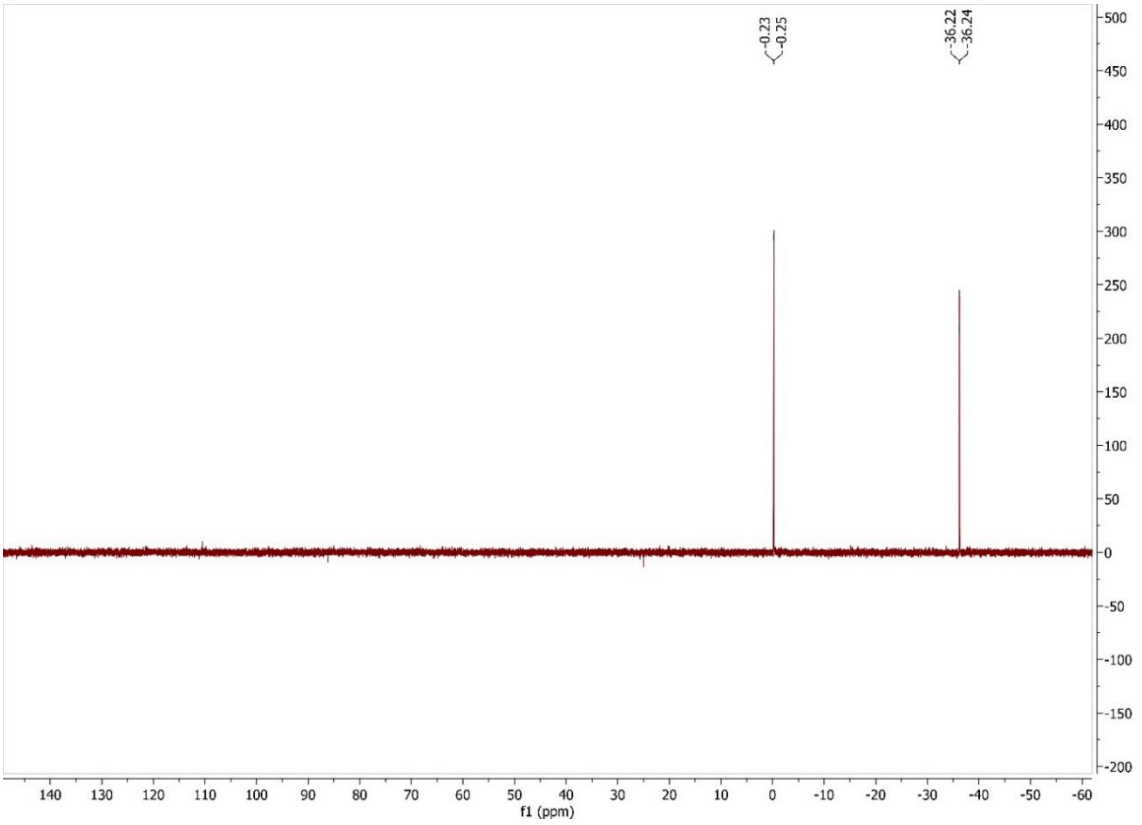

Figure 3. 49 ^{31}P NMR spectrum of **L3.3** in d_6-acetone at 202 MHz

Synthesis of amino phosphine **3.8**

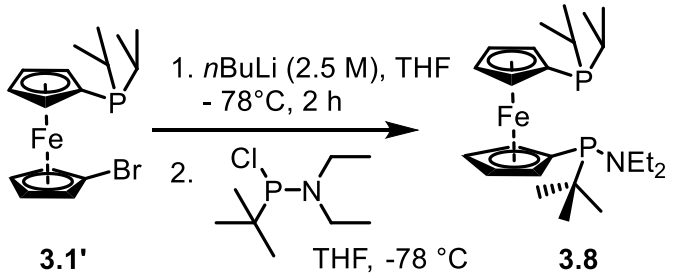

In a nitrogen filled glovebox, an oven dried and silanized 300 mL long-neck Schlenk flask was charged with FC-1b (4.9990 g, 13.121 mmol), THF (45 mL), and magnetic stir bar. The flask was sealed with a rubber septum and removed from the glovebox. The flask was connected to a Schlenk line with positive pressure of nitrogen gas, then placed in a dry ice and acetone bath. Once the temperature had equilibrated with the cold bath, *n*-butyl lithium (2.5 M) (5.4 mL, 13.515 mmol) was added dropwise via syringe over the course of 20 minutes. The mixture was stirred in the cold

bath for 1 hour. In the glovebox, a dried scintillation vial was used to measure the chlorophosphine (2.7041 g, 0.0138 mol), which was then dissolved in THF (9 mL) and taken up into a syringe. The chlorophosphine solution was then added to cold reaction mixture dropwise over the course of 30 minutes. The resulting mixture was stirred at room temperature and kept rigorously air free for 24 hours. The reaction vessel was then sealed with a rubber septum and taken into the glovebox via antechamber. The reaction mixture was filtered through a glass fritted funnel, then concentrated under reduced pressure to yield an orange solid of mass 5.6447 g, 93%.

^{1}H NMR ($CDCl_3$, 400 MHz): δ 4.42 – 4.07 (m, 8H), 3.11 (p, *J* = 7.5, 4H), 1.93 (br, 2H), 1.18 – 0.98 (m, 27H)

^{31}P NMR ($CDCl_3$, 162 MHz): δ 73.40, -0.42

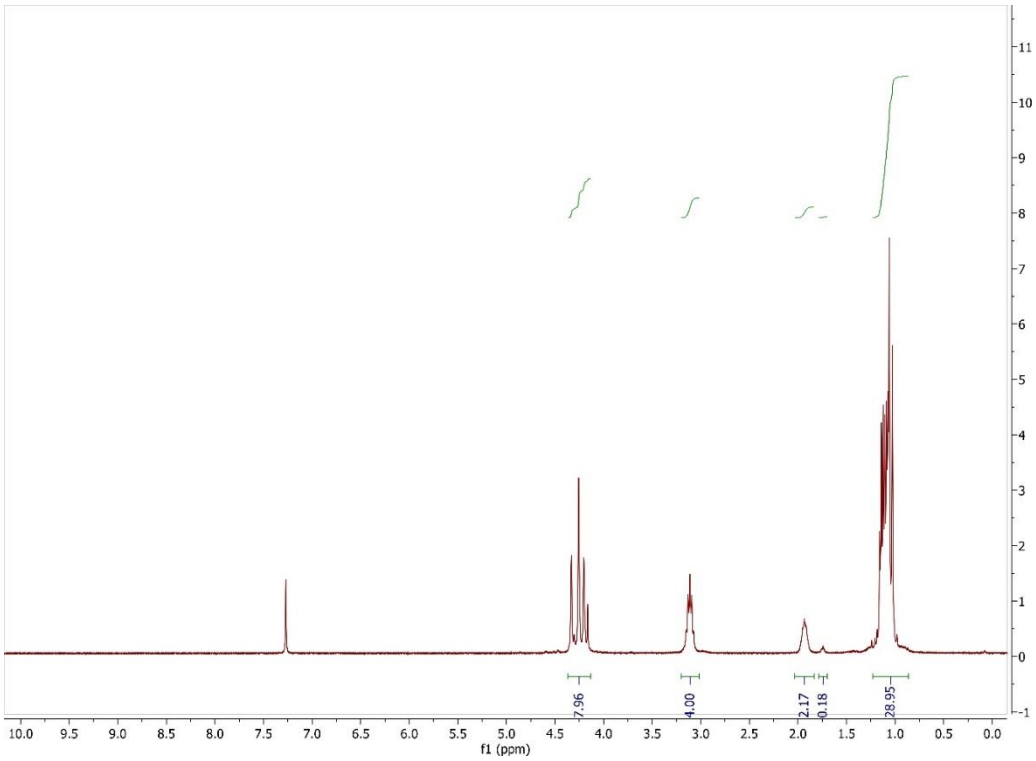

Figure 3. 50 ^{1}H NMR spectrum of **3.8** in $CDCl_3$ at 400 MHz

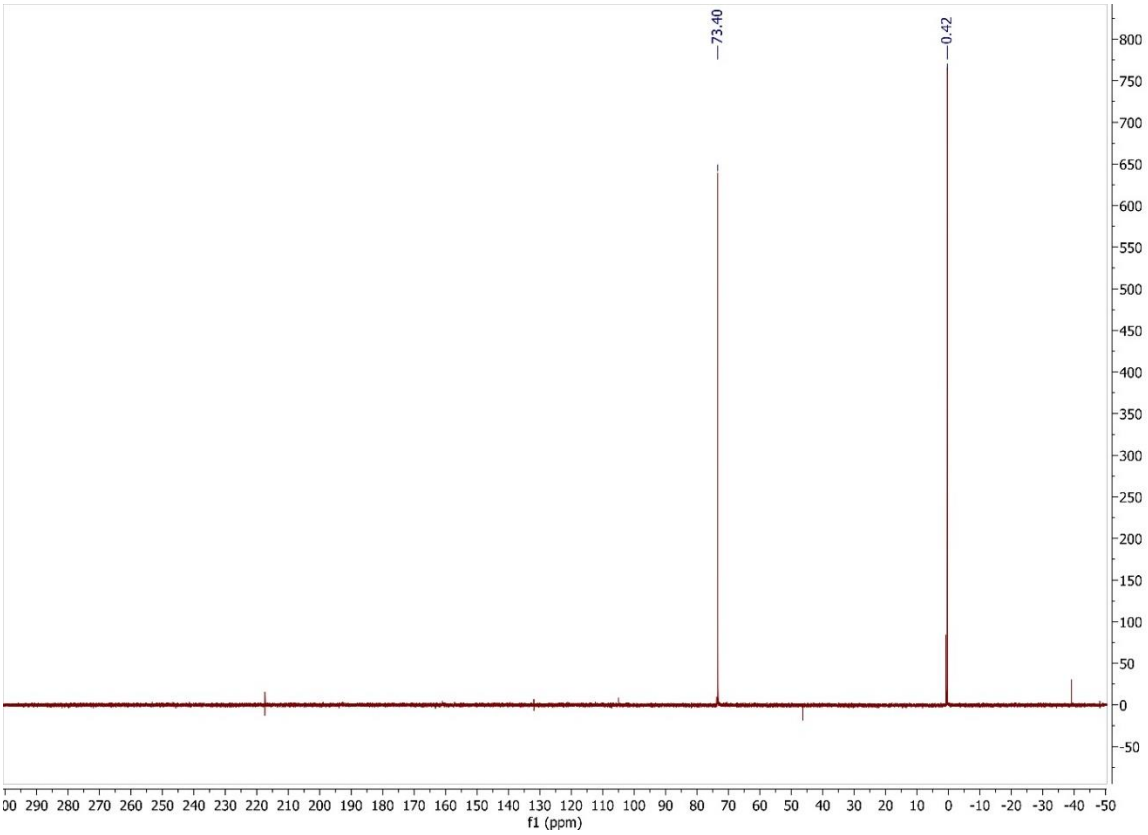

Figure 3. 51 ^{31}P NMR spectrum of **3.8** in $CDCl_3$ at 162 MHz

Synthesis of **3.9**

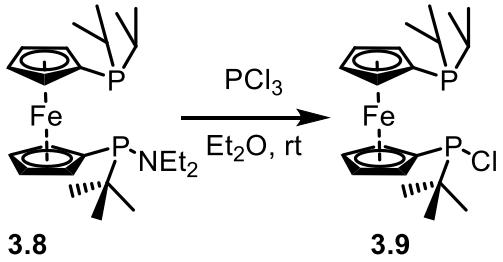

3.8 **3.9**

In a nitrogen filled glovebox, an oven dried and silanized 250 mL Schlenk flask was charged with aminophosphine (5.6447, 0.0122 mol), diethyl ether (40 mL), and a magnetic stir bar. The phosphorus trichloride was measured in dried vial and taken up into a syringe. The phosphorus trichloride was added to the diethyl ether solution of the amino phosphine and the resulting mixture was stirred at room temperature for 24 hours. When the reaction was judged to

have reached completion the volatiles were evaporated under reduced pressure. Extra caution was taken to collect all volatiles and quench with methanol. The resulting colorless liquid was used for the next step without further purification.

^{1}H NMR (C_6D_6, 500 MHz): δ 4.51 – 4.04 (m, 8H), 1.82 (m, 2H), 1.10 – 1.01 (m, 12H), 0.98 (d, *J* = 13.5, 9H)

^{31}P-NMR (C_6D_6, 202 MHz) δ 112.69, -0.71

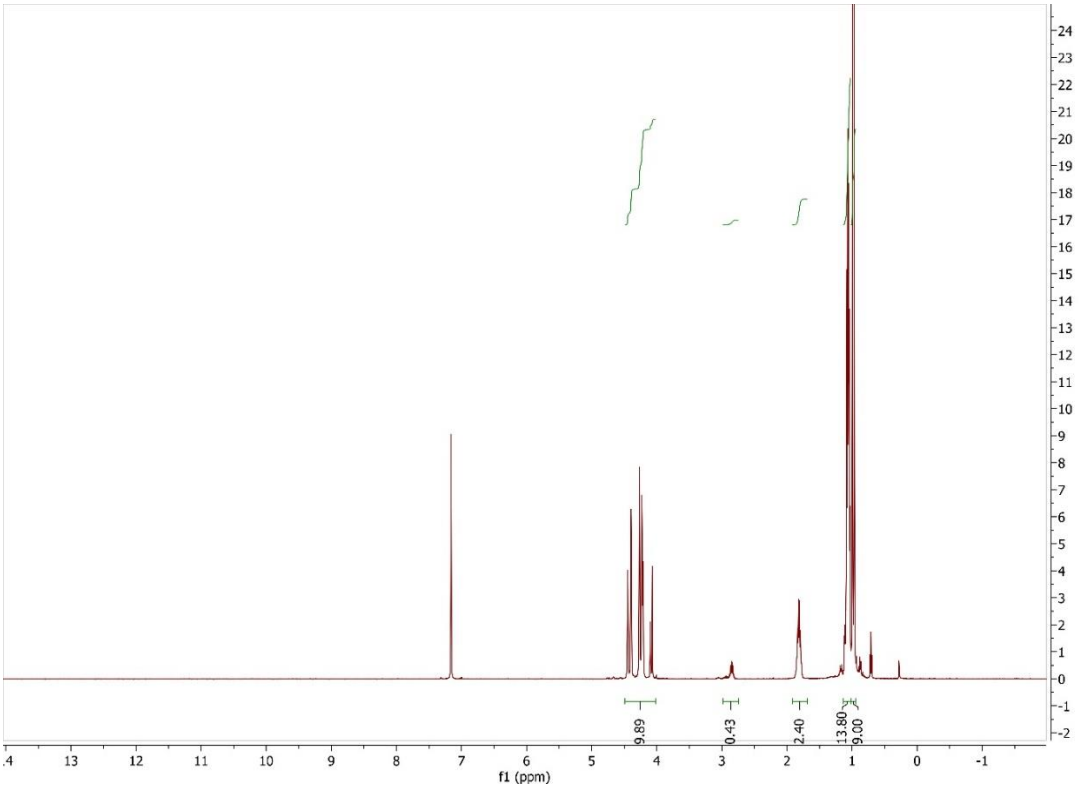

Figure 3. 52 ^{1}H NMR spectrum of **3.9** in C_6D_6 at 500 MHz

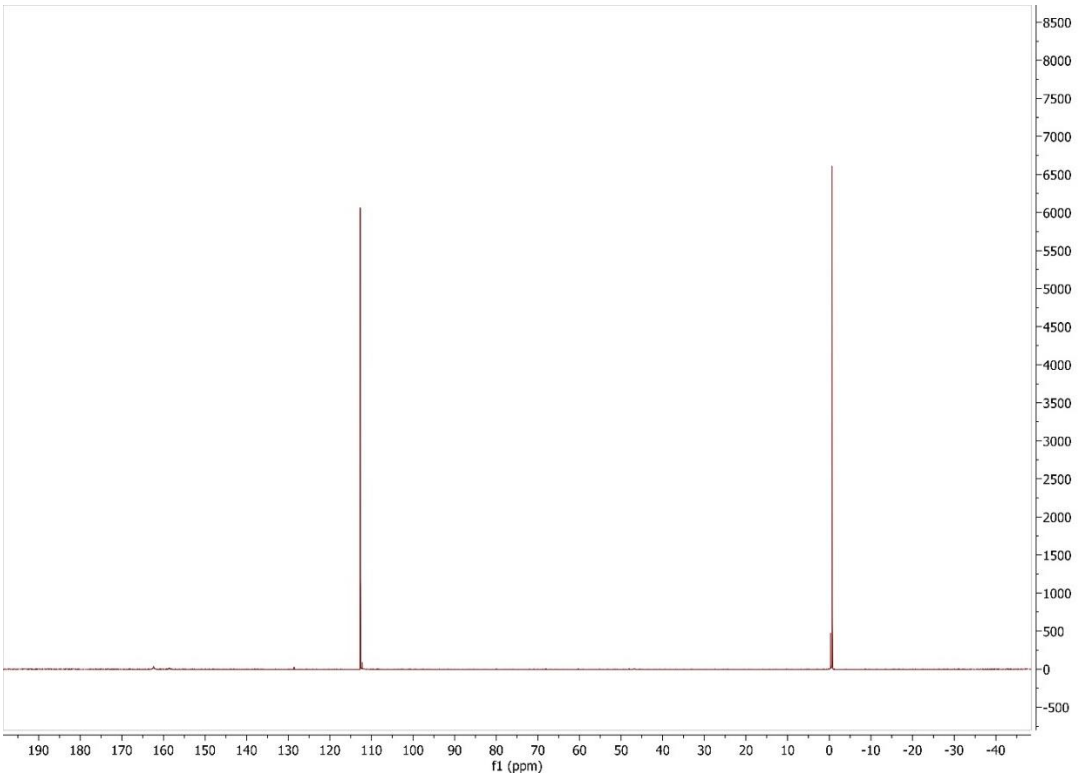

Figure 3. 53 ^{31}P NMR spectrum of **3.9** in C_6D_6 at 202 MHz

Synthesis of **L3.4**

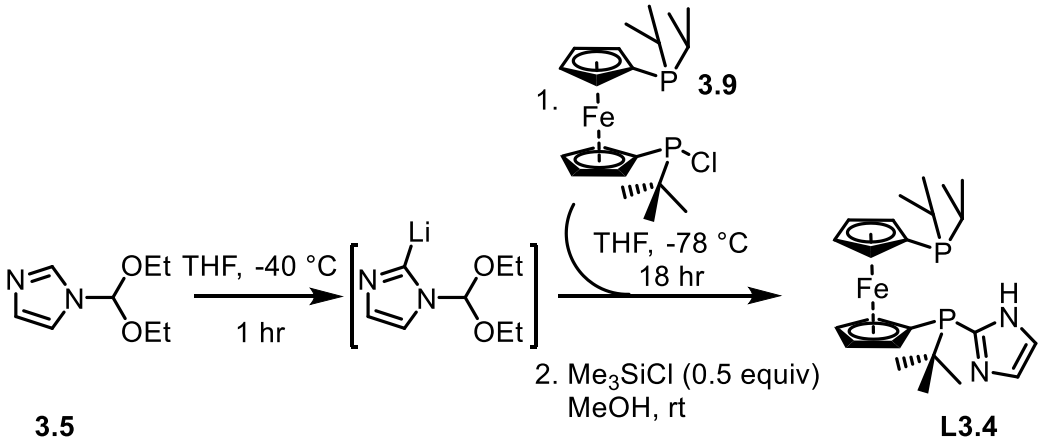

In a nitrogen filled glovebox, an oven dried 100 mL Schlenk flask was charged with bs477 (430.0 mg, 2.526 mmol), THF (12 mL), and magnetic stir bar. The flask was sealed with a rubber stopper, removed from the glovebox, then connected to a Schlenk line with positive pressure of nitrogen gas. The flask was then placed in a bath of acetonitrile and liquid nitrogen was added until

a liquid slurry was formed. Next, *n*-butyl lithium (2.5 M) (0.98 mL, 2.45 mmol) was added via syringe over 2 minutes. The mixture was stirred in the acetonitrile and liquid nitrogen bath for 1 hour. Next the reaction flask was transferred to an acetone dry ice bath. In the glovebox, a dried scintillation vial was charged with **3.9** (1.0278 g, 2.42 mmol) and THF (5 mL). The THF solution of the chlorophosphine was then added via syringe to the reaction mixture over the course of 6 minutes. The reaction was stirred in the acetone and dry ice bath and the dry ice was slowly evaporated as the reaction stirred for the next 24 hours. To quench any remaining reactive intermediates acetone (0.8 mL) was added via syringe, the mixture was stirred for 20 minutes at room temperature, then all volatiles were removed under reduced pressure. The residue was then dissolved in diethyl ether (20 mL) and filtered through a glass fritted funnel. The filtrate was then concentrated under reduced pressure. The solid residue was dissolved in methanol (10 mL) and chlorotrimethylsilane (0.13 mL, 1.78 mmol) was added. The mixture was stirred at room temperature for 1 hour, then filtered through a glass fritted funnel loaded with Amber-Jet -OH beads to quench remaining acidic species. The filtrate was concentrated under reduced pressure. The remaining solid was then purified by crystallization of a concentrated acetone solution in a -40 °C freezer to yield orange / yellow crystals of mass 448.3 mg, 42%.

^{1}H NMR (d_6-acetone, 400 MHz): δ 11.68 (br, 1H), 7.32 (m, 1H), 7.29 (m, 1H), 5.04 (m, 1H), 4.30 – 4.25 (m, 3H), 4.07 – 4.03 (m, 1H), 3.94 – 3.92 (m, 1H), 3.88 – 3.85 (m, 1H), 3.80 – 3.76 (m, 1H), 1.90 – 1.80 (m, 2H), 1.08 – 0.92 (m, 12H), 0.98 (d, J = 12.9, 9H)

^{31}P NMR (d_6-acetone, 162 MHz): δ – 0.64, -18.47

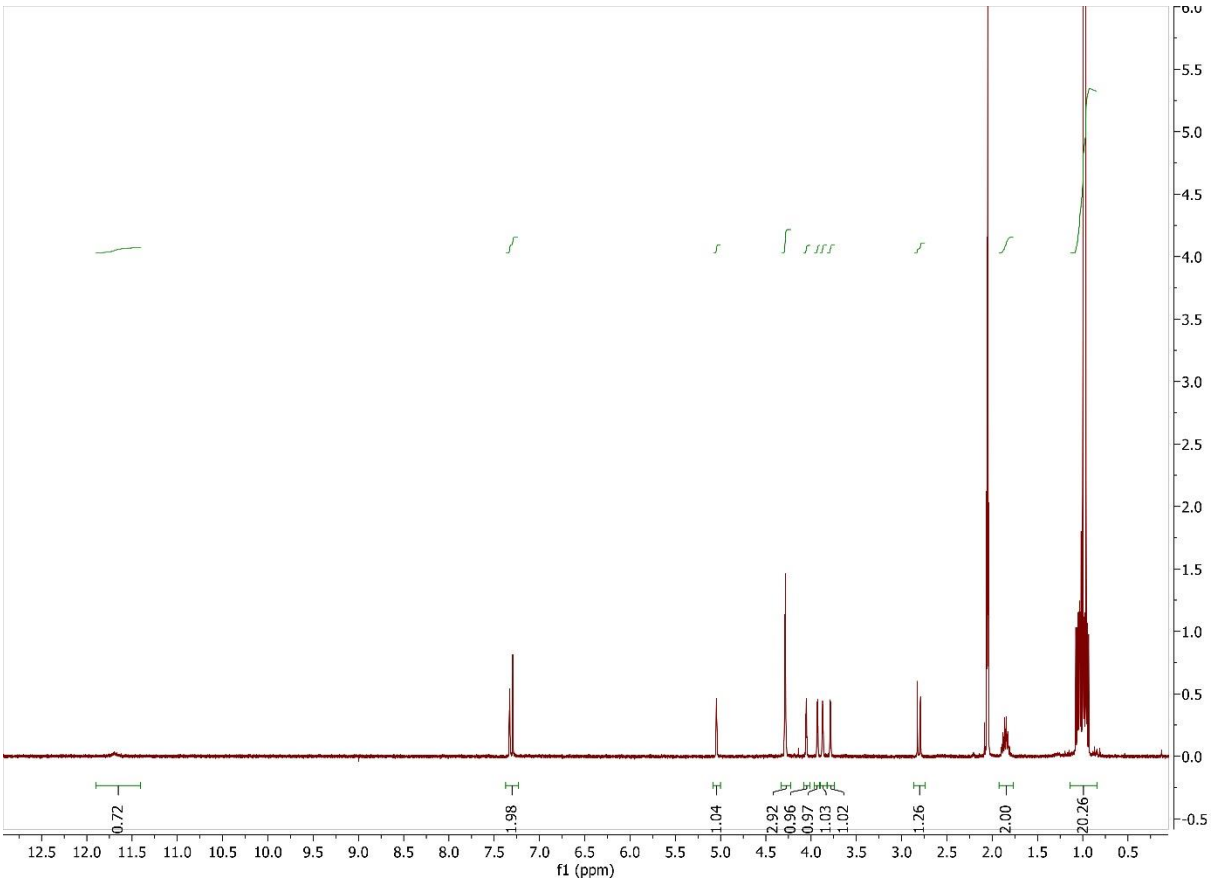

Figure 3. 54 ^{1}H NMR spectrum of **L3.4** in d_6-acetone at 400 MHz

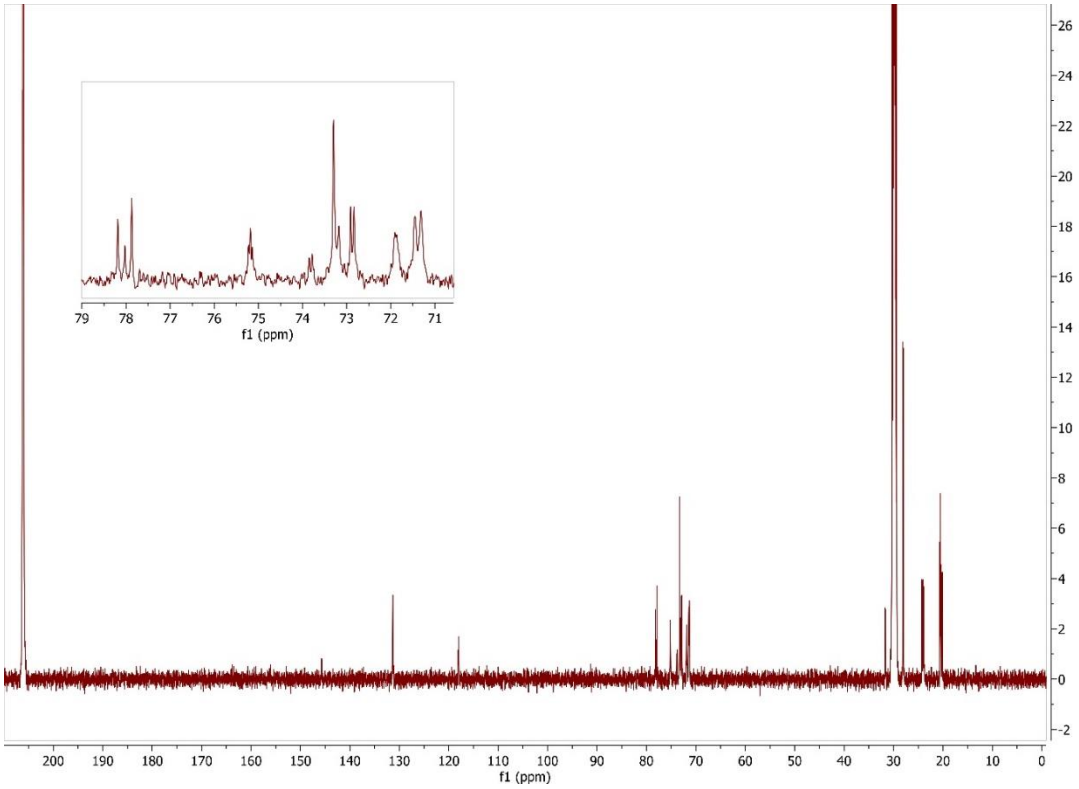

Figure 3. 55 $^{13}C\{^{1}H\}$ NMR spectrum of **L3.4** in d_6- acetone at 100 MHz

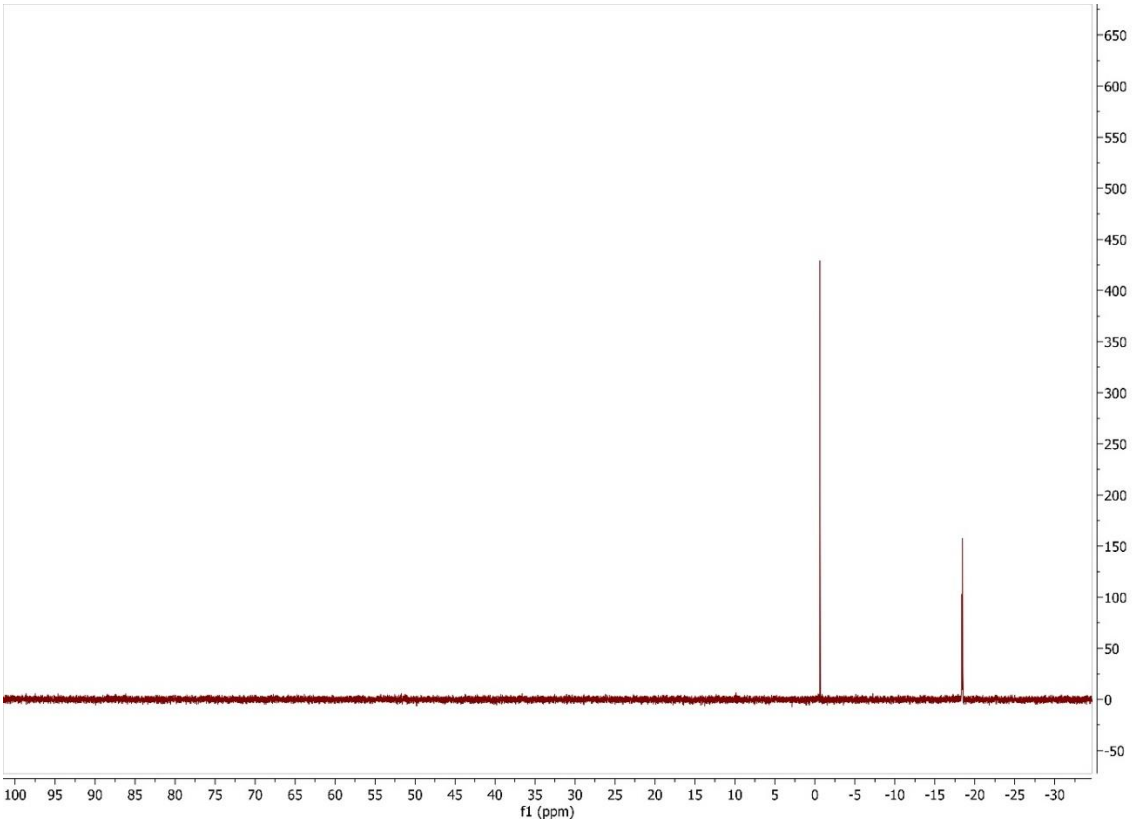

Figure 3. 56 ^{31}P NMR spectrum of **L3.4** in d_6-acetone at 162 MHz

Synthesis of **3.10**

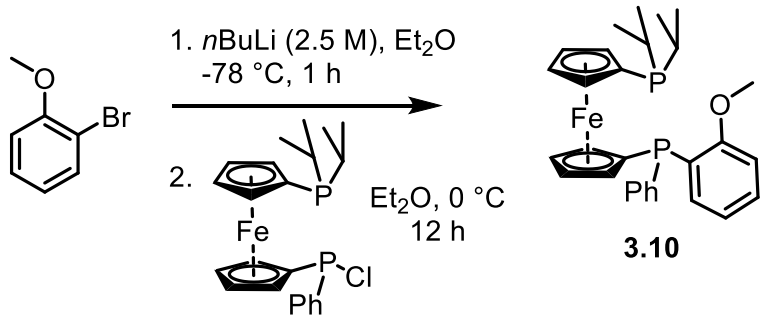

In a nitrogen filled glovebox, an oven dried and silanized 300 mL Schlenk flask was charged with 2-bromoanisole (645.1 mg, 3.449 mmol), diethyl ether (40 mL), and magnetic stir bar. The flask was sealed with a rubber septum, removed from the glovebox and connected to a

Schlenk line with positive pressure of nitrogen gas. The flask was then placed in a cooling bath of dry ice and acetone. Once the temperature of the flask contents equilibrated with the bath, *n*-butyl lithium (2.5 M) (1.3 mL, 3.25 mmol) was added via syringe over the course of 5 minutes. After the addition of the *n*-butyl lithium solution, the reaction flask was removed from the dry ice and acetone bath and placed into an ice water bath, then aged for 1 hour. In the glovebox, a dried scintillation vial was used to measure the chlorophosphine Fc-1d (1.3656 g, 3.098 mmol). The chlorophosphine was taken up in diethyl ether in a syringe. The chlorophosphine was then added to the reaction flask via syringe addition over the course of 20 minutes. The reaction was slowly warmed to room temperature as the dry ice sublimed and stirred for 24 hours. To quench any remaining P-Cl bonds or remaining lithium species, acetone (0.5 mL) was added to the reaction mixture. The volatiles were then removed under reduced pressure. The residue was taken up in hexanes and filtered through a glass fritted funnel with a small silica plug in the glovebox. The filtrate was concentrated dryness and a mass of 303.8 mg, 19%. It is suspected that the chlorophosphine Fc-1d may have undergone some decomposition before using in this protocol, as some insoluble orange solid was left over during the addition of the diethyl ether solution of Fc-1d. Such decomposition would account for the poor yield.

^{1}H NMR ($CDCl_3$, 400 MHz): δ 7.48 – 7.40 (m, 2H), 7.37 – 7.23 (m, 4H), 6.92 – 6.80 (m, 3H), 4.40 – 3.79 (m, 8H), 3.72 (s, 3H), 1.85 (m, 2H), 1.16 – 0.91 (m, 12H)

^{31}P NMR ($CDCl_3$, 162 MHz): δ 0.54, -29.84

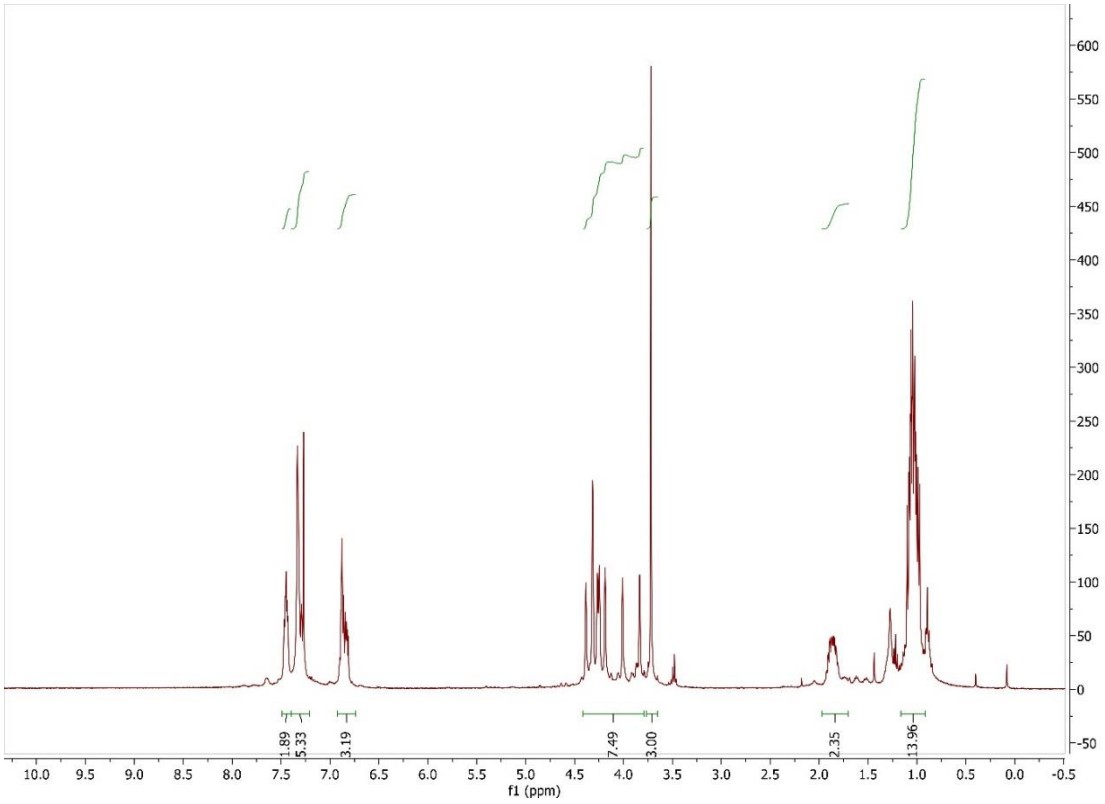

Figure 3. 57 ^{1}H NMR spectrum of **3.10** in $CDCl_3$ at 400 MHz

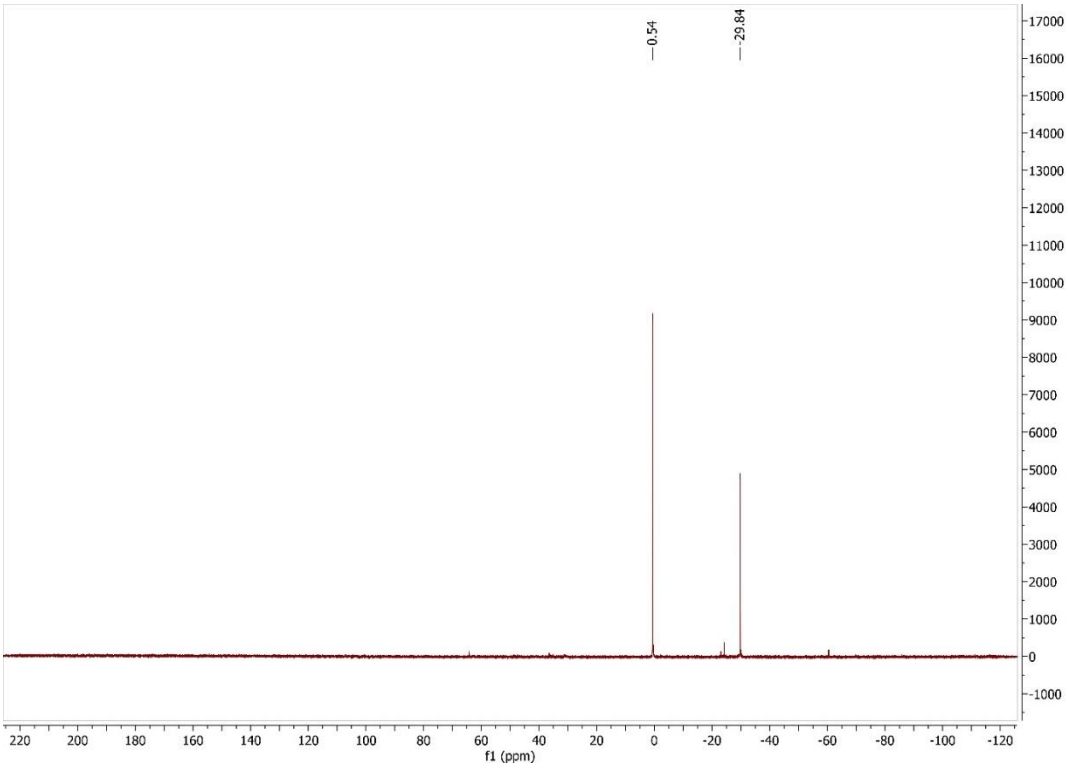

Figure 3. 58 ^{31}P NMR spectrum of **3.10** in $CDCl_3$ at 162 MHz

Synthesis of **L3.8**

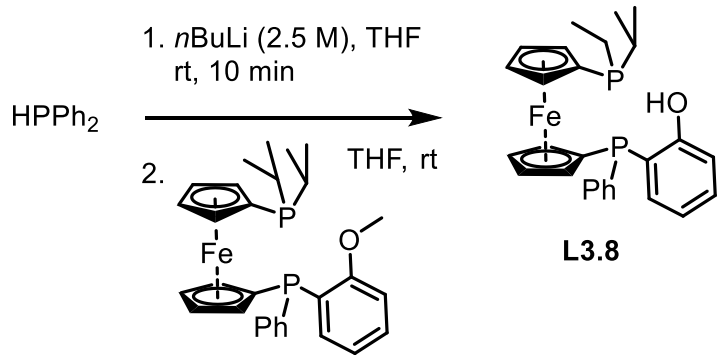

In a nitrogen filled glovebox, an oven dried and silanized 100 mL Schlenk flask was charged with diphenylphosphine (148.4 mg, 0.799 mmol), THF (1 mL), and magnetic stir bar. A syringe was used to measure a portion of *n*-butyl lithium (2.5 M) (0.33 mL, 0.825 mmol). The *n*-butyl lithium solution was added to the diphenylphosphine solution at room temperature, and immediately a color change was observed. The clear and colorless solution quickly turned to a deep red. The ferrocenyl phosphine **3.10** (339.0 mg, 0.656 mmol) was measured in the glovebox, and taken up in THF (2.4 mL). The resulting solution was added to the reaction flask via syringe addition. The mixture was stirred at room temperature for 8 hours. NMR analysis indicated a mixture of species, and more of the phosphorus anion was generated. In the glovebox, diphenylphosphine (166.6 mg, 0.895 mmol) was dissolved in THF (1 mL) and *n*-butyl lithium (2.5 M) (0.42 mL, 1.05 mmol) was added via syringe. The resulting deep red solution was added to the original reaction flask. The mixture was stirred at room temperature for 24 hours. The reaction mixture was then concentrated to dryness under reduced pressure. The orange residue was washed with pentane, then NH_4Cl (aq) (5 mL) was added. The mixture was extracted with diethyl ether (20 mL) three times. The combined organic fractions were dried over $MgSO_4$, filtered, then concentrated under reduced pressure. The crude product was then subject to column chromatography on silica gel. Due to the air-sensitive phosphorus (III) reagents, the

chromatography was run inside the glovebox. The mobile phase consisted of hexanes and diethyl ether, starting with 95% hexanes and 5% diethyl ether and ending with 70% hexanes and 30% diethyl ether. The product was collected as the second fraction of mass 77.6 mg, 24%.

^{1}H NMR ($CDCl_3$, 400 MHz): δ 7.33 – 7.27 (m, 1H), 7.15 (t, *J* = 6.6, 1H), 6.96 (dd, *J* = 8.2, 4.8, 1H), 6.89 (t, *J* = 7.5, 1H), 6.65 (d, *J* = 5.9, 1H), 4.44 – 4.00 (m, 8H), 1.89 (dtd, *J* = 14.1, 7.0, 3.0, 2H), 1.11 – 0.97 (m, 12H)

^{13}C NMR ($CDCl_3$, 125 MHz): δ

^{31}P NMR ($CDCl_3$, 202 MHz): δ 0.08, 0.05, 41.89, 41.92

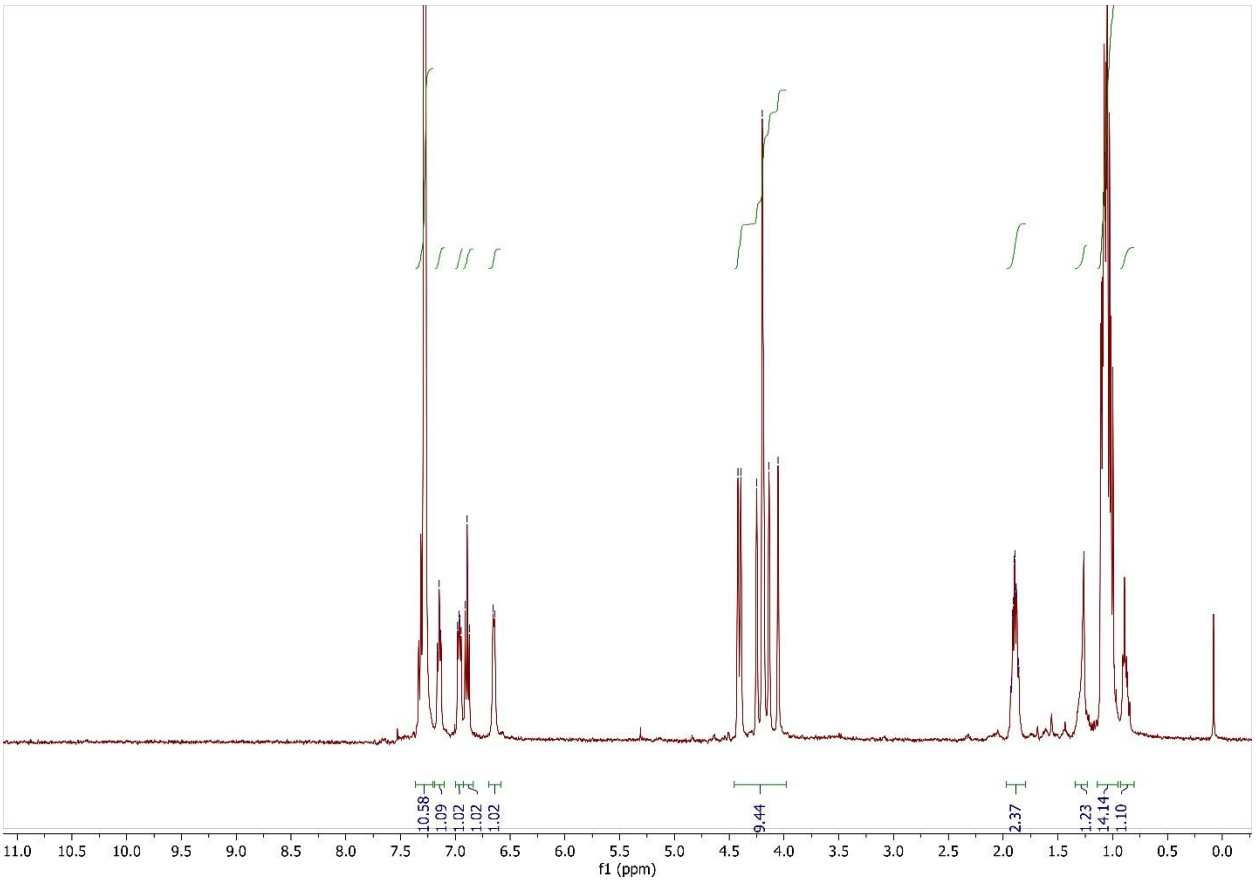

Figure 3. 59 ^{1}H NMR spectrum of **L3.8** in $CDCl_3$ at 400 MHz

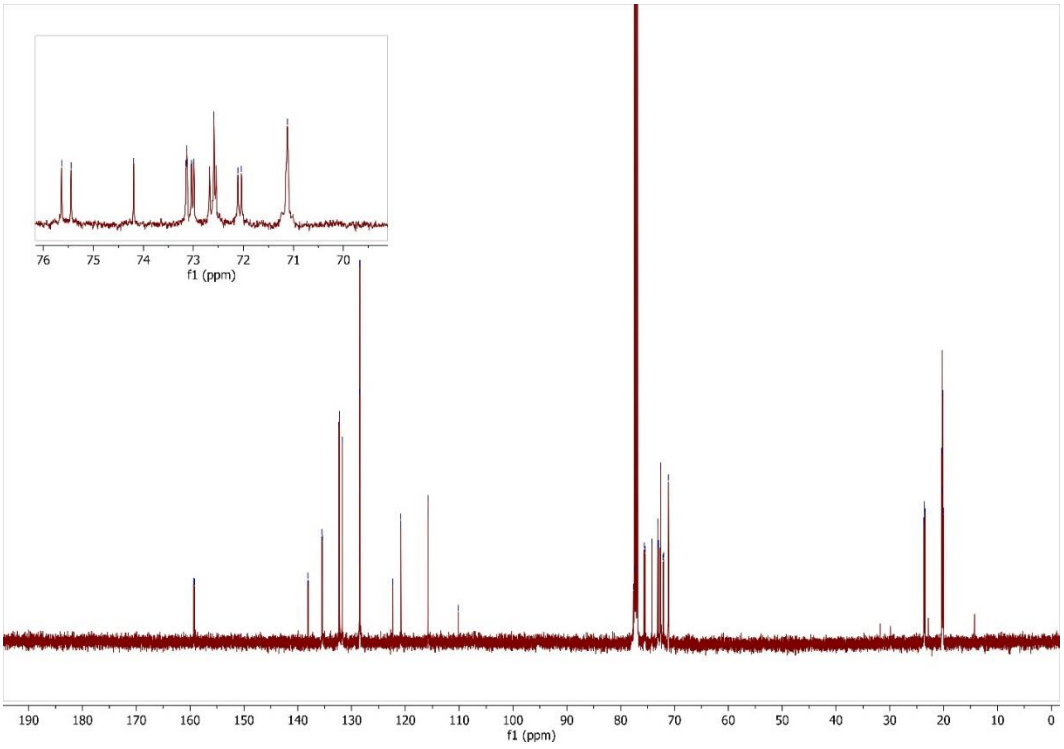

Figure 3. 60 $^{13}C\{^{1}H\}$ NMR spectrum of **L3.8** in $CDCl_3$ at 125 MHz

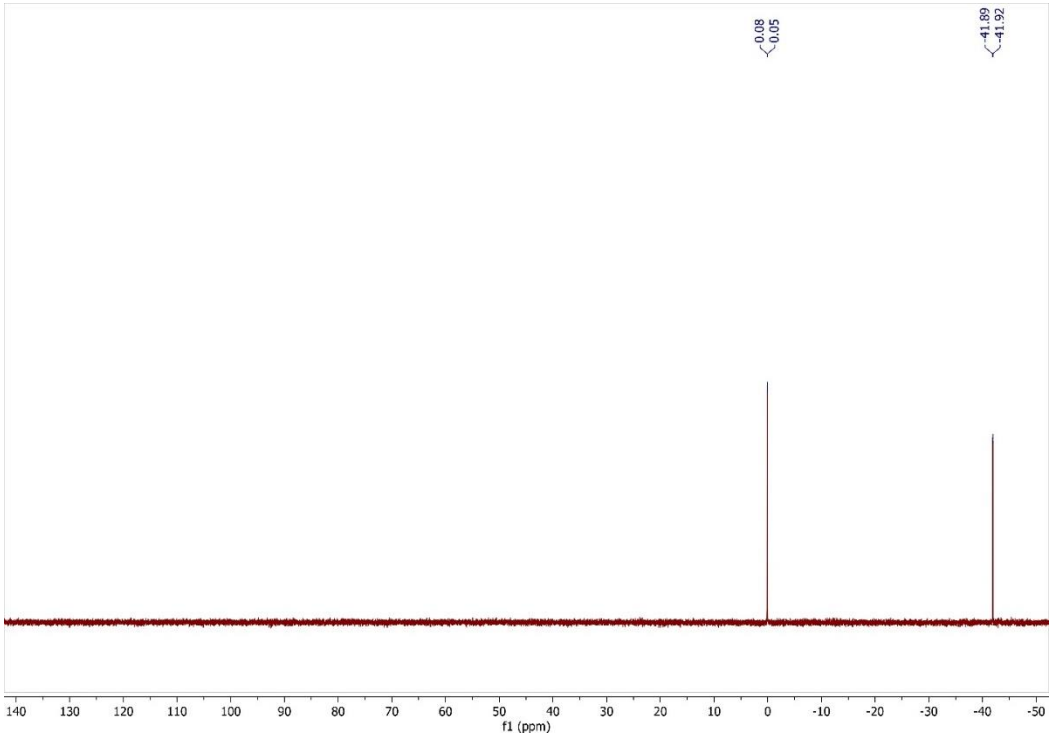

Figure 3. 61 ^{31}P NMR spectrum of **L3.8** in $CDCl_3$ at 202 MHz

Synthesis of L3.6

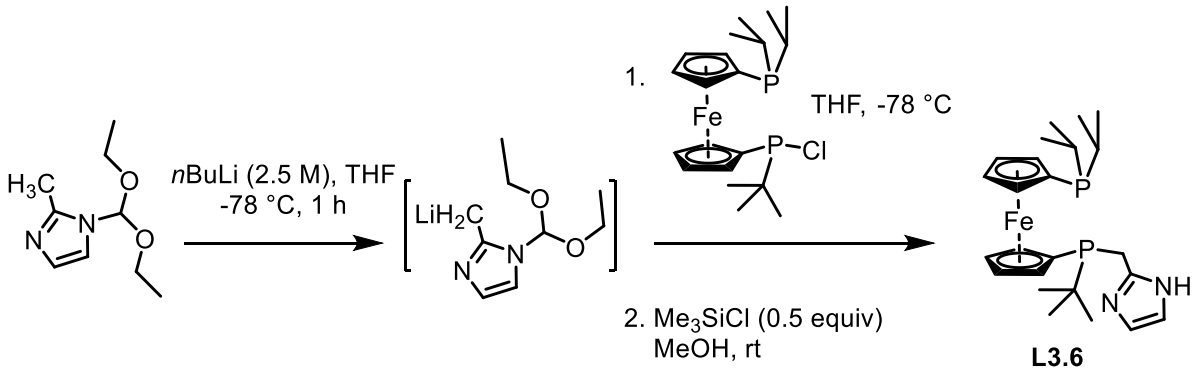

In a nitrogen filled glovebox, an oven dried and silanized 100 mL Schlenk flask was charged with methyl im' (416.2 mg, 2.259 mmol), THF (8 mL), and magnetic stir bar. A syringe was used to measure *n*-butyl lithium (2.5 M) (0.88 mL, 2.20 mmol). The vessels were sealed with rubber septa, removed from the glovebox, and connected to a Schlenk line with positive pressure of nitrogen gas. The reaction flask was placed in a bath of dry ice and acetone. Once the temperature equilibrated between the bath and the contents of the reaction flask, the *n*-butyl lithium solution was added via syringe over the course of 3 minutes. The mixture was aged for 1 hour and the cooling bath maintained. In the glovebox, a dried scintillation vial was used to measure chlorophosphine (914.0 mg, 2.152 mmol), then THF (18 mL) was used to dissolve the solid and contain it within a syringe. The THF solution of the chlorophosphine was then added dropwise over the course of 14 minutes. The reaction was stirred for the next 19 hours and gradually warmed to room temperature as the dry ice sublimed. All volatiles were removed under reduced pressure, then the reaction flask was brought into the glovebox via antechamber. Hexanes (30 mL) was added, the mixture stirred for 30 minutes, then was filtered through a glass fritted funnel, and concentrated under reduced pressure. The orange residue was dissolved in methanol (15 mL) and chlorotrimethylsilane (150 μL) was added. The mixture stirred at room temperature for 1 hour. The reaction was then filtered through a glass fritted funnel loaded with Amber-Jet-OH beads to

quench the acid. The crude product was purified through a plug of silica, with the mobile phase consisting of 5 different stages. The evolution of the mobile phase was hexanes (100%), hexanes (50%) and diethyl ether (50%), diethyl ether (100%), CH_2Cl_2 (100%), and CH_2Cl_2 (90%) and methanol (10%). The final portion of mobile phase cause elution of the orange color, indicative of the ferrocene component. The product was collected as an orange solid of mass 272.7 mg, 27%.

^{1}H NMR ($CDCl_3$, 400 MHz): δ 9.77 (br, 1H), 7.01 (s, 2H), 4.39 – 4.07 (m, 8H), 3.46 (d, *J* = 15.3, 1H), 3.30 (dd, *J* = 15.4, 2.9, 1H), 2.00 – 1.81 (m, 2H), 1.14 – 0.97 (m, 12H), 0.87 (d, *J* = 12.2, 9H)

^{31}P NMR ($CDCl_3$, 162 MHz): δ -0.86, -0.90, -5.96, -6.00

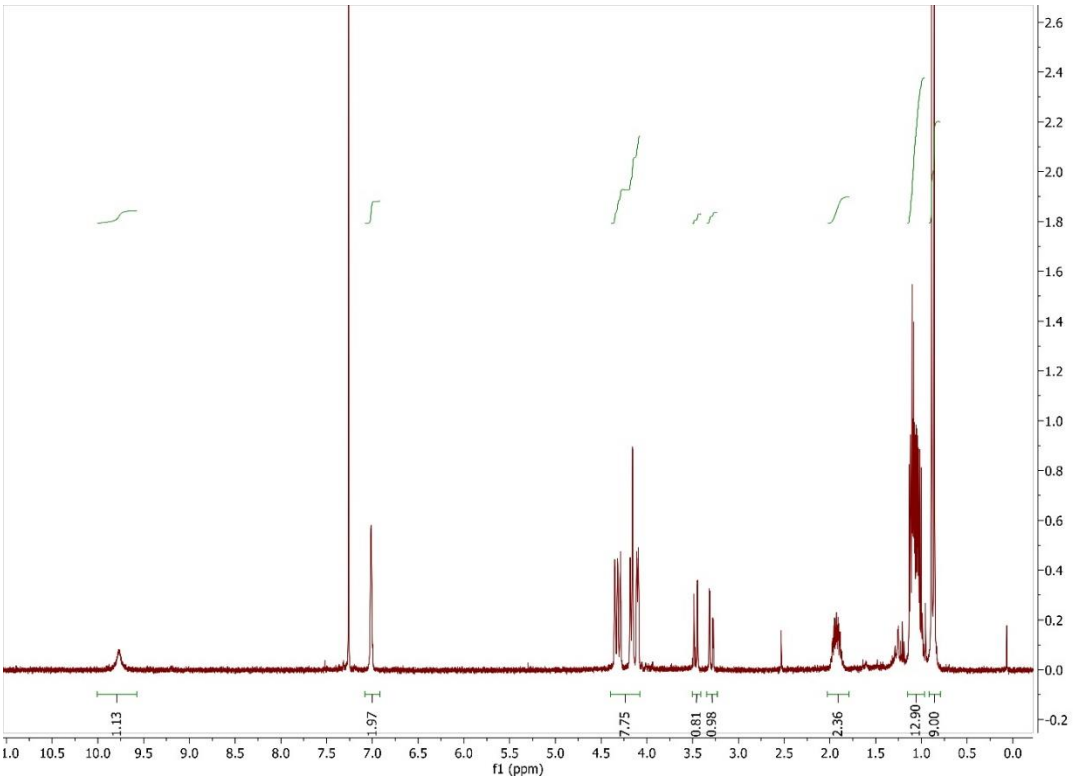

Figure 3. 62 ^{1}H NMR spectrum of **L3.6** in $CDCl_3$ at 400 MHz

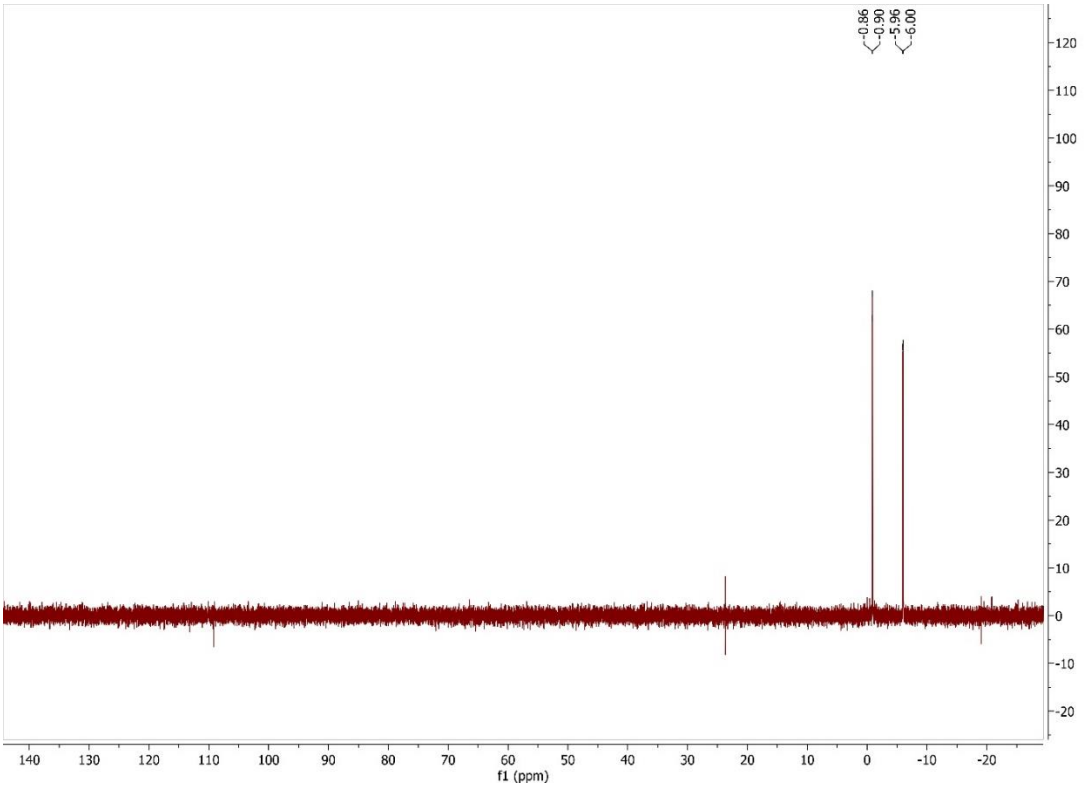

Figure 3. 63 ^{31}P NMR spectrum of **L3.6** in $CDCl_3$ at 162 MHz

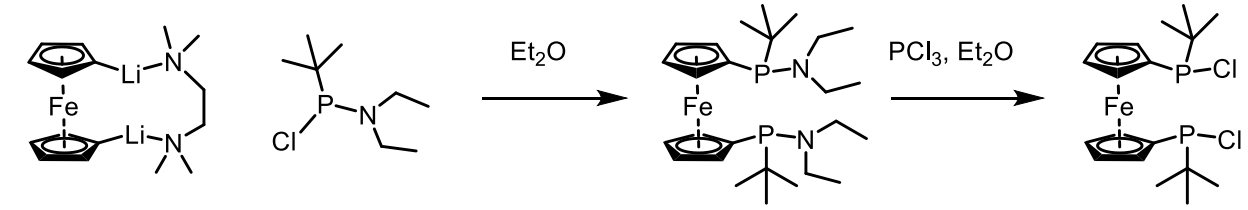

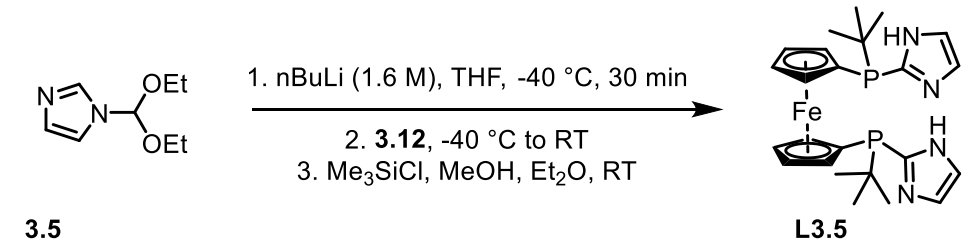

Synthesis of **3.11**

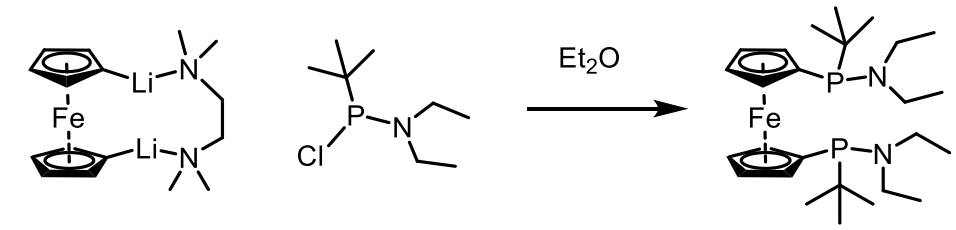

$FcLi_2$•DMEDA **3.4** **3.11**

In a nitrogen filled glove box, a dried and silanized 100 mL Schlenk flask was charged with magnetic stir bar, $FcLi_2$•DMEDA (946.7 mg), and Et_2O (35.0 mL). The flask was capped with rubber septum, removed from the glove box, put under a positive pressure of N_2 (g), and placed in an ice bath. A solution of *t*-BuPCl(NEt_2) (**3.4**) (930.2 mg) in $E_{t2}O$ (3 mL) was then slowly added via syringe and needle over 2 min. The resulting mixture was stirred with the bath temperature held below 5 °C for 1.6 h, after which point the cooling bath was removed and the mixture was stirred for an additional 20 h. During this stirring time, a large amount of white precipitate has formed in the flask. The mixture was brought into the glovebox and filtered through an oven dried fritted funnel with a small cake of celite, then washed with additional Et_2O. The filtrate was concentrated in vacuo with an oil pump to yield **3.11** as a viscous orange oil (1.1302 g). The material was used for the next step without further purification.

^{1}H-NMR (CDCl3, 400 MHz) δ 4.50-4.42 (m, overlapping signals, 8H), 3.24-3.08 (m, 8H), 1.27 (d, *J* = 12.4, 18H), 1.18 (t, J = 7.0, 12H)

^{31}P-NMR (CDCl3, 162 MHz) δ 73.62 (s), 73.51 (s)

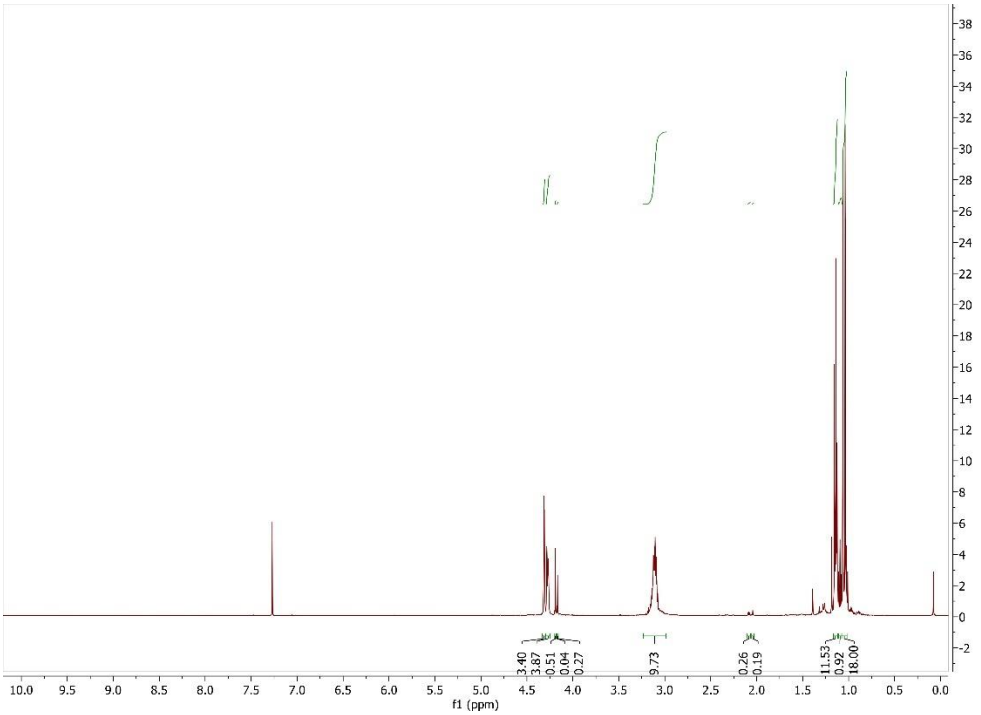

Figure 3. 64 ^{1}H NMR spectrum of **3.11** in $CDCl_3$ at 500 MHz

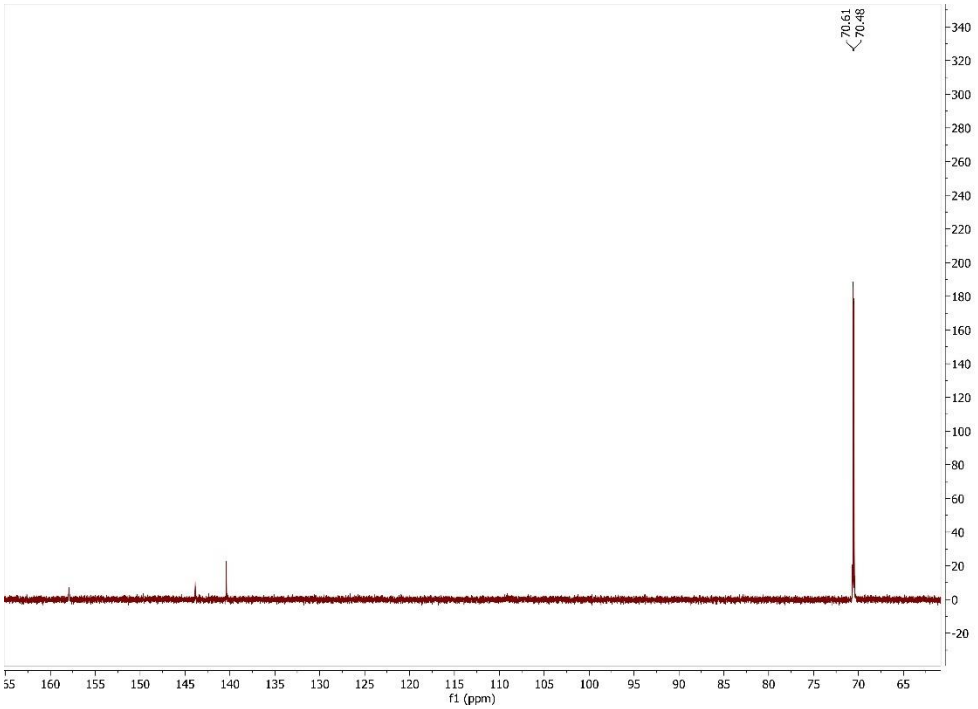

Figure 3. 65 ^{31}P NMR spectrum of **3.11** in $CDCl_3$ at 202 MHz

Synthesis of **3.12**

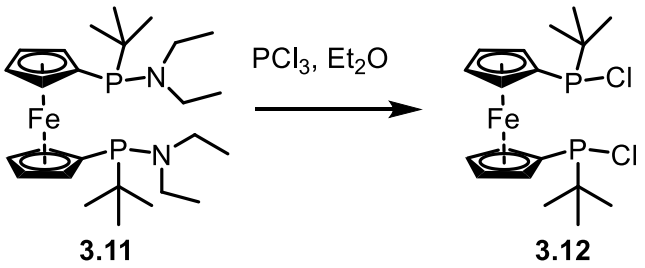

3.11 **3.12**

In a nitrogen filled glove box, a Schlenk flask was charged with magnetic stir bar**, 3.11** (273.8 mg, 0.542 mmool), and Et2O (5.0 mL). To the stirring solution was added a solution of PCl_3 (296.5 mg) in Et2O (1.0 mL) over 30 sec. The resulting mixture was stirred for 2 h, after which point the volatiles were removed with an oil pump. The orange residue (206.6 mg) was analyzed by ^{1}H- and ^{31}P-NMR and used for the next step without further purification.

^{1}H NMR ($CDCl_3$, 400 MHz): δ 4.48 (m, 2H), 4.40 – 4.35 (m, 6H), 0.95 (d, *J* = 13.5, 18H).

^{31}P-NMR ($CDCl_3$, 162 MHz) δ 111.5 (s), 111.4 (s).

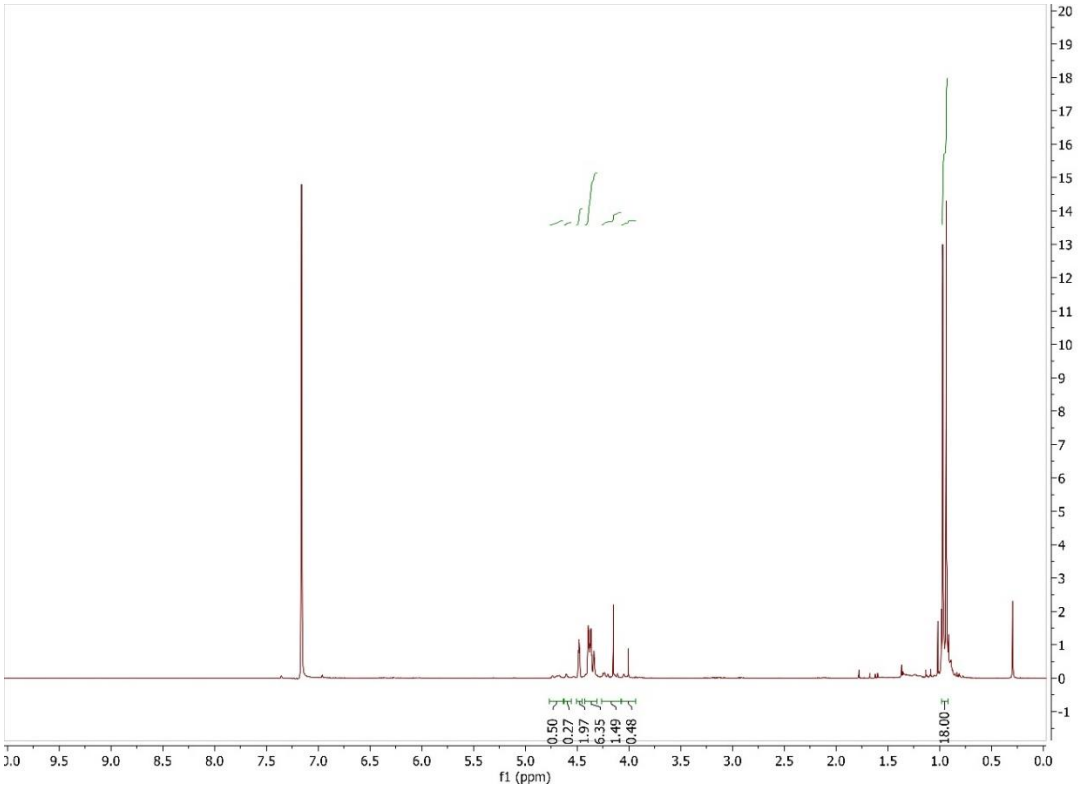

Figure 3. 66 ^{1}H NMR spectrum of **3.12** in C_6D_6 at 400 MHz

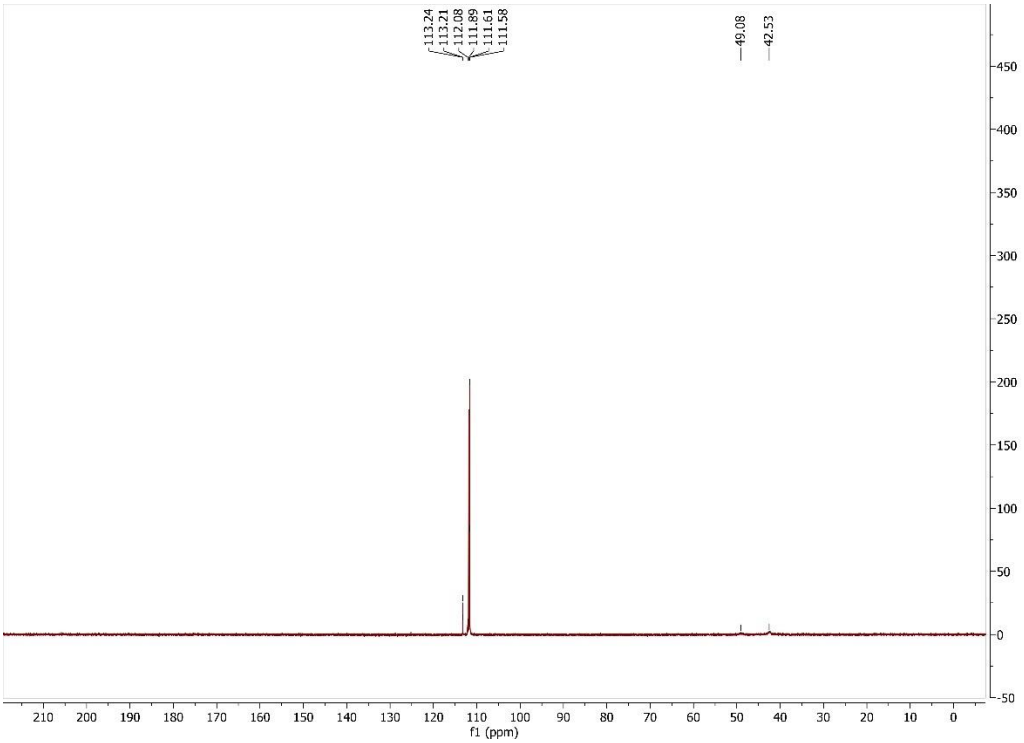

Figure 3. 67 ^{31}P NMR spectrum of **3.12** in C_6D_6 at 162 MHz

Synthesis of **L3.5**

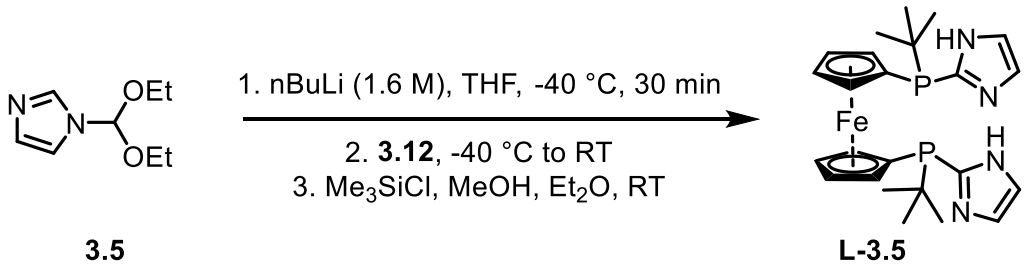

3.5 **L-3.5**

In a nitrogen filled glovebox, an oven dried 100 mL Schlenk flask was charged with **3.5** (744.8 mg, 4.375 mmol) and THF (25 mL). A magnetic stir bar was added to the flask, then a rubber septum was used to seal the flask before it was removed from the glovebox. The flask was connected to a flow of positive pressure of nitrogen gas via Schlenk line. The Schlenk flask was then placed in a cooling bath composed of CH_3CN and an amount of liquid nitrogen such that the bath is still liquid and free flowing. Next, *n*-butyllithium (1.6 M) (2.7 mL, 4.349 mmol) was added dropwise via syringe over the course of 6 minutes. The color of the reaction mixture changed from clear and colorless to a light yellow. The mixture was stirred with the cooling bath maintained for 30 minutes. Meanwhile, the chlorophosphine **3.12** was measured (937.5 mg, 2.175 mmol) and prepared as a THF solution (10 mL). The solution was taken up in a syringe and removed from the glovebox. The chlorophosphine was then added dtopwise to the reaction mixture over the course of 10 minutes. The mixture was then stirred for 24 hours in a rigorously air and water free environment. The volatile components were then evaporated under reduced pressure. The residue was taken up in MeOH (10 mL), and $(CH_3)_3SiCl$ (0.2 mL). The mixture was stirred at room temperature for 3 hours. The generated acid was quenched with the addition of K_2CO_3. The mixture was then diluted with K_2CO_3 (aq) (30 mL). Extraction with Et_2O (30 mL) was conducted three times, and the combined organic phase dried over Na_2SO_4, filtered through a glass fritted funnel, then concentrated under reduced pressure. The resiude was washed with pentane. The crude

product was then prepared for purification on alumina gel. The column was conducted in the glovebox with frequent purging. The mobile phase consisted of ethyl acetate, CH_2Cl_2. Fractions 6-11 were combined, and then crystallized from a cold and concentrated CH_2Cl solution of the bisphosphine. The total mass collected was 178.3 mg, 16 %

^{1}H-NMR (d_6-acetone,400 MHz): δ 11.67 (s, br, 2H), 7.33 (s, 2H), 7.28 (s, br, 2H), 4.74 (s, br, 2H), 4.17 (s, 2H). 3.81 (s, 2H), 3.73 (s, 2H), 0.94 (d, *J* = 13.1, 18)

^{13}C NMR (d_6-acetone, 100 MHz): δ 145.87 (d, *J* = 4.9), 131.27, 118.06 (d, *J* = 5.4), 78.54 (d, *J* = 40.5), 74.82 (d, *J* = 6.1), 73.79 (d, *J* = 7.8), 31.61 (d, *J* = 5.9), 28.01 (d, *J* = 15.2)

^{31}P-NMR (d_6-acetone, 100 MHz): δ -18.66

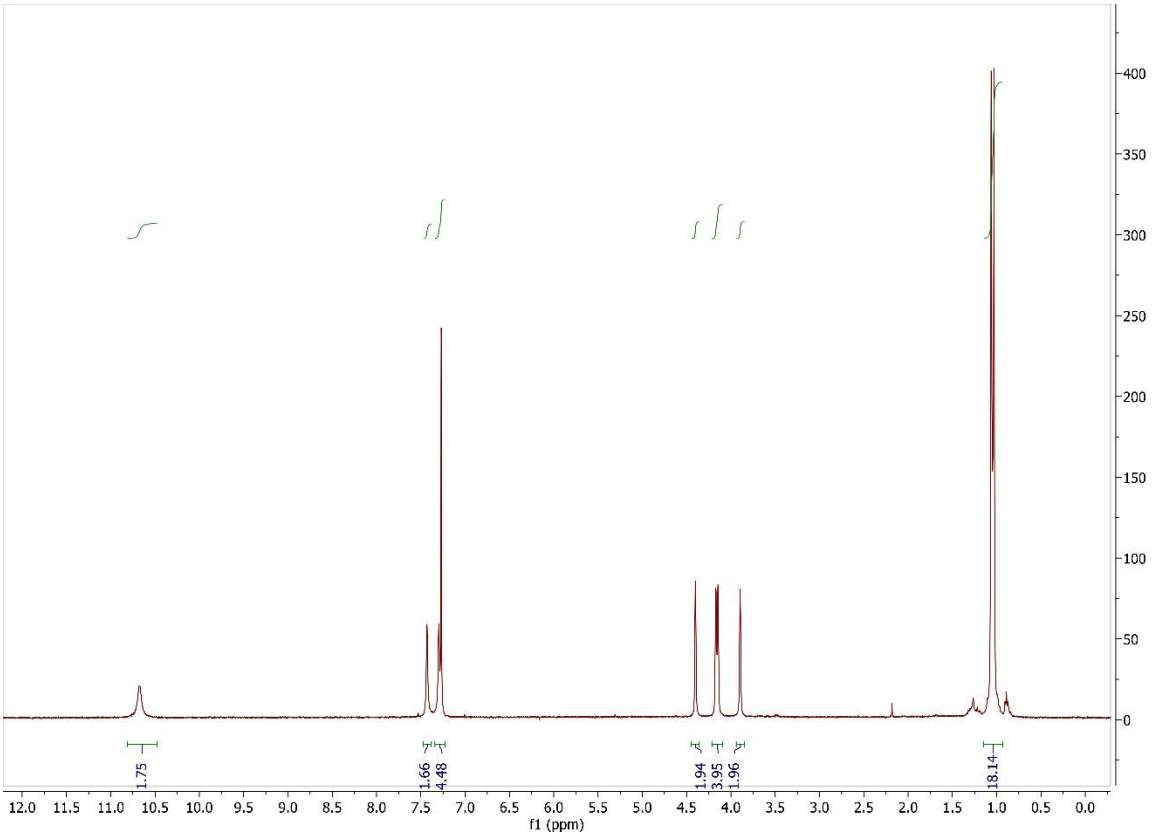

Figure 3. 68 ^{1} H NMR spectrum of **L3.5** in $CDCl_3$ at 400 MHz

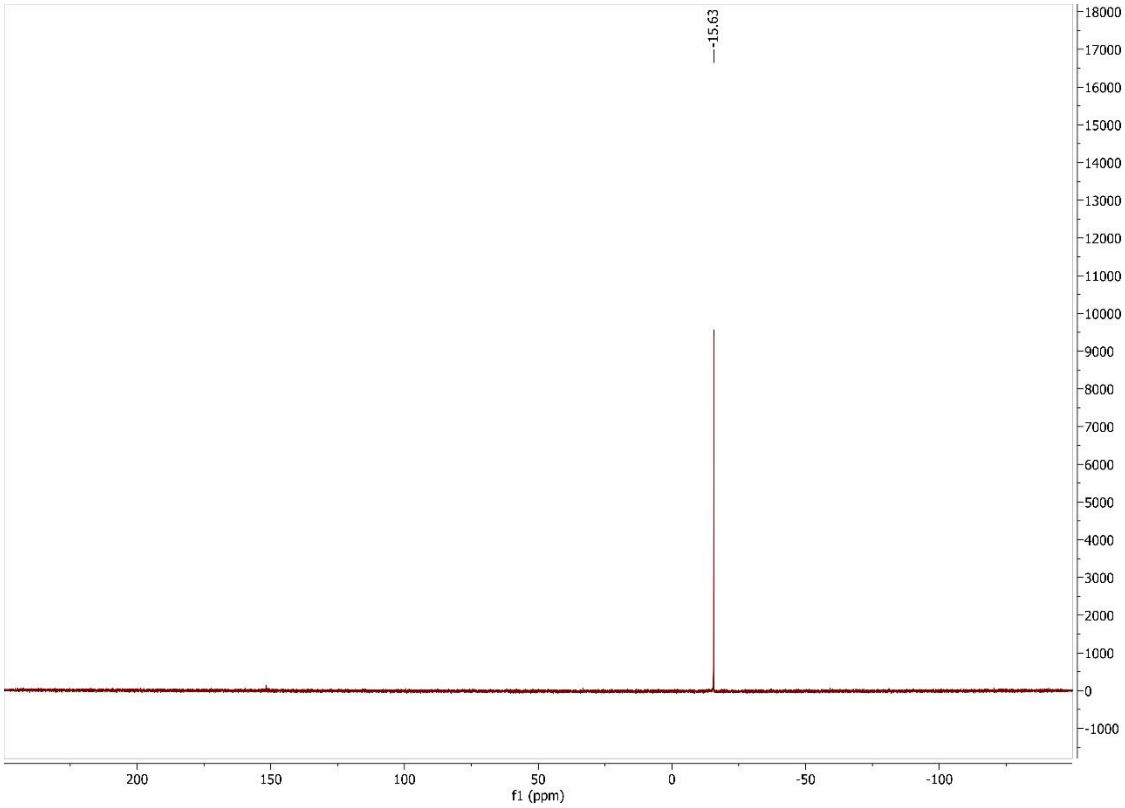

Figure 3. 69 ^{31}P NMR spectrum of **L3.5** in $CDCl_3$ at 162 MHz

Synthesis of nickel complexes

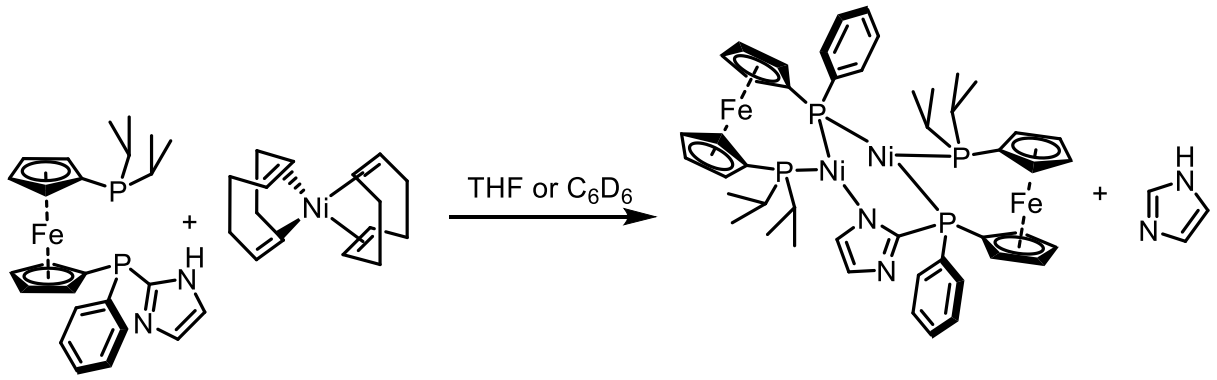

In a nitrogen filled glovebox, an oven dried J. Young NMR tube was charged with L3.3 (10.1 mg, 0.0212 mmol) and C_6D_6 (0.7 mL). The NMR tube allowed to mix for 10 minutes to allow time for all the added phosphine to dissolve. Next, $Ni(COD)_2$ (5.9 mg, 0.0212 mmol) was added to the NMR tube. A small portion of C_6D_6 was added to wash the solid from the top walls of the NMR tube. The initially orange solution had changed to green / brown within 5 to 10 minutes of mixing L3.3 and $Ni(COD)_2$. Confirmation of chemical structure was verified by x-ray crystal structure.

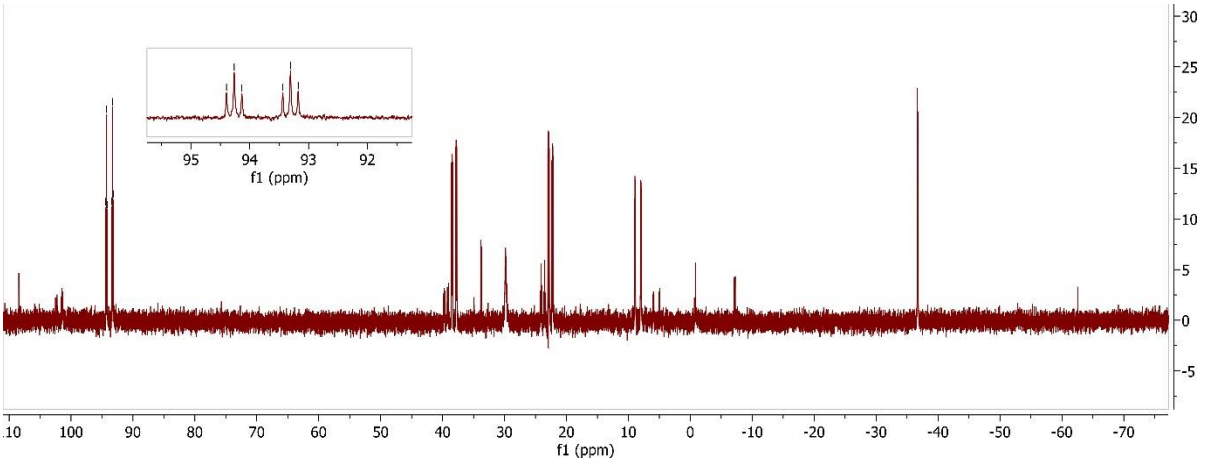

Figure 3. 70 ^{31}P NMR spectrum of reaction mixture of **L3.3** and $Ni(COD)_2$ in C_6D_6 at 162 MHz

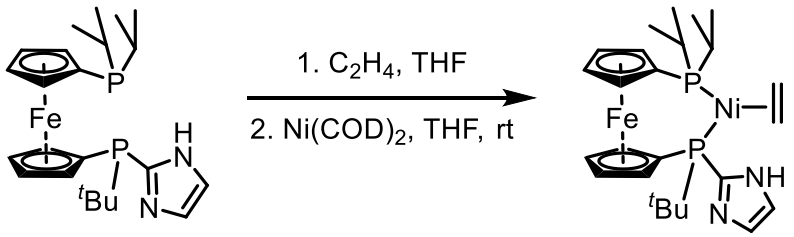

L3.2 **Ni-3.2**

In a nitrogen filled glovebox, an oven dried and silanized 50 mL Schlenk flask was charged with L3.2 (14.4 mg, 0.0316 mmol) and THF (1 mL). The flask was sealed with a rubber septum, removed from the glovebox, then connected to a Schlenk line with exposure to positive pressure of nitrogen gas. Ethylene gas was sparged through the solution for 1 minute. The flask was brought back into the glovebox via antechamber. $Ni(COD)_2$ (8.7 mg, 0.032 mmol) was added to the reaction flask, then the mixture was stirred for 1 hour. The volatiles were evaporated under reduced pressure to yield a solid of mass 21.54 mg. The solid was analyzed by NMR for characterization.

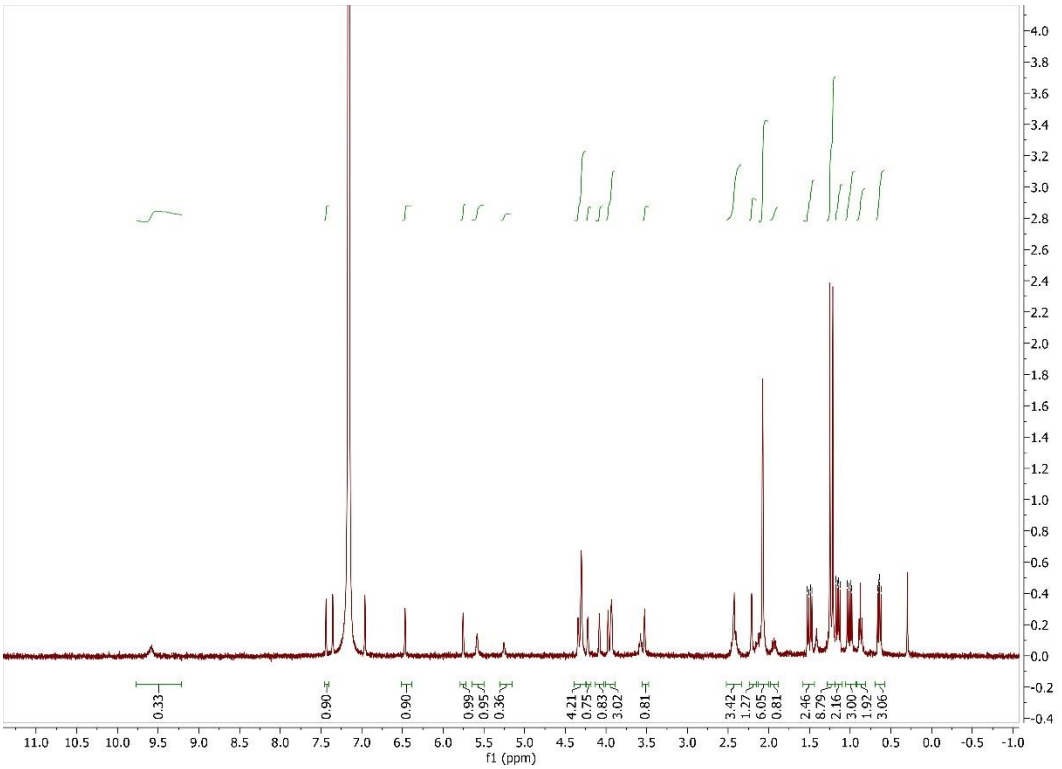

Figure 3. 71 ^{1}H NMR spectrum of **Ni-3.2** in C_6D_6 at 400 MHz

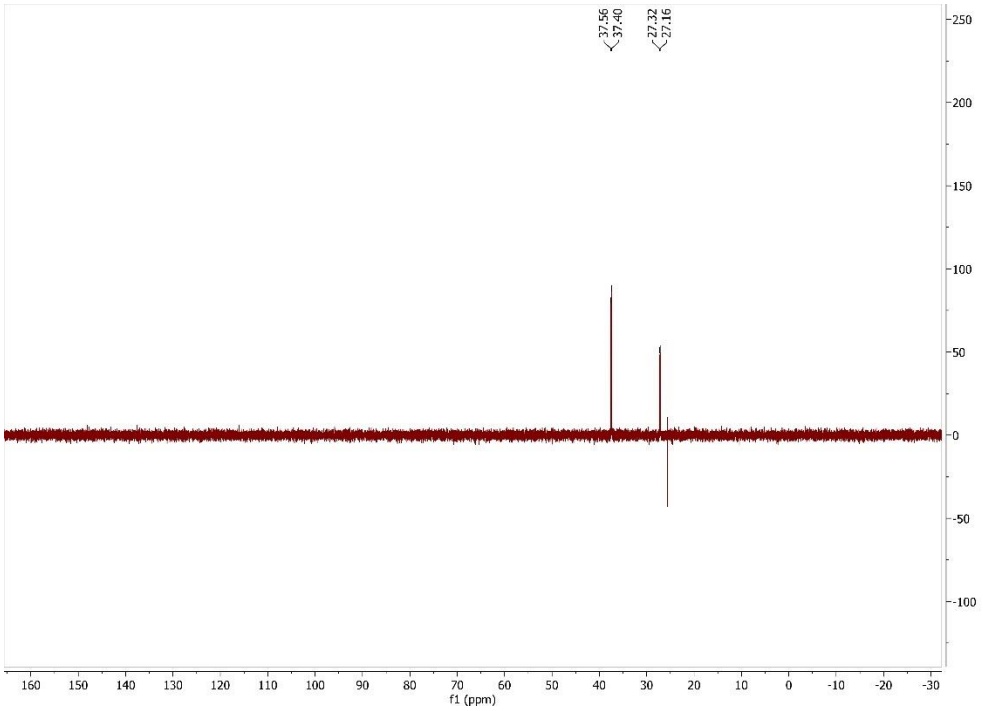

Figure 3. 72 ^{31}P NMR spectrum of **Ni-3.2** in C_6D_6 at 162 MHz

Synthesis of **Ni-3.3**

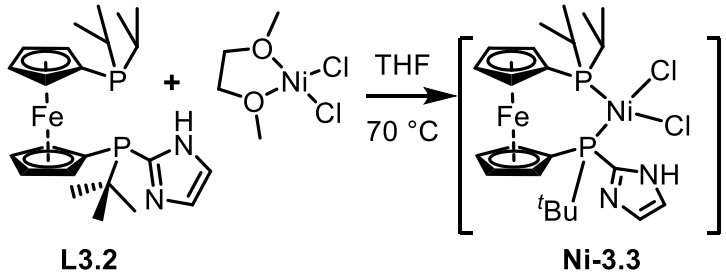

L3.2 **Ni-3.3**

In a nitrogen filled glovebox, an oven dried scintillation vial was charged with L3.2 (13.4 mg, 0.0284 mmol), $NiCl_2$•DME (6.5 mg, 0.0296 mmol), and THF (3 mL). The vial was sealed, removed from the glovebox, then placed in an oil bath heated to 70 °C for 7 hours. The vial was brought back into the glovebox via the antechamber, and all volatiles were removed under reduced pressure. The resulting green powder was redissolved in THF (1.5 mL), filtered through a short pad of celite 545, the futher rinsed with THF (2 mL). The volatiles were again removed under

reduced pressure to yield a dark powder of mass 20.5 mg (119%). It is likely the additional mass is residual DME, as the expected mass of the liberated DME is 2.7 mg, roughly the same as the additional mass of the residual powder.

Reduction of **Ni-3.3** with zinc powder

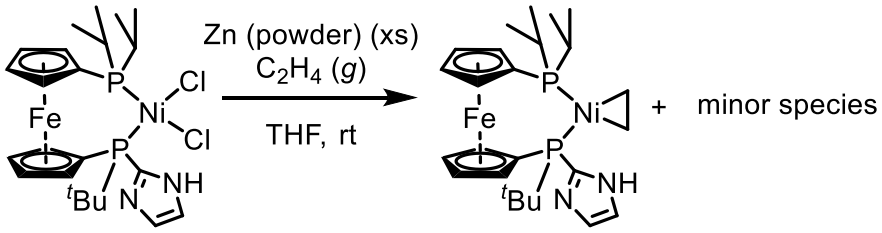

Ni-3.3 **Ni-3.2**

In a nitrogen filled glovebox, an oven dried 50 mL Schlenk flask was charged with zinc (s) poweder and THF (1 mL). The presumed nickel(II) dichloride complex Ni-3.3 (19.4 mg, 0.0331 mmol) was measured, THF (1.2 mL) added, and the mixture stirred for 20 minutes. The THF suspension of zinc powder was then removed from the glovebox and sparged with ethylene gas for 2 minutes. The THF solution of Ni-3.3 was then added via syringe to the Schlenk flask with zinc powder, ethylene, and THF. The mixture was stirred at room temperature for 12 hours. The mixture was then filtered and lightening of the color of the solution from dark to light green / yellow was observed. Ethylene gas was used to partially concentrate the solution of THF. Then the partially concentrated THF solution was aliquoted and diluted with d_8-THF for NMR analysis. Observation of the ^{31}P NMR spectrum revealed resonances consisted with the structure **Ni-3.2**

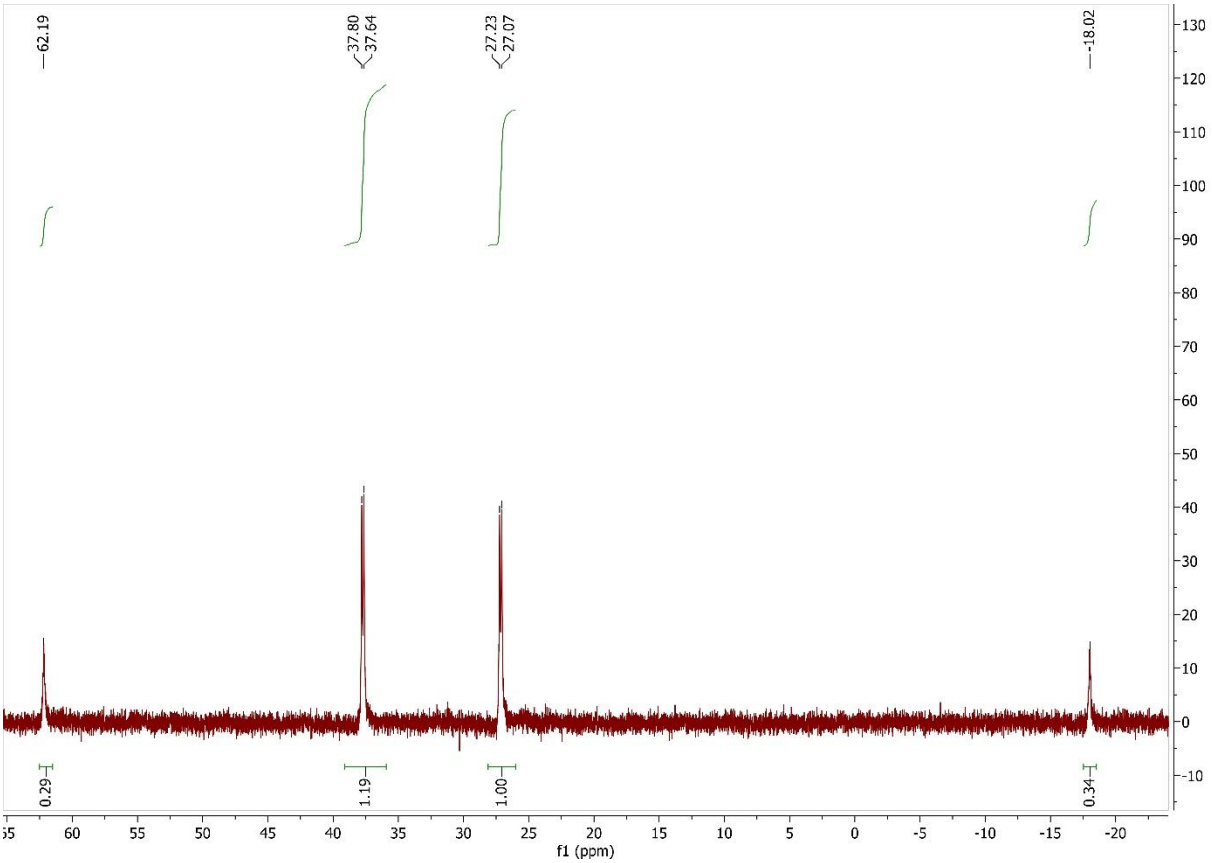

Figure 3. 73 ^{31}P NMR spectrum of reaction mixture for the reduction of **Ni-3.3** with zinc

Synthesis of **Pt-3.5**

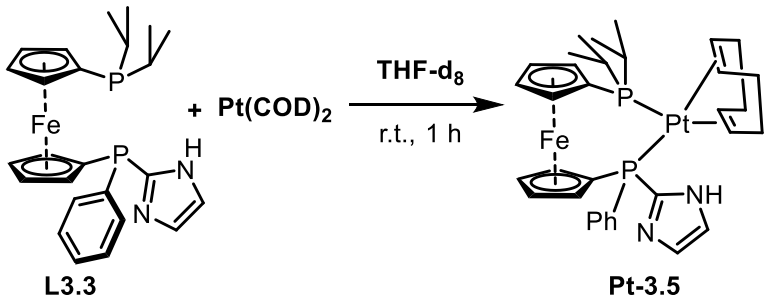

In a nitrogen filled glovebox, an oven dried scintillation vial was charged with **L3.3** (7.3 mg, 0.015 mmol), $((CH_3)_3Si)_4C$ (2.0 mg, 0.575 mmol), and d_8-THF (0.6 mL). The mixture was stirred for 10 minutes. In a separate oven dried vial, $Pt(COD)_2$ (6.3 mg, 0.015 mmol) was measured. The d_8-THF solution of **L3.3** was then added to the $Pt(COD)_2$ solid. The mixture formed an orange/ brown solution and was stirred for 2 hours. The solution was transferred from the vial to an oven dried J. Young NMR tube.

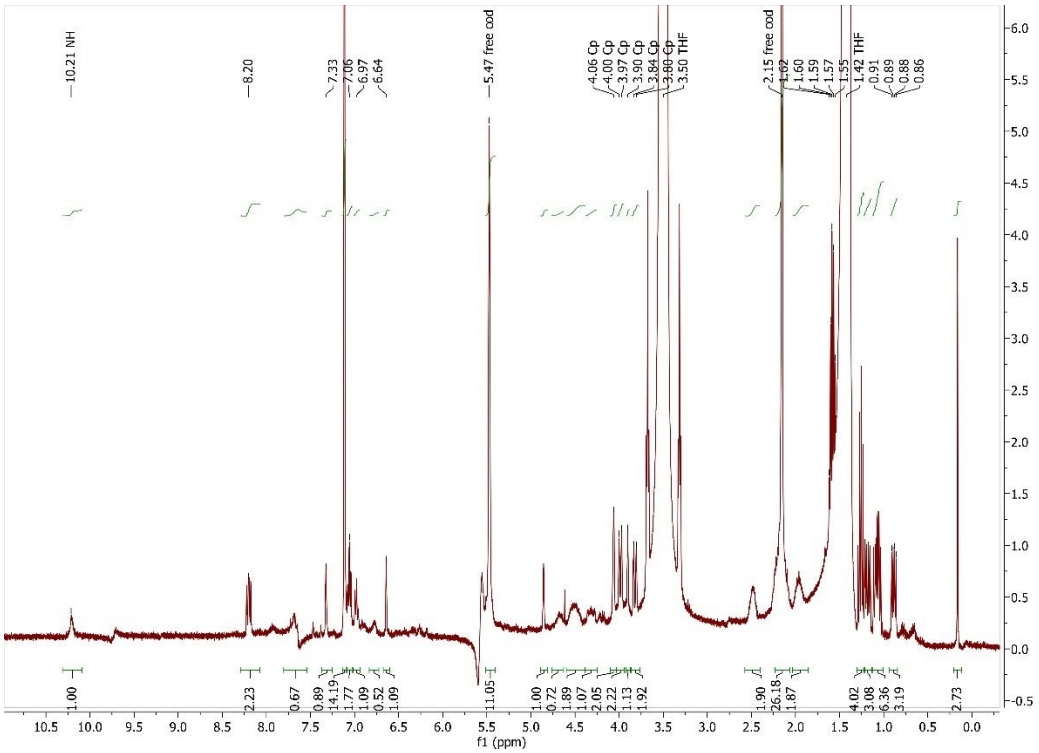

Figure 3. 74 ^{1}H NMR spectrum of **Pt-3.5** in C_6D_6 at 400 MHz

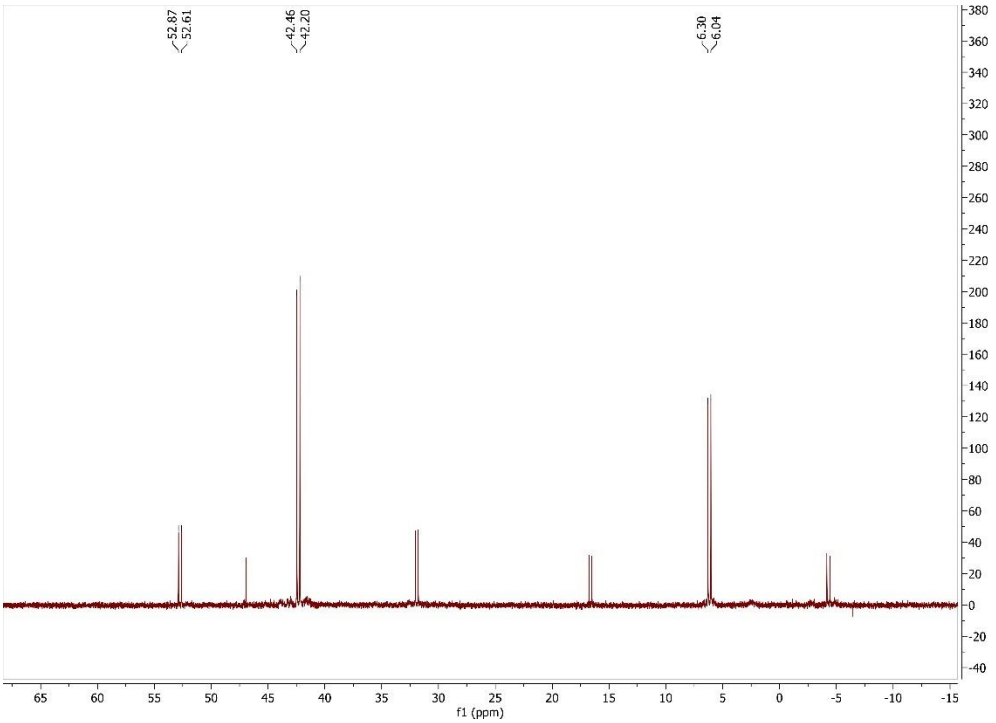

Figure 3. 75 ^{31}P NMR spectrum of **Pt-3.5** in C_6D_6 at 162 MHz

Synthesis of **Pt-3.6**

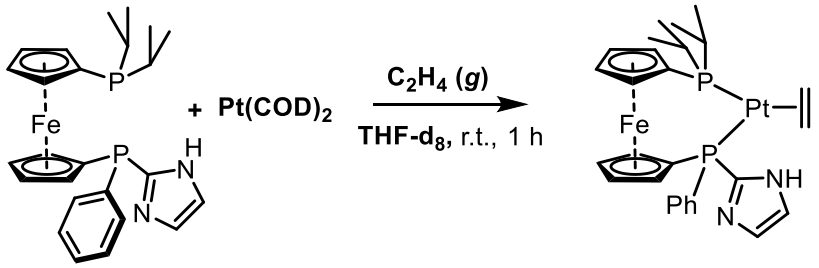

L3.3 **Pt-3.6**

In a nitrogen filled glovebox, an oven dried scintillation vial was charged with **L3.3** (10.2 mg, 0.0214 mmol) and d_6-acetone (1 mL). The vial was sealed and removed from the glovebox. The solution was then sparged with ethylene gas for 1 minute. The vial was sealed again and brough back into the glovebox via antechamber. Next, $Pt(COD)_2$ (8.6 mg, 0.0209 mmol) was measured into a separate oven dried vial. The d_6-acetone solution of **L3.3** and ethylene was transferred via syringe to the vial with the platinum complex. The mixture was stirred at room

temperature for 4 hours. The reaction mixture was then transferred to a J. Young NMR tube an observed for reactivity. During the preparation of the NMR, it was noted that a small amount of solid was visible on the bottom of the NMR tube. The observed ^{1}H NMR spectrum revealed non-coordinated cyclooctadiene (δ 2.34 ppm (s) and 5.53 ppm (s)) and a new broad signal at 3.00 ppm with a relative integration value for four protons. Interestingly, three signals appear up-field that correspond to the isopropyl methyl groups. Two of the signals (1.04 ppm and 1.21 ppm) represent a single methyl group each, and the signal at 1.30 ppm represents two methyl groups. Analysis of the ^{31}P NMR spectrum reveals two signals resonating at δ 44.62 (d, J = 37.7, $J_{Pt\text{-}P}$ = 3533.5) and 8.72 (d, J = 37.8, $J_{Pt\text{-}P}$ = 3589.2). Based on these spectra the structure was assigned as complex **Pt-3.6**.

^{1}H NMR (d_6-acetone, 400 MHz): δ 10.80 (br, 1H), 7.93 (m, 2H), 7.31 (br, 3H), 7.22 (s, br, 2H), 4.82 (s, 1H), 4.37 (s, br, 2H), 4.34 (s, br, 1H), 4.25 (s, 2H), 4.13 (s, 1H), 4.10 (s, 1H), 3.00 (br, 4H), 2.49 (m, 2H), 1.28 (dd, J = 14.9, 6.8, 6H), 1.20 (dd, J = 15.6, 7.1, 3H), 1.03 (dd, J = 13.5, 6.9, 3H). Uncoordinated 1,5-cyclooctadiene is observed at 2.34 ppm (s) and 5.53 ppm (s).

^{31}P NMR (d_6-acetone, 162 MHz): δ 44.62 (d, J = 37.7, $J_{Pt\text{-}P}$ = 3533.5) and 8.72 (d, J = 37.8, $J_{Pt\text{-}P}$ = 3589.2)

An attempt to isolate the complex as a solid was made. The volatile components were evaporated under reduced pressure, and the residue rinsed with a small portion of pentane. The residue was measured to be 9.3 mg. The residue was taken up in d_8-THF and observed with NMR analysis. Interestingly, the ^{31}P NMR spectrum matched identically to that initially observed in the d_6-acetone solution. However, inspection of the ^{1}H NMR spectrum shows the disappearance of the broad signal at 3.00 ppm that was assigned to coordinated ethylene. The resonances assigned to uncoordinated 1,5-cyclooctadiene are significantly smaller than in the initial d_6-acetone solution.

Comparison of the integrations of the 1,5-COD peaks before and after sample concentration indicate 78% removal of the 1,5-COD. The outstanding question remains, is there a coordinated ethylene unit within the structure? It is possible that the broad signal (or signals) between 2.17 – 1.81 ppm represent the C_2H_4 protons, however integration of this entire region only accounts for 2.9H. A resonance integrating close to 4H is expected for ethylene, thus the signal between 2.17 – 1.81 is not assigned to a coordinated ethylene.

In a separate experiment, Pt-3.6 was prepared identically to the described protocol, only after evaporation C_6D_6 was used as the solvent instead of d_8-THF. In this case, two broad resonances appear in the ^{1}H NMR spectrum at δ 2.43 ppm and 2.17 ppm. These signals integrate to a little over four protons, and we tentatively assign them to representing the coordinated ethylene.

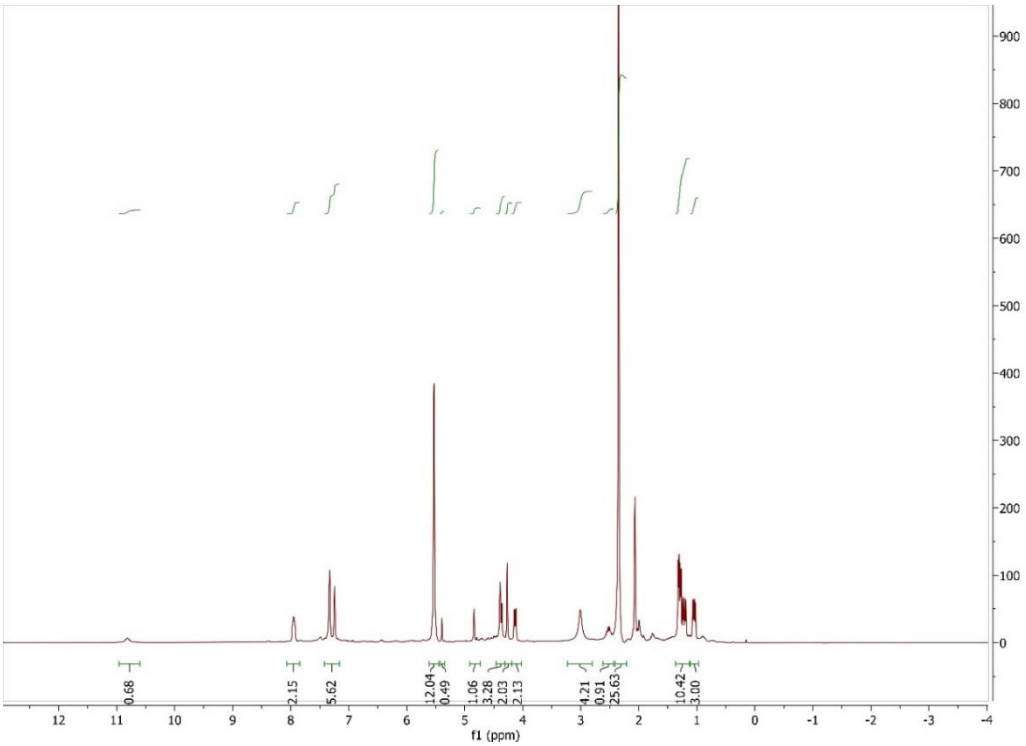

Figure 3. 76 ^{1}H NMR spectrum of **Pt-3.6** in d_6-acetone at 400 MHz

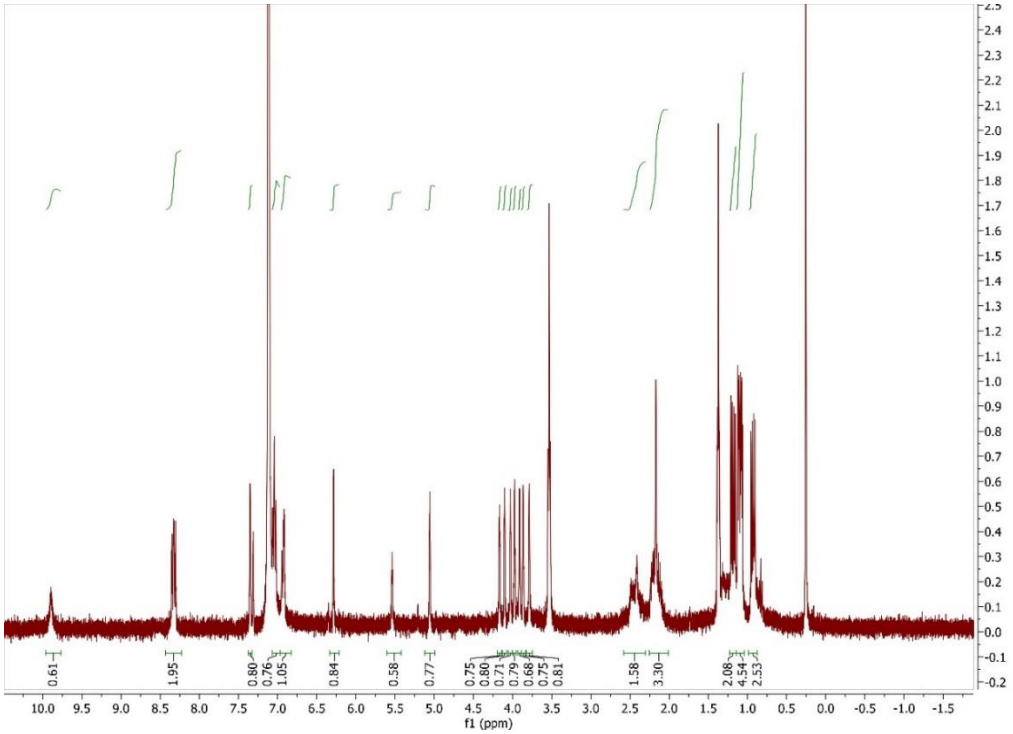

Figure 3. 77 ^{1}H NMR spectrum of **Pt-3.6** in C_6D_6 at 400 MHz

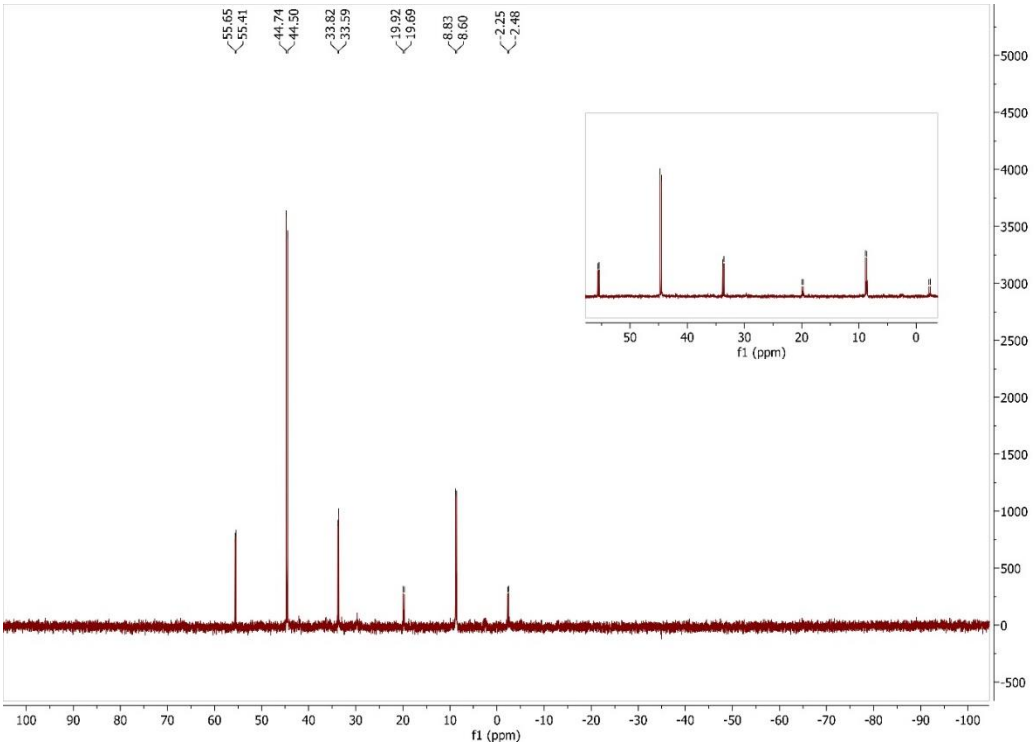

Figure 3. 78 ^{31}P NMR spectrum of **Pt-3.6** in d_6-acetone at 162 MHz

Synthesis of **Pt-3.7**

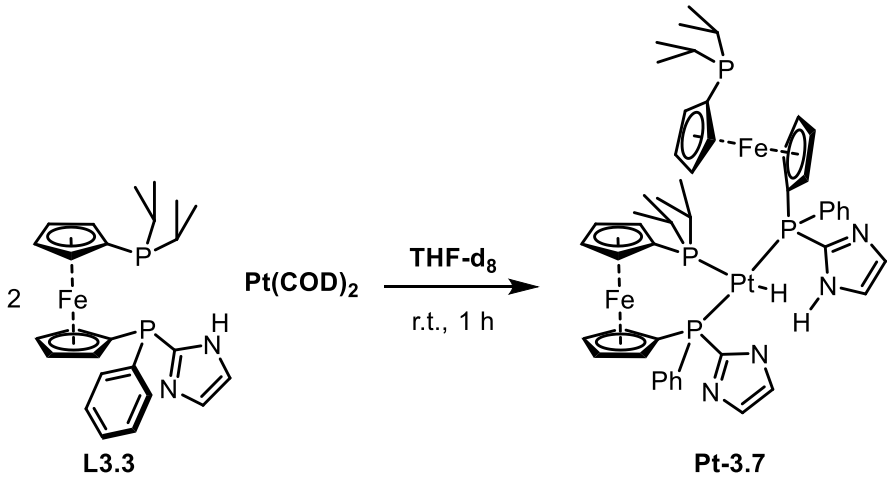

In a nitrogen filled glovebox, an oven dried scintillation vial was charged with $((CH_3)_3Si)_4C$ (1.5 mg), **L3.3** (12.9 mg, 0.0271 mmol), THF (2 mL), and magnetic stir bar. A separate oven dried vial was charged with $Pt(COD)_2$ (5.6 mg, 0.0135 mmol) and magnetic stir bar. The ligand solution was transferred to the vial with the platinum, and the mixture was stirred at room temperature for 30 minutes. The mixing solution was a dark yellow color. The mixture was then concentrated under reduced pressure to yield a residue of mass 19.4 mg. The residue was taken up in d_6-acetone, however a significant amount of precipitate was visible. The solution was filtered through a small celite plug in a glass pipette, then transferred to a J. Young NMR tube for analysis.

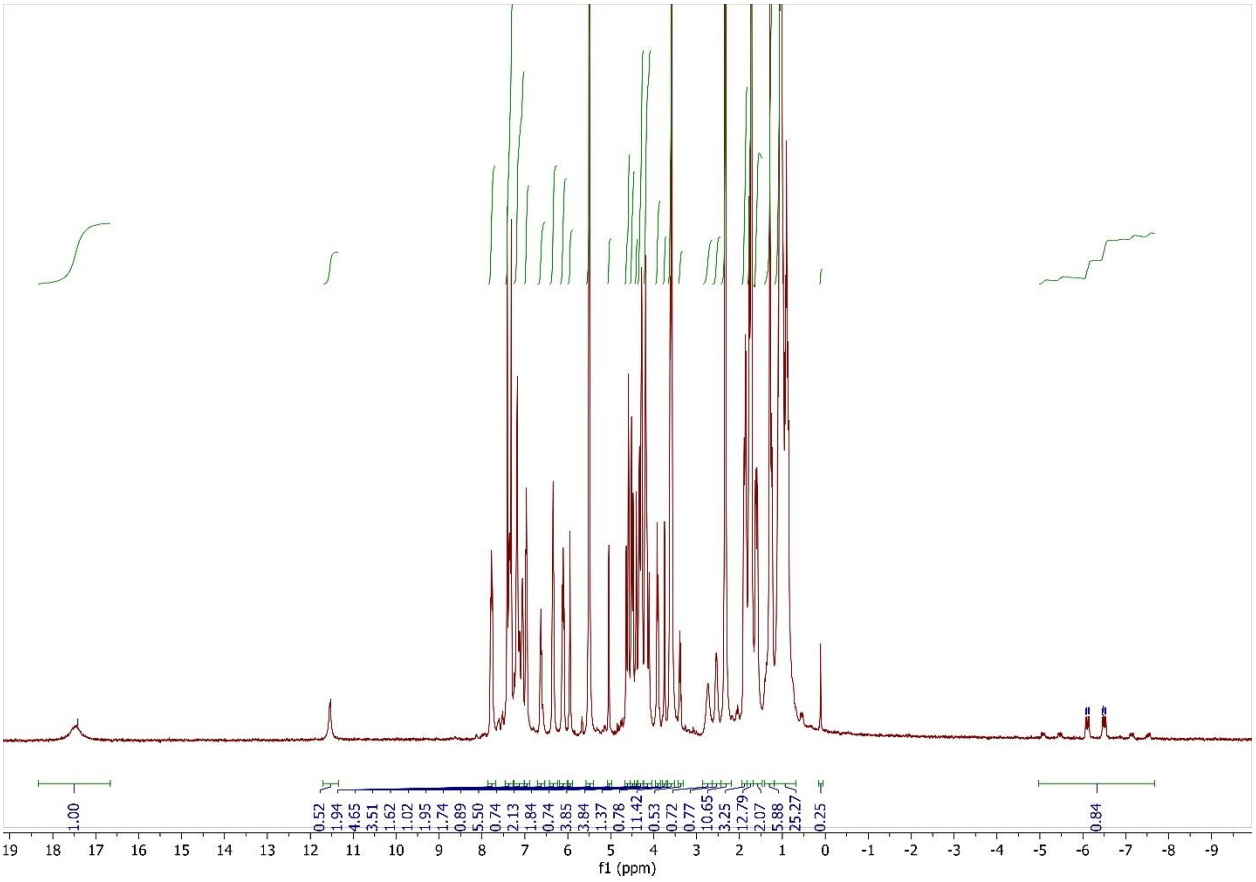

Figure 3. 79 ^{1}H NMR spectrum of **Pt-3.7** in d_6-acetone at 400 MHz

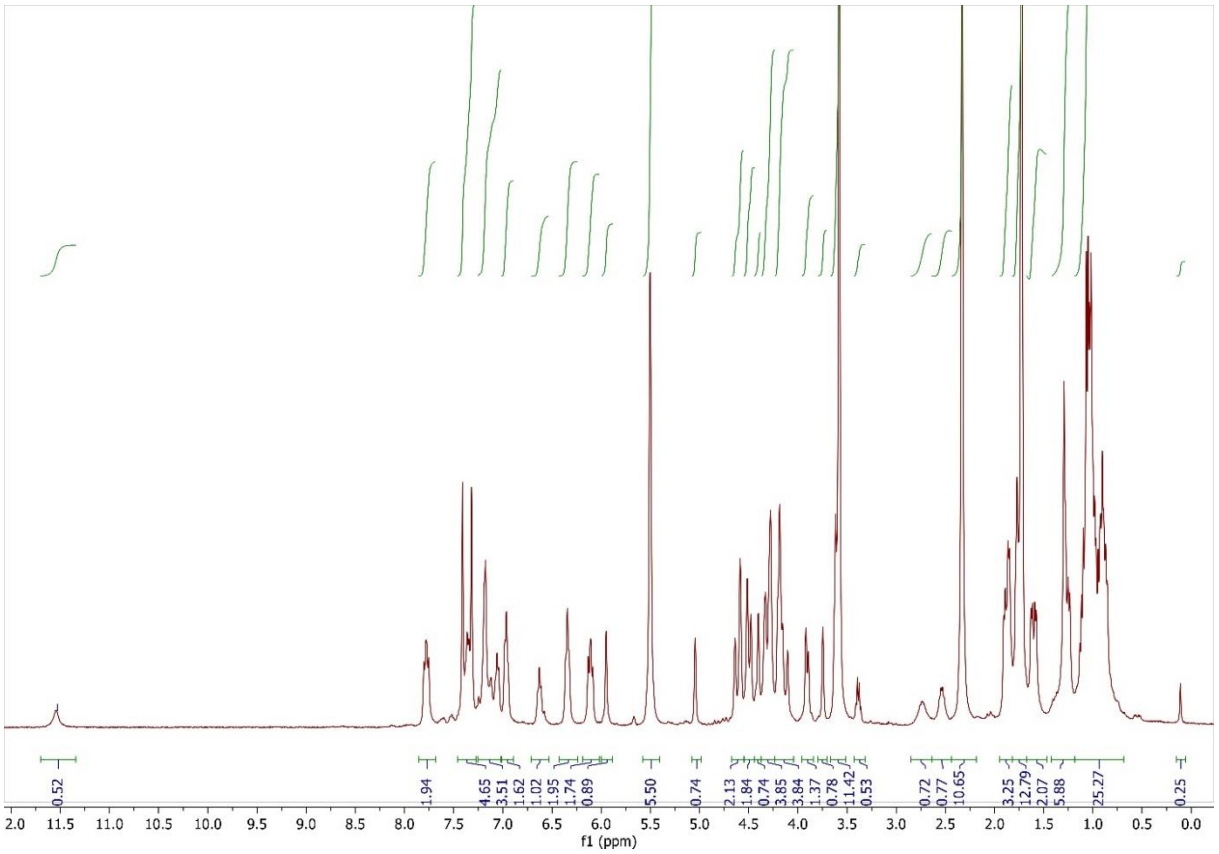

Figure 3. 80 Detailed view of ^{1}H NMR spectrum of **Pt-3.7** in d_6-acetone at 400 MHz

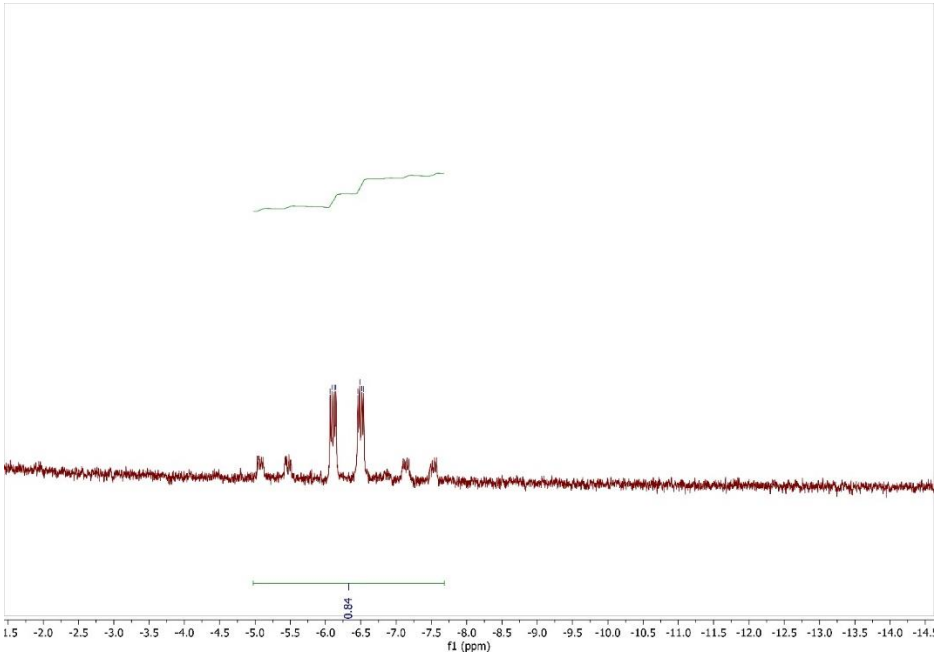

Figure 3. 81 Detailed view of ^{1}H NMR spectrum of **Pt-3.7** in d_6-acetone at 400 MHz

Synthesis of **Pt-3.10**

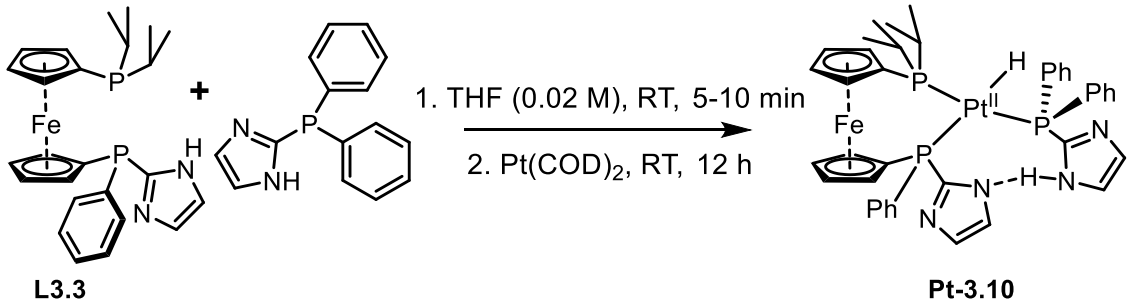

In a nitrogen filled glovebox, an oven dried scintillation vial was charged with **L3.3** (11.6 mg, 0.0243 mmol), diphenyl imidazolyl phosphine (6.1 mg, 0.0242), and THF (1.2 mL), and magnetic stir bar. The compound was stirred for 10 minutes. A separate oven dried scintillation vial was charged with $Pt(COD)_2$ (9.9 mg, 0.243 mmol). The THF solution of the phosphines was then added to the $Pt(COD)_2$ solution at room temperature and the mixture stirred for 14 hours. The volatiles were then removed under reduced pressure. A standout feature of the ^1H NMR spectrum is the resonance from 1,5-cyclooctadiene, δ 2.30 (s) and 5.49 (s). This indicates that COD is still present, but not coordinating to the Pt atom. Other key features of the ^1H NMR spectrum is the up-field signal at δ -6.35 (d, J = 157.8, $J_{Pt\text{-}H}$ = 819.1), and the down-field signal at δ17.42 (s, br). The far up-field signal is assigned to arise from a platinum-hydride. The far down-field signal is assigned to a strongly hydrogen bound proton that lies between the two imidazolyl nitrogen atoms.

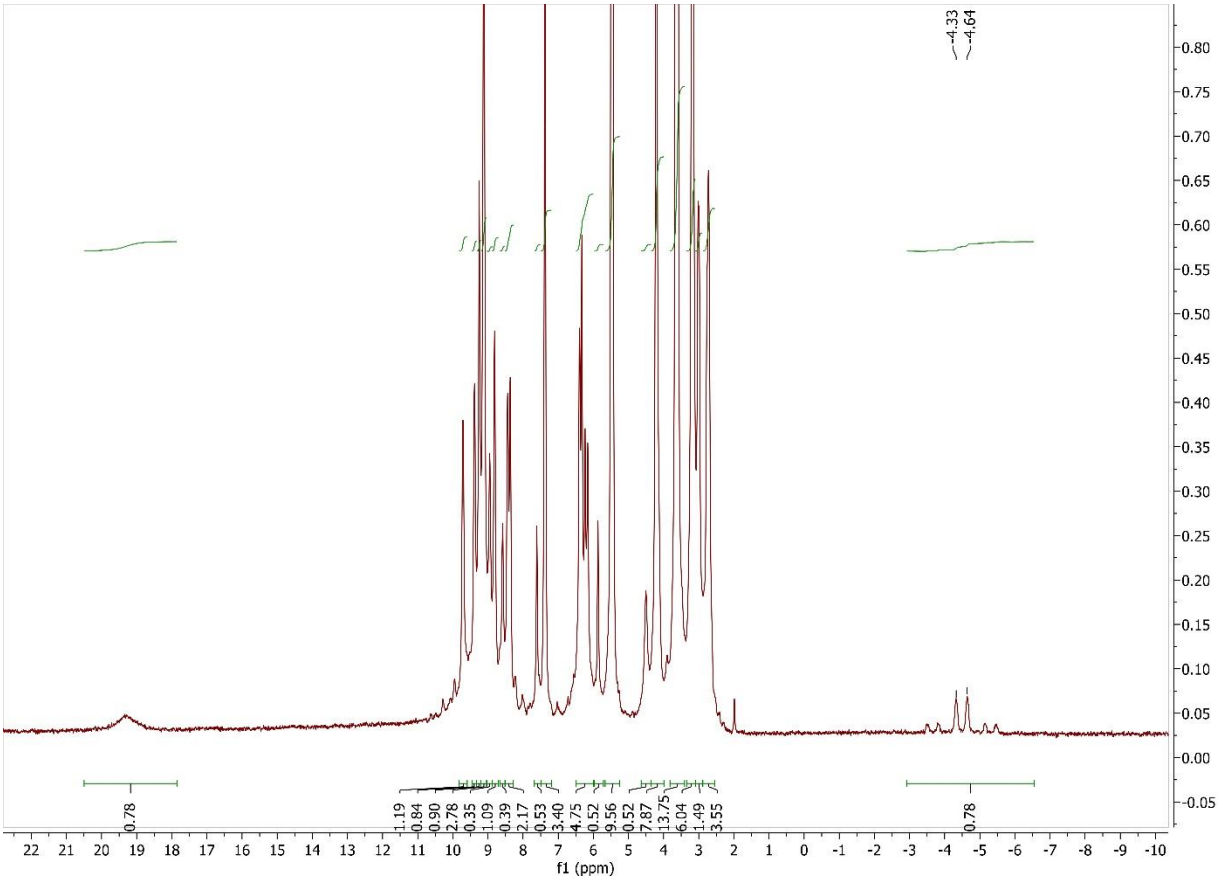

Figure 3. 82 ^{1}H NMR spectrum of **Pt-3.10** in d_8-THF at 500 MHz

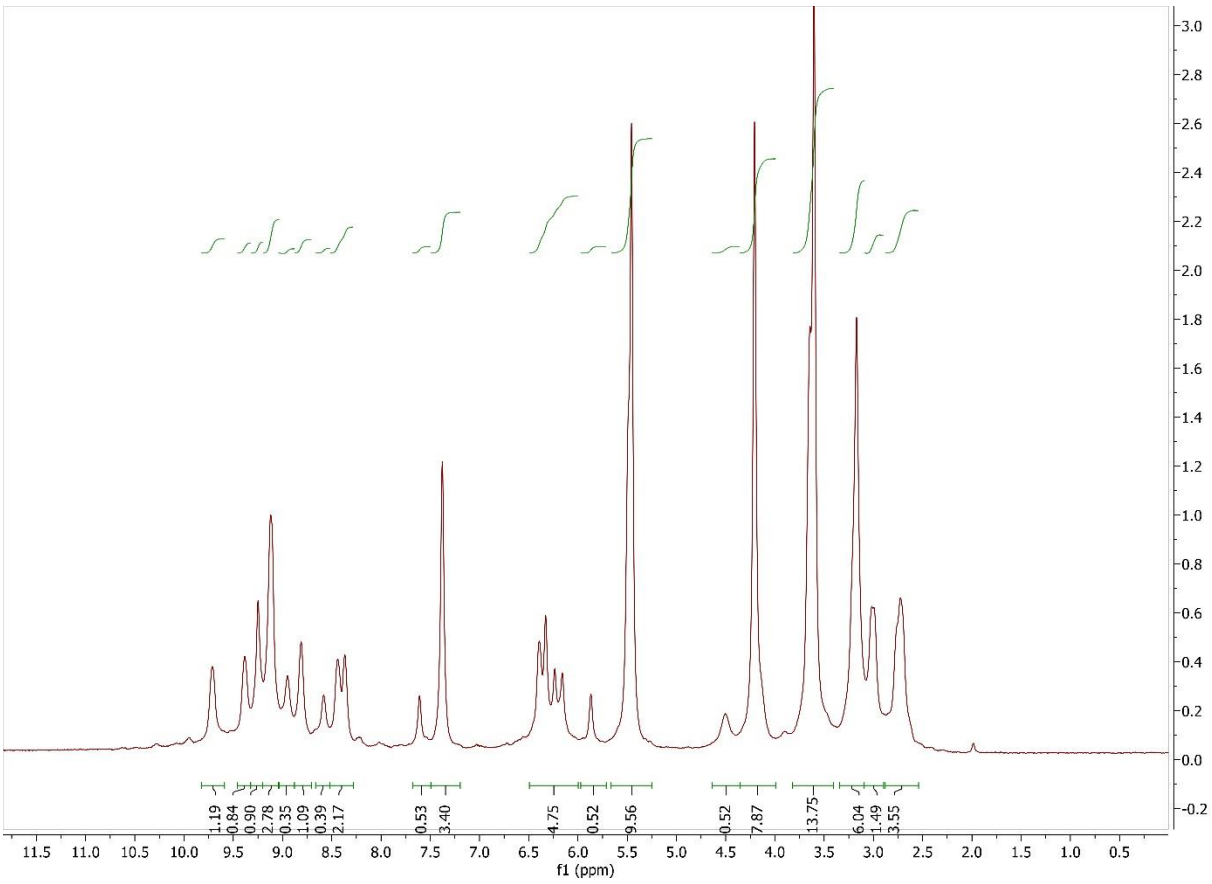

Figure 3. 83 Detailed view of ^{1}H NMR spectrum of **Pt-3.10** in d_8-THF at 500 MHz

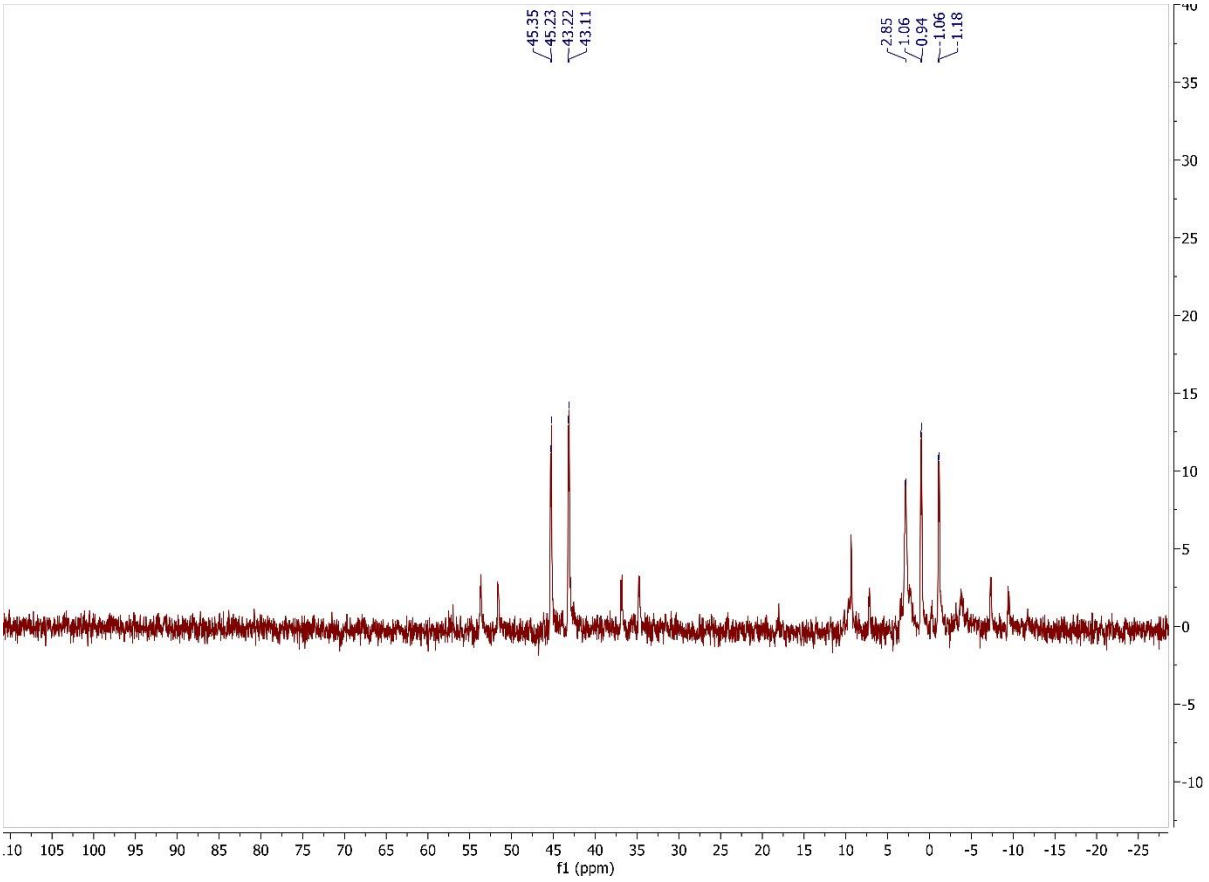

Figure 3. 84 ^{31}P NMR spectrum of **Pt-3.10** in d_8-THF at 162 MHz

Synthesis of **Pt-3.11**

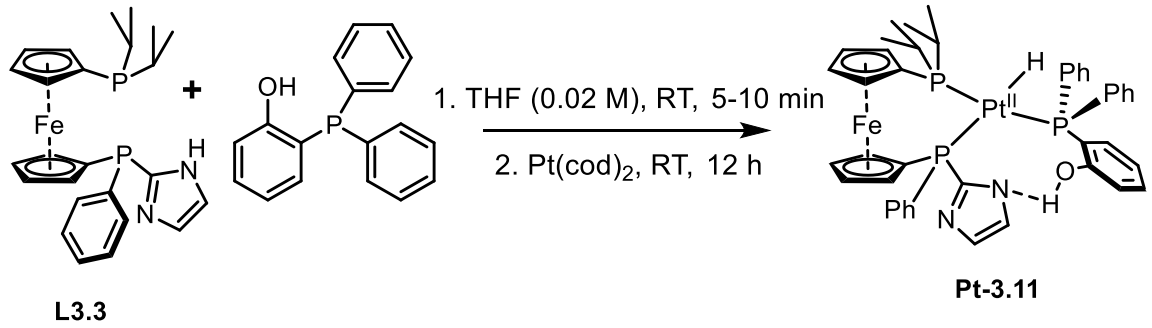

In a nitrogen filled glovebox, an oven dried flask was charged with L3.3 (11.7 mg, 0.0245 mmol), diphenylphosphinophenol (7.3 mg, 0.0262 mmol), d_8-THF (0.7 mL), and a magnetic stir bar. The mixture was stirred for 10 minutes. A separate oven dried flask was charged with $Pt(COD)_2$ (9.8 mg, 0.0238 mmol). The THF solution of the phosphines was then added to the flask

with the $Pt(COD)_2$. The mixture was stirred for 2 hours, then transferred to a J. Young NMR tube for observation. Key features of note from the ^1H NMR spectrum are the far up-field resonance at δ -6.34 (d, J = 159.6, J_{Pt-H} = 830.9) and the far down-field resonance at 17.19 (s, br). The up-field resonance is assigned as a platinum-hydride, and the down-field resonance is assigned as the phenolic proton tightly hydrogen bound between the phenol oxygen and the imidazolyl nitrogen.

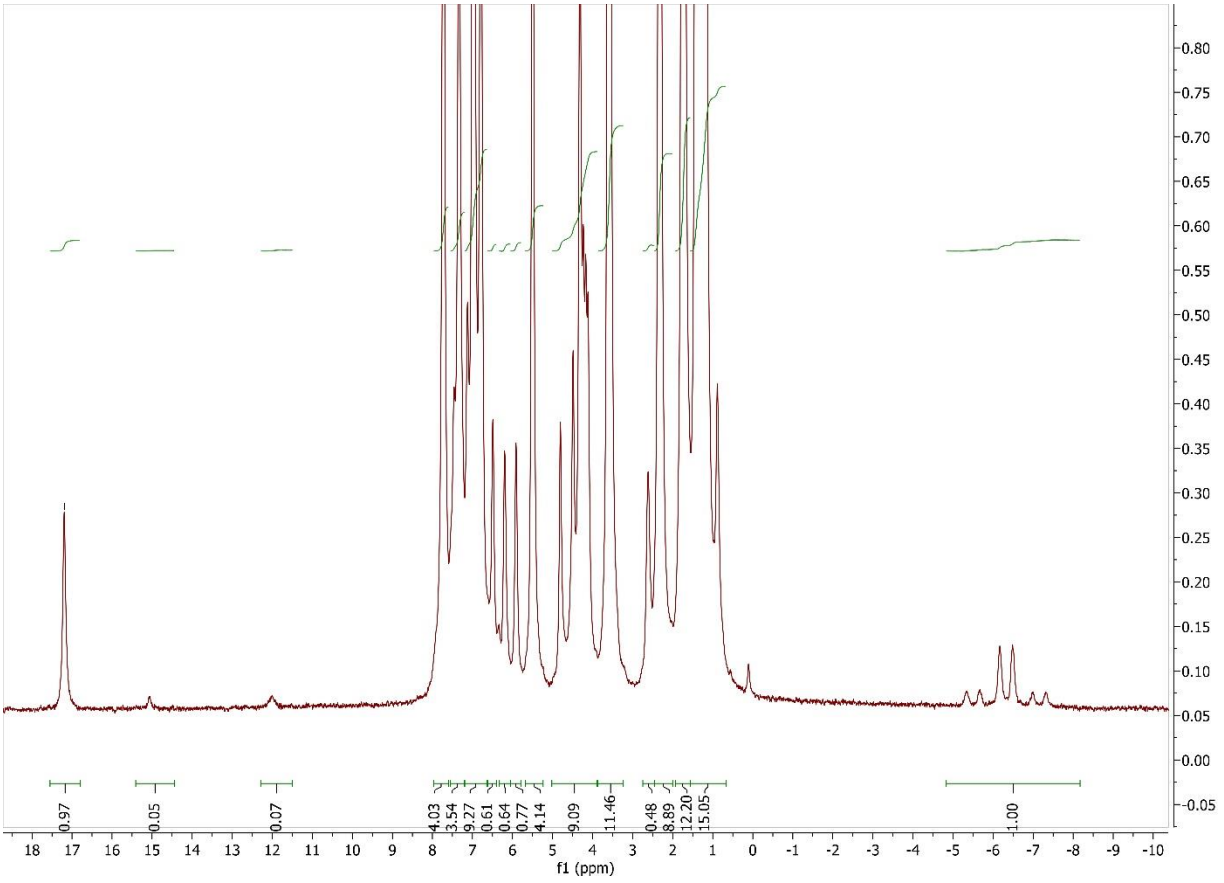

Figure 3. 85 ^1H NMR spectrum of **Pt-3.11** in d_8-THF at 500 MHz

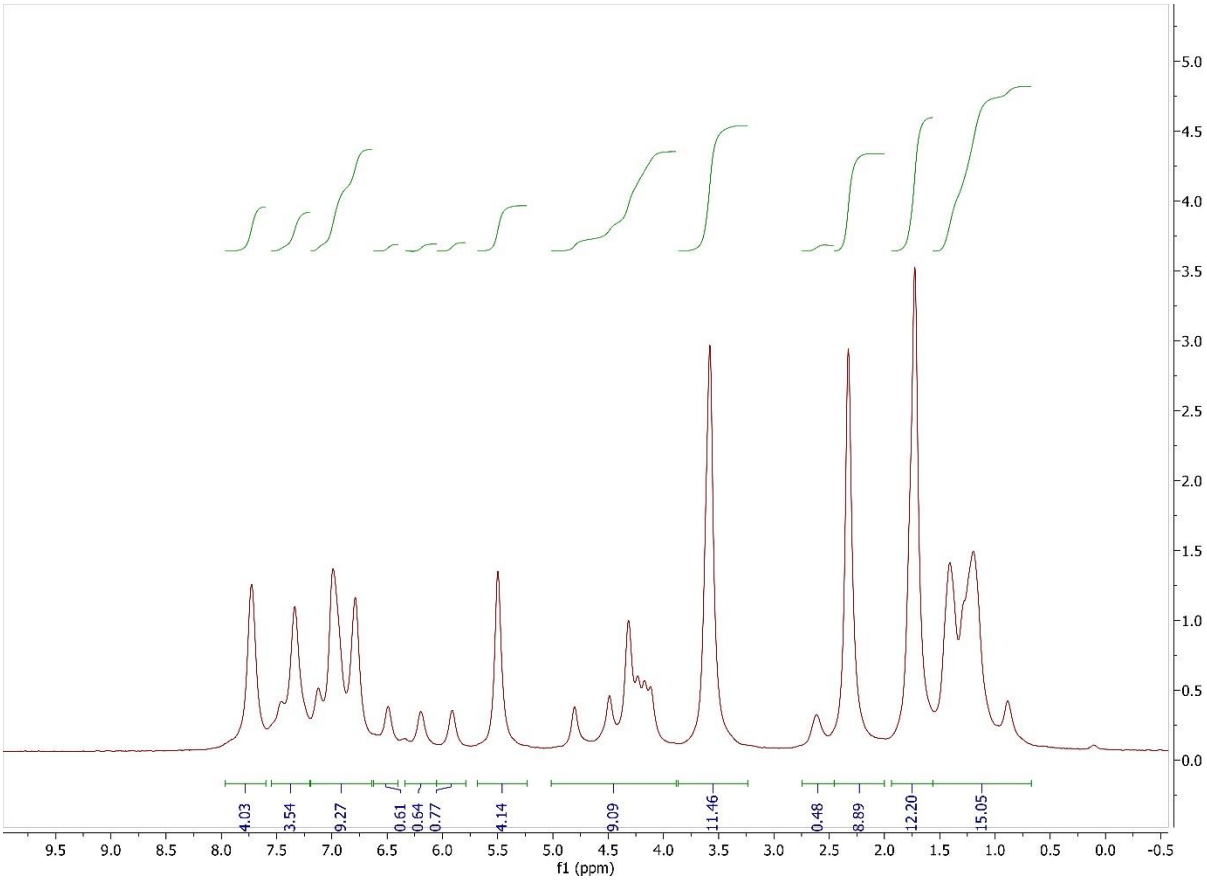

Figure 3. 86 ^{1}H NMR spectrum of **Pt-3.11** in d_8-THF at 500 MHz

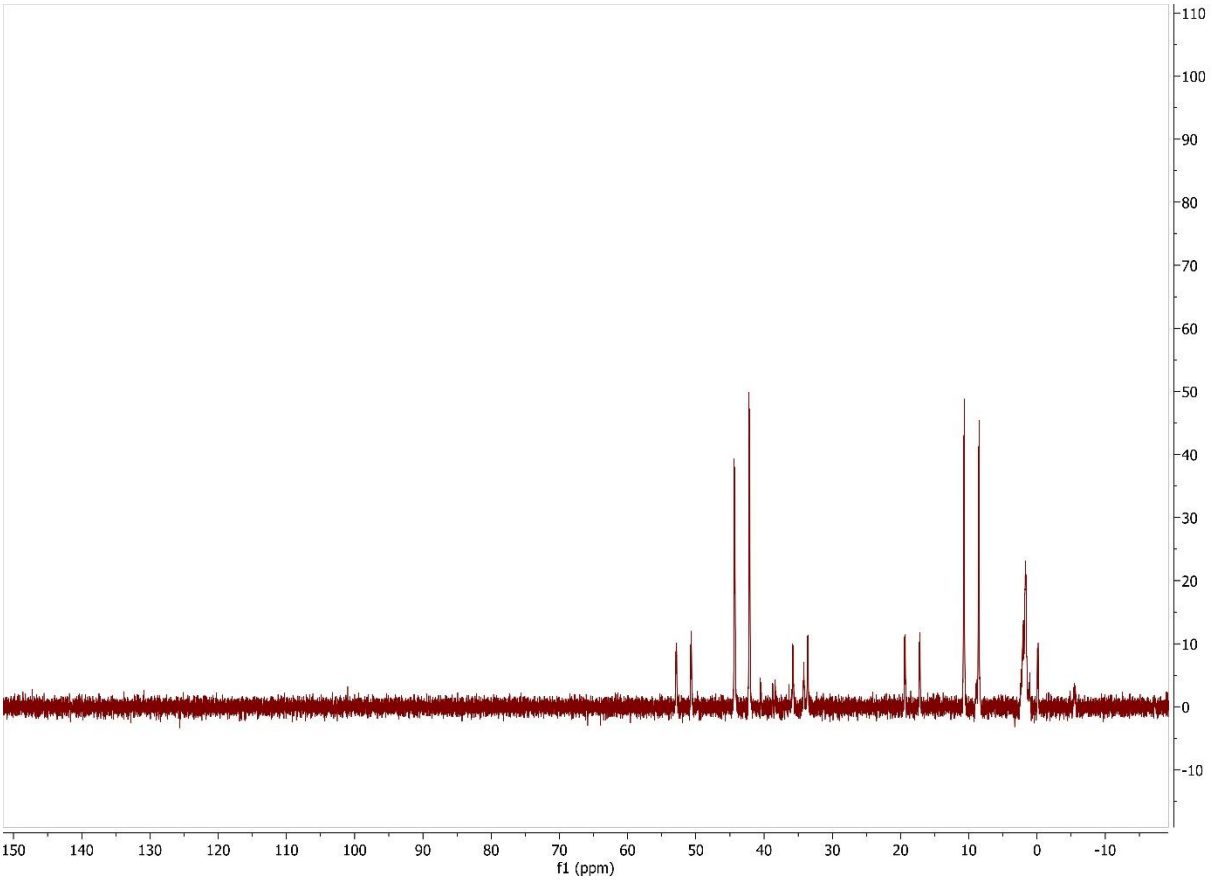

Figure 3. 87 ^{31}P NMR spectrum of **Pt-3.11** in d_8-THF at 162 MHz

Reaction of $Pt(COD)_2$ with **L3.3** and triphenylphosphine

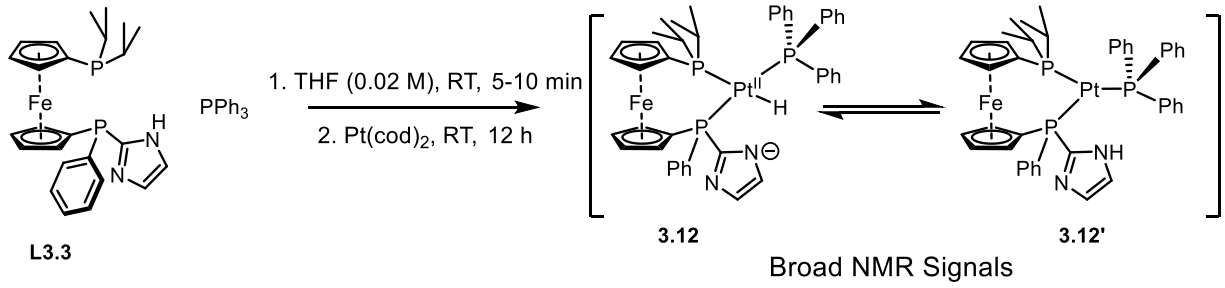

In a nitrogen filled glovebox, an oven dried flask was charged with **L3.3** (12.0 mg, 0.0252 mmol), triphenylphosphine (6.8 mg, 0.0259 mmol), THF (1.5 mL), and magnetic stir bar. The mixture was stirred for 5 minutes. Next $Pt(COD)_2$ (9.8 mg, 0.0238) was added. The mixture was stirred at room temperature for 20 hours. Attempts at crystallization were made by adding hexanes

and storing the mixture in a -40 °C freezer, no crystallization occurred. All volatiles were evaporated under reduced pressure. The solid residue was dissolved in d_8-THF and analyzed by NMR. Both the ^{1}H and ^{31}P NMR spectra had a significant amount of signal overlap, however there were some distinct signals visible. An up-field signal indicating hydride formation is visible at δ -6.33 (J = 155.5). The hydride signal is just distinguishable from the baseline noise, and the ^{195}Pt satellite signals are not readily apparent.

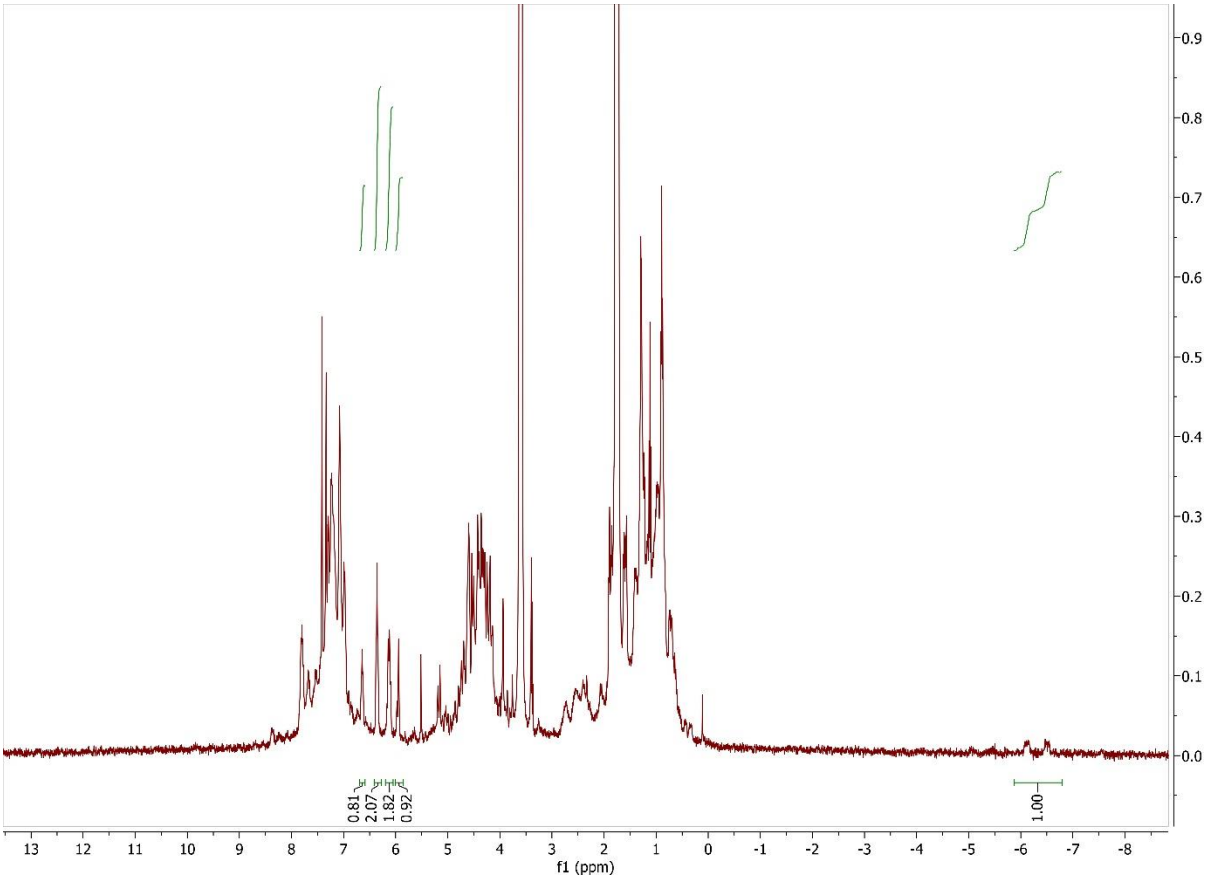

Figure 3. *88* ^{1}H NMR spectrum of **Pt-3.12** in d_8-THF at 400 MHz

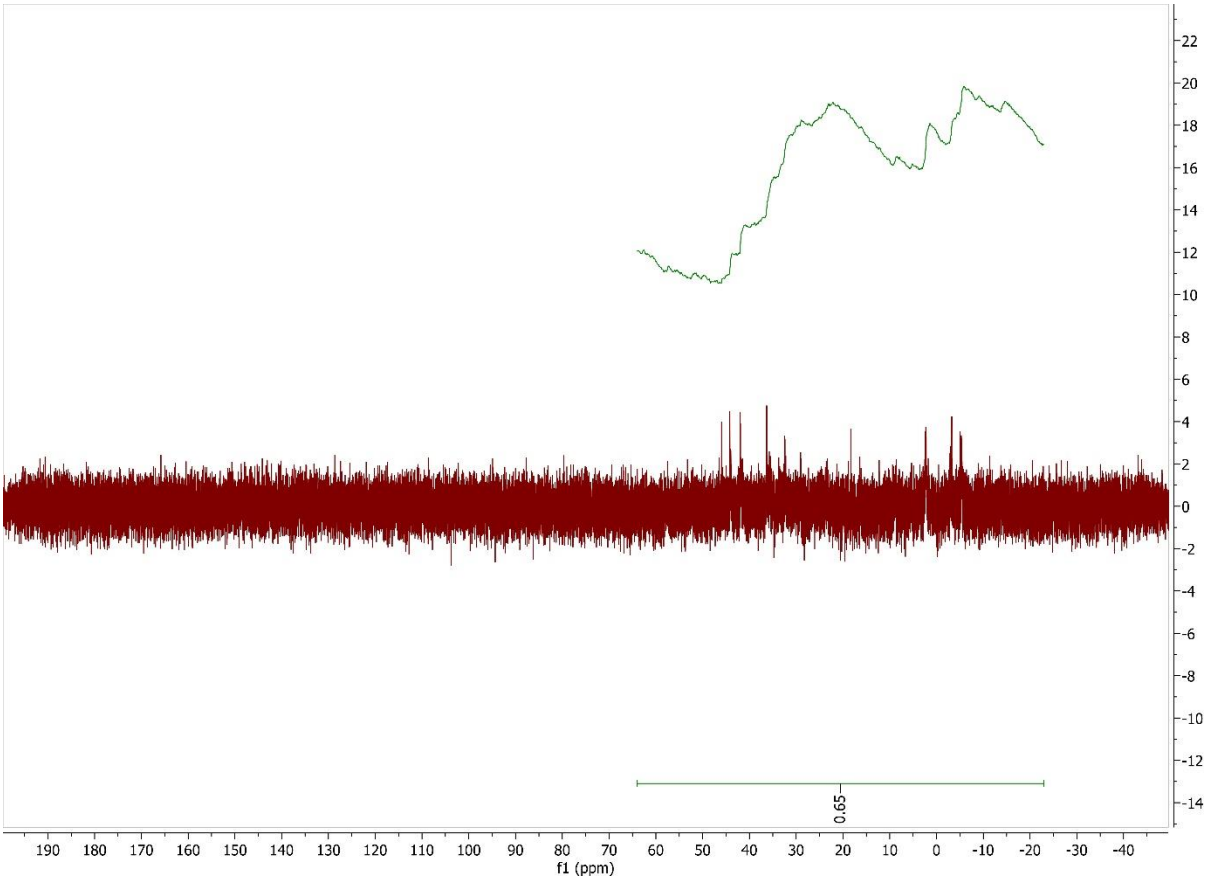

Figure 3. 89 ^{31}P NMR spectrum of **Pt-3.12** in d_8-THF at 162 MHz

ACKNOWLEDGEMENTS

Chapter 3 contains data currently being prepared for publication on the synthesis of hydrogen-bond-donor-functionalized ferrocenyl bisphosphines, and studies on the coordination chemistry of the novel bisphosphines with platinum and nickel. Development of the synthetic route to yielding the target compounds was necessary, and the major points of concern are discussed. The dissertation author was the sole investigator and author of this chapter.

References

(1) Armor, J. N. A History of Industrial Catalysis. *Catal. Today* **2011**. https://doi.org/10.1016/j.cattod.2009.11.019.

(2) Spence, M. *INTELLIGENCE REPORT: BUSINESS SHIFTS IN THE GLOBAL CATALYTIC PROCESS INDUSTRIES STUDY PRESENTATION The Seventeenth Biennial Edition*; 2013.

(3) Ertl, G. The nobel prize in chemistry 2001 https://www.nobelprize.org/prizes/chemistry/2001/summary/ (accessed Apr 7, 2020). https://doi.org/10.1142/9789814635660_0002.

(4) Ertl, G. The nobel prize in chemistry 2005 https://www.nobelprize.org/prizes/chemistry/2005/summary/ (accessed Apr 7, 2020). https://doi.org/10.1142/9789814635660_0002.

(5) The Nobel Prize in Chemistry 2010 https://www.nobelprize.org/nobel_prizes/chemistry/laureates/2010/ (accessed Jul 9, 2018).

(6) Anastas, P. T.; Warner, J. C. *Green Chemistry: Theory and Practice*; Oxford University Press, New York, 1998.

(7) Larsen, C. R.; Paulson, E. R.; Erdogan, G.; Grotjahn, D. B. A Facile, Convenient, and Green Route to (E)-Propenylbenzene Flavors and Fragrances by Alkene Isomerization. *Synlett* **2015**, *26* (17), 2462–2466. https://doi.org/10.1055/s-0035-1560205.

(8) W. Old, D.; P. Wolfe, J.; L. Buchwald, S. A Highly Active Catalyst for Palladium-Catalyzed Cross-Coupling Reactions: Room-Temperature Suzuki Couplings and Amination of Unactivated Aryl Chlorides. *J. Am. Chem. Soc.* **1998**, *120* (37), 9722–9723. https://doi.org/10.1021/ja982250+.

(9) Billingsley, K. L.; Anderson, K. W.; Buchwald, S. L. A Highly Active Catalyst for Suzuki-Miyaura Cross-Coupling Reactions of Heteroaryl Compounds. *Angew. Chemie - Int. Ed.* **2006**, *45* (21), 3484–3488. https://doi.org/10.1002/anie.200600493.

(10) Walker, S. D.; Barder, T. E.; Martinelli, J. R.; Buchwald, S. L. A Rationally Designed Universal Catalyst for Suzuki-Miyaura Coupling Processes. *Angew. Chemie - Int. Ed.* **2004**, *43* (14), 1871–1876. https://doi.org/10.1002/anie.200353615.

(11) Barder, T. E.; Walker, S. D.; Martinelli, J. R.; Buchwald, S. L. Catalysts for Suzuki-Miyaura Coupling Processes: Scope and Studies of the Effect of Ligand Structure. *J. Am. Chem. Soc.* **2005**, *127* (13), 4685–4696. https://doi.org/10.1021/ja042491j.

(12) Wolfe, J. P.; Singer, R. A.; Yang, B. H.; Buchwald, S. L. Highly Active Palladium Catalysts for Suzuki Coupling Reactions. *J. Am. Chem. Soc.* **1999**, *121* (41), 9550–9561. https://doi.org/10.1021/ja992130h.

(13) Yin, J.; Rainka, M. P.; Zhang, X. X.; Buchwald, S. L. A Highly Active Suzuki Catalyst for the Synthesis of Sterically Hindered Biaryls: Novel Ligand Coordination. *J. Am. Chem. Soc.* **2002**, *124* (7), 1162–1163. https://doi.org/10.1021/ja017082r.

(14) Billingsley, K.; Buchwald, S. L. Highly Efficient Monophosphine-Based Catalyst for the Palladium-Catalyzed Suzuki-Miyaura Reaction of Heteroaryl Halides and Heteroaryl Boronic Acids and Esters. *J. Am. Chem. Soc.* **2007**, *129* (11), 3358–3366. https://doi.org/10.1021/ja068577p.

(15) Okano, K.; Tokuyama, H.; Fukuyama, T. Total Synthesis of (+)-Yatakemycin. *J. Am. Chem. Soc.* **2006**, *128* (22), 7136–7137. https://doi.org/10.1021/ja0619455.

(16) Ebran, J. P.; Hansen, A. L.; Gøgsig, T. M.; Skrydstrup, T. Studies on the Heck Reaction with Alkenyl Phosphates: Can the 1,2-Migration Be Controlled? Scope and Limitations. *J. Am. Chem. Soc.* **2007**, *129* (21), 6931–6942. https://doi.org/10.1021/ja070321b.

(17) Cameron, M.; Foster, B. S.; Lynch, J. E.; Shi, Y. J.; Dolling, U. H. The Expedient Synthesis of 4,2′-Difluoro-5′-(7- Trifluoromethylimidazo[1,2-a]Pyrimidin-3-Yl)Biphenyl-2-Carbonitrile, a GABA A2/3 Agonist. *Org. Process Res. Dev.* **2006**, *10* (3), 398–402. https://doi.org/10.1021/op050217j.

(18) Gelman, D.; Buchwald, S. L. Efficient Palladium-Catalyzed Coupling of Aryl Chlorides and Tosylates with Terminal Alkynes: Use of a Copper Cocatalyst Inhibits the Reaction. *Angew. Chemie - Int. Ed.* **2003**, *42* (48), 5993–5996. https://doi.org/10.1002/anie.200353015.

(19) Milne, J. E.; Buchwald, S. L. An Extremely Active Catalyst for the Negishi Cross-Coupling Reaction. *J. Am. Chem. Soc.* **2004**, *126* (40), 13028–13032. https://doi.org/10.1021/ja0474493.

(20) Denmark, S. E.; Ober, M. H. Palladium-Catalyzed Cross-Coupling Reactions of Substituted Aryl(Dimethyl)Silanols. *Adv. Synth. Catal.* **2004**, *346* (13–15), 1703–1714. https://doi.org/10.1002/adsc.200404204.

(21) Denmark, S. E.; Butler, C. R. Vinylation of Aryl Bromides Using an Inexpensive Vinylpolysiloxane. *Org. Lett.* **2006**, *8* (1), 63–66. https://doi.org/10.1021/ol052517r.

(22) Mowery, M. E.; DeShong, P. Improvements in Cross Coupling Reactions of Hypervalent Siloxane Derivatives. *Org. Lett.* **1999**, *1* (13), 2137–2140. https://doi.org/10.1021/ol991186d.

(23) Nguyen, H. N.; Huang, X.; Buchwald, S. L. The First General Palladium Catalyst for the Suzuki-Miyaura and Carbonyl Enolate Coupling of Aryl Arenesulfonates. *J. Am. Chem. Soc.* **2003**, *125* (39), 11818–11819. https://doi.org/10.1021/ja036947t.

(24) Fox, J. M.; Huang, X.; Chieffi, A.; Buchwald, S. L. Highly Active and Selective Catalysts for the Formation of α-Aryl Ketones. *J. Am. Chem. Soc.* **2000**, *122* (7), 1360–1370. https://doi.org/10.1021/ja993912d.

(25) Vogl, E. M.; Buchwald, S. L. Palladium-Catalyzed Monoarylation of Nitroalkanes. *J. Org. Chem.* **2002**, *67* (1), 106–111. https://doi.org/10.1021/jo010953v.

(26) Martín, R.; Buchwald, S. L. A General Method for the Direct α-Arylation of Aldehydes with Aryl Bromides and Chlorides. *Angew. Chemie - Int. Ed.* **2007**, *46* (38), 7236–7239. https://doi.org/10.1002/anie.200703009.

(27) Lawrence Gray, B.; Schreiber, S. L. Skeletal Diversity in Small-Molecule Synthesis Using Ligand-Controlled Catalysis. *J. Comb. Chem.* **2007**, *9* (6), 1028–1035. https://doi.org/10.1021/cc7001028.

(28) Cooper, T.; Novak, A.; Humphreys, L. D.; Walker, M. D.; Woodward, S. User-Friendly Methylation of Aryl and Vinyl Halides and Pseudohalides with DABAL-Me3. *Adv. Synth. Catal.* **2006**, *348* (6), 686–690. https://doi.org/10.1002/adsc.200505405.

(29) Surry, D. S.; Buchwald, S. L. Biaryl Phosphane Ligands in Palladium-Catalyzed Amination. *Angew. Chemie - Int. Ed.* **2008**, *47* (34), 6338–6361. https://doi.org/10.1002/anie.200800497.

(30) Wolfe, J. P.; Tomori, H.; Sadighi, J. P.; Yin, J.; Buchwald, S. L. Simple, Efficient Catalyst System for the Palladium-Catalyzed Amination of Aryl Chlorides, Bromides, and Triflates. *J. Org. Chem.* **2000**, *65* (4), 1158–1174. https://doi.org/10.1021/jo991699y.

(31) Strieter, E. R.; Blackmond, D. G.; Buchwald, S. L. Insights into the Origin of High Activity and Stability of Catalysts Derived from Bulky, Electron-Rich Monophosphinobiaryl Ligands in the Pd-Catalyzed C-N Bond Formation. *J. Am. Chem. Soc.* **2003**, *125* (46), 13978–13980. https://doi.org/10.1021/ja037932y.

(32) Dhondi, P. K.; Chisholm, J. D. Rhodium-Catalyzed Addition of Alkynes to Activated Ketones and Aldehydes. *Org. Lett.* **2006**, *8* (1), 67–69. https://doi.org/10.1021/ol0525260.

(33) Dhondi, P. K.; Carberry, P.; Choi, L. B.; Chisholm, J. D. Addition of Alkynes to Aldehydes and Activated Ketones Catalyzed by Rhodium-Phosphine Complexes. *J. Org. Chem.* **2007**, *72* (25), 9590–9596. https://doi.org/10.1021/jo701643h.

(34) Movassaghi, M.; Hill, M. D. Single-Step Synthesis of Pyrimidine Derivatives. *J. Am. Chem. Soc.* **2006**, *128* (44), 14254–14255. https://doi.org/10.1021/ja066405m.

(35) Faller, J. W.; D'Alliessi, D. G. Planar Chirality in Tethered H6:H1-(Phosphinophenylenearene-P)Ruthenium(II) Complexes and Their Potential Use as Asymmetric Catalysts. *Organometallics* **2003**, *22* (13), 2749–2757. https://doi.org/10.1021/om030080q.

(36) Faller, J. W.; Fontaine, P. P. Resolution and Diels - Alder Catalysis with Planar Chiral Arene-Tethered Ruthenium Complexes. *Organometallics* **2005**, *24* (17), 4132–4138. https://doi.org/10.1021/om0501226.

(37) Haider, J.; Kunz, K.; Scholz, U. Highly Selective Copper-Catalyzed Monoarylation of

Aniline. *Adv. Synth. Catal.* **2004**, *346* (7), 717–722. https://doi.org/10.1002/adsc.200404011.

(38) Porcel, S.; Echavarren, A. M. Intramolecular Carbostannylation of Alkynes Catalyzed by Silver(I) Species. *Angew. Chemie Int. Ed.* **2007**, *46* (15), 2672–2676. https://doi.org/10.1002/anie.200605041.

(39) Cabello, N.; Rodríguez, C.; Echavarren, A. M. Gold-Catalyzed Cyclizations of 1,7-Enynes. *Synlett* **2007**, No. 11, 1753–1758. https://doi.org/10.1055/s-2007-984502.

(40) Nieto-Oberhuber, C.; López, S.; Echavarren, A. M. Intramolecular [4 + 2] Cycloadditions of 1,3-Enynes or Arylalkynes with Alkenes with Highly Reactive Cationic Phosphine Au(I) Complexes. *J. Am. Chem. Soc.* **2005**, *127* (17), 6178–6179. https://doi.org/10.1021/ja042257t.

(41) Nieto-Oberhuber, C.; López, S.; Muñoz, M. P.; Jiménez-Núñez, E.; Buñuel, E.; Cárdenas, D. J.; Echavarren, A. M. Gold(I)-Catalyzed Intramolecular Cyclopropanation of Dienynes. *Chem. - A Eur. J.* **2006**, *12* (6), 1694–1702. https://doi.org/10.1002/chem.200501089.

(42) Ferrer, C.; Amijs, C. H. M.; Echavarren, A. M. Intra- and Intermolecular Reactions of Indoles with Alkynes Catalyzed by Gold. *Chem. - A Eur. J.* **2007**, *13* (5), 1358–1373. https://doi.org/10.1002/chem.200601324.

(43) Jiménez-Núñez, E.; Claverie, C. K.; Nieto-Oberhuber, C.; Echavarren, A. M. Prins Cyclizations in Au-Catalyzed Reactions of Enynes. *Angew. Chemie Int. Ed.* **2006**, *45* (33), 5452–5455. https://doi.org/10.1002/anie.200601575.

(44) Herrero-Gómez, E.; Nieto-Oberhuber, C.; López, S.; Benet-Buchholz, J.; Echavarren, A. M. Cationic H1/H2-Gold(I) Complexes of Simple Arenes. *Angew. Chemie Int. Ed.* **2006**, *45* (33), 5455–5459. https://doi.org/10.1002/anie.200601688.

(45) Herrero-Gómez, E.; Nieto-Oberhuber, C.; López, S.; Benet-Buchholz, J.; Echavarren, A. M. Cationic H1/H2-Gold(I) Complexes of Simple Arenes. *Angew. Chemie - Int. Ed.* **2006**, *45* (33), 5455–5459. https://doi.org/10.1002/anie.200601688.

(46) Partyka, D. V.; Zeller, M.; Hunter, A. D.; Gray, T. G. Relativistic Functional Groups: Aryl Carbon-Gold Bond Formation by Selective Transmetalation of Boronic Acids. *Angew. Chemie - Int. Ed.* **2006**, *45* (48), 8188–8191. https://doi.org/10.1002/anie.200603350.

(47) Jiménez-Núñez, E.; Claverie, C. K.; Nieto-Oberhuber, C.; Echavarren, A. M. Prins Cyclizations in Au-Catalyzed Reactions of Enynes. *Angew. Chemie - Int. Ed.* **2006**, *45* (33), 5452–5455. https://doi.org/10.1002/anie.200601575.

(48) Ferrer, C.; Echavarren, A. M. Gold-Catalyzed Intramolecular Reaction of Indoles with Alkynes: Facile Formation of Eight-Membered Rings and an Unexpected Allenylation. *Angew. Chemie - Int. Ed.* **2006**, *45* (7), 1105–1109. https://doi.org/10.1002/anie.200503484.

(49) Paulson, E. R.; Moore, C. E.; Rheingold, A. L.; Pullman, D. P.; Sindewald, R. W.; Cooksy,

A. L.; Grotjahn, D. B. Dynamic Ï-Bonding of Imidazolyl Substituent in a Formally 16-Electron Cp Ru(2-P, N)+ Catalyst Allows Dramatic Rate Increases in (E)-Selective Monoisomerization of Alkenes. *ACS Catal.* **2019**, *9* (8), 7217–7231. https://doi.org/10.1021/acscatal.8b04345.

(50) Cao, T. C.; Cooksy, A. L.; Grotjahn, D. B. Origins of High Kinetic (E)-selectivity in Alkene Isomerization by a CPRu(PN) Catalyst: A Combined Experimental and Computational Approach. *ACS Catal.* **2020**, *10* (24), 15250–15258. https://doi.org/10.1021/acscatal.0c03497.

(51) Grotjahn, D. B.; Lev, D. A. A General Bifunctional Catalyst for the Anti-Markovnikov Hydration of Terminal Alkynes to Aldehydes Gives Enzyme-Like Rate and Selectivity Enhancements. *J. Am. Chem. Soc.* **2004**, *126*, 12232–12233.

(52) Nair, R. N. Development of Bifunctional Phosphines, Metal Complexes and Catalysts for Various Organic Transformations, University of California, San Diego; San Diego State University, 2011.

(53) Erdogan, G. Metal Complexes with Bifunctional Imidazolyl Phosphines for Catalytic Organic Transformations: Applications in Homogeneous and Polymer Supported Alkene Isomerization , and Hydrogen Deuterium Exchange, University of California, San Diego; San Diego State University, 2012.

(54) Wang, Y.; Wang, Z.; Li, Y.; Wu, G.; Cao, Z.; Zhang, L. A General Ligand Design for Gold Catalysis Allowing Ligand-Directed Anti-Nucleophilic Attack of Alkynes. *Nat. Commun.* **2014**, *5*, 3470. https://doi.org/10.1038/ncomms4470.

(55) Wang, Z.; Wang, Y.; Zhang, L. Soft Propargylic Deprotonation: Designed Ligand Enables Au-Catalyzed Isomerization of Alkynes to 1,3-Dienes. *J. Am. Chem. Soc.* **2014**, *136* (25), 8887–8890. https://doi.org/10.1021/ja503909c.

(56) Li, T.; Zhang, L. Bifunctional Biphenyl-2-Ylphosphine Ligand Enables Tandem Gold-Catalyzed Propargylation of Aldehyde and Unexpected Cycloisomerization. *J. Am. Chem. Soc.* **2018**, *140* (50), 17439–17443. https://doi.org/10.1021/jacs.8b12478.

(57) Wang, Z.; Ying, A.; Fan, Z.; Hervieu, C.; Zhang, L. Tertiary Amino Group in Cationic Gold Catalyst: Tethered Frustrated Lewis Pairs That Enable Ligand-Controlled Regiodivergent and Stereoselective Isomerizations of Propargylic Esters. *ACS Catal.* **2017**, *7* (5), 3676–3680. https://doi.org/10.1021/acscatal.7b00626.

(58) Liao, S.; Porta, A.; Cheng, X.; Ma, X.; Zanoni, G.; Zhang, L. Bifunctional Ligand Enables Efficient Gold-Catalyzed Hydroalkenylation of Propargylic Alcohol. *Angew. Chemie Int. Ed.* **2018**, *57* (27), 8250–8254. https://doi.org/10.1002/anie.201802533.

(59) Molander, G. A.; Trice, S. L. J.; Kennedy, S. M. Scope of the Two-Step, One-Pot Palladium-Catalyzed Borylation/Suzuki Cross-Coupling Reaction Utilizing Bis-Boronic Acid. *J. Org. Chem.* **2012**, *77* (19), 8678–8688. https://doi.org/10.1021/jo301642v.

(60) Wang, Z.; Wang, Y.; Zhang, L. Soft Propargylic Deprotonation: Designed Ligand Enables Au-Catalyzed Isomerization of Alkynes to 1,3-Dienes. *J. Am. Chem. Soc.* **2014**, *136* (25), 8887–8890. https://doi.org/10.1021/ja503909c.

(61) Gooßen, L. J.; Huang, L.; Arndt, M.; Gooßen, K.; Heydt, H. Late Transition Metal-Catalyzed Hydroamination and Hydroamidation. *Chem. Rev.* **2015**, *115* (7), 2596–2697. https://doi.org/10.1021/cr300389u.

(62) *CRC Handbook of Chemistry and Physics, 97th Edition*, 97th ed.; Haynes, W. M., Ed.; CRC Press, 2016. https://doi.org/https://doi.org/10.1201/9781315380476.

(63) Grotjahn, D. B.; Gong, Y.; DiPasquale, A. G.; Zakharov, L. N.; Rheingold, A. L. Bifunctional Imidazolylphosphine Ligands as Hydrogen Bond Donors Promote N-H and O-H Activation on Platinum. *Organometallics* **2006**, *25* (24), 5693–5695. https://doi.org/10.1021/om060880b.

(64) Grotjahn, D. B.; Kraus, J. E.; Amouri, H.; Rager, M. N.; Cooksy, A. L.; Arita, A. J.; Cortes-Llamas, S. A.; Mallari, A. A.; Dipasquale, A. G.; Moore, C. E.; Liable-Sands, L. M.; Golen, J. D.; Zakharov, L. N.; Rheingold, A. L. Multimodal Study of Secondary Interactions in Cp*Ir Complexes of Imidazolylphosphines Bearing an NH Group. *J. Am. Chem. Soc.* **2010**, *132* (23), 7919–7934. https://doi.org/10.1021/ja906712g.

(65) Mann, G.; Baranano, D.; Hartwig, J. F.; Rheingold, A. L.; Guzei, I. A. Carbon-Sulfur Bond-Forming Reductive Elimination Involving Sp-, Sp2-, and Sp3-Hybridized Carbon. Mechanism, Steric Effects, and Electronic Effects on Sulfide Formation. *J. Am. Chem. Soc.* **1998**, *120* (36), 9205–9219. https://doi.org/10.1021/ja981428p.

(66) Mann, G.; Shelby, Q.; Roy, A. H.; Hartwig, J. F. Electronic and Steric Effects on the Reductive Elimination of Diaryl Ethers from Palladium(II). *Organometallics* **2003**, *22* (13), 2775–2789. https://doi.org/10.1021/om030230x.

(67) Mann, G.; Baranano, D.; Hartwig, J. F.; Rheingold, A. L.; Guzei, I. A. Carbon-Sulfur Bond-Forming Reductive Elimination Involving Sp-, Sp2-, and Sp3-Hybridized Carbon. Mechanism, Steric Effects, and Electronic Effects on Sulfide Formation. *J. Am. Chem. Soc.* **1998**, *120* (36), 9205–9219. https://doi.org/10.1021/JA981428P/SUPPL_FILE/JA981428P_SA.PDF.

(68) Abis, L.; Sen, A.; Halpern, J. Intramolecular Reductive Elimination of Alkanes from Cis-Hydridoalkylbis(Phosphine)Platinum(II) Complexes. *J. Am. Chem. Soc.* **2002**, *100* (9), 2915–2916. https://doi.org/10.1021/JA00477A069.

(69) Grushin, V. V.; Marshall, W. J. Facile Ar-CF3 Bond Formation at Pd. Strikingly Different Outcomes of Reductive Elimination from [(Ph3P)2Pd(CF 3)Ph] and [(Xantphos)Pd(CF3)Ph]. *J. Am. Chem. Soc.* **2006**, *128* (39), 12644–12645. https://doi.org/10.1021/JA064935C/SUPPL_FILE/JA064935CSI20060816_070040.PDF.

(70) Fujita, K. I.; Yamashita, M.; Puschmann, F.; Alvarez-Falcon, M. M.; Incarvito, C. D.; Hartwig, J. F. Organometallic Chemistry of Amidate Complexes. Accelerating Effect of

Bidentate Ligands on the Reductive Elimination of N-Aryl Amidates from Palladium(II). *J. Am. Chem. Soc.* **2006**, *128* (28), 9044–9045. https://doi.org/10.1021/ja062333n.

(71) Guari, Y.; Van Strijdonck, G. P. F.; Boele, M. D. K.; Reek, J. N. H.; Kamer, P. C. J.; Van Leeuwen, P. W. N. M. Palladium-Catalyzed Amination of Aryl Bromides and Aryl Triflates Using Diphosphane Ligands: A Kinetic Study. https://doi.org/10.1002/1521-3765(20010119)7:2.

(72) Peacock, D. M.; Jiang, Q.; Cundari, T. R.; Hartwig, J. F. Reductive Elimination to Form C(Sp3)-N Bonds from Palladium(II) Primary Alkyl Complexes. *Organometallics* **2018**, *37* (19), 3243–3247. https://doi.org/10.1021/acs.organomet.8b00617.

(73) Matsunaga, T.; Hillhouse, G. L. Of-1.0. *J. Am. Chem. Soc.* **1993**, *115* (2), 2075–2077.

(74) Koo, K.; Hillhouse, G. L.; Rheingold, A. L. Oxygen-Atom Transfer from Nitrous Oxide to an Organonickel(II) Phosphine Complex. Syntheses and Reactions of New Nickel(II) Aryloxides and the Crystal Structure of (Me2PCH2CH2PMe2)Ni(O-o-C6H4CMe2CH2). *Organometallics* **1995**, *14* (1), 456–460. https://doi.org/10.1021/om00001a062.

(75) Han, R.; Hillhouse, G. L. Carbon-Oxygen Reductive-Elimination from Nickel(II) Oxametallacycles and Factors That Control Formation of Ether, Aldehyde, Alcohol, or Ester Products. *J. Am. Chem. Soc.* **1997**, *119* (34), 8135–8136. https://doi.org/10.1021/ja9714999.

(76) Hartwig, J. F. Electronic Effects on Reductive Elimination to Form Carbon-Carbon and Carbon-Heteroatom Bonds from Palladium(Ll) Complexes. *Inorg. Chem.* **2007**, *46* (6), 1936–1947. https://doi.org/10.1021/ic061926w.

(77) Frech, C. M.; Milstein, D. Direct Observation of Reductive Elimination of Methyl Iodide from a Rhodium(III) Pincer Complex: The Importance of Sterics. *J. Am. Chem. Soc.* **2006**, *128* (38), 12434–12435. https://doi.org/10.1021/ja064945d.

(78) Roy, A. H.; Hartwig, J. F. Reductive Elimination of Aryl Halides upon Addition of Hindered Alkylphosphines to Dimeric Arylpalladium(II) Halide Complexes. *Organometallics* **2004**, *23* (7), 1533–1541. https://doi.org/10.1021/om034277u.

(79) Terrett, J. A.; Cuthbertson, J. D.; Shurtleff, V. W.; MacMillan, D. W. C. Switching on Elusive Organometallic Mechanisms with Photoredox Catalysis. *Nature* **2015**, *524* (7565), 330–334. https://doi.org/10.1038/nature14875.

(80) Yamashita, M.; Cuevas Vicario, J. V.; Hartwig, J. F. Trans Influence on the Rate of Reductive Elimination. Reductive Elimination of Amines from Isomeric Arylpalladium Amides with Unsymmetrical Coordination Spheres. *J. Am. Chem. Soc.* **2003**, *125* (52), 16347–16360. https://doi.org/10.1021/ja037425g.

(81) Hitzel, S.; Färber, C.; Bruhn, C.; Siemeling, U. Phosphido Complexes Derived from 1,1′-Ferrocenediyl-Bridged Secondary Diphosphines. *Dalt. Trans.* **2017**, *46* (19), 6333–6348. https://doi.org/10.1039/c7dt00941k.

(82) Shafir, A.; Power, M. P.; Whitener, G. D.; Arnold, J.; Miller, P. W.; Long, N. J. 1,1′-Diaminoferrocene. *Inorg. Synth.* **2014**, *36*, 65–72.

(83) Lin, B.; Liu, L.; Fu, Y.; Luo, S.; Chen, Q.; Guo, Q. Comparing Nickel- and Palladium-Catalyzed Heck Reactions. **2004**, 2114–2123.

(84) Tasker, S. Z.; Jamison, T. F. Highly Regioselective Indoline Synthesis under Nickel/Photoredox Dual Catalysis. *J. Am. Chem. Soc.* **2015**, *137* (30), 9531–9534. https://doi.org/10.1021/JACS.5B05597.